

RATIONAL APPROACH TO DESIGN OF MELANOCORTIN LIGANDS AND RECEPTOR
CHIMERAS

By

KRISTA RENNER WILSON

A DISSERTATION PRESENTED TO THE GRADUATE SCHOOL
OF THE UNIVERSITY OF FLORIDA IN PARTIAL FULFILLMENT
OF THE REQUIREMENTS FOR THE DEGREE OF
DOCTOR OF PHILOSOPHY

UNIVERSITY OF FLORIDA

2008

© 2008 Krista Renner Wilson

To everyone who prayed me through my education.

ACKNOWLEDGMENTS

I would like to thank all who have been instrumental in my life and education. I especially thank my parents who have always been there to love and support me. Without their help I would not be who I am today. I also thank all the past and present members of the Haskell-Luevano laboratory for teaching me everything I know about chemistry and molecular biology. I especially thank Dr. Andrzej Wilczynski and Dr. Christine Joseph for teaching me peptide and organic synthesis and Dr. Bettina Proneth and Dr. Zhimin Xiang for teaching me molecular biology and pharmacology skills. I also thank all the technicians who were involved in assaying my compounds over the years; their contribution was essential to my success. Special thanks go to Jay Schaub for his help in proofreading this dissertation and helping with the list of abbreviations. I would like to thank my supervisory committee members; especially Dr. Carrie Haskell-Luevano, for her support over the years. I also thank Dr. Kenneth Sloan, Dr. Hendrik Luesch and Dr. Sally Litherland for their counsel. I would also like to thank Dr. Margaret James and Dr. Raymond Bergeron for their role in my success.

Finally I would like to thank my husband, Brandon Wilson. Without his love and encouragement I would never have made it this far. I thank him for driving me to the lab in the middle of the night to refill dry ice or check the HPLC and helping me label countless tubes and plates. I thank God every day for bringing him into my life.

I also acknowledge the University of Florida Alumni Association for supporting my education for the last 4 years and the NIH for providing grants that supported my research.

TABLE OF CONTENTS

	<u>page</u>
ACKNOWLEDGMENTS	4
LIST OF TABLES	8
LIST OF FIGURES	9
ABSTRACT	24
CHAPTER	
1 INTRODUCTION TO DRUG DISCOVERY	26
Rational Drug Design	26
Structure-Activity Relationship Studies of Peptides	27
Design of Peptidomimetics and Small Molecules	32
Secondary Structural Features of Peptides	32
Peptide Modification in the Design of Peptidomimetics	37
Global constraints	38
Local constraints	41
Design of Small Molecules	43
Receptor Mutagenesis and Chimeric Receptors	45
2 THE MELANOCORTIN SYSTEM	47
The Melanocortin Receptors	47
The Melanocortin Ligands	50
Diseases Associated with the Melanocortin System	57
3 GENERAL METHODOLOGIES 1: CHEMISTRY	61
Solid Phase Peptide Synthesis	61
Merrifield Approach	61
The Fmoc Synthetic Strategy	64
Resins for SPPS	65
Side chain protecting groups	68
Coupling methods	70
Colorimetric monitoring methods	76
Solid Phase 1,4-Benzodiazepine-2,5-dione Synthesis	77
Solid Phase Organic Synthesis	78
Colorimetric Monitoring	84
Experimental Details	85
Synthesis of MTII-based Cation- π Peptides	85
1,4-Benzodiazepine-2,5-diones	87
Ligand Purification and Analysis	90

	Reporter Gene Assay: β -Galactosidase	90
4	GENERAL METHODOLOGIES 2: MOLECULAR BIOLOGY	91
	Molecular Cloning.....	91
	Structure of DNA	91
	Replication of DNA	93
	Transcription of DNA	97
	Translation into protein.....	98
	The PCR reaction	101
	Restriction endonuclease digestion	103
	Gel electrophoresis.....	104
	Sequencing	106
	Bacterial Expression Vectors	107
	Cell Culture and Transfection.....	111
	Mammalian Cell Lines	111
	Transfection.....	112
	Functional Assay	113
	Pharmacology Definitions.....	113
	Luciferase Assay	115
	Functional Assay: cAMP Assay.....	117
	Experimental Methods.....	118
	Cell Culture and Transfection	118
	Site-Directed Receptor Mutagenesis	119
	Real Time Polymerase Chain Reaction (RT-PCR)	122
	Fluorescence-Activated Cell Sorting (FACS).....	124
	Luciferase Reporter Gene Assay	125
	Functional Assay: cAMP Assay.....	125
	Data Analysis.....	126
5	STRUCTURE-ACTIVITY RELATIONSHIP STUDIES OF PEPTIDES: A STUDY OF INTRAMOLECULAR CATION-II INTERACTIONS IN MELANOCORTIN AGONISTS AND THE EFFECTS ON AGONIST AND ANTAGONIST SELECTIVITY	127
	Introduction.....	127
	Background Pharmacology	133
	Results.....	137
	Discussion.....	143
	D-Phenylalanine	144
	Phenylalanine	145
	D-Naphthylalanine (2')	146
	Naphthylalanine (2').....	147
	D-Naphthylalanine (1')	148
	Naphthylalanine (1').....	149
	Conformation Effects	150
	Receptor Selectivity.....	150

Agonist vs. Antagonist Selectivity	152
Conclusions	152
6 DESIGN OF PEPTIDOMIMETICS AND SMALL MOLECULES: 1,4-BENZODIAZEPINE-2,5-DIONES AS NM MELANOCORTIN AGONISTS	153
Introduction.....	153
Results.....	166
Discussion.....	168
Receptor Specificities	179
Characterization Data	180
7 CONSTRUCTION AND CHARACTERIZATION OF MELANOCORTIN-2 AND -4 RECEPTOR CHIMERAS	198
Introduction.....	198
Results.....	205
Flag-tagged hMC2R	205
Real-time PCR.....	208
Chimera Construction.....	210
Fluorescence Activated Cell Sorting.....	212
Luciferase Assay	217
Functional Assay: cAMP.....	220
Discussion.....	221
Chimeras in HEK293 Cell Lines.....	221
Chimeras in OS3 Cell Lines.....	228
Conclusions and Future Directions	230
8 CONCLUDING REMARKS.....	232
Structure-Activity Relationship Studies Of Peptides: A Study Of Intramolecular Cation-II Interactions In Melanocortin Agonists And The Effects On Agonist And Antagonist Selectivity	232
Design Of Peptidomimetics And Small Molecules: 1,4-Benzodiazepine-2,5-Diones As nM Melanocortin Agonists	233
Construction And Characterization Of Melanocortin-2 And -4 Receptor Chimeras	234
APPENDIX	
A ¹ H-NMR of 1,4-Benzodiazepine-2,5-Diones	237
B DNA Sequences and Restriction Maps of Chimeras.....	258
C Histograms of FACS Chimera Data	273
LIST OF REFERENCES	302
BIOGRAPHICAL SKETCH	334

LIST OF TABLES

<u>Table</u>	<u>page</u>
1-1 Secondary structural features induced by common amino acids.....	35
1-2 Methods of disulfide and lactam bridge formation.....	38
2-1 Ligand potency series for the five melanocortin subtypes.....	51
2-2 Amino acid sequences of the endogenous and synthetic melanocortin agonists.....	51
2-3 Truncation study of ACTH tested at the mMC2R.....	54
3-1 Common types of resin used in SPPS.....	66
3-2 Side chain protecting groups commonly used in SPPS.....	69
3-3 Phosphonium and aminium-based coupling reagents.....	75
4-1 Diagram of mRNA codons translated to amino acid.....	99
4-2 Comparison of luciferase and cAMP assays.....	118
5-1 SAR Studies of Selected Melanocortin Tetrapeptides and Pharmacology Data of Arg Substitutions.....	134
5-2 Antagonists of the MC3R and MC4R containing DNal(2').	135
5-3 Analytical Data for Peptides Synthesized in the Cation- π Study	138
5-4 Pharmacology Data for Peptides in the Cation- π Study	139
6-1 Pharmacology data of compounds synthesized by Dr. Christine Joseph.....	163
6-2 Analytical data of 1,4-benzodiazepine-2,5-diones synthesized in this study.	164
6-3 Pharmacology data of 1,4-benzodiazepine-2,5-diones synthesized in this study by Krista Wilson.	165
7-1 Primers for insertion of Flag tag into hMC2R template.	206
7-2 Restriction enzyme recognition sites.	212
7-3 Primers for insertion of unique restriction sites in hMC2R and hMC4R templates.	212
7-4 Functional activity of α -MSH and ACTH(1-24) at selected chimeras.	220

LIST OF FIGURES

<u>Figure</u>	<u>page</u>
1-1	Flowchart of drug design from biologically active peptides.26
1-2	Graphical description of Structure-Activity Relationship (SAR) studies of peptides.28
1-3	L versus D forms of phenylalanine and effects on α -MSH and NDP-MSH potency.30
1-4	Potential ligand-receptor interactions at the binding pocket.....31
1-5	Peptide torsion angles defining secondary structures and conformation.....32
1-6	Representative Ramachandran plot depicting torsion angles defining common peptide secondary structural features.....33
1-7	Common secondary structural features of peptides.....35
1-8	Reverse turn structures found in peptides.....37
1-9	Disulfide Cyclization of Peptides.....39
1-10	Lactam bridge cyclization of peptides.....40
1-11	Small molecules and peptomimetics incorporating β - and γ -turn mimetic structures.....41
1-12	Unnatural, constrained amino acids to control peptide conformation.....42
1-13	Backbone modifications of peptides.....43
1-14	Privileged structures often used in small molecule design.....44
2-1	The Melanocortin system.....47
2-2	Posttranslational processing of POMC into the melanocortin agonists.....50
2-3	ACTH truncated to α -MSH.....53
2-4	Partial sequences of the melanocortin antagonists hAGRP and hAgouti depicting the five disulfide bonds in each ligand.....55
3-1	General method of solid phase peptide synthesis including deprotection, coupling and cleavage steps.....62
3-2	General Boc chemistry synthesis strategy.....63
3-3	Proposed mechanism for acid-catalyzed Boc deprotection.....63

3-4	General Fmoc synthetic strategy.....	64
3-5	Proposed mechanism for base-catalyzed Fmoc removal.....	65
3-6	Diketopiperazine formation during synthesis using a hydroxymethyl linker and proline as the first amino acid.....	67
3-7	Common side reactions observed during amino acid activation.	70
3-8	Mechanism of amino acid coupling using carbodiimide coupling reagents.....	71
3-9	Mechanism of amino acid coupling using carbodiimides through symmetrical anhydride formation.....	72
3-10	Structures of common hydroxybenzotriazoles used in coupling.....	72
3-11	Proposed mechanism of amino acid coupling through active ester formation using carbodiimides and HOBt as coupling reagents.....	73
3-12	Proposed mechanism of oxazolone formation leading to amino acid coupling when carbodiimides are used as coupling reagents.....	73
3-13	Structures of phosphonium and aminium salts used in coupling reactions.....	74
3-14	N-terminal guanidation of peptide chain when HBTU is the coupling reagent.	74
3-15	Possible mechanism of primary amine detection using ninhydrin.	77
3-16	Complex formed from the reaction of chloranil with a secondary amine.	77
3-17	Structures of common benzodiazepine templates.....	78
3-18	Bunin <i>et al.</i> synthesis of a 1,4-benzodiazepine-2-one.....	79
3-19	Boojamra <i>et al.</i> synthesis of a 1,4-benzodiazepine-2,5-dione.....	80
3-20	Keating <i>et al.</i> synthesis of 1,4-benzodiazepine-2,5-diones.....	81
3-21	Bhalay <i>et al.</i> synthesis of 1,4-benzodiazepine-2-ones.....	81
3-22	Mayer <i>et al.</i> synthesis of 1,4-benzodiazepine-2-ones.....	82
3-23	Lee <i>et al.</i> synthesis of 1,5-benzodiazepine-2-ones.....	83
3-24	Zhang <i>et al.</i> synthesis of 1,4-benzodiazepine-2-ones.....	83
3-25	Reaction of an aldehyde with DNPH to give a red complex.....	85
4-1	Structure of DNA and bases.....	91

4-2	Formation of a phosphodiester bond during DNA synthesis.....	92
4-3	Structure of the replication fork.....	94
4-4	DNA replication of circular and linear DNA.....	95
4-5	The rolling circle method of DNA replication in prokaryotes.....	96
4-6	Structures of DNA and RNA nucleotides.....	97
4-7	Model of DNA transcription.....	98
4-8	Model of DNA translation.....	100
4-9	The PCR reaction.....	102
4-10	Reagents for gel electrophoresis.....	105
4-11	Model showing how BDT sequencing is read by the detector.....	107
4-12	Bacterial growth curve.....	108
4-13	Pharmacology curves.....	115
4-14	Luciferase reporter gene assay.....	116
5-1	Cation- π interaction between the positive charge of arginine and the negative potential on the face of the Phe aromatic system.....	127
5-2	Structure of natural and unnatural amino acids used in this study.....	128
5-3	Benzene.....	129
5-4	Cation- π interactions of Arg and Lys with Phe and water.....	131
5-5	Structure and pharmacology of the synthetic melanocortin agonist MTII and the synthetic melanocortin antagonist SHU9119.....	132
5-6	Schematic of a cation- π interaction between the cationic side chain of Arg and the negative potential of the π systems of DPhe and DNaI(2').	137
5-7	Bar graph of peptides 15, 21 and 22 with DPhe as the aromatic system at the mMC1,3-5R.....	145
5-8	Bar graph of peptides 16, 23 and 24 with Phe as the aromatic system at the mMC1,3-5R.....	146
5-9	Bar graph of peptides 17, 25 and 26 with DNaI(2') as the aromatic system at the mMC1,3-5R.....	147

5-10	Bar graph of peptides 18, 27 and 28 with Nal(2') as the aromatic system at the mMC1,3-5R.	148
5-11	Bar graph of peptides 19, 29 and 30 with DNal(1') as the aromatic system at the mMC1,3-5R.	149
5-12	Bar graph of peptides 20, 31 and 32 with Nal(1') as the aromatic system at the mMC1,3-5R.	150
6-1	Structures of benzodiazepines.....	153
6-2	Small molecules with activity at the melanocortin receptors and based on privileged structure templates.	155
6-3	Structures of 1,4-benzodiazepine-2,5-diones synthesized in this study by KRW.	161
6-4	Structures of building blocks used to synthesize 1,4-benzodiazepine-2,5-diones 39-58.....	162
6-5	Structure of Compound 37, a nanomolar agonist at all melanocortin receptors tested. .	171
7-1	Amino acid alignment of human melanocortin receptors 1-5.	199
7-2	α -MSH is formed from the endogenous truncation of ACTH.	200
7-3	Schematic of chimeras.	201
7-4	Addition of Flag tag to the hMC2R gene.....	205
7-5	Characterization of HEK293 and OS3 cells stably expressing the Flag-hMC2R.	207
7-6	Gene expression assay of hMC2R-OS3, hMC4R-HEK, and OS3 cells.....	208
7-8	Schematic of chimera construction.....	211
7-9	Diagram of unique restriction sites used during this study and their locations in the receptor.	211
7-10	Schematic of FACS experiment.....	213
7-11	Summary of FACS data of wild type receptors and chimeras expressed in HEK293 cells.	214
7-12	Summary of FACS data of wild type receptors and chimeras expressed in OS3 cells. .	215
7-13	Histograms of FACS data from thr Flag-hMC4R construct expressed in both OS3 and HEK cell lines.	216

7-14	Summary of functional data from the luciferase assay performed on hMC2R wild type receptors and chimeras expressed in HEK293 cells.	218
7-15	Summary of functional data from the luciferase assay performed on hMC4R wild type receptors and chimeras expressed in HEK293 cells.	219
7-16	Correlation plots of HEK hMC2R chimera data.....	224
7-17	Amino acid alignment of all melanocortin receptors and chimeras.	227
7-18	Time course of HEK and OS3 cell lines transiently transfected with GFP.	229
A-1	Compound 39 (KRW9-70E) ¹ H-NMR, 3-(4-aminobutyl)-1-benzyl-3,4-dihydro-1H-benzo[e][1,4]diazepine-2,5-dione.	238
A-2	Compound 40 (KRW5-37) ¹ H-NMR, 3-Benzyl-1-biphenyl-2-ylmethyl-3,4-dihydro-1H-benzo[e][1,4]diazepine-2,5-dione.	239
A-3	Compound 41 (KRW 9-70J) ¹ H-NMR, 1-(3-(1-(biphenyl-2-ylmethyl)-2,5-dioxo-2,3,4,5-tetrahydro-1H-benzo[e][1,4]diazepin-3-yl)propyl)urea.	240
A-4	Compound 42 (KRW9-70F) ¹ H-NMR, 3-(4-aminobutyl)-1-(biphenyl-2-ylmethyl)-3,4-dihydro-1H-benzo[e][1,4]diazepine-2,5-dione.	241
A-5	Compound 43 (KRW9-70A) ¹ H-NMR, 3-benzyl-1-(naphthalen-1-ylmethyl)-3,4-dihydro-1H-benzo[e][1,4]diazepine-2,5-dione.	242
A-6	Compound 44 (KRW9-70K) ¹ H-NMR, 1-(3-(1-(naphthalen-1-ylmethyl)-2,5-dioxo-2,3,4,5-tetrahydro-1H-benzo[e][1,4]diazepin-3-yl)propyl)urea.	243
A-7	Compound 45 (KRW9-70G) ¹ H-NMR, 3-(4-aminobutyl)-1-(naphthalen-1-ylmethyl)-3,4-dihydro-1H-benzo[e][1,4]diazepine-2,5-dione.	244
A-8	Compound 46 (KRW4-91) ¹ H-NMR, 3-Benzyl-1-propyl-3,4-dihydro-1H-benzo[e][1,4]diazepine-2,5-dione.	245
A-9	Compound 47 (KRW5-25) ¹ H-NMR, 3-Benzyl-1-butyl-3,4-dihydro-1H-benzo[e][1,4]diazepine-2,5-dione.	246
A-10	Compound 48 (KRW9-70B) ¹ H-NMR, 1,3-dibenzyl-8-methyl-3,4-dihydro-1H-benzo[e][1,4]diazepine-2,5-dione.	247
A-11	Compound 49 (KRW9-70L) ¹ H-NMR, 1-(3-(1-benzyl-9-methyl-2,5-dioxo-2,3,4,5-tetrahydro-1H-benzo[e][1,4]diazepin-3-yl)propyl)urea.	248
A-12	Compound 50 (KRW9-70H) ¹ H-NMR, 3-(4-aminobutyl)-1-benzyl-9-methyl-3,4-dihydro-1H-benzo[e][1,4]diazepine-2,5-dione.	249

A-13	Compound 51 (KRW9-70C) ¹ H-NMR, 1-(3-(1-benzyl-8-chloro-2,5-dioxo-2,3,4,5-tetrahydro-1H-benzo[e][1,4]diazepin-3-yl)propyl)urea.	250
A-14	Compound 52 (KRW6-121A) ¹ H-NMR, N-[3-(1-Benzyl-8-chloro-2,5-dioxo-2,3,4,5-tetrahydro-1H-benzo[e][1,4]diazepin-3-yl)-propyl]-guanidine.	251
A-15	Compound 53 (KRW9-70D) ¹ H-NMR, 3-benzyl-1-(biphenyl-2-ylmethyl)-8-chloro-3,4-dihydro-1H-benzo[e][1,4]diazepine-2,5-dione.....	252
A-16	Compound 54 (KRW9-70M) ¹ H-NMR, 1-(3-(1-(biphenyl-2-ylmethyl)-8-chloro-2,5-dioxo-2,3,4,5-tetrahydro-1H-benzo[e][1,4]diazepin-3-yl)propyl)urea.	253
A-17	Compound 55 (KRW9-70I) ¹ H-NMR, 3-(4-aminobutyl)-1-(biphenyl-2-ylmethyl)-8-chloro-3,4-dihydro-1H-benzo[e][1,4]diazepine-2,5-dione.....	254
A-18	Compound 56 (KRW5-49) ¹ H-NMR, 3-Benzyl-8-chloro-1-naphthalen-2-ylmethyl-3,4-dihydro-1H-benzo[e][1,4]diazepine-2,5-dione.....	255
A-19	Compound 57 (KRW9-70N) ¹ H-NMR, 1-(3-(8-chloro-1-(naphthalen-1-ylmethyl)-2,5-dioxo-2,3,4,5-tetrahydro-1H-benzo[e][1,4]diazepin-3-yl)propyl)urea.	256
A-20	Compound 58 (KRW7-05A) ¹ H-NMR, 3-(4-Amino-butyl)-8-chloro-1-naphthalen-2-ylmethyl-3,4-dihydro-1H-benzo[e][1,4]diazepine-2,5-dione.....	257
B-1	Flag-hMC2R DNA Sequence	259
B-2	Chimera 2C1 DNA Sequence	260
B-3	Chimera 2C2 DNA Sequence	261
B-5	Chimera 2C4 DNA Sequence	263
B-6	Chimera 2C5 DNA Sequence	264
B-7	Chimera 2C6 DNA Sequence	265
B-8	Flag-hMC4R DNA Sequence	266
B-9	Chimera 4C1 DNA Sequence	267
B-10	Chimera 4C2 DNA Sequence	268
B-11	Chimera 4C3 DNA Sequence	269
B-12	Chimera 4C4 DNA Sequence	270
B-13	Chimera 4C5 DNA Sequence	271
B-14	Chimera 4C6 DNA Sequence	272

C-1	Flag-hMC2R in HEK cells FACS Histogram.....	274
C-2	Chimera 2C1 in HEK cells FACS Histogram.....	275
C-3	Chimera 2C2 in HEK cells FACS Histogram.....	276
C-4	Chimera 2C3 in HEK cells FACS Histogram.....	277
C-5	Chimera 2C4 in HEK cells FACS Histogram.....	278
C-6	Chimera 2C5 in HEK cells FACS Histogram.....	279
C-7	Chimera 2C6 in HEK cells FACS Histogram.....	280
C-8	Flag-hMC4R in HEK cells FACS Histogram.....	281
C-9	Chimera 4C1 in HEK cells FACS Histogram.....	282
C-10	Chimera 4C2 in HEK cells FACS Histogram.....	283
C-11	Chimera 4C3 in HEK cells FACS Histogram.....	284
C-12	Chimera 4C4 in HEK cells FACS Histogram.....	285
C-13	Chimera 4C5 in HEK cells FACS Histogram.....	286
C-14	Chimera 4C6 in HEK cells FACS Histogram.....	287
C-15	Flag-hMC2R in OS3 cells FACS Histogram.....	288
C-16	Chimera 2C1 in OS3 cells FACS Histogram.....	289
C-17	Chimera 2C2 in OS3 cells FACS Histogram.....	290
C-18	Chimera 2C3 in OS3 cells FACS Histogram.....	291
C-20	Chimera 2C5 in OS3 cells FACS Histogram.....	293
C-21	Chimera 2C6 in OS3 cells FACS Histogram.....	294
C-22	Flag-hMC4R in OS3 cells FACS Histogram.....	295
C-23	Chimera 4C1 in OS3 cells FACS Histogram.....	296
C-24	Chimera 4C2 in OS3 cells FACS Histogram.....	297
C-25	Chimera 4C3 in OS3 cells FACS Histogram.....	298
C-26	Chimera 4C4 in OS3 cells FACS Histogram.....	299

C-27	Chimera 4C5 in OS3 cells FACS Histogram.....	300
C-28	Chimera 4C6 in OS3 cells FACS Histogram.....	301

LIST OF ABBREVIATIONS

2-Cl-Z	2-Chlorobenzyloxycarbonyl
3-Bom	3-Benzyloxymethyl
A	Ala, Alanine
AA	Amino Acid
Acm	Acetomidomethyl
AcOH	Acetic Acid
ACS	American Chemical Society
ACTH	Adrenocorticotropic Hormone
AGRP	Agouti Related Protein
Alloc	Allyloxycarbonyl
Anc	Amino-2-Naphthylcarboxylic Acid
AOP	(7-Azabenzotriazol-1-Yloxy)-Tris(Dimethylamino)Phosphonium Hexafluorophosphate
APC	Allophycocyanin
ASP	Agouti Signaling Peptide
AT1/AT2	Angiotensin I/II Receptor
Atc	Amino-Tetrahydro-2-Naphthylcarboxylic Acid
ATP	Adenosine Triphosphate
BAL	Backbone Amide Linker Resin
BBB	Blood Brain Barrier
BMI	Body Mass Index
Boc	<i>Tert</i> -Butyloxycarbonyl
BOP	Benzotriazol-1-Yl-N-Oxy-Tris(Dimethylamino)Phosphonium Hexafluorophosphate
BSA	Bovine Serum Albumin

Bu ₃ P	Tributylphosphine
Bzl	Benzyl
C	Cys, Cysteine
cAMP	Cyclic 5'-Adenosine Monophosphate
CCK	Cholecystokinin
Choranil	2,3,5,6-Tetrachloro-1,4-Benzoquinone
CO ₂	Carbon Dioxide
COF ₃	Cobalt (III) Fluoride
CPE	Carboxypeptidase E
CRE	cAMP Response Element
CRH	Corticotropin Releasing Hormone
CRLR	Calcitonin Receptor-Like Receptor
CTR	Calcitonin Receptor
D	Asp, Aspartic Acid
DCC	Dicyclohexylcarbodiimide
DCM	Dichloromethane
DIC	Diisopropylcarbodiimide
DIEA	N,N-Diisopropylethylamine
DMAP	4-Dimethylaminopyridine
DMEM	Dulbecco Modified Eagle's Media (Dulbecco Modified Eagle's Minimal Essential Medium)
DMF	N,N-Dimethylformamide
DMS	Dimethylsulfide
DMSO	Dimethyl Sulfoxide
DNA	Deoxyribonucleic Acid
DNal(1')	D-1-Naphthylalanine

DNal(2')	D-2-Naphthylalanine
DNPH	Dinitrophenylhydrazine
Dpr	Diaminopropionic Acid
E	Glu, Glutamic Acid
EDC	1-[3-(Dimethylamino)Propyl]-1'-Ethylcarbodiimide Hydrochloride
Et ₃ N	Triethyl Amine
F	Phe, Phenylalanine
FACS	Fluorescence-Activated Cell Sorting
Falp	Fat Tissue-Specific Low Molecular Weight Protein
FGD	Familial Glucocorticoid Deficiency
Fmoc	9-Fluorenylmethyloxycarbonyl
For	Formyl
G	Gly, Glycine
GABA	γ -Aminobutyric Acid
GPCR	G Protein Coupled Receptor
H	His, Histine
HATU	N-[(Dimethylamino)-1H-1,2,3-Triazolo[4,5]Pyridine-1-Yl)methylmethanaminium Hexafluorophosphate N-Oxide
HBTU	N-[1H-Benzotriazole-1-Yl)(Dimethylamino)Methylamino)Methylene]-N-Methylmethanaminium Hexafluorophosphate N-Oxide
HEK293	Human Embryonic Kidney Cell Line 293
HF	Hydrogen Fluoride
Hg(II)	Mercury (II)
HIV	Human Immunodeficiency Virus
HOAt	1-Hydroxy-7-Azabenzotriazole
HOBt	3-Hydroxybenzotriazole

HPA Axis	Hypothalamic-Pituitary-Adrenal Axis
I	Ile, Isoleucine
IBMX	Isobutylmethylxanthine
ICV	Intracerebroventricular
IL-1	Interleukin 1
IL-10	Interleukin 10
IL-6	Interleukin 6
IP ₃	Inositol Triphosphate
K	Lys, Lysine
KCl	Potassium Chloride
KO	Knockout
L	Leu, Leucine
M	Met, Methionine
MC1R	Melanocortin-1 Receptor
MC2R	Melanocortin-2 Receptor
MC3R	Melanocortin-3 Receptor
MC4R	Melanocortin-4 Receptor
MC5R	Melanocortin-5 Receptor
MCM	Minichromosome Maintenance
MCR	Melanocortin Receptor
MeOH	Methanol
MgCl ₂	Magnesium Chloride
MRAP	Melanocortin-2 Receptor Accessory Protein
mRNA	Messenger Ribonucleic Acid
MsCl	Mesyl Chloride

MSH	Melanocyte Stimulating Hormone
MT-I	Melanotan I
MTII	Melanotan II
N	Asn, Asparagine
Na/NH ₃	Sodium/Ammonia
NaBH(OAc) ₃	Sodium Triacetoxyborohydride
NaH	Sodium Hydride
NaOH	Sodium Hydroxide
NaOtBu	Sodium <i>Tert</i> -Butoxide
NAT	N-Acetyltransferase
nBuLi	N-Butyllithium
NDP-MSH	Norleucine, D-Phenylalanine-Melanocyte Stimulating Hormone
NHANES	National Health And Nutrition Examination Survey
Nle	Norleucine
nM	Nanomolar
NMP	N-Methyl Pyrollidinone
NMR	Nuclear Magnetic Resonance
Nup 50	Nucleopore 50
OAllyl	Allyl Ester
OD	Optical Density
ONPG	<i>Ortho</i> -Nitrophenyl-β-Galactoside
ORC	Origin Recognition Complex
Orn	Ornithine
OtBu	<i>Tert</i> -Butyl Ester
P	Pro, Proline

PAM	Peptidyl A-Amidating Monooxygenase
Pbf	7-Pentamethyldihydro-Benzofuran-5-Sulfonyl
PC1	Prohormone Convertase 1
PC2	Prohormone Convertase 2
Ph ₃ PPd	Palladium Triphenylphosphine
PKC	Protein Kinase C
pM	Picomolar
POMC	Proopiomelanocortin
PyAOP	(7-Azabenzotriazol-1-Yloxy)-Tris(Pyrrolidino)Phosponium Hexafluorophosphate
PyBOP	Benzotriazol-1-Yl-N-Oxy-Tris(Pyrrolidino)Phosponium Hexafluorophosphate
PyBrOP	[Bromotris]-(Pyrrolidino)Phosponium Hexafluorophosphate
Q	Gln, Glutamine
R	Arg, Arginine
RAMP	Receptor Activity Modifying Protein
RP-HPLC	Reverse Phase High Performance Liquid Chromatography
rRNA	Ribosomal RNA
RT	Room Temperature
RT-PCR	Real-Time Polymerase Chain Reaction
S	Ser, Serine
SAR	Structure Activity Relationship
SEM	Standard Error Of The Mean
SnCl ₂	Tin (II) Chloride
SPPS	Solid Phase Peptide Synthesis
StBu	<i>Tert</i> -Butyl Thioether
T	Thr, Threonine

TATU	N-[(Dimethylamino)-1H-1,2,3-Triazolo[4,5]Pyridine-1-Ylmethylene]-N-Methylmethanaminium Tetrafluoroborate N-Oxide
TBTU	N-[1H-Benzotriazole-1-Yl(Dimethylamino)Methylene]-N-Methylmethanaminium Tetrafluoroborate N-Oxide
tBu	<i>Tert</i> -Butyl
TFA	Trifluoroacetic Acid
THF	Tetrahydrofuran
Tic	Amino-1,2,3,4-Tetrahydroisoquinoline-Carboxylic Acid
TM	Transmembrane
TNF α	Tumor Necrosis Factor Alpha
Tos	Tosyl
tRNA	Transfer RNA
Trt	Trityl
UV	Ultraviolet
V	Val, Valine
W	Trp, Tryptophan
Y	Tyr, Tyrosine
α -MSH	Alpha-Melanocyte Stimulating Hormone
β -MSH	Beta-Melanocyte Stimulating Hormone
γ -MSH	Gamma-Melanocyte Stimulating Hormone
μ M	Micromolar

Abstract of Dissertation Presented to the Graduate School
of the University of Florida in Partial Fulfillment of the
Requirements for the Degree of Doctor of Philosophy

RATIONAL APPROACH TO DESIGN OF MELANOCORTIN LIGANDS AND RECEPTOR
CHIMERAS

By

Krista Renner Wilson

May 2008

Chair: Carrie Haskell-Luevano
Major: Pharmaceutical Sciences

The melanocortin system is made up of five G protein-coupled receptors (GPCRs), the endogenous agonists α -MSH, β -MSH, γ_1 -MSH, γ_2 -MSH, and adrenocorticotrophic hormone (ACTH), and the only two known antagonists of GPCRs, agouti and agouti-related protein (AGRP). Many physiological processes have been linked to the melanocortin system, such as skin pigmentation, energy and weight homeostasis, and steroidogenesis.

Obesity (BMI >30) is a condition increasing in morbidity across the United States, and which may lead to serious complications such as type II diabetes mellitus, hypertension, stroke, heart disease, and cancer. It has been shown through targeted disruption of the MC4R that this receptor plays a role in the development of obesity. Structure-activity relationship studies of the endogenous agonist α -MSH have identified key amino acids involved in ligand binding to the receptor and have aided in the design of synthetic ligands more potent than α -MSH at the MC4R. It is hypothesized that potent agonists selective for the MC4R may be used as therapeutic agents to treat obesity.

This dissertation investigates three experimental methods used to provide information about putative ligand-receptor interactions for the design of drugs targeting the melanocortin system:

- Structure-Activity Relationship Studies of Peptides
- Design of Peptidomimetics and Small Molecules
- Receptor Mutagenesis and Chimeric Receptors

The first section reports the synthesis and evaluation of derivatives of the melanocortin synthetic ligands MTII and SHU9119. It is hypothesized that there may be a cation- π interaction between an Arg and the adjacent aromatic amino acid which may be involved in agonist and antagonist activity. To investigate this theory, a series of peptides was synthesized which incorporate six aromatic amino acids: DPhe, Phe, DNal(2'), Nal(2'), DNal(1') and Nal(1') coupled with either Arg, Lys, or Ala. A cation- π interaction is indicated by the potency series Arg > Lys > Ala.

The second section describes the synthesis of a series of 1,4-benzodiazepine-2,5-diones as small molecule ligands of the melanocortin receptors. These compounds were designed based on the core tetrapeptide sequence His-Phe-Arg-Trp present in all melanocortin agonists. Compounds were synthesized with significant agonist activity at all receptors.

The final section involves the construction and characterization of a series of hMC2R (human Melanocortin-2 Receptor) and hMC4R (human Melanocortin-4 Receptor) chimeras in order to clarify the unique properties of the hMC2R. It is hypothesized that the MC2R and ACTH may be involved in the homeostasis of human hypertension, and therefore correlated to heart disease and stroke. The study proposed herein attempts to understand the molecular mechanism of how ACTH stimulates the MC2R.

The results of these studies illustrate important intermolecular interactions present in melanocortin ligands which may be used in the future to design more potent and bioavailable drugs.

CHAPTER 1 INTRODUCTION TO DRUG DISCOVERY

Rational Drug Design

Over the past few decades the focus of drug research has switched from the concept of drug discovery (that is, serendipity) to that of rational drug design. With advances in molecular biology, genetics, and chemistry, it is now possible to design potential lead compounds based on a known biological target.

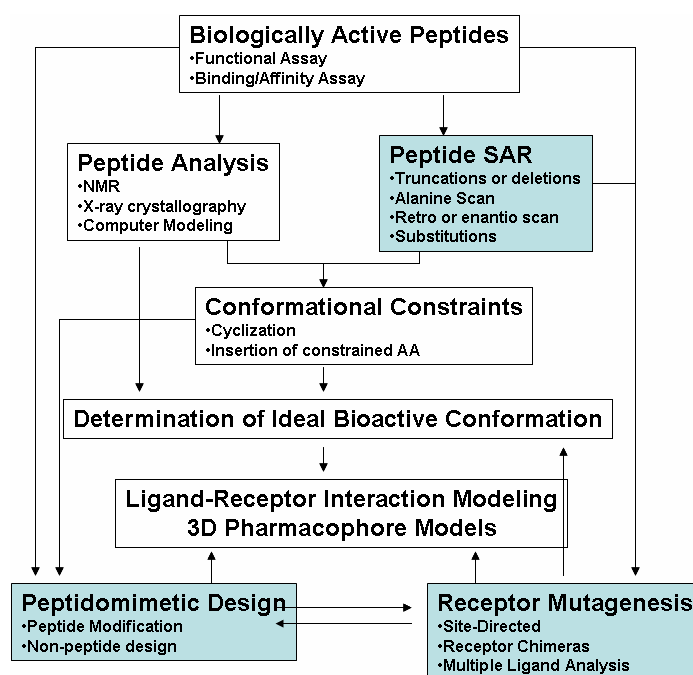


Figure 1-1. Flowchart of drug design from biologically active peptides. Highlighted boxes indicate methods considered in our study.

Rational drug design is a method for developing potential new therapeutic agents for the treatment of disease based on a known biological target. One common method involves the use of biologically active peptides as a starting point (Figure 1-1).¹ This process begins with the identification of a biological receptor system that is stimulated by a specific peptide. Functional assay and competitive binding studies may then be performed to characterize the endogenous ligand-receptor interaction. This is followed by structure-activity relationship (SAR) studies in which the molecular basis for the ligand-receptor interaction is probed using substituted peptides

and also by biophysical peptide analysis. This information can then be used to design conformationally constrained peptides and peptidomimetics to investigate the ideal bioactive conformation required for ligand binding and stimulation. 3-D computer modeling and molecular dynamics studies can also be used to predict ligand-receptor interactions. These studies can then be used in the design of small molecule ligands with biological activity. An additional receptor-based approach may also be used in which specific amino acid residues in the receptor are mutated to determine which portions of the receptor are interacting with the ligand.

This dissertation investigates three experimental methods used to provide information about putative ligand-receptor interactions for the design of drugs targeting the melanocortin system:

- Structure-Activity Relationship Studies of Peptides
- Design of Peptidomimetics and Small Molecules
- Receptor Mutagenesis and Chimeric Receptors

Structure-Activity Relationship Studies of Peptides

Once a biological target has been identified, it is a common approach in drug design to take the endogenous biological effectors (ie. peptides, steroids, small molecules) and submit them to extensive analysis. During this process, the amino acid sequence required for binding to and activating the endogenous receptor is investigated and lead peptide sequences optimized, meaning amino acid sequences are modified in order to produce synthetic peptides that are more potent than the endogenous peptide.

The processes by which peptides are analyzed and sequences optimized are known as structure-relationship studies (SAR) or structure-function studies. There are many methods to determine the ideal amino acid sequence including the use of truncation studies,² alanine scans,³

D-amino acid scans,⁴ enantio scans,⁵ retro synthesis,⁵ retro-enantio scans⁵ and the use of single or multiple amino acid substitution⁶⁻⁹ (Figure 1-2).

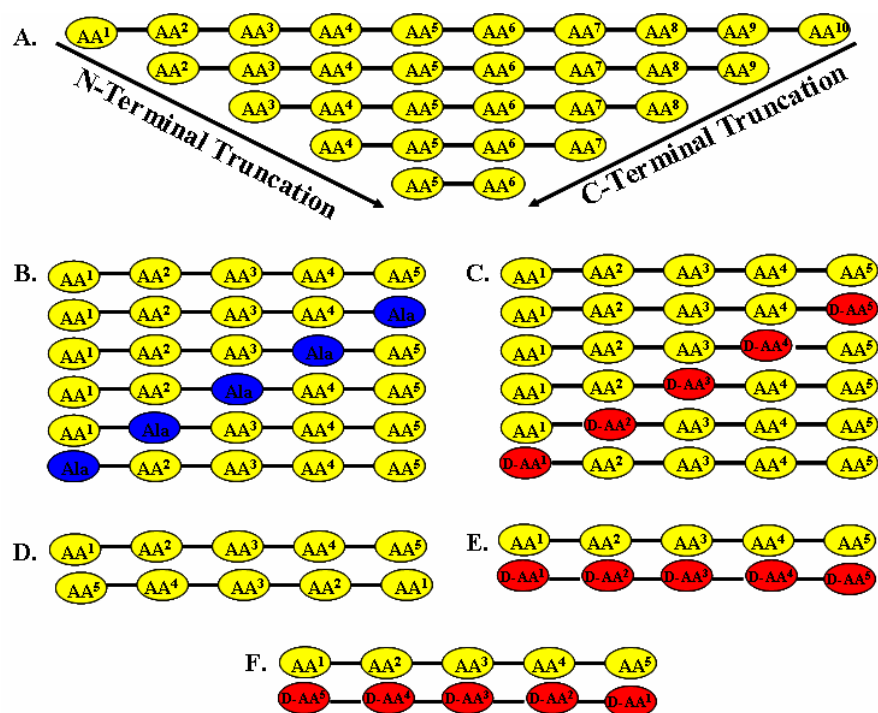


Figure 1-2. Graphical description of Structure-Activity Relationship (SAR) studies of peptides. **A.** N-terminal and C-terminal truncation. **B.** Alanine scan. **C.** D-amino acid scan. **D.** Retro scan. **E.** Enantio scan. **F.** Retro-enantio scan.

Truncation studies. The first method of SAR that is discussed is truncation or deletion studies (Figure 1-2A).² This method involves the sequential truncation of individual amino acids from either the N-terminus or the C-terminus of the endogenous peptide. As amino acids are removed, functional assay reveals whether or not the truncated peptide can still elicit a biological response. If there is no change in potency when an amino acid is removed, then it may be inferred that that amino acid is not necessary for ligand binding or signaling. If there is a significant decrease in potency upon deletion of an amino acid, then that amino acid may be involved in either ligand binding or signaling. Using this method, the shortest amino acid chain still able to elicit a biological response may be determined. This is important, as it is desirable for the design of small molecules to know the minimum sequence needed for stimulation.

Alanine scan. Another method common to peptide SAR studies is the alanine scan (Figure 1-2B).³ In this study, each amino acid in the sequence is sequentially replaced with an alanine. Alanine is a small, hydrophobic amino acid where $R = CH_3$. When other amino acids are replaced by alanine, the intermolecular interactions between that amino acid side chain and either the receptor or the ligand may be interrupted. For example, if the peptide contains a serine that is replaced by an alanine, the hydrogen bonding and hydrophilicity of the serine are replaced with a hydrophobic group. This, in turn, affects the binding of the ligand to the receptor or the folding of the peptide, causing a change in potency of the ligand. When an amino acid is replaced with alanine and there is a large decrease in potency associated with the substitution, it may be inferred that that amino acid is involved in either binding to the receptor or in signaling.

D-Amino acid scan. In biological systems, all amino acids are in the L configuration. This means that a chain of amino acids linked by peptide bonds will often behave in predictable ways when assuming the secondary structure based on the sequence of amino acids.^{1,10} The peptide will form a series of α -helices or β -sheets with the side chains of the amino acids projecting in predictable patterns. One method used to investigate the effects of a change in configuration on the potency of a ligand is the D-amino acid scan, where each amino acid is replaced with the D form of that amino acid, in turn (Figure 1-2C).⁴ Often, it may be discovered that the ligand is even more potent when specific amino acids are changed to the D configuration. An important example of this phenomenon is seen in the development of the synthetic melanocortin agonist NDP-MSH from the endogenous peptide α -MSH. D-amino acid studies of α -MSH revealed that when the phenylalanine residue was replaced with a D-phenylalanine, the resulting peptide was significantly more potent at the melanocortin receptors.⁴ This change was so significant, that many future synthetic ligands of melanocortin agonists have incorporated the D form of

phenylalanine (Figure 1-3). Incorporation of D-amino acids is also beneficial in the development of peptides that are more resistant to degradation as peptidases in the body do not recognize the D amino acids as their substrate, resulting in a peptide with a longer half-life.⁴

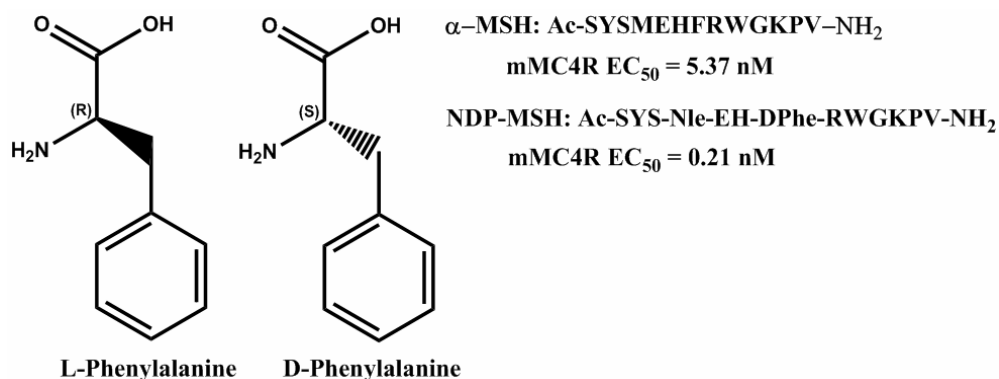


Figure 1-3. L versus D forms of phenylalanine and effects on α -MSH and NDP-MSH¹¹ potency.¹²

Retro, enantio, and retro-enantio scans. A less used form of studying ligand-receptor interactions through SAR studies is the use of retro, enantio, and retro-enantio scans.⁵ A retro scan involves synthesizing the reverse amino acid sequence of the original peptide (Figure 1-2D). This switches the N→C directionality of the peptide. This reveals information about whether the peptide is only active when synthesized in the physiological direction or whether it is only the sequence of amino acids that matters. Additionally, an enantio study is where all amino acids are replaced with the D form of the amino acid at the same time⁵ (Figure 1-2E). This completely changes the conformation of the peptide. Finally, a retro-enantio scan involves synthesizing the peptide in reverse order with all amino acids in the D-form⁵ (Figure 1-2F). While not as useful as the truncation studies, alanine scan, or D-amino acid scan, these methods are often used to explore the effects of changes in conformation and peptide direction.

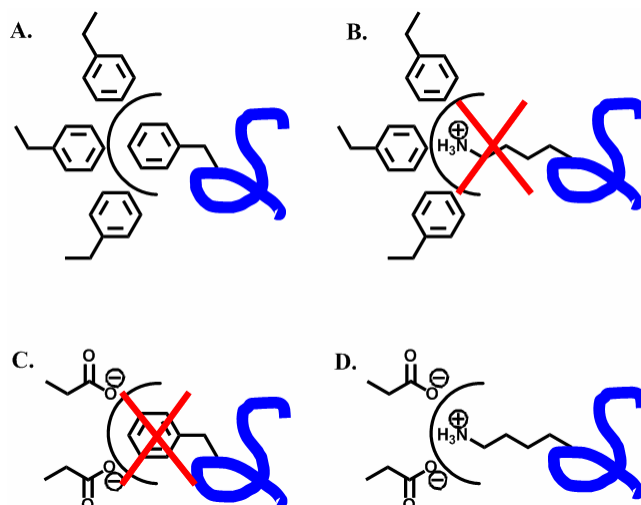


Figure 1-4. Potential ligand-receptor interactions at the binding pocket. Blue represents ligand; side chains represent receptor residues. **A.** Favorable interaction between aromatic ligand and hydrophobic binding pocket. **B.** Unfavorable interaction between hydrophobic binding pocket and charged ligand. **C.** Unfavorable interaction between negatively-charged binding pocket and aromatic ligand. **D.** Favorable interaction between negatively-charged binding pocket and positively-charged ligand.

Single or multiple substitutions. Once the important amino acid side chains have been determined by use of other SAR studies, it is possible to investigate more specifically the side chain functional groups which are important for ligand-receptor interactions. In these studies, amino acids possessing different chemical properties may be substituted for an important amino acid. For example, each residue may be replaced with a hydrophilic residue (ie. serine), a hydrophobic residue (ie. leucine), an aromatic residue (ie. phenylalanine), a basic residue (ie. lysine), an acidic residue (ie. aspartic acid), or with proline, which induces a turn or kink in the peptide chain.¹⁰ Information about the intermolecular interactions between ligand and receptor may be obtained here, enabling the proposal of possible binding pockets in the receptor. For example, if an aromatic or hydrophobic amino acid is well-tolerated and substitution with a charged or hydrophilic amino acid abolishes functional activity, then it may be postulated that this particular amino acid fits into a hydrophobic binding pocket in the receptor (Figure 1-4A,B). Conversely, if charged side chains produce a ligand with good potency, that region of the ligand

may be interacting with a charged or hydrophilic pocket in the receptor (Figure 1-4C,D). These studies are very important in the determination of the ideal peptide sequence needed to bind to and stimulate a target receptor. All the SAR data may be combined and then used to create peptides more potent than the endogenous peptide, or peptidomimetics and/or small molecules which are able to mimic the bioactive conformation of a given peptide.¹

Design of Peptidomimetics and Small Molecules

Peptides are very difficult to formulate as drugs because of their high molecular weight, abundance of hydrogen bonding sites, high rates of degradation in the body and long synthesis.^{13,14} For these and other reasons, it is often desirable to develop molecules which mimic the 3-D conformation of important functional groups in the active peptide. These molecules which mimic the peptide are often known as peptidomimetics.^{13,14} Common methods of peptide modification include cyclization, backbone modification and incorporation of unnatural, constrained amino acids.¹ Additionally, turn mimetics may be introduced into the molecule to induce a particular conformation.¹⁵⁻¹⁷

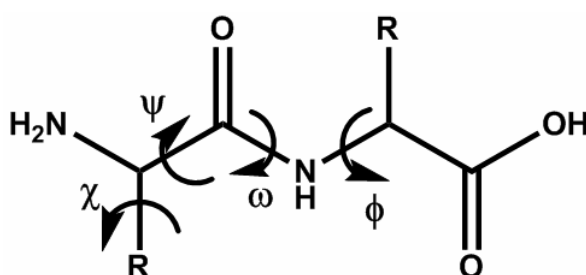


Figure 1-5. Peptide torsion angles defining secondary structures and conformation.

Secondary Structural Features of Peptides

Peptidomimetics are often designed to mimic the secondary structure of a peptide.^{13,14} There are several secondary structural features common to endogenous peptides and proteins. These are the α -helix, β -sheet, β -turn, and γ -turn.^{10,18} These secondary structural motifs are

defined by peptide torsion angles, defined in Figure 1-5. The angles are defined as follows: ϕ = the angle formed between the NH and the alpha carbon ($C\alpha$) of the peptide backbone; ψ = the angle formed between $C\alpha$ and the carbonyl carbon; ω = the angle formed between the carbonyl carbon and the NH; and χ = the angle formed between the first atom of the side chain and the peptide backbone. When the ϕ and ψ torsion angles are plotted against each other, a Ramachandran plot¹⁰ is obtained, which depicts the expected secondary structure of the peptide based on the specific ϕ and ψ angles. A representative Ramachandran plot showing the locations of the α -helix and β -sheet is shown in Figure 1-6¹⁰. In this diagram, the white regions correspond to structural conformations that are disallowed due to steric overlap of atoms, blue regions are allowable in certain situations, and red areas correspond to conformations where there is no steric hindrance. The red regions correspond to the two most common secondary structural features of peptides and proteins, the α -helix and the β -sheet.

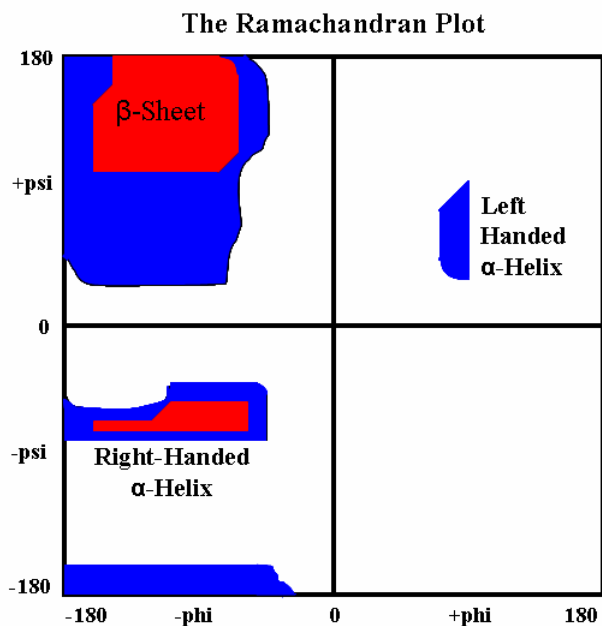


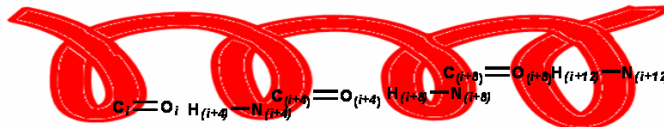
Figure 1-6. Representative Ramachandran plot¹⁰ depicting torsion angles defining common peptide secondary structural features.

The α -helix. The right-handed α -helix is characterized by negative phi (-60) and psi (-50) values.¹⁰ Hydrogen bonding between the backbone atoms results in a helical structure which repeats every 5.4 Å.¹⁹ There are 3.6 amino acids per turn of the helix and 1.5 Å rise between each amino acid.¹⁹ Each carbonyl oxygen is hydrogen bonded to the NH of the amino acid four residues away (O_i to N_{i+4})¹⁹ (Figure 1-7A). This forms a repeatable, regular, stable structure. Within the helix, all C=O groups point in one direction, and all H-N groups point in the opposite direction. Side chains extend outward from the helix and slightly toward the N-terminus.¹⁹ Certain amino acids are associated as being compatible with the α -helical structure (Table 1-1). These are Ala, Leu, Met, Phe, Glu, Gln, His, Lys, and Arg. Bulky, hydrophobic residues such as Tyr, Trp, Ile, Val, and Thr, and the large sulfur atom of Cys do not favor the α -helix, and instead prefer the β -sheet. Other amino acids such as Gly, Pro, Asp, Asn, and Ser tend to disrupt secondary structures, and are therefore more common in turn structures. The left-handed α -helix is much less common due to steric crowding of the C=O next to the amino acid side chains, and is thus only found in short segments of Gly-rich proteins.

The β -sheet. The other most common secondary structural feature of peptides and proteins is the β -sheet.²⁰ In contrast to the α -helix, psi values of β -sheets are positive, centered at approximately +130.¹⁰ Phi values are negative, centered around $\phi = -140$ degrees.¹⁰ Amino acids in a β -sheet are spaced 3.5 Å apart,²⁰ and are arranged in an extended, roughly linear manner. The structure is held together by hydrogen bonding between the C=O and N-H of the backbone of adjacent strands.²⁰ These strands can run either parallel or anti-parallel to each other.²⁰ Along a strand, the C=O and N-H are arranged opposite one another, and alternate side chains point in opposite directions oriented 90° from the backbone²⁰ (Figure 1-7B). Bulky and hydrophobic amino acids such as Tyr and Trp favor the β -sheet, as well as branched hydrophobics like Ile and

Val, and Cys, which contains a large sulfur atom attached to the β -carbon of the side chain, making it difficult to arrange in a α -helix.

A. α -Helix



B. β -Sheet (Antiparallel)

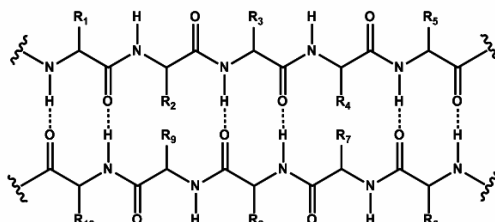


Figure 1-7. Common secondary structural features of peptides. **A.** α -helix. **B.** β -sheet.

Table 1-1. Secondary structural features induced by common amino acids.

Amino Acid	Secondary Structure	Comments
Ala	α -helix	
Cys	β -sheet	Large sulfur group on β -carbon
Asp	Disrupts structure	Hydrogen bond on side chain
Glu	α -helix	
Phe	α -helix	
Gly	Disrupts structure	No side chain to stabilize helix
His	α -helix	
Ile	β -sheet	Branched at β -carbon
Lys	α -helix	
Leu	α -helix	
Met	α -helix	
Asn	Disrupts structure	
Pro	Turns	Kinks chain, causes turns
Gln	α -helix	
Arg	α -helix	
Ser	Disrupts structure	Hydrogen bond on side chain
Thr	β -sheet	
Val	β -sheet	Branched at β -carbon
Trp	β -sheet	Bulky aromatic
Tyr	β -sheet	Bulky aromatic

The reverse turn. Many peptides and proteins also contain specialized structural features such as turns, which serve to change the direction of the peptide chain.^{10,18} The most common of these are the β -turn and the γ -turn. The β -turn (Figure 1-8A), also known as the reverse turn, serves as a site for chain reversal and may be involved in molecular recognition, antibody recognition, receptor binding, or posttranslational modification.¹⁸ The reverse turn is defined by the following conditions: positions i , $i+1$, $i+2$, and $i+3$ are not in an α -helix, and the distance between $Ca(i)$ and $Ca(i+3)$ is less than 7\AA .¹⁸ There are several types of β -turns, the most common being of Type I or Type II. Type I β -turns occur when the amino acids in positions $i+1$ and $i+2$ are in the L conformation. Type I bond angles are defined as follows: $\phi(i+1) = -60$; $\psi(i+1) = -30$; $\phi(i+2) = -90$; $\psi(i+2) = 0$.²¹ Type II β -turns occur when the amino acids in position $i+1$ is in the L conformation, and the amino acid in position $i+2$ is in the D conformation. Type II bond angles are defined as follows: $\phi(i+1) = -60$; $\psi(i+1) = 120$; $\phi(i+2) = -90$; $\psi(i+2) = 0$.²¹

The other turn motif is the γ -turn. This turn is similar to the β -turn, except that it only involves three amino acids. A gamma turn is defined for three residues i , $i+1$ and $i+2$ if residues i and $i+2$ are connected by a hydrogen bond, and the dihedral angles of $i+1$ fall into one of two categories: classic where $\phi = 75$ and $\psi = -64$; or inverse where $\phi = -79$ and $\psi = 69$ (Figure 1-8B).^{18,22} Like the β -turn, the γ -turn has been shown to be involved in molecular and antibody recognition as well as receptor binding.²³

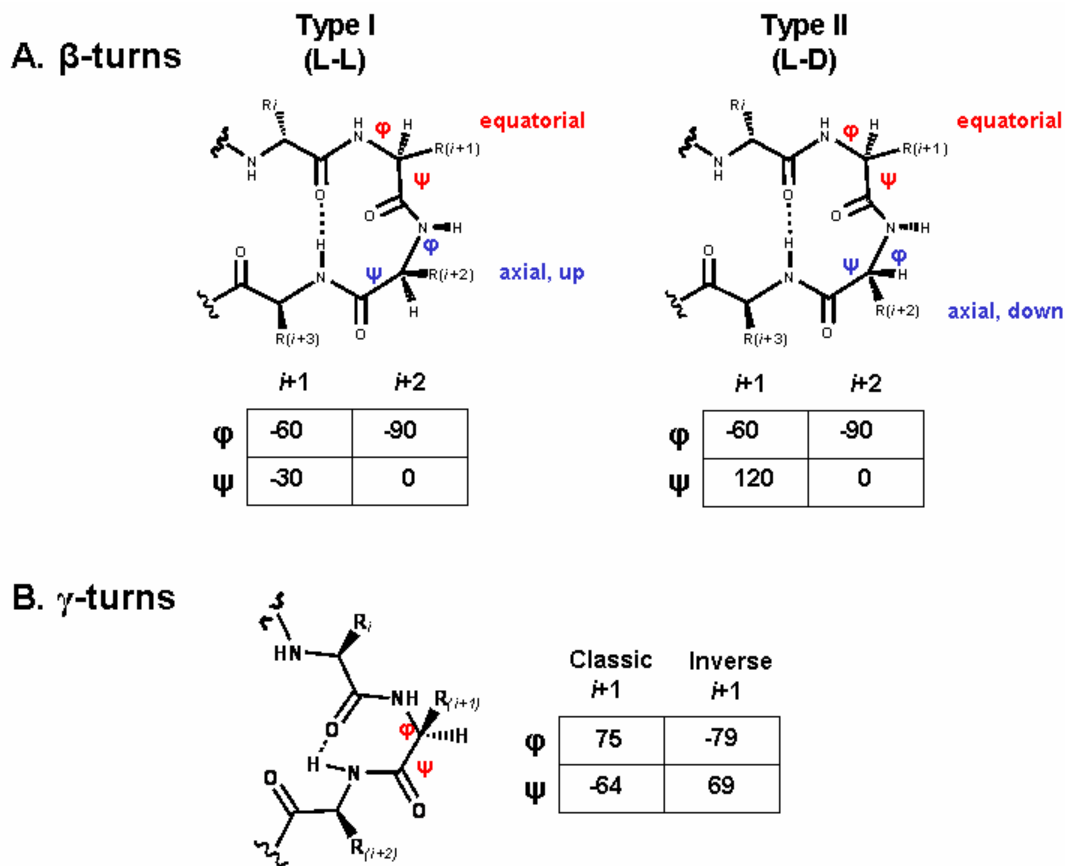


Figure 1-8. Reverse turn structures found in peptides. **A.** Type I and II β -turns along with torsion angles. **B.** γ -turn and torsion angles.

Peptide Modification in the Design of Peptidomimetics

Peptide SAR studies are essential in that they provide necessary information about the secondary structural characteristics and functional groups important for ligand binding and signaling. The next step is to take this information and modify the peptide in such a way as to increase potency and to increase the bioavailability of the molecule. This is often done by “locking” the molecule into its bioactive conformation by cyclization or by insertion of constrained amino acids.¹ Introduction of unnatural amino acids or mimetics into the peptide chain also serves to make the molecule more resistant to proteolytic degradation in the body by making the peptide less recognizable to peptidases.^{13,14}

Global constraints

Cyclization. Most endogenous peptides are linear and therefore often very flexible in solution. This gives rise to a large number of possible conformations that the peptide may adopt. In order to increase the potency of a peptide, it is often desirable to increase the number of molecules which are in the bioactive conformation. This can be done by “locking” the peptide into the bioactive conformation in many ways, including cyclization.

Endogenous peptides and proteins often contain disulfide bridges between Cys residues to help the protein adopt the correct 3-D conformation. This technique can also be used in solid phase peptide synthesis (SPPS) to bias the peptide toward the ideal bioactive conformation. The most common cyclization methods are formation of a disulfide bridge or a lactam bridge.¹ The disulfide bridge is formed between two cysteine residues contained in the peptide sequence. A peptide may contain one or more disulfide bridges. This is done through the selective protection and deprotection of cysteine pairs followed by oxidation (Figure 1-9 and Table 1-2).²⁴ The ease of cyclization depends on ring size and specific amino acid composition. Disulfide formation is most often done after cleavage in solution phase, though there are on-resin strategies that may be compatible with certain resins.²⁴

Table 1-2. Methods of disulfide and lactam bridge formation.

Cyclization Type	Chemistry	Solid or Solution Phase?	Protecting Group	Deprotection
Disulfide	Fmoc	Solution	Trt	TFA or HF
Disulfide	Boc or Fmoc	Solution	Acm	Iodine
Disulfide	Boc	Solution	Bzl	Na/NH ₃
Disulfide	Boc or Fmoc	Solution	<i>t</i> Bu	HF or Hg(II)
Disulfide	Boc or Fmoc	Solution	<i>S</i> tBu	RSH or Bu ₃ P
Lactam	Boc	Solid	Fmoc	Piperidine
Lactam	Fmoc	Solid	Alloc/OAllyl	Ph ₃ PPd

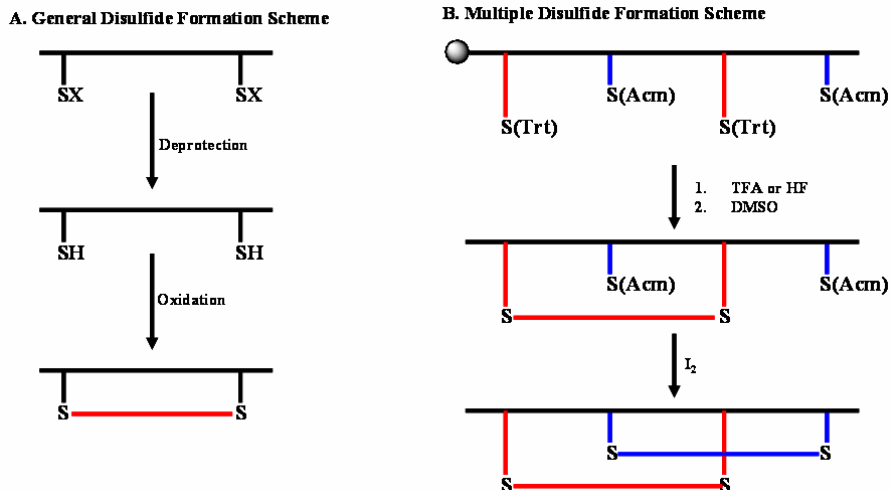


Figure 1-9. Disulfide Cyclization of Peptides. **A.** General disulfide formation scheme in which cysteine residues are protected with identical groups which may be deprotected separately from peptide-chain protecting groups, followed by oxidation to form a disulfide bridge. **B.** Multiple disulfide formation scheme used for the synthesis of multiple disulfide bonds on one peptide chain. Each pair of cysteines may be protected and deprotected selectively, ensuring correct disulfide pair formation.

Another common method of cyclization that has gained popularity in recent years is the lactam bridge.²⁵ This is essentially the formation of a peptide bond between an amine and a carboxylic acid. Lactam bridge cyclizations can be formed in several ways, including head-to-tail (between the N- and C-termini of a single peptide), head-to-side chain or tail-to-side chain (between a terminal residue or backbone and a side chain), and side chain-to-side chain cyclization (Figure 1-10).²⁵ Current methodology allows for the selective protection and deprotection of side chains to be cyclized on solid phase, and coupling reactions using the same coupling reagents as standard amino acid coupling (see Chapter 3). Either Boc or Fmoc chemistry may be used by employing suitable protection methods (Table 1-2). Common amino acids used for this cyclization are ones that contain an amine functional group (ie. Lys, Orn, Dpr), or a carboxylic acid (ie. Asp, Glu).

Pseudocyclization. Another method to globally constrain the structure of a peptide is through the stabilization of secondary structural features such as α -helices, β -sheets, β -turns, and

γ -turns. As was discussed previously, these secondary structural features may be important for binding and ligand recognition at the receptor. Peptides may be designed with a bias toward a particular secondary structure through the insertion of specialized amino acids, or through the incorporation of a small molecule moiety into the peptide chain which causes the peptide to form a turn structure.¹⁵⁻¹⁷

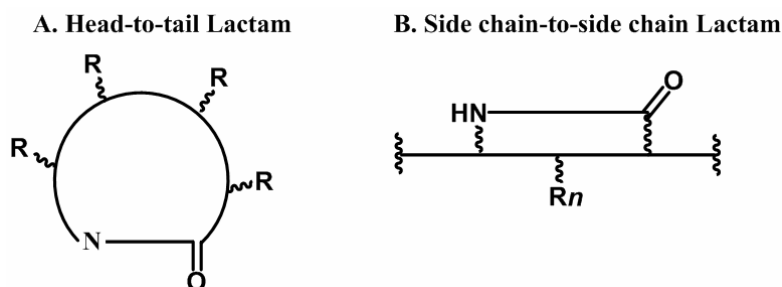


Figure 1-10. Lactam bridge cyclization of peptides. **A.** Head-to-tail cyclization. **B.** Side chain-to-side chain cyclization.

Peptidomimetic and non-peptide libraries have been constructed which incorporate β -turns that are melanocortin agonists.^{26,27} Haskell-Luevano *et al.* reported the synthesis of the first heterocyclic non-peptide molecules that were melanocortin agonists (Figure 1-11A,B).²⁶ These compounds were based on a β -turn motif, and were shown to be micromolar agonists at the mMC1R.²⁶ Bondebjerg *et al.* also did a study in which a thioether cyclized scaffold was used to mimic the β -turn found in the endogenous and synthetic peptides.²⁷ These molecules were shown to be nanomolar agonists at the mMC1R, and the mMC3-5R (Figure 1-11C).²⁷ Recent unpublished studies in the Haskell-Luevano lab have also identified a novel peptidomimetic that contains a β -turn and exhibits nanomolar agonist activity at the mMC1R, mMC4R, and mMC5R, but no functional activity at the mMC3R (Figure 1-11F).

Recently, Johannesson *et al.* have identified novel bicyclic motifs (Figure 1-11D,E) that exhibit activity at the Angiotensin receptors.^{15,16} When an acetal derivative of Asp was incorporated into the Angiotensin II template, cyclization occurred toward the C-terminus, and

the compounds exhibited reverse turn-inducing properties.¹⁶ Incorporation of the Glu acetal derivative resulted in cyclization toward the N-terminus.¹⁵

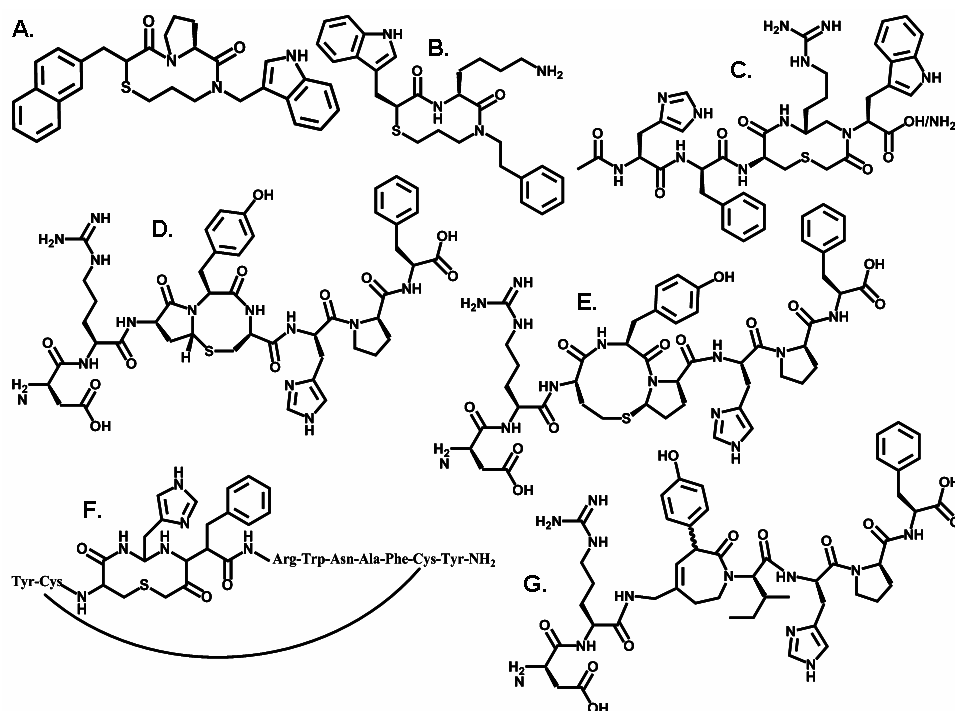


Figure 1-11. Small molecules and peptomimetics incorporating β - and γ -turn mimetic structures. **A,B.** First reported melanocortin small molecule agonists.²⁶ **C.** Thioether cyclized melanocortin agonists.²⁷ **D,E.** Angiotensin derivatives incorporating a β -turn mimetic.^{15,16} **F.** Unpublished melanocortin agonist. **G.** Angiotensin derivative encompassing a γ -turn mimetic.²³

Angiotensin analogues have also been the subject of studies to insert a γ -turn structure into the endogenous peptides. Figure 1-11G depicts an Angiotensin II analog with an azepine mimetic that has full agonist activity at the AT₁ receptor.²³

Local constraints

Substitution of constrained amino acids. The use of local constraints to bias a peptide towards its preferred bioactive conformation can also be done through the substitution of conformationally constrained amino acids.¹ The simplest of these is proline, which tends to introduce a bend or kink in the chain, and removes a degree of rotation from the peptide due to its secondary amine functionality.²⁸ Other cyclic derivatives of amino acids have been tested as

well and effectively serve to limit chain flexibility or define *cis-trans* isomerism.^{29,30} Figure 1-12 depicts the structures of three conformationally constrained amino acids often used to limit side-chain flexibility. The Tic residue has been shown to selectively adopt the *cis* isomer, and insertion of this amino acid into μ -opioid antagonist templates³¹ and ACE inhibitors³² has resulted in potent and selective compounds. In melanocortin tetrapeptide studies, when Anc was substituted for the His in the Ac-His-Phe-Arg-Trp-NH₂ template, the compound was converted from an agonist to an antagonist at the mMC3R and mMC4R.⁶

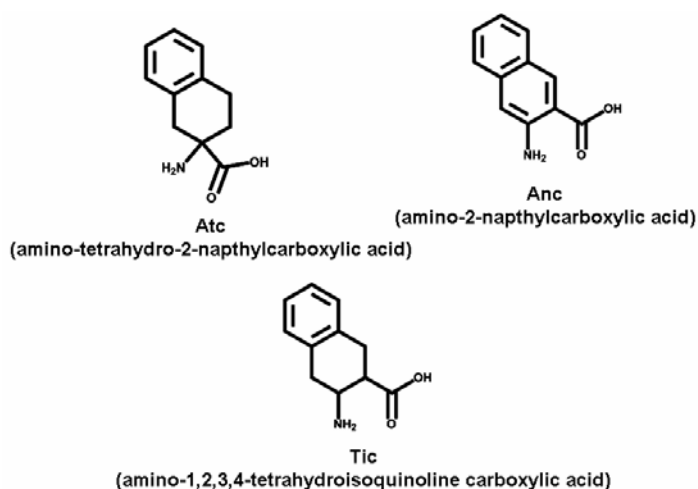


Figure 1-12. Unnatural, constrained amino acids to control peptide conformation.

Backbone modification. Three methods of peptide backbone modification are N-methylation, use of a CH₂NH reduced bond, or substitution with D-amino acids or aza-amino acids.³³ Additionally, the N-terminal and C-terminal may be modified by capping groups.³⁴ Both N-methylation (Figure 1-13A) and reduction (Figure 1-13B) serve to reduce the hydrogen bonding potential of the structure as well as make the peptide less recognizable to peptidases, and thus more stable. Changing the number of potential hydrogen bonds may serve to change the secondary structure of the peptide and modify the way it interacts with a receptor. These changes may increase or decrease binding and signaling depending on the receptor. N- or C-terminal capping with a long aliphatic chain (Figure 1-13C) may serve to make the peptide more

lipophilic. This may allow it to cross cell membranes more easily, or just to disguise it from amino- or carboxypeptidases. A study by Holder *et al.* showed that capping the N-terminal of the melanocortin His-DPhe-Arg-Trp-NH₂ tetrapeptide with an octanoyl group resulted in a compound with nanomolar activity at the mouse melanocortin receptors, and 14-fold increased potency over the endogenous peptide α -MSH.³⁴ Finally, Figure 1-13D shows an aza-substituted peptide template, where the general NH₂-CH(R¹)-COOH amino acid structure is replaced by NH₂-NH(R¹)-COOH.³³ These peptides have a tendency to form β -turn structures, and also help prevent enzymatic degradation of the peptide.

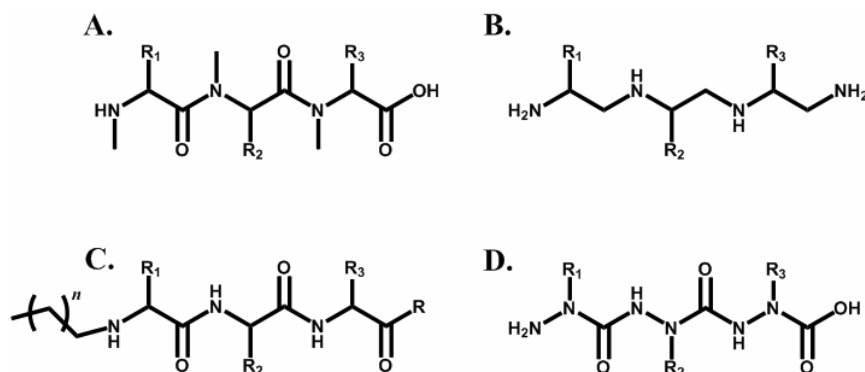


Figure 1-13. Backbone modifications of peptides. A. N-methylation. B. Reduction of amide bonds. C. N- or C-terminal capping. D. Aza-substitution.

Design of Small Molecules

An important aspect of drug design is the development of small molecule templates with biological activity. Although much research is focused on improving the oral bioavailability of peptides, it is still difficult to create a peptide drug that can withstand the harsh conditions of the digestive tract. Small molecules can be designed that are more stable to the acid environment of the stomach and able to cross lipid membranes with greater ease.

One method that has proved effective in the design of small molecule ligands is based on the principle of “privileged structures.”

Privileged structures. The term “privileged structure” was coined in 1988 to describe selected structural elements that, when functionalized, have the potential to produce high affinity ligands for more than one type of receptor.³⁵ Extensive analysis of commercially available drugs has identified a number of substructures that are able to elicit a biological response at many receptors. A number of these have been depicted in Figure 1-14.

The benzodiazepine template has been extensively studied as a privileged structure.³⁶⁻⁴⁰ In fact, this group of compounds was being studied when the idea of privileged structures was first proposed.³⁵ Benzodiazepines have been identified as sedatives, hypnotics, antidepressants, muscle relaxants, anti-amnesiacs, and anticonvulsants in the central nervous systems, as well as opioid receptor agonists,⁴¹ cholecystokinin antagonists,³⁶ oxytocin antagonists,^{37,38} HIV-Tat antagonists,³⁹ and HIV reverse transcriptase inhibitors⁴⁰ among many others. This class of compounds is discussed more extensively in Chapter 6.

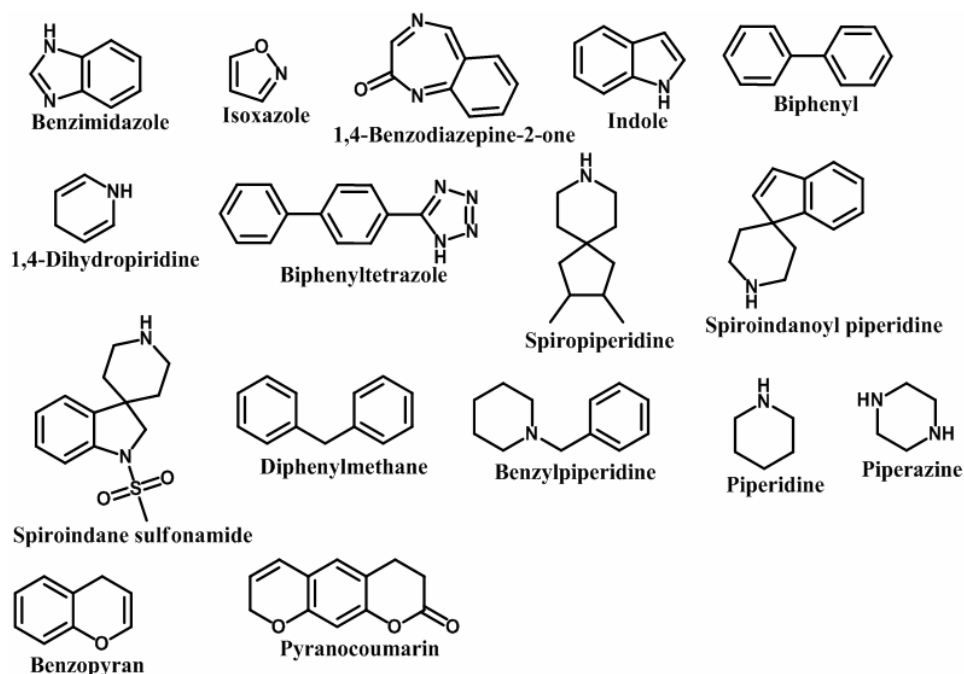


Figure 1-14. Privileged structures often used in small molecule design.

Receptor Mutagenesis and Chimeric Receptors

The final method of drug design that is discussed here is the concept of a receptor-based approach as opposed to a ligand-based approach. In traditional medicinal chemistry, a ligand is designed to interact with a given wild type receptor system. In this method, a known ligand is tested at mutant receptors to identify important ligand-receptor interactions and to design ligands that may correct for inactivity at naturally-occurring mutant receptors.⁴²

Site-directed receptor mutagenesis. A common method for generating mutant receptors is site-directed receptor mutagenesis.⁴³ This involves creating point mutations in the receptor DNA sequence that will only change one amino acid residue in the translated protein. Often an approach similar to the alanine scan of peptides is used in which key residues are changed to alanine. If binding or stimulation is changed, then that amino acid may be interacting either with the ligand or in the signal transduction mechanism. Amino acids may also be changed to investigate the presence of specific binding pockets in the receptor. If there is a hydrophobic binding pocket and one of the side chains is changed to a highly polar or charged residue, then the ligand-receptor interactions may be disturbed and the binding or potency may be altered. Receptor mutagenesis studies of the melanocortin receptors have identified key receptor residues that interact with the endogenous ligands.⁴³⁻⁵⁰ These studies have provided valuable information about the nature of the binding pocket in the mMC1R^{44,45} and the mMC4R,^{43,46-50} allowing for the design of peptides and small molecules that interact specifically with those areas of the receptor.

Chimeric receptors. Another approach to generating mutant receptors involves taking large sections of one receptor and cloning them into another receptor.⁵¹ Novel restriction enzyme sites are cloned into each receptor, and then the receptors are digested with the given enzymes to form two “pieces” of DNA. The excised DNA can then be ligated into the opposite receptor.

This type of study is valuable because it can be used to identify large regions of the receptor important for ligand binding and signal transduction. Sometimes point mutations do not give enough information because it may be the tertiary interactions of large numbers of amino acids working in a concerted fashion to produce the observed results. Chimeric receptor design can identify regions of each receptor necessary for their individual actions.

Uses in drug design. The study of mutant receptors is a very important tool in drug design. They can be created to mimic natural polymorphisms found in humans and characterized based on their interactions with natural ligands. Additionally, synthetic ligands can be tested at the mutant receptors to determine if function may be restored. A ligand that converts an inactive polymorphic receptor into a functional receptor is a very powerful tool in treating individuals with genetically inactive receptors.

CHAPTER 2 THE MELANOCORTIN SYSTEM

The Melanocortin Receptors

The melanocortin system (Figure 2-1) consists of five receptors, MC1-5,⁵²⁻⁵⁷ which are members of the superfamily of G protein coupled receptors (GPCRs). The MC1R and the MC3-5R are stimulated by the endogenous agonists α -MSH, β -MSH, γ_1 -MSH, γ_2 -MSH and ACTH and activate the cAMP second messenger signaling pathway.⁵⁸ The MC2R is unique in that it is only stimulated by ACTH.^{53,59} The melanocortin receptors are also antagonized by the only two known endogenous antagonists of GPCRs, Agouti^{60,61} and Agouti-related protein (AGRP).^{62,63}

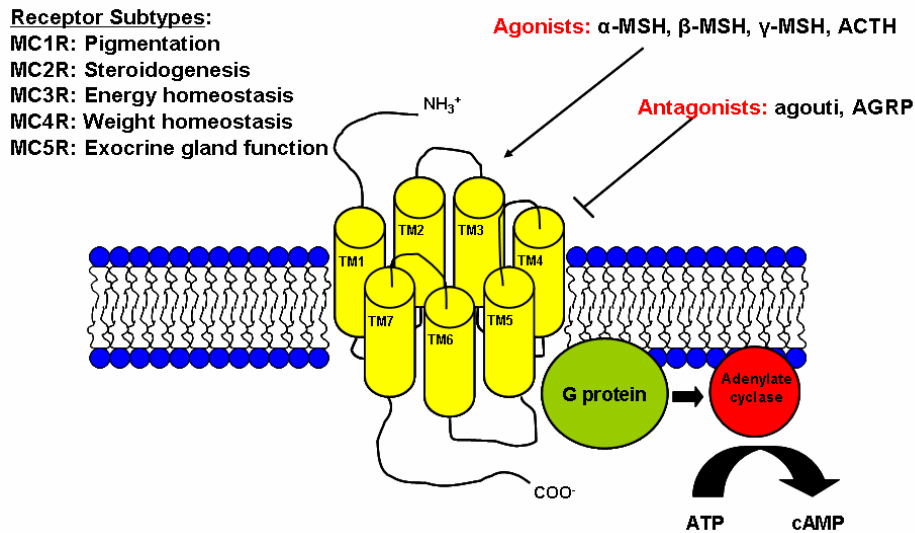


Figure 2-1. The Melanocortin system.

The MC1R is expressed in melanocytes and is involved in the production of melanin, the pigment responsible for skin and coat coloration.^{53,64-67} There are two types of pigments, eumelanin and pheomelanin.⁶⁸ Eumelanin is the brown/black pigment produced by the binding of α -MSH to the MC1R.⁶⁸ Eumelanin produces a photoprotective effect, reducing damage due to UV radiation.^{69,70} Pheomelanin is the red/yellow pigment produced in the absence of α -MSH.⁶⁸ It has been shown that Agouti is able to displace α -MSH at the MC1R, resulting in the production of pheomelanin.^{65,71} This makes the individual less likely to tan and heightens the

risk for UV damage.⁶⁷ It has been shown that α -MSH is produced in the skin following UV exposure.⁷² The MC1R has also been shown to be expressed in monocytes, neutrophils and macrophages, where it aids in the mediation of the anti-inflammatory response.⁷³ α -MSH antagonizes the effects of proinflammatory cytokines such as IL-1, IL-6, and TNF α ,^{72,74} and downregulates the production of interferon γ .⁷⁵ Additionally, α -MSH upregulates the production of IL-10, an immunosuppressive cytokine.⁷⁶

The MC2R is expressed in the adrenal cortex where it mediates the production of glucocorticoids and aldosterone.⁵³ The MC2R is the smallest melanocortin receptor⁷⁷ and is unique in that it is only stimulated by ACTH, and not by any of the other melanocortin agonists.^{53,59} Mutations in the MC2R have been linked to the autosomal recessive disorder, Familial Glucocorticoid Deficiency (FGD).⁷⁸⁻⁸³ FGD is characterized by the nonresponsiveness of the body to the actions of ACTH. This results in hypoglycemia, bacterial infections, and increased skin pigmentation. Pharmacological characterization of the MC2R has traditionally been difficult due to the fact that a functional MC2R is only expressed in cells of adrenal origin. Cells of non-adrenal origin, such as the HEK293 cell line, expresses the MC2R on the cell surface, but there is no functional or binding activity when stimulated with ACTH.^{84,85} Recent studies into this phenomenon have identified two accessory proteins, MRAP^{84,86} and Nup 50,⁸⁷ which have been shown to co-precipitate with the MC2R. MRAP has been shown to restore functional activity to the MC2R receptors when co-transfected into non-adrenal cell lines.⁸⁶

The MC3R is expressed in the brain, heart, gastrointestinal tract, and placenta,^{54,88} and has been shown to be involved in energy homeostasis, though the mechanism of action is not yet known.^{89,90} Mice who do not express the MC3R have an increased fat mass and a decreased lean mass, although they maintain the same body weight as their wild type littermates.^{89,90} In addition

to stimulating the production of cAMP, the MC3R has also been shown to cause an increase in intracellular Ca^{2+} levels, indicating a potential action through induction of inositol triphosphate (IP3) and Protein Kinase C (PKC).^{91,92}

The MC4R is expressed in the brain^{55,56} and testis, and is involved in energy and weight homeostasis,⁹³ feeding behavior,⁹³ and sexual function.^{94,95} MC4R knockout (KO) mice exhibit hyperphagia, hyperinsulinaemia, hyperglycemia and increased linear growth when compared to their wild type littermates which leads to severe obesity.⁹³ The endogenous agonist α -MSH stimulates the MC4R and results in a decrease in feeding behavior.⁹⁶ Mice which lack an MC4R are insensitive to α -MSH, leading to increased feeding and severe obesity. AGRP is able to antagonize the effects of α -MSH at the MC4R, resulting in an increase in food intake and body weight.⁶² Structure-activity relationship studies of α -MSH have identified key amino acids involved in ligand binding to the receptor and have aided in the design of synthetic ligands more potent than α -MSH at the MC4R. Ligands have also been discovered that exhibit high selectivity for the MC4R over the other melanocortin receptors. It is hypothesized that potent agonists selective for the MC4R may be used as therapeutic agents to treat obesity.⁹⁷ Additionally, the MC4R has been shown to play a role in erectile function in both man and mice.^{94,95,98,99} Administration of MC4R agonists in mice, such as the synthetic cyclic agonist MTII, results in increased sexual and grooming activity.⁹⁹ MTII has also been shown to stimulate penile erections in man.¹⁰⁰

The MC5R is expressed in peripheral tissues and is involved in the secretion of lipids from exocrine glands.^{57,101} MC5R knockout mice exhibit decreased water repulsion on their skin due to a decrease in sebaceous lipids.¹⁰¹ Additionally, these mice show a reduced capacity to thermoregulate their body temperature.¹⁰¹

The Melanocortin Ligands

Agonists. The melanocortin agonists are derived from the prohormone proopiomelanocortin (POMC)^{102,103} (Figure 2-2). POMC is expressed in the pituitary gland, skin, immune system, and brain.¹⁰⁴⁻¹⁰⁹ POMC is sequentially cleaved at dibasic cleavage sites by prohormone convertases (PC1-2)^{110,111} into the five melanocortin agonists, α -, β -, γ_1 -, γ_2 - and ACTH, as well as β -endorphin.¹¹¹ In the case of α -MSH, C-terminal cleavage by Carboxypeptidase E removes basic amino acids, followed by N-acetylation by N-acetyltransferase and amidation by PAM (peptidyl α -amidating monooxygenase) [reviewed in¹¹²]. The melanocortin agonists can be characterized by the way they interact with each receptor subtype. Table 2-1 shows the potency series for each receptor.¹¹³ In all cases, α -MSH is the most potent. ACTH is the only peptide able to stimulate all five receptors, and the only known peptide able to stimulate the MC2R.^{53,59}

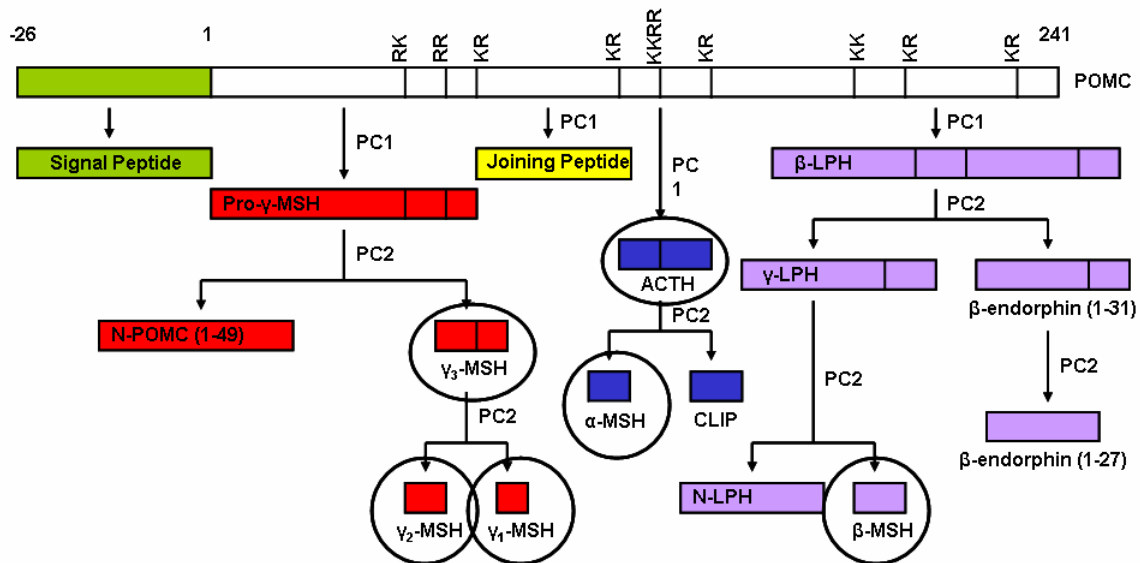


Figure 2-2. Posttranslational processing of POMC into the melanocortin agonists.

The most well-known melanocortin agonist is α -MSH (Table 2-2). Extensive structure-activity relationship (SAR) studies have been performed on α -MSH and have provided valuable information about the intermolecular interactions necessary for signaling at the melanocortin

receptors. Truncation studies of α -MSH have revealed that the minimal sequence able to stimulate the melanocortin receptors is the tripeptide Phe-Arg-Trp-NH₂.^{114,115} Alanine scans of this peptide have also provided valuable information. Alanine scans of α -MSH confirms that the tetrapeptide His-Phe-Arg-Trp is the core sequence of the melanocortin peptides and is responsible for binding to the receptors.³ D-amino acid scans of a peptide can also provide valuable information about the conformation of the amino acid side chains. These studies have shown that replacing the Phe in His-Phe-Arg-Trp with a DPhe results in a dramatic increase in activity at the melanocortin receptors.⁴

Table 2-1. Ligand potency series for the five melanocortin subtypes.

Receptor	Ligand Potency Series
MC1R	α -MSH = ACTH > β -MSH > γ -MSH
MC2R	ACTH only
MC3R	α -MSH = ACTH = β -MSH = γ -MSH
MC4R	α -MSH = ACTH > β -MSH > γ -MSH
MC5R	α -MSH > ACTH > β -MSH > γ -MSH

Table 2-2. Amino acid sequences of the endogenous and synthetic melanocortin agonists. The core tetrapeptide sequence His-Phe-Arg-Trp is in bold.

Ligand	Sequence
α -MSH	Ac-Ser-Tyr-Ser-Met-Glu- His-Phe-Arg-Trp -Gly-Lys-Pro-Val-NH ₂
ACTH(1-24)	Ser-Tyr-Ser-Met-Glu- His-Phe-Arg-Trp -Gly-Lys-Pro-Val-Gly-Lys-Lys-Arg-Arg-Pro-Val-Lys-Val-Tyr-Pro
β -MSH	Ala-Glu-Lys-Lys-Asp-Glu-Gly-Pro-Tyr-Arg-Met-Glu- His-Phe-Arg-Trp -Gly-Ser-Pro-Pro-Lys-Asp
γ 1-MSH	Tyr-Val-Met-Gly- His-Phe-Arg-Trp -Asp-Arg-Phe-NH ₂
γ 2-MSH	Tyr-Val-Met-Gly- His-Phe-Arg-Trp -Asp-Arg-Phe-Gly-OH
NDP-MSH	Ac-Ser-Tyr-Ser-Nle-Glu- His-DPhe-Arg-Trp -Gly-Lys-Pro-Val-NH ₂
MTII	Ac-Nle-c[Asp- His-DPhe-Arg-Trp -Lys]-NH ₂

These data were used in the design of the synthetic melanocortin agonists, NDP-MSH and MTII (Table 2-2).^{4,116-118} NDP-MSH is identical to the endogenous α -MSH except the methionine was replaced with a norleucine to make the peptide more stable to oxidation, and

DPhe is used in place of Phe in the core tetrapeptide sequence.⁴ NDP-MSH has been shown to be more potent at the melanocortin receptors than α -MSH.¹¹ NDP-MSH, also known as MT-I, is currently in clinical trials as a therapeutic agent to increase skin pigmentation.

MTII is a synthetic cyclic peptide based on amino acids 4-10 of α -MSH.^{116,117} SAR studies of α -MSH were used to identify amino acids essential for activity.^{116,117,119} These studies showed that the amino acids in positions 1,2,3,11,12, and 13 were not essential for activity and were removed in the design of MTII. Additionally, Glu was replaced with Asp to shorten the cyclic chain length, Gly was replaced with the basic amino acid Lys for cyclization purposes, and a Nle was added in place of the endogenous Met⁴ to prevent oxidation. Previous D-amino acid studies on α -MSH revealed that replacing LPhe with DPhe resulted in a much more potent compound, so a DPhe was used in position 7. These studies resulted in the development of a linear peptide agonist, Ac-[Nle⁴, Asp⁵, DPhe⁷, Lys¹⁰] α -MSH[4-10]-NH₂ that exhibited an increase in biological potency over the endogenous ligand.¹¹⁶ This linear compound was then cyclized through the use of a lactam bridge between the side chains of the Asp⁵ and Lys¹⁰ amino acids resulting in the formation of a 23-membered ring. This cyclic peptide, known as Melanotan II or MTII, was shown to be equipotent with α -MSH in the frog skin bioassay and 90-100 times more potent than α -MSH in the lizard skin assay.¹¹⁷ Prolongation studies showed that MTII continued to influence biological activity for up to 48 hours after removal of the compound from the assay media.¹¹⁷ This prolonged response was not observed for either α -MSH or the linear Ac-[Nle⁴, Asp⁵, DPhe⁷, Lys¹⁰] α -MSH[4-10]-NH₂ analogs.

SAR studies in which the DPhe of MTII was substituted with bulky aromatic amino acids such as DNal(2') resulted in the generation of a potent antagonist at the MC3R and the MC4R, known as SHU9119.¹¹⁸ SHU9119 is a partial agonist and antagonist at the mMC3R, a

competitive antagonist at the mMC4R, and retains full agonist activity at the mMC1R and mMC5R.¹¹⁹ ICV administration of SHU9119 to fasted mice and rats causes a dose-dependent increase in food intake which starts slowly and increases over a 12-hour period of time.⁹⁷ Additionally, co-administration of SHU9119 and MTII results in abolishment of the anorectic effects of MTII, indicating that SHU9119 acts by competitive antagonism of the melanocortin receptors.^{97,120}

MTII administered by intracerebroventricular (ICV),^{97,120-122} paraventricular,^{123,124} or intraperitoneal^{121,125} routes resulted in a dose-dependent decrease in food intake and a related decrease in body weight in mice.¹²² It is postulated that this primary effect on feeding is mediated through the MC4R. It has been observed that when MTII was administered to MC4R-knockout mice, the corresponding decrease in feeding behavior and weight loss was not observed,^{125,126} indicating that the MC4R is involved in the mechanism of action. MTII also has been shown to exhibit erectogenic and tanning effects in humans.^{100,127,128} MTII has been studied in Phase I and II Clinical Trials in healthy men¹⁰⁰ and in men with psychogenic¹²⁷ and organic¹²⁸



causes of erectile dysfunction.

Figure 2-3. ACTH truncated to α-MSH. α-MSH represents the first thirteen amino acids of ACTH.

Adrenocorticotropin hormone (ACTH) (Table 2-2) is a 39-amino acid peptide released from the adrenal glands where it is responsible for the regulation of glucocorticoid and aldosterone release.^{53,129} Changes in circulating levels of ACTH have been connected with

diseases such as Cushings and Addison's, as well as Familial Glucocorticoid Deficiency.⁷⁸⁻⁸³

ACTH is the only melanocortin agonist which binds to all five receptor subtypes.⁵⁹ It is the only peptide able to bind and stimulate the MC2R.^{53,59} α -MSH represents the first thirteen amino acids of ACTH⁶⁶ (Figure 2-3). ACTH retains the C-terminal amino acids as well as a basic KKRR tetrapeptide which has been shown to be important for stimulation of the MC2R.¹³⁰ Truncation studies of ACTH have revealed that the truncated peptide ACTH(1-24) is equipotent with full-length ACTH.¹³¹ Recent studies in our laboratory have tested truncated derivatives of ACTH at the hMC2R expressed in OS3 cells.¹³⁰ A cAMP functional assay has shown that deletion of the C-terminal amino acids is tolerated well until the KKRR tetrapeptide sequence begins to be deleted (Table 2-3). Removal of Arg¹⁸ results in a 114-fold decrease in potency and removal of Arg¹⁷ results in a 1000-fold decrease in potency; truncation of Lys¹⁶ and Lys¹⁵ each result in a complete loss of activity at the hMC2R in OS3 cells. These results indicate that there may be unique interactions with ACTH at the hMC2R that are responsible for ligand selectivity.

Table 2-3. Truncation study of ACTH tested at the mMC2R.¹³⁰

Peptide	Structure	mMC2R	
		EC ₅₀ (nM)	Fold Difference
ACTH(1-24)	SYSMEHFRWGKPVGKKRRPVKVYP-OH	1.45±1.02	1
ACTH(1-23)	SYSMEHFRWGKPVGKKRRPVKVY-OH	8.8±6.0	
ACTH(1-22)	SYSMEHFRWGKPVGKKRRPVKV-OH	1.19±0.52	
ACTH(1-21)	SYSMEHFRWGKPVGKKRRPVK-OH	0.91±0.38	
ACTH(1-20)	SYSMEHFRWGKPVGKKRRPV-OH	0.28±0.07	
ACTH(1-19)	SYSMEHFRWGKPVGKKRRP-OH	2.39±1.12	
ACTH(1-18)	SYSMEHFRWGKPVGKKRR-OH	1.51±0.79	
ACTH(1-17)	SYSMEHFRWGKPVGKKR-OH	11.3±0.8	8
ACTH(1-16)	SYSMEHFRWGKPVGKK-OH	165±50	114
ACTH(1-15)	SYSMEHFRWGKPVGK-OH	1450±400	1000
ACTH(1-14)	SYSMEHFRWGKPVG-OH	>100µM	No stim
ACTH(1-13)	SYSMEHFRWGKPV-OH	>100µM	No stim

Less is known about β - and γ -MSH (Table 2-2) than the other melanocortin agonists. Both peptides contain the core His-Phe-Arg-Trp tetrapeptide shown to be responsible for stimulation of the melanocortin receptors. SAR studies of γ -MSH have shown that this sequence is important for binding, although replacement of Phe with DPhe resulted in a decrease in potency.¹³² Instead, potency was increased by replacing Trp with DTrp.¹³³

Antagonists. The melanocortin system is unique in that it contains the only two known endogenous antagonists of G protein coupled receptors, Agouti^{65,71} and Agouti-Related Protein (AGRP).^{62,63} Agouti (Figure 2-4) is a competitive antagonist of α -MSH at the MC1R, MC3R, and MC4R.^{65,71} AGRP (Figure 2-4) has been shown to antagonize the action of α -MSH at the MC3R and the MC4R.^{62,63} Additional studies have shown that AGRP also acts as an inverse agonist at the MC4R.^{47,134,135} In this capacity, AGRP may be able to regulate cAMP levels in the absence of an agonist.¹³⁴ When agouti is overexpressed in mice, competitive displacement of α -MSH by agouti causes the cell to decrease production of the normal brown/black eumelanin pigment, and increase production of red/yellow pheomelanin,⁶⁰ these mice additionally show an obese phenotype.

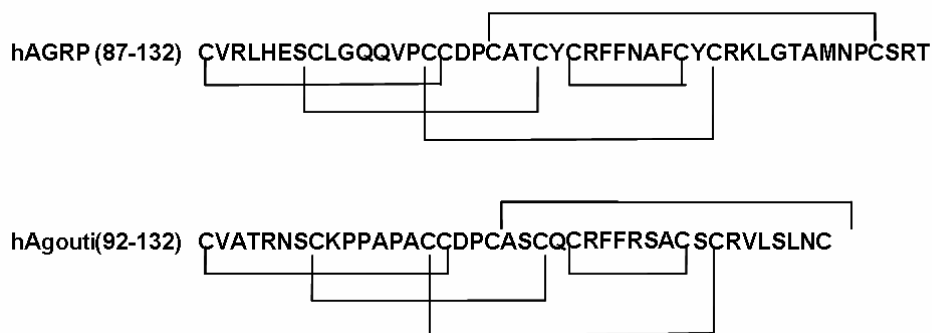


Figure 2-4. Partial sequences of the melanocortin antagonists hAGRP and hAgouti depicting the five disulfide bonds in each ligand.

The melanocortin antagonists can be classified as orexigenic peptides, which indicate an increase in food intake upon administration.^{62,136} Transgenic mice were created which expressed

the human AGRP gene. These mice exhibited increased weight gain compared to their wild type littermates at four weeks of age, as well as an increase in body length and food consumption.^{62,136} It has been reported that AGRP transgenic mice become obese, exhibiting a phenotype similar to that observed in the MC4R-deficient mice.⁹³ Therefore, it has been proposed that AGRP mediates its effects through the MC4R in the central nervous system.⁶²

Both agouti and AGRP contain ten cysteine residues which are able to form five disulfide bonds (Figure 2-4).^{62,71,137,138} One of the most significant core loops in AGRP is an octapeptide, [Cys-Arg-Phe-Phe-Asn-Ala-Phe-Cys].^{139,140} Of these eight amino acids, three residues have been shown to be critical for ligand binding: these are the Arg-Phe-Phe¹¹¹⁻¹¹³ triplet,¹⁴⁰ which is also found in the agouti protein. As it appears that the antagonists act by competitively binding to the receptor at the agonist binding site, it has been postulated that the Arg-Phe-Phe antagonist motif mimics the His-Phe-Arg-Trp motif found in all endogenous melanocortin agonists.^{140,141} This theory was tested through the design of several peptides. It was shown that a peptide based on the octapeptide loop of AGRP, Tyr-c[Cys-Arg-Phe-Phe-Asn-Ala-Phe-Cys]Tyr [hAGRP (109-118)], is a μ M agonist at the MC1R and an antagonist at the MC4R.¹⁴¹ As the minimal active sequence to show agonist activity at the MC1R is the tetrapeptide Ac-Phe-Arg-Trp-NH₂,^{114,115} it has been proposed that the conserved antagonist Arg-Phe-Phe triplet is mimicking the His-Phe-Arg-Trp tetrapeptide found in the melanocortin agonists.¹⁴¹ Additional studies have been performed using chimeric ligands which substitute the Arg-Phe-Phe triplet of hAGRP(109-118) with the His-Phe-Arg-Trp tetrapeptides of the agonists. When these compounds were tested at the melanocortin receptors, it was shown that these compounds are full agonists at the MC1R and MC3R-MC5R, providing further evidence that Arg-Phe-Phe is responsible for antagonist activity.¹⁴²

Diseases Associated with the Melanocortin System

Obesity. Obesity is a serious condition which can cause complications such as type II diabetes mellitus, cardiovascular disease, and hypertension, as well as increase the risk of certain types of cancer. A recent survey by the National Health and Nutrition Examination Survey (NHANES) has estimated that the prevalence of overweight and obese individuals in the United States has been steadily increasing since 1960.^{143,144} The Body Mass Index (BMI) also known as Quetelet's Index, is the standard measurement for the determination of overweight and obesity and is calculated from the individual's weight in pounds divided by their height in inches squared multiplied by 703. Quetelet's Index was used to determine the average ratio of weight and height. A value of 18.5 or less was considered underweight, 18.5-24.9 was considered normal, an index of 25-29.9 was overweight, 30-39.9 was considered obese, and an index above 40 was considered severely obese. These values are still used today to determine an individual's weight status.¹⁴⁵

Four national surveys have been conducted by NHANES since 1960, in which a subset of the population was analyzed according to their BMI.^{143,144} It was found that since 1994, the prevalence of overweight individuals (BMI 25-29.9) has increased from 55.9% to 64.3%.^{143,144} The prevalence of obesity (BMI 30-39.9) was 13.4% in 1960, rose to 15.0% by 1980, and in 2000 the prevalence of obesity was 30.9%.^{143,144} Additionally, the prevalence of extreme obesity (BMI >40) has increased from 2.9% in 1994 to 4.7% in 2000.^{143,144} As BMI increases, the chance increases for the individual to develop severe health complications.

Recent developments in molecular biology, genetics, and chemistry have enabled researchers to identify numerous pathways in the body that contribute to the regulation of feeding behavior and weight homeostasis. It has become evident that the melanocortin system is involved in this complicated network and that the MC4R is involved in this process. Targeted

disruption of the MC4R in mice leads to hyperphagia and adult-onset obesity, suggesting a role of the melanocortin system in the control of appetite and body weight.⁹³ It has been shown that AGRP, an endogenous antagonist of the MC4R⁶² is able to competitively displace the agonist α -MSH at the MC4R, resulting in an increase in food intake and weight gain.⁶² An MC4R-selective agonist may have the effect of decreasing appetite and weight gain.⁹⁷

ACTH-related diseases. The Hypothalamic-Pituitary-Adrenal axis is the system through which the brain sends endocrine signals through the bloodstream and to the adrenal glands.¹⁴⁶ The signal begins in the hypothalamus, which is a region of the brain responsible for beginning the endocrine cascade by releasing hypothalamic hormones. In this case, the paraventricular nucleus of the hypothalamus releases corticotropin releasing hormone (CRH) into the hypothalamic-hypophyseal-portal system, where it is transported to the anterior pituitary gland. Here, CRH binds to corticotroph cells which release ACTH into the bloodstream. ACTH then travels to the adrenal gland, where it binds to melanocortin-2 receptors on the adrenal cortex.⁵³ This stimulates a signal cascade which results in the biosynthesis and release of glucocorticoids such as cortisol.¹⁴⁶ Cortisol then acts on the hypothalamus in a negative feedback system to decrease the production of CRH.¹⁴⁶ In this way, cortisol levels are regulated to maintain proper homeostasis.

Cortisol is a glucocorticoid released from the adrenal cortex. In healthy individuals it serves to maintain blood pressure and cardiovascular function, slow the inflammatory response, balance the effects of insulin in breaking down glucose, regulate metabolism of proteins, carbohydrates, and fats, help maintain proper arousal and a sense of well-being, and to help the body respond to stress.¹⁴⁶ It is known as the “stress hormone” as it is released during times of acute stress in the “fight or flight” response. In this capacity it provides short-term benefits such

as a quick burst of energy, increased memory functions, increased immune functions, and a decrease in pain sensitivity. However, in times of chronic stress, excess cortisol can result in impaired cognitive and thyroid functions, hyperglycemia, and a decrease in bone density, muscle tissue, and immune response, as well as high blood pressure and increased abdominal fat which may increase the chances of a heart attack or stroke.¹⁴⁶

These symptoms are becoming more common in today's population due to the high-stress lifestyles many people lead. In these cases increased cortisol is the result of an environmental factor, but there are diseases which result in high circulating levels of cortisol from biological sources. One example of these conditions is Cushing's Syndrome.

Cushing's Syndrome, also known as hypercortisolism, is an endocrine disorder caused by chronic exposure to high levels of cortisol.¹⁴⁶ It primarily affects individuals between the ages of 20-50, and is seen in 10-15 individuals out of every million people per year. Signs and symptoms of this disease include upper body obesity, rounded face, increased neck fat, thinning of the extremities, thin skin which bruises easily and heals slowly, presence of stretch marks, weak bones, muscle weakness and severe fatigue, as well as high blood pressure, high blood sugar, and mental conditions including irritability, anxiety, and depression.¹⁴⁶ There are many causes for Cushing's, including pituitary adenoma, which is a benign tumor of the pituitary which secretes excess ACTH, resulting in high cortisol levels. It can also be caused by Ectopic ACTH Syndrome, in which tumors outside of the pituitary release large amounts of ACTH, or by adrenal tumors, such as adrenal carcinomas, which secrete excess cortisol into the blood. Familial Cushing's Syndrome occurs in individuals who have an increased genetic tendency to develop endocrine tumors.¹⁴⁶

Some diseases are caused by not enough cortisol or ACTH. Addison's Disease, or "hypocortisolism" occurs when the adrenal glands do not produce enough cortisol and aldosterone.¹⁴⁶ In this condition, individuals suffer weight loss, muscle weakness, fatigue, hypoglycemia, and low blood pressure. Over 70% of Addison's cases are caused by autoimmune disorders in which the body destroys the adrenal cortex, reducing cortisol levels.¹⁴⁶ The most common cause of Addison's is a secondary adrenal insufficiency condition caused by the removal of a pituitary or other ACTH-producing tumor, resulting in a lack of ACTH, and thus a lack of cortisol.¹⁴⁶

Mutations in the MC2R⁷⁸⁻⁸³ have been connected to Familial Glucocorticoid Deficiency (FGD), a rare autosomal recessive disorder. The disease is characterized by nonresponsiveness to ACTH, lowered glucocorticoid production, and elevated serum levels of ACTH.¹⁴⁷ The disease normally presents in childhood with the onset of severe hypoglycemia and episodes of bacterial infection. These signs are accompanied by excessive skin pigmentation. An understanding of the hMC2R may help in the development of a therapeutic treatment for this disease.

Due to the lack of understanding of the mechanism by which ACTH interacts with the hMC2R, it may be difficult to understand the diseases caused when there is an imbalance in the body. Knowledge of this system may help to treat and/or prevent many diseases related to cortisol, leading to a decrease in cardiovascular disease and stroke as well as other syndromes. This may lead to an increase in the quality of life for individuals suffering from these conditions.

CHAPTER 3
GENERAL METHODOLOGIES 1: CHEMISTRY

Solid Phase Peptide Synthesis

Merrifield Approach

Prior to the introduction of the notion of Solid Phase Peptide Synthesis (SPPS) in 1963 by Bruce Merrifield,¹⁴⁸ peptide synthesis was accomplished in solution phase.¹⁴⁹ Each step required extensive separation, purification and characterization, making this method highly labor- and reagent-intensive, and fraught with problems such as very low yield and high occurrence of side products. Merrifield worked to solve this problem by creating an insoluble solid support to which the growing peptide is attached during synthesis. The peptide remains attached to the resin until cleaved. The method is shown in Figure 3-1: Synthesis begins with the attachment of an amino acid which has been protected at the α -amine with a temporary protecting group and side-chain protected with a permanent protecting group which is not removed until cleavage. The next α -amino-protected amino acid is attached to the growing peptide chain after the temporary amine protecting group on the growing chain is removed. The cycle of deprotection and coupling is repeated until the peptide is the desired length, and then the peptide is cleaved from the resin and the side chain protecting groups removed in one step.

This new method of synthesis was far superior to the solution phase reaction for several reasons. First, unused reagents could be simply washed away after the reaction was complete, eliminating the need for extraction during each step and washing away any non-resin-bound side reaction products. This method also decreased undesirable side reactions and provided a way to drive the reaction to completion through the addition of excess reagents. Pure peptide yields were also significantly increased over the solution phase method as there was little loss between steps.

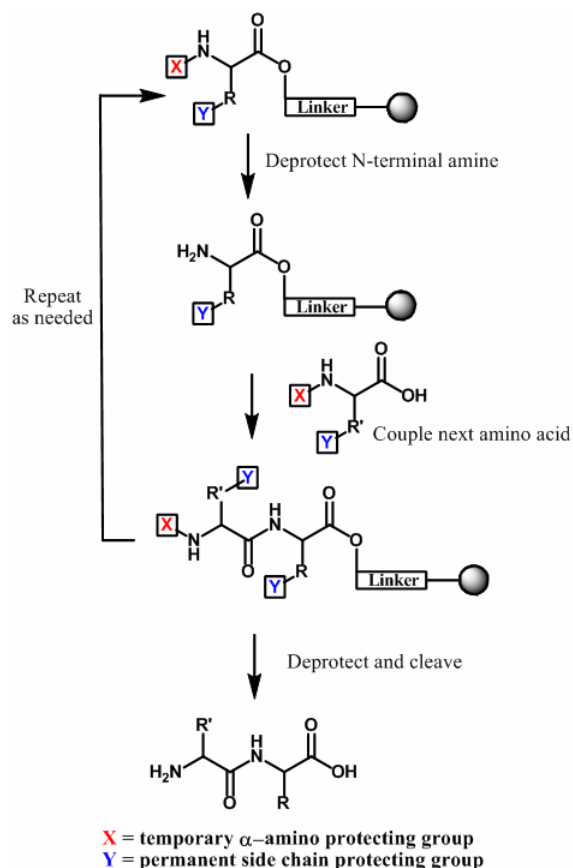


Figure 3-1. General method of solid phase peptide synthesis including deprotection, coupling and cleavage steps.

Successive publications by Merrifield¹⁵⁰⁻¹⁵² continued to improve on what is now called the Merrifield approach to SPPS. The Merrifield approach (Figure 3-2) makes use of a *tert*-butoxycarbonyl (Boc) protecting group at the α -amino group which can be cleaved using trifluoroacetic acid (TFA). Figure 3-3 depicts a possible acid-catalyzed mechanism for the removal of the Boc group. Side chain protecting groups consisted of benzyl-based, acid-labile groups that were stable to TFA, but cleaved in the presence of anhydrous hydrogen fluoride (HF). Coupling was accomplished by the use of dicyclohexylcarbodiimide (DCC) in dichloromethane (DCM) to form a peptide bond between the free amine attached to the resin and the activated carboxylic acid of a new amino acid.

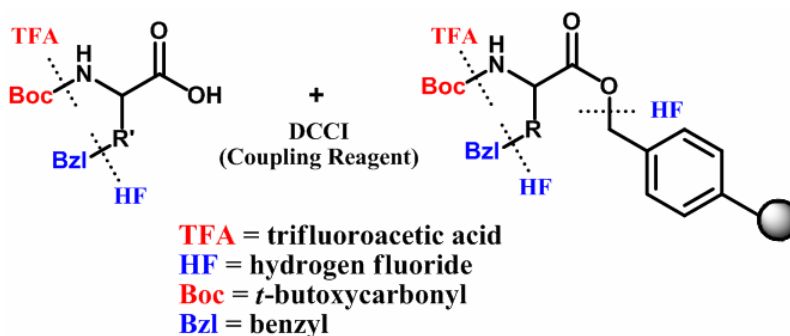


Figure 3-2. General Boc chemistry synthesis strategy. Temporary α -amino protecting groups are removed with TFA. Cleavage of side chain protecting groups and from resin is accomplished using HF.

The Boc approach to peptide synthesis was truly revolutionary, allowing the rapid, clean synthesis of peptides in days which before would have taken months by solution phase approaches. This method has been used ever since with great success, although it did not take long for peptide chemists to discover the need for a synthetic method which could be accomplished with milder cleavage conditions, due to the inherent danger and expensive equipment required for HF cleavage. Additionally, as both the temporary and permanent protecting groups were acid-labile, there was a certain amount of loss experienced due to premature side chain deprotection and cleavage from resin. It was therefore desirable to develop a method that uses different chemistries for the removal of each type of protecting group.

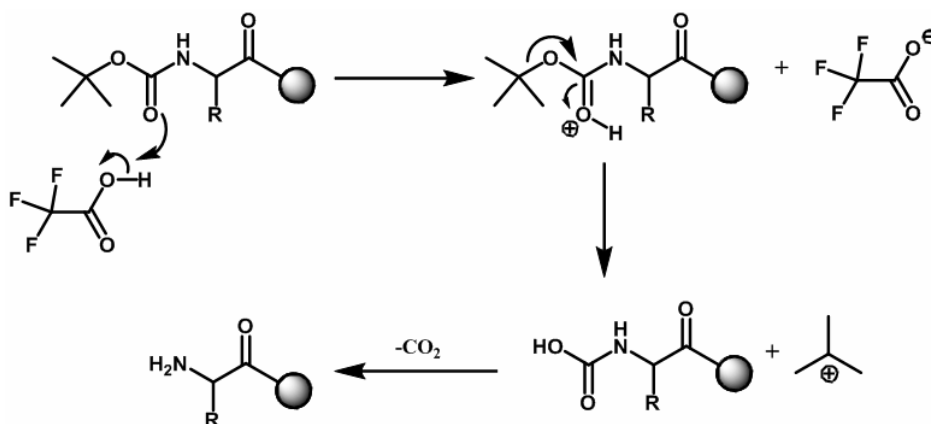


Figure 3-3. Proposed mechanism for acid-catalyzed Boc deprotection.

The Fmoc Synthetic Strategy

The new method of SPPS was introduced in 1970 by Carpini.^{153,154} Instead of the graduated acidolysis used in the Merrifield strategy, this method utilized an orthogonal protecting group strategy, where the α -amino group was protected by the base-labile 9-fluorenylmethoxycarbonyl (Fmoc) group (Figure 3-4). This group could be removed using 20% piperidine in DMF, and the acid-labile side chain protecting groups were not affected. This allowed selective amino deprotection without worry of cleaving the peptide or its side chain protecting groups prematurely. Additionally, since no acid was needed to deprotect, the side chain protecting groups and the linker between the peptide and resin could be removed with the milder acid TFA instead of HF. This opened up a wide possibility of options for side chain protection as well as linker functionalization, allowing for the design of linkers that will functionalize the C-terminus of the peptide when cleaved. Figure 3-5 depicts a possible mechanism for the base-catalyzed deprotection of the Fmoc group.

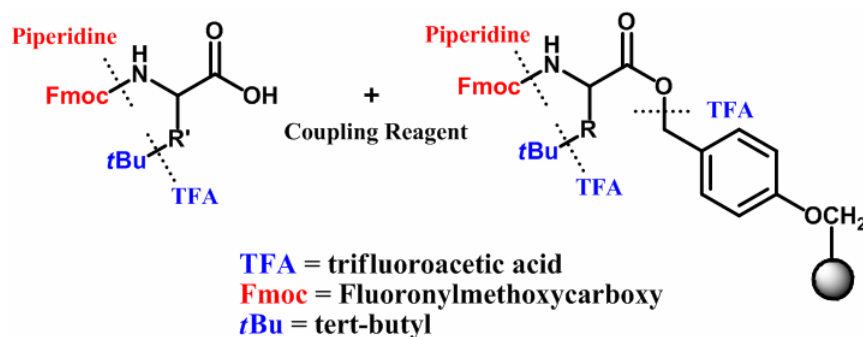


Figure 3-4. General Fmoc synthetic strategy. Temporary α -amino protecting groups are removed with piperidine. Removal of side chain protecting groups and cleavage from resin are accomplished using TFA.

The new Fmoc method was faster and cleaner than the Boc method and made use of much milder and safer reagents, making it a very popular method for peptide synthesis. Additionally, amino acids were easily functionalized with the Fmoc moiety, which resulted in functionalized

amino acids being available commercially. This also contributed to the popularity of the new SPPS method.

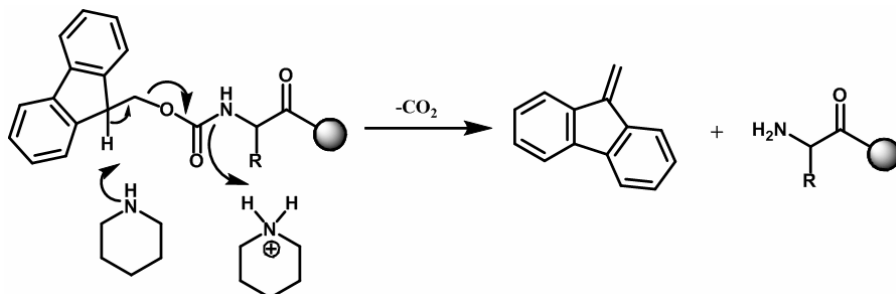


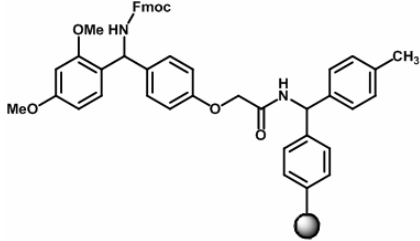
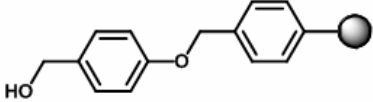
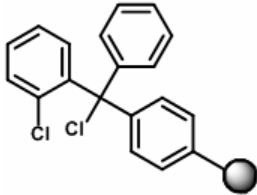
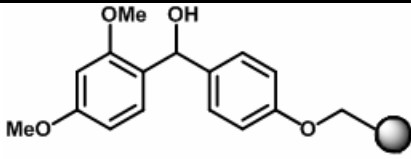
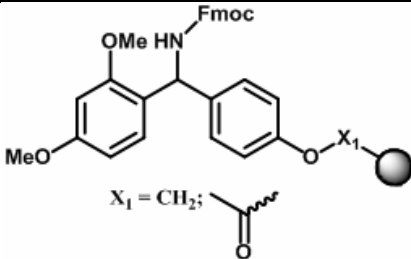
Figure 3-5. Proposed mechanism for base-catalyzed Fmoc removal.

Resins for SPPS

Resins for SPPS are most commonly made of 1% divinylbenzene cross-linked polystyrene.¹⁴⁹ This polymer is useful as it readily swells in common solvents for peptide synthesis such as DMF (N,N-dimethylformamide), DCM (1,2-dichloromethane), and NMP (N-methyl pyrrolidinone).¹⁴⁹ Additionally, it is easily functionalized with many different types of linkers.¹⁴⁹ These linkers serve to act as a tie between the peptide and the polymer support. They can be made to be cleavable by either HF or TFA and different linkers will result in various C-terminal functionalities upon cleavage, the most common post-cleavage functional groups being either an amide or an acid. Table 3-1 shows some common Boc and Fmoc resins used in this dissertation as well as their cleavage conditions, residual functionalities, and the type of chemistry it is compatible with.

The first amino acid to be attached to the resin requires different coupling conditions based on the type of resin used. The three common types of resin are hydroxymethyl-based resins, aminomethyl-based resins, and trityl chloride resins.¹⁴⁹ Attachment of the first amino acid is a critical step, as the initial loading determines the final peptide yield. Incomplete attachment of the first amino acid lowers yields, and can result in C-terminally truncated peptides.

Table 3-1. Common types of resin used in SPPS.

Resin	Linker	Cleavage	Functionality	Type of Chemistry
Rink-Amide MBHA		HF	Amide	Boc
Wang		TFA	Acid	Fmoc
2-chlorotrityl		TFA	Acid	Fmoc
Rink Acid		TFA	Acid	Fmoc
Rink Amide		TFA	Amide	Fmoc

Hydroxymethyl-based resin. For these types of resins, first amino acid attachment is accomplished by esterification of the amino acid to a linked hydroxyl group.¹⁴⁹ Examples of this type of resin are Wang resin¹⁵⁵ and Rink Acid¹⁵⁶ (Table 3-1). The esterification reaction is more difficult than formation of an amide bond, as it requires harsher conditions that can lead to problems such as low substitution, enantiomerization,¹⁵⁷ and dipeptide formation. The presence

of water increases the possibility of these side reactions, so the reaction should be carried out in anhydrous conditions. Generally DCC or DMAP is used as the catalyst, though these can cause partial racemization of the amino acid, so should only be used in catalytic amounts. It is very difficult to attach the amino acids Cys, His, Pro, Met, and Trp to these resins, and significant side reactions can occur, so it is recommended that a chlorotriyl-based resin is used if these amino acids are the first to be attached to the resin.¹⁵⁸ With the advent of pre-loaded resins, it is possible to purchase the resin with the desired first amino acid already attached, eliminating the need for the esterification reaction.

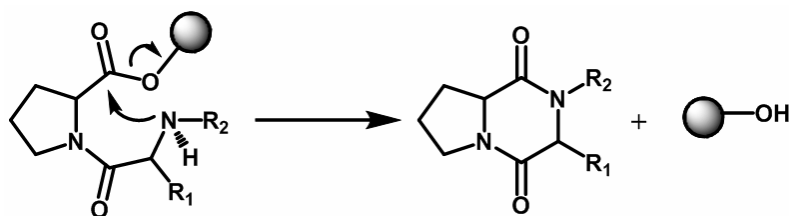


Figure 3-6. Diketopiperazine formation during synthesis using a hydroxymethyl linker and proline as the first amino acid.

When the first amino acid is proline, there is a higher occurrence of premature cleavage by diketopiperazine formation¹⁴⁹ (Figure 3-6) due to the unique secondary structure produced by the secondary amine. This results in cleavage of a dipeptide at the beginning of the sequence, and subsequent loss of peptide yield. To prevent this, when proline or N-alkylated amino are used as the first amino acid to be attached, the more sterically hindered chlorotriyl resin should be used instead.¹⁵⁸

Aminomethyl-based resins. Aminomethyl-based resins, such as Rink Amide^{156,159} (Fmoc) or Rink Amide MBHA (Boc) (Table 3-1) are the easiest to load with the initial amino acid, as they contain a free amine which may be coupled to the first amino acid using general peptide bond formation. Methods for coupling are discussed later in this section.

Chlorotrityl resins. If the resin to be used is a chloromethyl resin,¹⁶⁰ such as the 2-chlorotrityl resin^{158,160,161} (Table 3-1), the esterification proceeds by refluxing the desired first amino acid in DMF with the resin for several days. One problem with this method is that it is usually not possible to replace all chlorine atoms with the amino acid. If there are any free chlorine atoms, then in the presence of a tertiary amine the Cl can be replaced with the amine, forming a quaternary amine, which will interfere with subsequent coupling reactions.^{158,160,161} It is therefore essential to ensure the resin is fully substituted to prevent significant decreases in peptide yield. The advantage of this resin over hydroxymethyl derivatives is that there is no racemization of the first amino acid observed, and dipeptide formation is eliminated as well.¹⁵⁸ This makes them ideal for use when the first amino acid is Cys, Met, Pro, or Trp.¹⁵⁸ These resins can also be purchased with the first residue pre-loaded, allowing for standard chain elongation without the first esterification step.

It should be pointed out that the 2-chlorotrityl resin is unique in that the linker is hyperacid labile, meaning that very low concentrations of TFA can cleave the peptide in a short period of time. The side chain protecting groups, however, require stronger acidic conditions, meaning that this resin may yield peptides which are still fully side chain protected. A fully deprotected peptide may be obtained by longer treatment with higher acid concentration.

Side chain protecting groups

Over half of the common amino acids used in synthesis contain a reactive functionality on the side chain. In order to prevent deleterious side reactions these functional groups must be capped during synthesis. The capping groups are normally removed during the cleavage process, but must be stable to reaction conditions encountered during the synthesis. For Boc chemistry, the protecting group must be relatively stable to TFA, but must be removed with HF. Fmoc

chemistry allows the use of more acid-labile groups which are removed with TFA, but stable to base.

Common side chain protecting groups and the amino acids with which they are most commonly used are presented in Table 3-2. Special protecting groups may also be used which are removed by additional reagents either before or after cleavage. Examples are AcM, which is removed by iodine after cleavage for selective disulfide formation,¹⁴⁹ and the OAll and Alloc groups, which are removed with a palladium reagent.¹⁶² These are generally used for protection of side chains which will be deprotected during synthesis and used to form lactam bridge cyclizations. The lactam bridge can also be formed in Boc chemistry, by protecting with the Fmoc group, which can be selectively removed during synthesis using piperidine.

Table 3-2. Side chain protecting groups commonly used in SPPS.

Type Of Chemistry	Protecting Group Abbreviation	Cleavage Conditions	Amino acids
Boc	AcM	Iodine	Cys
	3-Bom	HF	His
	Bzl	HF	Asp, Cys, Glu, Ser, Thr, Tyr
	2-Cl-Z	HF	Arg
	Fmoc	piperidine	Lys, Asp, Glu
Fmoc	For	HF	Trp
	Tos	HF	Arg, His
	AcM	Iodine	Cys
	Alloc	Pd(Ph ₃ P)	Lys, Orn, Dap
	Boc	TFA	His, Lys, Orn, Trp
	OAll	Pd(Ph ₃ P)	Asp, Glu
	OtBu	TFA	Asp, Glu, Ser, Thr, Tyr
	Pbf	TFA	Arg
	Trt	TFA	Asn, Gln, Cys, His, Ser, Thr, Tyr

Coupling methods

The most important part of the peptide synthetic process is the coupling of one amino acid to another via formation of a peptide bond.¹⁴⁹ It is crucial to the success of the synthesis that the coupling method used is reliable, relatively quick, proceeds close to 100% completion and is free of deleterious side reactions. In order to ensure good coupling, the new amino acid must be activated at its C-terminus. This involves the addition of a reagent that will promote the nucleophilic attack of the resin-bound amine and release of the activating agent as a leaving group to form the peptide bond. This reagent must also proceed without loss of chiral specificity of the amino acid (See Figure 3-7 for common enantiomerization reactions of amino acids). Amino acid activation can be accomplished either by the addition of coupling reagents to the amino acid or by purchasing amino acids with an activating group already attached to the C-terminal of the amino acid. By far the most common method is the addition of coupling reagents which activate the C-terminus.¹⁴⁹ These can be divided into two categories, carbodiimide coupling reagents, and onium coupling reagents.¹⁴⁹

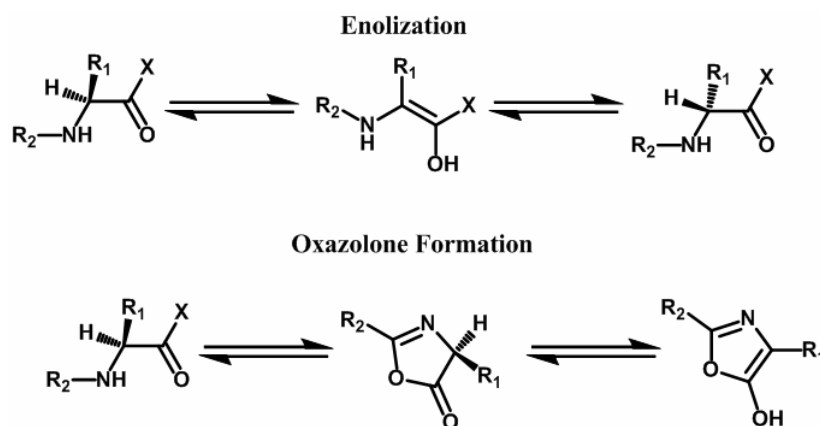


Figure 3-7. Common side reactions observed during amino acid activation.

Carbodiimides. Since Merrifield's development of SPPS,¹⁶³ carbodiimides have been widely utilized as coupling reagents along with HOBT (3-hydroxybenzotriazole) as the carboxyl activating agent.¹⁴⁹ Traditionally, DCC¹⁶⁴ (dicyclohexylcarbodiimide) was used, but has been

widely replaced by DIC¹⁶⁴⁻¹⁶⁶ (diisopropylcarbodiimide) for its ease of use and the increased solubility of the urea formed. Figure 3-8 depicts the possible mechanisms of carbodiimide-catalyzed coupling.¹⁴⁹

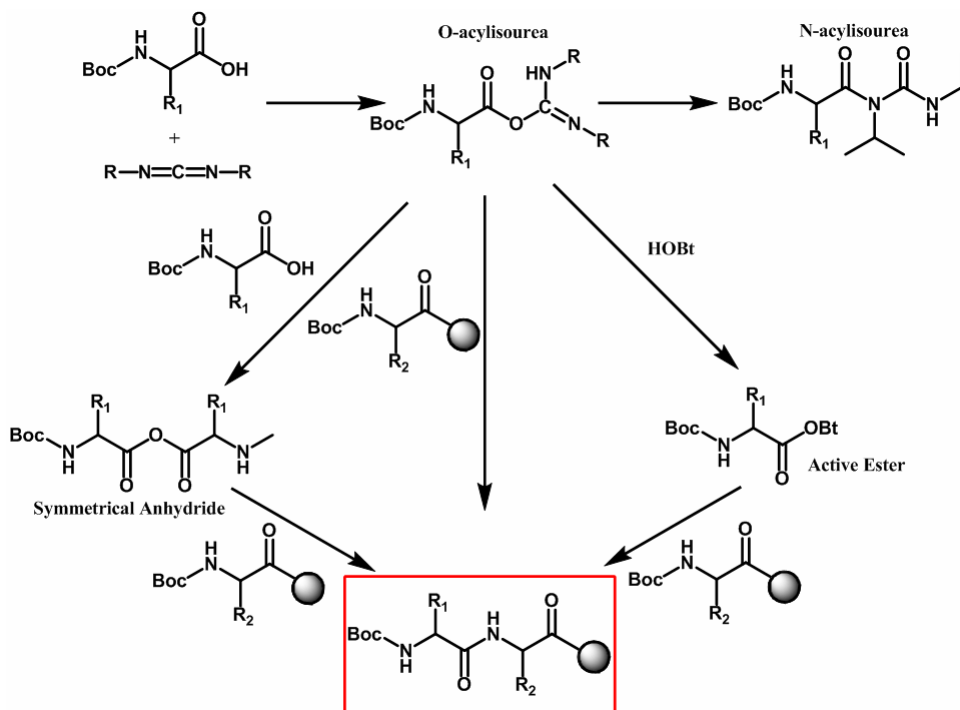


Figure 3-8. Mechanism of amino acid coupling using carbodiimide coupling reagents.

The synthesis can proceed through two intermediates, the symmetrical anhydride or the active ester. The reaction goes through the symmetrical anhydride intermediate when the amino acid: DIC ratio is 2:1 and there is no HOBT added.¹⁴⁹ In the presence of DIC, the O-acyl urea is formed. This intermediate is highly reactive, and may rearrange to form the N-acylisourea, which decreases the amount of amino acid available for coupling (Figure 3-8). Attack by another amino acid results in the symmetrical anhydride. This anhydride is then attacked by the amino group of the resin-bound amino acid, resulting in the formation of an amide bond (Figure 3-9).¹⁴⁹ Symmetrical anhydrides are best formed when DCM is the solvent, though some Fmoc amino acids require the addition of DMF to fully dissolve.¹⁴⁹ Additionally, the presence of base should be avoided as this will prevent the initial protonation of the carbodiimide and inhibit the

formation of the O-acylisourea. After amino acid activation, base may be added to increase the rate of carboxylate attack and subsequent anhydride formation.¹⁴⁹

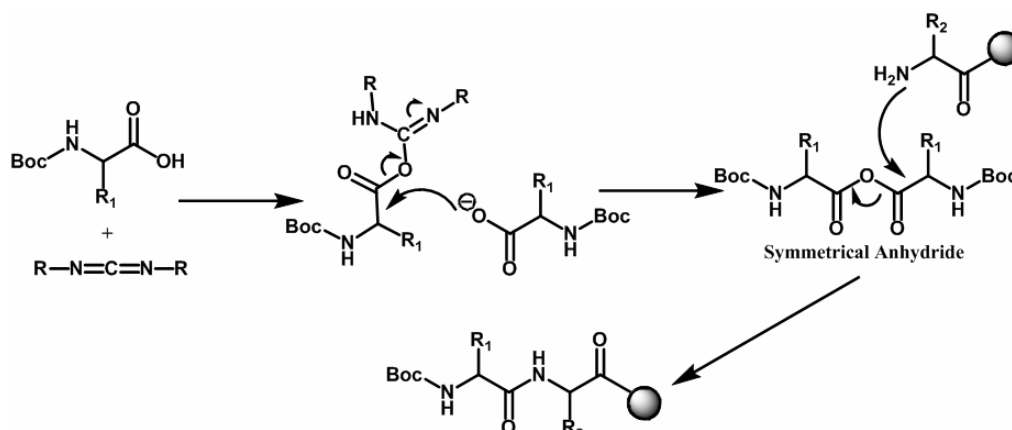


Figure 3-9. Mechanism of amino acid coupling using carbodiimides through symmetrical anhydride formation.

Addition of DMF favors the formation of other intermediates such as the active ester or oxazolone, which may contribute to loss of chirality.¹⁴⁹ Active ester formation takes place when an activating reagent such as HOBt (3-hydroxybenzotriazole) or HOAt (1-hydroxy-7-azabenzotriazole) are added (Figure 3-10).¹⁴⁹ In the presence of these nucleophiles, the active –OBt ester of the amino acid is formed. The –OBt ester intermediate is a very good leaving group, which makes subsequent amino attack and –OBt release relatively fast (Figure 3-11). The concentration of active ester may be increased with the addition of one equivalent of hydroxylamine. This serves to concentrate the ester by reacting with the O-acylisourea, preventing the formation of other intermediates. Addition of base after amino acid activation may serve to increase the rate of the coupling reaction.¹⁶⁷

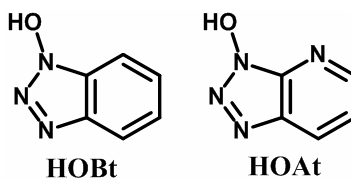


Figure 3-10. Structures of common hydroxybenzotriazoles used in coupling.

Another reactive intermediate that may be formed is the oxazolone (Figure 3-12),¹⁴⁹ this is most commonly formed if the amino acid is an N-carboxamide or by attack of a neighboring carbonyl.¹⁴⁹ This intermediate is undesirable as it increases the possibility of amino acid racemization (Figure 3-7).¹⁴⁹ Addition of a less reactive nucleophile, such as HOBt or hydroxylamines, may be added to reduce formation of the oxazolone and thus decrease the chances of racemization.

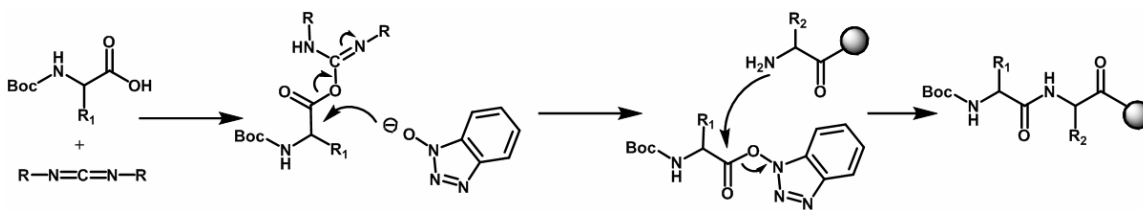


Figure 3-11. Proposed mechanism of amino acid coupling through active ester formation using carbodiimides and HOBt as coupling reagents.

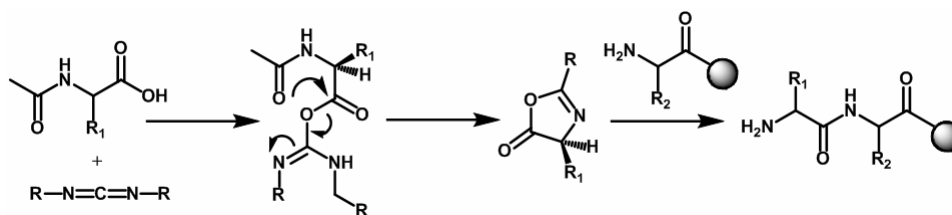


Figure 3-12. Proposed mechanism of oxazolone formation leading to amino acid coupling when carbodiimides are used as coupling reagents.

Phosphonium and aminium coupling reagents. Another widely used coupling method makes use of onium salts.¹⁴⁹ These are compounds based on two basic salts, phosphonium and aminium (Figure 3-13), coupled with a benzotriazole. Table 3-3 contains the names and structures of nine common onium coupling reagents.

The mechanism for the onium-assisted coupling of two amino acids has not been fully elucidated, although it is believed to proceed through highly reactive intermediates. In the case of phosphonium reagents, the reactive species may be an acyloxyphosphonium ion, which goes on to form either a symmetrical anhydride or active ester, depending on the presence of a hydroxybenzotriazole base.^{165,167-173} Aminium reagents may proceed through the

acyloxyguanidino intermediate, which reacts rapidly with the HOBt in solution to form the active ester.^{168,174-178} In either case, the presence of base in the reaction mixture is essential for the deprotonation of hydroxybenzotriazole. This reaction must be very fast in order to prevent the reactive onium intermediates from remaining in the solution too long and causing unwanted side reactions. One common side reaction is the N-terminal guanidation of the peptide chain (Figure 3-14) caused by aminium reagents.¹⁷⁹ This caps the N-terminal of the peptide chain, preventing chain elongation. To help prevent this, it is good to pre-activate the amino acid with 0.9 equivalents of aminium reagent before addition to resin.¹⁸⁰

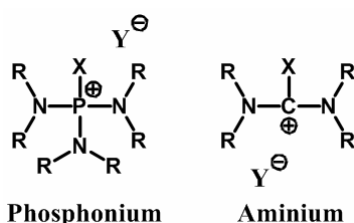


Figure 3-13. Structures of phosphonium and aminium salts used in coupling reactions.

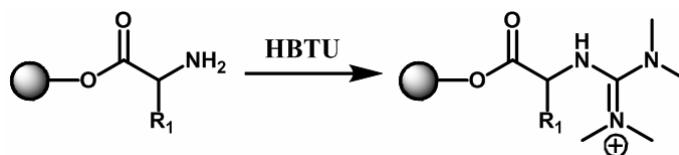


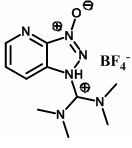
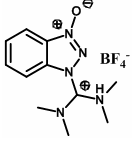
Figure 3-14. N-terminal guanidation of peptide chain when HBTU is the coupling reagent.

The first of these salts to gain popularity for use in SPPS was the phosphonium salt BOP (benzotriazol-1-yl-N-oxy-tris(dimethylamino)phosphonium hexafluorophosphate).^{181,182} One drawback of the use of this salt is the generation of a highly toxic side product, hexamethylphosphorotriamide,^{182,183} to avoid this side product, the BOP derivatives PyBOP (benzotriazol-1-yl-N-oxy-tris(pyrrolidino)phosphonium hexafluorophosphate)¹⁸⁴ and PyBrOP ([bromotris]-(pyrrolidino)phosphonium hexafluorophosphate)¹⁸⁵ were developed. The aminium reagents HBTU (N-[1H-benzotriazole-1-yl](dimethylamino)methylamino)methylene]-N-

methylmethanaminium hexafluorophosphate N-oxide),^{186,187} HATU (N-[(dimethylamino)-1H-1,2,3-triazolo[4,5]pyridine-1-ylmethylmethanaminium hexafluorophosphate N-oxide),¹⁶⁵ TBTU (N-[1H-benzotriazole-1-yl(dimethylamino)methylene]-N-methylmethanaminium tetrafluoroborate N-oxide), and TATU (N-[(dimethylamino)-1H-1,2,3-triazolo[4,5]pyridine-1-ylmethylene]-N-methylmethanaminium tetrafluoroborate N-oxide) do not produce this toxic side product.

Table 3-3. Phosponium and aminium-based coupling reagents.

Coupling Reagent	Abbreviation	Structure
Benzotriazol-1-yl-N-oxy-tris(dimethylamino)phosponium hexafluorophosphate	BOP	
Benzotriazol-1-yl-N-oxy-tris(pyrrolidino)phosponium hexafluorophosphate	PyBOP	
[Bromotris]-(pyrrolidino)phosponium hexafluorophosphate	PyBrOP	
(7-Azabenzotriazol-1-yloxy)-tris(dimethylamino)phosponium hexafluorophosphate	AOP	
(7-Azabenzotriazol-1-yloxy)-tris(pyrrolidino)phosponium hexafluorophosphate	PyAOP	
N-[1H-Benzotriazole-1-yl](dimethylamino)methylamino)methylene]-N-methylmethanaminium hexafluorophosphate N-oxide	HBTU	

N-[(Dimethylamino)-1H-1,2,3-triazolo[4,5]pyridine-1-ylmethylmethanaminium hexafluorophosphate N-oxide	HATU	
N-[1H-Benzotriazole-1-yl(dimethylamino)methylene]-N-methylmethanaminium tetrafluoroborate N-oxide	TBTU	
N-[(Dimethylamino)-1H-1,2,3-triazolo[4,5]pyridine-1-ylmethylene]-N-methylmethanaminium tetrafluoroborate N-oxide	TATU	

Colorimetric monitoring methods

There are two widely used on-resin colorimetric methods used to monitor the presence or absence of primary or secondary amines during SPPS. The most common method for detecting primary amines is the Kaiser¹⁸⁸ test, which makes use of the reagent ninhydrin, which reacts with free primary amines to produce the purple dye Ruhemann's purple (Figure 3-15). After Boc or Fmoc deprotection a test is done to detect the presence of free amine (dark blue), and after coupling another test is performed to monitor the completion of the reaction (absence of free amine, yellow color). This method is very useful for short (~2-30) amino acid sequences, though its utility decreases for long or aggregated sequences. Additionally, the test does not work for secondary amines such as proline, and the blue color is not always seen for amino acids such as serine, asparagine, and aspartic acid.¹⁴⁹

The Kaiser test is not suitable for the detection of secondary amines (ie proline) due to the fact that ninhydrin does not interact with secondary amines. To monitor reactions of proline and other secondary amines, the chloranil test¹⁸⁹ is used. Chloranil (2,3,5,6-tetrachloro-1,4-benzoquinone) reacts with both primary and secondary amines to form 2,3,5-trichloro-6-(2-

pyrrolidinyl-vinyl)-[1,4]benzoquinone (Figure 3-16), which causes the resin beads to turn a green-blue color in acetone.

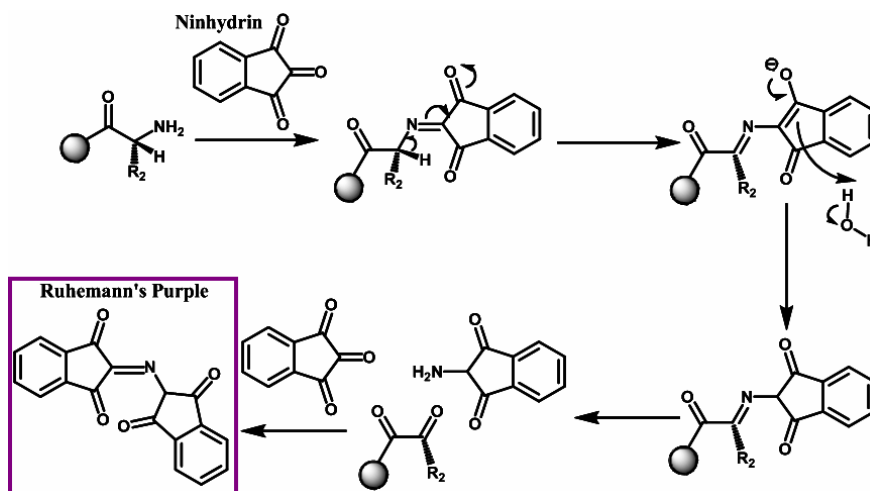


Figure 3-15. Possible mechanism of primary amine detection using ninhydrin.

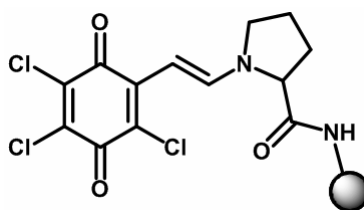


Figure 3-16. Complex formed from the reaction of chloranil with a secondary amine.

Solid Phase 1,4-Benzodiazepine-2,5-dione Synthesis

The 1,4-benzodiazepines are an important class of privileged templates,³⁵ and numerous derivatives have been identified that have selective activities against a diverse array of biological targets.³⁶⁻⁴⁰ Three common types of benzodiazepines are the 1,4-benzodiazepin-2-one (Figure 3-17A), 1,5-benzodiazepine-2-one (Figure 3-17B), and 1,4-benzodiazepine-2,5-dione (Figure 3-17C). 1,4-benzodiazepin-2,5-diones have been reported to possess anticonvulsant, anxiolytic, and antitumor properties, as well as being cholecystokinin receptor (CCK), opiate receptor and platelet glycoprotein IIb-IIIa antagonists,¹⁹⁰⁻¹⁹³ as well as having herbicidal properties.¹⁹⁴ In addition, the 1,4-benzodiazepine-2,5-dione core appears in a number of natural products, including asperlicin.¹⁹⁵⁻¹⁹⁷

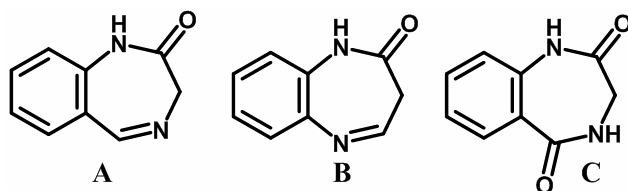


Figure 3-17. Structures of common benzodiazepine templates. **A.** 1,4-benzodiazepine-2-one. **B.** 1,5-benzodiazepine-2-one. **C.** 1,4-benzodiazepine-2,5-dione.

Solid Phase Organic Synthesis

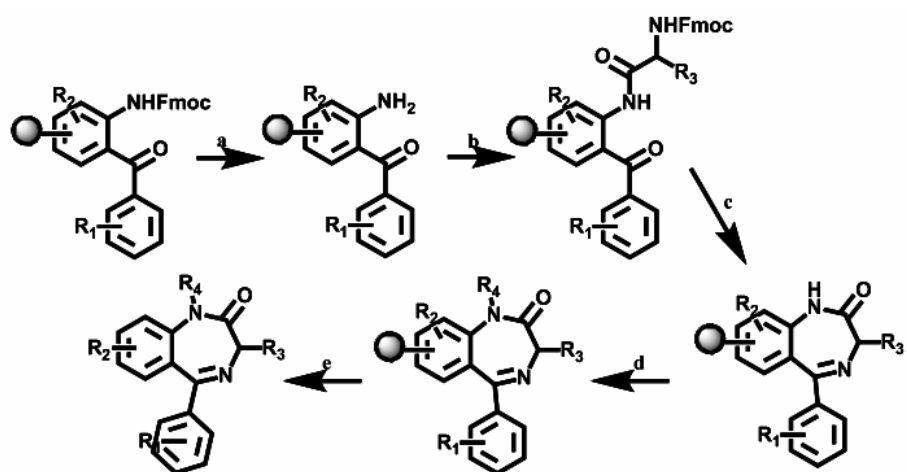
The syntheses of a vast number of organic heterocycles have been described for solution phase synthetic approaches for many decades, benzodiazepine synthesis included.¹⁹² The application of solid phase synthesis to organic molecules has only recently begun to gain in popularity.^{193,194,198-203} Solid phase is much preferable to solution phase for many reasons. The first is that reagents can be easily washed away by filtration after each step, eliminating the need for extensive extraction, purification, and characterization between each step. This simple washing also removes non-resin bound side products that may form. Additionally, excess reagents can be added in order to drive the reaction as close to completion as possible, maximizing yield. Solid phase organic synthesis can also be performed using the same equipment as solid phase peptide chemistry, resulting in a low start-up expense for laboratories already doing SPPS. Because the compounds are synthesized on resin, a large number of spatially separate molecules can be constructed in a short period of time with less labor and reagent cost. These compounds can be individually cleaved and analyzed in high-throughput applications to generate large diverse libraries for biological testing.

The benzodiazepine privileged structure provides an ideal framework for application to combinatorial solid phase approach due to the conserved core structure, many well-defined points of diversity, commercial availability of reagents, and the possibility of multiple points of attachment to resin.¹⁹² As benzodiazepines have already been shown to have potential for the

development of drugs, a simple, rapid, and robust method of synthesizing large numbers of compounds is highly desirable.

Several solid phase and solution phase methodologies for the rapid synthesis of benzodiazepine derivatives have been published recently. Each synthesis discussed is unique in the starting materials and specific methodologies, though most contain the same basic formula: attachment of the first amino acid-based moiety, acylation, cyclization, alkylation, and finally cleavage from resin.

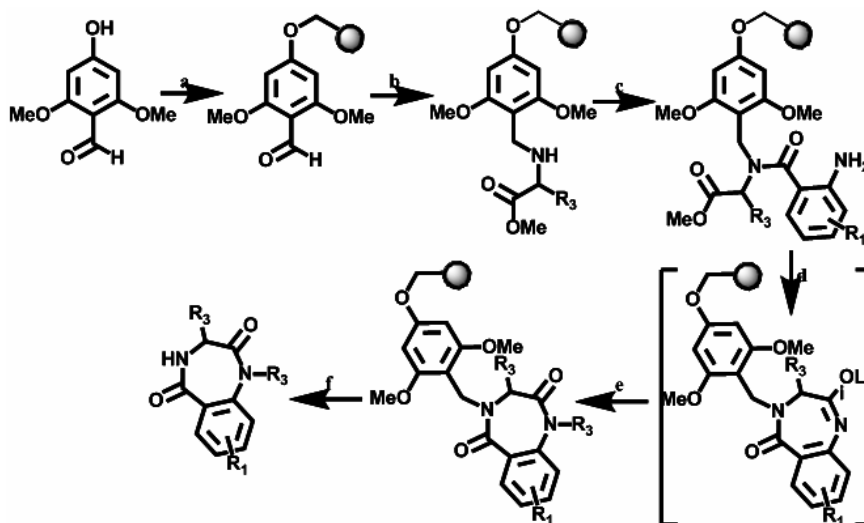
In 1994, Bunin *et al.* described the synthesis of a 1,4-benzodiazepine-2-one library from 2-aminobenzophenones, amino acids, and alkylating agents (Figure 3-18).¹⁹⁹ A pin apparatus was used in which the 2-aminobenzophenone was coupled to the solid support and the Fmoc protecting group removed. This was followed by coupling of an amino acid fluoride to the aryl amine. The acid-catalyzed cyclization was followed by alkylation, and finally cleavage. In this manner 192 separate compounds were synthesized and tested at the cholecystokinin A



a. 20% piperidine in DMF; b. N-Fmoc-amino acid fluoride in DCM; c. 5% acetic acid in DMF; d. lithiated 5-phenylmethyl-2-oxazolidinone in DMF/THF, 1:10 vol/vol, followed by alkylating agent in DMF; e. TFA/H₂O/Me₂S, 95:5:10 (vol/vol).

receptor.¹⁹⁹

Figure 3-18. Bunin *et al.*¹⁹⁹ synthesis of a 1,4-benzodiazepine-2-one.



a. NaH/DMF, then chloromethyl polystyrene resin, 50°C, 36h; **b.** amino acid ester, NaBH(OAc)₃ in 1% acetic acid/DMF; **c.** anthranilic acid and EDC in NMP; **d.** acetanilide lithium salt in THF/DMF, 30h; **e.** alkylating agent; **f.** TFA/DMS/H₂O.

Figure 3-19. Boojamra *et al.*^{194,200} synthesis of a 1,4-benzodiazepine-2,5-dione.

Boojamra *et al.* published a synthesis of 1,4-benzodiazepin-2,5-diones in 1995 that also utilized solid support (Figure 3-19).^{194,200} Merrifield resin was derivatized with 4-hydroxy-2,6-dimethoxybenzaldehyde to yield the resin-bound aldehyde which was then coupled to an amino acid ester via reductive amination. This formed the tertiary amine necessary for efficient lactamization. Cyclization was base-catalyzed using a lithium salt of acetanilide, which was basic enough to catalyze lactam-ring formation, but not basic enough to deprotonate other functionalities. Alkylation provided the final diversity point, and acid-catalyzed cleavage from the resin resulted in the desired compound in good yield and purity, with little to no observed racemization.

Rapid one-pot solution phase syntheses of benzodiazepines have also been recently examined.¹⁹² Keating *et al.* reported a solution phase synthesis utilizing the Ugi four-component condensation, which utilizes the combination of a carboxylic acid, an amine, an aldehyde or ketone, and an isocyanide to yield an α -acylamino amide (Figure 3-20).¹⁹² This compound then

cyclizes in the presence of acid to form a 1,4-benzodiazepine-2,5-dione. This is a useful reaction if a solution phase synthesis is desired, however it does require the use of column chromatography for purification, and the final compound is presented as a racemic mixture as the Ugi reaction results in the generation of a new stereocenter.

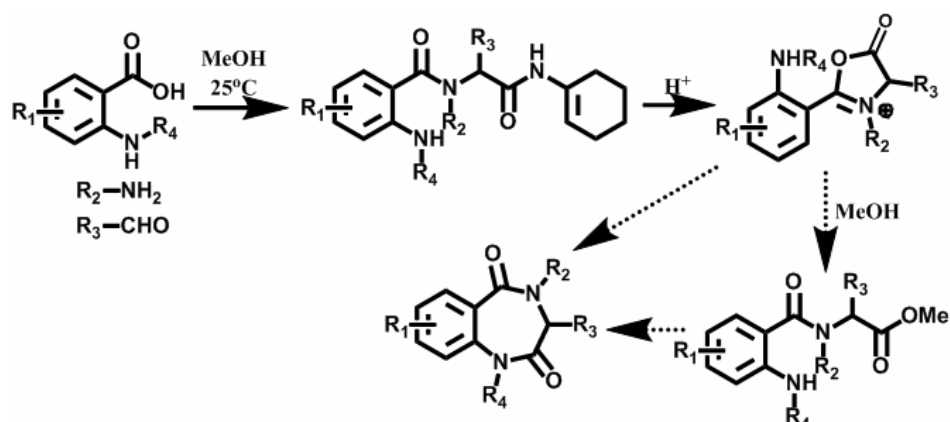
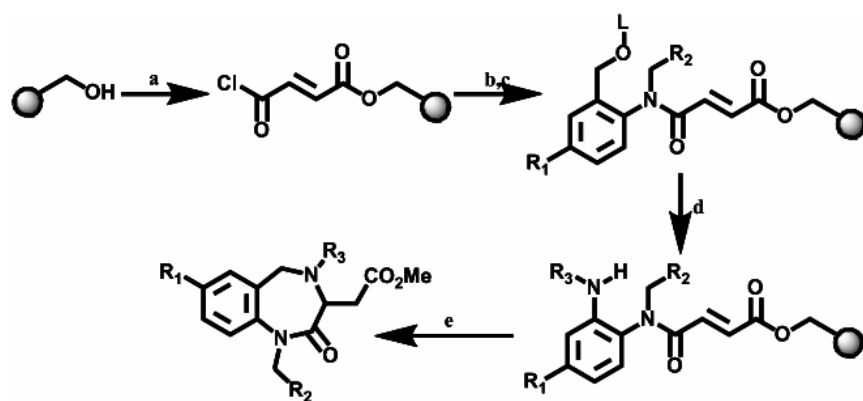


Figure 3-20. Keating *et al.*¹⁹² synthesis of 1,4-benzodiazepine-2,5-diones.



a. Fumaryl chloride, THF, rt, 10h; **b.** amino alcohol, DCM, rt, 10h; **c.** MsCl, Et₃N, DCM, 0°C to RT, 4h; **d.** alkyl amine, DMF, RT, 10h; **e.** NaOMe, THF/MeOH (4:1 v/v), RT, 10h.

Figure 3-21. Bhalay *et al.*²⁰¹ synthesis of 1,4-benzodiazepine-2-ones.

Another method reported by Bhalay *et al.* makes use of Wang resin on which to build 1,4-benzodiazepin-2-ones from amino alcohols, anthranilic esters, acid chlorides, and amines to produce 120 compounds with three points of diversity (Figure 3-21).²⁰¹ The reaction makes use of amino alcohols, which are synthesized from the corresponding acid chloride and anthranilic

ester, and then added to a resin bound acid chloride. A primary amine displaces a mesylate (L) to give a secondary aryl amine. Cyclization and cleavage take place concurrently with the addition of sodium methoxide and THF to give the final compound.

In the search for short, rapid methods to apply solid phase benzodiazepine synthesis to high throughput applications, Mayer *et al.* developed a strategy of synthesizing 1,4-benzodiazepin-2,5-diones using Wang resin functionalized with an amino acid, and then reacting this with either an *o*-nitrobenzoic acid or Fmoc-protected *o*-anthranilic acids (Figure 3-22).¹⁹³ Either way, the amine is produced on the aryl ring and then a base-promoted cyclization reaction occurs, which causes the molecule to be released from the resin. This results in an increase in final purity, as only compounds which have cyclized are released from the solid support. The ability to use either nitrobenzoic or anthranilic acids allows for an increase in diversity over other synthetic methods.

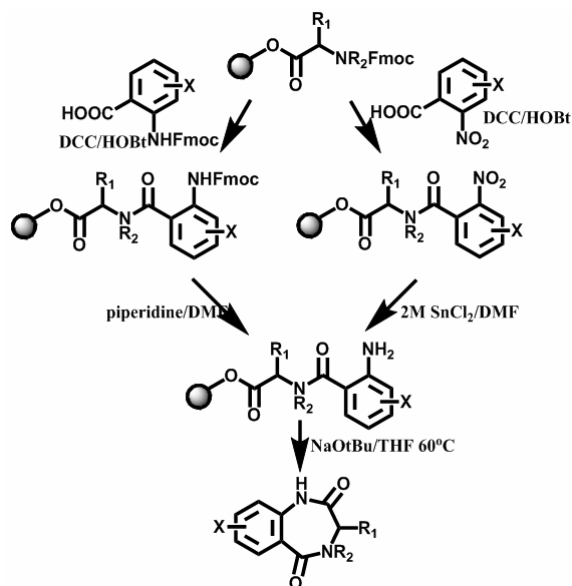
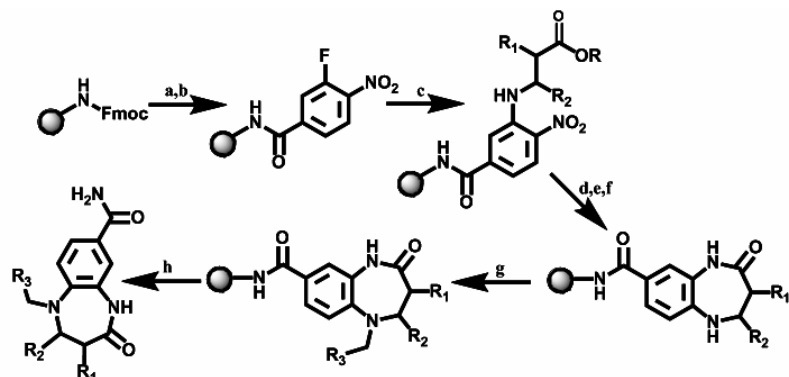


Figure 3-22. Mayer *et al.*¹⁹³ synthesis of 1,4-benzodiazepine-2-ones.

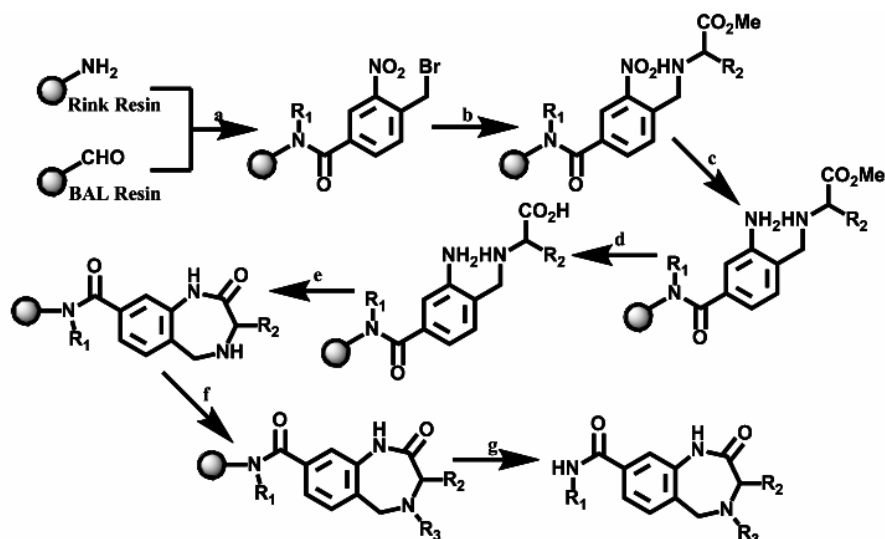
An interesting synthesis was reported in 1999 by Lee *et al.* which made use of synthesized α -substituted β -amino esters as the basis for the seven-membered ring (Figure 3-23).²⁰² They

took aryl fluorides with a nitro group ortho to the fluorine and substituted the fluorine with an α -substituted β -amino ester. The nitro group was reduced to an amine, and the ester hydrolyzed. Cyclization in DIC and HOBt provided the desired 1,5-benzodiazepin-2-one. The resulting molecule was alkylated and then cleaved from the resin.



a. DMF/piperidine; b. (4-F-3-NO₂)PhCO₂H, HATU, DIEA, DMF; c. H₂NCH(R₂)CH(R₁)CO₂R, DIEA, DMF; d. SnCl₂, DMF; e. 1N NaOH, THF; f. DIC, HOBt, DMF; g. R₃CH₂Br, K₂CO₃, CH₃COCH₃, 55°C; h. TFA/H₂O (95:5).

Figure 3-23. Lee *et al.*²⁰² synthesis of 1,5-benzodiazepine-2-ones.



a. Primary amine; b. R₂CH(NH₂)CO₂Me in NMP, 1.5h; c. SnCl₂ in NMP, 12h; d. NaOH in dioxane/H₂O, 55°C, 12h; e. DIC/HOBt in DMF; f. R₃CHO, NaBH(OAc)₃ in acetic acid/DMF; g. 20% TFA in DCM.

Figure 3-24. Zhang *et al.*²⁰³ synthesis of 1,4-benzodiazepine-2-ones.

The final synthesis discussed here was presented by Zhang *et al.* in 2002 (Figure 3-24).²⁰³

This synthesis of 1,4-benzodiazepine-2,5-diones begins with either a Rink amide resin or BAL

resin which is functionalized with an aldehyde. The resin is reacted with a primary amine and 4-(bromomethyl)-3-nitrobenzoic acid and then the aryl bromide is displaced with an α -amino ester. The nitro group is then reduced and the ester hydrolyzed, and intramolecular lactamization affords the cyclized structure. The compound is alkylated and then released from the solid support by treatment with TFA.

Each of these syntheses has its advantages and disadvantages and provides the framework for different points of diversity. For this work the synthesis by Boojamra^{194,200} was chosen as the basis for the synthesis of a library of 1,4-benzodiazepin-2,5-diones. This synthesis was attractive due to the available diversity and ease of synthesis as well as its applicability to solid phase synthesis techniques already in place. The basic synthesis remained the same, except BAL resin was used, which already had the aldehyde functionality attached. This allowed for the attachment of the amino ester to be the first step, followed by acylation, lactamization, alkylation, and cleavage. Library design and specific methods are discussed in Chapter 6.

Colorimetric Monitoring

Colorimetric tests were used during the benzodiazepine synthesis to monitor the progress of the reaction. The ninhydrin and chloronil tests have been discussed in the previous section.^{204,205} These tests were used to monitor the conversion of the secondary amine to the tertiary amine after acylation.

At the beginning of the synthesis, the reductive amination of the amino acid ester and the aldehyde was monitored by the DNPH test for aldehydes (Figure 3-25).²⁰⁶ In this test, 2,4-dinitrophenylhydrazine reacts with the resin-bound aldehyde to produce a red color. The reaction is monitored based on the disappearance of the aldehyde, marked by no color change in the test.

The other test used was the bromophenol blue test for tertiary amines.²⁰⁷ In the presence of a tertiary amine, bromophenol blue changes the resin beads from yellow to a dark green/blue. This test is valuable for monitoring the formation of a tertiary amine during acylation.

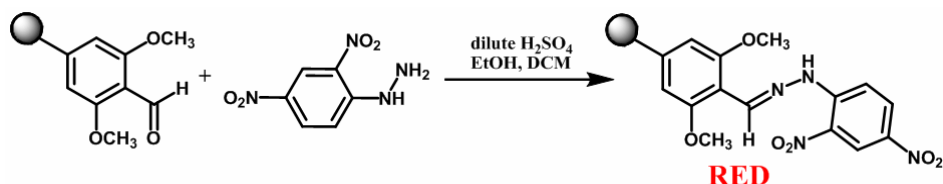


Figure 3-25. Reaction of an aldehyde with DNPH to give a red complex.

Experimental Details

Synthesis of MTII-based Cation- π Peptides

All amino acids and reagents were used without further purification. Boc-Ala-OH, Boc-Asp(O^tFm)-OH, Boc-DPhe-OH, Boc-His(3-Bom)-OH, Boc-Lys(2-chloro-Z)-OH, Boc-Lys(Fmoc)-OH, Boc-Nle-OH, Boc-Trp(For)-OH, Boc-Phe-OH, Boc-D-2-Nal-OH, Boc-DNal(1')-OH, and Boc-Nal(1')-OH were purchased from Bachem (Torrence, CA). Boc-Nal(2')-OH, N-Hydroxybenzotriazole (HOBt), and Benzotriazole-1-yl-oxy-tris-(dimethylamino)-phosphonium hexafluorophosphate (BOP) were purchased from Peptides International (Louisville, KY). N-Diisopropylethylamine (DIEA), piperidine, anisole, thioanisole, m-cresol and diisopropylcarbodiimide (DIC) were purchased from Sigma-Aldrich (St. Louis, MO). Dichloromethane, glacial acetic acid, acetonitrile, trifluoroacetic acid, and ethyl ether were purchased from Fisher (Fair Lawn, NJ). N,N-Dimethylformamide was purchased from Burdick and Jackson (McGaw Park, IL).

Peptide Synthesis was accomplished by standard Boc chemistry.²⁰⁸ pMBHA Resin (0.28 meq/g substitution) was used. The resin was placed in a manual reaction vessel (Peptides International), and allowed to swell for one hour in dichloromethane. 10% DIEA in DCM was used to neutralize the resin, and a Kaiser test³⁹ performed to detect the presence of a primary

amine. After a positive test (purple color), the first Boc amino acid (3-fold excess) was mixed with HOBt (Anhydrous) in 3-fold excess. The mixture was added to the resin along with a 3-fold excess of DIC, and the solution mixed with nitrogen gas for two hours. After coupling, the resin was washed with DMF twice for one minute each, and DCM seven times for one minute each. A Kaiser test was performed after coupling to ensure the absence of any primary amines, indicating that the reaction had gone to completion. After a negative Kaiser test (yellow solution), the resin was washed with DCM four times for one minute each. The Boc group on the amino terminus of the attached amino acid was next removed (deprotected) using a mixture of 50% TFA, 48% DCM, and 2% anisole (to prevent the free Boc group from reacting with the peptide chain) once for two minutes, and once for 20 minutes. After the resin was washed with DCM four times for one minute each, and a positive Kaiser test obtained, the resin was neutralized with 10% DIEA and the next amino acid added in the same way as the previous one. This cycle was repeated for all amino acids in the chain. Cyclization of the peptide was performed in solution prior to adding the final amino acid. The Fmoc groups protecting the side chains of the amino acids Boc-Lys(Fmoc)-OH, and Boc-Asp(OFm)-OH, were removed using a 20% piperidine solution in DMF for 30 minutes. After obtaining a positive Kaiser test, the resin was mixed with a 5-fold excess of BOP Reagent, HOBt (Anhydrous) (or HBTU), and DIEA in DCM at 37°C for up to two weeks in an Advanced Chemtech automatic synthesizer (440 MOS, Louisville, KY) until a negative Kaiser test was obtained. After the final amino acid was added, the final amino acid in the chain was deprotected, and the resin dried overnight in a desiccator.

Cleavage by hydrogen fluoride is very dangerous, and measures were taken to ensure the safety of the operator. Resin was placed in a Teflon reaction vessel along with a magnetic stir bar and the scavengers m-cresol and thioanisole in equimolar amounts (1 μ L scavenger per 2mg

resin). Scavengers are added to react with the free protecting groups in solution to prevent them from interacting with the newly deprotected side chain groups of the peptide. The vessel was attached to the HF vacuum apparatus and chilled in liquid nitrogen. The water and water pump were turned on and all stopcocks opened to check for leaks in the vacuum. If there were no leaks present, the anhydrous HF was stirred with CoF_3 and then transferred from the HF reservoir into a Teflon reaction vessel (approximately 3mL per 100g of resin). The reaction vessel was removed from the liquid nitrogen (-78°C) and placed in an ice bath to increase the temperature to 0°C , at which point the HF melted. At this point in time, the reaction was left stirring for one hour. After one hour, a Teflon waste trap was placed in liquid nitrogen and the HF transferred from the reaction vessel to the waste trap. When all HF had been removed, the reaction vessel(s) were removed from the apparatus and filled with ethyl ether to remove scavengers and form a white precipitate. Finally, the waste trap was removed from the liquid nitrogen and placed in sodium bicarbonate overnight.

After addition of ethyl ether to the peptide after cleavage, the mixture was filtered using a fritted glass funnel into a conical flask. The precipitate was washed a second time with ethyl ether. Glacial acetic acid was used to dissolve the peptide, and filtered into a round-bottomed flask. Filtering with acetic acid was performed three to four times using 20mL each time. After all the peptide was collected, the filtrate was frozen using dry ice in acetone, and lyophilized to remove the solvent, resulting in a dry powder.

1,4-Benzodiazepine-2,5-diones

Synthesis was performed in a manual reaction vessel (Peptides International, Louisville, KY), mixing was accomplished with nitrogen. All reagents used were ACS grade or better and used without further purification. BAL resin (Backbone amide linker resin) was purchased from Advanced ChemTech (Louisville, KY). Dichloromethane, acetic acid, N-methyl pyrrolidinone,

acetonitrile, acetone, and methanol were purchased from Fisher (Fair Lawn, NJ). N,N-Dimethylformamide was purchased from Burdick and Jackson (McGaw Park, IL). Sodium triacetoxyborohydride, 1-[3-(dimethylamino)propyl]-1'-ethylcarbodiimide hydrochloride, acetanilide, N-butyllithium (10M in hexanes), benzyl bromide, 2-(bromomethyl)-naphthalene, 2-phenylbenzylbromide, dimethylsulfide, 1-iodopropane, 1-iodobutane, tetrahydrofuran, triisopropylsilane and trifluoroacetic acid were purchased from Sigma-Aldrich (St. Louis, MO). 2-Amino-4-chlorobenzoic acid and 2-amino-3-methylbenzoic acid were purchased from Acros Organics (Morris Plains, NJ). Arginine-(Pbf) methyl ester, and lysine-(Boc) methyl ester were purchased from Bachem (Torrence, CA). Phenylalanine methyl ester was purchased from Advanced Chemtech (Louisville, KY). Tryptophan methyl ester was purchased from Fluka (St. Louis, MO). 2-Aminobenzoic acid was purchased from Alfa Aesar (Ward Hill, MA).

Synthesis was performed on solid phase using the method described in Schemes 6-1 and 6-2. BAL resin (0.3 mmol) was swollen in DCM for one hour and tested for the presence of an aldehyde using the DNPH method.²⁰⁶ The first step of the synthesis involves the reductive amination of an aldehyde and the methyl ester derivative of an amino acid. Three-fold excess of $\text{NaBH}(\text{OAc})_3$ (10 eq, 3.0 mmol) was dissolved in 1 % AcOH/DMF, generating a white suspension. An amino acid methyl ester in 3-fold excess (10 eq, 3.0 mmol) was added to the reaction mixture and stirred for 3-4 h. The resin was filtered and washed with DMF (3 x 20 ml), DCM (3 x 20 ml), MeOH (2 x 20 ml) and DCM (3 x 20 ml). A sample of the resin was removed and tested for the presence of a secondary amine (chloranil test) and the absence of an aldehyde (DNPH test for aldehydes²⁰⁶).

The next step involved the acylation of a secondary amine with a 2-aminobenzoic acid. The resin was dissolved in N-methyl pyrrolidinone (NMP) followed by the addition of excess 1-

[3-(dimethylamino)propyl]-1'-ethylcarbodiimide hydrochloride (EDC). After the EDC was completely dissolved, the 2-aminobenzoic acid was added slowly to minimize side reaction that may occur with an unprotected amine, and the reaction was mixed with nitrogen overnight. The resin was filtered and washed with NMP (2 x 20 ml), DMF (3 x 20 ml), DCM (3 x 20 ml), MeOH (2 x 20 ml) and DCM (3 x 20 ml). A sample of the resin was removed and tested for the absence of a secondary amine (chloranil test) and the presence of a tertiary amine (bromophenol blue test²⁰⁷).

Lactamization to form the seven-membered benzodiazepine ring required the synthesis of a lithiated acetanilide salt. A round-bottomed flask was oven-dried and acetanilide (24 eq, 7.2 mmol) dissolved in 10 mL THF was added. The flask was purged with argon gas and cooled to -78°C in a dry ice/acetone bath. A hexane solution of n-BuLi (20 eq, 6.0 mmol) was added dropwise over 10 min followed by rapid stirring for 30min at -78°C (Scheme 6-2). After 30 min, 10 mL DMF was added to homogenize the solution and the mixture stirred gently for 15 min. The flask was then allowed to slowly come to room temperature. The lithium salt was transferred to to a round-bottomed flask containing the resin and purged with argon and the resin stirred gently for 30 h at room temperature.

Following cyclization, the pH of the solution was tested with pH paper (pH~13-14) and an alkylating agent (40 eq, 12.0 mmol) was added and stirred at room temperature until the pH of the solution was approximately 5 as determined by pH paper. The resin was then transferred back to a reaction vessel and washed with DMF (7 x 20 mL), DCM (7 x 20 mL), MeOH (3 x 20 mL), and DCM (3 x 20 mL). The resin was air-dried and then cleaved with a cleavage cocktail of TFA/Me₂S/H₂O (90:5:5) for 50 h. The cleaved resin was removed by filtration and the filtrate was evaporated and lyophilized.

Ligand Purification and Analysis

Ligands were purified by Reverse Phase-High Performance Liquid Chromatography (RP-HPLC) using a Shimadzu chromatography system with a photodiode array detector and a semi-preparative RP-HPLC C18 bonded silica column (Vydac 218TP1010, 1.0 x 25 cm) and lyophilized. The purified peptides were analyzed using RP-HPLC with an analytical Vydac C18 column (Vydac 218TP104). Molecular mass was determined by Mass Spectrometry on a Voyager-DE Pro (University of Florida protein core facility). ¹H-NMR was performed on a 400MHz Varian instrument using DMSO-*d*₆ as solvent and TMS as reference. ¹H-NMR of compound 2 was performed on a 600MHz Bruker Advance Console using DMSO-*d*₆ as solvent and TMS as reference.

Reporter Gene Assay: β-Galactosidase

Pharmacological analysis was performed by β-galactosidase reporter gene assay.²⁰⁹ HEK-293 cells stably expressing the melanocortin receptors were transiently transfected with CRE/β-galactosidase reporter gene. Forty-eight hours post-transfection the cells were stimulated with 100μL peptide (10^{-4} - 10^{-10} M) or forskolin (10^{-4} M) control in assay medium (DMEM containing 0.1mg/mL BSA and 0.1 mM IBMX) for 6 h. To the cell lysate plates, 150 μL substrate buffer (60 mM sodium phosphate, 1 mM MgCl₂, 10 mM KCl, 5 mM β-mercaptoethanol, 2 mg/1 mL ONPG) was added to each well and the plates were incubated at 37°C. The sample absorbance, OD₄₀₅, was measured using a 96 well plate reader (Molecular Devices). Data points were normalized both to the relative protein content and non-receptor dependent forskolin stimulation.

CHAPTER 4
GENERAL METHODOLOGIES 2: MOLECULAR BIOLOGY

Molecular Cloning

Structure of DNA

DNA, or Deoxyribonucleic acid, is the thread that holds the fabric of life together. DNA contains all of the information necessary to build every protein in the organism and how the proteins go together to form cells and tissues as well as synthesize non-protein biological molecules. DNA is made up of units known as nucleotides. Each nucleotide consists of a deoxyribose sugar, an organic base, and a phosphate group. Each monomer is linked together through a sugar-phosphate bond, which makes the backbone of the molecule, with bases extending from the backbone as side chains. There are four bases in DNA, these are adenine, thymine, cytosine, and guanine. Adenine and guanine are purines, which consist of a fused ring system, and thymine and cytosine are pyrimidines, which are single ring molecules. The DNA molecule is made up of repeating nucleotides in a specific order. The order of the nucleotides determines the sequence of amino acids that makes up the protein that gene codes for.

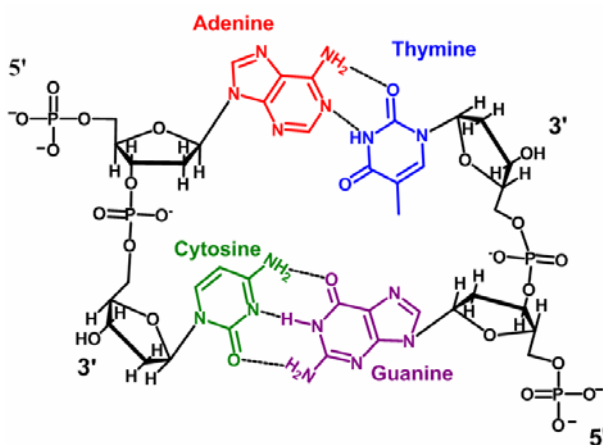


Figure 4-1. Structure of DNA and bases. Adenine and thymine base pair and form two hydrogen bonds. Cytosine and guanine form three hydrogen bonds. The sugar-phosphate backbone is shown in black.

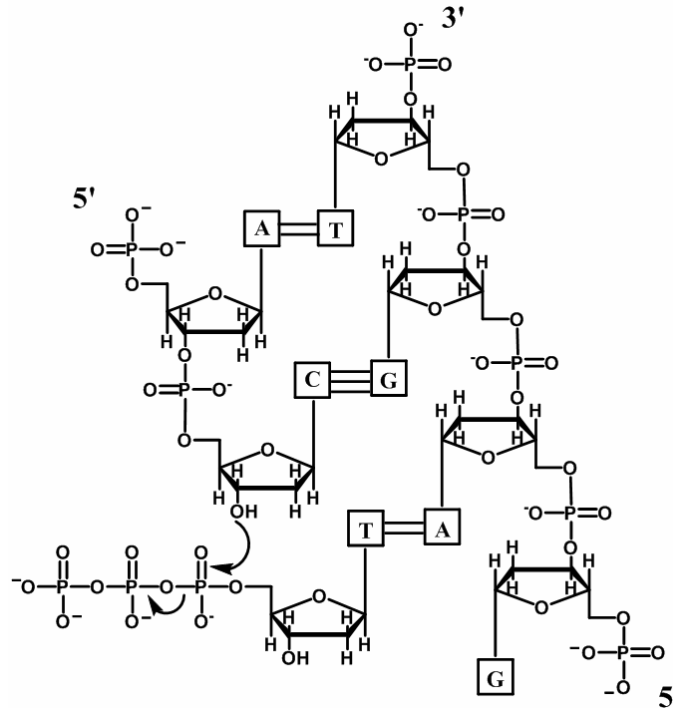


Figure 4-2. Formation of a phosphodiester bond during DNA synthesis. The bases pair and DNA polymerase catalyzes the nucleophilic attack of the 3'OH on the phosphate of the new base, releasing a diphosphate.

DNA is a double-stranded molecule. The two strands of repeating nucleosides are held together by hydrogen bonds between bases. The bases pair according to Chargaff's rules, which state that adenine and thymine always pair together, connected by two hydrogen bonds, and cytosine and guanine always base pair forming three hydrogen bonds (Figure 4-1). For this reason the two DNA strands are antiparallel and complementary, one running from the 5' to 3' direction, and the other running from the 3' to the 5' direction. As the DNA molecule is built, each nucleotide base is added through a phosphodiester bond between the 3' sugar and the 5' phosphate of the incoming nucleoside (Figure 4-2). As the DNA molecule grows, it twists, forming the characteristic double helix shape. The DNA double helix was proposed by James D. Watson and Francis Crick in 1953 based on X-ray diffraction studies of the DNA molecule by Rosalind Franklin.²¹⁰ Watson and Crick received the Nobel Prize in 1963 for their work with DNA, though Franklin passed away before the award was presented. The DNA double helix in

its most common form, the B-form,²¹¹ is about 22-26Å wide.²¹² Each nucleotide is approximately 3.3Å long.²¹² This results in a structure that undergoes one complete turn every 10.4 base pairs.²¹³ The turn of the helix results in two grooves, the major groove, which is 22Å wide, and the minor groove, which is 12Å wide.²¹⁴ The major groove serves as the recognition site for many DNA-associated transcription factors.²¹⁵ The B-form of DNA is a right-handed helix. Other forms of DNA are A-DNA, which is a wider right-handed spiral and may be associated with dehydrated DNA, DNA-RNA hybrids, or enzyme-DNA complexes.^{216,217} Z-DNA is much less common and forms a left-hand spiral.²¹⁸

The strength of the DNA double helix is based on its C-G content. As the C-G base pair is held together by three hydrogen bonds as opposed to the two hydrogen bonds of the A-T base pair, it is more difficult to separate C and G. The relative amount of C-G base pairs may be used to determine the melting temperature (T_m) of a particular DNA strand. This is especially important during the PCR reaction. The C-G content of the hybridization primers determines how strongly they associate with the template DNA, and the C-G content of the template DNA determines how easily the strands denature between each elongation step.

The DNA molecule contains a permanent copy of the genetic code of an organism. The information is encoded in the base pair sequence, and converted into protein through the processes of transcription and translation. Additionally, the genetic code is replicated and passed to each daughter cell during mitotic cell division. These important cellular processes are detailed below.

Replication of DNA

In order to maintain the flow of genetic information from one generation to another there must exist a mechanism to create identical copies of a cell's genome to pass on to daughter cells during mitotic division. Before each round of cell division, the entire genome must be replicated

in a reliable manner. Three manners of DNA replication are discussed here, including bacterial replication, plasmid replication in bacterial systems, and eukaryotic DNA replication. All replication methods use a similar array of proteins to create a new copy of DNA.

In prokaryotes, replication is initiated and carried out by a series of proteins known as the pre-replication complex. This consists of a helicase (dnaA) which is responsible for unwinding the two strands of DNA, a primase (dnaG or RNA polymerase) which begins synthesis by adding an RNA primer which the DNA polymerases need to start elongation of the DNA strand, and the DNA holoenzyme. This enzyme complex actually performs replication of the DNA and contains DNA polymerases. In bacteria, there are two main polymerases, Pol I and Pol III. Pol III is the main polymerase responsible for chain elongation and takes over after the primase adds the RNA primer. Pol III cannot initiate synthesis de novo, and thus requires a short RNA primer added by the primase, which recognizes the replication start site and adds a short sequence of RNA. Later, Pol I will use its 3'→5' exonuclease activity to remove the RNA primer and replace it with DNA nucleotides.

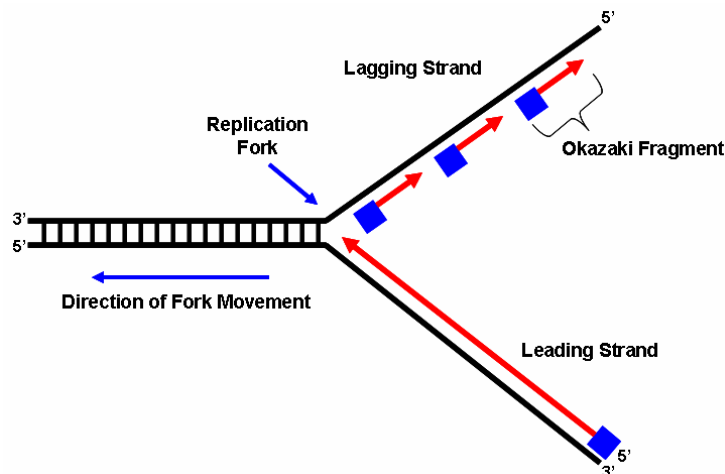


Figure 4-3. Structure of the replication fork. Blue boxes represent RNA primers, red arrows represent newly synthesized DNA.

In eukaryotes, replication is initiated by the Origin Recognition Complex (ORC) which is analogous to *dnaA* in prokaryotes. The ORC recruits regulatory proteins Cdc6 and Cdt1 which then recruit the MCM complex, or Minichromosome Maintenance proteins, which is a helicase-primase complex which unwinds the DNA and adds an RNA primer. The primase complex is made of an RNA polymerase and a DNA polymerase known as Pol α which adds several DNA bases after the RNA. Replication is then taken over by Pol δ . Though the proteins are somewhat different, following initiation, DNA replication is similar in both prokaryotic and eukaryotic cells.

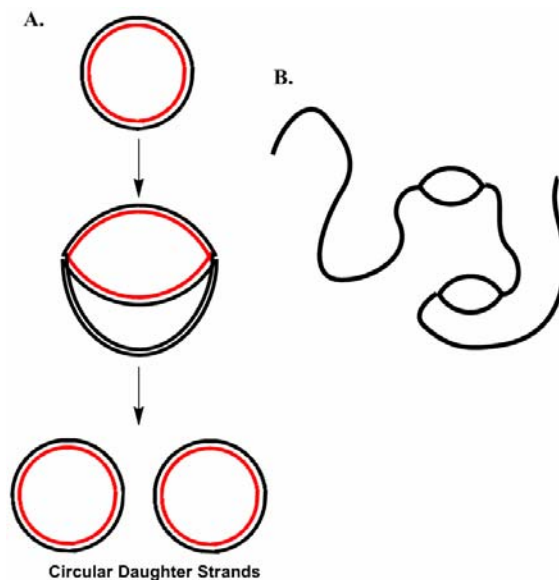


Figure 4-4. DNA replication of circular and linear DNA. A. Replication of circular DNA to form two circular daughter strands. B. Two replication bubbles forming during replication of linear DNA.

Following initiation of replication, elongation takes place at the replication fork (Figure 4-3). Since DNA synthesis only occurs in the 5'→3' direction, each strand of DNA is replicated differently. The leading strand is the one which opens in the 5'→3' direction, and synthesis occurs continuously. On the other strand, however, the replication fork opens in the opposite direction. This strand is known as the lagging strand because synthesis takes place in short pieces known as Okazaki fragments. As the DNA unwinds, new RNA primers are added and DNA

polymerase adds DNA bases until it reaches the previous fragment. At this point, in prokaryotic cells Pol I removes the RNA primer and replaces it with DNA bases. DNA ligase then joins the fragments together resulting in a complete DNA strand. As the DNA is unwound, supercoiling at the replication fork is relieved by DNA gyrase in prokaryotes and Topoisomerases in eukaryotes. In both circular and linear DNA, there may be multiple replication forks on each DNA strand (Figure 4-4). This results in more rapid DNA synthesis.

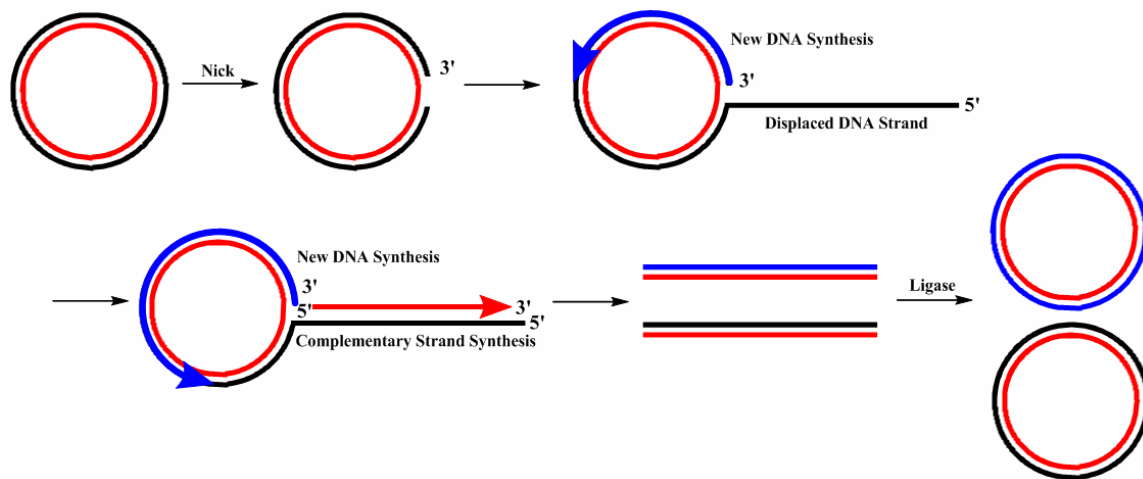


Figure 4-5. The rolling circle method of DNA replication in prokaryotes.

Another method of rapid DNA replication occurs in bacterial systems that contain plasmid DNA. In order to create large numbers of copies of the plasmid, bacteria use a method known as rolling circle replication (Figure 4-5). In this method, one DNA strand is nicked and begins to unwind. The 3' end of the nicked strand serves as a primer for replication of the unnicked strand by Pol III. Replication then proceeds around the circle, displacing the nicked strand as single-strand DNA. Multiple copies of DNA may be produced as head-to-tail concatemers. These concatemers are converted to dsDNA through leading strand synthesis by Pol III. Pol I serves to remove the RNA primer and then DNA ligase joins the ends of the DNA together to create double-strand circular DNA.

Transcription of DNA

Transcription is the process by which the information in DNA is encoded into messenger RNA (mRNA) for translation into protein. In prokaryotes this takes place in the cytoplasm, and in eukaryotes it occurs in the nucleus and then the mRNA is translocated to the cytoplasm for translation. As eukaryotic transcription is highly complex, the prokaryotic model is presented here. Transcription in eukaryotes is essentially the same only complicated by many more transcription factors and the presence of heterochromatin which limits the accessibility of the DNA for transcription.

RNA, or ribonucleic acid, differs from DNA in two important ways. First is the use of ribose as the sugar in the backbone as opposed to deoxyribose which is used in DNA. Also, in RNA the base thymine is replaced with uracil (U). These differences are shown in Figure 4-6. The base pairing is the same except that adenine pairs with uracil instead of thymine.

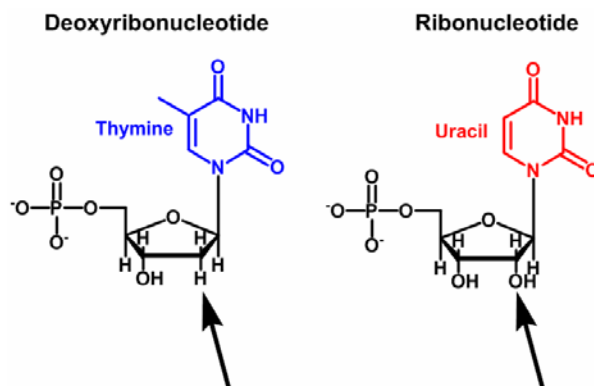


Figure 4-6. Structures of DNA and RNA nucleotides. Black arrows indicate sites of sugar differences between DNA and RNA. The DNA base thymine is shown in blue, and the RNA base uracil is shown in red.

A sequence of DNA which is transcribed into a single mRNA is known as a Transcription Unit (TU). The TU consists of upstream promoter units which recruit the transcription machinery to the proper place, the DNA template, and 5' and 3' untranslated regions (UTR). These UTRs are not translated, but are important for regulation of transcription and translation. Since DNA is

double-stranded, there is a coding strand and a template strand. The coding strand runs from 5'→3' and contains the exact coding sequence. However, this strand is not translated as RNA synthesis only proceeds from 5'→3' and transcription would result in an mRNA complementary to the coding sequence. For this reason, the opposite strand, known as the template strand, is the one transcribed starting at the 3' end. This results in an mRNA transcript exactly the same as the coding sequence.

Transcription consists of three stages: initiation, elongation, and termination (Figure 4-7). Transcription is initiated by RNA polymerase (RNAP) binding to the promoter upstream of the transcription start site. The RNAP then “melts” the DNA duplex, opening up a “transcription bubble”, then adds several RNA nucleotides. Elongation is the process by which RNAP processes down the template, adding RNA bases until it reaches the end of the transcript. Transcription may be terminated by one of two methods. In rho-dependent termination, the rho protein causes the polymerase to fall off the template. In rho-independent termination, the transcript forms a hairpin loop followed by a series of U’s which destabilizes the RNAP-DNA complex and terminates transcription. Following transcription, the mRNA may be processed to remove introns or modify bases.

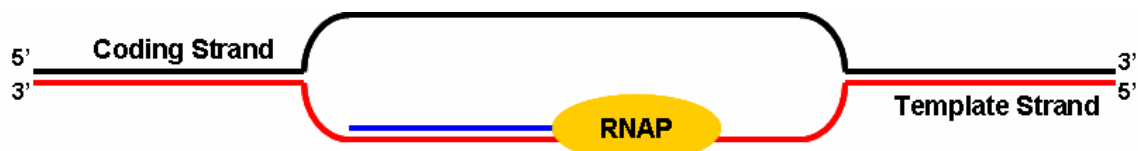


Figure 4-7. Model of DNA transcription. The coding strand is shown in black and the template strand in red. RNA polymerase (RNAP) synthesizes a new strand of mRNA (blue) using the template strand.

Translation into protein

Following mRNA synthesis, the mRNA template is used to synthesize a new protein in a process known as translation. Due to the complexity of eukaryotic translation, the prokaryotic

process is detailed here. The main steps of translation remain the same between prokaryotic and eukaryotic protein synthesis.

Table 4-1. Diagram of mRNA codons translated to amino acid. The first letter is read first on the left, then the second letter across, and the third letter down on the right. The intersection of the three letters indicates the amino acid coded for by that codon.

First Letter↓	Second Letter→				Third Letter↓
	U	C	A	G	
U	Phenylalanine	Serine	Tyrosine	Cysteine	U
	Phenylalanine	Serine	Tyrosine	Cysteine	C
	Leucine	Serine	Stop	Stop	A
	Leucine	Serine	Stop	Tryptophan	G
C	Leucine	Proline	Histidine	Arginine	U
	Leucine	Proline	Histidine	Arginine	C
	Leucine	Proline	Glutamine	Arginine	A
	Leucine	Proline	Glutamine	Arginine	G
A	Isoleucine	Threonine	Asparagine	Serine	U
	Isoleucine	Threonine	Asparagine	Serine	C
	Isoleucine	Threonine	Lysine	Arginine	A
	Start/Methionine	Threonine	Lysine	Arginine	G
G	Valine	Alanine	Aspartate	Glycine	U
	Valine	Alanine	Aspartate	Glycine	C
	Valine	Alanine	Glutamate	Glycine	A
	Valine	Alanine	Glutamate	Glycine	G

Translation occurs in the cytoplasm of the cell, at the rough endoplasmic reticulum (RER). There are four steps of translation: activation, initiation, elongation, and termination. During activation, a tRNA is charged with a corresponding amino acid. Transfer RNA (tRNA) is a non-coding RNA which serves to deliver the new amino acid to the ribosome. There are 20 tRNA molecules, each of which corresponds to the 20 natural amino acids. Each amino acid is coded for by a three-base sequence known as a codon. A table of codons and their corresponding amino acids is shown in Table 4-1. Each tRNA contains an anticodon which is complementary to the codon on the mRNA. The codon and anticodon base pair during translation to ensure the addition of the correct amino acid. There are only 20 amino acids and 64 codons. This is because the

genetic code is degenerate and unambiguous. This means that though an amino acid can be coded for by several different codons, no codon codes for more than one amino acid. During activation, a tRNA that contains the proper anticodon is charged with a specific amino acid by aminoacyl tRNA synthetase.

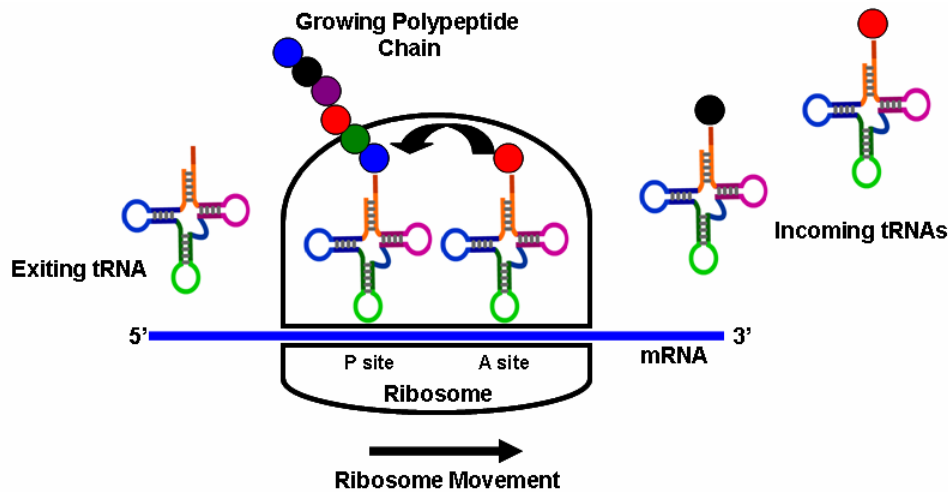


Figure 4-8. Model of DNA translation. The ribosome reads the mRNA in the 5'→3' direction. New tRNAs with an anticodon complementary to the codon on the mRNA enter into the A site and the attached amino acid forms a peptide bond with the amino acid attached to the tRNA in the P site. After bond formation, the ribosome shifts to the right and a new tRNA moves into the A site.

During the initiation step, a ribosome is recruited to the mRNA to be translated. A ribosome is an organelle made up of rRNA and protein which catalyzes protein synthesis. It is made up of a large and a small subunit which are assembled separately. First, the small ribosomal subunit is recruited to the mRNA strand by recognition of the ribosome binding site on the mRNA (Shine-Dalgarno sequence in prokaryotes, Kozak sequence in eukaryotes). This sequence serves to properly position the ribosome at the site of the start codon, AUG. This codes for a special Met that has been formylated and is recognized as the universal start of protein synthesis. The large ribosomal subunit then binds to the fMet-tRNA and translation is ready to begin.

The ribosome contains three tRNA binding sites: the A site, the P site, and the E site. The A site is the point of entry for new aminoacylated tRNAs. The tRNA binds to the codon through base pairing with its anticodon. A peptide bond is then formed between the amino acids attached to the tRNAs in the A site and the P site. The process known as translocation then causes the ribosome to shift three bases toward the 3' end of the mRNA, moving the tRNA in the P site into the E site and the tRNA in the A site to the P site. An empty tRNA in the E site is released into the cytoplasm. A new charged tRNA then moves into the A site and elongation continues until a stop codon is reached. This process is shown in Figure 4-8.

During termination of protein synthesis, a codon is reached which does not code for an amino acid. There are three stop codons, UAA, UGA, and UAG. No tRNA enters the A site causing release factors to catalyze the release of the newly formed peptide and the dissociation of the translation complex.

In vivo, peptides are synthesized from the N-terminus to the C-terminus. Following synthesis, they may undergo post-translational modification of specific amino acids to form an active protein. The protein products of translation form the proteosome, which is responsible for all cellular structural and enzymatic processes.

The PCR reaction

The polymerase chain reaction (PCR) was first described by Kleppe *et al.* in 1971.²¹⁹ It was not widely accepted though, until 1983 when Kary Mullis popularized the technique. Mullis received the Nobel Prize in Chemistry in 1993 for his efforts, though patent wars are still pending.

PCR is a process by which fragments of DNA may be amplified exponentially. It may be used in the isolation of genomic DNA for purposes of genotyping or establishing a “DNA fingerprint” for an individual. It is commonly used for the amplification and quantification of

plasmid or linear DNA for research purposes, or for the deliberate insertion of specific mutations.

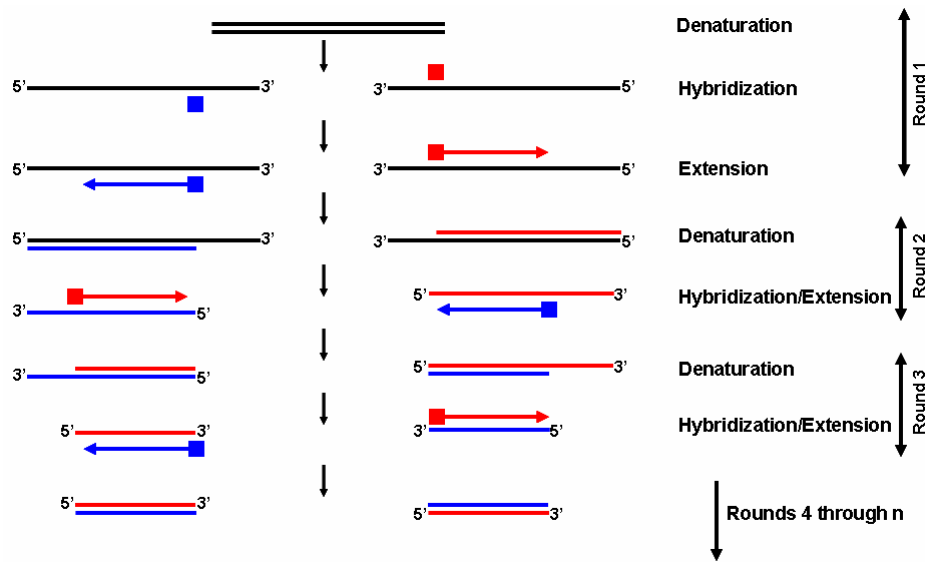


Figure 4-9. The PCR reaction. Template DNA is denatured, primers anneal to the desired sequence, and DNA polymerase synthesizes a new strand of DNA. This process is repeated many times resulting in an exponential increase in the number of amplified DNA sequences.

The PCR reaction requires several components. The first is a DNA template to be amplified. DNA primers corresponding to the 5' and 3' ends of the desired sequence are added. These primers are around 20 base pairs long and match the template with high affinity. The G-C content should correspond to about 60% of the base composition to ensure a strong bond. A DNA polymerase is also needed. This polymerase must be able to survive the periods of high temperature required for DNA denaturation, therefore polymerases are used from thermophilic bacteria that grow in geysers and are able to withstand temperatures above 110°C. The most widespread polymerase used is from *Thermus aquaticus*, known as *Taq* polymerase.²²⁰ *Taq* is stable at high temperatures, though prone to errors as it does not possess 3'→5' exonuclease proofreading activity.²²¹ A new polymerase was isolated from the thermophilic archaeon *Pyrococcus furiosus* (*Pfu*).²²² *Pfu* is superior to *Taq* as it contains a high fidelity 3'→5'

proofreading exonuclease system. This results in substantially fewer PCR-induced mutations. The remaining ingredients in the PCR mixture include dNTPs (deoxyribonucleotide triphosphates) from which to build the new DNA, a suitable buffer for maximal activity of the polymerase, divalent cations such as Mg^{2+} or Mn^{2+} , and potassium ions.

The general PCR reaction consists of six main steps (Figure 4-9). First is an initialization step of 94-96°C to activate the polymerase. This is followed by a denaturation step of 94-98°C for 20-30 seconds to denature the DNA. An annealing step at 50-65°C for 20-40 seconds is then performed to allow the primers to bind to their complementary sequences on the template. The annealing step should be performed at only a few degrees above the melting temperature of the primers to ensure that only sequences with high fidelity matches bind to the template. Annealing is followed by an elongation step at the optimal temperature for the polymerase, usually around 75-80°C. The length of this step varies with the length of the desired amplified sequence. It may be assumed that the polymerase will add about 1000 bases per minute. The denaturation, annealing, and extension steps are repeated 20-30 times. Each new DNA sequence may serve as a template for the next cycle resulting in exponential increases in the number of amplified DNA sequences. After the last cycle, a final elongation step is performed to ensure the extension of any remaining single-stranded DNA. The PCR mixture may then be held at 4°C for short-term storage.

The PCR reaction has become an indispensable tool in molecular biology and forensics. It has opened the door to a vast realm of possibilities in DNA manipulation and cloning.

Restriction endonuclease digestion

A Restriction Enzyme, also known as a Restriction Endonuclease, is an enzyme which recognizes specific DNA sequences and cuts the DNA backbone at specific locations without interfering with the base. The term “restriction” came from the observation that *E. coli* seemed to

be restricting infection by bacteriophages and it was inferred that this was a mechanism used to resist viral attack. Further research revealed a plethora of bacterial enzymes that could be used to cut DNA at specific sequences. In 1978 Daniel Nathans won the Nobel Prize for his discovery of restriction enzymes which led to the development of recombinant DNA technology.

Restriction enzymes generally recognize sequences of four, five, six, or seven bases. Often these sequences are palindromic, this means that both strands read the same from the 5'→3' direction. Restriction fragments may have blunt ends or sticky ends. Blunt ends means that the enzyme cuts at the same place on both strands. These fragments may be ligated to any other blunt end fragment. Sticky ends result from an enzyme which cuts at two ends of the recognition sequence, resulting in a single-stranded overhang. These fragments may be ligated with another DNA fragment that has been cut with the same enzyme. DNA ligase is used to repair the breaks in the backbone and create a new DNA sequence.

One of the main uses of restriction enzymes is the cutting of a fragment of DNA and religating into a plasmid, known as “cloning.” The plasmid can then be inserted into bacterial vectors or mammalian cells for expression of the desired gene. In this way restriction enzymes have played a vital role in the identification and manipulation of a vast number of genes and have made the process of DNA recombination and cloning possible.

Gel electrophoresis

Gel electrophoresis is a method used to separate DNA fragments of differing size and conformation. It is based on the principle that when DNA is placed in neutral or alkaline conditions, the phosphate groups become ionized, giving DNA an overall negative charge. When a current is applied to the negatively charged DNA it will migrate towards the positive anode. Two types of gels are commonly used, agarose and acrylamide. As acrylamide is toxic, agarose is more commonly used. Agarose is purified from agar, which is a polysaccharide found in the

cell walls of some types of algae and seaweed (Figure 4-10A). Agarose is neutrally charged and forms large pores that make it ideally suited for separation of large biomolecules.

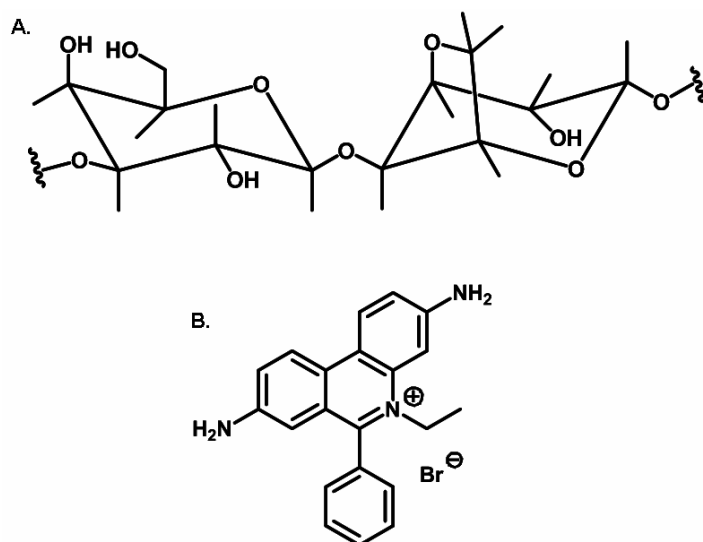


Figure 4-10. Reagents for gel electrophoresis. A. Structure of the crosslinking unit of agarose. B. Structure of ethidium bromide.

A sample of DNA is loaded onto a gel along with a loading buffer. The loading buffer contains a denaturing agent such as SDS or urea to prevent any enzymatic reactions, glycerol to weight down the DNA at the bottom of the well so it does not come out, and dyes which are used as mobility markers. These markers are commonly bromophenol blue and xylene cyanol. They migrate with the DNA for a visual representation of the progress of the DNA down the gel. The gel is run in a buffer such as TAE (Tris-acetate EDTA buffer) which carries the charge from the anode and cathode through the gel.

DNA migrates through agarose gels based on its size and conformation. Large pieces of DNA will not travel as fast as small fragments, allowing for size separation. Restriction enzyme digests of plasmids or DNA segments can result in characteristic gel patterns based on the size of the fragments. The conformation of a DNA molecule also determines its movement through the gel. Circular DNA will move faster than linear DNA, allowing for differentiation between nicked and circular plasmids.

Following DNA migration through the gel it is necessary to view the DNA. Since DNA is invisible to the naked eye, a chemical known as ethidium bromide is commonly used to view the DNA bands. Ethidium bromide (Figure 4-10B) is a carcinogen which intercalates between the DNA bases. When exposed to UV light it fluoresces orange, allowing for the visualization of DNA. The DNA bands may be cut out of the gel and the DNA purified for further experiments.

Sequencing

An important part of DNA manipulation is sequencing. It is often useful to know the exact sequence of nucleotides. In the seventies Sanger *et al.* developed a method for chain-termination sequencing.²²³ In this method, four tubes are used. Each tube is loaded with template DNA, primers, and regular dNTPs, but each tube also gets a ddNTP (dideoxynucleotide triphosphate) corresponding to one of the four bases. Incorporation of the ddNTP results in chain termination as there is no 3'OH to continue building the chain. The reaction mixtures can then be run on a gel. Based on how far each band travels it can be inferred how long the chain is. As only one ddNTP is added to each tube, it is known that the last base corresponds to that ddNTP.

A more recent method automates this process and only requires one reaction mixture. It is known as the Big Dye Terminator (BDT) method. Each ddNTP is coupled to a donor and an acceptor dye. The donor dye is 6-carboxyfluorescein (6-FAM). When coupled to different forms of rhodamine, the dyes fluoresce at different wavelengths, allowing for the identification of the terminal base. The acceptor dyes are commonly as follows: dichloro-R6G (dichloro-rhodamine 6G) attached to adenine, dichloro-ROX (dichloro-rhodamine X) for cytosine, dichloro-R110 (dichloro-rhodamine 110) is attached to guanine, and dichloro-TAMRA (dichloro-tetramethylrhodamine) is used for thymine. The BDT reaction mixture, template DNA, a sequencing primer and buffer are mixed and amplified using PCR. As the chain grows, the dye-labeled ddNTPs are incorporated resulting in a mixture of DNA sequences of every length. After

PCR, the purified PCR product is run on a specialized machine which runs the reaction mixture through a special polymer. As with gel electrophoresis, small DNA fragments run faster than large segments. As each fragment passes through an argon ion laser, the 6-FAM donor dye is excited, which then transfers its energy to the acceptor molecule. A detector reads each dye and differentiates between the dyes. A computer program then interprets the fluorescence and assigns a specific base to each position and plots the sequence on an electropherogram (Figure 4-11). This sequence can then be used for sequence confirmation and further experiments.

Some drawbacks to this method include inefficient ddNTP incorporation or “dye blobs” resulting from clumping of the dyes and causing artifacts in DNA traces. These problems are overcome through use of highly efficient polymerases and through continual development of the chemistry used. Though expensive, BDT sequencing is highly reliable and produces high fidelity sequences.

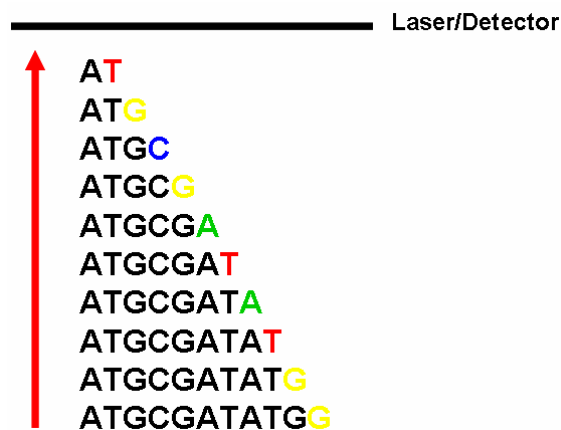


Figure 4-11. Model showing how BDT sequencing is read by the detector. Sequences are run through a polymer which separate the sequences by size. As they pass by the detector, the fluorescent label on the 3' end is read and the base identified.

Bacterial Expression Vectors

Escherichia coli. *E. coli* is a gram-negative, rod-shaped bacterium of the family Enterobacteriaceae that is most commonly used in genetic manipulation. It is used because its

genome is well-characterized and it is easy to grow in the laboratory. The bacteria are ideal for use in plasmid amplification and can be made chemically competent for transformation. *E. coli* grows well in LB-media (Luria-Bertani) and can be grown either on agar plates or in broth suspensions. *E. coli* was discovered in 1885 by the German pediatrician and bacteriologist Theodor Escherich. The bacteria are commonly found as part of the normal flora of the mammalian large intestine, and thus is an important indicator organism for fecal contamination. Some strains can cause food poisoning, such as the publicized O157:H7 strain.

The strain used in this work is the DH5a strain of *E. coli*. This is a strain that is competent for transformation. It is sensitive to antibiotics such as ampicillin and kanamycin so plasmids containing resistance genes may be transformed for antibiotic selection of transformed bacteria.

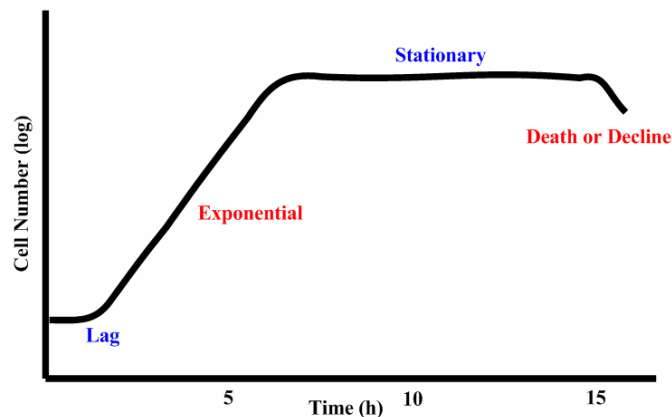


Figure 4-12. Bacterial growth curve.

The bacterial growth curve (Figure 4-12) is common to most prokaryotic species. A new culture starts with the lag phase, where there is little growth until the bacteria acclimate to their new environment. This is followed by the exponential phase where bacterial growth occurs very rapidly. When media resources become depleted the bacteria enter a stationary phase where the bacteria are alive but do not divide. Finally, if no new nutrients are added, the population will reach a death phase where the bacteria begin to die. For plasmid amplification it is necessary to maintain the culture in the exponential phase for optimal results.

Cloning plasmids. Plasmids are small, circular, double-stranded DNA that exist outside of the chromatin and are stably inherited. They may be used to insert genes of interest into both bacterial and mammalian cells. Most synthetic plasmids contain genes that confer resistance to certain antibiotics to allow selection of cells based on their incorporation of the plasmid.

There are several characteristics of an ideal cloning plasmid. The first is that it should have an easily selectable phenotype. This allows for distinction between cells that express the plasmid and cells that do not. Plasmids should also have a large number of unique restriction sites. Most plasmids have a multiple cloning site (MCS) that contains a large number of restriction sites not found anywhere else in the plasmid. This allows the researcher to match the restriction enzymes with their gene of interest. Plasmids should also be fairly small to allow for greater stability and ease of transformation. Finally, the plasmid should have a relaxed replication control to allow it to replicate in large quantities in bacterial vectors for rapid amplification.

Several plasmids are used in this work. These are pBK-CMV, pcDNA3, and pMV-CRE-Luc. pBK-CMV is a bacterial plasmid useful for site-directed mutagenesis. The gene is cut out and replaced into pcDNA3 before transfection into mammalian cells. pcMV-CRE-Luc is a reporter gene plasmid transiently transfected before functional assays.

Transformation. Transformation is the process by which plasmid DNA is taken up by bacterial cells and replicated for plasmid purification. The process is detailed as follows. Competent bacteria are placed on ice and a small quantity of plasmid DNA is added to the cells. The bacteria are then incubated on ice for 20-30 minutes while the bacteria take up the DNA. The bacteria are then submitted to heat shock for 45-60 seconds at 42°C. This causes them to produce heat shock proteins so they don't expel the foreign DNA right away. They are incubated on ice for another 2 minutes to stop the heat shock process and then rich SOC media is added

and the bacteria are gently shaken at 210 rpm at 37°C for at least an hour. During this time the bacteria begin to grow. They are then plated on LB-agar plates supplemented with the antibiotic of choice and grown overnight at 37°C. If the bacteria have taken up the plasmid DNA they will be resistant to the antibiotic and colonies will form on the agar in about 12-16 hours. Single colonies can then be subcloned into an antibiotic LB broth and grown for plasmid isolation.

Plasmid purification. In order to obtain enough plasmid for sequencing, restriction digests or transfection, the plasmids are amplified by insertion into a bacterial expression system, as described above. For small-scale reactions, a Miniprep kit from Qiagen was used. This provided about 30 µL of 0.3 µg/µL DNA for sequencing or digestion. For large-scale isolation reactions, the Maxiprep kit from Qiagen was used to provide anywhere from 100-2000 µL of 1-2 µg/µL DNA which may be used for any application including stable transfection into mammalian cells.

The general procedure is the same for both small- and large-scale reactions. A quantity of bacteria expressing the desired plasmid is grown in LB broth supplemented with ampicillin overnight at 37°C and 275rpm. Bacteria are collected by centrifugation and growth media is discarded. The bacteria are resuspended (Qiagen- Buffer P1) and then subjected to alkaline lysis (Qiagen- Buffer P2). The lysis solution contains a NaOH-SDS solution in the presence of RNaseA. SDS, or sodium dodecylsulfate, is used to solubilize the proteins and phospholipids of the cell membrane, leading to membrane breakage and release of the cell contents. NaOH is used to denature the chromosomal DNA, plasmid DNA, and proteins to prevent enzymatic reactions. Following lysis, a neutralization buffer (Qiagen- Buffer P3) containing acidic potassium acetate is added. The high salt concentration precipitates KDS (potassium dodecylsulfate), trapping the cellular debris in a salt-detergent complex. This debris contains proteins, chromosomal DNA, and other cellular components. The plasmid DNA, however, remains in solution as it is smaller

and covalently circular, allowing it to renature quickly after precipitation of the detergent. The precipitate is removed by centrifugation and the lysate containing plasmid DNA is applied to a column containing a specialized resin (Qiagen) which selectively binds plasmid DNA. The column is washed with a medium salt buffer (Qiagen- Wash Buffer QC) which serves to remove contaminants such as degraded RNA and proteins without affecting the bound plasmid DNA. The wash buffer also disrupts non-specific interactions of proteins with the DNA allowing for removal of nucleic acid binding proteins without having to use phenol. Ethanol in the buffer disrupts any non-specific hydrophobic interactions resulting in an increased purity of the plasmid DNA. At this point, the DNA is either eluted with a high salt buffer (Qiagen- Buffer QF) in the case of a Maxiprep, or water for Minipreps. The Miniprep DNA is ready for use; however the Maxiprep undergoes several more purification steps. Isopropanol is added to desalt and concentrate the DNA, and then centrifuged. The DNA is then washed with ethanol, which is easier to remove than isopropanol, and then resuspended in a suitable buffer such as TE Light (pH~8.0). DNA concentration may then be determined by spectrophotometric methods or by agarose gel electrophoresis. The DNA is ready to use for any experimental application needed.

Cell Culture and Transfection

Mammalian Cell Lines

The HEK293 cell line. The HEK293 cell line was developed in the early seventies in the laboratory of Alex Van der Eb in Leiden, Holland.²²⁴ A culture of human embryonic kidney cells were transformed with sheared DNA from the adenovirus 5 virus.²²⁴ Later it was shown that the transformation was brought about by incorporation of a 4.5kb insert from the left arm of the viral genome into chromosome 19 of the cells.²²⁵ This resulted in an immortal cell line which is able to grow in solution without changing for an indeterminate length of time. Further studies on the

origin of the HEK293 cell line indicate that it is possible that the line originated from a neuronal cell present in the kidney culture that was transfected.²²⁶

HEK293 cells were quickly shown to be a valuable cell line for molecular biology and biotechnology applications. They are easy to grow and transfect with close to 100% transfection efficiency with the calcium phosphate precipitation method.²²⁷ Though the cell line is not a good model for normal or cancer cells, it has become extremely useful in protein expression and functional assays. Its high transfection rates make it ideal for transfection of a gene of interest and subsequent protein expression analyses. In the biotechnology industry, HEK293 cells have become valuable as a way to produce therapeutic viruses and proteins for gene therapy applications.

The OS3 cell line. The OS3 cell line was derived from the murine Y1 adrenocortical tumor cell line along with the Y6 cell line. These cell lines contain a wild type MC2R gene, however this DNA sequence is not functional due to growth in the presence of forskolin.²²⁸ The cells do, however, contain an intact cAMP signal transduction pathway, resulting in a functional transfected MC2R.^{228,229} This cell line is used as it is able to produce a functional transfected MC2R, however its drawbacks are that it grows slowly and is very difficult to transfect with a gene of interest (<2% efficiency).

Transfection

Transfection is the process by which foreign DNA is introduced into a eukaryotic cell. This is often done to test gene expression or functionality and is an important tool in molecular biology. Once inserted, the gene may be transiently or stably transfected. In transient transfection, the plasmid containing the gene is expressed for only one or two generations, and eventually is lost during mitotic divisions. The gene expression is initially very high but transfection levels vary between experiments. The gene may also be stably transfected. In this

type of transfection, a selective pressure is placed on the cell to force it to retain the plasmid and stably express the gene for a long period of time. The antibiotic Geneticin, or G418, is often used for this process. G418 is an aminoglycoside antibiotic isolated from *Micromonospora rhodorangea*. It is toxic to both prokaryotic and eukaryotic cells, but resistance may be inferred through transfection of the neo gene, which is often present in plasmids designed for mammalian transfection. Once stable expression is achieved, the cells produce the protein of interest in stable quantities for a long period of time.

Many methods exist for the transfection of DNA into eukaryotic cell lines. The most common and cost-effective is the calcium phosphate method developed by Graham *et al.*²²⁷ In this method, a HEPES-buffered saline solution containing phosphate ions is combined with calcium chloride and the DNA to be transfected. A precipitate of calcium phosphate forms, binding DNA. Through a mechanism that is not fully understood, the cell takes up the precipitate along with the foreign DNA.

Another method involves the use of lipid-based reagents. These reagents form liposome-like structures around the DNA. The liposomes bind to the cell membrane, releasing DNA into the cell. This process is often known as lipofection, and the formulas for the reagents is highly proprietary.

Lesser used methods for transfection include electroporation, heat shock, magnetofection, use of the gene gun, in which DNA is coupled to an inert nanoparticle and then “shot” into the nucleus, as well as the use of viral DNA carriers.

Functional Assay

Pharmacology Definitions

A discussion of functional pharmacology requires an understanding of the physical graphical representation of the data. Examples of these graphs are shown in Figure 4-13. Figure

4-13A depicts some agonist curves. The log concentration of the ligand is shown in the x axis and the percent stimulation in the y axis. Curve A (red) depicts a typical full agonist. Curve B (green) shows a full agonist that is less potent than A. As the potency decreases, the curve shifts to the right. Curve C (purple) is an example of a partial agonist. A partial agonist has the same shape as a full agonist and a maximum stimulation is reached, but the maximum is less than 100% when compared to forskolin control. Curve D (red) shows a ligand that has no agonist activity, and Curve E (black) is an example of an inverse agonist. An inverse agonist is a compound that is able to decrease cAMP levels below basal levels.

In this work antagonist values are obtained using a Schild analysis.²³⁰ This involves costimulation of the receptor with a known agonist and a suspected antagonist. The curve is shown in Figure 4-13B. The blue represents the agonist, and the green curves represent the agonist combined with increasing concentrations of antagonist. If the compound is an antagonist, then increasing concentrations will result in a shift to the right of the agonist curve. This assay tests for competitive antagonists only. It is effective because a competitive antagonist competes with an agonist for the same binding site. When the antagonist binds, however, there is no receptor stimulation. This gives the appearance of a less potent agonist. If no right shift occurs when antagonist concentration is increased, then the compound is not an antagonist. Sometimes a ligand might have what is known as mixed pharmacology. In this case the ligand may have some partial agonist activity but also have antagonist activity. These compounds are not well understood but may be important for continued receptor or ligand characterization.

Figure 4-13C shows how an EC_{50} value is determined. An EC_{50} value is the concentration of a ligand which results in 50% stimulation of the receptor as compared to forskolin control. This value is widely used to describe the functional activity of a ligand at a particular receptor. A

higher EC₅₀ value suggests a less potent ligand (shift to the right) while a smaller EC₅₀ value suggests a more potent ligand (shift to the left).

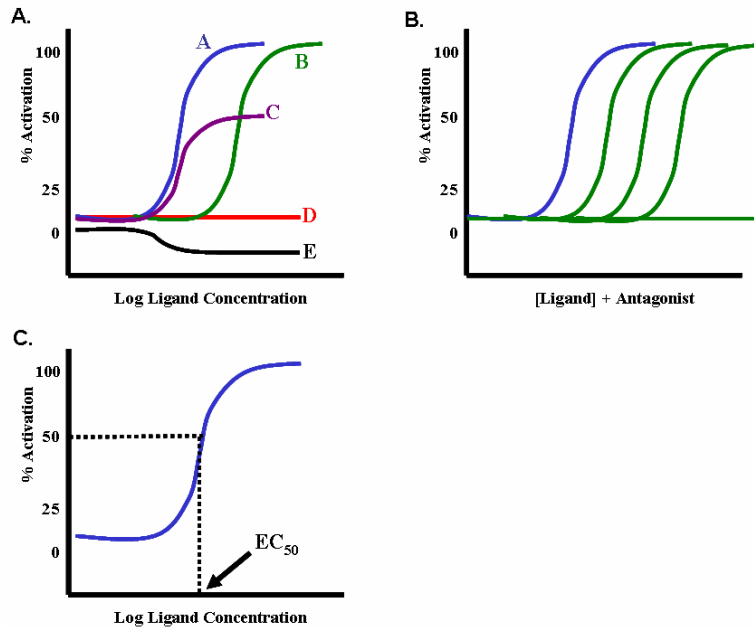
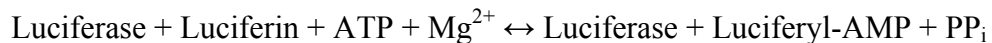


Figure 4-13. Pharmacology curves. A. Shows various agonist curves. Curve A = full agonist, Curve B = less potent full agonist, Curve C = partial agonist, Curve D = no agonist, Curve E = inverse agonist. B. Model of a Schild analysis. Blue curve is the known agonist. Green curves represent the agonist costimulated with increasing concentrations of antagonist. C. Determination of EC₅₀ value from a dose response curve.

Luciferase Assay

Firefly luciferase from the North American firefly *Photinus pyralis* has been extensively studied for its role in bioluminescence.²³¹ The endogenous substrate of luciferase is luciferin, and the reactions catalyzed by luciferase are as follows:



The reaction begins with the formation of enzyme-bound luciferyl-AMP which then is oxidatively decarboxylated to form oxyluciferin and light. The yellow-green light is emitted at pH 7.5 to 8.5 at a peak emission of 560nm. When the luciferase enzyme is supplemented with excess luciferin, ATP, and oxygen, studies have shown that the light produced is proportional to

the amount of luciferase in the solution.²³² It is this property of the enzyme that allows for its use in quantitative assays.

Prior to the development of the luciferase assay, the CAT (bacterial chloramphenicol acetyltransferase) enzyme was used as a method of monitoring eukaryotic promoter activity.^{233,234} The luciferase assay, however, is superior to this method as it is less expensive, more sensitive, and does not require the use of radioactive substrates.

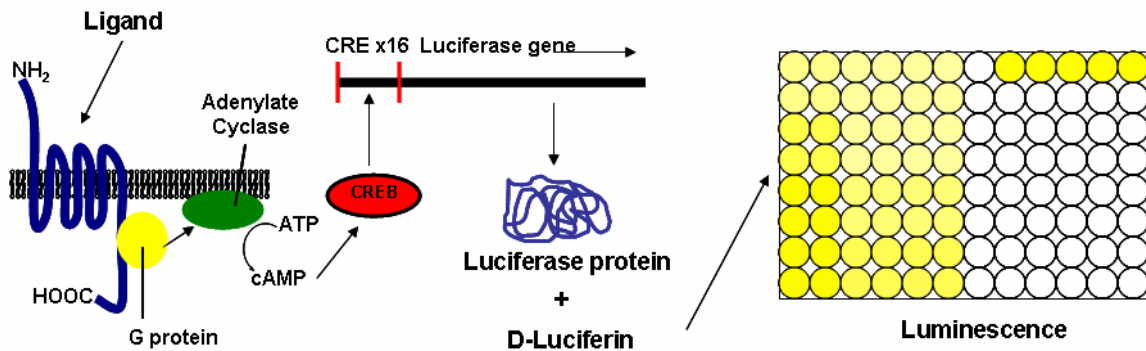


Figure 4-14. Luciferase reporter gene assay. When a ligand stimulates the GPCR, G protein activates adenylate cyclase which converts ATP to cAMP. cAMP binds to CREB which binds to CRE units on the reporter gene causing transcription of the luciferase gene. The cell makes luciferase protein. When the luciferase substrate D-luciferin is added, light is released. The luminescence can be read on a luminometer. Here, dark yellow indicates a high level of luminescence and light yellow low levels.

The luciferase reporter gene assay is described in Figure 4-14. A plasmid containing the luciferase gene and a suitable promoter is transfected into a mammalian cell line stably expressing a receptor of interest. The plasmid used in this study contains the luciferase gene preceded by 16 CRE units.²³⁵⁻²³⁸ When a ligand is added to the cell culture which activates the receptor, second messenger systems in the cell stimulate the promoter element on the plasmid, causing transcription of the luciferase gene. The mRNA is translated into the luciferase protein. The amount of luciferase produced is proportional to the level of stimulation of the receptor by the ligand. Cell lysates are then supplemented with luciferin, ATP, Mg^{2+} and oxygen, and the light intensity measured using a luminometer. The intensity of light can be analyzed, leading to a

quantitative measurement of the amount of luciferase produced and therefore the activity of the ligand at the receptor.

Functional Assay: cAMP Assay

The cAMP assay is a radioassay which measures the amount of cAMP produced in a cell. cAMP is a second messenger produced when G protein is activated by binding of a ligand to a GPCR, causing activation of adenylate cyclase and conversion of ATP to cAMP. The cAMP then binds to CREB which binds to promoter CRE units on DNA, stimulating transcription of certain genes. This assay differs from reporter gene assays in an important way. Reporter gene assays measure a protein produced from activation of the CRE-coupled genes. The cAMP assay directly measures the amount of cAMP produced from stimulation of the receptor.

After receptor stimulation, cell lysates are isolated and tritiated cAMP ($^3\text{H-cAMP}$) and a cAMP binding protein are incubated with the lysates. The cAMP and $^3\text{H-cAMP}$ compete for binding to the binding protein. A standard curve with known concentrations of cAMP incubated with a constant concentration of $^3\text{H-cAMP}$ is also made and the unknowns compared with the standards to determine the amount of cAMP in the unknown samples. High levels of unlabeled cAMP will result in a greater amount of unlabeled cAMP bound to the binding protein, and thus lower levels of radioactivity detected in a scintillation counter. Low levels of cAMP will result in a greater amount of bound $^3\text{H-cAMP}$ and a higher scintillation counter reading. These data may be used to determine the amount of cAMP produced across several concentrations of ligand and may be used to plot a dose-response curve and determine EC_{50} values of the ligand.

Though a very reliable assay, the cAMP assay has several drawbacks. First, it requires the use of radioactive substrates and specialized training and certification is required. Second, it is quite expensive and generally used only when more cost effective options are exhausted.

Additionally, the assay is labor-intensive and not compatible with high-throughput operations. A table comparing the luciferase assay and the cAMP assay is shown in Table 4-2.

Table 4-2. Comparison of luciferase and cAMP assays.

	Luciferase Assay	cAMP Assay
Detection	Luminescence	Radioactivity
High-Throughput?	Yes	No
Cost	\$\$	\$\$\$\$
Ease of Assay	Easy	Moderate
Special Equipment?	Yes	Yes
Certification Required?	No	Yes

Experimental Methods

Cell Culture and Transfection

HEK293 cells were grown in media consisting of DMEM (Dulbecco's Modified Eagle Medium) supplemented with 50 mL NCS (Newborn Calf Serum) and 5 mL Penicillin/Streptomycin. Cells were split by adding 1 mL of a 0.1% trypsin solution and incubating for two minutes. The trypsin was then diluted with 5 mL of media and the cells dislodged by gentle pipetting. The cells were aliquotted to new plates and 10 mL of media added. Cells were grown at 37°C and 5% CO₂.

OS3 cells were grown in media consisting of F10 Media supplemented with 75 mL horse serum, 12 mL FBS (Fetal Bovine Serum), 5 mL Penicillin/Streptomycin, and 84 mg G418. Cells were split in the same way except OS3 cells must be removed from the plate with a cell scraper as they adhere more strongly to the plate surface.

Transfection of HEK293 cells was performed using the calcium phosphate method in which 5-10 µL of DNA was combined with CaCl₂ and water in a 1:100 ratio to make 500 µL of solution. 2X-BBS (500 µL) was added and the mixture incubated at room temperature for 15 minutes before being added to cells growing on a 10cm plate. Cells were incubated overnight at

35°C and 3% CO₂. For stable transfection, media was changed to G418 media (regular growth media supplemented with 500 mg G418) and the media changed every few days until a stable population of cells began to grow.

Transfection of OS3 cells was accomplished using Fugene 6 Transfection reagent (Roche). DNA and Fugene were combined in a 3:1 ratio. Fugene and serum-free media were combined for a total volume of 500 µL and incubated at room temperature for 5 min. DNA was then added and incubated at room temperature before being added to cells grown in a 10cm dish. Incubation and stable transfection were accomplished in the same manner as HEK293 cells.

Site-Directed Receptor Mutagenesis

Insertion of Flag tag. The Flag tag was inserted on the 5' end of the receptor gene as follows. Primers were designed which incorporated the Kozak sequence, start codon, and Flag tag (see chapter 7). DNA was combined with the primers, dNTPs, *Taq* polymerase, buffer and PCR Taq Master Mix (Brinkman Inst, Inc). The PCR reaction was run as follows:

1. 95°C, 2 min
2. 95°C, 30 sec
3. 56°C, 1 min
4. 72°C, 2 min
5. Go to 2 for 34 repetitions
6. 72°C, 10 min
7. Hold 4°C

Following PCR, the reaction was run on agarose gel and the amplified fragment excised and ligated into pBKS. The plasmid was transformed into DH5α cells, and grown in a Miniprep to isolate DNA. The DNA was sequenced to confirm the presence of the Flag tag.

Mutant PCR. Mutant PCR was performed as follows. Template DNA, dNTPs, *Pfu* polymerase (Stratagene), primers containing the desired mutation, and buffer were subjected to the following PCR reaction:

1. 95°C, 30 sec
2. 95°C, 30 sec

3. 55°C, 1 min
4. 68°C, 9 min
5. Go to 2 for 12 repetitions
6. Hold 4°C

Following PCR, the reaction mixture was purified by PCR Purification (Qiagen) and incubated with Dpn1 overnight to digest template DNA. The DNA was then transformed into DH5 α cells and the plasmid isolated by Miniprep. The sequence was confirmed and the mutant receptor excised and ligated into pcDNA3 for transfection.

Transformation. Chemically competent DH5 α cells (100 μ L) were gently mixed with 1-20 μ L of DNA and incubated on ice for 20-30 minutes. The bacteria were then heat shocked for 40-60 seconds at 42°C and then incubated on ice for 2 minutes. SOC media (150 μ L) (tryptone, yeast extract, NaCl, KCl, MgCl₂, MgSO₄, glucose and water) was added to the tubes and then gently shaken at 210 rpm and 37°C for at least one hour. The bacteria were then spread onto LB-agar plates (tryptone, NaCl, yeast extract, agar and water) supplemented with 100 μ g/ μ L ampicillin and grown in a 37°C incubator overnight.

Miniprep. Procedure was taken from Qiagen Handbook. Bacterial cultures were prepared by picking a single clone from the LB-agar plates and growing overnight in 5 mL LB broth (tryptone, NaCl, yeast extract and water) supplemented with 100 μ g/ μ L ampicillin at 275 rpm and 37°C. The bacteria were harvested by centrifuging 1.5 mL of culture in a microcentrifuge for 8 min at 6000 rpm and discarding growth medium. This procedure was repeated twice and the bacterial pellet resuspended in Buffer P1. Lysis buffer P2 was added and the tubes gently mixed and held for two minutes. Neutralization Buffer P3 was then added and the tubes inverted several times to mix. The mixture was centrifuged for 10 min at 14000 rpm and the supernatant applied to a Qiagen spin column and centrifuged for 1 min at 14000 rpm. The flowthrough was discarded and 750 μ L wash buffer added to the column. The column was centrifuged twice for 1 min each

at 14000 rpm, then 40 μ L of water was then added and centrifuged for 1 min at 14000 rpm to collect the DNA in a fresh 1.5 mL Eppendorf tube.

Maxiprep. A bacterial culture was grown overnight in 500 mL LB broth supplemented with 100 μ g/ μ L ampicillin. The bacteria was harvested by centrifugation for 10 min at 6000 rpm and 4°C and the growth medium discarded. The pellet was resuspended in 10 mL Buffer P1 and then lysed for 5 min in 10 mL of Buffer P2. Neutralization Buffer P3 (10 mL) was added and the suspension incubated on ice for 20 min. The supernatant was obtained by centrifuging for 30 min at 14000 rpm and 4°C. The supernatant was applied to an equilibrated Qiagen column and allowed to drain by gravity. The column was washed twice with 30 mL each of wash buffer and then the DNA was eluted with 15 mL of Buffer QF. DNA was precipitated with 1.7 volumes of isopropanol and centrifuged for 30 min at 8800 rpm and 4°C. The solution was decanted and the DNA pellet collected using 70% ethanol in water. The DNA was centrifuged in a microcentrifuge for 10 min at 14000 rpm and 4°C, then the solution was decanted and the DNA air dried for 10 min. The pellet is resuspended in 100 μ L of TE Light buffer (Tris and EDTA, pH=8.0). Following DNA concentration determination, the DNA was diluted to 1 μ g/ μ L with TE Light buffer.

Plasmid sequencing. Plasmid sequencing using the BDT sequencing method was accomplished as follows. DNA, a suitable sequencing primer, BDT buffer, and BDT reaction mixture were combined and run in a PCR reaction as follows:

1. 96°C, 10 sec
2. 50°C, 5 sec
3. 60°C, 4 min
4. Go to 1 for 24 repetitions
5. Hold 4°C

Following PCR, the reaction was purified by ethanol precipitation, dried, and submitted for sequencing.

Real Time Polymerase Chain Reaction (RT-PCR)

Stimulation. For HEK cells: 1.8 mL media (1960 μ L DMEM, 20 μ L IBMX (100x), 20 μ L 1% BSA in PBS) was added to a 10 cm plate (cell confluency 90-100%). ACTH (1-24) (200 μ L, 10^{-7} M) was added, and cells were incubated at 37°C for 6 hours.

For OS3 cells: 1.8 mL media (1980 μ L OS3 media, 20 μ L IBMX (100x)) was added to a 10 cm plate (cell confluency 90-100%). ACTH (1-24) (200 μ L, 10^{-7} M) was added, and cells were incubated at 37°C for 6 hours.

Isolation of RNA. RNA was isolated using the RNeasy Mini Kit (Qiagen Sciences, Maryland, USA). Growth media was aspirated from cells and 600 μ L Buffer RLT (6 mL RLT (Qiagen Sciences, Maryland, USA) + 60 μ L β -mercaptoethanol) was added. The cells were transferred to a 1.5 mL Eppendorf tube and homogenized by passing the lysate through a 20-gauge needle ten times. One volume of ethanol was added to the homogenized lysate and mixed. The sample was placed on an RNeasy mini column (Qiagen Sciences, Maryland, USA) and centrifuged for 15 sec at 10,000 rpm. Flowthrough was discarded, and 700 μ L Buffer RWI (Qiagen Sciences, Maryland, USA) was added to the column and centrifuged for 15s at 10,000 rpm. The flowthrough was discarded and 500 μ L of Buffer RPE (Qiagen Sciences, Maryland, USA) was added and centrifuged for 15 s at 10,000 rpm to dry the column. The flowthrough was discarded and 500 μ L of Buffer RPE (Qiagen Sciences, Maryland, USA) was added and centrifuged 1 min at 10,000 rpm. To elute the RNA, 40 μ L of RNase-free water was placed on the silica-gel membrane and centrifuged 1 min at 10,000 rpm. The elution step was repeated with 40 μ L of RNase-free water. RNA concentration was determined by adding 4 μ L RNA to 796 μ L ddH₂O and the OD₂₆₀ was measured with a spectrophotometer. The concentration was calculated from the absorbance using the equation $C = OD_{260} \times (V_T/4) \times 40$ where C = concentration, and V_T = total volume. RNA quality was determined by gel electrophoresis on a 1% agarose gel.

Synthesis of cDNA. All cDNA reagents purchased from Applied Biosystems (Foster City, CA). To an optical PCR tube was added 10 μL 10x Reverse Transcription Buffer, 4 μL 25x dNTPs, 10 μL 10x random primers, 5 μL MultiScribe Reverse Transcriptase (50 U/ μL), 50 μL TaqMan 2x Universal PCR Master Mix, and 71 μL RNA + ddH₂O (10 μg RNA was calculated from measured RNA concentration). The PCR tubes were placed in an Eppendorf Mastercycler Gradient PCR machine, program: 10 min at 25°C, 120 min at 37°C.

Real Time PCR. To set up the RT-PCR experiment, cDNA was first diluted to 20 ng/ μL (20 μL cDNA + 80 μL ddH₂O). For 18S ribosomal cDNA detection, the 20 ng/ μL cDNA was further diluted to 1 ng/2.5 μL (2 μL 20 ng/ μL cDNA + 98 μL ddH₂O). Assay media was prepared as follows: for each gene to be detected, 1.25 μL of RT-PCR Assay on Demand (Applied Biosystems, Foster City, CA) was added to a tube followed by 6.25 μL ddH₂O and 12.5 μL TaqMan 2x Universal PCR Master Mix (Applied Biosystems, Foster City, CA). The 18S ribosomal assay media was prepared using reagents from the TaqMan Ribosomal RNA Control Reagent Kit (Applied Biosystems, Foster City, CA). For each well, 9.625 μL ddH₂O, 0.125 μL forward primer, 0.125 μL reverse primer, 0.125 μL probe, and 12.5 μL of TaqMan 2x Universal PCR Master Mix (Applied Biosystems, Foster City, CA) were mixed. In a 96-well optical reaction plate, 20 μL assay and 5 μL 20 ng/ μL cDNA were added to each well for unknown gene detection, and 22.5 μL assay and 2.5 μL 1 ng/2.5 μL cDNA was added to separate wells for 18S ribosomal detection. For each assay type, a no cDNA sample was tested, using 20 μL assay and 5 μL ddH₂O. The plate was covered with an optical plastic cover, centrifuged, and placed in an ABI Prism 7000 Sequence Detection System RT-PCR machine (Applied Biosystems, Foster City, CA), program: 2 min 50°C (1x), 10 min at 95°C (1x), 15 s at 95°C then 1 min at 60°C (40x).

Fluorescence-Activated Cell Sorting (FACS)

OS3 and HEK293 cells stably expressing the Flag-hMC2R gene were grown to 80-90% confluency. The cells were washed with 2 mL DPBS, then released from the plate by 5 min incubation at 4°C in 2 mL dissociation buffer (1x PBS, 0.02% EDTA). The cells were transferred to a 50 mL conical tube and centrifuged at 600xg for 5 min at room temperature. The supernatant was aspirated and cells were resuspended in 1 mL FACS buffer (1% RIA grade bovine serum albumin, 0.1% sodium azide, and 1x PBS pH 7.2). The cell suspension (200 µL) was aliquoted into each of four FACS tubes, labeled as such: no label, isotype, surface, and total. Mouse IgG (1.5 µL) was added to each tube to block Fc receptors, and incubated 10 min at room temperature. To the tube containing the isotype control, 1 µL APC-labeled mouse IgG1 k₁ isotype control was added. To the surface and total tubes, 1 µL anti-Flag-APC was added. All tubes were incubated at room temperature for 45 min. After incubation, 4% formaldehyde in 1x PBS was added to each tube for a final concentration of 2% (v/v). Tubes were held at room temperature for 15 min, then centrifuged at 600xg for 5 min at room temperature. The supernatant was decanted, and 1 mL saponin buffer (1% RIA grade bovine serum albumin, 0.1% sodium azide, 0.5% saponin, 1x PBS pH 7.2) was added to each tube and incubated 20 min. The tubes were centrifuged at 600xg for 5 min at room temperature and the supernatant decanted. To the isotype control tube 1 µL of APC-labeled mouse IgG1 k₁ isotype control was added and to the tube for total expression 1 µL anti-Flag-APC was added then incubated at room temperature for 1 hour. All tubes were washed three times with saponin buffer as follows: 1 mL saponin buffer was added then the tubes were centrifuged at 600xg for 5 min at room temperature and the supernatant was decanted. Tubes were held at 4°C until analyzed. Flow cytometry was performed on a FACSCalibur by Becton Dickinson. Cells were prepared for deconvolution microscopy by adding 1 mL of DAPI stain to all tubes, then cytopinning the samples at 600xg

for 4 min at room temperature. Slides were washed in 1x PBS, air dried, and mounted with Biomedica Gel Mount. Slides were stored at 4°C until analyzed.

Luciferase Reporter Gene Assay

Pharmacological analysis was performed by luciferase reporter gene assay. On the day of transfection 96-well black-wall clear-bottom luminescence plates were treated with 100 µL working collagen solution per well. HEK-293 cells stably expressing the melanocortin receptors were transiently transfected with CRE/luciferase reporter gene and 0.5 µg of GFP plasmid per cell type to test transfection efficiency. Twenty-four hours post-transfection the plates were washed with 200 µL DMEM per well and transfected cells were plated at 100 µL per well. Forty-eight hours post-transfection the cells were stimulated with 100 µL peptide (10^{-4} - 10^{-10} M) or forskolin (10^{-4} M) control in assay medium (DMEM containing 0.1 mg/mL BSA and 0.1 mM IBMX) for 6 h then the cells were lysed using lysis buffer (0.1M potassium phosphate buffer pH=7.8, 1% Triton X-100, 1 mM DTT, 2 mM EDTA). Protein analysis was performed by adding 10 µL of cell lysate to 200 µL protein dye in 96-well assay plates. Protein content was measured at OD₅₉₅ using a 96-well plate reader (Molecular Devices). To the remaining cell lysate 100 µL of luciferase assay buffer (30 mM tricine, 2 mM ATP, 15 mM MgSO₄, 10 mM DTT) and 100 µL 1mM D-luciferin were added. Luminescence was measured using a luminometer. Data points were normalized both to the relative protein content and non-receptor dependent forskolin stimulation.

Functional Assay: cAMP Assay

cAMP TRK432 kit purchased from Amersham Biosciences. EBSS Assay buffer (1 mL of 1 M HEPES pH 7.4, 1 mL 200 mM Glutamine, 6.3 mL 17.5 g NaHCO₃/500 mL stock, 100 mg bovine serum albumin, 91.7 mL 1X EBSS) was prepared first and then 1X IBMX in EBSS buffer was made for compound dilutions (1 mL 100x IBMX per 100 mL EBSS assay buffer).

Compound dilutions of ACTH (1-24) 10^{-6} - 10^{-11} M were prepared in assay buffer containing IBMX. Growth media was aspirated from the cells and cells were washed with EBSS assay buffer. Cells were incubated for 30 min at 37°C in 500 μ L EBSS assay buffer. After incubation, 500 μ L of compound dilution were added per well and cells incubated for 6 h at 37°C. Cells were lysed cells with 1 mL 100% ethanol and transferred to labeled 1.5 mL Eppendorf tubes which were placed on ice for 30 min. Tubes were centrifuged at 4°C for 10 min at 1900 g and the supernatant transferred to labeled 12x75mm glass tubes. The supernatant was evaporated at 55°C in a water bath under a stream of nitrogen gas until dry. cAMP standards were prepared (16 pmol/mL - 1 pmol/mL). The dry supernatant was resuspended in 150 μ L Tris EDTA buffer (50 mM Tris/HCl, 4 mM EDTA pH 7.5), and vortexed to mix. An aliquot of each sample (50 μ L) was transferred to labeled 1.5 mL Eppendorf tubes. 3 H-cAMP tracer (50 μ L) and 100 μ L binding protein was added to each tube, vortexed, and incubated at 4°C for 2 h up to overnight. Charcoal suspension (100 μ L) was added to all tubes, vortexed, and centrifuged for 5 min at maximum speed. The supernatant from each tube (200 μ L) was added to a separate scintillation vial filled with 5 mL ScintiVerse scintillation fluid. Vials were counted using a scintillation counter for 1 min per sample.

Data Analysis

Real Time PCR, luciferase, and cAMP data analysis was performed using Microsoft Excel and Graphpad Prism 4.0. FACS analysis was performed using CellQuest as well as Microsoft Excel and Graphpad Prism 4.0. All experiments were performed a minimum of three times.

CHAPTER 5
STRUCTURE-ACTIVITY RELATIONSHIP STUDIES OF PEPTIDES: A STUDY OF
INTRAMOLECULAR CATION- π INTERACTIONS IN MELANOCORTIN AGONISTS
AND THE EFFECTS ON AGONIST AND ANTAGONIST SELECTIVITY

Peptides in this study (peptides 21-32) were synthesized, purified and analytically characterized by Krista R. Wilson. Pharmacology was performed by Michael S. Wood, Nicholas B. Sorenson, Dong V. Phan, and Zhimin Xiang of the same laboratory. Data Analysis was performed by Carrie Haskell-Luevano and Krista R. Wilson.

Introduction

Noncovalent interactions play an important role in stabilization of the secondary and tertiary structure of proteins and peptides as well as in protein-protein, ligand-receptor, and DNA-protein interactions.^{239,240} Over the past decade it has become clear that the electrostatic interaction between a cation and the negative potential found on the face of a π system may be significantly involved in ligand-receptor interactions as well as in peptide and protein folding.^{239,240}

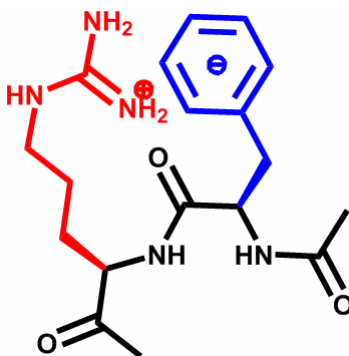


Figure 5-1. Cation- π interaction between the positive charge of arginine and the negative potential on the face of the Phe aromatic system.

Many factors are involved in shaping a polypeptide chain into a bioactive molecule. Secondary and tertiary structural determinations are driven by noncovalent interactions between backbone and side chain molecular elements as well as interaction with solvent and other proteins in the environment.^{239,240} These noncovalent interactions can be quite strong and involve

forces such as hydrogen bonding, electrostatic (ionic) interactions, hydrophobic attraction, dispersion forces, aromatic π - π interactions, dipole-dipole interactions, and dipole-quadrupole interactions just to name a few.^{239,240} One noncovalent force that has recently been identified as having a significant impact on protein and peptide structure is the cation- π interaction.^{239,240} In general, the cation- π interaction is the association of a cation or partial positive charge with the negatively charged face of an aromatic π system (Figure 5-1). In proteins, these interactions can be quite complex, and have been shown to be involved in secondary α -helix, β -sheet and turn stabilization, protein and peptide folding, ligand-receptor binding and signaling, protein-protein interaction, DNA-protein interactions and antibody-antigen recognition.^{239,240} In native proteins, cation- π interactions occur between specific amino acid side chains. The cation of Arg, Lys, and His may interact with the aromatic systems of Trp, Tyr, and Phe (Figure 5-2).^{239,240}

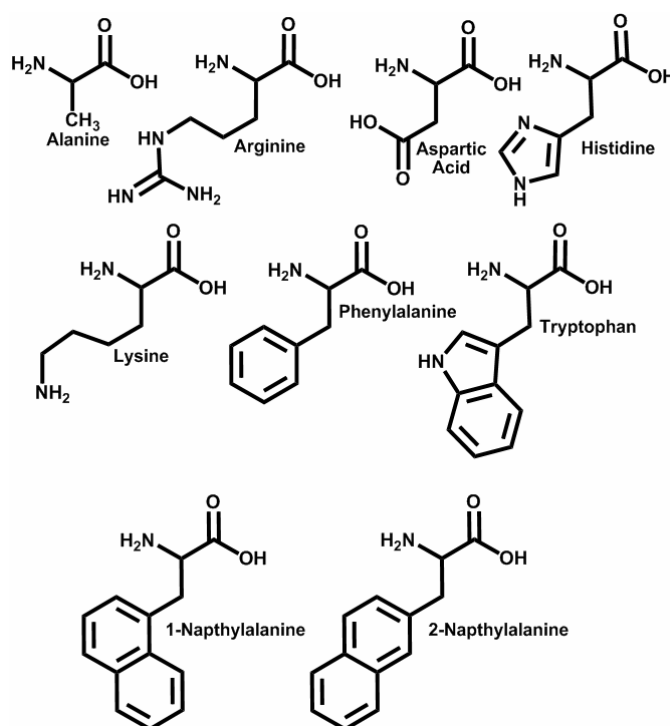


Figure 5-2. Structure of natural and unnatural amino acids used in this study.

Benzene is the prototypic example of a simple aromatic system, and is used here as a basis for understanding the aromatic systems of Trp, Tyr, and Phe. For general purposes, benzene is often considered a nonpolar molecule (Figure 5-3A). Though it does not exhibit a permanent dipole moment, this does not mean that the molecule does not contain a charge distribution. The π orbitals of the aromatic system are arranged in such a manner as to produce six dipole moments, which give benzene a permanent, substantial quadrupole moment ($-28.3 \text{ kcal/mol} \pm 1.2$) (Figure 5-3B,C).²⁴¹ This results in a significant charge distribution where the interior of the aromatic ring contains a negative charge and the outer ring is positively charged (Figure 5-3D). The negatively charged face can then interact with surrounding positive charges in a manner similar to the electrostatic interaction of two ions.

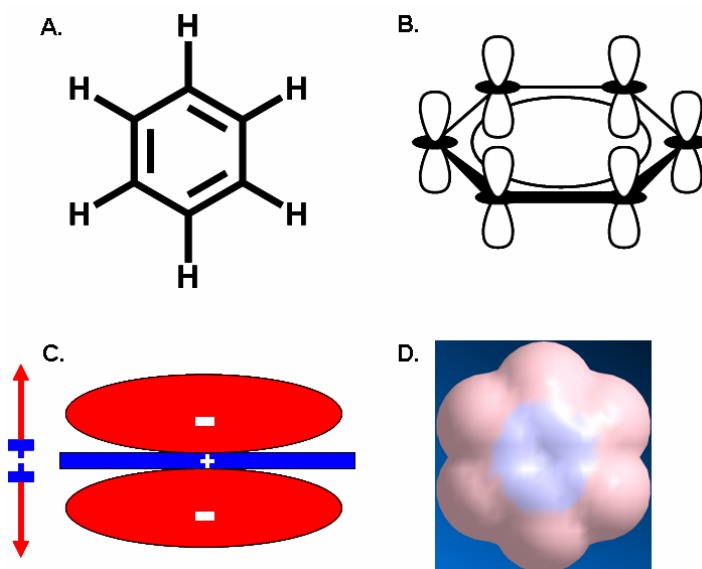


Figure 5-3. Benzene. A. Structure of benzene. B. Pi orbitals of benzene from a side view. C. Schematic of the quadrupole moment of benzene, side view. D. Charge distribution of benzene; blue indicates a negative charge, red indicates a positive charge.

It has been known for some time that small metal cations were able to bind strongly to benzene, with smaller atoms binding stronger than larger atoms.²⁴² It was therefore postulated that this phenomenon could be applied to systems with partial positive charges and to organic cations such as the ammonium ion.^{243,244} In fact, it has been shown that aromatic π systems can

interact with both full and partial charges, such as those found in highly polarized molecules such as water and amines.^{243,244} In peptides and proteins this results in a significant amount of stabilization obtained from the interaction of cationic amino acid side chains (ie. arginine, lysine, histidine) with aromatic amino acid side chains (ie. phenylalanine, tyrosine, tryptophan).^{243,244} As Arg, Lys, and His are ionized at physiological pH, they may interact with the aromatic systems in a cation- π interaction.

Though these interactions were first observed in the gas phase, studies by the Dougherty laboratory²⁴⁵ designed artificial receptor systems that were able to exhibit cation- π interactions in an aqueous environment.²⁴⁵ In fact, the aromatic “receptors” were able to pull cations out of water and bind them in an aromatic environment.²⁴⁵ This is significant as noncovalent interactions must compete with the solvation energy of the positive charge interacting with the polar groups of water. To bind the aromatic system, the cation must undergo a “desolvation penalty”²⁴⁶⁻²⁴⁸ to break its aqueous interactions and bind to the aromatic. This change in energy due to desolvation has been used to describe the differing binding strengths of arginine and lysine.

In general, arginine associates more strongly with aromatic π systems than lysine.^{243,244} The guanidyl group is chemically different from a primary amine and thus associates differently with aromatic systems. Interestingly, in the gas phase the ammonium ion interacts more strongly than the guanidinium ion.²⁴⁹ This may be related to the small size of the ammonium ion (smaller ions associate more strongly than larger ones) and the charge distribution on the guanidinium ion. Since arginine is much more likely to be involved in a cation- π interaction, there must be factors other than electrostatic effects involved in these interactions. One theory relates desolvation energy to strength of interaction (Figure 5-4).²⁵⁰ The guanidinium ion has two

potential sites for ionization (Figure 5-4A). This decreases the desolvation penalty because one ion can interact with the aromatic system and the other cation can maintain interactions with the aqueous environment, lowering the energy related to desolvation.²⁵⁰ The ammonium ion only has one site for ionization and thus must relinquish its interactions with water to bind the aromatic system (Figure 5-4B). This results in a much greater desolvation penalty associated with lysine binding to aromatics than arginine.²⁵⁰ This desolvation penalty may be reduced in lysine due to the partial positive charge associated with the ϵ carbon. This carbon is highly polarized and maintains a partial positive charge that can interact with either an aromatic or water. This interaction is not as strong as a full cation, but may decrease the desolvation penalty.²⁵¹ These observations may be used to explain the differences associated with arginine versus lysine selectivity.

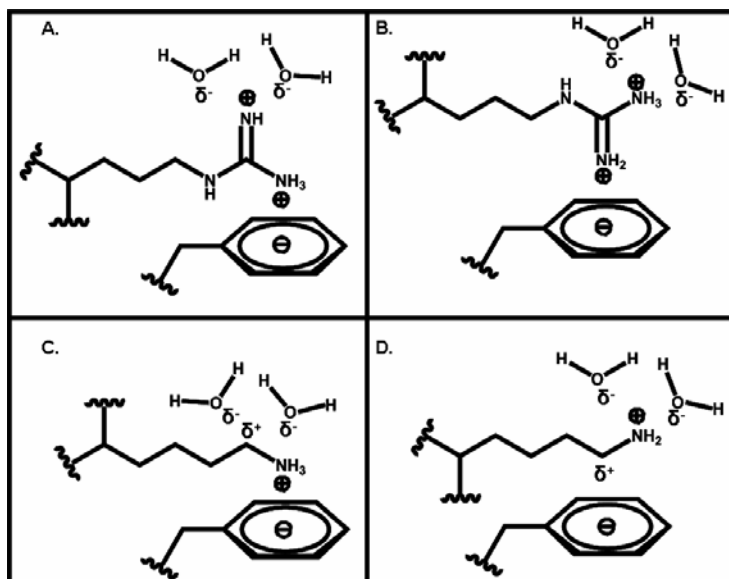


Figure 5-4. Cation- π interactions of Arg and Lys with Phe and water. A. and B. show two different conformations by which Arg may interact with Phe. C. and D. show conformations of interaction between Lys and Phe.

The three most common hydrophobic amino acids involved in cation- π interactions are phenylalanine, tyrosine, and tryptophan.^{243,244} In the gas phase, an indole moiety binds cations much stronger than either phenol or benzene.^{239,252,253} In protein database searches, 26% of all

tryptophan residues are located near cations.²⁵¹ This is in agreement with the observation that tryptophan is the aromatic amino acid most likely to be involved in cation- π interactions as it has the greatest negative potential. The side chains of phenylalanine and tyrosine have similar binding properties;²⁵³ however, if the hydroxyl of tyrosine is hydrogen bonded, or if the negative potential of the oxygen interacts directly with the cation, the binding properties of tyrosine increase as compared to phenylalanine.²⁵¹

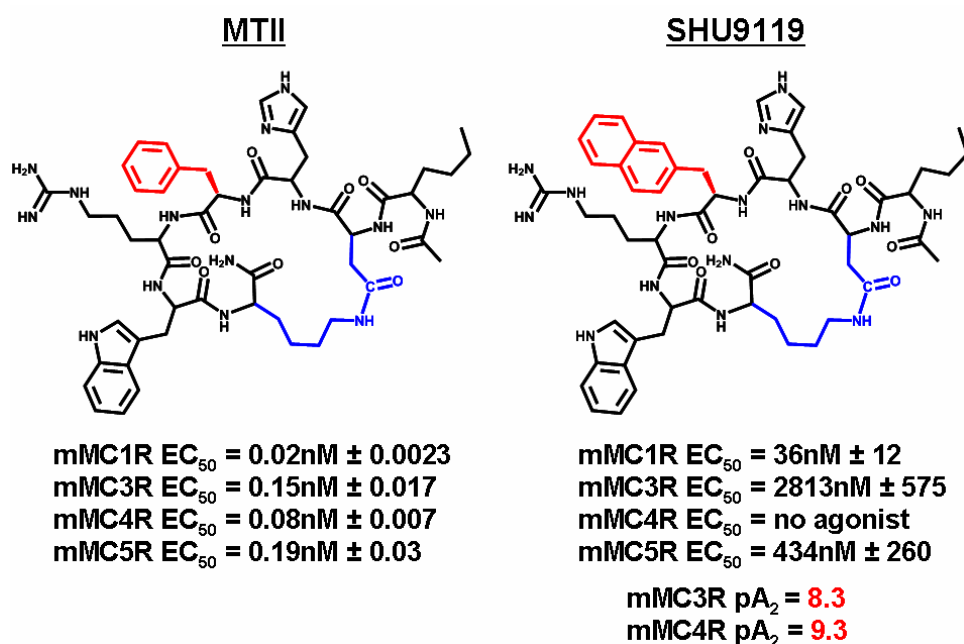


Figure 5-5. Structure and pharmacology of the synthetic melanocortin agonist MTII (left) and the synthetic melanocortin antagonist SHU9119 (right). The lactam bridge is shown in blue and the differing aromatic systems [MTII = Phe; SHU9119 = DNal(2')] are in red. EC₅₀ values in nM are shown below the structures along with associated errors. Antagonist pA₂ values are shown for SHU9119 at the mMC3R and mMC4R.²⁵⁴

All known endogenous melanocortin peptides contain the same core tetrapeptide sequence, His-Phe-Arg-Trp. These four residues are essential for potent activity at the melanocortin receptors.¹¹⁵ SAR studies of α -MSH have shown that the minimal essential sequence for stimulation is Ac-Phe-Arg-Trp-NH₂, though addition of His results in a significant increase in ligand potency.^{114,115} These SAR studies resulted in the discovery of NDP-MSH, a derivative of α -MSH in which the Met was replaced with a Nle to prevent oxidation and the Phe is replaced

with a DPhe to significantly increase potency.⁴ This molecule was much more potent than the endogenous peptide. Further cyclization and deletion studies of NDP-MSH resulted in the development of MTII (Ac-Nle-[Asp-His-DPhe-Arg-Trp-Lys]-NH₂) (Figure 5-5), a small cyclic agonist that is more potent than either α -MSH or NDP-MSH.^{117,118,255} During the course of this investigation, it was discovered that replacement of DPhe with a DNal(2') resulted in a compound (SHU9119, Figure 5-5) (Ac-Nle-[Asp-His-DNal(2')-Arg-Trp-Lys]-NH₂) with potent antagonist activity at the mMC3 and mMC4R.^{117,118,255} It is hypothesized that there may be a cation- π interaction between the arginine and the adjacent aromatic residue and that the differences between the interaction with DPhe and DNal(2') and arginine may have an effect on agonist and antagonist selectivity.⁴³

Background Pharmacology

Holder *et al.* synthesized a number of single-substitution derivatives of the core tetrapeptide sequence His-Phe-Arg-Trp in order to investigate the ideal structural features for melanocortin activity.⁶⁻⁹ They systematically replaced each amino acid with a number of natural and unnatural amino acids. During the course of these studies, it was observed that the Phe and Arg positions had very specific requirements for activity, and that the Phe position seems to be significantly involved in agonist versus antagonist activity. Some significant compounds synthesized during this study are shown in Table 5-1.

Table 5-1. SAR Studies of Selected Melanocortin Tetrapeptides^{116-14,6-9} and Pharmacology Data of Arg Substitutions²⁵⁶⁻²⁰

		mMC1R	mMC3R	mMC4R	mMC5R
#	Structure	EC₅₀ (nM)	EC₅₀ (nM)	EC₅₀ (nM)	EC₅₀ (nM)
1	Ac-His-Phe-Arg-Trp-NH ₂	7690±3590	4370±535	2110±243	103±28
2	Ac-His-DPhe-Arg-Trp-NH ₂	20.1±0.57	156±9.2	17.2±2.78	3.96±0.94
3	Ac-His- Ala -Arg-Trp-NH ₂	30000±6100	>100000	>100000	>100000
4	Ac-His-(pI)DPhe-Arg-Trp-NH ₂	60.4±13.4	PA pA ₂ = 7.25±0.18	25.0±9.78	1.60±0.35
5	Ac-His-Nal(1')-Arg-Trp-NH ₂	15200±3100	>100000	>100000	11200±2300
6	Ac-His-DNal(1')-Arg-Trp-NH ₂	356±64	4100±1000	303±65	51.4±4.07
7	Ac-His-Nal(2')-Arg-Trp-NH ₂	22000±5600	>100000	>100000	7400±1800
8	Ac-His-DNal(2')-Arg-Trp-NH ₂	167±41	PA pA ₂ = 6.53±0.09	pA ₂ = 7.78±0.18	34.7±6.75
9	Ac-His-DPhe- Ala -Trp-NH ₂	3400±1600	42000±8900	23000±4100	6900±1500
10	Ac-His-DPhe- Lys -Trp-NH ₂	770±500	25500±1900	830±140	320±14
11	Ac-His-DPhe- Orn -Trp-NH ₂	6100±2200	55600±2800	6500±1900	540±30
12	Ac-His-DPhe- Dap -Trp-NH ₂	9300±3100	38900±5800	3800±893	610±40
13	Ac-His-DPhe- Asp -Trp-NH ₂	43400±9700	>100000	>100000	16400±7900
14	Ac-His-DPhe- Glu -Trp-NH ₂	42900±9700	65400±9100	15500±2200	2000±970
15	Ac-Nle-c[Asp-His-DPhe-Arg-Trp-Lys]-NH ₂	0.02±0.002	0.14±0.016	0.04±0.007	0.27±0.03
16	Ac-Nle-c[Asp-His-Phe-Arg-Trp-Lys]-NH ₂	23.2±12.8	1.73±0.12	45±7.5	1.62±1.0
17	Ac-Nle-c[Asp-His-DNal(2')-Arg-Trp-Lys]-NH ₂	0.20±0.08	pA ₂ = 9.54±0.23 50%@10µM	pA ₂ = 10.14±0.20	1.79±0.65
18	Ac-Nle-c[Asp-His-Nal(2')-Arg-Trp-Lys]-NH ₂	122±32	21.9±4.8 80%@10µM	81±7.2 60%@10µM	1.85±0.60
19	Ac-Nle-c[Asp-His-DNal(1')-Arg-Trp-Lys]-NH ₂	0.68±0.39	1.23±0.27	0.38±0.07 70%@10µM	3.2±0.7
20	Ac-Nle-c[Asp-His-Nal(1')-Arg-Trp-Lys]-NH ₂	380±150	246±170 85%@10µM	142±27	11.1±8.0

Compounds 15-20 were synthesized in the Haskell-Luevano laboratory at the University of Florida. Compounds 15,18,19 and 20 were synthesized by J. Ryan Holder, Compound 16 was synthesized by Jay W. Schaub, and Compound 17 was synthesized by Fernanda Marques. Indicated errors represent the standard error of the mean for at least three independent experiments. >100000 indicates that no agonist activity was observed at agonist concentrations up to 100µM concentrations. PA = partial agonist. Compounds not possessing full agonist activity were assayed for antagonist activity using the Schild analysis against the agonist MTH.

SAR at the Phe position⁷ revealed that similar to previous studies, replacing the LPhe with a DPhe resulted in a compound that is >100-fold more potent at the mMC4R. Additionally, replacement with an Ala significantly decreased the agonist potency at the mMC1R, and completely abolished all activity at the mMC3-5R, indicating that the aromatic ring is important for activity. Replacing the single aromatic ring of Phe with either a double aromatic system (naphthylalanine [Nal]) or with a para-substituted phenyl ring gave interesting results. When Phe was replaced with either a (pI)DPhe or a DNal(2') residue the tetrapeptide showed antagonist activity.⁷ The (pI)DPhe compound showed mixed pharmacology with both partial agonist and antagonist activity at the mMC3R and full agonist activity at the mMC4R, and the DNal(2') compound was an antagonist at both the mMC3R and the mMC4R, as well as a partial agonist at the mMC3R.⁷

Table 5-2. Antagonists of the MC3R and MC4R containing DNal(2').

Compound Name	Sequence	Reference
PG-914	Ac-Nle-c[Asp-Che-DNal(2')-Arg-Trp-Lys]-NH ₂	257
SHU9119	Ac-Nle-c[Asp-His-DNal(2')-Arg-Trp-Lys]-NH ₂	117,255,258
HS014	c[Cys-Glu-His-DNal(2')-Arg-Trp-Gly]-Pro-Pro-Lys-Asp-NH ₂	259
HS024	c[Cys-Nle-Arg-His-DNal(2')-Arg-Trp-Gly-Cys]	260
HS9510	c[Cys-Glu-His-DNal(2')-Arg-Trp-Cys]	261

The effects of substituting a DNal(2') for DPhe have been well characterized. Its effect on melanocortin potency was observed during SAR studies of MTII, which resulted in the discovery of the potent mMC3R and mMC4R antagonist SHU9119.^{117,255,258,262,263} SHU9119 is an agonist at the mMC1,5R and a partial agonist at the mMC3R, but is a potent antagonist at the mMC3,4R.^{117,255,258,262,263} Table 5-2 depicts several peptides containing the DNal(2') moiety which are antagonists at the MC3R and MC4R.^{117,255,257-259,261,263,264} A plethora of SAR studies have been performed on SHU9119 which consistently demonstrate that the substitution of DPhe

with a DNal(2') results in a compound with selective antagonist activity at the MC3R and MC4R.^{257,259-261,265-273}

For LNal(2') or either the D- or L- forms of Nal(1'), there was no antagonist activity observed, and the compounds were much less potent than the DPhe or DNal(2') compounds. This data, along with data from MTII and SHU9119, has led to the hypothesis that the Phe position may be involved in the determination of agonist vs antagonist potency at the mMC3R and mMC4R.

Tetrapeptide SAR studies at the Arg position^{9,274,275} revealed that the cationic character of the guanidine side chain is important for agonist activity. When Arg was replaced with an Ala there was a significant decrease in agonist activity observed at all melanocortin receptors.^{9,274,275} Additionally, decreasing the cationic character with a Lys resulted in a compound with intermediate potency (less than Arg, more than Ala). Decreasing the chain length beginning with Lys (4C), then Orn (3C), and finally Dap (2C) resulted in a stepwise decrease in potency. Furthermore, replacement with an anionic amino acid such as Asp and Glu resulted in either a complete loss of activity (Asp) or a significant decrease in activity (Glu). This data indicates that there may be an anionic binding pocket that requires a cation in the ligand for efficient binding.

Data from these studies were used in the design of compounds in the present work. In this study, MTII,^{117,258} a cyclic synthetic melanocortin peptide, was modified at the arginine and D-phenylalanine positions to investigate the role cation- π interactions may play in the agonist or antagonist potency of this ligand at the melanocortin receptors. It is hypothesized that when combined with any one of six aromatic π systems [Phe, DPhe, Nal(1'), DNal(1'), Nal(2'), or DNal(2')], peptides with an arginine should exhibit the greatest potency and those with an alanine should have a significant loss of activity, with lysine peptides exhibiting an intermediate

potency. Additionally, in accordance with the melanocortin antagonist SHU9119, compounds containing a DNal(2') should exhibit antagonist activity. Naphthylalanine derivatives are used because the double aromatic ring results in a greater negative electrostatic potential than the single ring of phenylalanine, and thus should interact more strongly with the cation (Figure 5-6).

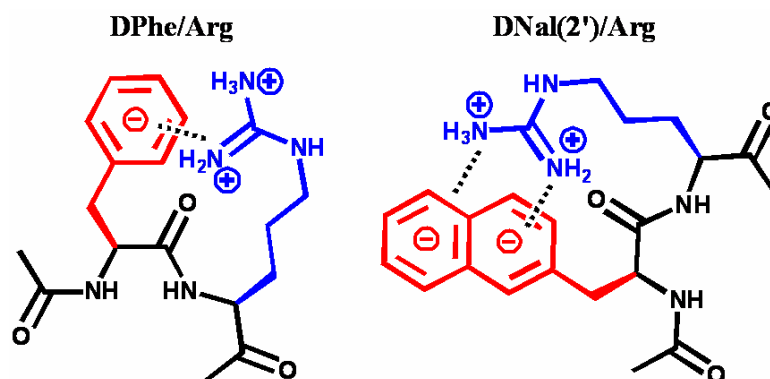


Figure 5-6. Schematic of a cation- π interaction (dotted lines) between the cationic side chain of Arg (blue) and the negative potential of the π systems of DPhe and DNal(2') (red).

Results

Peptide synthesis. All peptides were synthesized using standard Boc chemistry in a manual reaction vessel (Peptides International, Louisville, KY). The peptides were purified to homogeneity by semi-preparative reversed-phase high-performance liquid chromatography (RP-HPLC). Peptide purity was determined using mass spectrometry and analytical RP-HPLC in two solvent systems (Table 5-3)

Table 5-3. Analytical Data for Peptides Synthesized in the Cation- π Study

#	HPLC k' (System 1)	HPLC k' (System 2)	% Yield	m/z (M, calcd)	m/z (M+1, exptl)
21	6.22	11.13	>95%	995.5	996.8
22	6.70	10.88	>95%	938.5	939.7
23	6.20	10.96	>98%	995.5	997.3
24	5.71	11.35	>98%	938.5	939.9
25	7.17	12.47	>95%	1046.2	1047.0
26	6.81	12.06	>98%	989.1	990.9
27	6.71	11.09	>95%	1046.2	147.5
28	6.61	12.76	>98%	989.1	990.8
29	6.98	12.41	>95%	1046.2	1047.7
30	6.80	13.16	>98%	989.1	989.9
31	6.59	11.54	>98%	1046.2	1046.8
32	6.63	12.96	>98%	989.1	989.8

HPLC k' = [(peptide retention time – solvent retention time)/(solvent retention time)] in solvent system 1 (10 % acetonitrile in 0.1 % trifluoroacetic acid/water and a gradient to 90 % acetonitrile over 35 min) or solvent system 2 (10 % methanol in 0.1 % trifluoroacetic Acid/water and a gradient to 90 % methanol over 35 min). An analytical Vydac C18 column (Vydac 218TP104) was used with a flow rate of 1.5 ml/min. The peptide purity was determined by HPLC at a wavelength of 214 nm by comparison of the area under the curve of compound peak compared to all other peaks.

Table 5-4. Pharmacology Data for Peptides in the Cation- π Study

#	Structure	mMC1R		mMC3R		mMC4R		mMC5R	
		EC ₅₀ (nM)	Fold Diff	EC ₅₀ (nM)	Fold Diff	EC ₅₀ (nM)	Fold Diff	EC ₅₀ (nM)	Fold Diff
α -MSH	Ac-Ser-Tyr-Ser-Met-Glu-His-Phe-Arg-Trp-Gly-Lys-Pro-Val-NH ₂	0.7±0.23		2.14±0.46		2.56±0.29		2.0±0.20	
NDP-MSH	Ac-Ser-Tyr-Ser-Nle-Glu-His-DPhe-Arg-Trp-Gly-Lys-Pro-Val-NH ₂	1.0±0.79		0.09±0.02		0.1±0.01		0.22±0.03	
21	Ac-Nle-[Asp-His-DPhe-Lys-Trp-Lys]-NH ₂	0.13±0.12	6	2.29±0.70	16	0.66±0.37	17	0.86±0.65	3
22	Ac-Nle-[Asp-His-DPhe-Ala-Trp-Lys]-NH ₂	1.77±0.58	89	4.97±1.08	36	2.19±0.98	55	0.57±0.20	2
23	Ac-Nle-[Asp-His-Phe-Lys-Trp-Lys]-NH ₂	311±106	13	76±14	44	45±7.5	37	1.62±1.0	0.8
24	Ac-Nle-[Asp-His-Phe-Ala-Trp-Lys]-NH ₂	1400±315	60	1064±160	615	700±260	574	19.7±3.56	10
25	Ac-Nle-[Asp-His-DNal(2')-Lys-Trp-Lys]-NH ₂	2.04±0.90	10	pA ₂ = 8.38±0.1	14	pA ₂ = 9.03±0.3	13	8.98±2.49	5
26	Ac-Nle-[Asp-His-DNal(2')-Ala-Trp-Lys]-NH ₂	8.44±1.7	42	pA ₂ = 7.44±0.2	125	pA ₂ = 8.54±0.4	40	2.33±0.80	1.3
27	Ac-Nle-[Asp-His-Nal(2')-Lys-Trp-Lys]-NH ₂	1000±370	8	420±100 50%@10 μ M	19	1240±400	15	72.4±47	40
28	Ac-Nle-[Asp-His-Nal(2')-Ala-Trp-Lys]-NH ₂	1820±700	15	14000±5300	640	>100000		430±57	230
29	Ac-Nle-[Asp-His-DNal(1')-Lys-Trp-Lys]-NH ₂	0.98±0.36	1	30.9±16	25	4.27±1.43	11	3.20±0.7	8
30	Ac-Nle-[Asp-His-DNal(1')-Ala-Trp-Lys]-NH ₂	5.38±2.79	8	74.8±22	61	44.6±7.1	117	7.41±1.1	18
31	Ac-Nle-[Asp-His-Nal(1')-Lys-Trp-Lys]-NH ₂	1800±700	5	4800±900	20	1900±800	13	255±112	23
32	Ac-Nle-[Asp-His-Nal(1')-Ala-Trp-Lys]-NH ₂	2600±150	7	3500±250 60%@10 μ M	14	2600±470 60%@10 μ M pA ₂ = 6.15±0.2	18	3200±930	288

Indicated errors represent the standard error of the mean for at least three independent experiments. >100000 indicates that no agonist activity was observed at agonist concentrations up to 100 μ M concentrations. PA = partial agonist. Compounds not possessing full agonist activity were assayed for antagonist activity using the Schild analysis against the agonist MTII. Antagonist fold differences were determined using K_i values; K_i = -logpA₂. For each aromatic system, the Arg compound is defined as 1, with the fold differences of Lys and Ala compounds calculated compared to Arg (Arg compounds in Table 5-1).

Biological evaluation. Table 5-4 compares the cAMP stimulation determined by the β -galactosidase reporter gene assay²⁰⁹ of the MTII derivatives at the mMC1,3-5R with the endogenous peptide α -MSH and the known synthetic agonist MTII as controls. Compounds with the Arg substitution are shown in Table 5-1.

When DPhe was the aromatic system, the order of potency of arginine>lysine>alanine was observed at all four receptors. At the mMC1R, the DPhe-Arg compound 15 (MTII) is a subnanomolar agonist with 0.02 nM activity. When the arginine is converted to a lysine (compound 21) there was a 6-fold decrease in potency, and when an alanine (compound 22) was inserted, there was an 89-fold decrease in potency as compared to compound 15. At the mMC3R, MTII is a 0.14 nM agonist. Addition of lysine in compound 21 results in a 16-fold decrease in potency and the presence of alanine in compound 22 causes a 36-fold decrease in potency. At the mMC4R, MTII is a 0.04 nM agonist, but substitution of the arginine for a lysine or an alanine results in a 17-fold and 55-fold decrease in potency, respectively. The potency trend is not observed at the mMC5R, however, as all three compounds are within 3-fold experimental error (error inherent in all laboratory experiments) of each other and are therefore equipotent. The values for compound 15 (MTII, DPhe-Arg), and compound 22 (DPhe-Ala) are in agreement with previous SAR studies of MTII.^{117,255,258}

When the aromatic system is Phe, there was a decrease in potency observed compared to the DPhe compounds. At the mMC1R, compound 16 (Phe-Arg) is a 23.2 nM agonist. Compound 23 (Phe-Lys) exhibits a 13-fold decrease in potency and compound 24 (Phe-Ala) exhibits a 60-fold decrease in potency as compared to compound 16. At the mMC3R, compound 16 is a 1.73 nM agonist while compounds 23 and 24 are 44- and 615-fold less potent than the arginine compound 16, respectively. At the mMC4R, compound 16 is a 1.22 nM agonist. As before, the

lysine compound 23 is 55-fold less potent and the alanine compound 24 is 574-fold less potent than the arginine compound 16. At the mMC5R, the arginine compound 16 and the lysine compound 23 are equipotent, while the alanine compound 24 exhibits a 10-fold decrease in potency.

SHU9119 is identical to MTII except that the DPhe of MTII is replaced with DNal(2'). Previous studies have shown that this compound is a subnanomolar full agonist at the mMC1R and the mMC5R, and an antagonist and partial agonist at the mMC3R and an antagonist at the mMC4R.^{117,118,255} The results reported here for compound 17 (DNal(2')-Arg) are similar to previously reported values.^{117,118,255} Compound 17 is a 0.20 nM agonist at the mMC1R with partial agonist activity. The DNal(2')-Lys compound 25 exhibits a 10-fold decrease in potency compared to compound 17, and the DNal(2')-Ala compound 26 is 42-fold less potent than compound 17 at the mMC1R. At the mMC3R, all three compounds are antagonists with partial agonist activity observed in compound 17 only. Still the same potency trend continues, as compound 17 (Arg) is the most potent antagonist, followed by compound 25 (Lys) and then compound 26 (Ala). This antagonist trend is the same at the mMC4R, though all three compounds are more potent antagonists than the same compound at the mMC3R. Once again, the potency trend changes for compounds tested at the mMC5R. The lysine compound 25 is 5-fold less potent than the arginine compound 17, while the alanine compound 26 is equipotent with the alanine compound 17.

When the aromatic system is changed from DNal(2') to Nal(2') the pharmacology differs significantly. These compounds are much less potent agonists and are not antagonists at any of the receptors. At the mMC1R, compound 18 [Nal(2')-Arg] is a 122 nM agonist. When the cation is changed to a lysine in compound 27, there is an 8-fold decrease in potency, and when it is

changed to an alanine in compound 28, there is a 15-fold decrease in potency. At the mMC3R, compound 18 [Nal(2')-Arg] is a 430 nM agonist, and only exhibits partial agonist activity. Compound 27 [Nal(2')-Lys] is 19-fold less potent than compound 18, and compound 27 [Nal(2')-Ala] is 640-fold less potent than compound 18, though they are both full agonists while compound 18 is a partial agonist. At the mMC4R, the arginine compound 18 is an 81 nM partial agonist, while the lysine compound 27 is a 15-fold less potent full agonist. When the cation is removed by inserting an alanine in compound 28, the compound does not exhibit any agonist or antagonist activity at the mMC4R. At the mMC5R compounds 18, 27, and 28 follow the same arginine>lysine>alanine potency trend as the other receptors. At the mMC5R, compound 18 is a potent 1.85 nM full agonist, while compound 27 [Nal(2')-Lys] is 40-fold less potent and compound 28 [Nal(2')-Ala] is 230-fold less potent than compound 18.

The next aromatic system tested was DNal(1'). At the mMC1R, compound 19 [DNal(1')-Arg] and compound 29 [DNal(1')-Lys] were equipotent subnanomolar agonists. Compound 30 [DNal(1')-Ala] was 8-fold less potent than the other compounds at the mMC1R. At the mMC3R, the arginine compound 19 is a 1.23 nM agonist. The lysine compound 29 is 25-fold less potent than compound 19 and the alanine compound 30 is 61-fold less potent than compound 19. At the mMC4R, compound 19 is a 0.38 nM agonist, compound 29 exhibits an 11-fold decrease in potency, and compound 30 exhibits a 117-fold decrease in potency. At the mMC5R, the potency trend is followed, as the alanine compound 30 is 18-fold less potent than the arginine compound 19 while the lysine compound 29 is 8-fold less potent than compound 19.

The final aromatic system tested was Nal(1'). These compounds are less potent than the corresponding DNal(1') compounds. At the mMC1R, compound 20 [Nal(1')-Arg] is a 380 nM agonist. The lysine compound 31 is 5-fold less potent, and the alanine compound 32 is 7-fold

less potent. At the mMC3R, compound 20 is a 246 nM partial agonist while compound 31 is a 20-fold less potent full agonist. Compound 32, however, is only 14-fold less potent than the arginine compound 20, making it more potent than the lysine compound 31, though it is a partial agonist. The potency trend returns at the mMC4R. Compound 20 [Nal(1)-Arg] is a 142 nM agonist and the lysine compound 31 is 13-fold less potent. Surprisingly, when an alanine is included in compound 32, the compound becomes a partial agonist and an antagonist at the mMC4R. Finally, at the mMC5R, compound 20 is an 11.1 nM agonist, compound 31 is 23-fold less potent, and compound 32 exhibits a 288-fold decrease in potency with an EC₅₀ value of 3200 nM at the mMC5R.

Discussion

The interaction between a cation and an aromatic π system has recently gained popularity as a significant noncovalent interaction in biological systems.^{239,240} Recent analysis of the Protein Databank (PDB) has indicated that there is one cation- π for every 77 amino acids in proteins.²⁵¹ Additionally it was observed that Arg is found in cation- π interactions more often than Lys and over 70% of Arg residues are close to an aromatic.^{251,276} Tryptophan is the most common aromatic residue to associate with a cation, with over 25% of all Trp residues being located near a cation²⁵¹ and 7.3% of all cation- π interactions are found between adjacent amino acid residues (by X-ray crystallography) helping to establish the 3-D conformation of the protein or peptide.²⁵¹ Cation- π interactions are also commonly found in the *i* and *i*+4 positions, indicating their importance in the stabilization of the α -helix.^{251,277}

Cation- π interactions have been found in many different capacities. They have been shown to play a role in transcription activation,^{278,279} DNA binding to proteins,²⁸⁰ antibody-antigen interactions,²⁸¹⁻²⁸³ and membrane protein interactions^{284,285} just to name a few. They have been shown to be important in the binding of ligand and receptor in acetylcholine receptors,²⁸⁶⁻²⁹²

serotonin receptors,^{290,293,294} GABA receptors,²⁹⁵⁻²⁹⁸ NPY,²⁹⁹ angiotensin 2 receptors,³⁰⁰ and in antimicrobial peptide action.³⁰¹ Recently, the cation- π interaction has been exploited as a tool in synthetic organic chemistry as reviewed.³⁰²

In the present study, the differential cation- π interactions between arginine and lysine were used to investigate the presence of a cation- π interaction in the melanocortin synthetic agonist MTII. Arginine, lysine, and alanine were coupled with six aromatic systems, Phe, DPhe, Nal(1'), DNal(1'), Nal(2'), and DNal(2'). It was hypothesized that if there is a cation- π interaction between the Arg and DPhe of MTII, then when the Arg is replaced with Lys there will be an observable decrease in potency and when Ala is substituted there will be an even greater decrease in potency resulting from a decrease in cation- π interaction strength. Additionally, as MTII (Arg-DPhe) is an agonist, and SHU9119 [Arg-DNal(2')] is an antagonist, it is hypothesized that the difference in the interaction between Arg and either DPhe and DNal(2') may be responsible for agonist versus antagonist selectivity at the hMC3,4R.

D-Phenylalanine

The first aromatic system investigated was DPhe, which is the aromatic amino acid present in MTII.^{117,255,258} These peptides (peptides 15, 21 and 22) were the most potent compounds tested in this study, with all values in the sub- to low-nanomolar range. At the mMC1,3, and 4R the reported values agree with the hypothesis that Arg > Lys > Ala. At each of these receptors, the Arg compound is significantly more potent than the Lys compound, with the Ala compound being the least potent compound. These data indicate that there may be a cation- π interaction which is important for ligand activity. At the mMC5R, however, all three compounds were within 3-fold experimental error of each other and no significant differences were observed. This may indicate that the cation- π interaction is more important for activity at the mMC1,3, and 4R

than at the mMC5R. Bar graphs showing the differences in potency at each receptor are shown in Figure 5-7.

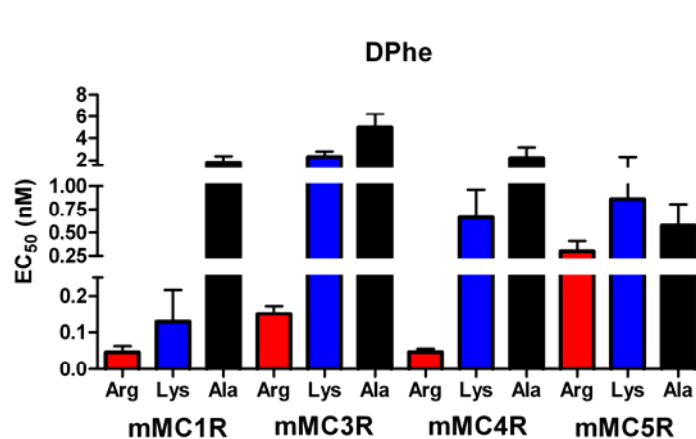


Figure 5-7. Bar graph of peptides 15, 21 and 22 with DPhe as the aromatic system at the mMC1,3-5R.

Phenylalanine

The next group of peptides (peptides 16, 23 and 24) contain an LPhe in place of the DPhe. These compounds differ from the DPhe compounds only in the conformation of the Phe side chain. It has already been reported that changing the LPhe in the endogenous melanocortin ligand α -MSH to a DPhe (to make NDP-MSH) results in a significant increase in potency.⁴ The results reported herein agree with this difference in potency. As compared to the DPhe compounds, the LPhe compounds were significantly less potent. However, the same trends are observed at the mMC1,3, and 4R as before. At each of these receptors, the Arg compounds were the most potent, followed by a significant loss of potency when a Lys was inserted, and an even greater loss of potency when the cation was substituted with an Ala. Once again, these data support the hypothesis of a significant cation- π interaction between Arg and Phe. A different trend was observed at the mMC5R. The Arg and Lys compounds were equipotent, and the Ala compound was 10-fold less potent than the other two compounds. This data may indicate that at this receptor, the identity of the cation is less important, and potency is maintained as long as a

positive charge is present. When the positive charge is completely removed, however, the potency is decreased, though not as significantly as at the other receptors. These data are depicted in Figure 5-8.

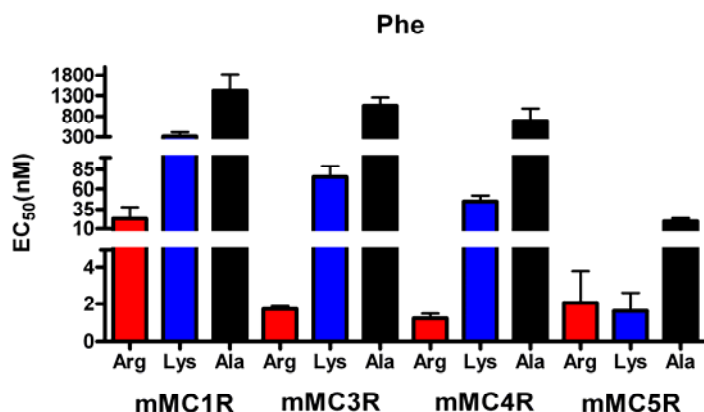


Figure 5-8. Bar graph of peptides 16, 23 and 24 with Phe as the aromatic system at the mMC1,3-5R.

D-Naphthylalanine (2')

SHU9119 is a cyclic melanocortin antagonist developed during SAR studies of MTII.^{117,118,255} The only difference between the two ligands is that SHU9119 contains a bulky naphthalene aromatic group in place of the DPhe in MTII.^{117,118,255} It has been suggested that the antagonist activity of SHU9119 is due to an interaction between DNal(2') and the adjacent Arg in which the aromatic modifies the conformation of Arg resulting in unique molecular interactions with the mMC3R and mMC4R.⁴³ As is depicted in Figure 5-6, the aromatic character of DPhe and DNal(2') are different and interact differently with Arg and the receptors. To test the theory that a cation- π interaction is involved in SHU9119's antagonist activity, the Arg was substituted with Lys and Ala (peptides 25 and 26) to investigate the effect of cation strength on antagonist activity.

When a Lys was substituted for Arg in compound 25, there was a decrease in potency at the mMC1R and mMC5R as compared to Arg, but the ligand retained its agonist activity. Like

SHU9119, peptide 25 is an antagonist at the mMC3R and mMC4R, except the affinity for the receptors is decreased as evidenced by K_i values ($K_i = -\log pA_2$).²³⁰ When Arg is replaced with Ala in peptide 26, the cation- π effect is removed, and the potency is decreased at the mMC1, 3 and 4R, though antagonist activity was retained at the mMC3R and mMC4R. At the mMC5R, however, there was no significant difference between peptides 17 and 26, indicating that the cation- π interaction may not be as important for activity at this receptor. Figure 5-9 shows a bar graph representation of these data.

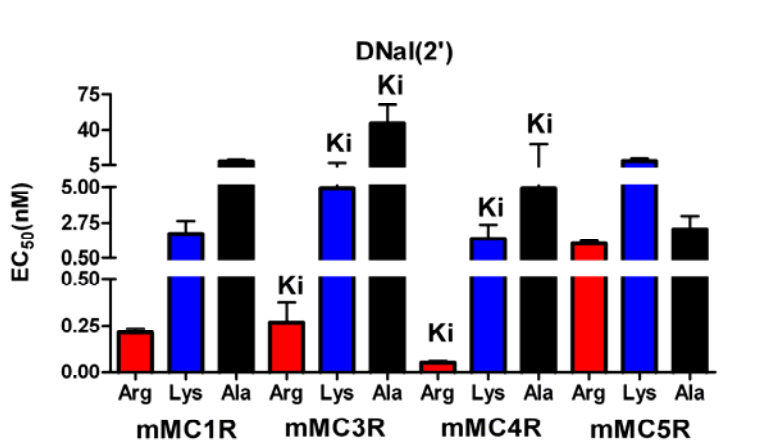


Figure 5-9. Bar graph of peptides 17, 25 and 26 with DNal(2') as the aromatic system at the mMC1,3-5R. Values at the mMC3R and mMC4R are antagonist K_i values.

Naphthylalanine (2')

Peptides 18, 27 and 28 differ from the DNal(2') compounds only in the positioning of the aromatic moiety. In this series an LNal(2') was used in conjunction with Arg, Lys, and Ala. Interestingly, while the D conformation of the aromatic produces peptides which are potent antagonists at the mMC3R and mMC4R, changing the conformation to the L form results in compounds with significantly decreased agonist activity. The expected Arg > Lys > Ala potency series was observed at all receptors, though the Ala peptide 28 was a high micromolar agonist at the mMC3R and did not possess any stimulatory activity at the mMC4R. The most potent compound in this series is the Arg peptide 18 at the mMC5R, with low nanomolar activity.

Substitution of the Arg resulted in significant decreases in potency, however. This is different from the other mMC5R series observed so far because the cation- π interaction seems to be more important when the aromatic is Nal(2') than when it is DPhe, Phe, or DNal(2'). A bar graph representation of these data is found in Figure 5-10.

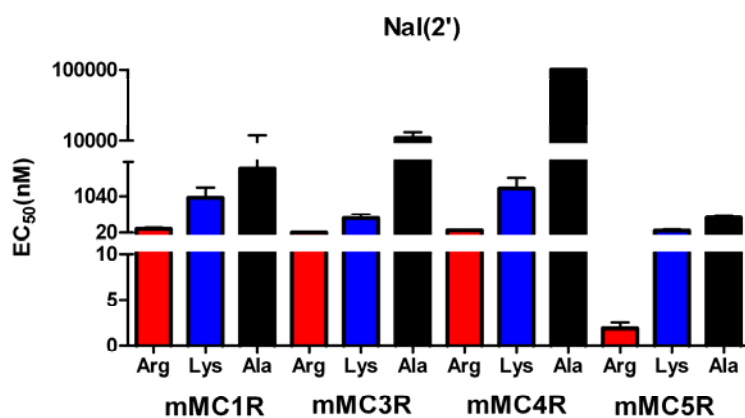


Figure 5-10. Bar graph of peptides 18, 27 and 28 with Nal(2') as the aromatic system at the mMC1,3-5R.

D-Naphthylalanine (1')

The next aromatic system investigated was DNal(1') (peptides 19, 29 and 30). DNal(1') differs from DNal(2') in the point of attachment of the naphthyl ring to the methyl linker. This results in a different interaction with the Arg cation and with the receptor. At the mMC1R, all three peptides were either sub- or low-nanomolar agonists, with no difference between the Arg and Lys peptides and only a slight 8-fold decrease in potency for the Ala peptide. At the other three receptors, all peptides were agonists and the potency series Arg > Lys > Ala is maintained, indicating the importance of the cation- π interaction at these receptors.

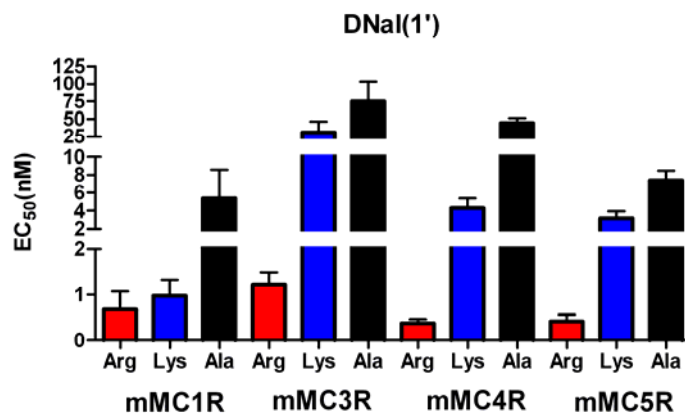


Figure 5-11. Bar graph of peptides 19, 29 and 30 with DNal(1') as the aromatic system at the mMC1,3-5R.

Naphthylalanine (1')

The final aromatic amino acid that was included was Nal(1') (peptides 20, 31 and 32). When compared with the D conformation of this amino acid, the potency was significantly decreased with the L form. Additionally, at the mMC1R there is little change in potency between Arg, Lys, and Ala. At the mMC3R, the Arg compound is the most potent, though the Lys and Ala compounds are approximately equipotent. An interesting effect is seen at the mMC4R. The expected Arg > Lys agonist trend was seen with the first two peptides, however the Ala peptide 32 was a partial agonist and antagonist at the mMC4R. There may be other unique interactions that are taking place between Nal(1'), Ala and the receptor which accounts for this antagonist activity. At the mMC5R the expected Arg > Lys > Ala trend is maintained.

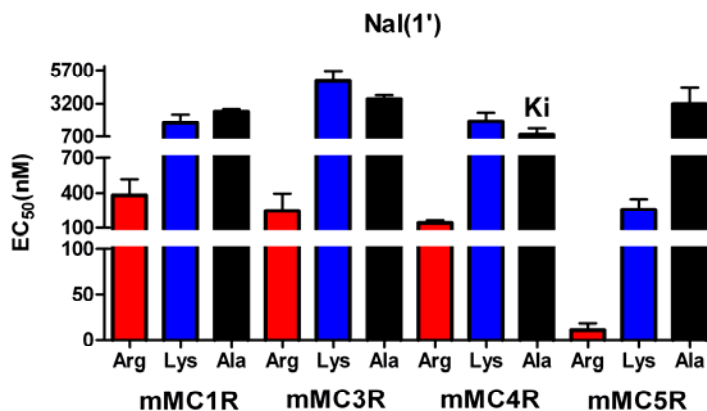


Figure 5-12. Bar graph of peptides 20, 31 and 32 with Nal(1') as the aromatic system at the mMC1,3-5R. The Ala compound 32 at the mMC4R is expressed as an antagonist Ki value.

Conformation Effects

An important observation that should be made from this study is that for each aromatic system investigated, the D form of the amino acid is significantly more potent than the L form. This is in accordance with previous studies investigating conformational differences at the aromatic position, especially in the case of the development of NDP-MSH from α -MSH.³⁰³ Holder *et al.* reported the differences between D and L conformations of the naphthylalanine derivatives (see Table 5-1), and also recognized the significant increase in potency when the L form was replaced with the D form.⁷ It is apparent that the D form of the aromatic amino acid allows for a more favorable interaction with the melanocortin receptors resulting in greater stimulatory activity.

Receptor Selectivity

Each receptor is unique in the way it responds to a particular ligand. Each melanocortin receptor has been characterized based on how it interacts with each endogenous and synthetic ligand and this is often the basis for the specific physiological activity of each receptor. It should be expected, therefore, that the strength and importance of the cation- π interaction at each receptor should be unique.

At the mMC1R, four aromatics: DPhe, Phe, DNal(2') and Nal(2') exhibited the hypothesized Arg > Lys > Ala potency series which suggests the importance of the cation- π interaction for activity. However, when the aromatics DNal(1') and Nal(1') were used, the cation- π effect was greatly decreased. In the case of DNal(1') the peptides still maintained subnanomolar activity, indicating that there are other important interactions responsible for activity at this receptor.

Cation- π interactions at the mMC3R seem to be very important for both agonist and antagonist activity. The only aromatic system that does not follow the Arg > Lys > Ala potency series is Nal(1'). Like the mMC3R, the Nal(1') system appears to interact through a unique mechanism. The only aromatic which exhibited antagonist activity was DNal(2'). No other naphthyl derivatives had any antagonist activity. It is concluded, therefore, that DNal(2') is unique in the way it interacts with Arg and the receptor to act as an antagonist.

The mMC4R is the receptor at which cation- π interactions seem to play the most important role in agonist activity. For all aromatic systems tested, Arg > Lys > Ala for both agonist and antagonist activity. Additionally, DNal(2') was the only aromatic system to have antagonist activity for all three peptides. No other naphthyl derivatives had antagonist activity at this receptor except for peptide 32, which contains the Nal(1')/Ala combination. It is unknown why this peptide has antagonist activity, but may be a result of the local unique environment created by this peptide.

The mMC5R has mixed cation- π specificities. When the aromatic is DPhe, Phe, or DNal(2') the cation- π interaction does not appear to be a significant factor affecting potency. The other aromatics Nal(2'), DNal(1'), and Nal(1'), however, appear to interact through a cation- π

interaction at this receptor. It is suspected that this is due to unique ligand-receptor interactions at the mMC5R.

Agonist vs. Antagonist Selectivity

Part of the original hypothesis for this study involved the agonist vs. antagonist selectivity between MTII and SHU9119.^{117,118,255} It has been proposed that the antagonist activity of SHU9119 is due to a unique interaction between the bulky aromatic DNal(2') group and the cationic character of Arg.⁴³ Based on the results of this study, it was observed that DNal(2') is the only naphthyl derivative in this work that had significant antagonist activity that was significantly affected by a cation- π interaction. The aromatic systems Nal(2'), DNal(1') and Nal(1') were not antagonists except for peptide 32, which was a weak antagonist at the mMC4R.

Conclusions

Several conclusions may be drawn from the information obtained in this study. First it appears that the original hypothesis is correct and there may be a significant cation- π interaction between the Arg and the adjacent aromatic amino acid in melanocortin ligands. This was confirmed by the observation that in the majority of peptides synthesized in this study the Arg compound was the most potent, followed by Lys, and finally Ala as the least potent compound. It was also observed that in each aromatic system tested, the D form of the amino acid was more potent than the L form. Additionally, DNal(2') is the only aromatic system tested which has antagonist activity at the mMC3R and mMC4R. An interesting observation is that the Nal(1')/Ala combination results in a peptide with antagonist activity at the mMC4R. These studies are significant as they provide important information which may be used in the future to design new peptide and non-peptide ligands for the melanocortin receptors.

CHAPTER 6
DESIGN OF PEPTIDOMIMETICS AND SMALL MOLECULES: 1,4-BENZODIAZEPINE-
2,5-DIONES AS nM MELANOCORTIN AGONISTS

Portions of this chapter are “in press” in the *Journal of Medicinal Chemistry*. 1,4-Benzodiazepine-2,5-diones were synthesized, purified, and analytically characterized by Krista R. Wilson in the Haskell-Luevano laboratory. Pharmacology was performed by Federico Portillo, Michael S. Wood, Nicholas B. Sorenson, Dong V. Phan, and Zhimin Xiang of the Haskell-Luevano laboratory. NMR analysis was done by Krista R. Wilson, Christine G. Joseph, and Rachel M. Witek of the Haskell-Luevano laboratory. NMR of compounds 40, 46, 47, 52, and 56 were performed by Jim Rocca of the University of Florida NMR Core Facility. Data analysis was performed by Krista R. Wilson and partially by Carrie Haskell-Luevano.

Introduction

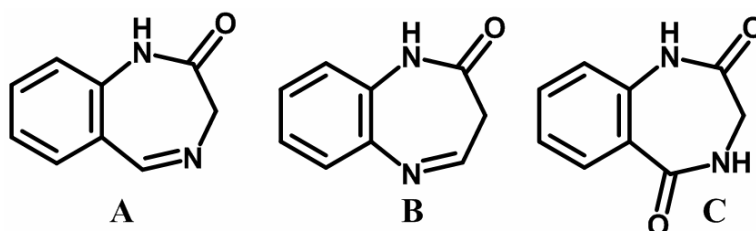


Figure 6-1. Structures of A. 1,4-benzodiazepine-2-one, B. 1,5-benzodiazepine-2-one and C. 1,4-benzodiazepine-2,5-dione templates.

The 1,4-benzodiazepines are an important class of privileged templates,³⁵ and numerous derivatives have been identified that have selective activities against a diverse array of biological targets.³⁶⁻⁴⁰ A subset of the 1,4-benzodiazepines, the 1,4-benzodiazepine-2,5-diones (Figure 6-1C), are the focus of this work. 1,4-Benzodiazepine-2,5-diones have been reported to possess anticonvulsant, anxiolytic, and antitumor properties, as well as being cholecystokinin receptor (CCK), opiate receptor and platelet glycoprotein IIb-IIIa antagonists,¹⁹⁰⁻¹⁹³ as well as having herbicidal properties.¹⁹⁴ In addition, the 1,4-benzodiazepine-2,5-dione core appears in a number of natural products.¹⁹⁵⁻¹⁹⁷

Information obtained from peptide related SAR studies may be used in the design of peptidomimetic and small molecule templates that are potent and selective for the melanocortin receptors. Peptides are not ideally suited for use as drugs due to their large molecular weight, high rate of first-pass metabolism in the stomach and small intestine, and extreme sensitivity to changes in pH or temperature; therefore it is desirable to obtain a small molecule drug. In the design of small molecules, the information obtained from the peptide SAR studies is used to create conformationally restrained peptides and/or small molecules. Further studies are done to optimize the molecule in regards to potency, selectivity, and toxicity. Small-molecule libraries have become an important part of the drug discovery process^{190,304-306} with particular emphasis placed upon the preparation and evaluation of libraries based upon privileged structures.³⁵ These structures display a number of different functionalities that result in a number of potent and specific drugs or candidates for different therapeutic targets.^{35,190,307}

Structure-activity relationship studies of the endogenous melanocortin agonists have shown that these ligands all contain the core tetrapeptide His-Phe-Arg-Trp.^{114,115} Based on these studies, synthetic peptide agonists of the melanocortin receptors were designed which are even more potent than the endogenous peptides, and contain a DPhe in place of the endogenous Phe.⁴ NMR studies of both endogenous and synthetic ligands have indicated the presence of a reverse turn mimetic in the Phe-Arg-Trp region.³⁰⁸⁻³¹⁰ A reverse turn, or β -turn, is a secondary structural motif found in peptides and proteins, and involving four amino acid side chains, termed i , $i+1$, $i+2$ and $i+3$.¹⁸ The carboxyl carbon of i and the N-H of $i+3$ are often hydrogen bonded to increase the stability of the structure. The reverse turn is defined by the following conditions: positions i , $i+1$, $i+2$, and $i+3$ are not in an α -helix, and the distance between $C\alpha(i)$ and $C\alpha(i+3)$ is less than 7\AA .¹⁸

agonists.^{26,27} The first heterocyclic non-peptide molecules that were identified as melanocortin agonists were based on a 9-membered heterocyclic ring system (Figure 6-2A,B).²⁶ These compounds were based on a β -turn motif, and were shown to be micromolar agonists at the mMC1R.²⁶ Bondebjerg *et al.* also did a study in which a thioether cyclized scaffold was used to mimic the β -turn found in the endogenous and synthetic peptides (Figure 6-2C).²⁷ These molecules were shown to be nanomolar agonists at the mMC1R, and the mMC3-5R.²⁷ These results indicate the importance of the reverse turn in the design of melanocortin ligands. As there are only a few bioactive conformations able to stimulate the receptors, it is desirable to design ligands with a more rigid template, which may increase the concentration of bioactive molecules in solution. The 1,4-benzodiazepine-2,5-dione template used in this study has been shown both to exhibit a reverse turn and to adopt a more rigid, planar conformation.^{326,327} The scaffold adopts a reverse turn-like conformation, enabling the modification of side chains to mimic the 3-dimensional conformation of amino acid side chains found in bioactive peptides. In this study, the template was modified to mimic the DPhe-Arg-Trp tetrapeptide in synthetic melanocortin ligands.

The term “privileged structure” was first coined in 1988 by John Ellman as a way to describe molecular substructures that were able to provide a framework for potent and selective ligands at multiple receptors.³⁵ At the time Ellman was studying the benzodiazepine structure, trying to develop potent CCK antagonists.³⁵ He noticed that there were subtle differences between structures that were active at the CCK, gastrin, or central benzodiazepine receptors. NMR analysis of the 3-D conformations of these molecules led him to hypothesize that these “privileged” substructures could be functionalized to create ligands that make specific interactions with different receptors.³⁵ Since then, extensive library analyses have identified a

plethora of substructures commonly found in small molecule drugs (See Figure 1-14 for more privileged templates).

Small molecule ligands based on many different privileged templates are shown in Figure 6-2. Figure 6-2D depicts an MC4R agonist containing the 2-phenyl-indole privileged template.³¹¹ Another template, the spiro-piperidine-indane substructure, was used in the design of Figure 6-2E, which is an agonist at the MC4R.³¹² Piperidine and its derivatives have been used to design several melanocortin ligands. Dyck *et al.* synthesized a series of aryl piperidine derivatives based on growth hormone secretagogue compounds that were potent and selective for the MC4R (Figure 6-2F).³¹³ Another group designed melanocortin ligands from the bis-piperazine template that were meant to inhibit the binding of AGRP to the MC4R. Though this end was not realized, the compound in Figure 6-2G was reported to antagonize the MC4R better than AGRP.³¹⁴ Richardson *et al.* also used the piperazine template to design potent MC4R ligands (Figure 6-2H).³²⁸ Finally, Xi *et al.* used a series of piperazine-succinamide derivatives to create small molecules with nM activity at the MC4R (Figure 6-2I).³²⁹

Merck scientists developed a group of molecules that contained the piperidine core as well as a tetrazole ring.³¹⁷ The compound in Figure 6-2J was able to selectively agonize the MC4R over the other melanocortin subtypes.³¹⁷ Herpin *et al.* was able to design small molecules based on piperidine that were selective for the MC1R over the MC4R (Figure 6-2K).³¹⁸ Finally, Ujjainwalla *et al.* reported a group of compounds that contained the pyridazinone core and was able to stimulate the MC4R.³¹⁹ Optimization of these compounds by Merck resulted in compounds with improved binding and potency at the MC4R (Figure 6-2L).³¹⁹

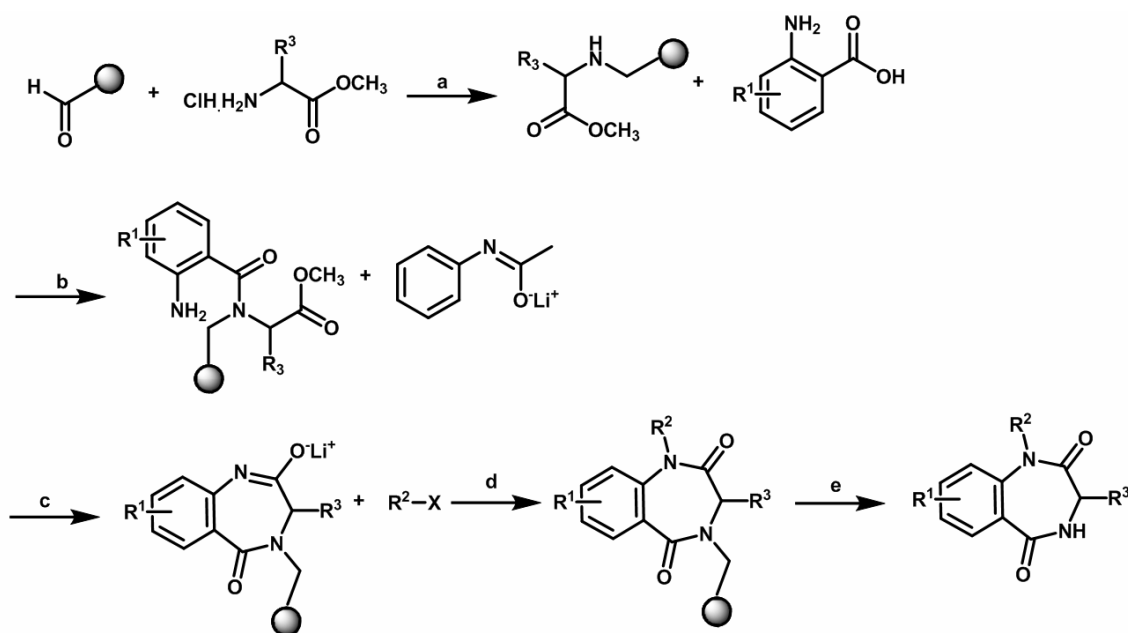
Several other templates have been used with some success. The tetrahydropyran scaffold was used to create the compound in Figure 6-2M, which is a partial agonist at the MC4R,^{320,321}

as well as the compound in Figure 6-2N, which mimics the side chain of arginine, but was only able to stimulate the MC1R at high concentrations and not the MC4R.^{320,321} Pan *et al.* designed compounds containing a 1,2,4-thiazolium ring which was able to bind MC4R and when injected into rats resulted in a decrease in food intake (Figure 6-2O).³²² Vos *et al.* used a cyclocondensed imidazole ring to design antagonists of the MC4R which were orally active and concentrated in the brain (Figure 6-2P).³²³ Finally, Cain *et al.* has recently reported a peptide mimetic that mimics the β -turn secondary structure and was able to selectively stimulate the MC1R (Figure 6-2Q).³²⁴

It is clear that there is a strong precedent for the use of privileged structures in the design of melanocortin ligands. Therefore it was hypothesized that a library of small molecule 1,4-benzodiazepine-2,5-diones may be created that mimic the side chains of the His-Phe-Arg-Trp melanocortin agonist core tetrapeptide resulting in agonist activity at the melanocortin receptors. Christine G. Joseph, a former graduate student in the Haskell-Luevano lab originally investigated this template as a way to create selective melanocortin ligands (Table 6-1). In order to achieve these goals, a number of synthetic schemes for the solid-phase organic synthesis of benzodiazepines were evaluated.^{191-194,198-203,330} The optimized synthesis approach utilized is shown in Schemes 6-1 and 6-2.^{190,194,200,304} It begins with the attachment of the α -amino ester to the solid support, followed by acylation with an anthranilic acid, base-catalyzed lactamization, alkylation, and cleavage. The sequence relies on the incorporation of three different components, anthranilic acids (R1), alkylating agents (R2), and α -amino esters (R3) which are available commercially with appropriate side-chain protection. Synthesis with this scheme also provided high yield and relatively clean crude products. Several compounds were synthesized, analytically characterized and pharmacologically characterized by Christine G. Joseph for functional agonist

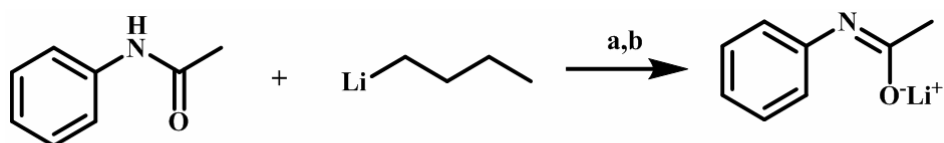
activity at the melanocortin receptors (MC1R, and MC3-5Rs). The results are shown in Table 6-

1.



Reaction conditions: (a) $\text{NaBH}(\text{OAc})_3$, DMF/ 1% AcOH, rt, 2h; (b) EDC in NMP, rt, overnight; (c) rt, 30h, under argon; (d) rt, until pH=5; (e) TFA/Me₂S/H₂O (90:5:5), rt, 50h.

Scheme 6-1. Solid-phase organic synthesis of 1,4-benzodiazepine-2,5-diones.



Reaction conditions: (a) -78°C , 30min, under argon; (b) DMF, -78°C , 15min.

Scheme 6-2. Synthesis of acetanilide-lithium salt.

Based on the results of Dr. Joseph's work in Table 6-1, an additional twenty compounds were designed by Krista Wilson to investigate the structural requirements necessary for activity at the melanocortin receptors, these are shown in Figure 6-3. Three aminobenzoic acid derivatives were used at the R1 position: a hydrogen, a 9-methyl, and an 8-chloro; five different alkylating agents were used at the R2 position: benzyl, biphenyl, naphthyl, propyl, and butyl; and three amino acid esters were used at the R3 position: benzyl (phenylalanine), propyl guanidine

(arginine), and 4-aminobutyl (lysine) (Figure 6-4). It was hypothesized that these compounds would allow the exploration of 3-D space in the molecular recognition and activation of the melanocortin receptors by the 1,4-benzodiazepine-2,5-dione class of privileged structures and to determine structural requirements for this interaction.

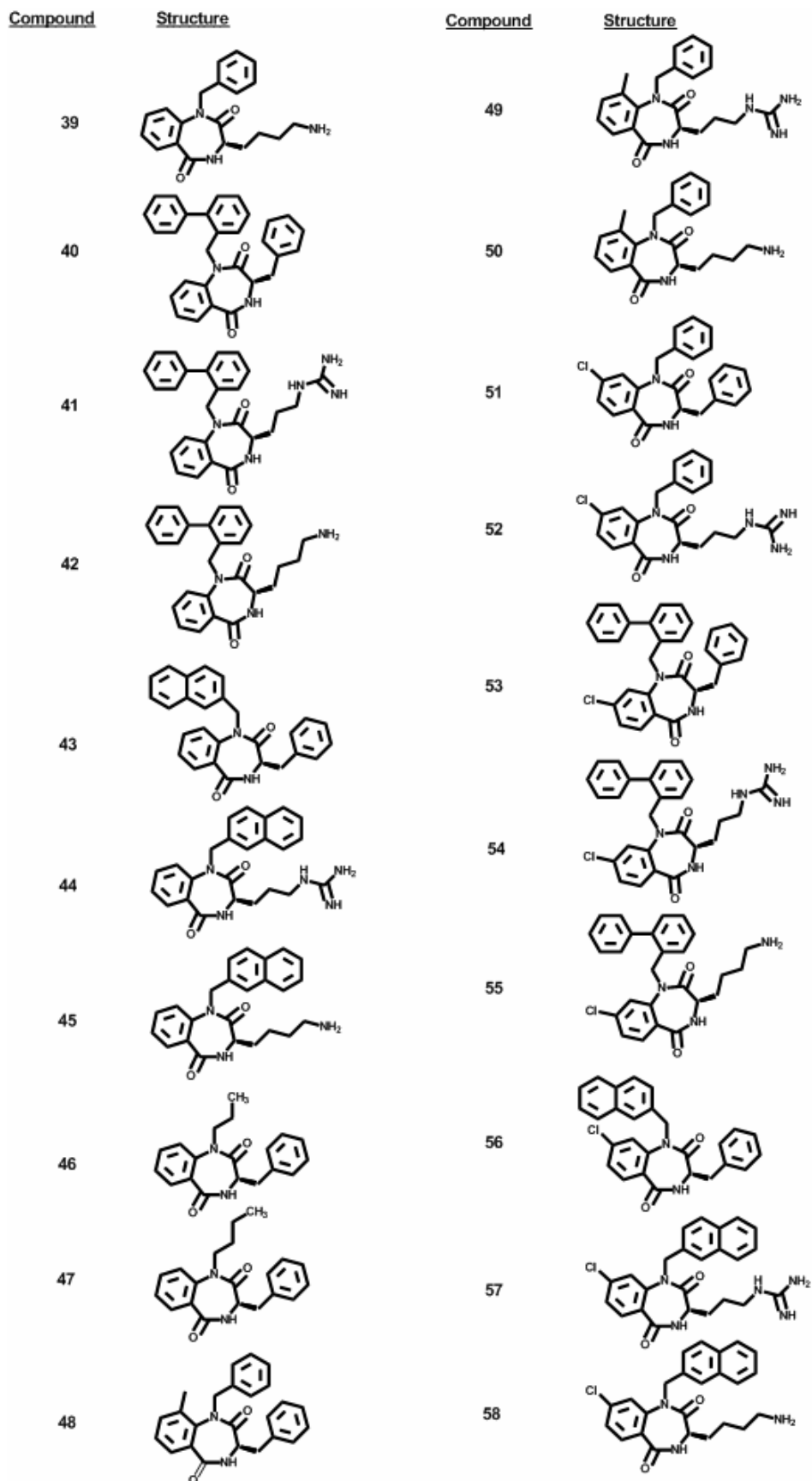


Figure 6-3. Structures of 1,4-benzodiazepine-2,5-diones synthesized in this study by KRW.

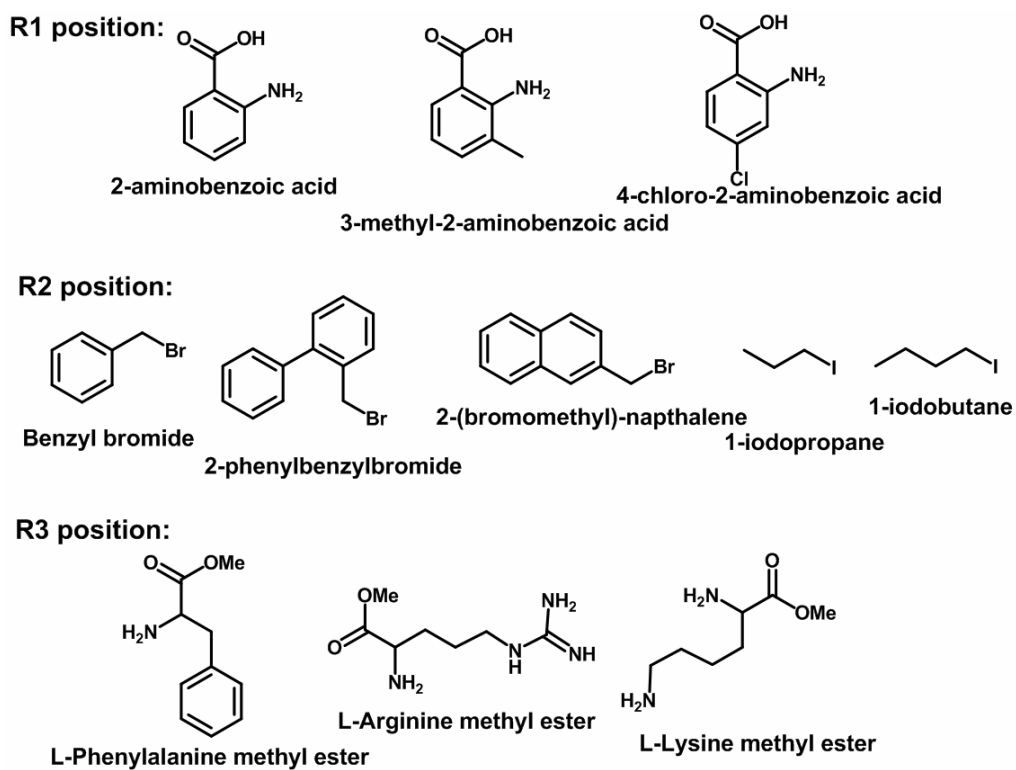
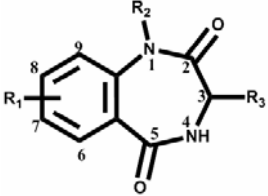


Figure 6-4. Structures of building blocks used to synthesize 1,4-benzodiazepine-2,5-diones 39-58.

Table 6-1. Pharmacology data of compounds synthesized by Dr. Christine Joseph.

		Agonist EC ₅₀ (μM)					
Compound	Structure	mMC1R	mMC3R	mMC4R	mMC5R		
α-MSH	Ac-Ser-Tyr-Ser-Met-Glu-His-Phe-Arg-Trp-Gly-Lys-Pro-Val-NH ₂	0.0007±0.00023	0.00214±0.00046	0.00256±0.00029	0.0020±0.00020		
Template: 							
	R ₁	R ₂	R ₃	mMC1R	mMC3R	mMC4R	mMC5R
33	H	Benzyl	Benzyl	32.9±8.2	No agonist	No agonist	No agonist
34	H	Benzyl	Propyl guanidine	16.5±6.0	No agonist	No agonist	No agonist
35	H	Benzyl	1H-indol-3-yl-methyl	4.6±2.5	No agonist	No agonist	No agonist
36	9-Methyl	Benzyl	1-Benzyl-1H-indol-3-yl-methyl	21.6±6.9	No agonist	No agonist	No agonist
37	8-Chloro	Benzyl	4-aminobutyl	0.048±0.023	0.32±0.08	0.24±0.075	0.087±0.038
38	8-Chloro	Napthalene-2-yl-methyl	1H-indol-3-yl-methyl	No agonist	No agonist	No agonist	No agonist

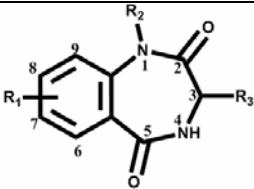
Indicated errors represent the standard error of the mean, determined from at least four independent experiments. “No agonist” indicates that no agonist activity was observed at up to 100 μM. Agonists that possessed some stimulatory response at 100 μM concentrations are indicated as percent response relative to the maximal response observed for the forskolin control.

Table 6-2. Analytical data of 1,4-benzodiazepine-2,5-diones synthesized in this study.

Compound	HPLC k' (system 1)⁹⁰	HPLC k' (system 2)⁹⁰	% purity	m/z (M, calcd)	m/z (M+1, expt)
39	5.5	6.8	>97	336.9	336.9
40	10.9	15.3	>98	432.5	433.1
41	8.1	10.8	>98	442.5	440.6
42	7.1	10.1	>97	413.5	412.6
43	10.8	13.4	>98	406.5	405.6
44	7.1	9.2	>98	416.5	414.6
45	6.9	9.1	>98	387.5	386.7
46	7.8	10.7	>98	308.4	309.5
47	8.5	12.3	>99	322.4	323.1
48	12.1	11.4	>95	370.4	369.9
49	5.8	8.1	>97	380.4	378.7
50	5.6	7.4	>95	351.4	350.8
51	10.6	13.3	>97	390.9	389.7
52	6.6	9.5	>99	399.9	401.1
53	12.5	13.6	>98	467.0	465.7
54	9.2	12.0	>97	477.0	474.6
55	8.1	11.4	>96	448.0	446.7
56	11.3	17.2	>99	440.9	440.6
57	7.7	10.8	>95	451.0	448.6
58	8.0	12.1	>97	421.9	422.5

HPLC k' = c[(peptide retention time – solvent retention time)/(solvent retention time)] in solvent system 1 (10 % acetonitrile in 0.1 % trifluoroacetic acid/water and a gradient to 90 % acetonitrile over 35 min) or solvent system 2 (10 % methanol in 0.1 % trifluoroacetic acid/water and a gradient to 90 % methanol over 35 min). An analytical Vydac C18 column (Vydac 218TP104) was used with a flow rate of 1.5 ml/min. The peptide purity was determined by HPLC at a wavelength of 214 nm by comparison of the area under the curve of compound peak compared to all other peaks. Mass spectroscopy was performed on a Voyager-DE Pro (University of Florida Protein Core).

Table 6-3. Pharmacology data of 1,4-benzodiazepine-2,5-diones synthesized in this study by Krista Wilson.

Compound	Structure	Agonist EC ₅₀ (μM)					
		mMC1R	mMC3R	mMC4R	mMC5R		
α-MSH	Ac-Ser-Tyr-Ser-Met-Glu-His-Phe-Arg-Trp-Gly-Lys-Pro-Val-NH ₂	0.0007±0.00023	0.00214±0.00046	0.00256±0.00029	0.0020±0.00020		
 <p>Template:</p>							
	R ₁	R ₂	R ₃	mMC1R	mMC3R	mMC4R	mMC5R
39	H	Benzyl	4-aminobutyl	50%@100μM	No Agonist	No Agonist	No Agonist
40	H	Biphenyl-2-yl-methyl	Benzyl	0.23±0.0027	4.2±0.07	1.97±1.23	60%@100μM
41	H	Biphenyl-2-yl-methyl	Propyl guanidine	38.8±8.9, 70%	No Agonist	No Agonist	No Agonist
42	H	Biphenyl-2-yl-methyl	4-aminobutyl	59.5±15.9	No Agonist	No Agonist	60%@100μM
43	H	Naphthalen-2-yl-methyl	Benzyl	50%@100μM	No Agonist	No Agonist	60%@100μM
44	H	Naphthalen-2-yl-methyl	Propyl guanidine	34.2±10.1, 70%	No Agonist	No Agonist	70%@100 μM
45	H	Naphthalen-2-yl-methyl	4-aminobutyl	71.6±20.1	No Agonist	No Agonist	69.7±18.3, 75%
46	H	Propyl	Benzyl	6.9±2.6	80%@100μM	35±16	3.3±1.0
47	H	Butyl	Benzyl	70%@100μM	No Agonist	No Agonist	No Agonist
48	9-Methyl	Benzyl	Benzyl	50%@100μM	No Agonist	No Agonist	No Agonist
49	9-Methyl	Benzyl	Propyl guanidine	60%@100μM	No Agonist	No Agonist	No Agonist
50	9-Methyl	Benzyl	4-aminobutyl	0.006±.004, 50%	No Agonist	No Agonist	No Agonist
51	8-Chloro	Benzyl	Benzyl	36.3±4.9, 75%	No Agonist	No Agonist	60%@100μM
52	8-Chloro	Benzyl	Propyl guanidine	1.8±0.10	30.7±23	60%@100μM	17±4.5
53	8-Chloro	Biphenyl-2-yl-methyl	Benzyl	50%@100μM	No Agonist	No Agonist	No Agonist
54	8-Chloro	Biphenyl-2-yl-methyl	Propyl guanidine	20.5±4.7, 75%	No Agonist	50%@100μM	No Agonist
55	8-Chloro	Biphenyl-2-yl-methyl	4-aminobutyl	No Agonist**	No Agonist	No Agonist	No Agonist
56	8-Chloro	Naphthalen-2-yl-methyl	Benzyl	4.7±1.3	23.3±2.5	80%@100μM	4.35±1.7
57	8-Chloro	Naphthalen-2-yl-methyl	Propyl guanidine	60%@100μM	No Agonist	No Agonist	70%@100μM
58	8-Chloro	Naphthalen-2-yl-methyl	4-aminobutyl	3.4±0.07	30%@100μM	30%@100μM	65%@10μM

Indicated errors represent the standard error of the mean, determined from at least four independent experiments. "No agonist" indicates that no agonist activity was observed at up to 100μM. Agonists that possessed some stimulatory response at 100 μM concentrations are indicated as percent response relative to the maximal response observed for the forskolin control.

**Compound 59 was toxic at the mMC1R at 100μM.

Results

Analytical characterization and agonist functional data for the 1,4-benzodiazepine-2,5-dione molecules synthesized in this study are summarized in Tables 6-2 and 6-3, respectively. All functional agonist data are expressed as μM EC_{50} values with the associated standard error of the mean (SEM) derived from at least three independent experiments provided. $^1\text{H-NMR}$ and proton assignments of compounds 39-58 may be found in Appendix A.

Compound 39 contains a hydrogen at R1, a benzyl group at R2, and a 4-aminobutyl group at R3. At the mMC1R, compound 39 exhibits 50% maximal response. No stimulatory response was observed at the mMC3-4R, but some agonist activity was seen at the mMC5R, with 40% maximal response as compared to the forskolin control at up to 100 μM concentrations.

Compounds 40-42 contain a hydrogen at the R1 position, a biphenyl-2-yl-methyl group at the R2 position and are differentially modified at the R3 position. Compound 40, containing a benzyl moiety at the R3 position, is a nM agonist at the mMC1R, is 18-fold mMC1R versus mMC3R selective, is ca 9-fold mMC1R versus mMC4R selective, exhibits μM agonist potency at the mMC3R and the mMC4R, and is able to stimulate a 60% maximal forskolin response at the mMC5R. When the R3 position is substituted with a propyl guanidine group in compound 41, the molecule now is a μM agonist at the mMC1R with 70% maximal activity, and exhibits no activity at the mMC3-5R. When R3 is a 4-aminobutyl group in compound 42, the molecule is a full micromolar agonist at the mMC1R, and possesses some stimulatory activity at the mMC5R, but no activity at the mMC3-4R.

Compounds 43-45 have an H in the R1 position, and a naphthalene-2-yl-methyl moiety at the R2 position, but they differ at R3. When R3 is a benzyl in compound 43, there is no stimulatory activity at the mMC3-4R, but 50% and 60% maximal activity was observed at the mMC1R and mMC5R respectively compared to maximal forskolin response. Compound 44

contains a propyl guanidine group at position R3, and is a micromolar agonist with 70% maximal activity at the mMC1R. There is no activity at the mMC3-4R and only 70% maximal activity was observed at the mMC5R. Compound 45 contains a 4-aminobutyl group at R3, and is a high μM agonist at the mMC1R. It does not contain any stimulatory activity at the mMC3-4R, and a micromolar agonist with 75% maximal response at 100 μM as compared to forskolin control.

Compounds 46-47 each have an H at R1 and a benzyl moiety at R3, though they differ at the R2 position. When R2 is a propyl group in compound 46, μM full agonist activity is observed at the mMC1R, mMC4R, and mMC5R with only a 80% maximal forskolin response at the mMC3R. When R2 position contains the butyl group in compound 47, only a 70% maximal forskolin stimulation response is observed at the mMC1R and no stimulatory response is observed at any of the other receptors.

Compounds 48-50 each contain a 9-methyl group at the R1 position and a benzyl at the R2 position, but differ at R3. When R3 is a benzyl group in compound 48, there is only 50% maximal stimulation at the mMC1R as compared to forskolin control, and no stimulatory response observed at the mMC3-5R. When position R3 contains a propyl guanidine moiety as in compound 49, 60% maximal activity is observed at the mMC1R, though no stimulatory effect was observed at the mMC3-5R. Compound 50 contains a 4-aminobutyl group at the R3 position, and interestingly is a nanomolar partial agonist at the mMC1R, but only 50% maximal activity was observed. No activity was seen at the other receptors.

Compounds 51-52 contain an 8-chloro substitution at R1 and a benzyl at R2, but differ at R3. Compound 51 contains a benzyl at R3, and is a micromolar agonist with 75% activity at the mMC1R. 51 does not stimulate the mMC3-4Rs, and exhibits only 60% maximal stimulation at the mMC5R as compared to forskolin control. Compound 52, containing a propyl guanidine

group at R3, resulted in full μM agonist activity at the mMC1, mMC3, and mMC5 receptors, and 60% maximal activity at the mMC4R.

Compounds 53-55 all contain an 8-chloro group at the R1 position and a biphenyl-2-yl-methyl moiety at the R2 position, but differ at R3. When R3 is a benzyl group in compound 53, no agonist activity was observed at the mMC3-5R, and only weak stimulatory activity was observed at the mMC1R. Compound 54 contains a propyl guanidine group at the R3 position, and exhibits μM agonist activity at the mMC1R, but no stimulatory activity was observed at the mMC3-4R, and only slight stimulatory activity was observed at the mMC5R. When the R3 position is substituted with a 4-aminobutyl group in compound 55, there is no agonist activity observed at the mMC1,3-5R. Interestingly, at the mMC1R, compound 55 was toxic at 100 μM concentrations.

Compounds 56-58 contain an 8-chloro at the R1 position and a naphthylene-2-yl-methyl group in the R2 position, with differential substitution at R3. Compound 56, containing a naphthyl side chain at R2 and a benzyl group at R3, resulted in a μM agonist at the mMC1R, mMC3R, and mMC5R but was only able to stimulate the mMC4R to 70% maximal activity observed for the forskolin control at 100 μM concentrations. Compound 57 contains a propyl guanidine group at R3 and only exhibits weak stimulatory activity at the mMC1R and mMC5R, with no activity at the mMC3-4R. Compound 58, differing from compound 56 by the presence of the 4-amino butyl moiety at the R3 position, is equipotent with compound 56 at the mMC1R yet was only able to generate weak stimulatory responses at the mMC3R, MC4R, and mMC5R at 100 μM concentrations.

Discussion

The benzodiazepine template has been widely studied as a scaffold for non-peptide drugs.³⁵ The core was first identified as a CCK antagonist with the isolation of asperlicin, a

natural product from *Aspergillus alliaceus*.³³¹⁻³³³ Though it showed antagonist activity at the CCK receptor, asperlicin did not exhibit good bioavailability, leading researchers to develop new ligands based on the benzodiazepine core. Many of these compounds have been shown to exhibit better pharmacokinetic properties than the natural product. Additional studies have resulted in compounds that are selective for the CCKA (gut) receptor versus the CCKB (brain) receptor.³³⁴⁻³³⁹ Derivatives have been identified which have properties as anxiolytics, κ -opioid receptor agonists,⁴¹ oxytocin receptor antagonists,^{37,38} endothelin antagonists,³⁴⁰ HIV Tat antagonists,³⁹ and reverse transcriptase inhibitors⁴⁰ among others. As many targets are members of the G-protein coupled receptor super family (i.e. cholecystinin, κ -opioid, oxytocin, and endothelin receptors), it was hypothesized that benzodiazepine derivatives could be designed as melanocortin ligands.

Traditionally, benzodiazepines have been used as anxiolytics and sedatives, in which they serve as allosteric enhancers of the GABA receptors. In this role, benzodiazepines bind to a distinct site on the GABA receptor, where they potentiate the effect of γ -aminobutyric acid (GABA), allowing for increased opening of postsynaptic chloride channels leading to hyperpolarization of cell membranes and resulting in sedative and hypnotic CNS effects. The lipophilic nature of these compounds combined with their small size enables them to cross the blood brain barrier (BBB), and exert their CNS effects. As the hMC4R is centrally expressed, a small molecule melanocortin drug would need to cross the BBB in order to bind to their target receptors. As the benzodiazepine template is able to cross the BBB and has been shown to have activity at other GPCRs, it may be possible to design small molecule ligands of the melanocortin receptors with significant *in vivo* CNS activity. One caveat of this template may be presence of undesirable side effects due to binding to the GABA receptor.

The 1,4-benzodiazepine-2,5-dione library synthesized in this study was designed to interact with proposed binding sites in the melanocortin receptors. Homology molecular modeling of the mMC1R^{44,341} and the mMC4R^{43,48-50,342} suggest the presence of hydrophobic and electrostatic binding pockets which are essential for binding of the melanocortin ligands to the receptor. Based on the results of this study, it is proposed that the p(Cl)-phenyl ring of the benzodiazepine and an aryl side chain may interact with the hydrophobic pockets and that a cationic component may interact with the anionic binding pocket.

The benzodiazepines reported herein were designed based on a set of 1,4-benzodiazepine-2,5-dione compounds synthesized by Christine G. Joseph of the Haskell-Luevano laboratory that were shown by functional analysis to have activity at the melanocortin receptors. These results are reported in Table 6-1 and a summary follows.

Compounds 33-38 in Table 6-1 represent those compounds synthesized by Christine G. Joseph. These studies revealed four compounds selective for the mMC1R and one compound with nanomolar activity at all melanocortin receptors. Compounds 33-35 are identical in that they all contain a hydrogen at position R1 and a benzyl at R2. They differ only at the R3 position, where 33 contains a benzyl, 34 a propyl guanidine, and 35 a 1H-indol-3-yl-methyl. These compounds were micromolar agonists at the mMC1R and had no activity at any of the other receptors. Potency increased from 33 through 35, showing the potency series 1H-indol-3-yl-methyl > propyl guanidine > benzyl where the indole compound is the most potent. Additionally, R1 substituents were varied, incorporating either a H, a 9-methyl, or an 8-chloro group. Compounds 33 and 36 were identical except for the substitution of a 9-methyl group for the hydrogen in compound 36. This compound was less potent than 33, but still maintained micromolar agonist potency at the mMC1R. When R1 was changed to an 8-chloro in compound

37, there was nanomolar activity observed at all melanocortin receptors tested, making this compound very promising for lead optimization. Finally, when a naphthalene group was inserted into position R3 in compound 38 there was no activity observed at any of the receptors.

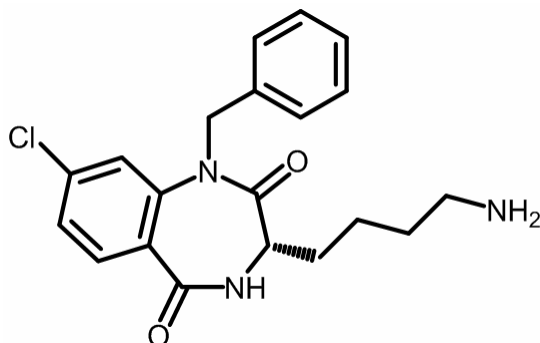


Figure 6-5. Structure of Compound 37, a nanomolar agonist at all melanocortin receptors tested.

These studies are highly significant as they have identified a small molecule compound, 37, which possesses nanomolar activity at the mMC1,3-5R (Figure 6-5). Micromolar mMC1R agonists were also identified. Based on these interesting pharmacology results, a new series of compounds (Compounds 39-58) were designed in order to investigate the structural requirements necessary for benzodiazepine activity at the melanocortin receptors, and to probe the structure-activity relationships at each point of diversity. The numbering system used as well as the location for the three points of diversity are shown in the figure labeled “Template” in Table 6-3. Building blocks are shown in Figure 6-4.

Position R1. Three different structural elements were used at position R1: a hydrogen (compounds 39-47), a 9-methyl (compounds 48-50), and an 8-chloro (compounds 51-58). This position was derived from the substituted 2-aminobenzoic acids used during synthesis (Figure 6-4). Electronically, these substituents represent three different electronic effects when coupled with an aromatic system. The hydrogen does not contribute any electronic effects to the aromatic ring, so the contribution to the pharmacophore represents only an aromatic ring. The methyl group, however, is an electron-donating substituent, which may lead to an increased electron

density on the face of the aromatic π system. The 8-chloro represents a highly electronegative moiety, which is electron-withdrawing, thereby decreasing the electron density on the aromatic face. Electronegative halogens have been shown to act as electron acceptors, and may interact with the π bonds of aromatics or with the π systems of peptide bonds. They may also interact with the lone pairs of N, O, or S. Studies of π - π stacking in peptides have suggested that the addition of an electron-withdrawing group in the para position on a phenyl ring increases activity.³⁴³⁻³⁴⁵ Addition of chlorine creates an electron-deficient ring which may interact favorably with the relatively electron-rich ring of tyrosine.³⁴⁶ Based on this information, it may be proposed that the halogenated ring of the benzodiazepine template may interact with the receptor to create a favorable π -stacking charge-transfer relationship, resulting in increased agonist activity.

When introduced into the 1,4-benzodiazepine-2,5-dione template, some general trends were observed. First is that when R1 is a hydrogen, almost all compounds have some activity at the mMC1R and mMC5R, but no activity at the mMC3-4R. Exceptions are compounds 40 and 46, which exhibit activity at all melanocortin receptors tested. Compounds substituted with a 9-methyl at R1 followed a similar trend, with all three compounds tested having activity only at the mMC1R. When R1 was an 8-chloro, the pharmacology was more complex, with some compounds having activity at between one and four receptors, and other compounds with no activity observed. Due to the complex pharmacology observed, it is proposed that though position R1 may be important for activity in combination with other factors, it does not appear that position R1 alone is responsible for individual effects, though the 8-chloro group does seem to confer more activity at the mMC3-4R, while the hydrogen and 9-methyl have more activity at the mMC1R, and some at the mMC5R.

Position R2. Another level of diversity was added at position R2. These five groups were derived from alkylation with the corresponding alkyl or aryl halide (Figure 6-4). The bromide derivatives were used for the benzyl, biphenyl, and naphthyl moieties, and the iodo derivative was used to add the propyl and butyl groups due to low reactivity of the bromo derivatives. Each of these derivatives was chosen for a reason based on previous peptide SAR data. The benzyl group was chosen due to its similarity with the Phe in the core tetrapeptide sequence His-Phe-Arg-Trp, which has been shown many times to be essential for activity at the melanocortin receptors.¹¹⁶ The biphenyl group, when substituted for Phe in the tetrapeptide Ac-His-Phe-Arg-Trp-NH₂ has been shown to stimulate the mMC1, 4, and 5 receptors with nanomolar activity when in the D form, and to have micromolar activity at the mMC1,5R in the L form.⁷ Naphthyl derivatives have been shown to have significant effects on pharmacology when introduced into melanocortin peptides. When DNal(2') was introduced into the synthetic cyclic agonist MTII, the molecule retained agonist activity at the mMC1,5R, but was converted into a potent antagonist at the mMC3,4R.^{116-118,255} Studies of the melanocortin tetrapeptide⁷ and other melanocortin ligands^{142,347} have identified more templates that are converted into antagonists at the mMC3,4R by addition of a DNal(2'). Interestingly, use of the L form of Nal(2') or the Nal(1') derivative results in ligands which are agonists at the melanocortin receptors, but with a significant decrease in potency as compared to Phe or DPhe derivatives.⁷ Propyl and butyl derivatives were chosen to see the effects of an alkyl substituent. Aliphatic chains have been shown to increase the potency and prolong the effects of the tetrapeptide His-Phe-Arg-Trp-NH₂ *in vitro*.³⁴ Additionally, it was desired to see the difference of an alkyl and aryl group at this position.

From the compounds synthesized by Christine G. Joseph, it appeared that the combination of hydrogen at R1 and a benzyl at R2 resulted in compounds with activity at the mMC1R (see

compounds 33-38, Table 6-1). This assessment seems to be accurate since compound 39 also had activity at the mMC1R and at no other receptors. When a benzyl at R2 was combined with a 9-methyl at R1, Dr. Joseph reported compound 36, which also had activity at only the mMC1R. Compounds 48-50 also contained this combination and were agonists at the mMC1R only. Finally, when Dr. Joseph coupled a benzyl with an 8-chloro at R1, compound 37 was created, which possessed nanomolar activity at all melanocortin receptors. In response, compounds 51 and 52 were synthesized. Compound 51 exhibited some activity at the mMC1,5R and no activity at the mMC3,4R, and compound 52 had micromolar activity at the mMC1, 3, and 5R, but only slight stimulatory activity at the mMC4R. From these studies it may be inferred that combining a benzyl at position R2 with either a hydrogen or 9-methyl at R1 results in compounds which are only active at the mMC1R. Compounds with an 8-chloro at R1 and a benzyl at R2 were shown to have increased activity at the mMC3,4R over the other compounds and appears to be important for conferring activity at the mMC3,4R.

The next R2 group that was investigated was the biphenyl moiety. When coupled with a hydrogen at R1, three compounds with distinct pharmacology were obtained (compounds 40-42). These compounds differed significantly in their activity at each receptor, and thus it is concluded that the differences are due to the R3 position and will be discussed below. When the biphenyl was grouped with an 8-chloro at R1, compounds 53-55 were obtained. These compounds had less activity than the hydrogen/biphenyl compounds and only two had activity at the mMC1R. Compound 55 had no activity at any of the receptors tested and in fact was toxic at the mMC1R, causing cells to die during stimulation. The 8-chloro/biphenyl combination does not appear to be tolerated well, and effects are highly variable based on the R3 substituent.

Only one compound containing a naphthyl group at the R2 position was synthesized by Dr. Joseph (compound 38) and this compound did not have any activity at the melanocortin receptors tested. Since the naphthyl moiety has been shown to convert ligands into melanocortin antagonists,^{117,118,255} this compound was also tested for antagonist activity at the mMC3,4R, however no activity was observed. To further investigate the effects of this group on ligand potency, the naphthyl was combined with either a hydrogen or 8-chloro at the R1 position. Compounds 43-45 contain the hydrogen/naphthyl combination and all compounds were micromolar mMC1R and mMC5R agonists. These results were very similar to the hydrogen/biphenyl combination and it does not appear that one is preferred over the other, though the benzyl compounds were more potent than either. Compounds 56-58 possess an 8-chloro at R1 and a naphthyl at R2. Although compound 57 only weakly stimulates the mMC1,5R, there is no activity at the mMC3,4R. Compounds 56 and 58, however, had activity at all four receptors. These results suggest that the 8-chloro/naphthyl combination is more highly favored at the melanocortin receptors than the 8-chloro/biphenyl combination, possibly because the naphthyl group is in a better position to make key ligand-receptor interactions.

Two aliphatic groups were tested at the R2 position, propyl (compound 46) and butyl (compound 47). These compounds were identical at positions R1 and R3, differing only at position R2. Additionally, the only difference between the substituents used at R2 is the addition of one methyl in compound 47. Interestingly, the propyl compound is active at all four melanocortin receptors, while the butyl compound has only slight agonist activity at the mMC1R. N-terminal capping of the tetrapeptide Ac-His-DPhe-Arg-Trp-NH₂ by Holder *et al.* revealed that activity increased with increasing chain length.³⁴ This is different from the current data, where the propyl is more potent than the butyl. This may be due to a different mechanism

of action. It was proposed that the capped tetrapeptide may have more activity because the aliphatic group associates with the plasma membrane, prolonging the association of the ligand with the receptor.³⁴ The R2 position of the 1,4-benzodiazepine-2,5-diones may interact differently than the tetrapeptide. It would be interesting to conduct further studies incorporating aliphatic groups of differing lengths, both longer and shorter than those already tested. It may be that incorporation of an ethyl, methyl, or hydrogen onto position R2 may result in greater potency. There is also the possibility that as chain length increases; the potency may gradually start to increase as well.

From the R1 and R2 data, some general conclusions may be drawn. At the mMC1R and mMC5R, the following potency series was observed: 8-chloro/benzyl > H/benzyl > H/propyl > 8-chloro/naphthyl > H/biphenyl > H/naphthyl > 8-chloro/biphenyl > H/butyl > 9-methyl/benzyl. At the mMC3R and mMC4R, the potency series changes: 8-chloro/benzyl > H/propyl > 8-chloro/naphthyl > H/biphenyl. Other combinations did not exhibit activity at the mMC3,4R.

Position R3. The final position to be discussed is the R3 position. This level of diversity was added through the addition of amino esters. Three different esters were used, the derivatives of phenylalanine, arginine, and lysine (Figure 6-4). The L forms of these amino acids were used, and these were chosen based on past SAR studies of melanocortin ligands. Both Phe and Arg have been shown to be involved in the core sequence of melanocortin ligands. When these amino acids are changed to alanine, there is a significant loss of potency at the melanocortin receptors.¹¹⁵ Lysine was chosen due to the fact that many small molecule ligands contain a primary amine. A basic residue has been shown to be important for interaction with a negatively-charged binding pocket in the melanocortin receptors.^{43,44,48-50,341,342} Arginine fulfills this requirement; however the guanidinyll side chain is large and less stable than the primary amine of

lysine. It would be expected, based on results presented in Chapter 5 of this dissertation, that the Arg compounds would be more potent than the Lys compounds, due to a cation- π interaction present in the peptide. These results are discussed below.

The first series contains a hydrogen in position R1, and a benzyl in position R2. The benzyl (compound 33) and aminobutyl (compound 34) compounds were synthesized by Christine G. Joseph. From Dr. Joseph's data it appeared that the arginine compound was more potent than the benzyl compound at the mMC1R, though the difference was less than the standard 3-fold experimental error. When the lysine compound (compound 39) was synthesized in this study, however, the compound only had weak stimulatory activity at the mMC1R.

When R1 is a hydrogen and R2 is a biphenyl (compounds 40-42), a different trend is observed. At the mMC1R, Phe > Arg > Lys. Additionally, at the mMC3,4R, compound 40 (H/biphenyl/Phe) has low micromolar activity, while the other two compounds do not have any stimulatory activity.

When R1 is a hydrogen and R2 is a naphthyl (compounds 43-45), the potency trends change again. At the mMC1R, Arg > Lys > Phe. There was no activity at the mMC3,4R, though there was activity at the mMC5R. At this receptor, there was micromolar activity when R3 was Lys (compound 45), though only slight activity was observed with the other two compounds.

Compounds 48-50 contain a 9-methyl at R1 and a benzyl at R2. These compounds had some activity at the mMC1R only. In these compounds, Lys > Arg > Phe. The Arg and Phe compounds only have weak stimulatory activity, but the Lys compound (compound 50) is a partial agonist with only 50% activity, but had a low nanomolar EC₅₀ value.

The most potent series of compounds involves compound 37, which was synthesized by Dr. Joseph, along with compounds 51 and 52 synthesized in this study. These compounds have

an 8-chloro in the R1 position and a benzyl in the R2 position. What is interesting about these compounds is that 37 is a nanomolar agonist at all receptors (R3 = Lys), compound 52 is a micromolar agonist at the mMC1,3,5R (R3 = Arg), and compound 51 is a micromolar agonist at the mMC1R only (R3 = Phe). As the R3 substituent goes from Lys to Arg to Phe, the potency decreases and activity is lost at certain receptors. This may give an idea about what interactions are important at which receptor. For example, the lysine is active at all four receptors, but when it is changed to an arginine, activity is lost at the mMC4R and decreased at the other receptors. When a phenylalanine is introduced, activity is lost at the mMC3R, the mMC4R, and the mMC5R and significantly decreased at the mMC1R. These receptor specificities may be important in designing ligands to specifically target certain receptors.

When R1 is an 8-chloro and R2 is a biphenyl (compounds 53-55), all activity is lost at the mMC3-5R. Also, the only compound with significant activity at the mMC1R is the Arg compound, 54, which is a micromolar agonist. The Phe compound 53 has only weak stimulatory activity at the mMC1R, and the Lys compound, 55, has no activity at any of the receptors and is cytotoxic at high concentrations. These results indicate that the 8-chloro/biphenyl combination is not tolerated well at the melanocortin receptors and is not a good candidate for further lead optimization.

The final group of compounds contains an 8-chloro at R1 and a naphthyl at R2 (compounds 56-58). Unlike the biphenyl compounds, these compounds have some activity at all receptors tested. When R3 is a Phe, micromolar activity was observed at all receptors except for the mMC4R, which had only weak stimulatory activity. When R3 was an Arg (compound 57), however, there was only weak activity observed at the mMC1,5R and no activity observed at the

mMC3,4R. When R3 was converted to a Lys (compound 58), the molecule was a low micromolar agonist at the mMC1R, and some weak activity was observed at all other receptors.

Receptor Specificities

In order to draw some general conclusions from this study, it is necessary to look at specific requirements at each receptor. First, the mMC1R will be discussed. This receptor seems to have the least strict requirements for activity. At least some stimulatory activity was seen at this receptor for all compounds tested, except for compound 55, which was toxic. All other combinations of building blocks tested resulted in compounds with activity, though the most potent compounds were 40 (H/biphenyl/benzyl), 46 (H/propyl/benzyl), 52 (8-chloro/benzyl/propyl guanidine), 56 (8-chloro/naphthyl/benzyl), and 58 (8-chloro/naphthyl/aminobutyl). These compounds are all very different structurally, so no specific conclusions can be drawn, indicating that the local 3-D conformations of each molecule are making unique and satisfactory interactions with the receptor to result in activity.

There were not many compounds tested that had activity at the mMC3R or the mMC4R. These compounds were 40 (H/biphenyl/benzyl), 46 (H/propyl/benzyl), 52 (8-chloro/benzyl/propyl guanidine), 56 (8-chloro/naphthyl/benzyl), and 58 (8-chloro/naphthyl/aminobutyl). All of these compounds also had activity at the mMC1R and the mMC5R, so there was no selectivity observed for these compounds at any specific receptor. Once again there does not appear to be any specific pharmacophore that may be elucidated from these results, indicating specific local ligand-receptor interactions may be influencing activity for each compound.

The mMC5R seems to have similar requirements as the mMC1R, however all ligands tested were less active at the mMC5R. The most potent compounds observed were 46

(H/propyl/benzyl), 52 (8-chloro/benzyl/propyl guanidine), and 56 (8-chloro/naphthyl/benzyl).

These compounds were also active at all other receptors tested.

Future studies of this class of compounds should focus on the incorporation of aliphatic groups at R2, as well as halogens at R1. The R3 position seems to be less strict, allowing for the incorporation of building blocks mimicking amino acid side chains of Phe, Lys, Arg, and Trp as well as others. The His side chain cannot be incorporated using this synthetic scheme due to the low stability of the imidazole side chain under the reductive environment necessary for its addition. It may also be interesting to incorporate substituted derivatives of Phe, as some of these have been shown to result in compounds with activity at the melanocortin receptors.⁷

In conclusion, this research has resulted in the identification of several benzodiazepine derivatives that exhibit agonist activity at the mouse melanocortin receptors. These compounds appear to have the most activity at the mMC1R, with only a few compounds exhibiting significant activity at the other receptors. These compounds are easy to synthesize due to the use of solid phase organic synthesis and may be readily purified allowing for the design of a large number of compounds. When substituted with building blocks that mimic the active sequence of peptide melanocortin ligands, this template has the potential to create compounds with increasing potency that may be used in the future as drugs to treat obesity.

Characterization Data

Structures of compounds may be found in Figure 6-3.

3-(4-Aminobutyl)-1-benzyl-3,4-dihydro-1H-benzo[e][1,4]diazepine-2,5-dione (39). BAL resin (333 mg, 0.9 mmol/g) was mixed with sodium triacetoxyborohydride [NaBH(OAc)₃] (636 mg, 3.0 mmol) and H-Lys(Boc)-OMe.HCl (890 mg, 3.0 mmol) in 1% acetic acid/DMF for 2 h and washed with DMF, DCM, and MeOH. The resin containing the amino ester was then treated with EDC (690 mg, 3.6 mmol) in NMP and 2-aminobenzoic acid (411 mg, 3.0 mmol) overnight

and washed as before. A solution of acetanilide (973 mg, 7.2 mmol) and n-butyllithium (252 μ L, 3.0 mmol) in THF was stirred for 30 min and then 15 ml of DMF was added; this solution was then added to the acylated resin and stirred under argon for 30 h. Benzyl bromide (1.4 ml, 12 mmol) was added following lactamization and stirred until the pH=5 as measured by pH paper. The resin was then washed and dried in a desiccator. The compound was cleaved from the resin using 90% TFA, 5% dimethylsulfide, and 5% H₂O for 50 h. Semi-preparative HPLC on an RP-HPLC C18 bonded silica column (Vydac 218TP1010, 1.0 x 25 cm) using a gradient of 22-32% acetonitrile in 0.1% TFA/H₂O over 10 min and collected from 6.7 - 7.6 min gave a compound that was >98% pure. M = 336.86 by mass spectrometry. ¹H NMR (400 MHz, DMSO-*d*₆) δ 8.70 (br, 1H), 7.65—7.63 (m, 1H), 7.56—7.47 (m, 2H), 7.30—7.18 (m, 4H), 7.09—7.08 (m, 2H), 5.33 (d, *J* = 9.75 Hz, 1H), 4.98 (d, *J* = 10.0 Hz, 1H), 3.73 (br, 1H), 2.75—2.60 (m, 2H), 1.85—1.75 (m, 1H), 1.75—1.65 (m, 1H), 1.50—1.45 (m, 2H), 1.40—1.25 (m, 2H).

3-Benzyl-1-biphenyl-2-ylmethyl-3,4-dihydro-1H-benzo[e][1,4]diazepine-2,5-dione (40). BAL resin (333 mg, 0.9 mmol/g) was mixed with sodium triacetoxyborohydride [NaBH(OAc)₃] (636 mg, 3.0 mmol) and L-Phe-OMe.HCl (647 mg, 3.0 mmol) in 1% acetic acid/DMF for 2 h and washed with DMF, DCM, and MeOH. The resin containing the amino ester was then treated with EDC (690 mg, 3.6 mmol) in NMP and 2-aminobenzoic acid (411 mg, 3.0 mmol) overnight and washed as before. A solution of acetanilide (973 mg, 7.2 mmol) and n-butyllithium (252 μ L, 3.0 mmol) in THF was stirred for 30 min and then 15 ml of DMF was added; this solution was then added to the acylated resin and stirred under argon for 30 h. 2-Phenylbenzylbromide (2.2 ml, 12 mmol) was added following lactamization and stirred until the pH=5 as measured by pH paper. The resin was then washed and dried in a desiccator. The compound was cleaved from the

resin using 90% TFA, 5% dimethylsulfide, and 5% H₂O for 50 h. Semi-preparative HPLC on an RP-HPLC C18 bonded silica column (Vydac 218TP1010, 1.0 x 25 cm) using a gradient of 55-65% acetonitrile in 0.1% TFA/H₂O over 10 min and collected from 7.1-7.9min gave a compound that was >95% pure. M = 433.1 by mass spectrometry. ¹H NMR (500 MHz, DMSO-*d*₆) δ 8.76 (d, *J* = 2.6 Hz, 1H), 7.56 (dd, *J* = 0.6, 3.0 Hz, 1H), 7.46- 7.37 (m, 4H), 7.29-7.15 (m, 11H), 7.07-7.03 (m, 2H), 5.15 (d, *J* = 6.4 Hz, 1H), 4.87 (d, *J* = 6.4 Hz, 1H), 4.01-3.97 (m, 1H), 3.14 (dd, *J* = 2.2, 6.4 Hz, 1H), 2.94—2.89 (m, 1H).

1-(3-(1-(biphenyl-2-ylmethyl)-2,5-dioxo-2,3,4,5-tetrahydro-1H-benzo[e][1,4]diazepin-3-yl)propyl)urea (41). BAL resin (333 mg, 0.9 mmol/g) was mixed with sodium triacetoxymethylborohydride [NaBH(OAc)₃] (636 mg, 3.0 mmol) and L-Arg(Pbf)-OMe.HCl (1321 mg, 3.0 mmol) in 1% acetic acid/DMF for 2 h and washed with DMF, DCM, and MeOH. The resin containing the amino ester was then treated with EDC (690 mg, 3.6 mmol) in NMP and 2-aminobenzoic acid (411 mg, 3.0 mmol) overnight and washed as before. A solution of acetanilide (973 mg, 7.2 mmol) and n-butyllithium (252 μL, 3.0 mmol) in THF was stirred for 30 min and then 15 ml of DMF was added; this solution was then added to the acylated resin and stirred under argon for 30 h. 2-Phenylbenzylbromide (2.2 ml, 12 mmol) was added following lactamization and stirred until the pH=5 as measured by pH paper. The resin was then washed and dried in a desiccator. The compound was cleaved from the resin using 90% TFA, 5% triisopropylsilane, and 5% H₂O for 50 h. Semi-preparative HPLC on an RP-HPLC C18 bonded silica column (Vydac 218TP1010, 1.0 x 25 cm) using a gradient of 33-40% acetonitrile in 0.1% TFA/H₂O over 10 min and collected from 6.7-7.4min gave a compound that was >98% pure. M = 440.59 by mass spectrometry. ¹H NMR (400 MHz, DMSO-*d*₆) δ 9.37 (br, 1H), 9.08 (br, 1H),

7.66—7.64 (m, 1H), 7.46—7.38 (m, 4H), 7.30—7.22 (m, 5H), 7.18—7.16 (m, 1H), 7.12—7.06 (m, 2H), 6.26 (br, 2H), 5.13 (d, $J = 10.0$ Hz, 1H), 4.87 (d, $J = 10.5$ Hz, 1H), 3.76 (br, 1H), 3.03 (br, 2H), 1.83 (s, 1H), 1.78—1.68 (m, 2H), 1.56—1.44 (m, 2H).

3-(4-aminobutyl)-1-(biphenyl-2-ylmethyl)-3,4-dihydro-1H-benzo[e][1,4]diazepine-2,5-dione (42). BAL resin (333 mg, 0.9 mmol/g) was mixed with sodium triacetoxyborohydride [NaBH(OAc)₃] (636 mg, 3.0 mmol) and H-Lys(Boc)-OMe.HCl (890 mg, 3.0 mmol) in 1% acetic acid/DMF for 2 h and washed with DMF, DCM, and MeOH. The resin containing the amino ester was then treated with EDC (690 mg, 3.6 mmol) in NMP and 2-aminobenzoic acid (411 mg, 3.0 mmol) overnight and washed as before. A solution of acetanilide (973 mg, 7.2 mmol) and *n*-butyllithium (252 μ L, 3.0 mmol) in THF was stirred for 30 min and then 15 ml of DMF was added; this solution was then added to the acylated resin and stirred under argon for 30 h. 2-Phenylbenzylbromide (2.2 ml, 12 mmol) was added following lactamization and stirred until the pH=5 as measured by pH paper. The resin was then washed and dried in a desiccator. The compound was cleaved from the resin using 90% TFA, 5% triisopropylsilane, and 5% H₂O for 50 h. Semi-preparative HPLC on an RP-HPLC C18 bonded silica column (Vydac 218TP1010, 1.0 x 25 cm) using a gradient of 32-42% acetonitrile in 0.1% TFA/H₂O over 10 min and collected from 6.5-7.25 min gave a compound that was >98% pure. $M = 412.58$ by mass spectrometry. ¹H NMR (400 MHz, DMSO-*d*₆) δ 8.66 (br, 1H) 7.65 (d, $J = 4.75$ Hz, 1H), 7.47—7.36 (m, 4H), 7.31—7.22 (m, 5H), 7.16—7.19 (m, 1H), 7.11—7.06 (m, 2H), 5.16 (d, $J = 10.25$ Hz, 1H), 4.87 (d, $J = 10.0$ Hz, 1H), 3.69 (br, 1H), 2.64 (t, $J = 4.75$ Hz, 2H), 1.86 (s, 2H), 1.78—1.70 (m, 1H), 1.68—1.61 (m, 1H), 1.46—1.38 (m, 2H), 1.36—1.11 (m, 1H), 1.10—1.14 (m, 1H).

3-Benzyl-1-(naphthalen-1-ylmethyl)-3,4-dihydro-1H-benzo[e][1,4]diazepine-2,5-dione (43).

BAL resin (333 mg, 0.9 mmol/g) was mixed with sodium triacetoxyborohydride [NaBH(OAc)₃] (636 mg, 3.0 mmol) and L-Phe-OMe.HCl (647 mg, 3.0 mmol) in 1% acetic acid/DMF for 2 h and washed with DMF, DCM, and MeOH. The resin containing the amino ester was then treated with EDC (690 mg, 3.6 mmol) in NMP and 2-aminobenzoic acid (411 mg, 3.0 mmol) overnight and washed as before. A solution of acetanilide (973 mg, 7.2 mmol) and n-butyllithium (252 μ L, 3.0 mmol) in THF was stirred for 30 min and then 15 ml of DMF was added; this solution was then added to the acylated resin and stirred under argon for 30 h. 2-(Bromomethyl)-naphthalene (2.7 g, 12 mmol) was added following lactamization and stirred until the pH=5 as measured by pH paper. The resin was then washed and dried in a desiccator. The compound was cleaved from the resin using 90% TFA, 5% triisopropylsilane, and 5% H₂O for 50 h. Semi-preparative HPLC on an RP-HPLC C18 bonded silica column (Vydac 218TP1010, 1.0 x 25 cm) using a gradient of 50-60% acetonitrile in 0.1% TFA/H₂O over 10 min and collected from 7.65-8.3 min gave a compound that was >98% pure. M = 405.64 by mass spectrometry. ¹H NMR (400 MHz, DMSO-*d*₆) δ 8.88 (d, *J* = 3.75 Hz, 1H), 7.86—7.84 (m, 1H), 7.80 (d, *J* = 5.5 Hz, 1H), 7.74—7.71 (m, 1H), 7.57 (d, *J* = 3.5 Hz, 2H), 7.53 (t, *J* = 3.75 Hz, 2H), 7.48—7.46 (m, 2H), 7.38 (d, *J* = 4.75 Hz, 2H), 7.28—7.19 (m, 5H), 5.51 (d, *J* = 9.5 Hz, 1H), 5.15 (d, *J* = 10 Hz, 1H), 4.12—4.06 (m, 1H), 3.21 (dd, *J* = 8.7, 4.5 Hz, 1H), 2.99 (dd, *J* = 8.9, 5.6 Hz, 1H).

1-(3-(1-(Naphthalen-1-ylmethyl)-2,5-dioxo-2,3,4,5-tetrahydro-1H-benzo[e][1,4]diazepin-3-yl)propyl)urea (44).

BAL resin (333 mg, 0.9 mmol/g) was mixed with sodium triacetoxyborohydride [NaBH(OAc)₃] (636 mg, 3.0 mmol) and L-Arg(Pbf)-OMe.HCl (1321 mg,

3.0 mmol) in 1% acetic acid/DMF for 2 h and washed with DMF, DCM, and MeOH. The resin containing the amino ester was then treated with EDC (690 mg, 3.6 mmol) in NMP and 2-aminobenzoic acid (411 mg, 3.0 mmol) overnight and washed as before. A solution of acetanilide (973 mg, 7.2 mmol) and n-butyllithium (252 μ L, 3.0 mmol) in THF was stirred for 30 min and then 15 ml of DMF was added; this solution was then added to the acylated resin and stirred under argon for 30 h. 2-(Bromomethyl)-naphthalene (2.7 g, 12 mmol) was added following lactamization and stirred until the pH=5 as measured by pH paper. The resin was then washed and dried in a desiccator. The compound was cleaved from the resin using 90% TFA, 5% triisopropylsilane, and 5% H₂O for 50 h. Semi-preparative HPLC on an RP-HPLC C18 bonded silica column (Vydac 218TP1010, 1.0 x 25 cm) using a gradient of 30-40% acetonitrile in 0.1% TFA/H₂O over 10 min and collected from 6.5-7.5 min gave a compound that was >98% pure. M = 414.63 by mass spectrometry. ¹H NMR (400 MHz, DMSO-*d*₆) δ 8.94 (d, *J* = 3.75 Hz, 1H), 8.45 (br, 1H), 7.86—7.83 (m, 1H), 7.80 (d, *J* = 5.5 Hz, 1H), 7.75—7.73 (m, 1H), 7.65—7.63 (m, 1H), 7.60 (br, 1H), 7.53—7.52 (m, 2H), 7.48—7.44 (m, 2H), 7.32 (br, 2H), 7.29—7.22 (m, 2H), 5.50 (d, *J* = 10.0 Hz, 1H), 5.15 (d, *J* = 10.0 Hz, 1H), 3.87—3.85 (m, 1H), 3.08 (br, 2H), 1.92—1.86 (m, 1H), 1.85 (s, 1H) 1.82—1.72 (m, 1H), 1.65—1.50 (m, 2H).

3-(4-Aminobutyl)-1-(naphthalen-1-ylmethyl)-3,4-dihydro-1H-benzo[e][1,4]diazepine-2,5-dione (45). BAL resin (333 mg, 0.9 mmol/g) was mixed with sodium triacetoxyborohydride [NaBH(OAc)₃] (636 mg, 3.0 mmol) and H-Lys(Boc)-OMe.HCl (890 mg, 3.0 mmol) in 1% acetic acid/DMF for 2 h and washed with DMF, DCM, and MeOH. The resin containing the amino ester was then treated with EDC (690 mg, 3.6 mmol) in NMP and 2-aminobenzoic acid (411 mg, 3.0 mmol) overnight and washed as before. A solution of acetanilide (973 mg, 7.2 mmol) and n-

butyllithium (252 μ L, 3.0 mmol) in THF was stirred for 30 min and then 15 ml of DMF was added; this solution was then added to the acylated resin and stirred under argon for 30 h. 2-(Bromomethyl)-naphthalene (2.7 g, 12 mmol) was added following lactamization and stirred until the pH=5 as measured by pH paper. The resin was then washed and dried in a desiccator. The compound was cleaved from the resin using 90% TFA, 5% triisopropylsilane, and 5% H₂O for 50 h. Semi-preparative HPLC on an RP-HPLC C18 bonded silica column (Vydac 218TP1010, 1.0 x 25 cm) using a gradient of 32-42% acetonitrile in 0.1% TFA/H₂O over 10 min and collected from 6.5-7.25 min gave a compound that was >97% pure. M = 412.58 by mass spectrometry. ¹H NMR (400 MHz, DMSO-*d*₆) δ 8.70 (br, 1H), 7.83—7.75 (m, 3H), 7.64—7.60 (m, 2H), 7.64 (br, 2H), 7.48—7.46 (m, 2H), 7.27—7.21 (m, 2H), 5.52 (d, *J* = 9.75 Hz, 1H), 5.13 (d, *J* = 10.0 Hz, 1H), 3.95 (br, 1H), 2.80—2.71 (m, 2H), 1.89 (s, 2H), 1.88—1.79 (m, 1H), 1.79—1.70 (m, 1H), 1.58—1.46 (m, 2H), 1.57—1.39 (m, 1H), 1.39—1.32 (m, 1H).

3-Benzyl-1-propyl-3,4-dihydro-1H-benzo[e][1,4]diazepine-2,5-dione (46). BAL resin (333 mg, 0.9 mmol/g) was mixed with sodium triacetoxyborohydride [NaBH(OAc)₃] (636 mg, 3.0 mmol) and L-Phe-OMe.HCl (647 mg, 3.0 mmol) in 1% acetic acid/DMF for 2 h and washed with DMF, DCM, and MeOH. The resin containing the amino ester was then treated with EDC (690 mg, 3.6 mmol) in NMP and 2-aminobenzoic acid (411 mg, 3.0 mmol) overnight and washed as before. A solution of acetanilide (973 mg, 7.2 mmol) and n-butyllithium (252 μ L, 3.0 mmol) in THF was stirred for 30 min and then 15 ml of DMF was added; this solution was then added to the acylated resin and stirred under argon for 30 h. 1-Iodopropane (1.2 ml, 12 mmol) was added following lactamization and stirred until the pH=5 as measured by pH paper. The resin was then washed and dried in a desiccator. The compound was cleaved from the resin using

90% TFA, 5% dimethylsulfide, and 5% H₂O for 50 h. Semi-preparative HPLC on an RP-HPLC C18 bonded silica column (Vydac 218TP1010, 1.0 x 25 cm) using a gradient of 40-50% acetonitrile in 0.1% TFA/H₂O over 10 min and collected from 6.4-7.1min gave a compound that was >95% pure. M = 309.5 by mass spectrometry. ¹H NMR (500 MHz, DMSO-*d*₆) δ 8.70 (d, *J* = 2.6 Hz, 1H), 7.60-7.57 (m, 2H), 7.48 (d, *J* = 3.2 Hz, 1H), 7.32-7.27 (m, 3H), 7.21 (t, *J* = 3.0 Hz, 2H), 7.17-7.14 (m, 1H), 4.25—4.19 (m, 1H), 3.88-3.84 (m, 1H), 3.61—3.57 (m, 1H), 3.13 (dd, *J* = 2.2, 5.6 Hz, 1H), 2.91 (dd, *J* = 3.6, 5.6 Hz, 1H), 1.43-1.40 (m, 1H), 1.30-1.26 (m, 1H), 0.70 (t, *J* = 2.8 Hz, 3H).

3-Benzyl-1-butyl-3,4-dihydro-1H-benzo[e][1,4]diazepine-2,5-dione (47). BAL resin (333 mg, 0.9 mmol/g) was mixed with sodium triacetoxyborohydride [NaBH(OAc)₃] (636 mg, 3.0 mmol) and L-Phe-OMe.HCl (647 mg, 3.0 mmol) in 1% acetic acid/DMF for 2 h and washed with DMF, DCM, and MeOH. The resin containing the amino ester was then treated with EDC (690 mg, 3.6 mmol) in NMP and 2-aminobenzoic acid (411 mg, 3.0 mmol) overnight and washed as before. A solution of acetanilide (973 mg, 7.2 mmol) and n-butyllithium (252 μL, 3.0 mmol) in THF was stirred for 30 min and then 15 ml of DMF was added; this solution was then added to the acylated resin and stirred under argon for 30 h. 1-Iodobutane (1.4 ml, 12 mmol) was added following lactamization and stirred until the pH=5 as measured by pH paper. The resin was then washed and dried in a desiccator. The compound was cleaved from the resin using 90% TFA, 5% dimethylsulfide, and 5% H₂O for 50 h. Semi-preparative HPLC on an RP-HPLC C18 bonded silica column (Vydac 218TP1010, 1.0 x 25 cm) using a gradient of 55-65% acetonitrile in 0.1% TFA/H₂O over 10 min and collected from 4.0-4.5min gave a compound that was >95% pure. M = 323.1 by mass spectrometry. ¹H NMR (500 MHz, DMSO-*d*₆) δ 8.69 (d, *J* = 2.6 Hz, 1H), 7.60-

7.56 (m, 2H), 7.48 (d, $J = 3.2$ Hz, 1H), 7.32-7.26 (m, 3H), 7.22 (t, $J = 2.8$ Hz, 2H), 7.17—7.14 (m, 1H), 4.31—4.25 (m, 1H), 3.87—3.82 (m, 1H), 3.63—3.57 (m, 1H), 3.12 (dd, $J = 2.2, 5.6$ Hz, 1H), 2.90 (dd, $J = 3.6, 5.6$ Hz, 1H), 1.36—1.22 (m, 2H), 1.14—1.09 (m, 2H), 0.75 (t, $J = 3.0$ Hz, 3H).

1,3-Dibenzyl-8-methyl-3,4-dihydro-1H-benzo[e][1,4]diazepine-2,5-dione (48). BAL resin (333 mg, 0.9 mmol/g) was mixed with sodium triacetoxyborohydride [NaBH(OAc)₃] (636 mg, 3.0 mmol) and L-Phe-OMe.HCl (647 mg, 3.0 mmol) in 1% acetic acid/DMF for 2 h and washed with DMF, DCM, and MeOH. The resin containing the amino ester was then treated with EDC (690 mg, 3.6 mmol) in NMP and 2-amino-3-methylbenzoic acid (453 mg, 3.0 mmol) overnight and washed as before. A solution of acetanilide (973 mg, 7.2 mmol) and n-butyllithium (252 μ L, 3.0 mmol) in THF was stirred for 30 min and then 15 ml of DMF was added; this solution was then added to the acylated resin and stirred under argon for 30 h. Benzyl bromide (1.4 ml, 12 mmol) was added following lactamization and stirred until the pH=5 as measured by pH paper. The resin was then washed and dried in a desiccator. The compound was cleaved from the resin using 90% TFA, 5% dimethylsulfide, and 5% H₂O for 50 h. Semi-preparative HPLC on an RP-HPLC C18 bonded silica column (Vydac 218TP1010, 1.0 x 25 cm) using a gradient of 44-54% acetonitrile in 0.1% TFA/H₂O over 10 min and collected from 8.1-8.6min gave a compound that was >95% pure. $M = 369.93$ by mass spectrometry. ¹H NMR (400 MHz, DMSO-*d*₆) δ 8.62 (d, $J = 4.0$ Hz, 1H), 7.48 (dd, $J = 4.5, 0.75$ Hz, 1H), 7.35 (dd, $J = 5.0$ Hz, 1.25 Hz, 1H), 7.28—7.27 (m, 1H), 7.26—7.25 (m, 2H), 7.24—7.22 (m, 1H), 7.21—7.20 (m, 1H), 7.19—7.15 (m, 3H), 7.04—7.01 (m, 2H), 5.38 (d, $J = 9.5$ Hz, 1H), 4.28 (d, $J = 9.25$ Hz, 1H), 3.85—3.81 (m, 1H), 3.08 (dd, $J = 9.0, 3.0$ Hz, 1H), 2.86 (dd, $J = 9.0, 5.75$ Hz, 1H), 2.41 (s, 3H).

1-(3-(1-Benzyl-9-methyl-2,5-dioxo-2,3,4,5-tetrahydro-1H-benzo[e][1,4]diazepin-3-yl)propyl)urea (49). BAL resin (333 mg, 0.9 mmol/g) was mixed with sodium triacetoxyborohydride [NaBH(OAc)₃] (636 mg, 3.0 mmol) and H-Arg(Pbf)-OMe.HCl (1321 mg, 3.0 mmol) in 1% acetic acid/DMF for 2 h and washed with DMF, DCM, and MeOH. The resin containing the amino ester was then treated with EDC (690 mg, 3.6 mmol) in NMP and 2-amino-3-methylbenzoic acid (453 mg, 3.0 mmol) overnight and washed as before. A solution of acetanilide (973 mg, 7.2 mmol) and n-butyllithium (252 μ L, 3.0 mmol) in THF was stirred for 30 min and then 15 ml of DMF was added; this solution was then added to the acylated resin and stirred under argon for 30 h. Benzyl bromide (1.4 ml, 12 mmol) was added following lactamization and stirred until the pH=5 as measured by pH paper. The resin was then washed and dried in a desiccator. The compound was cleaved from the resin using 90% TFA, 5% triisopropylsilane, and 5% H₂O for 50 h. Semi-preparative HPLC on an RP-HPLC C18 bonded silica column (Vydac 218TP1010, 1.0 x 25 cm) using a gradient of 25-33% acetonitrile in 0.1% TFA/H₂O over 10 min and collected from 5.95-6.5min gave a compound that was >97% pure. M_r = 378.70 by mass spectrometry. ¹H NMR (400 MHz, DMSO-*d*₆) δ 8.78 (br, 1H), 8.66 (br, 1H), 7.48 (dd, 2H, *J* = 4.5, 4.5 Hz), 7.36 (br, 1H), 7.32—7.28 (m, 1H), 7.16—7.15 (m, 2H), 7.2—6.8 (m, 2H), 6.25 (br, 2H), 5.39 (d, 1H, *J* = 9.25 Hz), 4.27 (d, 1H, *J* = 9.25 Hz), 3.63 (br, 1H), 3.02 (br, 2H), 2.41 (s, 3H), 1.86 (s, 1H), 1.74—1.64 (m, 2H), 1.56—1.44 (m, 2H).

3-(4-Aminobutyl)-1-benzyl-9-methyl-3,4-dihydro-1H-benzo[e][1,4]diazepine-2,5-dione (50). BAL resin (333 mg, 0.9 mmol/g) was mixed with sodium triacetoxyborohydride [NaBH(OAc)₃] (636 mg, 3.0 mmol) and H-Lys(Boc)-OMe.HCl (1187 mg, 3.0 mmol) in 1% acetic acid/DMF for

2 h and washed with DMF, DCM, and MeOH. The resin containing the amino ester was then treated with EDC (690 mg, 3.6 mmol) in NMP and 2-amino-3-methylbenzoic acid (453 mg, 3.0 mmol) overnight and washed as before. A solution of acetanilide (973 mg, 7.2 mmol) and *n*-butyllithium (252 μ L, 3.0 mmol) in THF was stirred for 30 min and then 15 ml of DMF was added; this solution was then added to the acylated resin and stirred under argon for 30 h. Benzyl bromide (1.4 ml, 12 mmol) was added following lactamization and stirred until the pH=5 as measured by pH paper. The resin was then washed and dried in a desiccator. The compound was cleaved from the resin using 90% TFA, 5% dimethylsulfide, and 5% H₂O for 50 h. Semi-preparative HPLC on an RP-HPLC C18 bonded silica column (Vydac 218TP1010, 1.0 x 25 cm) using a gradient of 20-30% acetonitrile in 0.1% TFA/H₂O over 10 min and collected from 7.4-8.0min gave a compound that was >95% pure. *M* = 350.77 by mass spectrometry. ¹H NMR (400 MHz, DMSO-*d*₆) δ 4.48 (d, *J* = 3.25 Hz, 1H), 7.50—7.48 (m, 1H), 7.44 (dd, *J* = 4.5, 0.75 Hz, 1H), 7.32—7.28 (m, 1H), 7.19—7.14 (m, 3H), 7.02—6.99 (m, 2H), 5.38 (d, *J* = 9.5 Hz, 1H), 4.27 (d, *J* = 9.5 Hz, 1H), 3.57 (br, 1H), 3.29 (br, 2H), 2.67—2.62 (m, 2H), 2.45—2.44 (m, 2H), 2.41 (s, 3H), 1.89 (s, 2H), 1.74—1.66 (m, 1H), 1.66—1.56 (m, 1H), 1.46—1.36 (m, 2H).

1-(3-(1-Benzyl-8-chloro-2,5-dioxo-2,3,4,5-tetrahydro-1H-benzo[e][1,4]diazepin-3-yl)propyl)urea (51). BAL resin (333 mg, 0.9 mmol/g) was mixed with sodium triacetoxymethylborohydride [NaBH(OAc)₃] (636 mg, 3.0 mmol) and L-Phe-OMe.HCl (647 mg, 3.0 mmol) in 1% acetic acid/DMF for 2 h and washed with DMF, DCM, and MeOH. The resin containing the amino ester was then treated with EDC (690 mg, 3.6 mmol) in NMP and 2-amino-4-chlorobenzoic acid (515 mg, 3.0 mmol) overnight and washed as before. A solution of acetanilide (973 mg, 7.2 mmol) and *n*-butyllithium (252 μ L, 3.0 mmol) in THF was stirred for 30

min and then 15 ml of DMF was added; this solution was then added to the acylated resin and stirred under argon for 30 h. Benzyl bromide (1.4 ml, 12 mmol) was added following lactamization and stirred until the pH=5 as measured by pH paper. The resin was then washed and dried in a desiccator. The compound was cleaved from the resin using 90% TFA, 5% dimethylsulfide, and 5% H₂O for 50 h. Semi-preparative HPLC on an RP-HPLC C18 bonded silica column (Vydac 218TP1010, 1.0 x 25 cm) using a gradient of 50-60% acetonitrile in 0.1% TFA/H₂O over 10 min and collected from 6.6-7.2min gave a compound that was >98% pure. M = 389.72 by mass spectrometry. ¹H NMR (400 MHz, DMSO-*d*₆) δ 8.86 (d, *J* = 3.75 Hz, 1H), 7.62 (br, 1H), 7.56 (d, *J* = 5.75 Hz, 1H), 7.34—7.30 (m, 3H), 7.25 (t, *J* = 4.6 Hz, 4H), 7.21—7.18 (m, 2H), 7.08 (d, *J* = 5.25 Hz, 2H), 5.39 (d, *J* = 10.0 Hz, 1H), 4.99 (d, *J* = 9.75 Hz, 1H), 4.14—4.06 (m, 1H), 3.16 (dd, *J* = 9.6, 3.0 Hz, 1H), 2.95 (dd, *J* = 8.75, 5.5 Hz, 1H).

N-[3-(1-Benzyl-8-chloro-2,5-dioxo-2,3,4,5-tetrahydro-1H-benzo[e][1,4]diazepin-3-yl)-propyl]-guanidine (52). BAL resin (333 mg, 0.9 mmol/g) was mixed with sodium triacetoxyborohydride [NaBH(OAc)₃] (636 mg, 3.0 mmol) and L-Arg(Pbf)-OMe.HCl (1321 mg, 3.0 mmol) in 1% acetic acid/DMF for 2 h and washed with DMF, DCM, and MeOH. The resin containing the amino ester was then treated with EDC (690 mg, 3.6 mmol) in NMP and 2-amino-4-chlorobenzoic acid (515 mg, 3.0 mmol) overnight and washed as before. A solution of acetanilide (973 mg, 7.2 mmol) and n-butyllithium (252 μL, 3.0 mmol) in THF was stirred for 30 min and then 15 ml of DMF was added; this solution was then added to the acylated resin and stirred under argon for 30 h. Benzyl bromide (1.4 ml, 12 mmol) was added following lactamization and stirred until the pH=5 as measured by pH paper. The resin was then washed and dried in a desiccator. The compound was cleaved from the resin using 90% TFA, 5%

dimethylsulfide, and 5% H₂O for 50 h. Semi-preparative HPLC on an RP-HPLC C18 bonded silica column (Vydac 218TP1010, 1.0 x 25 cm) using a gradient of 28-38% acetonitrile in 0.1% TFA/H₂O over 10 min and collected from 6.9-7.5min gave a compound that was >95% pure. M = 401.1 by mass spectrometry. ¹H NMR (500 MHz, DMSO-*d*₆) δ 8.74 (d, *J* = 2. Hz, 1H), 7.64 (d, *J* = 3.2 Hz, 1H), 7.59 (d, *J* = 0.8 Hz, 1H), 7.47—7.43 (m, 1H), 7.35 (dd, *J* = 0.8, 3.4 Hz, 1H), 7.27—7.18 (m, 3H), 7.08 (d, *J* = 2.8 Hz, 2H), 6.51 (s, 1H), 5.35 (d, *J* = 6.4 Hz, 1H), 5.00 (d, *J* = 6.4 Hz, 1H), 3.88—3.84 (m, 1H), 3.10—3.06 (m, 2H), 1.89-1.80 (m, 1H), 1.72-1.63 (m, 1H), 1.60-1.45 (m, 2H).

3-Benzyl-1-(biphenyl-2-ylmethyl)-8-chloro-3,4-dihydro-1H-benzo[e][1,4]diazepine-2,5-dione (53). BAL resin (333 mg, 0.9 mmol/g) was mixed with sodium triacetoxyborohydride [NaBH(OAc)₃] (636 mg, 3.0 mmol) and L-Phe-OMe.HCl (647 mg, 3.0 mmol) in 1% acetic acid/DMF for 2 h and washed with DMF, DCM, and MeOH. The resin containing the amino ester was then treated with EDC (690 mg, 3.6 mmol) in NMP and 2-amino-4-chlorobenzoic acid (515 mg, 3.0 mmol) overnight and washed as before. A solution of acetanilide (973 mg, 7.2 mmol) and n-butyllithium (252 μL, 3.0 mmol) in THF was stirred for 30 min and then 15 ml of DMF was added; this solution was then added to the acylated resin and stirred under argon for 30 h. 2-Phenylbenzylbromide (2.2 ml, 12 mmol) was added following lactamization and stirred until the pH=5 as measured by pH paper. The resin was then washed and dried in a desiccator. The compound was cleaved from the resin using 90% TFA, 5% triisopropylsilane, and 5% H₂O for 50 h. Semi-preparative HPLC on an RP-HPLC C18 bonded silica column (Vydac 218TP1010, 1.0 x 25 cm) using a gradient of 65-75% acetonitrile in 0.1% TFA/H₂O over 10 min and collected from 6.75-7.35min gave a compound that was >98% pure. M = 465.71 by mass

spectrometry. ^1H NMR (400 MHz, $\text{DMSO-}d_6$) δ 8.81 (d, $J = 4.0$ Hz, 1H), 7.54 (d, $J = 7.5$ Hz, 1H), 7.46—7.37 (m, 3H), 7.30—7.25 (m, 7H), 7.23—7.21 (m, 2H), 7.18—7.16 (m, 2H), 7.11—7.08 (m, 2H), 5.27 (d, $J = 10.0$ Hz, 1H), 4.83 (d, $J = 10.0$ Hz, 1H), 4.06—4.00 (m, 1H), 3.11 (dd, $J = 8.8, 3.25$ Hz, 1H), 2.90 (dd, $J = 8.75, 5.75$ Hz, 1H).

1-(3-(1-(Biphenyl-2-ylmethyl)-8-chloro-2,5-dioxo-2,3,4,5-tetrahydro-1H-

benzo[e][1,4]diazepin-3-yl)propyl)urea (54). BAL resin (333 mg, 0.9 mmol/g) was mixed with sodium triacetoxymethylborohydride [$\text{NaBH}(\text{OAc})_3$] (636 mg, 3.0 mmol) and H-Arg(Pbf)-OMe.HCl (1321 mg, 3.0 mmol) in 1% acetic acid/DMF for 2 h and washed with DMF, DCM, and MeOH. The resin containing the amino ester was then treated with EDC (690 mg, 3.6 mmol) in NMP and 2-amino-4-chlorobenzoic acid (515 mg, 3.0 mmol) overnight and washed as before. A solution of acetanilide (973 mg, 7.2 mmol) and n-butyllithium (252 μL , 3.0 mmol) in THF was stirred for 30 min and then 15 ml of DMF was added; this solution was then added to the acylated resin and stirred under argon for 30 h. 2-Phenylbenzylbromide (2.2 ml, 12 mmol) was added following lactamization and stirred until the pH=5 as measured by pH paper. The resin was then washed and dried in a desiccator. The compound was cleaved from the resin using 90% TFA, 5% triisopropylsilane, and 5% H_2O for 50 h. Semi-preparative HPLC on an RP-HPLC C18 bonded silica column (Vydac 218TP1010, 1.0 x 25 cm) using a gradient of 40-48% acetonitrile in 0.1% TFA/ H_2O over 10 min and collected from 5.4-5.9 min gave a compound that was >97% pure. $M = 474.59$ by mass spectrometry. ^1H NMR (400 MHz, $\text{DMSO-}d_6$) δ 9.02 (br, 1H), 8.67 (br, 1H), 7.65—7.61 (m, 1H), 7.46—7.39 (m, 3H), 7.33—7.22 (m, 5H), 7.17—7.15 (m, 1H), 7.12—7.09 (m, 2H), 6.25 (br, 2H), 5.26 (d, $J = 10.0$ Hz, 1H), 4.81 (d, $J = 10.25$ Hz, 1H), 3.76 (br, 1H), 3.03 (br, 2H), 1.84 (s, 1H), 1.78—1.64 (m, 2H), 1.66—1.42 (m, 2H).

3-(4-Aminobutyl)-1-(biphenyl-2-ylmethyl)-8-chloro-3,4-dihydro-1H-benzo[e][1,4]diazepine-2,5-dione (55). BAL resin (333 mg, 0.9 mmol/g) was mixed with sodium triacetoxyborohydride [NaBH(OAc)₃] (636 mg, 3.0 mmol) and H-Lys(Boc)-OMe.HCl (1187 mg, 3.0 mmol) in 1% acetic acid/DMF for 2 h and washed with DMF, DCM, and MeOH. The resin containing the amino ester was then treated with EDC (690 mg, 3.6 mmol) in NMP and 2-amino-4-chlorobenzoic acid (515 mg, 3.0 mmol) overnight and washed as before. A solution of acetanilide (973 mg, 7.2 mmol) and n-butyllithium (252 μ L, 3.0 mmol) in THF was stirred for 30 min and then 15 ml of DMF was added; this solution was then added to the acylated resin and stirred under argon for 30 h. 2-Phenylbenzylbromide (2.2 ml, 12 mmol) was added following lactamization and stirred until the pH=5 as measured by pH paper. The resin was then washed and dried in a desiccator. The compound was cleaved from the resin using 90% TFA, 5% triisopropylsilane, and 5% H₂O for 50 h. Semi-preparative HPLC on an RP-HPLC C18 bonded silica column (Vydac 218TP1010, 1.0 x 25 cm) using a gradient of 40-50% acetonitrile in 0.1% TFA/H₂O over 10 min and collected from 7.6-8.0min gave a compound that was >97% pure. M = 446.67 by mass spectrometry. ¹H NMR (400 MHz, DMSO-*d*₆) δ 8.66 (br, 1H), 7.62 (d, *J* = 5.25 Hz, 1H), 7.45—7.41 (m, 3H), 7.32—7.26 (m, 5H), 7.19—7.14 (m, 1H), 7.20—7.16 (m, 2H), 5.28 (d, *J* = 11.0 Hz, 1H), 4.81 (d, *J* = 9.75 Hz, 1H), 3.95 (br, 1H), 2.59 (br, 2H), 2.14—2.08 (m, 1H), 1.87 (s, 2H), 1.76—1.68 (m, 1H), 1.68—1.60 (m, 2H), 1.43—1.34 (m, 2H).

3-Benzyl-8-chloro-1-naphthalen-2-ylmethyl-3,4-dihydro-1H-benzo[e][1,4]diazepine-2,5-dione (56). BAL resin (333 mg, 0.9 mmol/g) was mixed with sodium triacetoxyborohydride [NaBH(OAc)₃] (636 mg, 3.0 mmol) and L-Phe-OMe.HCl (647 mg, 3.0 mmol) in 1% acetic

acid/DMF for 2 h and washed with DMF, DCM, and MeOH. The resin containing the amino ester was then treated with EDC (690 mg, 3.6 mmol) in NMP and 2-amino-4-chlorobenzoic acid (515 mg, 3.0 mmol) overnight and washed as before. A solution of acetanilide (973 mg, 7.2 mmol) and n-butyllithium (252 μ L, 3.0 mmol) in THF was stirred for 30 min and then 15 ml of DMF was added; this solution was then added to the acylated resin and stirred under argon for 30 h. 2-(Bromomethyl)-naphthalene (2.7 g, 12 mmol) was added following lactamization and stirred until the pH=5 as measured by pH paper. The resin was then washed and dried in a desiccator. The compound was cleaved from the resin using 90% TFA, 5% dimethylsulfide, and 5% H₂O for 50 h. Semi-preparative HPLC on an RP-HPLC C18 bonded silica column (Vydac 218TP1010, 1.0 x 25 cm) using a gradient of 55-65% acetonitrile in 0.1% TFA/H₂O over 10 min and collected from 7.5-8.2min gave a compound that was >95% pure. M = 440.5 by mass spectrometry. ¹H NMR (500 MHz, DMSO-*d*₆) δ 8.89 (d, *J* = 2.6 Hz, 1H), 7.85-7.84 (m, 1H), 7.80 (d, *J* = 3.4 Hz, 1H), 7.73-7.72 (m, 1H), 7.65 (d, *J* = 0.6 Hz, 1H), 7.57—7.54 (m, 2H), 7.50—7.45 (m, 2H), 7.35—7.33 (m, 2H), 7.30—7.24 (m, 3H), 7.22—7.18 (m, 2H), 5.55 (d, *J* = 6.6 Hz, 1H), 5.14 (d, *J* = 6.4 Hz, 1H), 4.17-4.13 (m, 1H), 3.20 (dd, *J* = 2.2, 5.6 Hz, 1H), 2.98 (dd, *J* = 3.4, 5.0 Hz, 1H).

1-(3-(8-Chloro-1-(naphthalen-1-ylmethyl)-2,5-dioxo-2,3,4,5-tetrahydro-1H-

benzo[e][1,4]diazepin-3-yl)propyl)urea (57). BAL resin (333 mg, 0.9 mmol/g) was mixed with sodium triacetoxyborohydride [NaBH(OAc)₃] (636 mg, 3.0 mmol) and H-Arg(Pbf)-OMe.HCl (1321 mg, 3.0 mmol) in 1% acetic acid/DMF for 2 h and washed with DMF, DCM, and MeOH. The resin containing the amino ester was then treated with EDC (690 mg, 3.6 mmol) in NMP and 2-amino-4-chlorobenzoic acid (515 mg, 3.0 mmol) overnight and washed as before. A

solution of acetanilide (973 mg, 7.2 mmol) and n-butyllithium (252 μ L, 3.0 mmol) in THF was stirred for 30 min and then 15 ml of DMF was added; this solution was then added to the acylated resin and stirred under argon for 30 h. 2-(Bromomethyl)-naphthalene (2.7 g, 12 mmol) was added following lactamization and stirred until the pH=5 as measured by pH paper. The resin was then washed and dried in a desiccator. The compound was cleaved from the resin using 90% TFA, 5% triisopropylsilane, and 5% H₂O for 50 h. Semi-preparative HPLC on an RP-HPLC C18 bonded silica column (Vydac 218TP1010, 1.0 x 25 cm) using a gradient of 34-44% acetonitrile in 0.1% TFA/H₂O over 10 min and collected from 7.0-7.8min gave a compound that was >95% pure. M = 448.63 by mass spectrometry. ¹H NMR (400 MHz, DMSO-*d*₆) δ 8.89 (br, 1H), 8.85 (br, 1H), 7.98 (br, 1H), 7.84—7.80 (m, 2H), 7.75 (d, *J* = 4.0 Hz, 1H), 7.66-7.60 (m, 3H), 7.48—7.47 (m, 1H), 7.34—7.32 (m, 1H), 7.21 (d, *J* = 5.75 Hz, 2H), 6.18 (br, 2H), 5.55 (d, *J* = 10.25 Hz, 1H), 5.15 (d, *J* = 10.25 Hz, 1H), 3.98—3.89 (m, 1H), 3.29 (br, 3H), 2.12—2.08 (m, 1H), 1.88 (s, 1H), 1.88—1.60 (m, 2H), 1.60—1.50 (m, 1H).

3-(4-Amino-butyl)-8-chloro-1-naphthalen-2-ylmethyl-3,4-dihydro-1H-

benzo[e][1,4]diazepine-2,5-dione (58). BAL resin (333 mg, 0.9 mmol/g) was mixed with sodium triacetoxyborohydride [NaBH(OAc)₃] (636 mg, 3.0 mmol) and L-Lys(Boc)-OMe.HCl (890 mg, 3.0 mmol) in 1% acetic acid/DMF for 2 h and washed with DMF, DCM, and MeOH. The resin containing the amino ester was then treated with EDC (690 mg, 3.6 mmol) in NMP and 2-amino-4-chlorobenzoic acid (515 mg, 3.0 mmol) overnight and washed as before. A solution of acetanilide (973 mg, 7.2 mmol) and n-butyllithium (252 μ L, 3.0 mmol) in THF was stirred for 30 min and then 15 ml of DMF was added; this solution was then added to the acylated resin and stirred under argon for 30 h. 2-(Bromomethyl)-naphthalene (2.7 g, 12 mmol)

was added following lactamization and stirred until the pH=5 as measured by pH paper. The resin was then washed and dried in a desiccator. The compound was cleaved from the resin using 90% TFA, 5% dimethylsulfide, and 5% H₂O for 50 h. Semi-preparative HPLC on an RP-HPLC C18 bonded silica column (Vydac 218TP1010, 1.0 x 25 cm) using a gradient of 35-45% acetonitrile in 0.1% TFA/H₂O over 10 min and collected from 6.0-6.8min gave a compound that was >95% pure. M = 422.5 by mass spectrometry. ¹H NMR (500 MHz, DMSO-*d*₆) δ 8.75 (br, 1H), 7.86-7.84 (m, 1H), 7.80 (d, *J* = 3.4 Hz, 1H), 7.76—7.74 (m, 1H), 7.68 (d, *J* = 0.8 Hz, 1H), 7.63—7.59 (m, 2H), 7.49—7.46 (m, 2H), 7.33 (dd, *J* = 0.8, 3.4 Hz, 1H), 7.20 (dd, *J* = 0.6, 3.4 Hz, 1H), 6.55 (br, 1H), 5.57 (d, *J* = 6.4 Hz, 1H), 5.13 (d, *J* = 6.4 Hz, 1H), 3.84 (br, 1H), 2.72 (t, *J* = 2.8 Hz, 2H), 1.85—1.78 (m, 1H), 1.77—1.68 (m, 1H), 1.56—1.28 (m, 4H).

CHAPTER 7 CONSTRUCTION AND CHARACTERIZATION OF MELANOCORTIN-2 AND -4 RECEPTOR CHIMERAS

All primer design, cloning, stable cell line generation, and pharmacology was performed by Krista Wilson. Dr. Xhimin Xiang and Bettina Proneth of the Haskell-Luevano laboratory provided valuable advice and training in cloning and pharmacology. The Flag tag was added to the hMC4R by Dr. Xhimin Xiang. Dr. Sally Litherland of the Department of Pathology provided training and data analysis advice for FACS analysis. Data analysis was performed by Krista Wilson and Dr. Carrie Haskell-Luevano. Luciferase Assay was performed with help from Dr. Hendrik Luesch.

Introduction

The Melanocortin-2 Receptor (MC2R), also known as the ACTH Receptor, or ACTHR, is unique among the melanocortin receptors.⁵⁹ It is one of the shortest known GPCRs, with only 297 amino acids and a predicted mass of 33 kDa.⁵³ It also has two glycosylation sites near the N-terminus, which results in an experimental mass of 43 kDa.¹²⁹ The human MC2R shares 39% sequence identity with the MC1R, 45% identity with the MC3R, 50% identity with the MC4R, and 46% sequence identity with the MC5R. These differences are mainly in the C-terminal domain as well as the first extracellular loop and the third intracellular loop. The MC2R aligned with all four melanocortin receptors is presented in Figure 7-1. The MC2R is coded by the ACTHR gene located on the small arm of chromosome 18 (18p11.21).³⁴⁸ The coding sequence is contained in one exon, exon 2, though a major transcription initiation site has been located upstream of exon 2.⁵³ The MC2R is expressed in the adrenal cortex,⁵³ though it has also been observed at low levels in human skin,³⁴⁹ ovarian steroid cell tumors,³⁵⁰ and in rodent adipocytes.³⁵¹

	N-Terminus (EC)	
hMC1R	MSSVVEFTMAVQGSQRRLGSLNSTPTAIPQLGLAANQTGARCLEVSIS	
hMC2R	MKHIINSYENINNTARNNSDCPRVVLV	
hMC3R	SSVVEFTMSIQKTYLEGDFVFPVSSSFLRTLLEPQLGSALLTAMNASCLLPSVQPTLPNGSEHLQAPFFSNQSSSAFCEQVFIK	
hMC4R	MVNSTHRGMHTSLHLWNRSSYRLHSNASESLGKGYSDGGCYEQLFVS	
hMC5R	MSSFHLHFLDLNLNATEGNLSGPNVKNKSSPCEDMGIA	
	TM1	Loop 1 (IC)
hMC1R	DGLFSLGLVSLVENALVVATIAK	NRNLHS
hMC2R	EEIFFTISIVGVLENLIVLLAVFK	NKNLQA
hMC3R	PEVFLSLGIVSLENILVILAVVR	NGNLHS
hMC4R	PEVFTLGVISLLENILVIVAIK	NKNLHS
hMC5R	VEVFTLGVISLLENILVIGAIK	NKNLHS
	TM2	Loop 2 (EC)
hMC1R	PMYCFICCLALSDDLVSQSNVLETAVILL	LEAGALVARAAVLQQL
hMC2R	PMYFFICSLAISDMLGSLYKILENILL	RNMGYLKPRGSFETTA
hMC3R	PMYFFLCSLAVADMLVSVSNALETIMIAIVHSDY	LT FED QFIQHM
hMC4R	PMYFFICSLAVADMLVSVSNGSETIVITL	LN STDTDAQSFTVNI
hMC5R	PMYFFVCSLAVADMLVSMSSAWETITIIYL	LNNKHLVIADAFVRHI
	TM3	Loop 3 (IC)
hMC1R	DNVIDVITCSSMLSSLCFLGAIIVDRYISI	FYALRYHSIVT
hMC2R	DDIIDLFLVLSLLGSIFLSVIAADRYITI	FHALRYHSIVT
hMC3R	DNIFDSMICISLVASICNLLAIAVDRYVTI	FYALRYHSIMT
hMC4R	DNVIDSVICSSLLASICLLSIAVDRYFTI	FYALQYHNIMT
hMC5R	DNVFDSMICISVVASMCSLLAIAVDRYVTI	FYALRYHHIMT
	TM4	Loop 4 (EC)
hMC1R	LPRARRAVAAIIVASVVFSTLFI	AYYDH
hMC2R	MRRTVVVLTVIWTFCTGTGITMV	IFSHH
hMC3R	VRKALTLIVAIWVCCGVC V V	FIVYS
hMC4R	VKRVGIIISCIWAACVSGILFI	IYSDS
hMC5R	ARRSGAIIAGIWAFACTGCGIVFI	LYSES
	TM5	Loop 5 (IC)
hMC1R	VA VLLCLVVFFLAMVLMAVLYVHMLARACQHAQG	IARLHKRQRPVHRPVHQ
hMC2R	VPT VITFTSL FPLMLVFILCLYVHMFLARSHTRK	ISTLP
hMC3R	ESKMVIVCLITMFFAMMLMGTYVHMFLFARLHVKR	IAALPPADGVAPQQH
hMC4R	SA VIICLITMFFTMLALMASLYVHMFLMARLHIKR	IAVLPGTGAIHQ
hMC5R	TY VILCLISMFFAMFLVLSLYIHMFLARLTHVKR	IAALPGASSARQRTSMQ
	TM6	Loop 6 (EC)
hMC1R	GFGLKGAVTLTILLGIFFLCWGPPFLHLLTLIVL	CPEHPTCGC
hMC2R	RANMKGAILTLTILLGVFIFCWAPFVHLVLLMTF	CPSNPYCAC
hMC3R	SCMKGAVTITILLGVFIFCWAPFLLHLVLIIT	CPTNPYCIC
hMC4R	GANMKGAILTLTILLGVFVVCWAPFLLHLIFYIS	CPQNPYCVC
hMC5R	GAVT VTMLLGVFTVCWAPFLLHLTLMLS	CPQNLVCSR
	TM7	C-terminus (IC)
hMC1R	IFKNFNFLFLALIIICNAIIDPLIYAFHSQ	ELRRTLKEVLTCSW
hMC2R	YMSLFQVNGMLIMCNAVIDPFIYAFRSP	ELRDAFKKMI FCSRYW
hMC3R	YTAHFNTYLVLMCNSVIDPLIYAFRSL	ELRNTFREILCGCNGMNLG
hMC4R	FMSHFNLYLILIMCNDIIDPLIYALRSQ	ELRKTfKEIICCYPLGGLCDLSSRY
hMC5R	FMSHFNMYLILIMCNSVMDPLIYAFRSQ	EMRKTfKEIICCRGFRIACSFPRRD

Figure 7-1. Amino acid alignment of human melanocortin receptors 1-5, arranged by transmembrane domain and loop. IC = Intracellular. EC = Extracellular. Transmembrane (TM) domains were determined by comparison with previous hMC1R and hMC4R alignments.⁴³ Spaces are placed in sequences for alignment purposes.

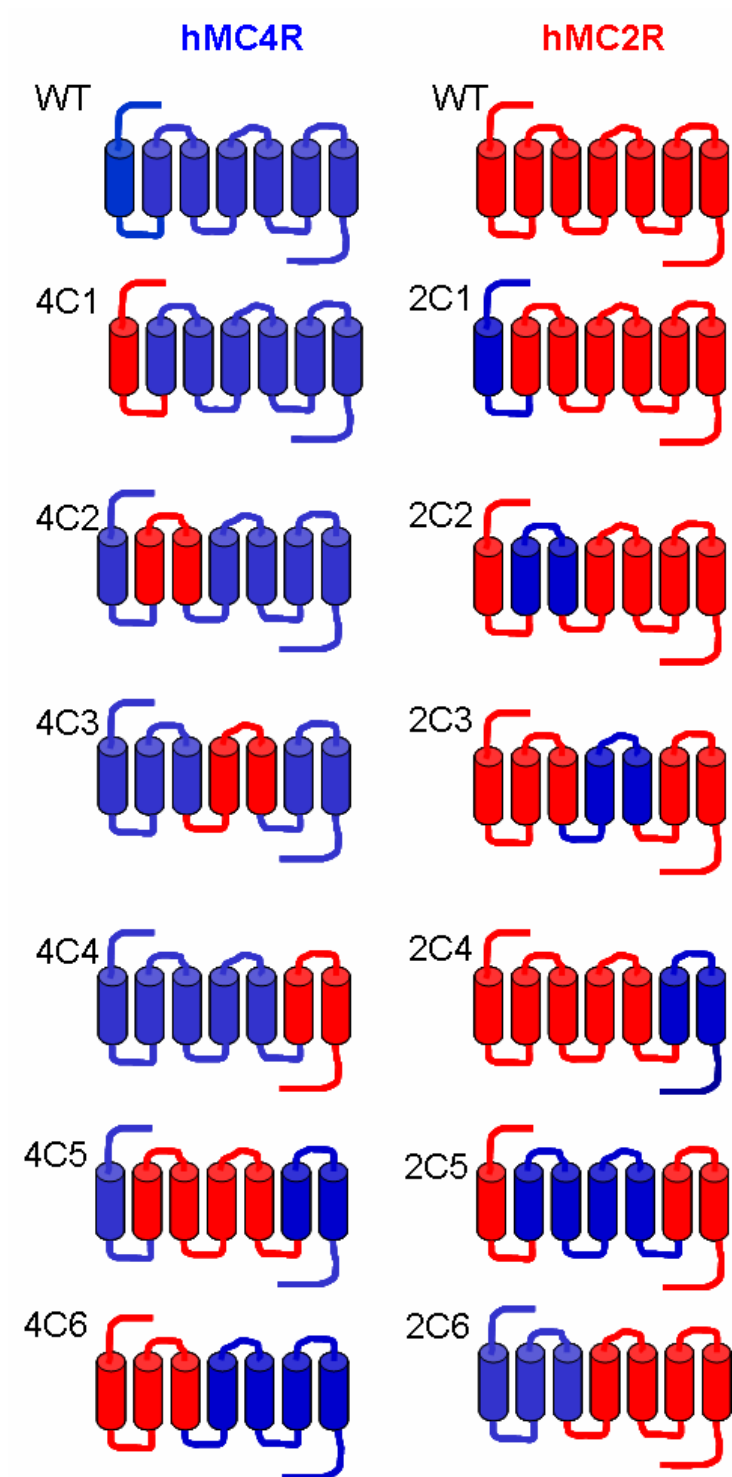


Figure 7-3. Schematic of chimeras. Blue cylinders = hMC4R TM domains; Red cylinders = hMC2R TM domains.

Cell lines of non-adrenal origin can be stably transfected with the receptor, but there is no functional response when stimulated with ACTH.⁵⁹ HEK293 cells are derived from human embryonic kidney cells. These cells are not of adrenal origin and do not contain the MC2R gene. Until this time, it was assumed that the reason the MC2R did not produce a functional response when expressed in HEK293 cells was due to the fact that the receptor was not expressed on the cell surface.⁸⁶ This work demonstrates that this may not be the case and the MC2R is expressed on the surface of HEK293 cells as determined by FACS (Figure 7-5C). It is hypothesized that the reason MC2R-HEK cells do not produce a functional response in the β -galactosidase assay is due to lack of an accessory protein which binds to the receptor and ligand, facilitating receptor stimulation. Alternatively, the MC2R is in an inactive conformation and thus is not able to bind the ligand.

These results lead to the idea that an additional factor may be needed to produce a functional MC2 receptor. The OS3 cells naturally express this receptor, therefore they would also express all proteins required for activity. HEK293 cells do not express this receptor naturally; therefore they may not express this unknown factor. Two classes of accessory proteins have gained popularity in receptor interaction. The first is a class known as RAMPs, or receptor activity modifying proteins, which have been identified as essential partners for the activity at the calcitonin receptor (CTR) and the calcitonin receptor-like receptor (CRLR).³⁵⁴ There are three RAMPs, RAMP1-3, that have been identified to date. RAMP1 is a 148 amino acid protein which shares only 30% homology with the other two RAMPs.³⁵⁴ All RAMPs share the same structure. They are made up of a large extracellular N-terminus, a single TM domain and a short intracellular C-terminal domain.³⁵⁴ They have been shown to form dimers with their target receptors in the endoplasmic reticulum and remain associated through the Golgi apparatus,

during insertion into the cell membrane, and through receptor activation, internalization and degradation.³⁵⁵⁻³⁵⁹ Additionally, RAMP association leads to glycosylation of the CRLR^{354,357} and plays a role in ligand-receptor binding as proposed by Foord *et al.*³⁶⁰ Due to its ubiquitous expression,³⁵⁴ it has been suggested that RAMPs may play a role in the function of other receptors. MRAP, or Melanocortin-2 Receptor Accessory Protein, was first identified as fat tissue-specific low molecular weight protein (Falp) expressed in adipocytes and the adrenal cortex.³⁶¹ Metherell *et al.* has identified that MRAP interacts with the MC2R and is required for MC2R activity in CHO cells.⁸⁶ The protein has been shown to be expressed in 3T3-L1 cells³⁶¹ as well as Y1 and Y6 cells,⁸⁶ all which express a functional MC2R. Recently, it has been shown that the MC2R is expressed on the surface of HEK293 cells without the presence of MRAP, but that cotransfection of MRAP is required for MC2R activity in this cell line.³⁶²

For many years ligands have been screened at the melanocortin receptors using the β -galactosidase assay.²⁰⁹ This assay works well with receptors expressed in HEK293 cells and the pCRE/ β -gal plasmid transiently transfected into the cells before stimulation.²⁰⁹ This method is effective for cells expressing the MC1R, MC3R, MC4R, or MC5R, however, when the MC2R is stably transfected into HEK 293 cells, there is no functional response in the β -galactosidase assay.⁸³

As has been previously stated, it is known that stimulation of OS3 cells stably transfected with the hMC2R gene results in a functional response.⁵⁹ Conversely, HEK293 cells that contain the hMC2R do not produce a functional response when stimulated.^{84,85} Amino acid alignment of the hMC2R with the hMC4R has identified key amino acid changes in the transmembrane regions which may be involved in ligand binding and/or signal transduction (Figure 7-1). To test the hypothesis that these amino acids are involved in the production of a functional hMC2

receptor in HEK293 cells, chimeric receptors were made to identify the role each transmembrane domain plays in ligand binding and signal transduction in the hMC2R. Entire transmembrane regions from the hMC4R were inserted into the hMC2R gene and these chimeric receptors were stably transfected into OS3 cells and HEK293 cells. Figure 7-3 depicts the chimeric receptors that were generated. Based on the regions of diversity in the transmembrane domains, hMC2R chimeras were created in which TM domains 2, 5, and 7 from the hMC4R replace the hMC2R sequence. Chimeras were also generated which contain the N-terminus, C-terminus, and middle three TM domains of the hMC4R, respectively. A site-directed mutagenesis approach will not be used because the differences may not be due to single amino acid differences, but due to the local tertiary structure of all amino acids in the vicinity. Identical chimeras in which hMC2R TM domains are inserted into the hMC4R were also generated to serve as internal controls. All chimeras were stably expressed in both the OS3 and HEK293 cells. The wild type receptors were also expressed in both cell types as controls. Figure 7-3 depicts the chimeras that were made. Blue TM domains are used to represent the sections from the hMC4R, and red TM domains are used to depict regions of the hMC2R.

Following construction of chimeras and generation of stable cell lines, the expression and localization of the receptor was determined using FACS (Fluorescence-Activated Cell Sorting). All receptors contain the Flag tag on the N-terminus, as demonstrated by our lab.^{363,364} A Flag tag is an amino acid sequence specific for an anti-Flag antibody that is attached to the receptor by PCR. When labeled with the anti-Flag-APC antibody, cells fluoresce, allowing the flow cytometer to determine relative fluorescence levels. Cells were first labeled on the extracellular surface, and then a group of cells were permeabilized and labeled again, to label the receptor on the inside of the cell. These cells are used to determine the total receptor expression. The cells

labeled only on the outside give cell surface expression. Relative surface expression of chimeras was determined based on relative to surface expression of the wild type receptors. Functional assay of all chimeras in HEK293 cells was also performed to measure the response of the receptor to agonist stimulation.

Results

Flag-tagged hMC2R

A Flag tag was added to the N-terminus of the hMC2R to enable detection with an antibody specific for the Flag sequence, DYKDDDDK.³⁶⁵ In order to insert the tag into the receptor sequence, a primer was designed that contained the Kozak sequence, which is necessary for ribosome recognition, a Met start codon, and the DNA sequence that codes for the Flag tag (Figure 7-4 and Table 7-1). The hMC2R gene with the new 5' sequence was amplified by PCR, then the new DNA was isolated and gel purified. During PCR, the HindIII restriction site was inserted at the 5' end and the XbaI restriction site inserted at the 3' end. Both the insert and a new pBKS or pcDNA₃ plasmid were cut with these two enzymes, and the insert ligated into the pBKS or pcDNA₃ plasmid. This resulted in a plasmid containing the Flag-hMC2R construct.

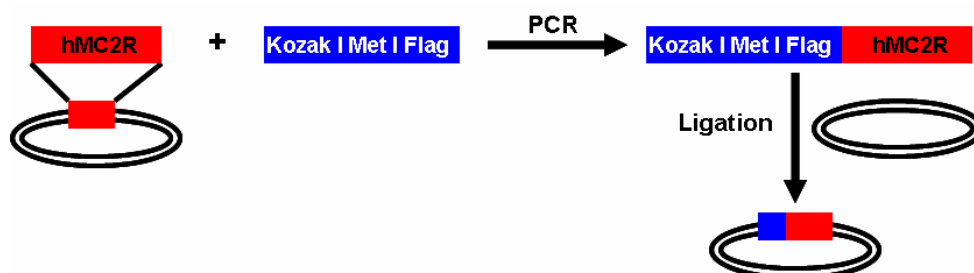


Figure 7-4. Addition of Flag tag to the hMC2R gene. A PCR approach was used to create a receptor preceded by the Kozak sequence, Met start codon, and Flag tag, and then the construct was ligated into a new expression plasmid.

This construct was stably transfected into both HEK293 and OS3 cells in order to test the surface expression and functional activity of the receptor. First, FACS analysis and deconvolution microscopy were used to test the surface expression of the receptor. One group of

cells was labeled with an anti-Flag antibody on the cell surface only, and another group was labeled on the outside and the inside of the cell. Flow cytometry allowed quantification of surface expression of the Flag-hMC2R in both cell types. Results are shown in Figure 7-5A and B. Figure 7-5A shows the percentage of cells expressing the receptor on the surface and in total above background levels. Figure 7-5B shows the mean fluorescence of each cell type and location above background. The mean fluorescence gives information about the amount of receptor in each cell. A high mean fluorescence indicates that individual cells are expressing large numbers of receptor while a low mean fluorescence indicates that individual cells are expressing low levels of receptors. Visualization of the surface expression of Flag-hMC2R was accomplished by deconvolution microscopy. Figure 7-5C shows an image of an HEK293 cell expressing the Flag-hMC2R and labeled on the cell surface only. Figure 7-5D shows the surface expression of the Flag-hMC2R in OS3 cells. It is apparent that the HEK cells express the receptor at much higher levels than OS3 cells, though much of the receptor was contained in the interior of the cell. OS3 cells have been shown to have low transfection efficiency, which is apparent here, but most of the receptor that is expressed is on the surface as opposed to the interior of the cell.

Table 7-1. Primers for insertion of Flag tag into hMC2R template. F = forward primer; R = reverse primer.

Primer	Primer Sequence
Flag-hMC2R-F	5'GATGAAGCTTGCCGCCCATGGACTACAAGGACGACGACGACAAGAAGCACAT TATCAACTCG3'
Flag-hMC2R-R	5'CGAGGCTGATCAGCGGGTTTAAACG3'

The Flag-hMC2R was also identified by Western blotting of the transfected HEK and OS3 cell lines. These results are shown in Figure 7-5E. Treatment of cellular extracts with an anti-Flag antibody reveals the presence of the Flag-tagged receptor in the cell.

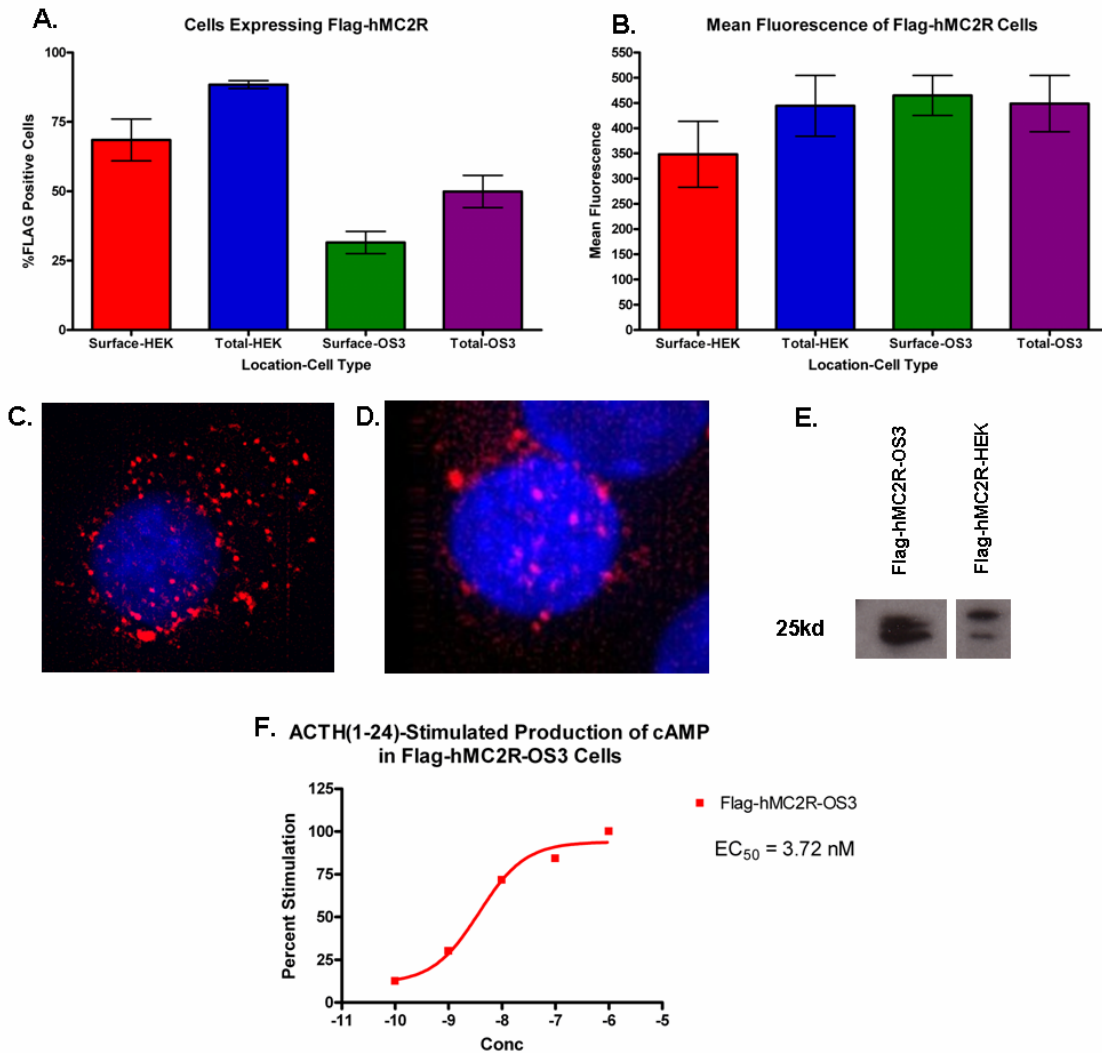


Figure 7-5. Characterization of HEK293 and OS3 cells stably expressing the Flag-hMC2R. A. Surface and total expression levels of Flag-hMC2R determined by FACS. B. Mean fluorescence levels of surface and total Flag-hMC2R expression in HEK and OS3 cells. C. Deconvolution microscopy image of Flag-hMC2R stably expressed in HEK cells and labeled with anti-Flag-APC antibody on the cell surface only. D. Deconvolution microscopy image of Flag-hMC2R stably expressed in OS3 cells and labeled with anti-Flag-APC antibody on the cell surface only. E. Western blot of HEK and OS3 cells stably expressing Flag-hMC2R. F. cAMP production determined by cAMP assay in OS3 cells stably expressing the Flag-hMC2R (cells obtained from Schimmer *et al.*) and stimulated with ACTH(1-24).

Functional activity of the receptor in each cell type was tested using the cAMP assay.

Results are shown in Figure 7-5F. As has been previously observed by other researchers, a

functional response was seen in OS3 cells expressing the Flag-hMC2R and stimulated with ACTH, however; no functional activity was observed in the HEK cells (data not shown).

Real-time PCR

Real-time PCR was performed in order to determine if the accessory proteins RAMP1, RAMP2, RAMP3, or MRAP were present in the HEK and OS3 cells. Probes for the hMC2R as well as the four accessory proteins were purchased from Applied Biosciences. Expression levels were tested in five cell types: hMC2R-OS3 cells, hMC4R-HEK cells, untransfected OS3 cells, and the hMC2R-OS3 and hMC4R-HEK cells stimulated with 10^{-7} M ACTH(1-24) for 6 h at 37°C. The hMC2R gene expressed in transfected OS3 cells was used as a 100% standard. All values were normalized to 18S ribosomal RNA levels. Each experiment was performed at least three times with at least two replicates per experiment.

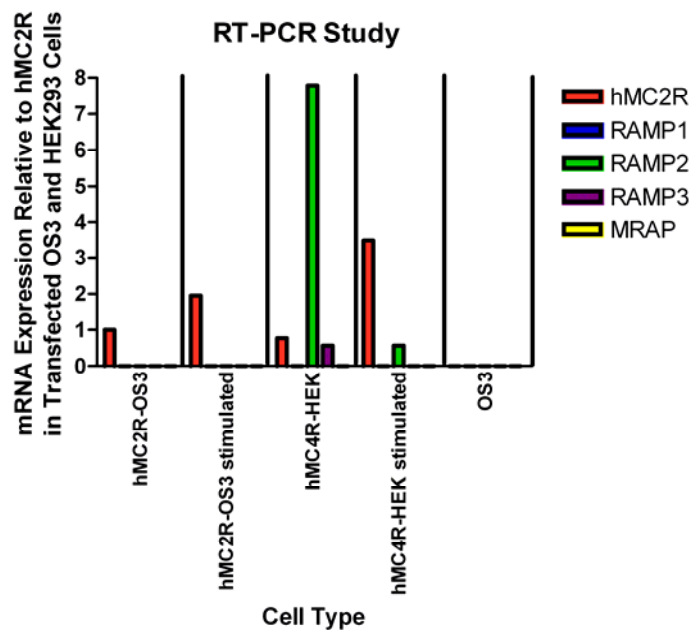


Figure 7-6. Gene expression assay of hMC2R-OS3, hMC4R-HEK, and OS3 cells. Stimulated cell lines were treated with 10^{-7} M ACTH(1-24) for 6 h prior to mRNA isolation.

Results are shown in Figure 7-6. OS3 cells transfected with the hMC2R showed expression of hMC2R mRNA, but no other test mRNA was detected. The stimulated hMC2R-OS3 cells

Chimera Construction

Chimeras were constructed using the following methods (Figure 7-8). Unique restriction sites were inserted into the wild type DNA using PCR (Figure 7-9). Care was used not to change the amino acid sequence. Following PCR, the DNA was incubated with DpnI to remove the wild type DNA, and then the DNA transformed into chemically competent DH5 α cells. Transformed bacteria were grown and DNA isolated via Miniprep and sequenced to confirm the presence of the unique restriction site. The bacteria was then grown for Maxiprep and DNA isolated and stored in TE Light buffer at a concentration of 1 μ g/ μ L. Enzymatic digestion of the plasmid allowed for the isolation of a short insert and a digested plasmid, which were isolated via gel extraction. At this point, the insert from the hMC4R was ligated into the digested hMC2R plasmid, and the hMC2R insert ligated into the hMC4R plasmid, resulting in chimeric receptors. The ligated DNA was transformed into chemically competent DH5 α cells, and amplified by miniprep and maxiprep. The chimeric receptors were fully sequenced to ensure that the receptors were free of unintentional PCR-induced changes. Full sequences of all wild type receptors and chimeras as well as restriction maps may be found in Appendix B.

Following chimera construction, the DNA was stably transfected into either HEK or OS3 cells. For HEK cells, 10 μ g of DNA was transfected using the calcium chloride precipitation method.²²⁷ For OS3 cells, 10 μ g of DNA was transfected using Fugene 6 transfection reagent (Roche). Stably transfected cells were selected using the antibiotic G418.

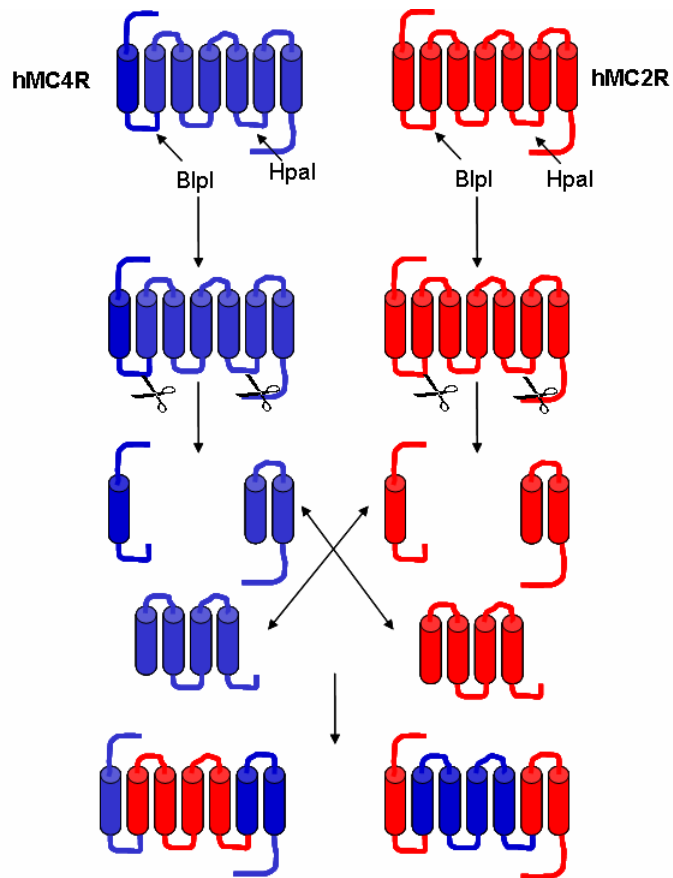


Figure 7-8. Schematic of chimera construction. Chimera E is used as example, BlnI and HpaI refer to restriction endonucleases. Actual experiments performed on plasmid DNA containing melanocortin receptor DNA, data presented here as protein for clarity. DNA fragments ligated using T4 ligase.

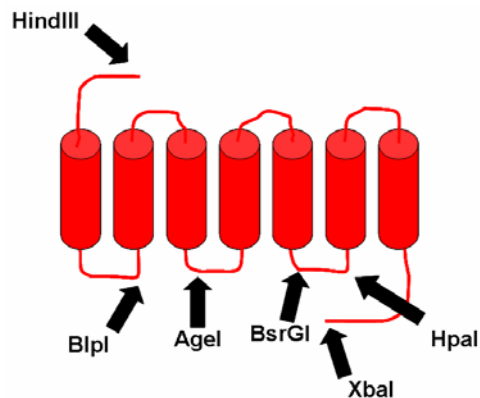


Figure 7-9. Diagram of unique restriction sites used during this study and their locations in the receptor.

Table 7-2. Restriction enzyme recognition sites. ↓ Indicates site of DNA digestion.

Restriction Enzyme	Recognition Sequence
Hind3	5'...A↓AGCTT...3' 3'...TTCGA↓A...5'
Blp1	5'...GC↓TNAGC...3' 3'...CGANT↓CG...5'
Age1	5'...A↓CCGGT...3' 3'...TGGCC↓A...5'
BsrG1	5'...T↓GTACA...3' 3'...ACATG↓T...5'
Hpa1	5'...GTT↓AAC...3' 3'...CAA↓TTG...5'
Xba1	5'...T↓CTAGA...3' 3'...AGATC↓T...5'

Table 7-3. Primers for insertion of unique restriction sites in hMC2R and hMC4R templates. F = forward primer; R = reverse primer. Restriction sites are underlined.

Primer	Primer Sequence
hMC2R-Blp1-F	5'CATCTGTAGCTTAGCCATATCTGATATGCTGGGC3'
hMC2R-Blp1-R	5'GCCAGCATATCAGATATGGCTAAGCTACAGATG3'
hMC2R-Age1-F	5'CCTGTCTGTGATTGCTGCGG <u>ACCGGT</u> ACATCACC3'
hMC2R-Age1-R	5'GGTGATGT <u>ACCGGT</u> CCCGACGCAATCACAGACAGG3'
hMC2R-BsrG1-F	5'CCTGTGCCTCTAT <u>GTACA</u> CATGTTCTGCTGGC3'
hMC2R-BsrG1-R	5'GCCAGCAGGAACATGTGT <u>ACAT</u> AGAGGCACAGG3'
hMC2R-Hpa1-F	5'CATGAAAGGGGCCATCACGTTA <u>ACC</u> ATCCTGCTCG5'
hMC2R-Hpa1-R	5'CGAGCAGGATGGTTA <u>AC</u> GTGATGGCCCTTTCATG3'
hMC4R-Blp1-F	5'CTTTTCATCTGCAGCTTAGCTGTGGCTGATATGC3'
hMC4R-Blp1-R	5'GCATATCAGCCACAGCTAAGCTGCAGATGAAAAAG3'
hMC4R-Age1-F	5'GCTTCAATTGCAGTGG <u>ACCGGT</u> ACTTTACTATCTTC3'
hMC4R-Age1-R	5'GAAGATAGTAAAGT <u>ACCGGT</u> CCACTGCAATTGAAAGC3'
hMC4R-BsrG1-F	5'CATGGCTTCTCTCTAT <u>GTACA</u> CATGTTCTGATGG3'
hMC4R-BsrG1-R	5'CCATCAGGAACATGTGT <u>ACAT</u> AGAGAGAAGCCATG3'
hMC4R-Hpa1-F	5'GAAGGGAGCGATTACGTTA <u>ACC</u> ATCCTGATTGG3'
hMC4R-Hpa1-R	5'CAAATCAGGATGGTTA <u>AC</u> GTAATCGCTCCCTTC3'

Fluorescence Activated Cell Sorting

Fluorescence-Activated Cell Sorting was used to determine the cellular localization of each chimeric receptor. For each cell type, four samples were prepared (Figure 7-10). The first sample was not labeled with any antibody, and the second sample was labeled with an isotype control.

This control was used to determine background fluorescence, which was subtracted from the experimental samples. The third sample was labeled with an Anti-Flag-APC antibody on the cell

surface only. The fourth sample was labeled on the surface, then permeabilized with saponin and labeled again with the Anti-Flag antibody. The fourth sample gave total expression of the receptor on the outside and inside of the cell. Three independent experiments were performed for each cell type.

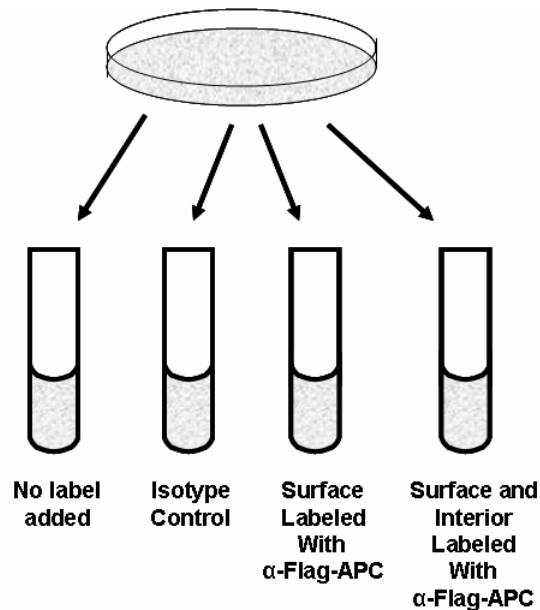


Figure 7-10. Schematic of FACS experiment. Cells are split into four groups as shown.

Results are shown in Figures 7-11 and 7-12. Figure 7-11 depicts expression data from the HEK cells expressing the chimeras. Data is represented in several ways. Figure 7-11A gives the raw data obtained for each cell type. Figure 7-11B shows the data normalized to the wild type receptor. From this data, it was observed that chimeras 2C1, 2C3, and 2C6 all exhibited increased surface expression as compared to the hMC2R wild type receptor, though total expression remained the same. Additionally, chimera 2C5 showed decreased surface and total expression as compared to wild type. When the hMC4R chimeras were examined, it was observed that most chimeras exhibited similar expression to the hMC4R wild type, though 4C1 and 4C4 showed slightly less surface expression.

Figure 7-11C and 7-11D show the mean fluorescence data from the HEK FACS experiments. The mean fluorescence (MF) is a measure of the relative fluorescence on each individual cell. Looking at the MF normalized to the wild type receptors, it was seen that chimeras 2C1, 2C2, and 2C6 had increased surface and total expression on each cell, and chimera 2C3 expressed similar total levels of receptor, however the surface density was significantly increased over wild type.

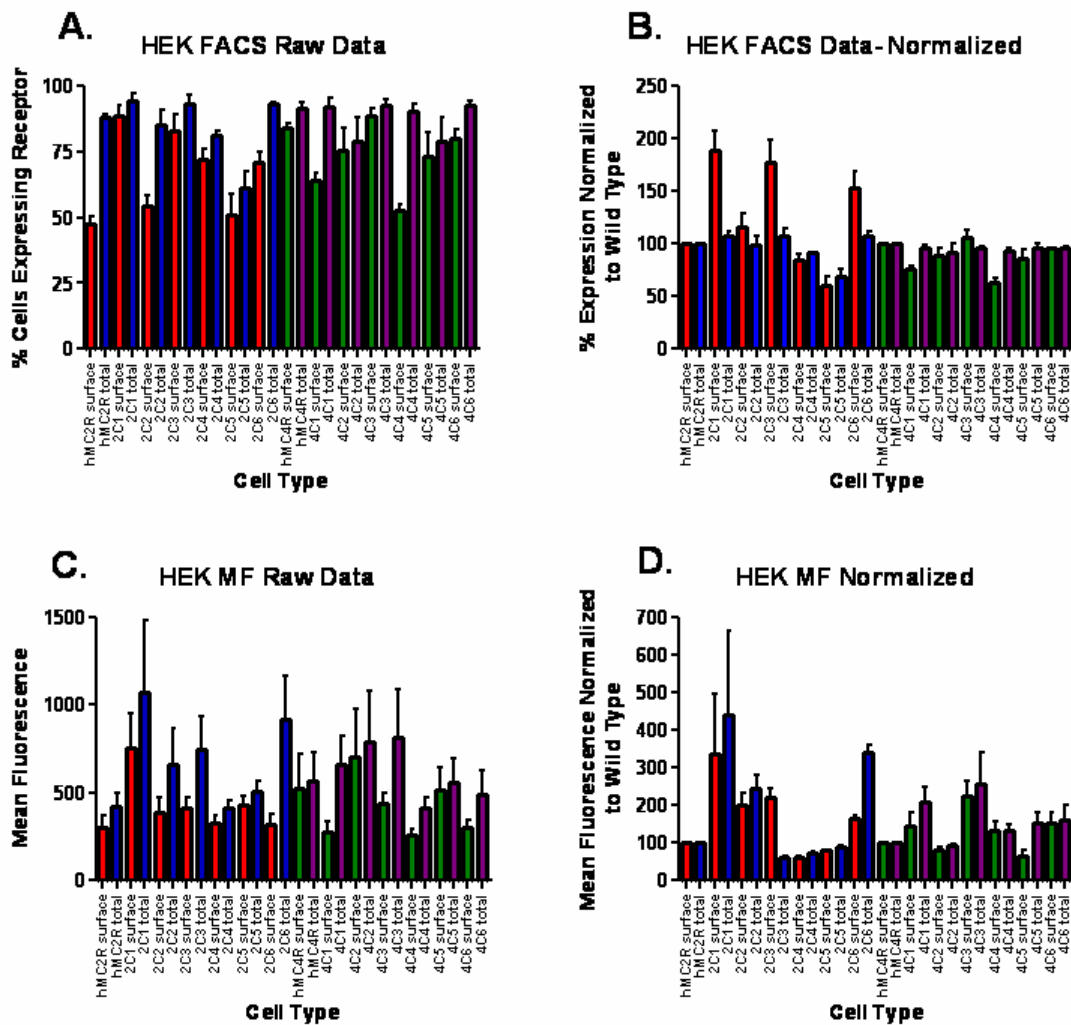


Figure 7-11. Summary of FACS data of wild type receptors and chimeras expressed in HEK293 cells.

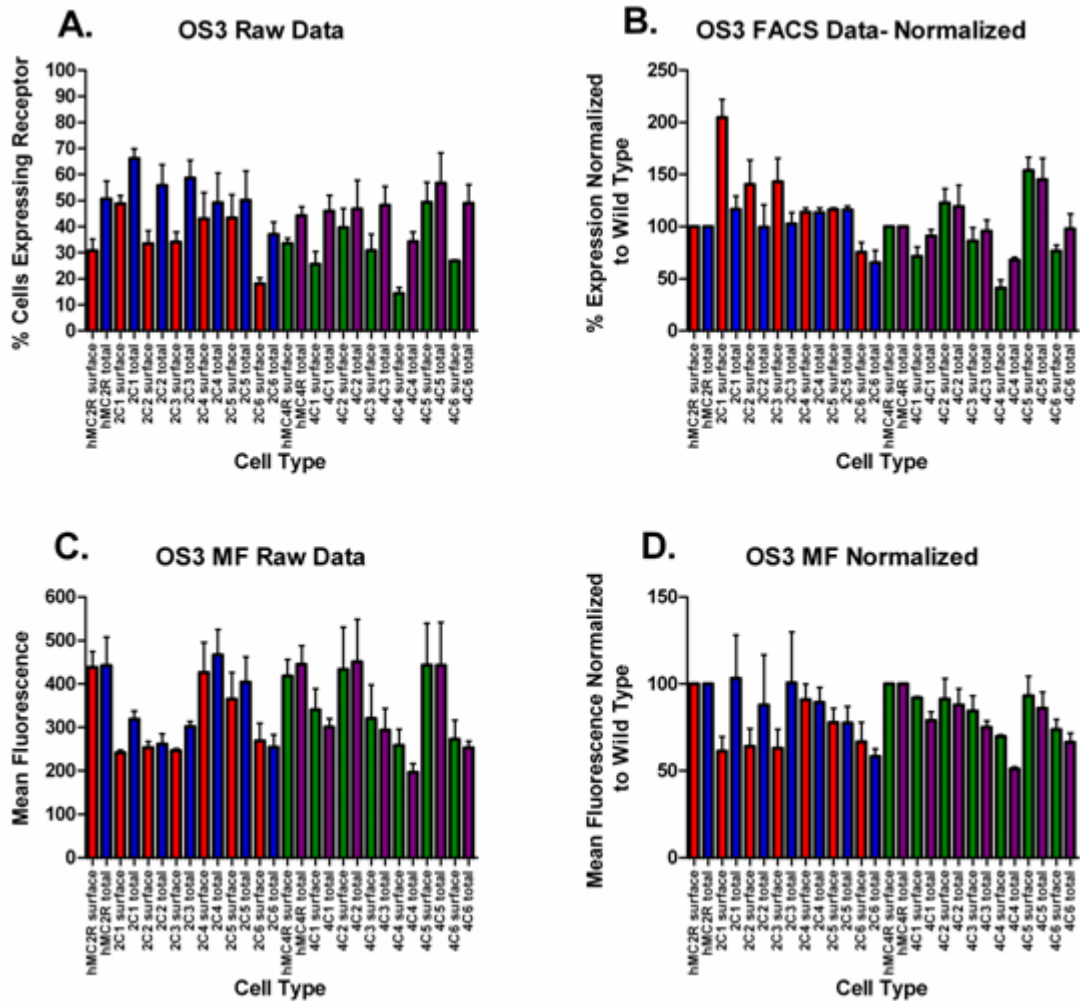


Figure 7-12. Summary of FACS data of wild type receptors and chimeras expressed in OS3 cells.

FACS analysis was also performed on OS3 cells. Figure 7-12 depicts this data. One significant observation is that the receptor expression and mean fluorescence were significantly decreased as compared to HEK cells (Figure 7-11A and Figure 7-12A). Figure 7-12A and 7-12B shows raw and normalized FACS data in OS3 cells. Similar to the HEK cells, chimeras 2C1 and 2C3 exhibit increased surface expression as compared to the hMC2R wild type receptor, though total expression remains fairly constant. hMC4R chimera expression was more variable. Chimeras 4C2 and 4C5 showed increased surface and total expression over wild type, while

chimeras 4C1 and 4C4 have decreased expression. Chimeras 4C3 and 4C6 showed similar expression to the wild type hMC4R receptor.

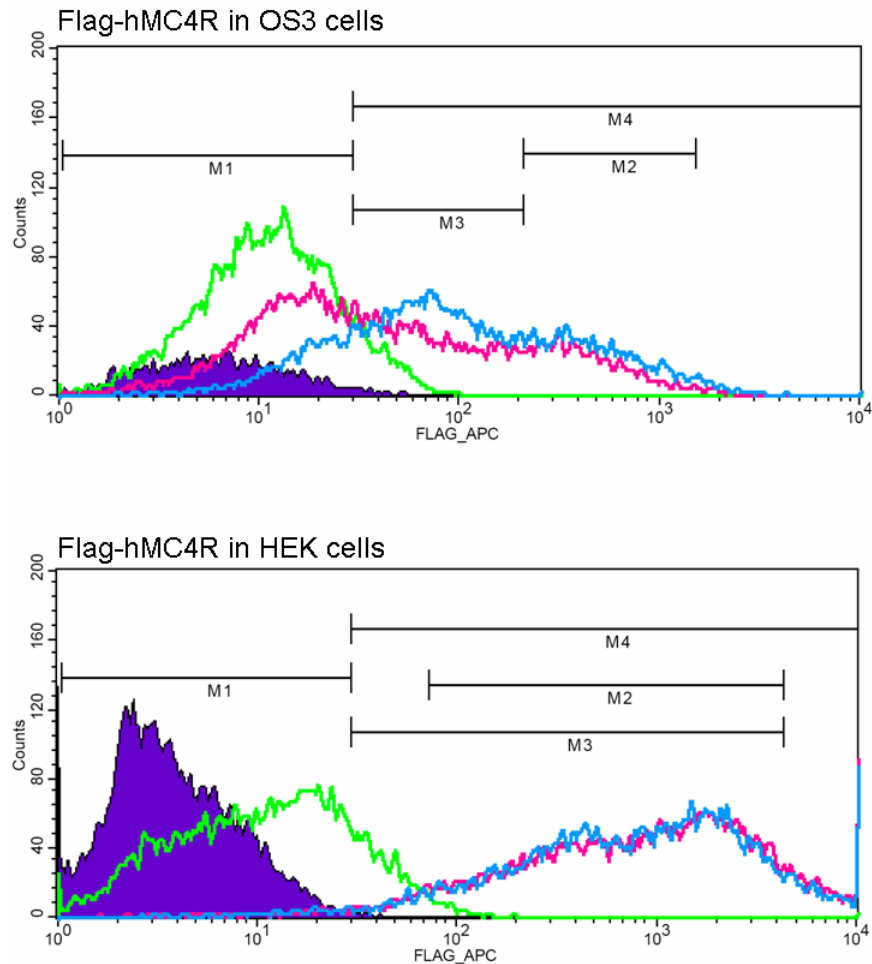


Figure 7-13. Histograms of FACS data from the Flag-hMC4R construct expressed in both OS3 (top) and HEK (bottom) cell lines. Purple (filled) peak represents cells not labeled with antibody. Green curve represents isotype control. Blue peak represents total expression and pink peak represents surface expression. M1 = No label and isotype control peaks. M2 = Surface and total expression peaks only. M3 = Surface and total expression peaks + low data. M4 = Surface and total expression peaks + high and low data.

OS3 mean fluorescence levels are shown in Figures 7-12C and 7-12D. While relative total expression remained the same among chimeras 2C1, 2C2, 2C3, and 2C4, surface expression was significantly less in chimeras 2C1, 2C2, 2C3, and 2C6, and total expression was decreased in

chimera 2C6 as compared to hMC2R wild type. Among the hMC4R chimeras, 4C4 and 4C6 had decreased expression while the other chimeras had similar expression to the wild type hMC4R.

FACS data expressed as histograms for all wild type receptors and chimeras in both HEK and OS3 cells may be found in Appendix C. Figure 7-13 depicts FACS histograms of the Flag-hMC4R construct expressed in both OS3 and HEK cell lines. It appears that there may be two populations of cells present, a high-affinity binding population and a lower-affinity population. It is unknown whether or not this trend affects functional activity.

Luciferase Assay

Functional assay was performed on the chimeras. The luciferase assay is a reporter gene assay utilizing the firefly luciferase gene²³¹ coupled to 16 CRE (cAMP response element) units.^{83,236,238,366-368} When the receptor is stimulated by an agonist, cAMP is produced, which binds CREB (cAMP response element binding protein), which binds to the CRE units, initiating transcription of the luciferase gene. Following stimulation, D-luciferin is added to the lysis mixture, which reacts with the luciferase producing a flash of light. Luminescence can be quantified using a luminometer. The more luminescence detected, the more potent the agonist.

It has been reported that the luciferase assay may be used with both HEK and OS3 cell types.²³⁸ However, after extensive testing on the cell lines generated in this study, no luciferase activity was observed in OS3 cells either with agonist stimulation or with forskolin stimulation, which increases cAMP levels without receptor involvement. Therefore the luciferase assay was performed only on HEK chimeras using the agonists ACTH(1-24) and α -MSH.

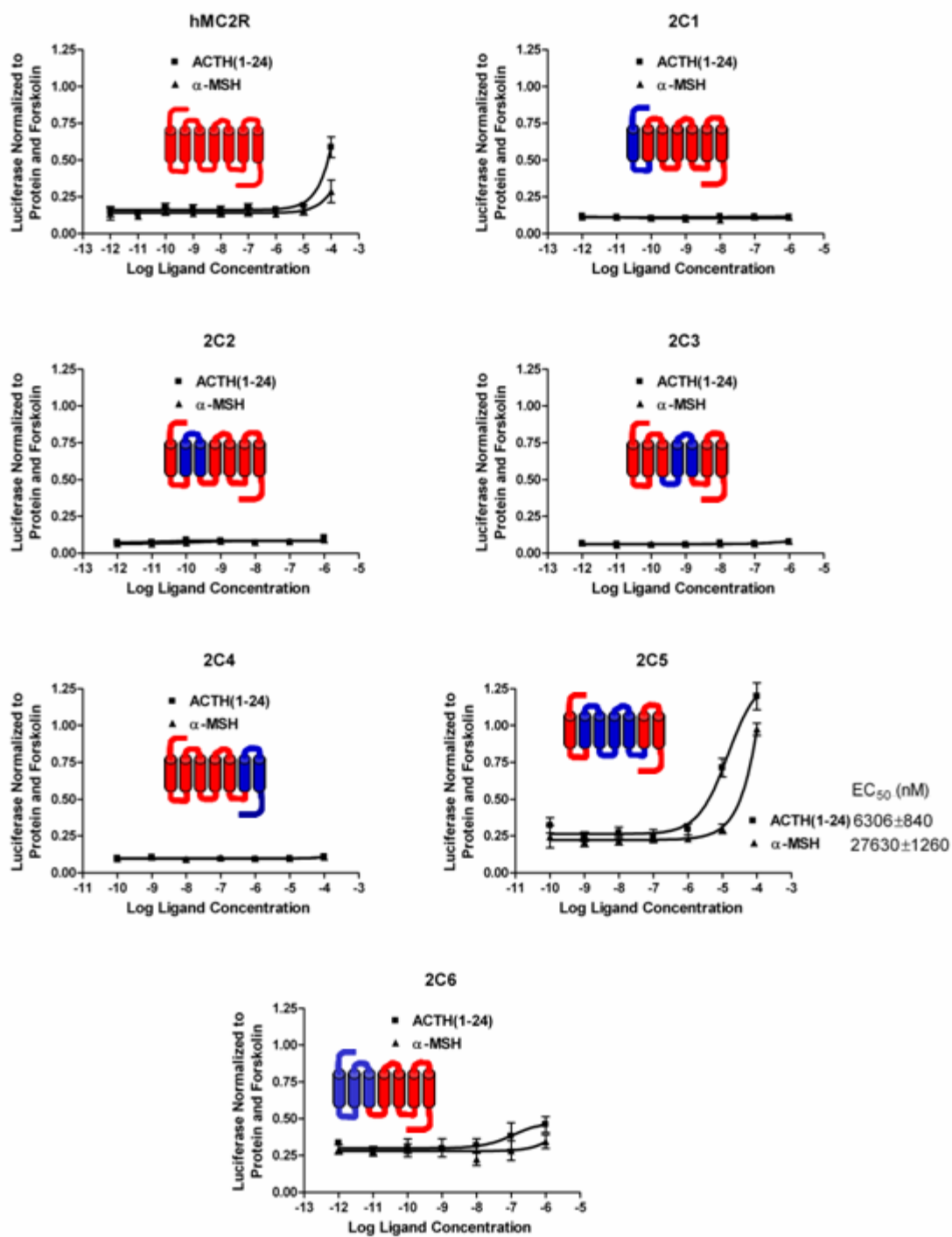


Figure 7-14. Summary of functional data from the luciferase assay performed on hMC2R wild type receptors and chimeras expressed in HEK293 cells.

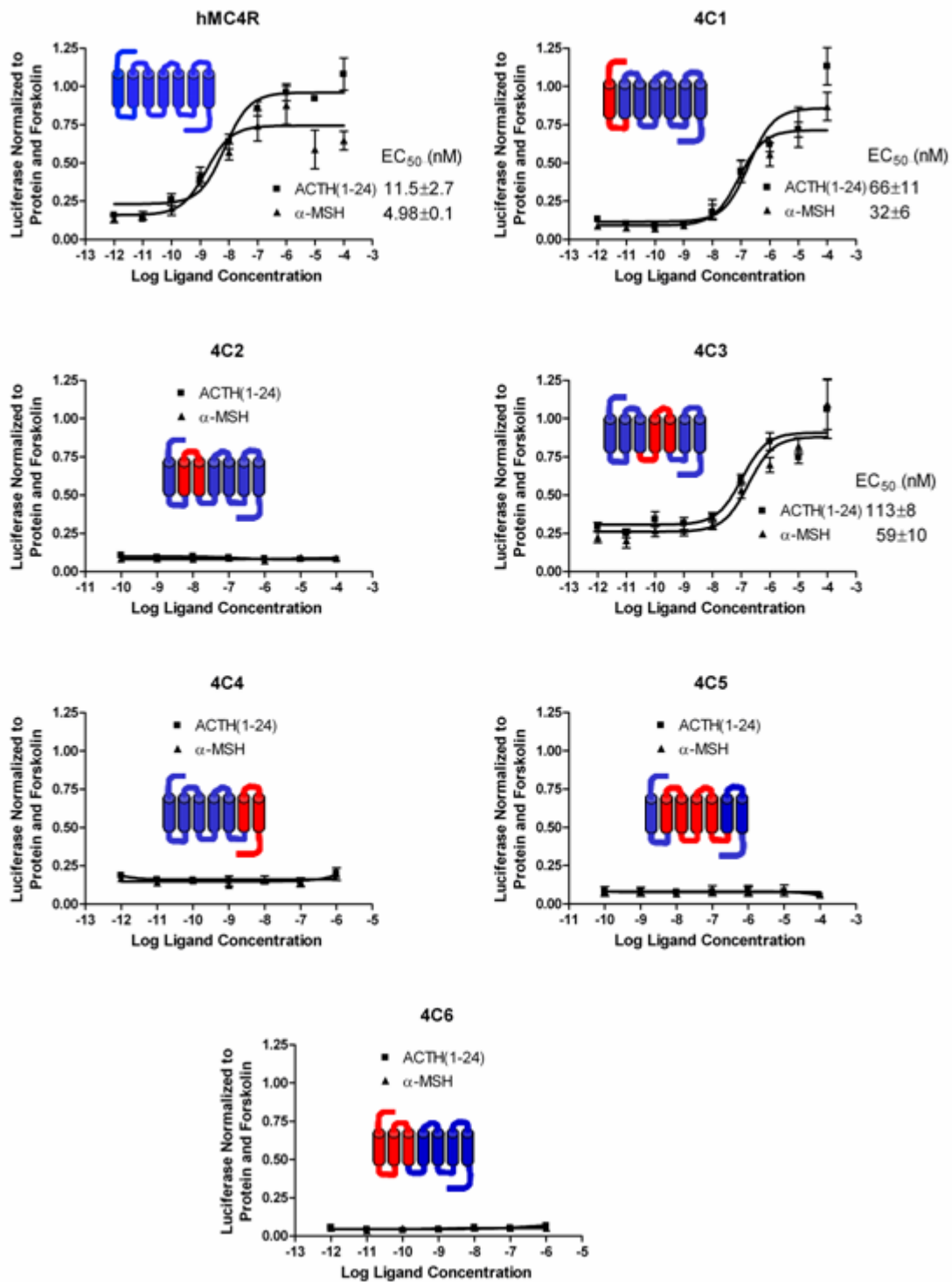


Figure 7-15. Summary of functional data from the luciferase assay performed on hMC4R wild type receptors and chimeras expressed in HEK293 cells.

Functional data is shown in Figures 7-14 and 7-15, and in Table 7-4. Both wild type receptors exhibited agonist EC₅₀ values within reported values. Most chimeras, however, did not have any activity when stimulated with ACTH(1-24) or α -MSH. These inactive receptors were 2C1, 2C2, 2C3, 2C4, 2C6, 4C2, 4C4, 4C5, and 4C6. Only three chimeras had activity with these ligands: 2C5, 4C1, and 4C3. Chimera 4C1 was the most potent, with only 6-fold decreased potency as compared to the hMC4R. Like the wild type receptor, α -MSH was twice as potent as ACTH. Chimera 4C3 is the next most potent receptor. It was 10-fold less potent than the wild type receptor, and α -MSH was twice as potent as ACTH. The only hMC2R chimera that exhibited any activity was 2C5. This receptor was significantly less potent than the wild type receptor, but α -MSH was still a full agonist. ACTH reached 100% stimulation as compared to the forskolin control, but was a micromolar agonist instead of a nanomolar agonist.

Table 7-4. Functional activity of α -MSH and ACTH(1-24) at selected chimeras.

Ligand	Cell Line EC ₅₀ (nM)			
	hMC4R	4C1	4C3	2C5
α -MSH	4.98±0.1	32±6	59±10	27630±1260
ACTH(1-24)	11.5±2.7	66±11	113±8	6306±840

EC₅₀ values calculated from the average of at least three experiments.

Functional Assay: cAMP

As the luciferase assay did not prove effective for assaying the chimeric receptors expressed in OS3 cells, the cAMP assay was used. However, once again no significant response was observed in the OS3 cells generated in this study. It is unknown why the cAMP assay failed as it was used earlier in this study to characterize the first Flag-hMC2R construct in OS3 cells. It may be that the receptor expression was too low to produce a significant response. As a result, no functional activity was obtained for OS3 cells.

Discussion

Chimeras in HEK293 Cell Lines

The HEK293 cell line is derived from a culture of human embryonic kidney cells transformed with sheared DNA from the adenovirus 5 virus.²²⁴ It is a valuable cell line often used for protein expression and functional receptor assays. The cell line does not contain any endogenous melanocortin receptors, but will express functional MC1,3-5 receptors upon transfection. The MC2R, however, is not functional when expressed in this cell line.^{84,85} The hMC2R is only functional in cell lines of adrenal origin such as the Y1, Y6, and OS3 cell lines.^{228,238} This study seeks to determine the reasons why the hMC2R is not functional in HEK293 cells and why the hMC2R is stimulated by ACTH but not by the other endogenous melanocortin ligands.

The first area of interest explored was the possibility of an accessory protein which may be expressed selectively in adrenal cells and is necessary for MC2R activity. Two classes of accessory proteins were investigated, the RAMPs and MRAP. The RAMP family has been shown to associate with calcitonin receptor family proteins and is essential for its activity. MRAP has recently been shown to be involved in MC2R expression and functional activity.⁸⁶ During the course of this dissertation work, it was reported that co-transfection of MRAP with the MC2R into HEK293 cells resulted in a functional receptor.³⁶² In this study, RT-PCR was used to determine the gene expression of RAMP1-3 and MRAP in HEK293 transfected with the hMC4R gene and OS3 cell lines transfected with the hMC2R gene. One group of cells of each type was stimulated with 10^{-7} M ACTH(1-24) for 6 h prior to mRNA isolation. Results are shown in Figure 7-6. The only accessory protein mRNA to be detected were RAMP 2 and 3 in unstimulated hMC4R-HEK cells. Upon ACTH stimulation of this cell type, RAMP2 expression levels were significantly inhibited and RAMP3 was no longer detected. No RAMPs were found

in the OS3 cells. These data indicate that the RAMP family of proteins is most likely not involved in hMC2R activity. MRAP mRNA was not detected in any cell types. This may be misleading, however, as the human MRAP gene probe was used in the experiments and the OS3 cell line is a mouse cell line (see Figure 7-7 for gene sequence alignment). Though the related Y1 and Y6 lines have been shown to express MRAP,⁸⁶ the OS3 cell line has not been tested in the literature. It is likely that MRAP would be present in the OS3 cells if a mouse probe were used. These data represent, to the best of the author's knowledge, the first examples of RAMP expression in HEK and OS3 cell lines.

Following the RT-PCR experiments, a chimeric receptor approach was applied to the problem of why the hMC2R is not expressed in HEK cells and why the hMC2R is only stimulated by ACTH. This method involves the substitution of large segments of one receptor with another receptor. This is done to investigate the effects of large groups of amino acids on receptor structure and function. Since the hMC4R is well-characterized, it was used along with the mMC2R to generate chimeric receptors. Figure 7-3 shows the chimeras generated in this study. A recent paper by Chen *et al.* describes the analysis of hMC4R chimeras created by the substitution of TM regions from the hMC2R in order to investigate the regions of the hMC4R necessary for α -MSH binding.³⁶⁹ It was determined that TM2, TM3 and TM6 of the hMC4R were involved in α -MSH binding.³⁶⁹ The chimeras generated here represent larger regions of the receptors, including intracellular and extracellular loops and both the hMC4R and its corresponding hMC2R chimera were made to serve as internal controls.

A summary of the FACS data is presented in Figure 7-11. Expression data and mean fluorescence are presented both as raw data and as data normalized to the wild type. Expression data gives information about where the receptor is localized within the cell. The chimera data can

be normalized to the wild type expression to show if the surface expression is increased or decreased. Surface expression is very important as the ligand cannot bind to the receptor if it is retained inside the cell. One detail noticed during FACS analysis can be seen on the histogram analyses in Appendix C and Figure 7-13. It appears that there are two populations of receptors in the cells. One group has a higher expression or Flag-antibody binding level than the other. It may be that there are possibly two cell populations, one with higher expression, or it could be that one population has a greater affinity between the Flag and anti-Flag antibody than the other. Another possibility is that some receptors may be in a conformation that hides or covers up the Flag tag so that the antibody cannot access the tag as efficiently.

FACS analysis revealed that chimeras 2C1, 2C3 and 2C6 have a similar total expression as the hMC2R wild type, but surface expression is increased significantly. Amongst the hMC4R chimeras, all chimeras have a similar surface and total expression as the hMC4R wild type, though 4C4 has slightly less surface expression. Another parameter that may be analyzed from FACS data is the mean fluorescence (MF). This reveals the relative receptor expression per cell. A high MF value indicates that each cell is expressing a high concentration of receptor. A low MF value indicates that each cell expresses a low level of receptor. When each chimera is plotted as surface expression versus MF (Figure 7-16) it is revealed that that the 2C1, 2C3 and 2C6 receptors, which had an increased surface expression compared to the hMC2R wild type, also all express high levels of receptor. Interestingly, when the chimeras were tested for functional activity using the luciferase assay (Figure 7-14 and 7-15, Table 7-4), the 2C5 chimera was the only hMC2R chimera to have functional activity. The hMC2R chimeras expressing high levels of receptor were not functional. This leads to the idea that overexpression of the receptor may be inhibiting activity. When extremely high levels of receptor are continually expressed, it becomes

difficult for the cellular machinery to keep up. With high levels of expression, one or more signaling factors may be titrated, leading to a loss of activity due to improper folding or membrane insertion. A positive forskolin response during stimulation indicates that the signal transduction machinery is probably still functional. Another theory is that with so much surface expression, there may simply be too many receptors in a small area, leading to overcrowding and improper receptor conformation. Chimera 2C5, which is the only active hMC2R chimera, expresses much lower levels of receptor than 2C1, 2C3 and 2C6, which are not active, lending a level of credence to this theory.

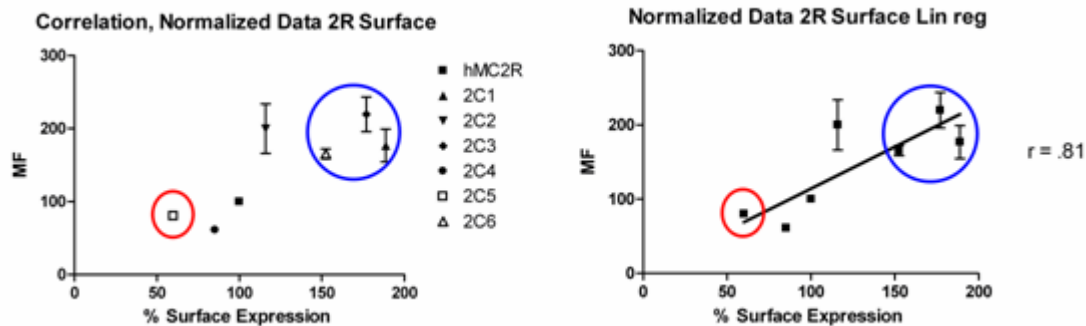


Figure 7-16. Correlation plots of HEK hMC2R chimera data; % Surface Expression vs. Mean Fluorescence. Blue circle surrounds chimeras 2C1, 2C3, and 2C6. Red circle shows chimera 2C5.

When the hMC4R receptors were tested for functional activity, only the wild type receptor, 4C1 and 4C3 displayed any activity. Additionally, among the chimeras with activity, there was no preference for one ligand over another. It should be noted that the EC_{50} value for α -MSH at the wild type hMC4R was over 10-fold higher than expected.^{42,43,56,370} This may be a result of transfection efficiency or other problems which may have occurred during detection.

Additionally, no difference in ligand selectivity was observed between the wild type hMC4R and the active chimeras 4C1, 4C3 and 2C5. This experiment did not answer the question about ligand selectivity. Functional assay of the chimeras in OS3 cells may have helped to clarify this

hMC1R DNVIDVITCSSMLSSLCLFLGAIIVDRYISI
hMC2R DDIIDSLFVLSLLGSIFSLSVIAADRYITI
hMC3R DNIFDSMICISLVSASICNLLAIAVDRYVTI
hMC4R DNVIDSVICSSLLASICSLLSIAVDRYFTI
hMC5R DNVFDSMICISVVASMCSSLLAIAVDRYVTI
2C1 DDIIDSLFVLSLLGSIFSLSVIAADRYITI
2C2 DNVIDSVICSSLLASICSLLSIAVDRYITI
2C3 DDIIDSLFVLSLLGSIFSLSVIAADRYFTI
2C4 DDIIDSLFVLSLLGSIFSLSVIAADRYITI
2C5 DNVIDSVICSSLLASICSLLSIAVDRYFTI
2C6 DNVIDSVICSSLLASICSLLSIAVDRYITI
4C1 DNXIDSVICSSLLASICSLLSIAVDRYFTI
4C2 DDIIDSLFVLSLLGSIFSLSVIAADRYFTI
4C3 DNVIDSVICSSLLASICSLLSIAVDRYITI
4C4 DNVIDSVICSSLLASICSLLSIAVDRYFTI
4C5 DDIIDSLFVLSLLGSIFSLSVIAADRYITI
4C6 DDIIDSLFVLSLLGSIFSLSVIAADRYFTI

FYALRYHSIVT
 FHALRYHSIVT
 FYALRYHSIMT
 FYALQYHNIMT
 FYALRYHHIMT
 FHALRYHSIVT
 FHALRYHSIVT
 FYALQYHNIMT
 FHALRYHSIVT
 FYALQYHNIMT
 FHALRYHSIVT
 FYALQYHNIMT
 FHALRYHSIVT
 FYALQYHNIMT
 FHALRYHSIVT
 FYALQYHNIMT
 FHALRYHSIVT
 FYALQYHNIMT

TM4

hMC1R LPRARRAVAAIIVVASVVFSTLFI
hMC2R MRRTVVVLTVIWTFCTGTGITMV
hMC3R VRKALTLIVAIWVCCGVCG V V
hMC4R VKRVGIIISCIWAACVSGILFI
hMC5R ARRSAGI IAGIWAFACTGCGIVFI
2C1 MRRTVVVLTVIWTFCTGTGITMV
2C2 MRRTVVVLTVIWTFCTGTGITMV
2C3 VKRVGIIISCIWAACVSGILFI
2C4 MRRTVVVLTVIWTFCTGTGITMV
2C5 VKRVGIIISCIWAACVSGILFI
2C6 MRRTVVVLTVIWTFCTGTGITMV
4C1 VKRVGIIISCIWAACVSGILFI
4C2 VKRVGIIISCIWAACVSGILFI
4C3 MRRTVVVLTVIWTFCTGTGITMV
4C4 VKRVGIIISCIWAACVSGILFI
4C5 MRRTVVVLTVIWTFCTGTGITMV
4C6 VKRVGIIISCIWAACVSGILFI

Loop 4 (EC)

AYYDH
 IFSHH
 FIVYS
 IYSDS
 LYSES
 IFSHH
 IFSHH
 IYSDS
 IFSHH
 IYSDS
 IFSHH
 IYSDS
 IFSHH
 IYSDS
 IFSHH
 IYSDS

TM5

hMC1R VA VLLCLVVFFLAMLVLMVLYVHMLARACQHAQG
hMC2R VPT VITFTSL FPLMLVFILCLYVHMFLARSHTRK
hMC3R ESKMVI VCLITMFFAMMLLGMTLYVHMFLFARLHVKR
hMC4R SA VIICLITMFFTMLALMASLYVHMFLMARLHIKR
hMC5R TY VILCLISMFFAMFLVLSLYIHMFLARLTHVKR
2C1 VPTVITFTSLFPLMLVFILCLYVHMFLARSHTRK
2C2 VPTVITFTSLFPLMLVFILCLYVHMFLARSHTRK
2C3 SAVIICLITMFFTMLALMASLYVHMFLARSHTRK
2C4 VPTVITFTSLFPLMLVFILCLYVHMFLARSHTRK
2C5 SAVIICLITMFFTMLALMASLYVHMFLMARLHIKR
2C6 VPTVITFTSLFPLMLVFILCLYVHMFLARSHTRK
4C1 SAVIICLITMFFTMLALMASLYVHMFLMARLHIKR
4C2 SAVIICLITMFFTMLALMASLYVHMFLMARLHIKR
4C3 VPTVITFTSLFPLMLVFILCLYVHMFLMARLHIKR
4C4 SAVIICLITMFFTMLALMASLYVHMFLMARLHIKR
4C5 VPTVITFTSLFPLMLVFILCLYVHMFLARSHTRK
4C6 SAVIICLITMFFTMLALMASLYVHMFLMARLHIKR

Loop 5 (IC)

IARLHKRQRPVHRPVHQ
 ISTLP
 IAALPPADGVAPQQH
 IAVLPGTGAIRO
 IAALPGASSARQRTSMQ
 ISTLP
 ISTLP
 ISTLP
 ISTLP
IAVLPGTGAIRO
 ISTLP
IAVLPGTGAIRO
 IAVLPGTGAIRO
IAVLPGTGAIRO
 IAVLPGTGAIRO
 ISTLP
 IAVLPGTGAIRO

TM6

hMC1R GFGLKGAVTLTILLGIFFLCWGPPFFLHLTLIVL
hMC2R RANMKGAILTLTILLGVFIFCWAPFVLHVLLMTF
hMC3R SCMKGAVTITILLGVFIFCWAPFVLHLVLIIT
hMC4R GANMKGAILTLTILLGVFVVCWAPFVLHLIFYIS
hMC5R GAVT VTMLLGVFTVCWAPFVLHLTLMLS
2C1 RANMKGAILTLTILLGVFIFCWAPFVLHVLLMTF

Loop 6 (EC)

CPEHPTCGC
 CPSNPYCAC
 CPTNPYCIC
 CPQNPYCV
 CPQNYCSR
 CPSNPYCAC

2C2	RANMKGAITLTILLGVFIFCWAPFVLHVLLMTF	CPSNPYCAC
2C3	RANMKGAITLTILLGVFIFCWAPFVLHVLLMTF	CPSNPYCAC
2C4	RANMKGAITLTILLGVFVVCWAPFFLHLIFYIS	CPQNPYCVC
2C5	GANMKGAITLTILLGVFIFCWAPFVLHVLLMTF	CPSNPYCAC
2C6	RANMKGAITLTILLGVFIFCWAPFVLHVLLMTF	CPSNPYCAC
4C1	GANMKGAITLTILLGVFVVCWAPFFLHLIFYIS	CPQNPYCVC
4C2	GANMKGAITLTILLGVFVVCWAPFFLHLIFYIS	CPQNPYCVC
4C3	GANMKGAITLTILLGVFVVCWAPFFLHLIFYIS	CPQNPYCVC
4C4	GANMKGAITLTILLGVFIFCWAPFVLHVLLMTF	CPSNPYCAC
4C5	RANMKGAITLTILLGVFVVCWAPFFLHLIFYIS	CPQNPYCVC
4C6	GANMKGAITLTILLGVFVVCWAPFFLHLIFYIS	CPQNPYCVC
	TM7	C-terminus (IC)
hMC1R	IFKNFNLFLALIICNAIIDPLIYAFHSQ	ELRRTLKEVLTCSW
hMC2R	YMSLFQVNGMLIMCNAVIDPFIYAFRSP	ELRDAFKKMIFCSRYW
hMC3R	YTAHFNTYLVLIMCNSVIDPLIYAFRSL	ELRNTFREILCGCNGMNLG
hMC4R	FMSHFNLYLILIMCNSIIDPLIYALRSQ	ELRKTfKEIICCYPLGGLCDLSSRY
hMC5R	FMSHFNMYLILIMCNSVMDPLIYAFRSP	EMRKTfKEIICCRGFRIACSFPRRD
2C1	YMSLFQVNGMLIMCNAVIDPFIYAFRSP	ELRDAFKKMIFCSRYW
2C2	YMSLFQVNGMLIMCNAVIDPFIYAFRSP	ELRDAFKKMIFCSRYW
2C3	YMSLFQVNGMLIMCNAVIDPFIYAFRSP	ELRDAFKKMIFCSRYW
2C4	FMSHFNLYLILIMCNSIIDPLIYALRSQ	ELRKTfKEIICCYPLGGLCDLSSRY
2C5	YMSLFQVNGMLIMCNAVIDPFIYAFRSP	ELRDAFKKMIFCSRYW
2C6	YMSLFQVNGMLIMCNAVIDPFIYAFRSP	ELRDAFKKMIFCSRYW
4C1	FMSHFNLYLILIMCNSIIDPLIYALRSQ	ELRKTfKEIICCYPLGGLCDLSSRY
4C2	FMSHFNLYLILIMCNSIIDPLIYALRSQ	ELRKTfKEIICCYPLGGLCDLSSRY
4C3	FMSHFNLYLILIMCNSIIDPLIYALRSQ	ELRKTfKEIICCYPLGGLCDLSSRY
4C4	YMSLFQVNGMLIMCNAVIDPFIYAFRSP	ELRDAFKKMIFCSRYW
4C5	FMSHFNLYLILIMCNSIIDPLIYALRSQ	ELRKTfKEIICCYPLGGLCDLSSRY
4C6	FMSHFNLYLILIMCNSIIDPLIYALRSQ	ELRKTfKEIICCYPLGGLCDLSSRY

Figure 7-17. Amino acid alignment of all melanocortin receptors and chimeras. IC = intracellular, EC = extracellular, IL = intracellular loop, EL = extracellular loop. Significant differences between the hMC2R and hMC4R and chimeras with functional activity are highlighted. Blank spaces inserted for alignment purposes.

Based on preliminary FACS and functional data, the roles of each receptor were not clearly seen. Therefore all melanocortin receptors and chimeras were aligned with divisions between the proposed loop and TM regions based on previous melanocortin alignments (Figure 7-17).^{43,49} These amino acid alignments revealed interesting information about the structural differences between the hMC2R and the other melanocortin receptors. When looking at the sequences, the first major difference is seen in EL2. The hMC1, 3-5R all contain significant sequence similarity, however, the hMC2R differs greatly from the other receptors. Additionally, IL5 is significantly different in the other melanocortin receptors than in the hMC2R. As all wild type receptors and chimeras that express the combination of EL2 and IL5 similar to the hMC4R are active in HEK

cells (4C1, 4C3, 2C5), and the hMC2R and chimeras that contain either the EL2 or IL5 from hMC2R are not active in HEK cells, it is possible that these loops are necessary for activity in HEK cells. A protein database search of the IL5 of the MC1,3-5R revealed that there is some sequence similarity between this loop and other GPCRs. Among the classes of receptors that contain homologous sequences are the olfactory receptors of several species³⁷¹⁻³⁷⁵ and taste receptors, which have been shown to be active in HEK cells,³⁷⁶ among many others. In order to prove whether or not these loops are essential for activity in HEK cells, hMC2R chimeras should be made which incorporate the EL2 and/or IL5 from the hMC4R into the hMC2R template. Functional assay of these new chimeras should show whether activity is conferred on the hMC2R with the introduction of one or both of these loops.

Chimeras in OS3 Cell Lines

Along with the HEK293 cell line, all chimeras were stably transfected into OS3 cells, which is an adrenal cell line developed from the Y1 adrenocortical tumor cell line. These cell lines contain a wild type MC2R gene, however this DNA sequence is not functional due to growth in the presence of forskolin.²²⁸ The cells do, however, contain an intact cAMP signal transduction pathway, resulting in a functional transfected MC2R.^{228,229}

FACS analysis of OS3 wild type receptors and chimeras resulted in similar expression patterns as was seen in HEK cells. The main difference is that expression levels were significantly lower in OS3 cells. Figure 7-12 summarizes the FACS data showing percent expression and mean fluorescence levels. When compared to wild type receptors, chimera 2C1, 2C2, and 2C3 showed increased surface expression and 2C5 expression was similar to the hMC2R expression. Chimeras 4C2 and 4C5 exhibited increased expression as compared to hMC4R wild type, though 4C4 showed significantly decreased expression levels. When MF data is compared to wild type, chimeras 2C1, 2C2, 2C3, 2C5 and 2C6 all had decreased MF values as

compared to the hMC2R, and chimera 4C4 showed significantly decreased fluorescence levels compared to the hMC4R, but the other hMC4R chimeras had similar expression as compared to wild type.

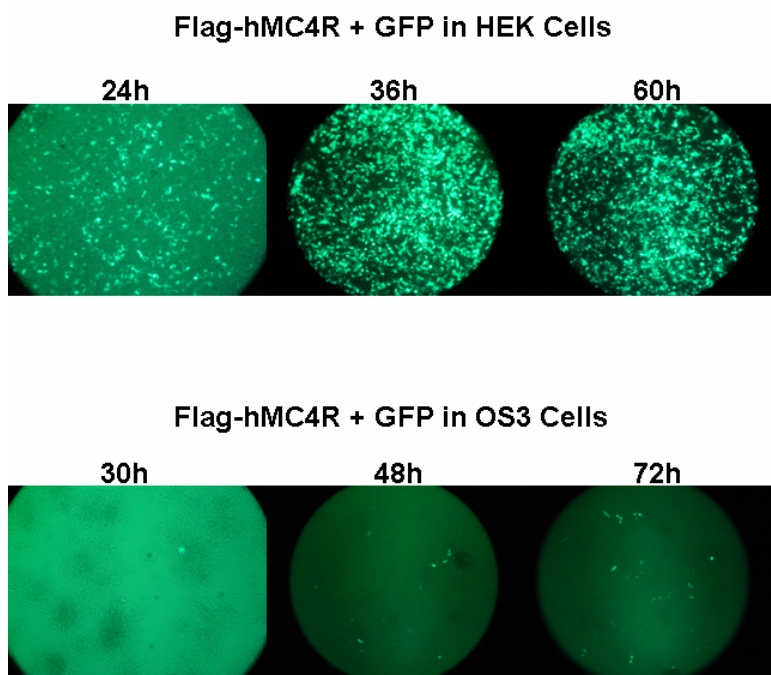


Figure 7-18. Time course of HEK and OS3 cell lines transiently transfected with GFP and incubated at 35°C and 3% CO₂. HEK cells were transfected using the calcium phosphate method. OS3 cells were transfected using Fugene 6 (Roche).

It has been reported that the luciferase assay may be used with both HEK and OS3 cell types.²³⁸ However, after extensive testing, no luciferase activity was observed in OS3 cells either with agonist stimulation or with forskolin stimulation, which increases cAMP levels without receptor involvement. Furthermore, the cAMP assay, which has been extensively used to test the hMC2R in OS3 cells, was not able to detect a functional response in these studies. It is unknown why the assays did not work in this case. One issue is possibly transfection efficiency. OS3 cells are notoriously difficult to transfect (<2% transfection efficiency), and these are no different. Figure 7-12 shows FACS analysis data from the OS3 chimeras. Compared with HEK293 chimeras (Figure 7-11) receptor levels were significantly lower in the OS3 cells. Figure 7-18

shows both HEK and OS3 cells transfected with a GFP plasmid (experiments performed with the help of Dr. Hendrik Luesch). Previous studies had shown that the calcium phosphate method is ineffective using OS3 cells (data not shown), so the lipid transfection reagent Fugene 6 (Roche) was used to transfect the OS3 cells. A time course is shown in Figure 7-18, and it is clear that HEK cells transfect very efficiently, but the OS3 cell line does not take up the DNA very efficiently. It may be that the stable cell lines simply did not express enough of the receptor to produce a functional response. In the future, it may be possible to use a different cell line which may transfect better than OS3 cells to test function of the hMC2R chimeras.

Conclusions and Future Directions

In summary, this study has identified new receptor chimeras of the hMC2R and hMC4R which have activity when stimulated with ACTH(1-24) and α -MSH, though no ligand selectivity was observed. All chimeras were expressed on the surface of both HEK and OS3 cells, though OS3 expression was very low. Chimeras 4C1, 4C3 and 2C5 are the only chimeras to have functional activity in HEK cells when tested with the luciferase assay. These chimeras are unique in that they are the only chimeras made which contain both the EL3 and IL5 from the hMC4R. It is suggested that these domains may be important for activity in HEK cells. Future studies should include the construction of hMC2R chimeras which contain one or both of these loops from the hMC4R to test their importance for HEK activity. Another important experiment that should be performed is binding studies of the chimeras with either iodinated ACTH or NDP-MSH. These studies would allow the evaluation of the ligand-receptor interaction and determination of regions of the receptors required for ligand binding versus signal transduction.

OS3 cells stably transfected with the chimeras were shown to express the receptor on the cell surface, however expression levels were very low and no functional activity was observed. It may be possible to use a different cell line which is able to express a functional hMC2R to test

these chimeras for activity. Binding studies would also be extremely valuable in the characterization of these chimeras.

Gene expression assays performed on HEK and OS3 cells represent the first studies into the expression of RAMP1-3 and MRAP in these cell lines. No RAMPs were observed in the OS3 cells, though RAMP2 and 3 were present in unstimulated HEK cells but expression was significantly decreased when the cells were stimulated with ACTH(1-24). No MRAP was observed in any cell lines, but the human probe was used on the murine OS3 cell line so it is unknown whether mouse Mrap is present in this cell line. Future studies of hMC2R expression in HEK cells should include co-transfection of MRAP as it has recently been shown to confer activity to the hMC2R in HEK cells.³⁶²

These studies represent important advancements in the characterization of the hMC2R. Novel chimeras were created that have activity in HEK293 cells, which are not able to functionally express the wild type receptor. Further studies are required to fully elucidate the functional and binding activity of these chimeras. It is hoped that these discoveries may someday aid in the understanding of the role of the hMC2R in stress and adrenal disorders.

CHAPTER 8 CONCLUDING REMARKS

Structure-Activity Relationship Studies Of Peptides: A Study Of Intramolecular Cation- π Interactions In Melanocortin Agonists And The Effects On Agonist And Antagonist Selectivity

In this study, MTII, a cyclic synthetic melanocortin peptide, was modified at the arginine and D-phenylalanine positions to investigate the role cation- π interactions may play in the agonist or antagonist potency of this ligand at the melanocortin receptors. It was hypothesized that when combined with any one of six aromatic π systems [Phe, DPhe, Nal(1'), DNal(1'), Nal(2'), or DNal(2')], peptides with an arginine should exhibit the greatest potency and those with an alanine should have a significant loss of activity, with lysine peptides exhibiting an intermediate potency. Additionally, in accordance with the melanocortin antagonist SHU9119, compounds containing a DNal(2') should exhibit antagonist activity. Naphthylalanine derivatives were used because the double aromatic ring results in a greater negative electrostatic potential than the single ring of phenylalanine, and thus should interact more strongly with the cation.

Several conclusions may be drawn from the information obtained in this study. First it appears that the original hypothesis is correct and there may be a significant cation- π interaction between the Arg and the adjacent aromatic amino acid in melanocortin ligands. This was confirmed by the observation that in the majority of peptides synthesized in this study the Arg compound was the most potent, followed by Lys, and finally Ala as the least potent compound. It was also observed that in each aromatic system tested, the D form of the amino acid was more potent than the L form. Additionally, DNal(2') is the only aromatic system tested which has antagonist activity at the mMC3R and mMC4R. An interesting observation is that the Nal(1')/Ala combination results in a peptide with antagonist activity at the mMC4R. These

studies are significant as they provide important information which may be used in the future to design new peptide and non-peptide ligands for the melanocortin receptors.

Design Of Peptidomimetics And Small Molecules: 1,4-Benzodiazepine-2,5-Diones As nM Melanocortin Agonists

The benzodiazepine template has been widely studied as a scaffold for non-peptide drugs. As many targets are members of the G-protein coupled receptor super family (i.e. cholecystokinin, κ -opioid, oxytocin, and endothelin receptors), it was hypothesized that benzodiazepine derivatives could be designed as melanocortin ligands.

The 1,4-benzodiazepine-2,5-dione library synthesized in this study was designed to interact with proposed binding sites in the melanocortin receptors. Homology molecular modeling of the mMC1R^{44,341} and the mMC4R^{43,48-50,342} suggest the presence of hydrophobic and electrostatic binding pockets which are essential for binding of the melanocortin ligands to the receptor. Based on the results of this study, it was proposed that the p(Cl)-phenyl ring of the benzodiazepine and an aryl side chain may interact with the hydrophobic pockets and that a cationic component may interact with the anionic binding pocket.

The benzodiazepines reported herein were designed based on a set of 1,4-benzodiazepine-2,5-dione compounds synthesized by Christine G. Joseph of the Haskell-Luevano laboratory that were shown by functional analysis to have activity at the melanocortin receptors.

Based on these interesting pharmacology results, a new series of compounds (Compounds 39-58) were designed in order to investigate the structural requirements necessary for benzodiazepine activity at the melanocortin receptors, and to probe the structure-activity relationships at each point of diversity.

Future studies of this class of compounds should focus on the incorporation of aliphatic groups at R2, as well as halogens at R1. The R3 position seems to be less strict, allowing for the

incorporation of building blocks mimicking amino acid side chains of Phe, Lys, Arg, and Trp as well as others. The His side chain cannot be incorporated using this synthetic scheme due to the low stability of the imidazole side chain under the reductive environment necessary for its addition. It may also be interesting to incorporate substituted derivatives of Phe, as some of these have been shown to result in compounds with activity at the melanocortin receptors.⁷

In conclusion, this research has resulted in the identification of several benzodiazepine derivatives that exhibit agonist activity at the mouse melanocortin receptors. These compounds appear to have the most activity at the mMC1R, with only a few compounds exhibiting significant activity at the other receptors. These compounds are easy to synthesize due to the use of solid phase organic synthesis and may be readily purified allowing for the design of a large number of compounds. When substituted with building blocks that mimic the active sequence of peptide melanocortin ligands, this template has the potential to create compounds with increasing potency that may be used in the future as drugs to treat obesity.

Construction And Characterization Of Melanocortin-2 And -4 Receptor Chimeras

For many years ligands have been screened at the melanocortin receptors using the β -galactosidase assay. This assay works well with receptors expressed in HEK293 cells and the pCRE/ β -gal plasmid transiently transfected into the cells before stimulation.²⁰⁹ This method is effective for cells expressing the MC1R, MC3R, MC4R, or MC5R, however, when the MC2R is stably transfected into HEK 293 cells, there is no functional response in the β -galactosidase assay.⁸³

As has been previously stated, it is known that stimulation of OS3 cells stably transfected with the hMC2R gene results in a functional response. Conversely, HEK293 cells that contain the hMC2R do not produce a functional response when stimulated.^{84,85} Amino acid alignment of the hMC2R with the hMC4R has identified key amino acid changes in the transmembrane

regions which may be involved in ligand binding and/or signal transduction (Figure 7-1). To test the hypothesis that these amino acids are involved in the production of a functional hMC2 receptor in HEK293 cells, chimeric receptors were made to identify the role each transmembrane domain plays in ligand binding and signal transduction in the hMC2R. Entire transmembrane regions from the hMC4R were inserted into the hMC2R gene and these chimeric receptors stably transfected into OS3 cells and HEK293 cells. Following construction of chimeras and generation of stable cell lines, the expression and localization of the receptor was determined using FACS (Fluorescence Activated Cell Sorting). Functional assay of all chimeras in HEK293 cells was also performed to measure the response of the receptor to agonist stimulation.

In summary, this study has identified new receptor chimeras of the hMC2R and hMC4R which have activity when stimulated with ACTH(1-24) and α -MSH, though no ligand selectivity was observed. All chimeras were expressed on the surface of both HEK and OS3 cells, though OS3 expression was very low. Chimeras 4C1, 4C3 and 2C5 are the only chimeras to have functional activity in HEK cells when tested with the luciferase assay. These chimeras are unique in that they are the only chimeras made which contain both the EL3 and IL5 from the hMC4R. It is suggested that these domains may be important for activity in HEK cells. Future studies should include the construction of hMC2R chimeras which contain one or both of these loops from the hMC4R to test their importance for HEK activity. Another important experiment that should be performed is binding studies of the chimeras with radioactively labeled ACTH or NDP-MSH. These studies would allow the evaluation of the ligand-receptor interaction and determination of regions of the receptors required for ligand binding versus signal transduction.

OS3 cells stably transfected with the chimeras were shown to express the receptor on the cell surface, however expression levels were very low and no functional activity was observed. It

may be possible to use a different cell line which is able to express a functional hMC2R to test these chimeras for activity. Binding studies would also be extremely valuable in the characterization of these chimeras.

Gene expression assays performed on HEK and OS3 cells represent the first studies into the expression of RAMP1-3 and MRAP in these cell lines. No RAMPs were observed in the OS3 cells, though RAMP2 and 3 were present in unstimulated HEK cells but expression was significantly decreased when the cells were stimulated with ACTH(1-24). No MRAP was observed in any cell lines, but the human probe was used on the murine OS3 cell line so it is unknown whether mouse Mrap is present in this cell line. Future studies of hMC2R expression in HEK cells should include co-transfection of MRAP as it has recently been shown to confer activity to the hMC2R in HEK cells.³⁶²

These studies represent important advancements in the characterization of the hMC2R. Novel chimeras were created that have activity in HEK293 cells, which are not able to functionally express the wild type receptor. Further studies are required to fully elucidate the functional and binding activity of these chimeras. It is hoped that these discoveries may someday aid in the understanding of the role of the hMC2R in stress and adrenal disorders.

APPENDIX A
¹H-NMR OF 1,4-BENZODIAZEPINE-2,5-DIONES

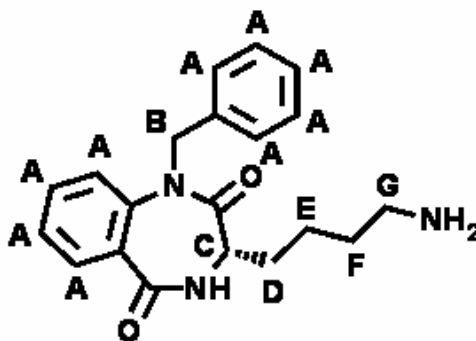
All compounds were dissolved in DMSO-*d*6 and spectra were obtained at room temperature.

Std Proton parameters

Automation directory:
Sample : BZD **BE**

Pulse Sequence: s2pu1
Solvent: dms0
Temp. 22.0 C / 295.1 K
Operator: witek
Mercury-400BB "nmr400"

Relax. delay 1.000 sec
Pulse 45.0 degrees
Acq. time 1.998 sec
Width 6402.0 Hz
32 repetitions
OBSERVE H1, 400.1218989 MHz
DATA PROCESSING
FT size 32768
Total time 1 min, 40 sec



A = 9 aromatic H, 7.65—7.08
B = 2H, 5.33 and 4.98
C = 1H, 3.73
D = 2H, 1.85—1.65
E = 2H, 1.40—1.25
F = 2H, 1.50—1.45
G = 2H, 2.75—2.60

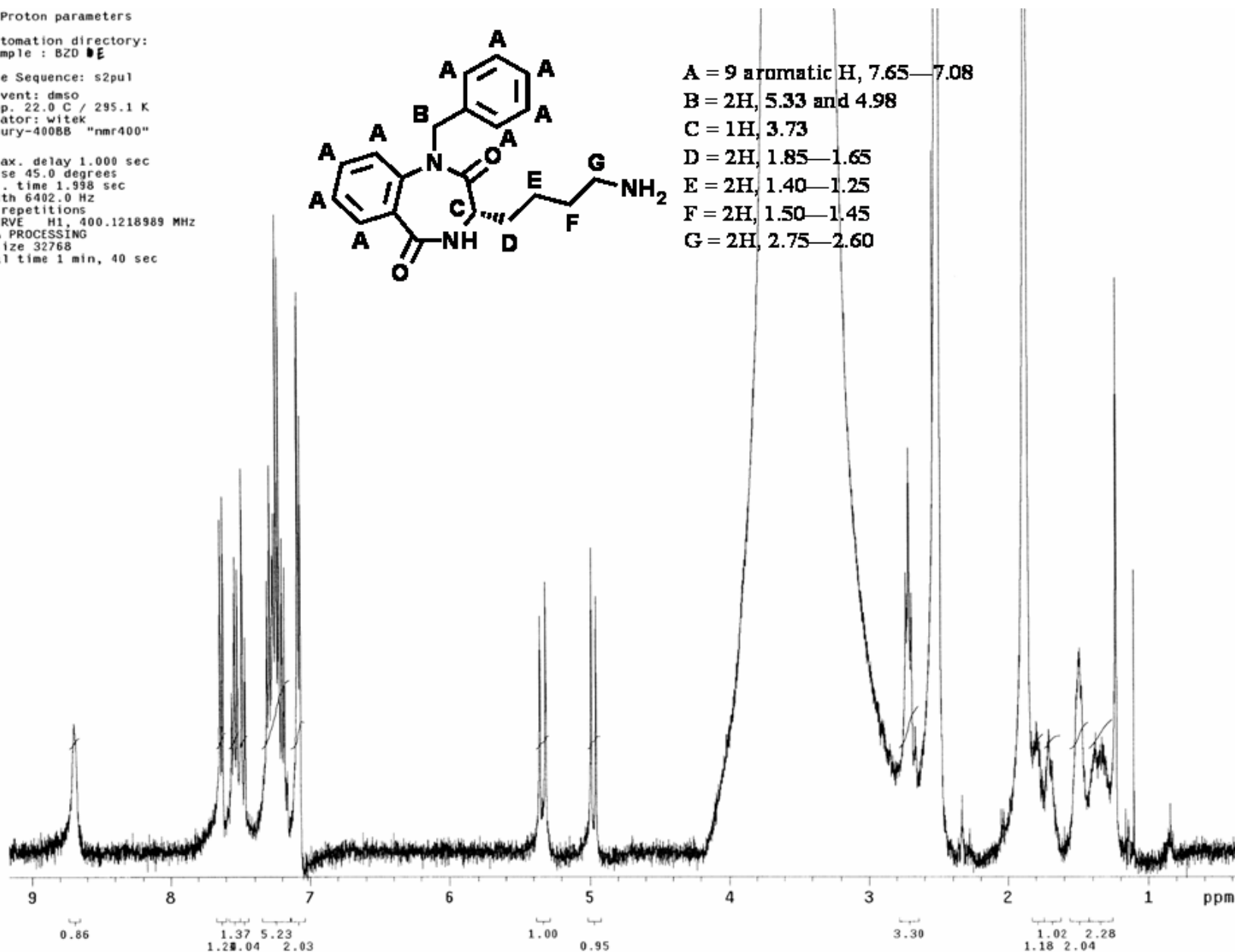


Figure A-1. Compound 39 (KRW9-70E) ¹H-NMR, 3-(4-aminobutyl)-1-benzyl-3,4-dihydro-1H-benzo[e][1,4]diazepine-2,5-dione.

Krista Wilson, KRW-5-37 in DMSO-D6
5 mm BBO Probe, Temp= 27 C, Non Spun, Bruker Avance 500 Console, Magnex 11.75 T/54 mm Magnet
Advanced Magnetic Resonance Imaging and Spectroscopy, McKnight Brain Institute, University of Florida
Jim Rocca, AMRIS

A = 18 aromatic H, 7.57—7.03

B = 2H, 5.15 and 4.87

C = 1H, 4.01—3.97

D = 2H, 3.14 and 2.94—2.89

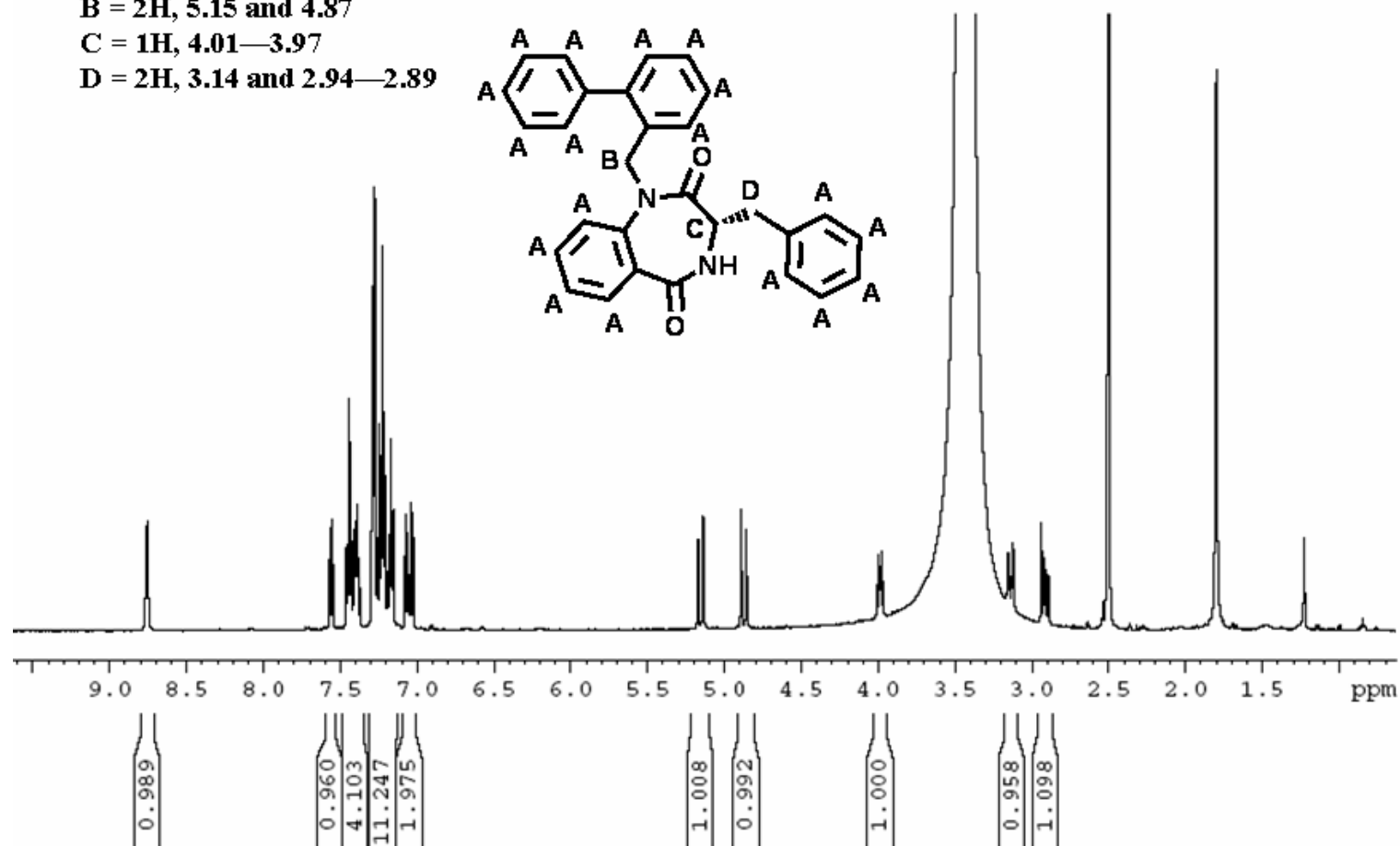


Figure A-2. Compound 40 (KRW5-37) ¹H-NMR, 3-Benzyl-1-biphenyl-2-ylmethyl-3,4-dihydro-1H-benzo[e][1,4]diazepine-2,5-dione.

Std Proton parameters

Automation directory:
Sample : BZD J

Pulse Sequence: s2pu1
Solvent: dms0
Temp. 22.0 C / 295.1 K
Operator: witek
Mercury-400BB "nmr400"

Relax. delay 1.000 sec
Pulse 45.0 degrees
Acq. time 1.938 sec
Width 6402.0 Hz
32 repetitions
OBSERVE H1, 400.1219000 MHz
DATA PROCESSING
FT size 32768
Total time 1 min, 40 sec

- A = 13 aromatic H, 7.66—7.06
- B = 2H, 5.13 and 4.87
- C = 1H, 3.76
- D = 2H, 1.78—1.68
- E = 2H, 1.56—1.44
- F = 2H, 3.03

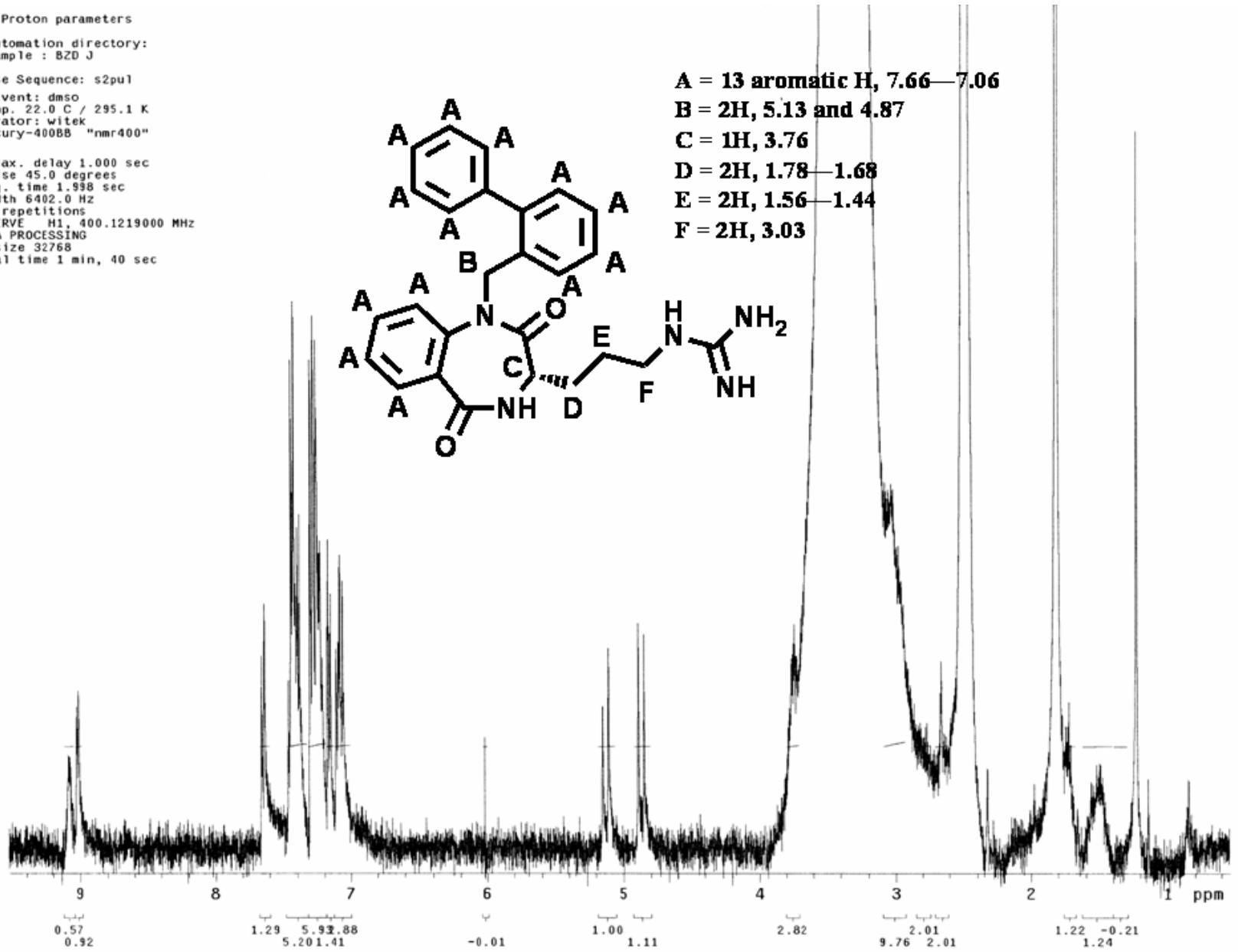
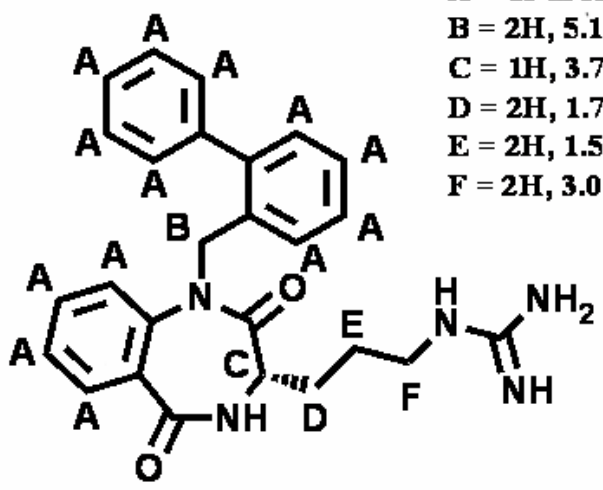


Figure A-3. Compound 41 (KRW 9-70J) ¹H-NMR, 1-(3-(1-(biphenyl-2-ylmethyl)-2,5-dioxo-2,3,4,5-tetrahydro-1H-benzo[e][1,4]diazepin-3-yl)propyl)urea.

Std Proton parameters

Automation directory:
Sample : B2D F

Pulse Sequence: s2pu1

Solvent: dms0
Temp. 22.0 C / 295.1 K
Operator: witek
Mercury-400BB "nmr400"

Relax. delay 1.000 sec
Pulse 45.0 degrees
Acq. time 1.998 sec
Width 6402.0 Hz
32 repetitions
OBSERVE H1, 400.1218996 MHz
DATA PROCESSING
FT size 32768
Total time 1 min, 40 sec

A = 13 aromatic H, 7.65—7.07

B = 2H, 5.16 and 4.87

C = 1H, 3.69

D = 2H, 1.78—1.61

E = 2H, 1.36—1.11

F = 2H, 1.46—1.38

G = 2H, 2.64

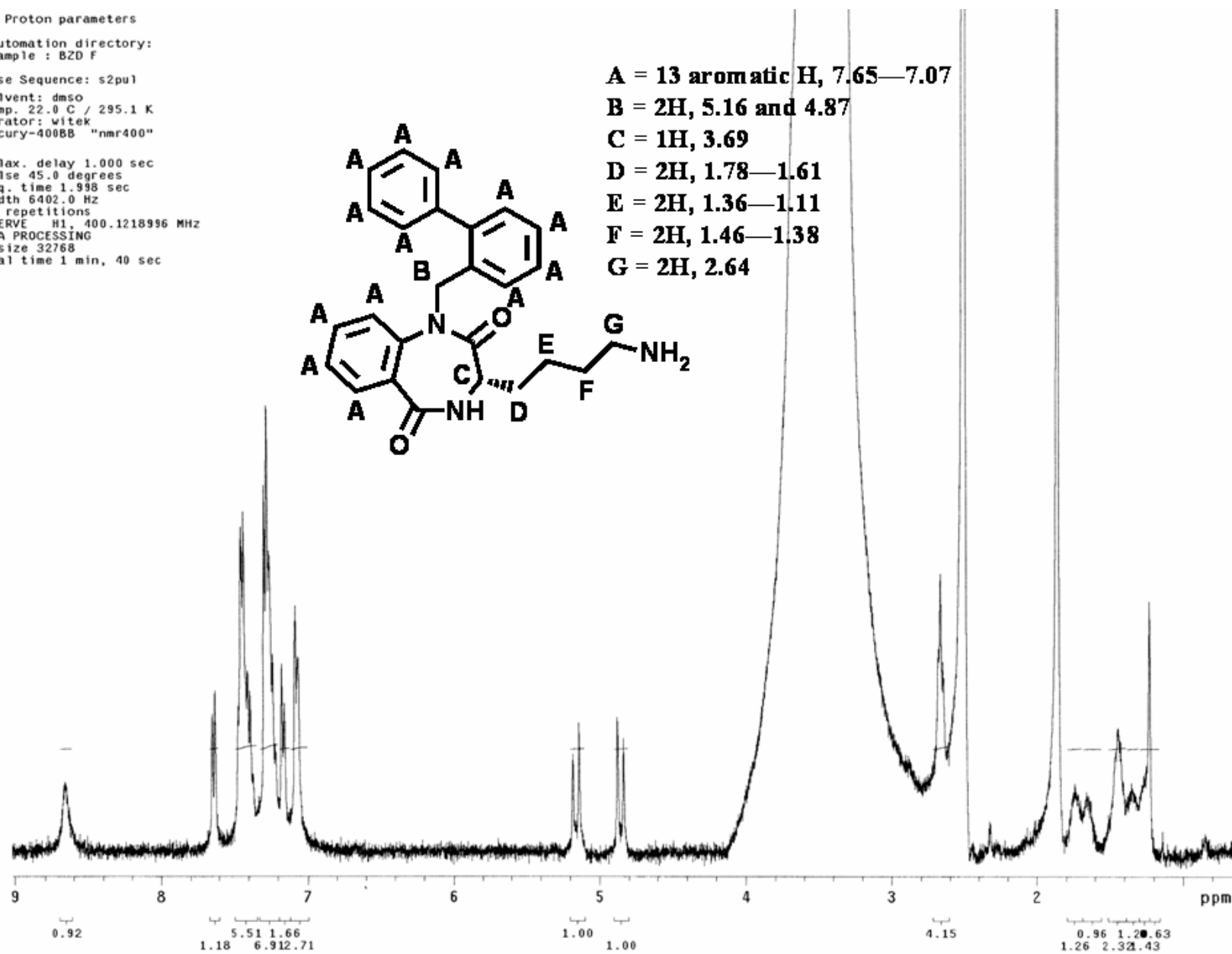
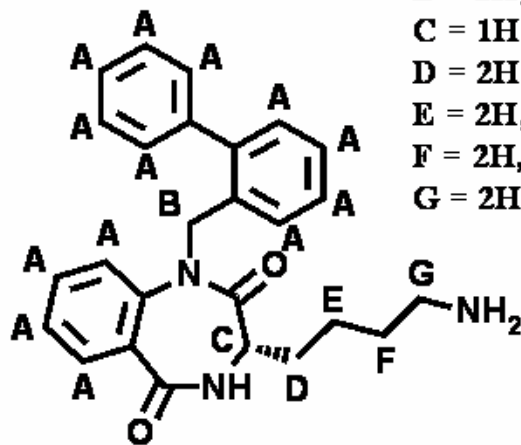


Figure A-4. Compound 42 (KRW9-70F) ¹H-NMR, 3-(4-aminobutyl)-1-(biphenyl-2-ylmethyl)-3,4-dihydro-1H-benzo[e][1,4]diazepine-2,5-dione.

Std Proton parameters

Automation directory:
Sample : B2D A
Pulse Sequence: s2pul
Pulse Program: s2pul
Solvent: DMSO
Ambient temperature
Operator: haslach
Mercury-400BB "nmr400"

Relax. delay 1.000 sec
Pulse 45.0 degrees
Acq. time 1.998 sec
Width 6402.0 Hz
32 repetitions
OBSERVE H1, 400.1218996 MHz
DATA PROCESSING
FT size 32768
Total time 1 min, 40 sec

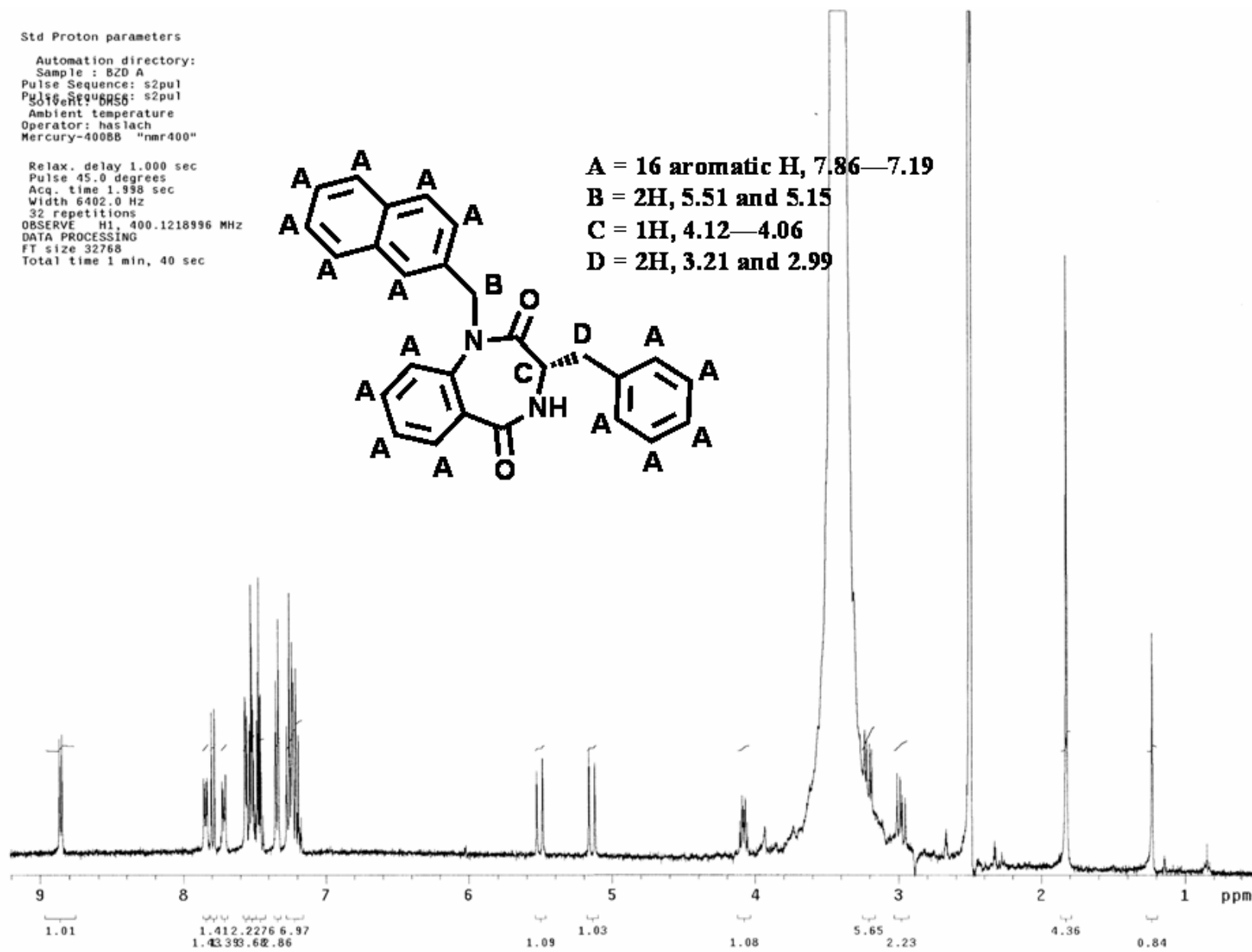
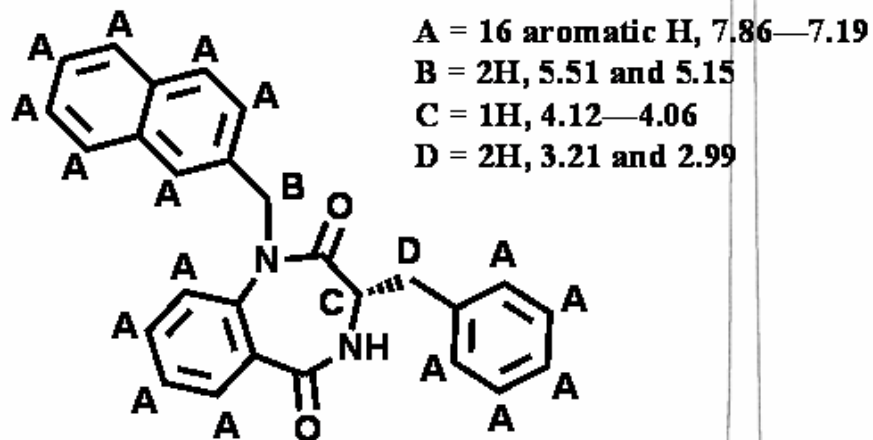


Figure A-5. Compound 43 (KRW9-70A) ¹H-NMR, 3-benzyl-1-(naphthalen-1-ylmethyl)-3,4-dihydro-1H-benzo[e][1,4]diazepine-2,5-dione.

Std Proton parameters
Automation directory:
Sample : B2D K
Pulse Sequence: s2pu1
Solvent: dms0
Temp. 22.0 C / 295.1 K
Operator: witek
Mercury-400BB "nmr400"
Relax. delay 1.000 sec
Pulse 45.0 degrees
Acq. time 1.998 sec
Width 6402.0 Hz
32 repetitions
OBSERVE H1, 400.1218996 MHz
DATA PROCESSING
FT size 32768
Total time 1 min, 40 sec

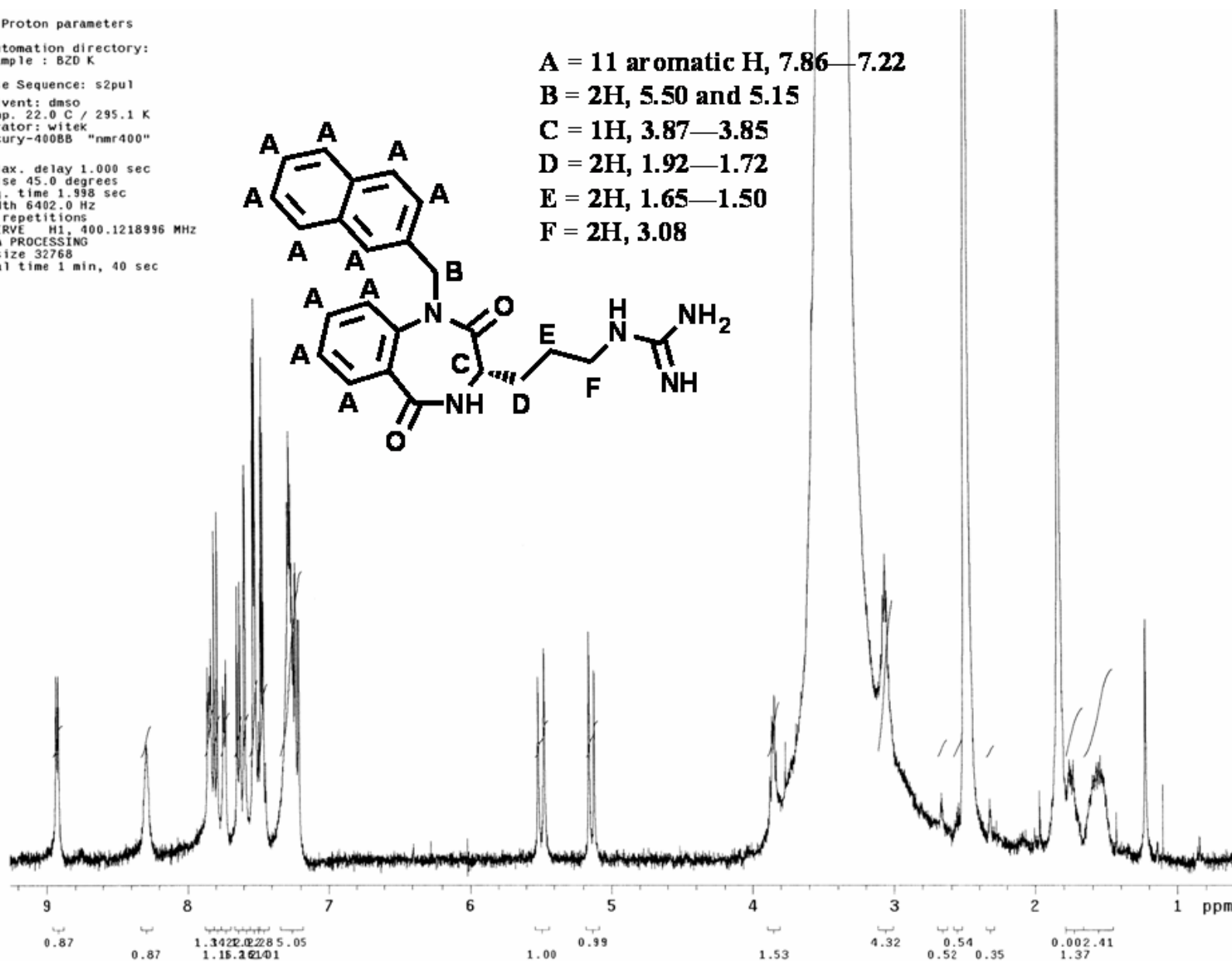
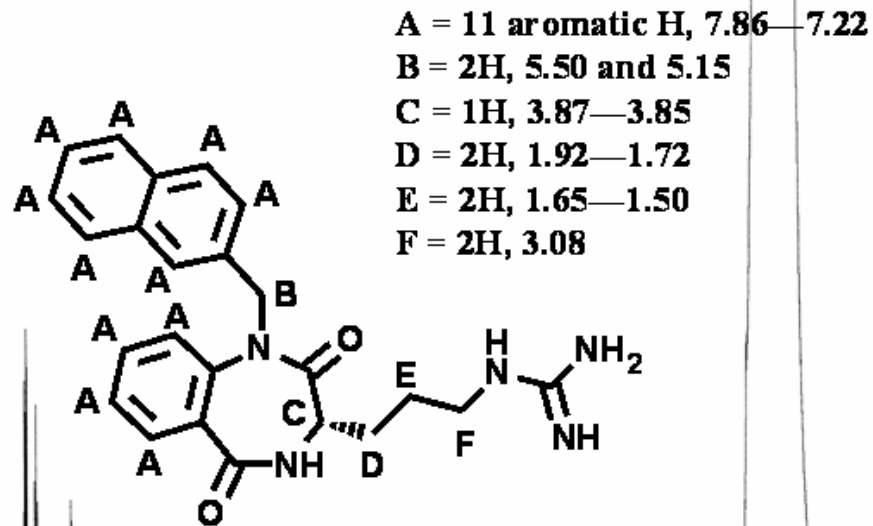


Figure A-6. Compound 44 (KRW9-70K) ¹H-NMR, 1-(3-(1-(naphthalen-1-ylmethyl)-2,5-dioxo-2,3,4,5-tetrahydro-1H-benzo[e][1,4]diazepin-3-yl)propyl)urea.

Std Proton parameters

Automation directory:
Sample : 820 #C₄

Pulse Sequence: s2pu1

Solvent: dms0
Temp. 22.0 C / 295.1 K
Operator: witek
Mercury-400BB "nmr400"

Relax. delay 1.000 sec
Pulse 45.0 degrees
Acq. time 1.998 sec
Width 6402.0 Hz
32 repetitions
OBSERVE H1, 400.1219000 MHz
DATA PROCESSING
FT size 32768
Total time 1 min, 40 sec

A = 11 aromatic H, 7.83—7.21

B = 2H, 5.52 and 5.13

C = 1H, 3.95

D = 2H, 1.88—1.70

E = 2H, 1.57—1.32

F = 2H, 1.58—1.46

G = 2H, 2.75

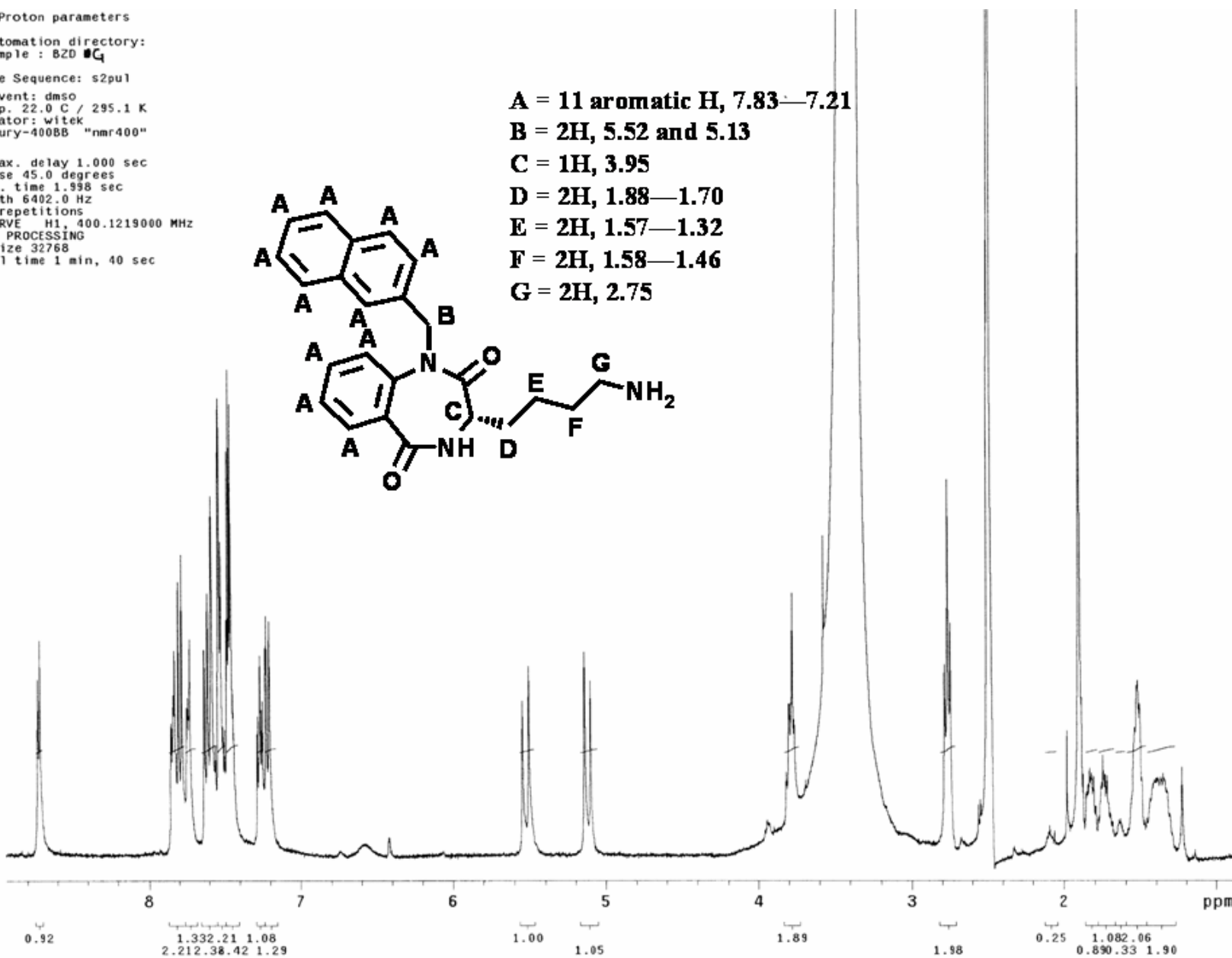
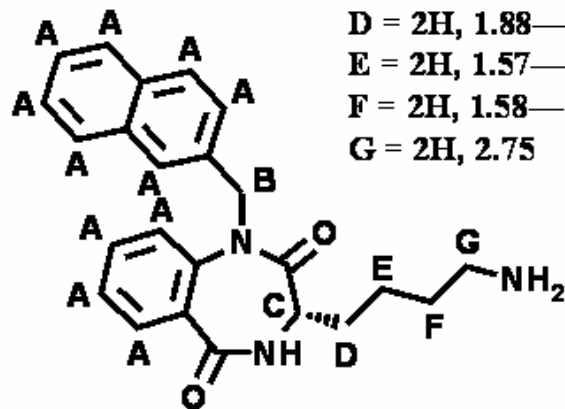


Figure A-7. Compound 45 (KRW9-70G) ¹H-NMR, 3-(4-aminobutyl)-1-(naphthalen-1-ylmethyl)-3,4-dihydro-1H-benzo[e][1,4]diazepine-2,5-dione.

Krista Wilson, KRW-4-91 in DMSO-D6
5 mm BBO Probe, Temp= 27 C, Non Spun, Bruker Avance 500 Console, Magnex 11.75 T/54 mm Magnet
Advanced Magnetic Resonance Imaging and Spectroscopy, McKnight Brain Institute, University of Florida
Jim Rocca, AMRIS

A = 9 aromatic H, 7.60—7.14

B = 2H, 3.88—3.84 and 3.62—3.57

C = 2H, 1.43—1.40 and 1.30—1.26

D = 3H, 0.70

E = 1H, 4.25—4.19

F = 2H, 3.13 and 2.91

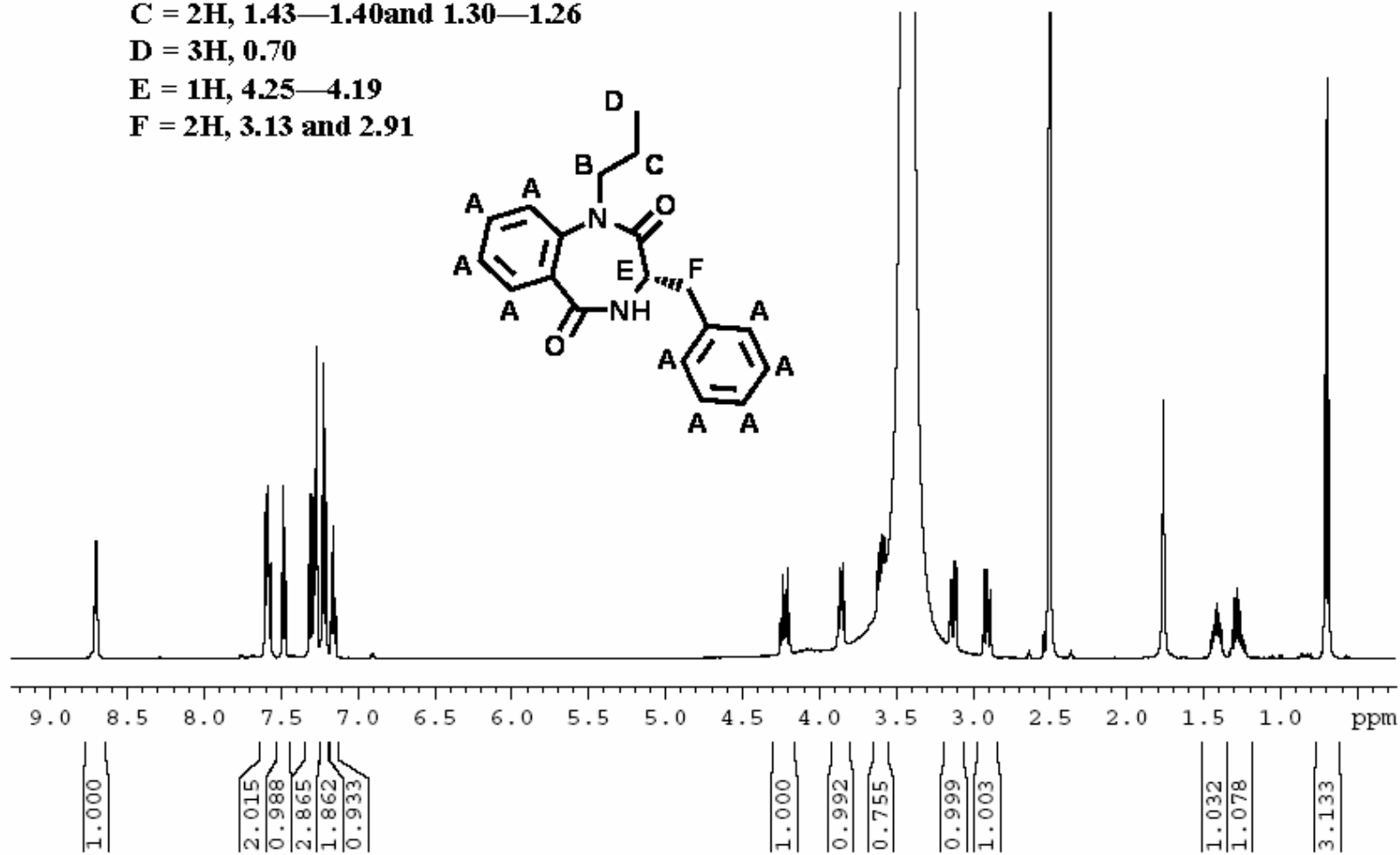


Figure A-8. Compound 46 (KRW4-91) ¹H-NMR, 3-Benzyl-1-propyl-3,4-dihydro-1H-benzo[e][1,4]diazepine-2,5-dione.

Krista Wilson, KRW-5-25 in DMSO-D6
5 mm BBO Probe, Temp= 27 C, Non Spun, Bruker Avance 500 Console, Magnex 11.75 T/54 mm Magnet
Advanced Magnetic Resonance Imaging and Spectroscopy, McKnight Brain Institute, University of Florida
Jim Rocca, AMRIS

A = 9 aromatic H, 7.60—7.14
B = 2H, 3.87—3.82 and 3.63—3.57
C = 4H, 1.36—1.22 and 1.14—1.09
D = 3H, 0.75
E = 1H, 4.31—4.25
F = 2H, 3.12 and 2.90

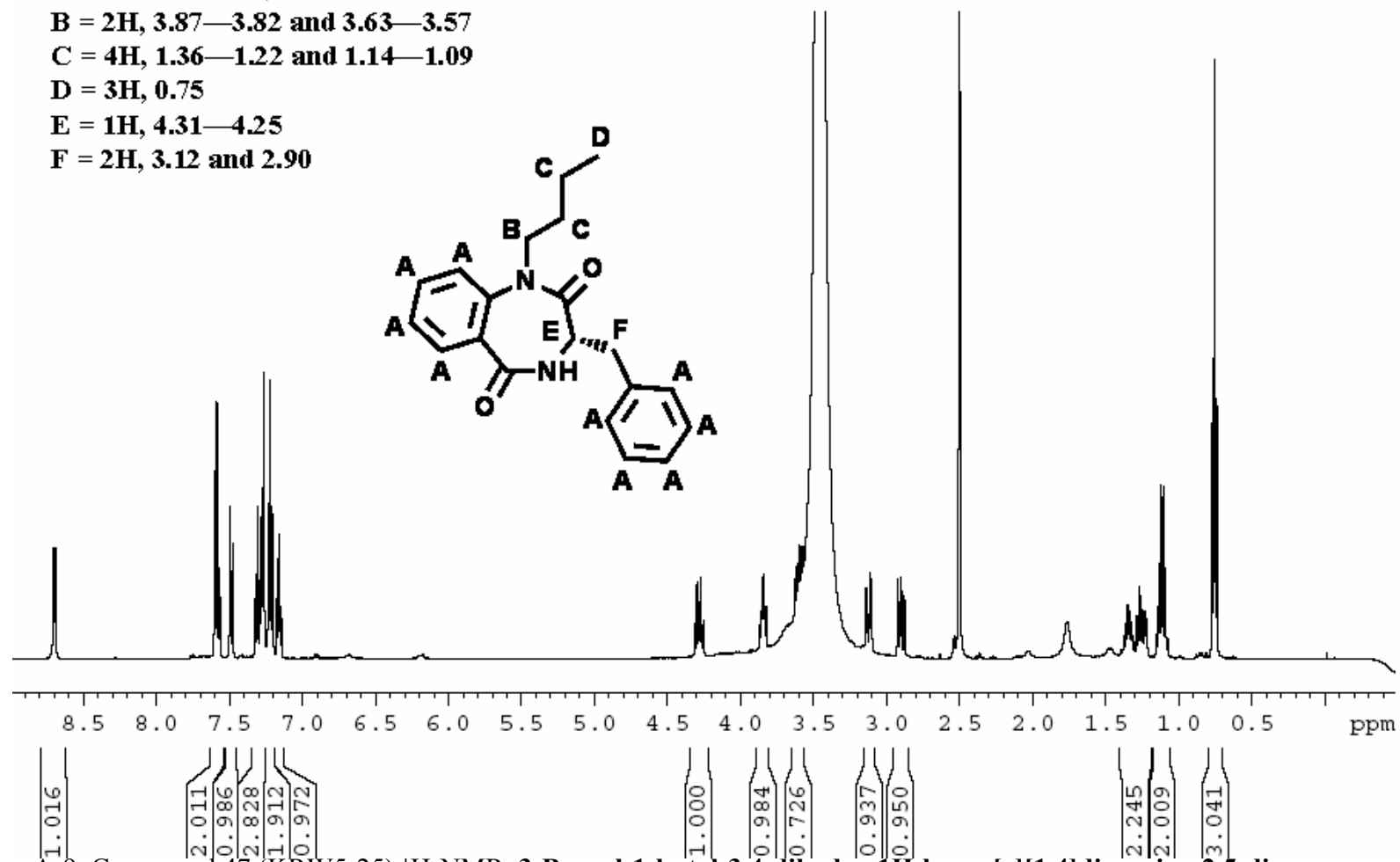


Figure A-9. Compound 47 (KRW5-25) ¹H-NMR, 3-Benzyl-1-butyl-3,4-dihydro-1H-benzo[e][1,4]diazepine-2,5-dione.

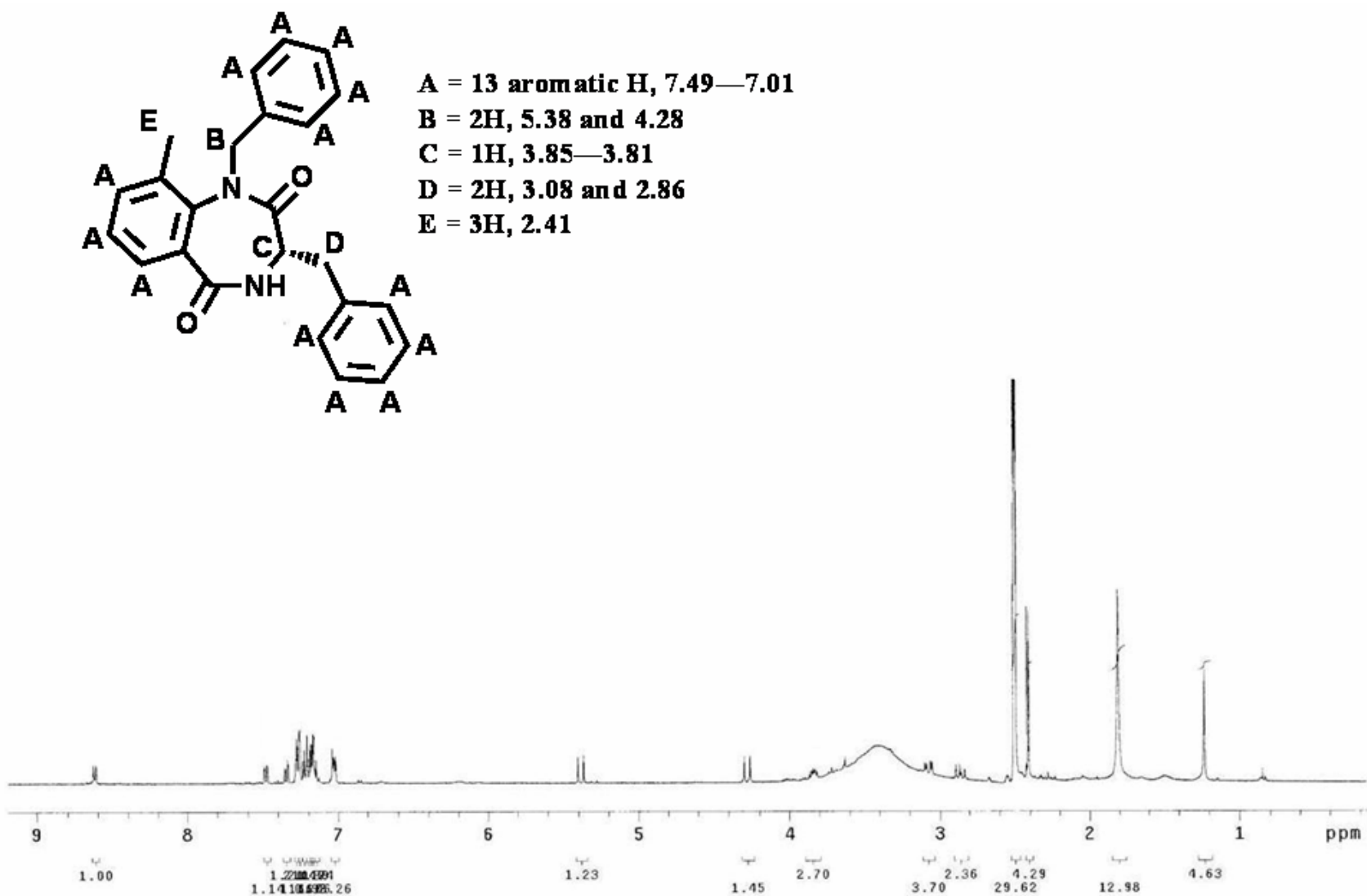


Figure A-10. Compound 48 (KRW9-70B) $^1\text{H-NMR}$, 1,3-dibenzyl-8-methyl-3,4-dihydro-1H-benzo[e][1,4]diazepine-2,5-dione.

Std Proton parameters

Automation directory:
Sample : B20 L

Pulse Sequence: s2pul

Solvent: dms0
Temp. 22.0 C / 295.1 K
Operator: witek
Mercury-400BB "nmr400"

Relax. delay 1.000 sec
Pulse 45.0 degrees
Acq. time 1.998 sec
Width 6402.0 Hz
32 repetitions
OBSERVE H1, 400.1219000 MHz
DATA PROCESSING
FT size 32768
Total time 1 min, 40 sec

A = 8 aromatic H, 7.48—7.01

B = 2H, 5.39 and 4.27

C = 1H, 3.63

D = 2H, 1.74—1.64

E = 2H, 1.56—1.44

F = 2H, 3.02

G = 3H, 2.41

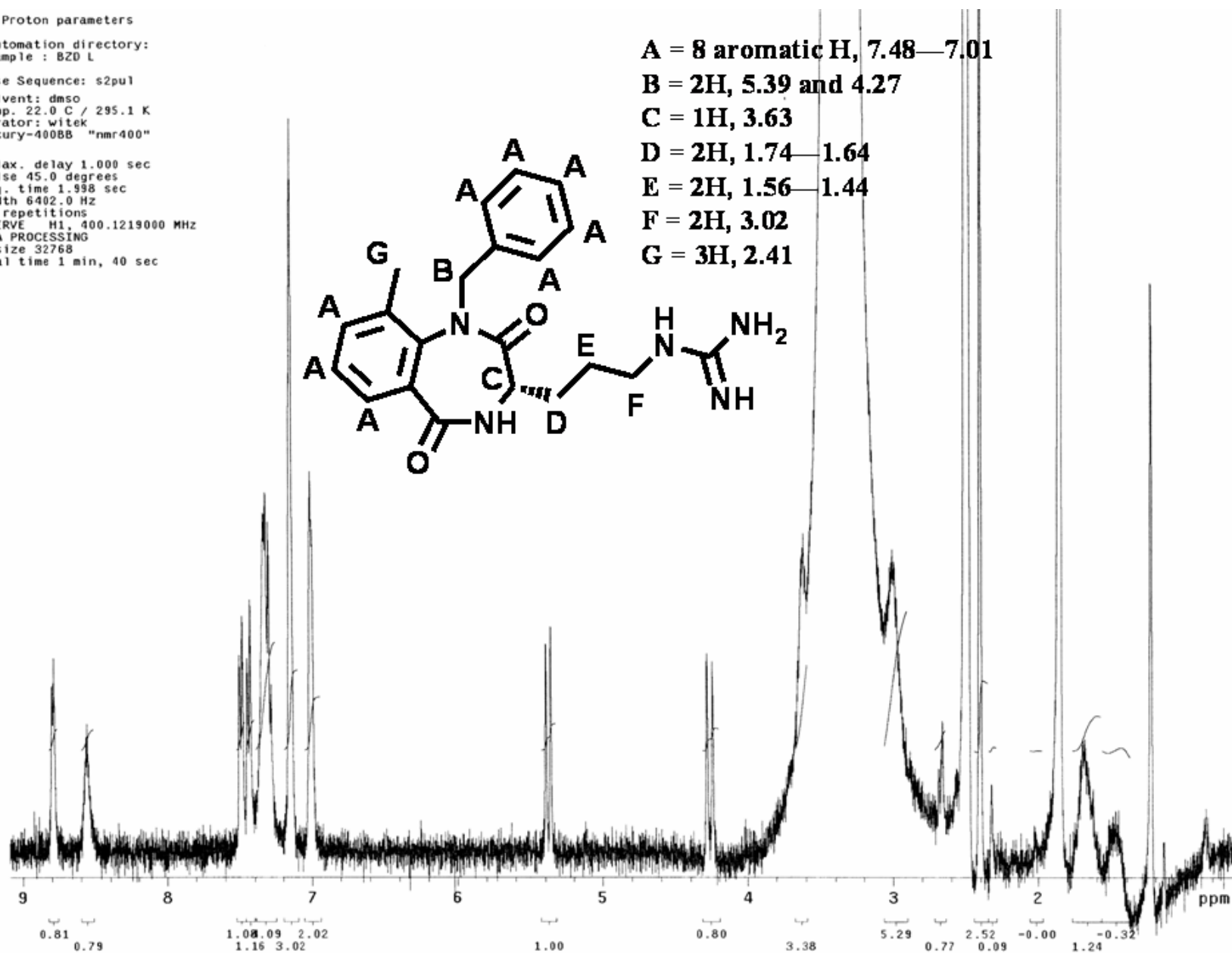


Figure A-11. Compound 49 (KRW9-70L) ¹H-NMR, 1-(3-(1-benzyl-9-methyl-2,5-dioxo-2,3,4,5-tetrahydro-1H-benzo[e][1,4]diazepin-3-yl)propyl)urea.

Std Proton parameters

Automation directory:
Sample : B20 H

Pulse Sequence: s2pul

Solvent: dms0
Temp. 22.0 C / 295.1 K
Operator: witek
Mercury-400BB "nmr400"

Relax. delay 1.000 sec
Pulse 45.0 degrees
Acq. time 1.998 sec
Width 6402.0 Hz
64 repetitions
OBSERVE H1, 400.1218989 MHz
DATA PROCESSING
FT size 32768
Total time 3 min, 20 sec

A = 8 aromatic H, 7.50—6.99

B = 2H, 5.38 and 4.27

C = 1H, 3.57

D = 2H, 2.33—2.32

E = 2H, 1.41—1.39

F = 2H, 1.71—1.60

G = 2H, 2.67—2.62

H = 3H, 2.41

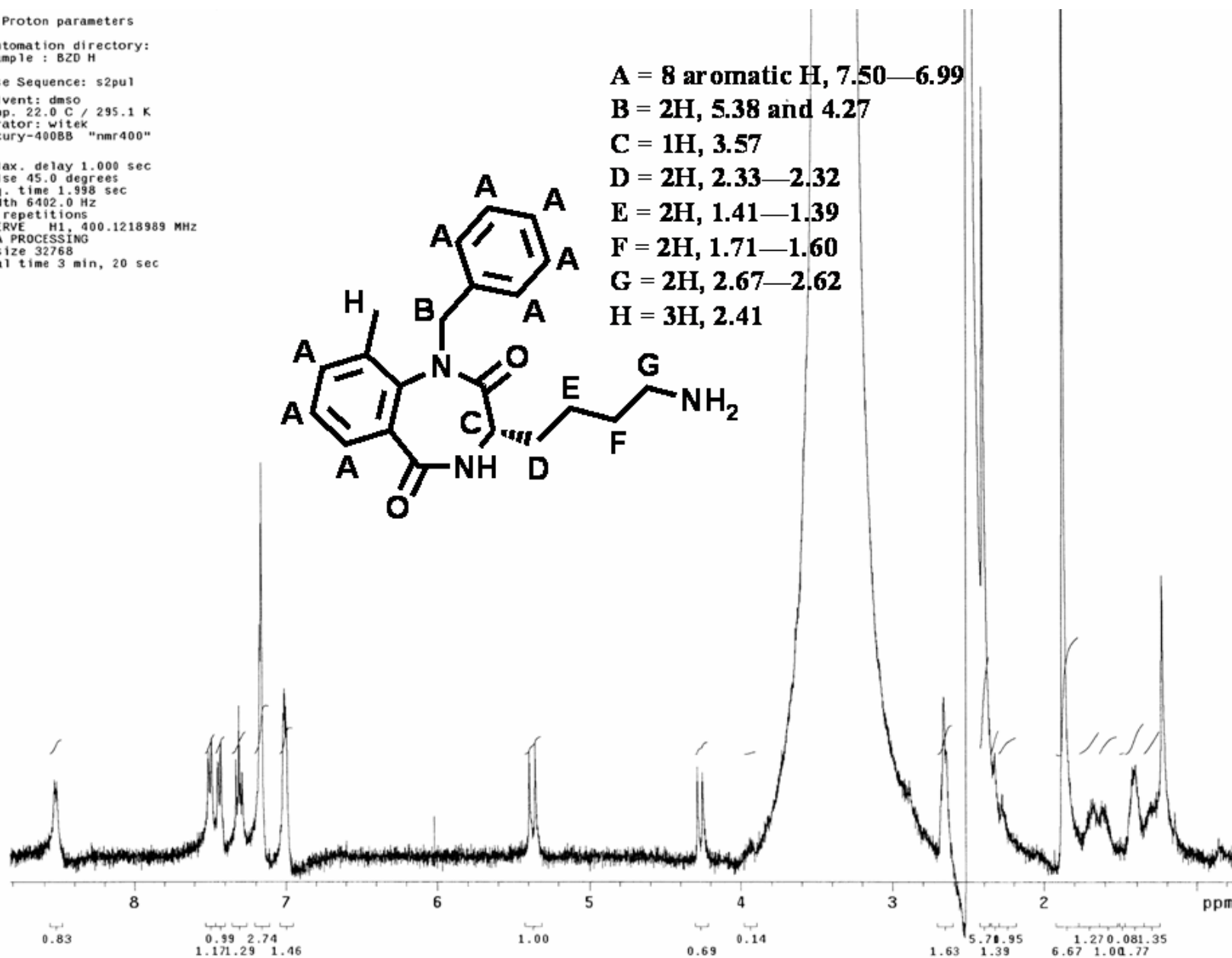
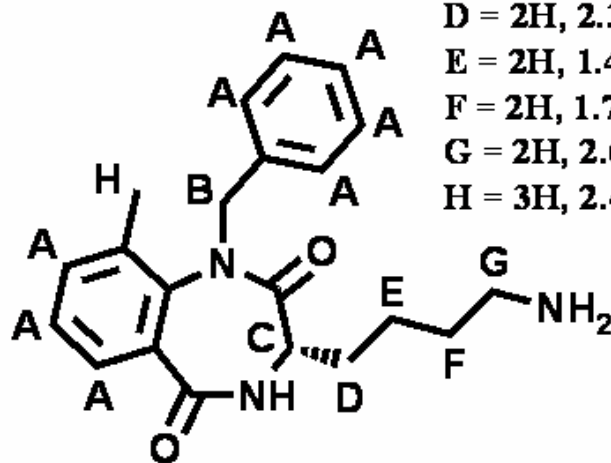


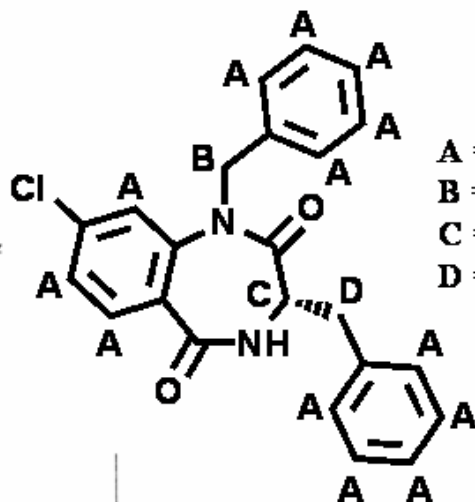
Figure A-12. Compound 50 (KRW9-70H) ¹H-NMR, 3-(4-aminobutyl)-1-benzyl-9-methyl-3,4-dihydro-1H-benzo[e][1,4]diazepine-2,5-dione.

Std Proton parameters

Automation directory:
Sample : BZD C

Pulse Sequence: s2pu1
Solvent: dms0
Temp. 22.0 C / 295.1 K
Operator: witek
Mercury-400BB "nmr400"

Relax. delay 1.000 sec
Pulse 45.0 degrees
Acq. time 1.998 sec
Width 6402.0 Hz
32 repetitions
OBSERVE H1, 400.1218996 MHz
DATA PROCESSING
FT size 32768
Total time 1 min, 40 sec



A = 13 aromatic H, 7.62—7.07

B = 2H, 5.39 and 4.99

C = 1H, 4.10

D = 2H, 3.16 and 2.95

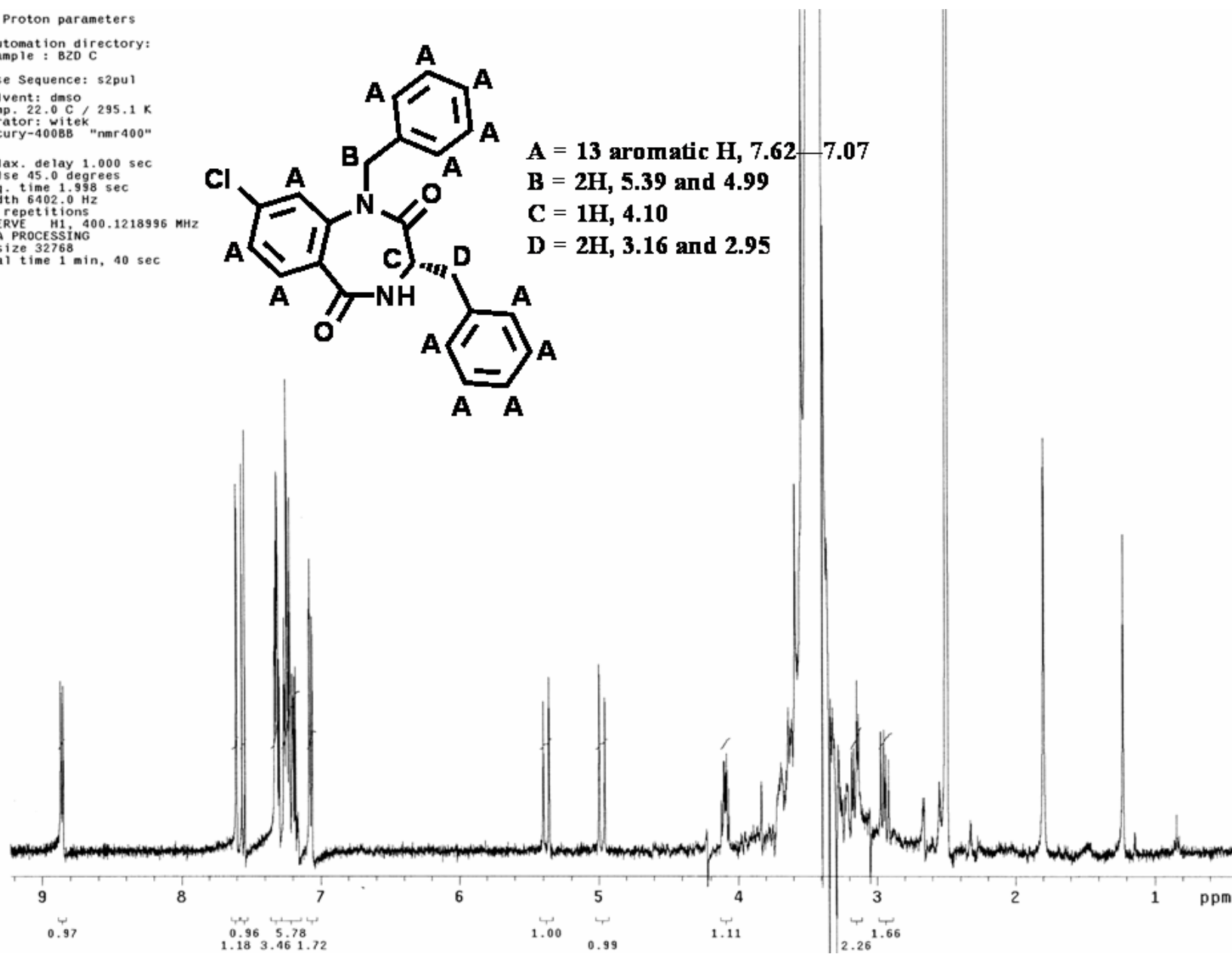


Figure A-13. Compound 51 (KRW9-70C) ¹H-NMR, 1-(3-(1-benzyl-8-chloro-2,5-dioxo-2,3,4,5-tetrahydro-1H-benzo[e][1,4]diazepin-3-yl)propyl)urea.

Krista Wilson, KRW-6-121A in DMSO-D6
5 mm BBO Probe, Temp= 27 C, Non Spun, Bruker Avance 500 Console, Magnex 11.75 T/54 mm Magnet
Advanced Magnetic Resonance Imaging and Spectroscopy, McKnight Brain Institute, University of Florida
Jim Rocca, AMRIS

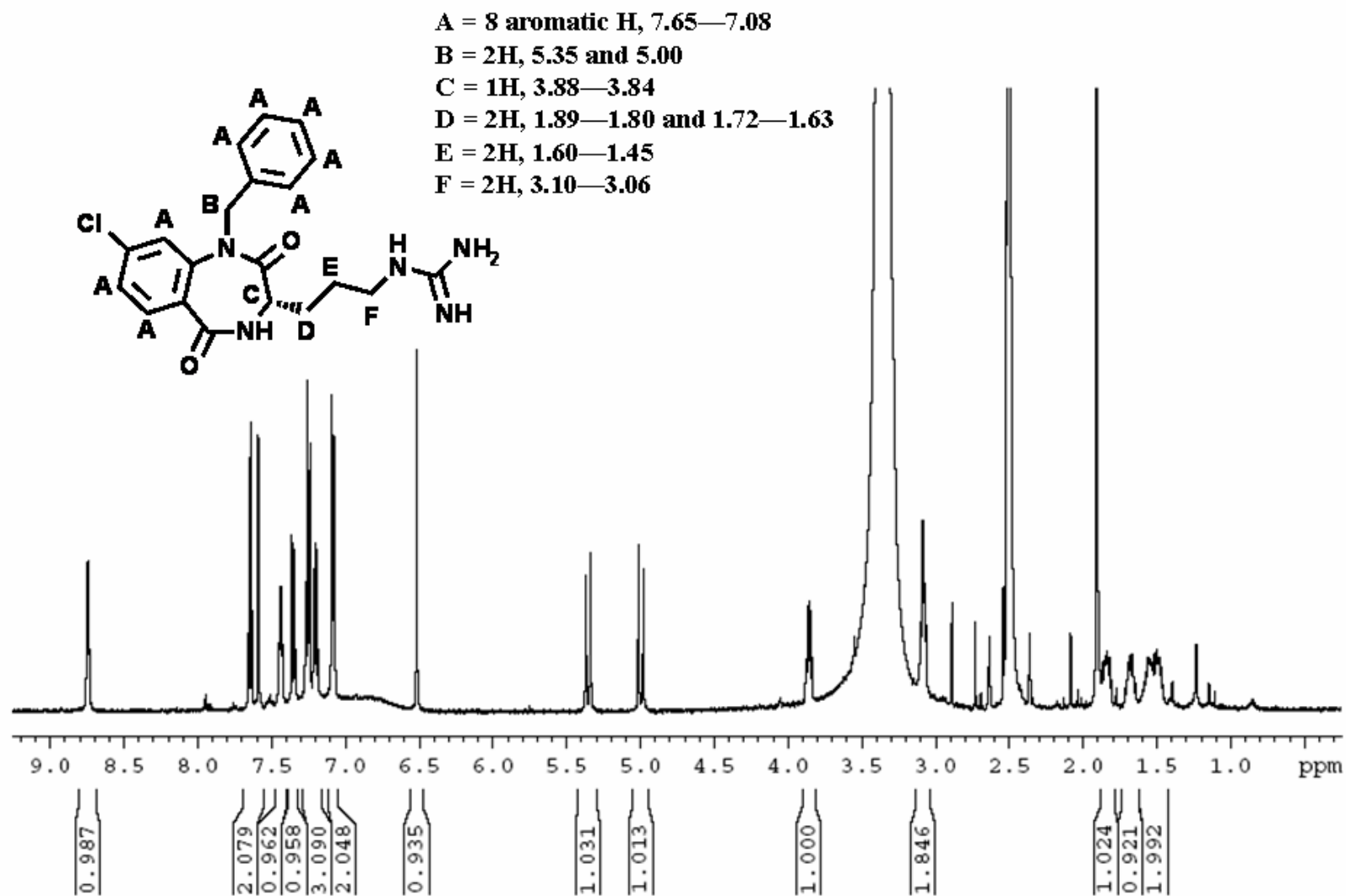


Figure A-14. Compound 52 (KRW6-121A) ¹H-NMR, N-[3-(1-Benzyl-8-chloro-2,5-dioxo-2,3,4,5-tetrahydro-1H-benzo[e][1,4]diazepin-3-yl)-propyl]-guanidine.

Std Proton parameters

Automation directory:
Sample : BZD D

Pulse Sequence: s2pul

Solvent: dms0
Temp. 22.0 C / 295.1 K
Operator: witek
Mercury-400BB "nmr400"

Relax. delay 1.000 sec
Pulse 45.0 degrees
Acq. time 1.998 sec
Width 6402.0 Hz
16 repetitions
OBSERVE H1, 400.1219000 MHz
DATA PROCESSING
FT size 32768
Total time 0 min, 50 sec

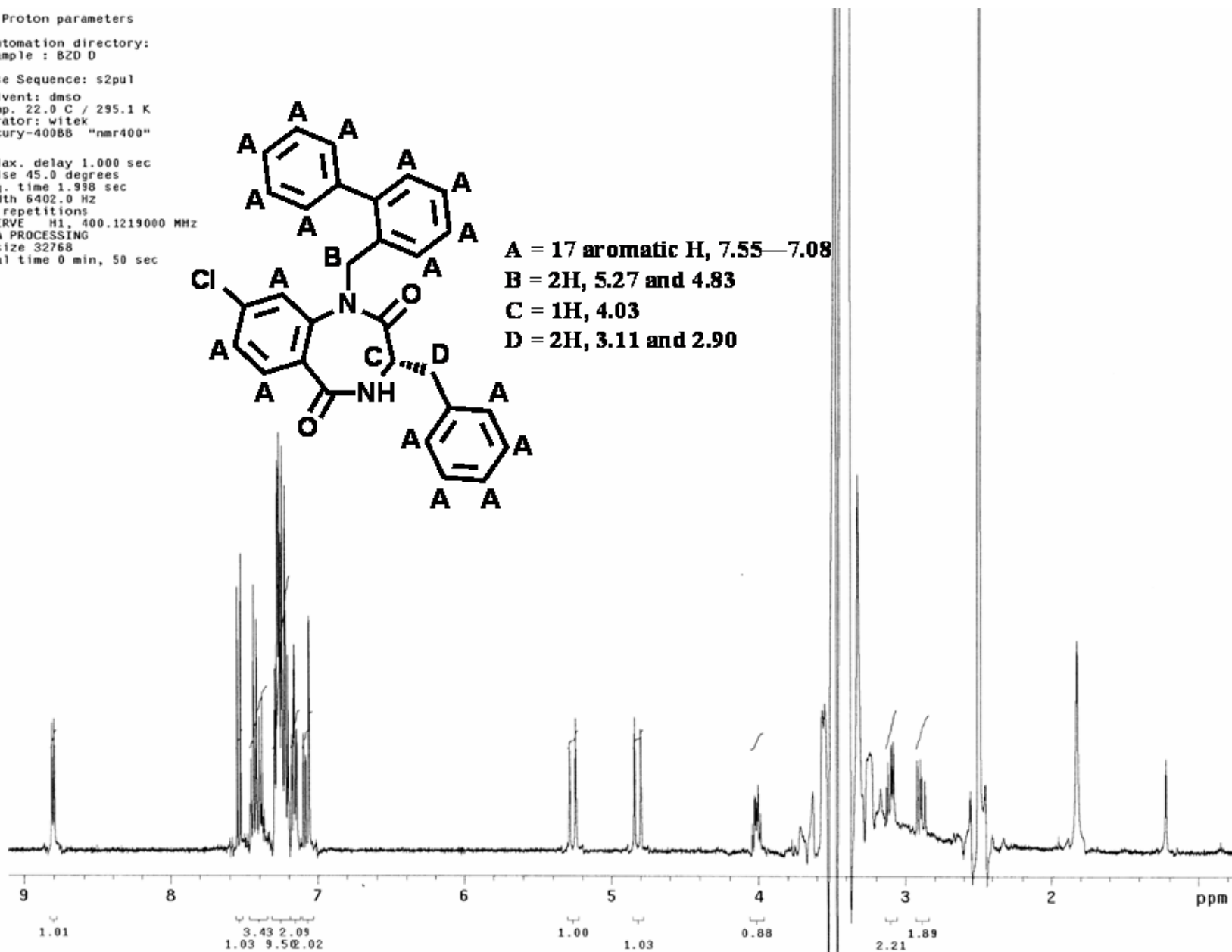
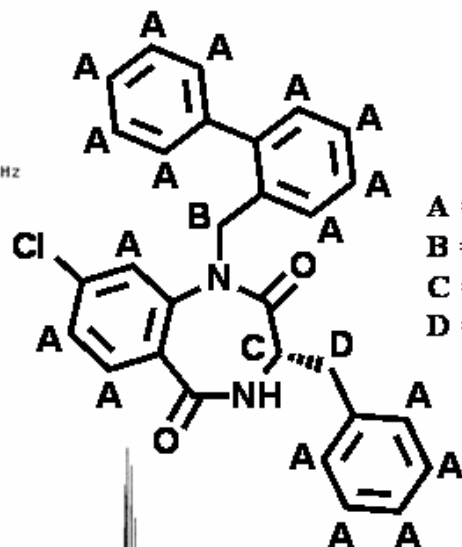


Figure A-15. Compound 53 (KRW9-70D) ¹H-NMR, 3-benzyl-1-(biphenyl-2-ylmethyl)-8-chloro-3,4-dihydro-1H-benzo[e][1,4]diazepine-2,5-dione.

Std Proton parameters

Automation directory:
Sample : B20 M

Pulse Sequence: s2pul

Solvent: dms0
Temp. 22.0 C / 295.1 K
Operator: witek
Mercury-400BB "nmr400"

Relax. delay 1.000 sec
Pulse 45.0 degrees
Acq. time 1.998 sec
Width 6402.0 Hz
32 repetitions
OBSERVE H1, 400.1218989 MHz
DATA PROCESSING
FT size 32768
Total time 1 min, 40 sec

A = 12 aromatic H, 7.65—7.09

B = 2H, 5.26 and 4.81

C = 1H, 3.76

D = 2H, 1.78—1.64

E = 2H, 1.66—1.42

F = 2H, 3.03

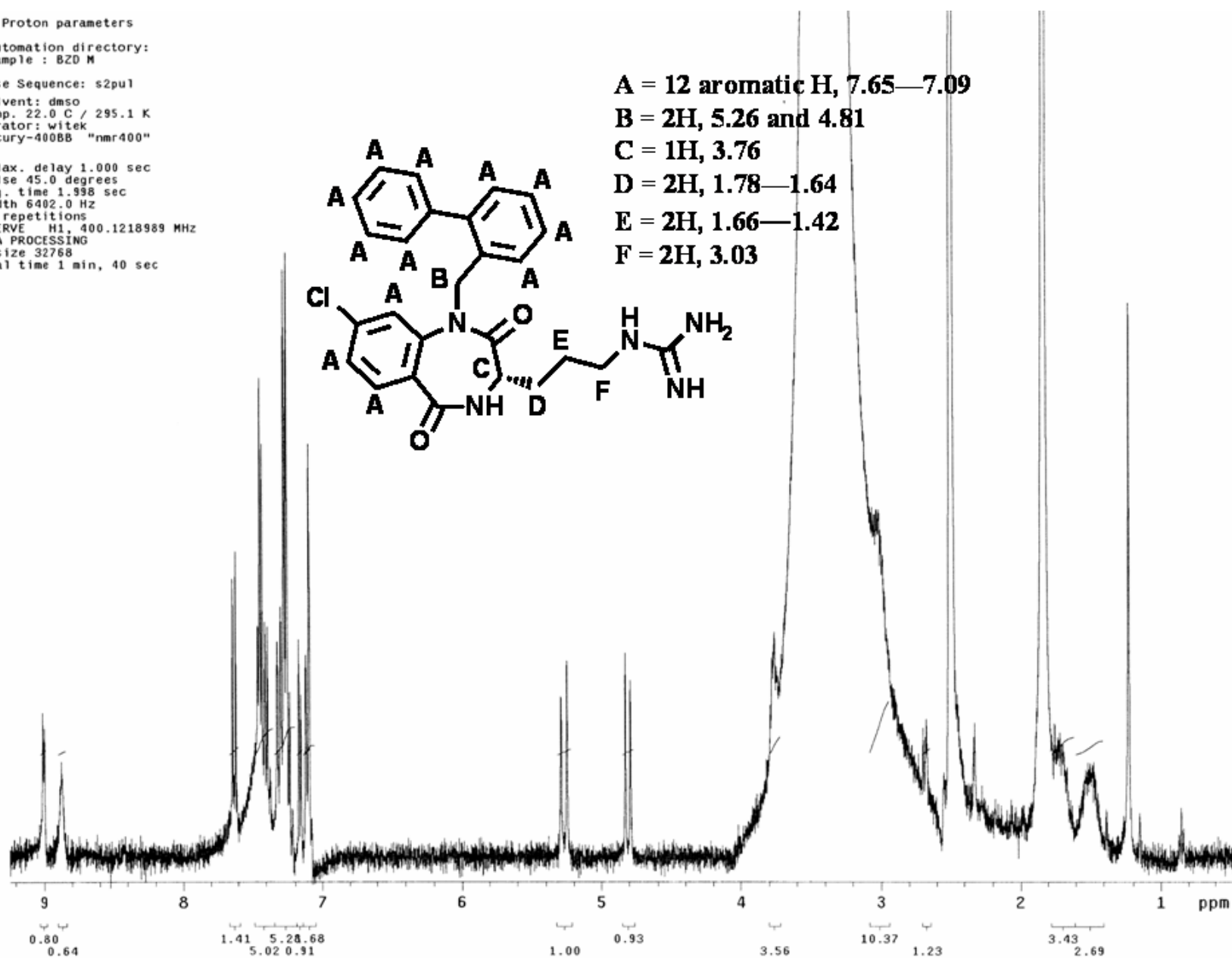


Figure A-16. Compound 54 (KRW9-70M) ¹H-NMR, 1-(3-(1-(biphenyl-2-ylmethyl)-8-chloro-2,5-dioxo-2,3,4,5-tetrahydro-1H-benzo[e][1,4]diazepin-3-yl)propyl)urea.

Std Proton parameters

Automation directory:
Sample: B2D

Pulse Sequence: s2pu1

Solvent: dms0
Temp: 22.0 C / 295.1 K
Operator: witek
Mercury-400BB "nmr400"

Relax. delay 1.000 sec
Pulse 45.0 degrees
Acq. time 1.998 sec
Width 6402.0 Hz
32 repetitions
OBSERVE H1, 400.1219000 MHz
DATA PROCESSING
FT size 32768
Total time 1 min, 40 sec

A = 12 aromatic H, 7.63—7.16

B = 2H, 5.28 and 4.81

C = 1H, 3.95

D = 2H, 2.14—2.08

E = 2H, 1.43—1.34

F = 2H, 1.68—1.60

G = 2H, 2.59

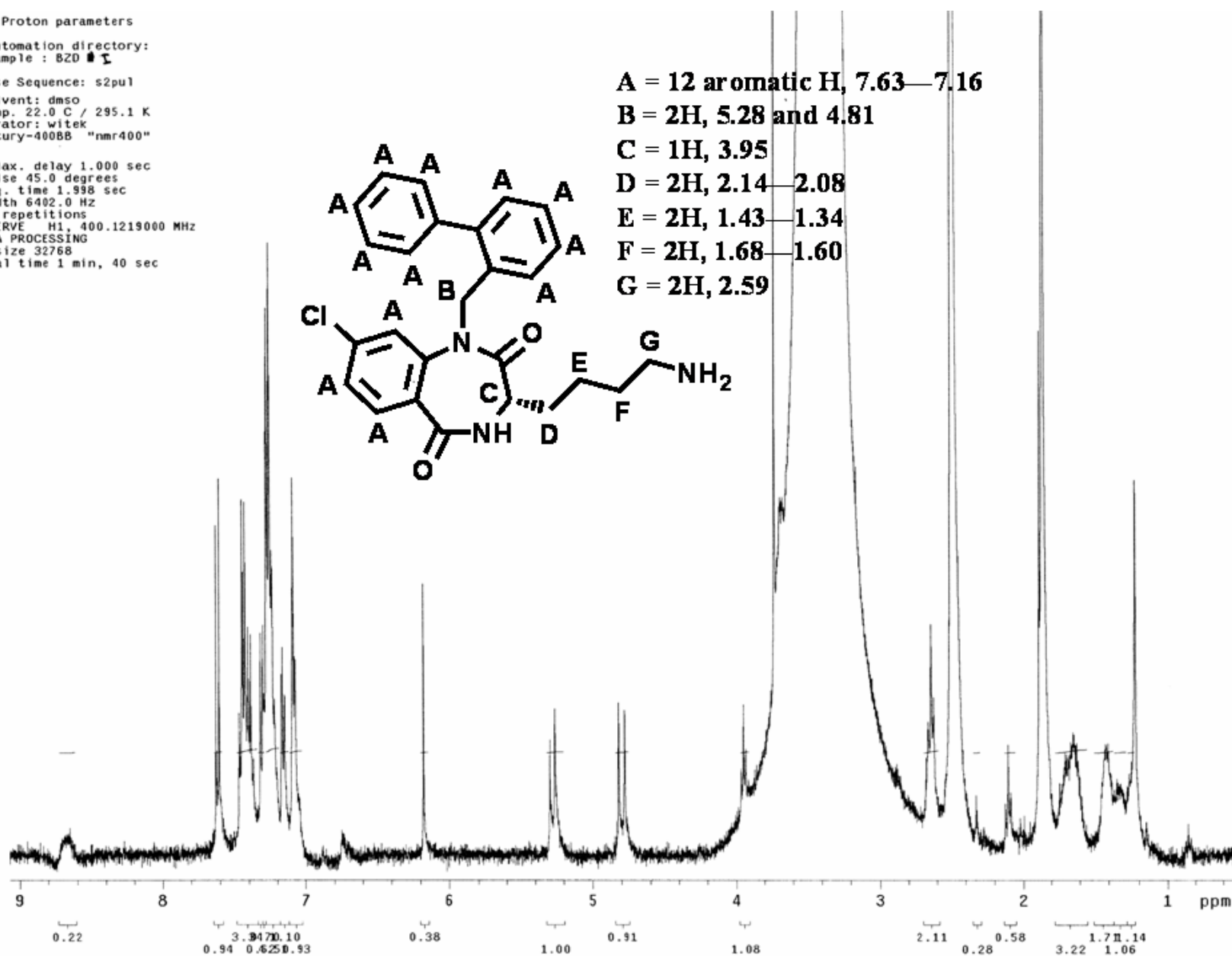


Figure A-17. Compound 55 (KRW9-701) ¹H-NMR, 3-(4-aminobutyl)-1-(biphenyl-2-ylmethyl)-8-chloro-3,4-dihydro-1H-benzo[e][1,4]diazepine-2,5-dione.

Krista Wilson, KRW-5-49 in DMSO-D6
5 mm BBO Probe, Temp= 27 C, Non Spun, Bruker Avance 500 Console, Magnex 11.75 T/54 mm Magnet
Advanced Magnetic Resonance Imaging and Spectroscopy, McKnight Brain Institute, University of Florida
Jim Rocca, AMRIS

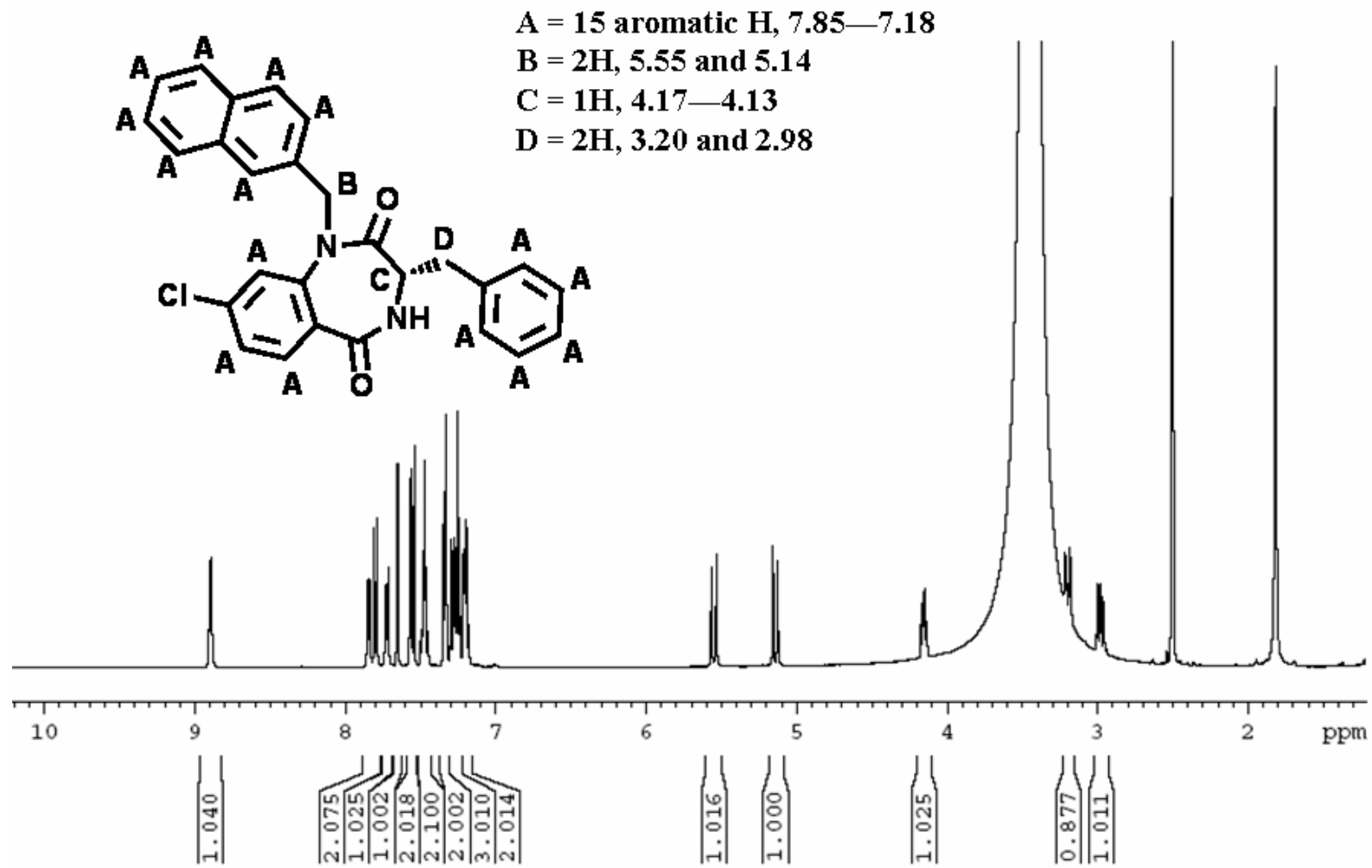


Figure A-18. Compound 56 (KRW5-49) ¹H-NMR, 3-Benzyl-8-chloro-1-naphthalen-2-ylmethyl-3,4-dihydro-1H-benzo[e][1,4]diazepine-2,5-dione.

Std Proton parameters

Automation directory:
Sample : B20 N

Pulse Sequence: s2pul
Solvent: dms0
Temp. 22.0 C / 295.1 K
Operator: witek
Mercury-400BB "nmr400"

Relax. delay 1.000 sec
Pulse 45.0 degrees
Acq. time 1.398 sec
Width 6402.0 Hz
32 repetitions
OBSERVE H1, 400.1218996 MHz
DATA PROCESSING
FT size 32768
Total time 1 min, 40 sec

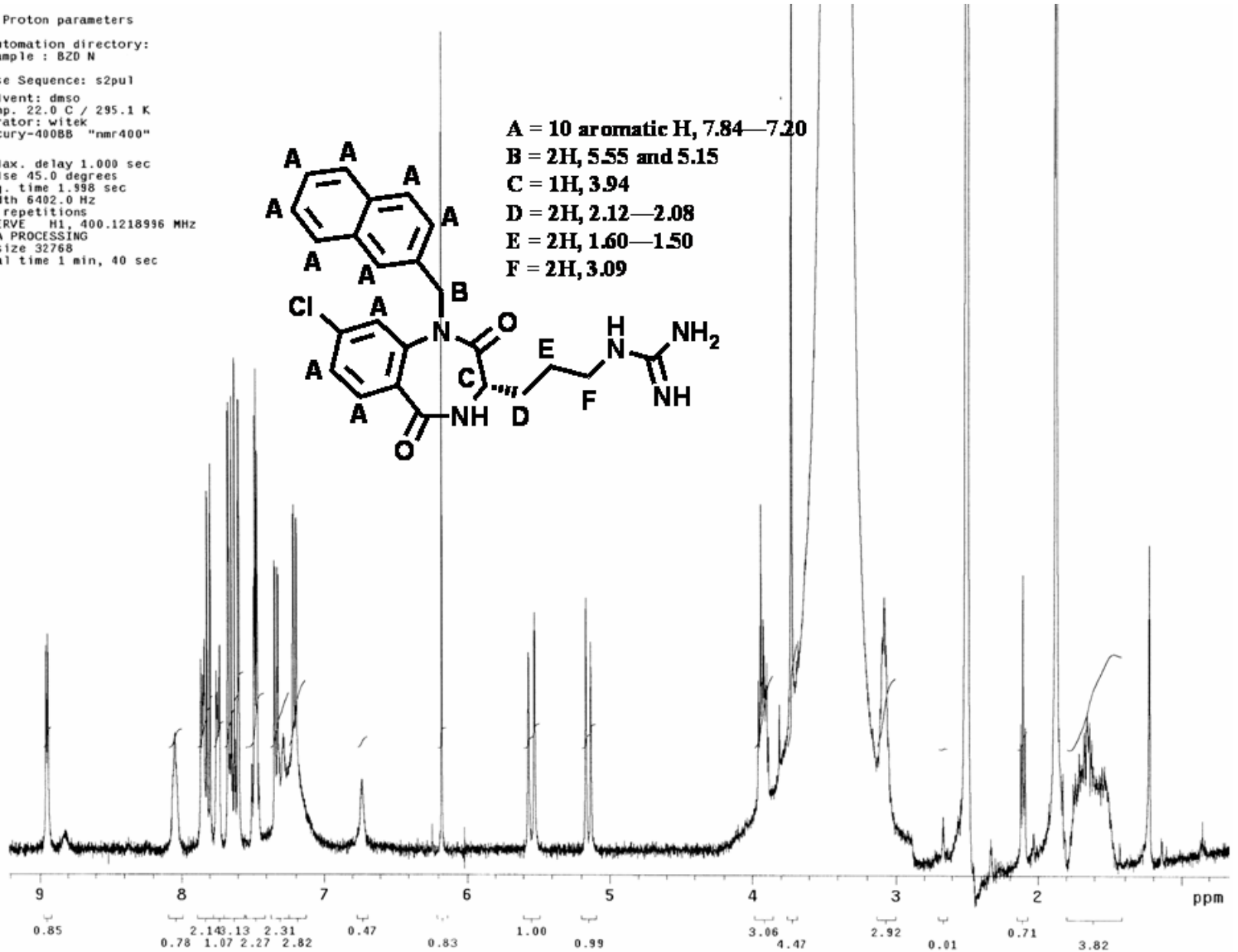
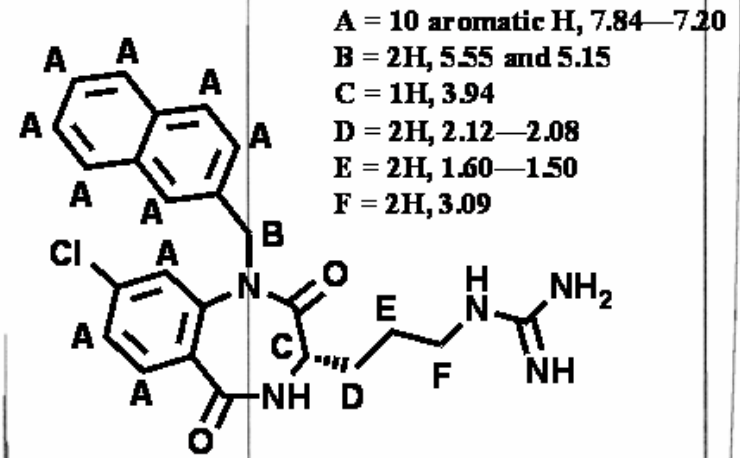


Figure A-19. Compound 57 (KRW9-70N) ¹H-NMR, 1-(3-(8-chloro-1-(naphthalen-1-ylmethyl)-2,5-dioxo-2,3,4,5-tetrahydro-1H-benzo[e][1,4]diazepin-3-yl)propyl)urea.

Krista Wilson, KRW-7-05A in DMSO-D6
5 mm BBO Probe, Temp= 27 C, Non Spun, Bruker Avance 500 Console, Magnex 11.75 T/54 mm Magnet
Advanced Magnetic Resonance Imaging and Spectroscopy, McKnight Brain Institute, University of Florida
Jim Rocca, AMRIS

A = 10 aromatic H, 7.86—7.19

B = 2H, 5.57 and 5.13

C = 1H, 3.84

D = 2H, 1.85—1.78 and 1.77—1.68

E = 4H, 1.56—1.28

F = 2H, 2.72

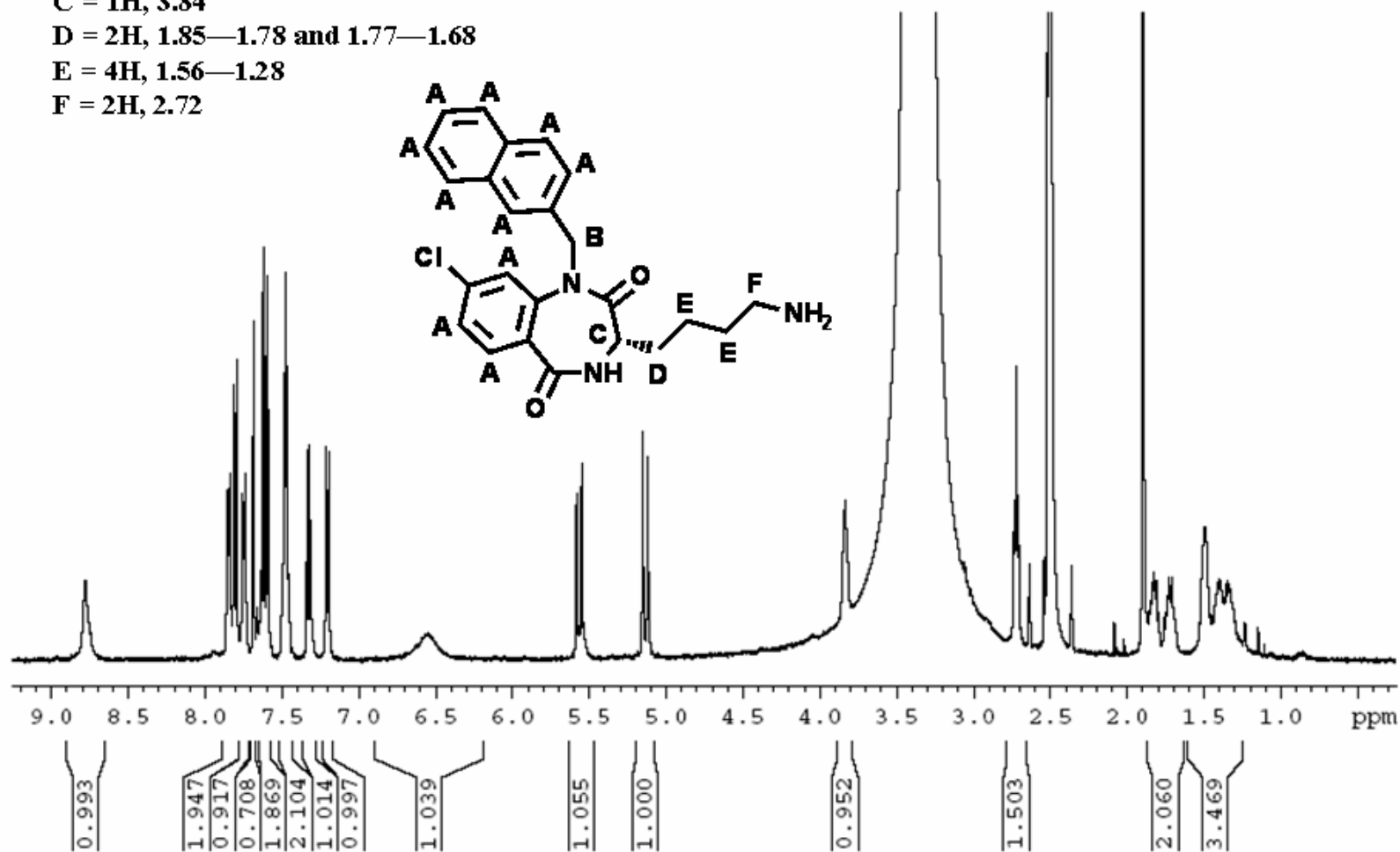


Figure A-20. Compound 58 (KRW7-05A) ¹H-NMR, 3-(4-Amino-butyl)-8-chloro-1-naphthalen-2-ylmethyl-3,4-dihydro-1H-benzo[e][1,4]diazepine-2,5-dione.

APPENDIX B
DNA SEQUENCES AND RESTRICTION MAPS OF CHIMERAS

Red text indicates sequences inserted from the opposite receptor.

Figure B-1. Flag-hMC2R DNA Sequence

Complete Sequence of Flag-hMC2R in pcDNA3

AAGCTTGGCCGCGCCATGGACTACAAGGACGACGACGACAAGAAGCACATTATCAACTCGTATGAAAACATCAACAACACAGCAAGAATAATCCGACTGTCCTCGTGGTTTTGCCGGAGGAGATA
 TTTTCAAAATTTCCATTTGTTGGAAATCTGATCGTCTGCTGGCTGTGTTCAAGAATAAGAATCTCCAGGCACCATGTACTTTTTCATCTGTAGCTTGGCCATATCTGATATGCTGGCC
 AGCCTATATAAGATCTTGGAAAATATCCTGATCATATTGAGAAACATGGGCTATCTCAAGCCACGTGGCAGTTTTGAAACCACAGCCGATGACATCATCGACTCCCTGTTTGTCTCTCCCTGCTTGGC
 TCCATCTTCAGCCTGTCTGTGATTTGCTGGGACCGCTACATCACCATCTTCCAGCAGCTGGGTACCACAGCATCGTGACCATGCGCCGCACTGTGGTGGTCTTACGGTCACTGGAGCTTCTGCACG
 GGGACTGGCATCACCATGGTATCTTCCATCATGTGCCACAGTGATCACCTTCCAGCTGCTGTTCCCGCTGATGCTGGTCTTTCATCCTGTGCCCTATATGGACATGTTCTGTGGCTCGATCC
 CACACCAGGAAGATCTCCACCTCCCGAGCCAAACATGAAAGGGGCAATCACACTGACCATCTGCTCGGGTCTTTCATCTTCTGTGGGCCCCCTTTGTGCTTATGCTCTTGTGATGACATTCTGC
 CCAAGTAACCCCTACTGCGCTGTACATGTCTCTCTCCAGGTGAACGGCATGTTGATCATGTGCAATGCCCTCATTGACCCCTTCATATATGCCTCCGGAGCCAGAGCTCAGGACCGCATTCAAA
 AAGATGATCTTCTGCAGCAGTACTGGTAGCTCGAGTCTAGA

Restriction Map

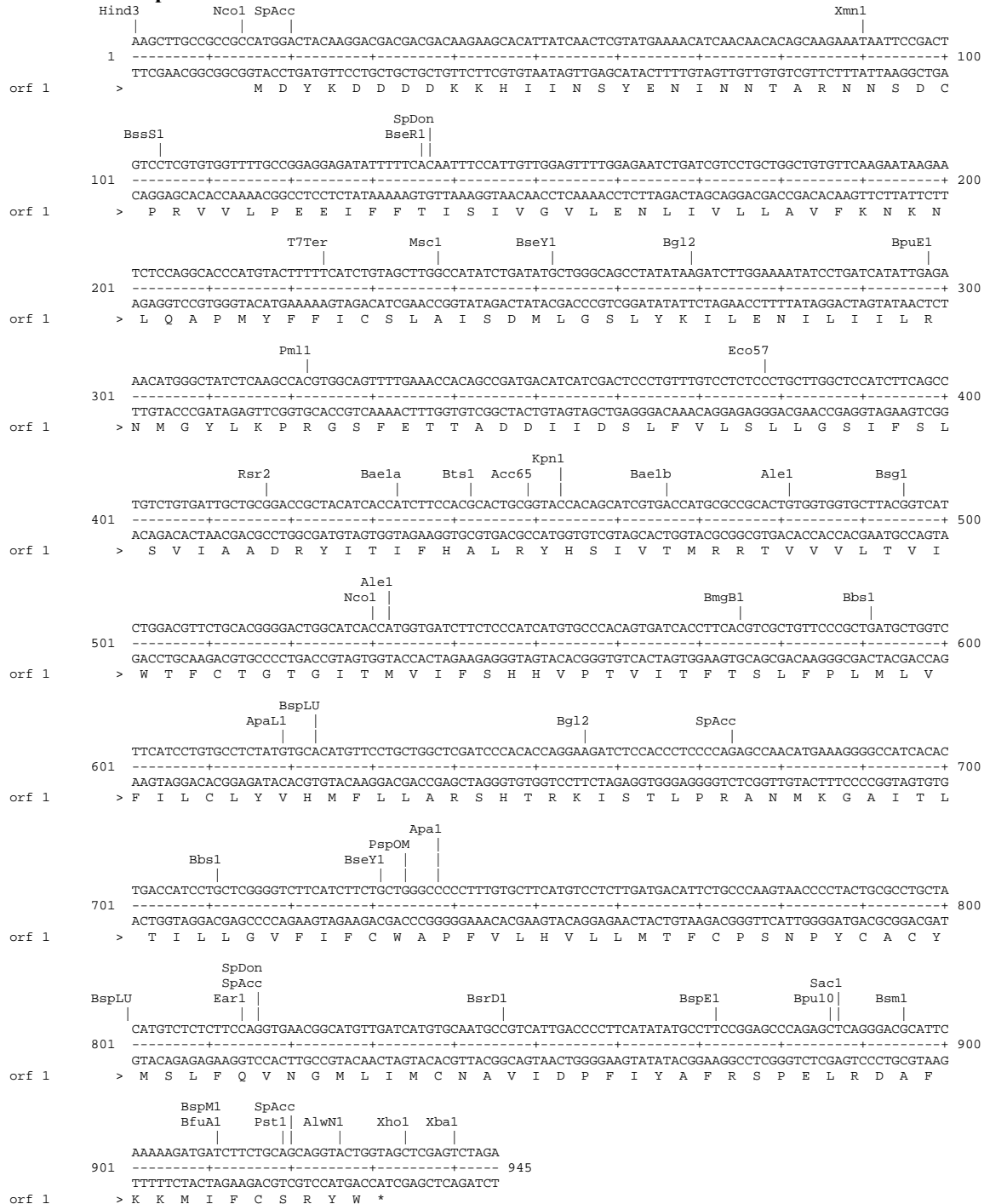


Figure B-2. Chimera 2C1 DNA Sequence

Complete sequence of Flag-hMC2R/2C1/pcDNA3

AAGCTTGGTACCGAGCTCGGATCCACTAGTCCAGTGTGGTGAATTCGGCTTGGCCGCCCATGGACTACAAGGACGACGACGACAAGGTGAACCTCCACCACCGTGGGATGCACACTTCTCTGCACCT
 CTGGAAACCGCAGCAGTTACAGACTGCACAGCAATGCCAGTGGTCCCTTGGAAAAGGCTACTCTGTATGGAGGGTCTACGAGCAACTTTTGTCTCTCCCTGAGGTGTTTGTGACTCTGGGTGTCATCAG
 CTGTGGAGAAATATCTTAGTGTGTGGCAATAGCCAAGAACAAAGAACTCGATTCCACCATGACTTTTTCATCTGCAGCTTAGCCATATCTGATATGCTGGGCAGCCTATATAAGATCTTGGAAAA
 TATCCTGATCATATGAGAAACATGGGCTATCTCAAGCCACGTGGCAGTTTGAACACACAGCCGATGACATCATCGACTCCCTGTTTGTCTCCCTGCTGGCTCCACTTTCAGCCTGTCTGTGAT
 TGCTGCGGACCGCTACATCACCATCTTCCACGCACTGCGGTACCACAGCATCGTGACCATGCGCCGCACTGTGGTGGTCTTACGGTCACTTGGAGCTTCTGCACGGGACTGGCATCACCATGGTGT
 CTCTCCCATCATGTGCCACAGTATCACCTTACGTCGTGTCCCGCTGATGTGTCTTTCATCTCTGCTCTATGTGCACATGTCTCTGCTGGCTCGATCCACACAGGAAGATCTCCACCCT
 CCCAGAGCAACATGAAAGGGCCATCACACTGACCATCTGCTCGGGTCTTCACTTCTGCTGGGCCCTTTGTGCTTTCATGTCTCTTGTGATGACATTTGCCAAAGTAAACCCCTACTCGCCCTG
 CTACATGTCTCTTCCAGGTGAACGGCATGTTGATCATGTGCAATGCCCTATTGACCCCTTCATATATGCCTTCCGGAGCCAGAGCTCAGGGACGCATTCAAAAAGATGATCTTCTGCAGCAGGTA
 CTGGTAGCTCGAGTCTAGA

Restriction Map

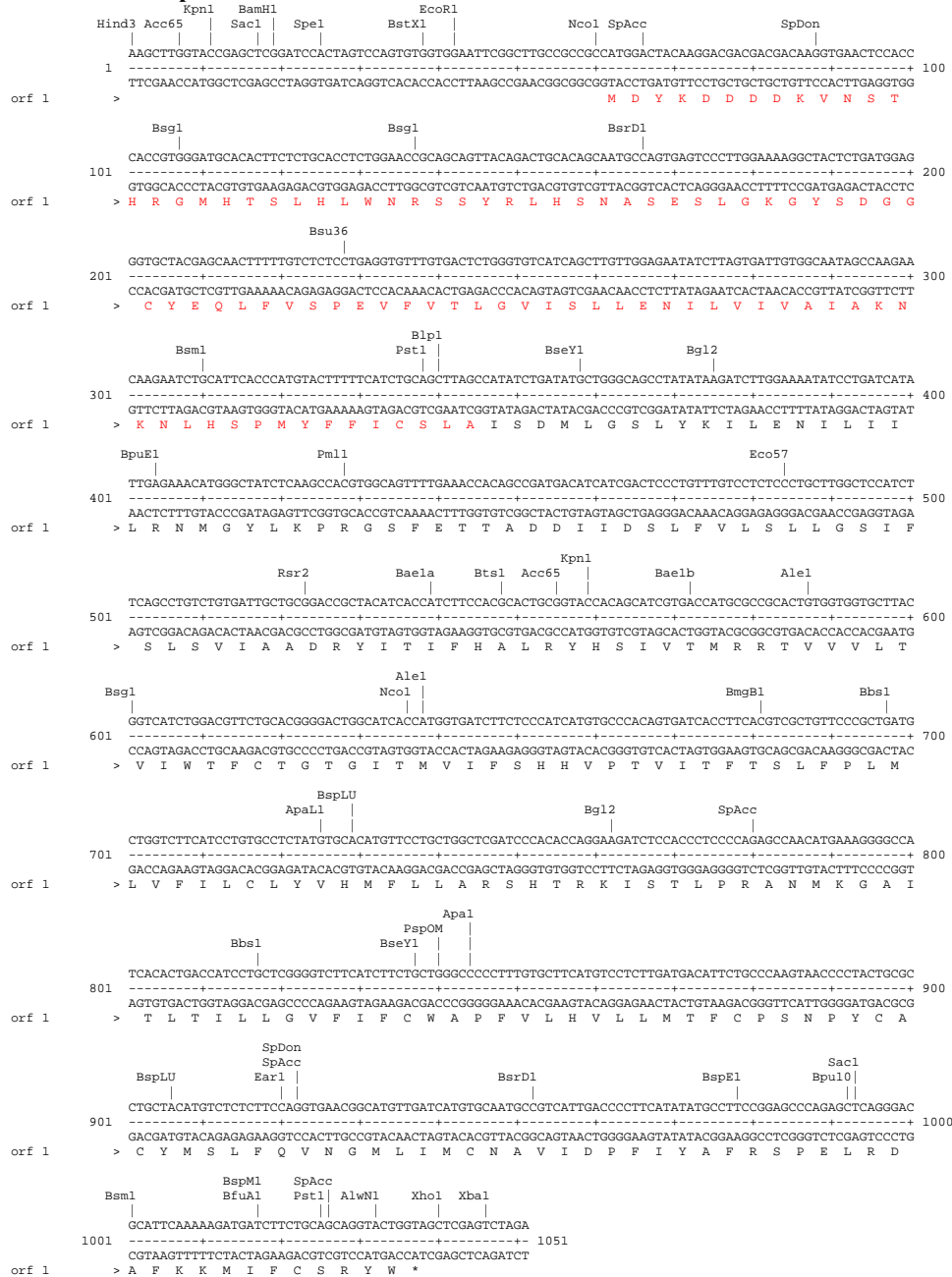


Figure B-3. Chimera 2C2 DNA Sequence

Complete sequence of Flag-hMC2R/2C2/pcDNA3

AAGCTTGGCCGCGCCATGGACTACAAGGACGACGACAAGAAGCACATTATCAACTCGTATGAAAACATCAACAACACAGCAAGAATAATCCGACTGTCCTGTGGTGTTCGCCGGAGGAGATA
 TTTTTCACAATTCCATTGTTGGAGTTTGGAGAACTGATCGTCTGCTGGCTGTGTTCAAGAATAAGAATCTCCAGGCACCCATGTACTTTTTCATCTGTAGCTTAGCTGGCTGATATGCTGGTG
 AGCGTTTCAAATGGATCAGAAACCATTGTATCACCCTATTAACAGTACAGATACGGATGCACAGAGTTTACACAGTGAATATTGATAATGTCAATTGACTCGGTGATCTGTAGCTCCTGTTCATCC
 ATTTGCAGCTGCTTTCAATTGCAGTGGACCGGTACATCACCATCTTCCACGCACTGGGTACCAAGATCGTGACCATGCGCCGCACTGTGGTGGTGTTCACGGTCACTGGACGTTCTGCACGGGG
 ACTGGCATCACCATGGTGTCTTCTCCCATCATGTGCCACAGTATCACCTTCAAGTCTGCTTCCCGTGTGCTTCCATCCTGTGCCTCTATGTGCACATGTTCCCTGGCTCGATCCAC
 ACCAGGAAGATCTCCACCTCCAGAGCAACATGAAAGGGGCCATCAGCTGACCATCTGCTGGGGTCTTCACTTCTGCTGGGGCCCTTTGTCTTATGTCCTCTTGTGACATCTGCCCCA
 AGTAACCCCTACTGCGCTGCTACATGTCTCTCTCCAGTGAACGGCATGTTGATCATGTGCAATGCCGTCAATGACCCCTCATATATGCCTCCGGAGCCAGAGCTCAGGAGCCATTCAAAAAG
 ATGATCTTCTGCAGCAGTACTGGTAGCTCGAGTCTAGA

Restriction Map

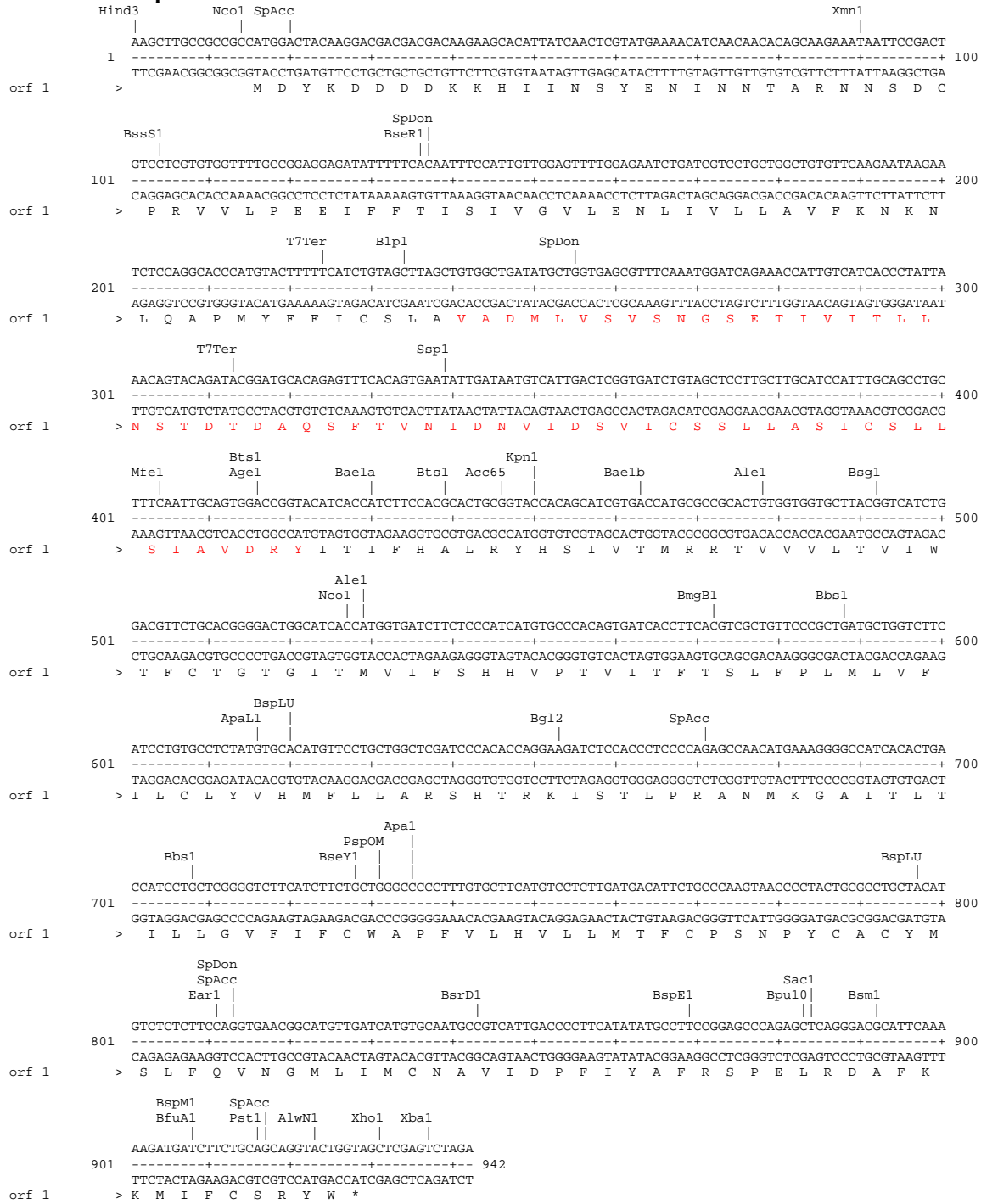


Figure B-4. Chimera 2C3 DNA Sequence

Complete sequence of Flag-hMC2R/2C3/pcDNA3

AAGCTTGGCCGCGCCATGGACTACAAGGACGACGACGACAAGAAGCACATTATCAACTCGTATGAAAACATCAACAACACAGCAAGAATAATCCGACTGTCCTCGTGGTTTTGCCGGAGGAGATA
 TTTTCAACAATTCATTTGGAGTTTGGAGAACTGATCGTCTGCTGGCTGTGTTCAAGAATAAGAATCTCAGGCACCCATGTACTTTTCATCTGTAGCTTGGCCATATCTGATATGCTGGCC
 AGCCTATATAAGATCTTGGAAAATATCCTGATCATATTGAGAAACATGGGCTATCTCAAGCCACGTGGCAGTTTTGAAACCACAGCCGATGACATCATCGACTCCCTGTTGTCTCTCCCTGCTTGGC
 TCCATCTTCAGCCTGTCTGTGATTCGTCGGGACCGGTACTTTACTATCTTCTATGCTCTCCAGTACCATAACATTTATGACAGTTAAGCGGGTTGGGATCATATAAGTTGTATCTGGGCAGCTTGCAAG
 GTTTCAGGCATTTTGTTCATCATTACTCAGATAGTAGTCTGTCATCATCTGCCTCATACCATGTTCTTCACCATGCTGGCTCTCATGGCTTCTCTATGTACACATGTTCTGCTGGCTCGATCC
 CACACCAGGAAGATCTCCACCCTCCCGAGCCAAACATGAAAGGGGCCATCACACTGACCATCTGCTCGGGTCTTCATCTTCTGCTGGCCCCCTTTGTGCTTATGCTCTTGTATGACATTCTGC
 CCAAGTAACCCCTACTGCGCTGTACATGTCTCTCTCCAGGTGAACGGCATGTTGATCATGTCAATGCCGTCATTGACCCTTCATATATGCCTCCGGAGCCAGAGCTCAGGACCGCATTCAAA
 AAGATGATCTTCTGCAGCAGTACTGGTAGCTCGAGTCTAGA

Restriction Map

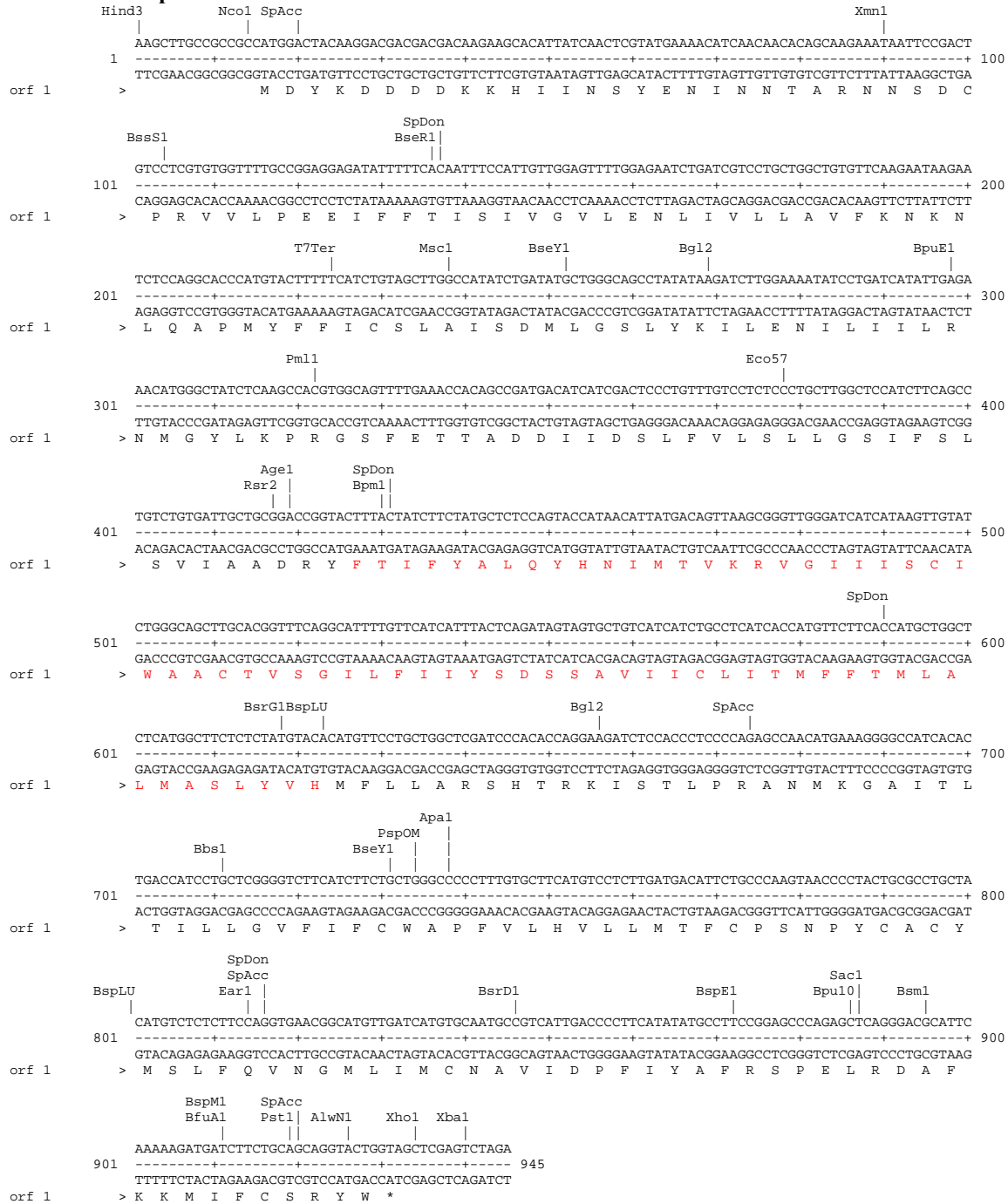


Figure B-5. Chimera 2C4 DNA Sequence

Complete sequence of Flag-hMC2R/2C4/pcDNA3

AAGCTTGGCCGCGCCATGGACTACAAGGACGACGACGACAAGACACATTAACAACGATGAAACACACAGCAAGAATAATCCGACTGTCCTCGTGGTTTTGCCGGAGGAGATA
 TTTTTCACAATTTCCATTTGGAGTTTGGAGAACTCGATCTCTCTGGCTGTGTTCAAGAAATAAGAAATCTCCAGGCACCCATGTACTTTTTCATCTGTAGCTTGGCCATATCTGATATGCTGGC
 AGCCTATATAAGATCTTGGAAAATATCCTGATCATATTGAGAAACATGGGCTATCTCAAGCCACGTTGGCGCTTTTGAACCCACAGCCGATGACATCATCGACTCCCTGTTTGTCTCTCCCTGCTTGGC
 TCCATCTTCAGCCTGTCTGTGATTTGCTGGGACCGCTACATCACCATCTTCCAGCAGCTGCGGTACCACAGCATCGTGACCATGCGCCGCACTGTGGTGGTCTTACGGTCACTGGACGTTCTGCACG
 GGGACTGGCATCACCATGGTATCTTCCATCATGTGCCACAGTGATCACCTTCCAGTGTCTTCCGCTGATGCTGGTCTTCCATCCTGTGCCCTATGTGCACATGTTCTGCTGGCTGATCC
 CACACCAGGAAGATCTCCACCTCCCGAGCCAAACATGAAAGGGCCATCACGTTAAACCATCTGATGGCGCTTTTGTGTCTGTGGGCCCATTTCTCTCCACTTAATATTTACATCTCTTGT
 CCTCAGAATCCATATTGTGTGCTTTCATGTCTCACTTTAACTTGTATCTCATACTGATCATGTGAATTAATCAATCATCGATCCTCTGATTTATGCACTCCGGAGTCAAGAACTGAGGAAAACCTTCAA
 GAGATCATCTGTGCTATCCCTGGGAGCCCTTTGTGACTTGTCTAGCAGATATTAATGGGGACAGACGCAATATAGAAGCCGAATTTCTGAGATATCCAGCACAGTGGCGCCGCTCGAGTCTA
 GA

Restriction Map

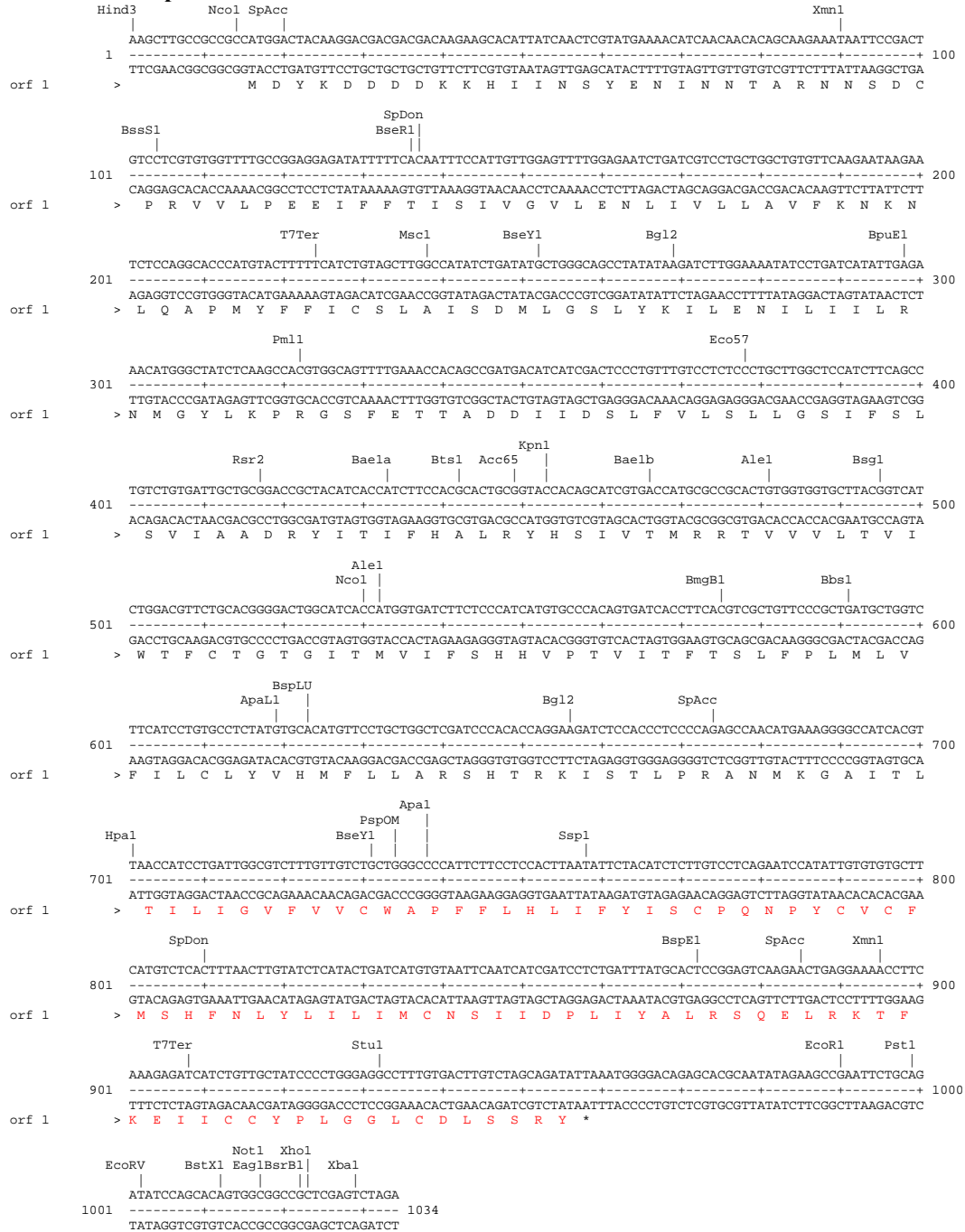


Figure B-6. Chimera 2C5 DNA Sequence

Complete sequence of Flag-hMC2R/2C5/pcDNA3

AAGCTTGGCCGCGCCATGGACTACAAGGACGACGACGACAAGAAGCACATTATCAACTCGTATGAAAACATCAACAACACAGCAAGAATAATCCGACTGTCCTGTGGTTTTGCCGGAGGAGATA
 TTTTCAACAATTTCCATTTGGAGATTTGGAGAATCTGATCGTCTGCTGGCTGTTCAAGAATAAGAATCTCCAGGCACCATGTACTTTTTCATCTGTAGCTTAGCTGTGGCTGATGCTGGTG
 AGCCTTTCAAATGGATCAGAAACCATTGTATCACCCCTATTAACAGTACAGATACGGATGCACAGAGTTTACACAGTGAATATTGATAATGTCATTGACTCGGTGATCTGTAGCTCCTGTGTCATCC
 ATTTGCAGCTGCTTCAATTCAGTGGACAGGTACTTTACTATCTTCTATGCTCTCCAGTACCATAAATTATGACAGTTAAGCGGGTTGGGATCATATAAGTTGATCTGGGCAGCTGACAGGTT
 TCAGGCATTTTGTTCATTTACTCAGATAGTAGTGTCTCATCTGCTCATCTGCCCTATCACCATGTTCTTCCATGCTGGCTCTCATGGCTTCTCTATGTCACATGTTCCGTATGGCCAGGCTTCC
 ATTAAGAGGATGCTGCTCCCGGCACCTGGTCCATCCGCCAAGTGCCAAATATGAAGGGAGCGATTACGTTAAACATCTCTGCTCGGGTCTTATCTTCTGCTGGGCCCTTTGTGCTTATGTC
 CTCTTGATGACATTTCCCAAGTAACCCCTACTGCGCTGTACATGTCTCTCCAGGTGAACGGCATGTTGATCATGTGCAATGCCGTCATTGACCCTTTCATATATGCCTTCCGGAGCCAGAG
 CTCAGGGACGATTCAAAGATGATCTTCTGCAGCAGTACTGGTAGCTCAGTCTAGA

Restriction Map

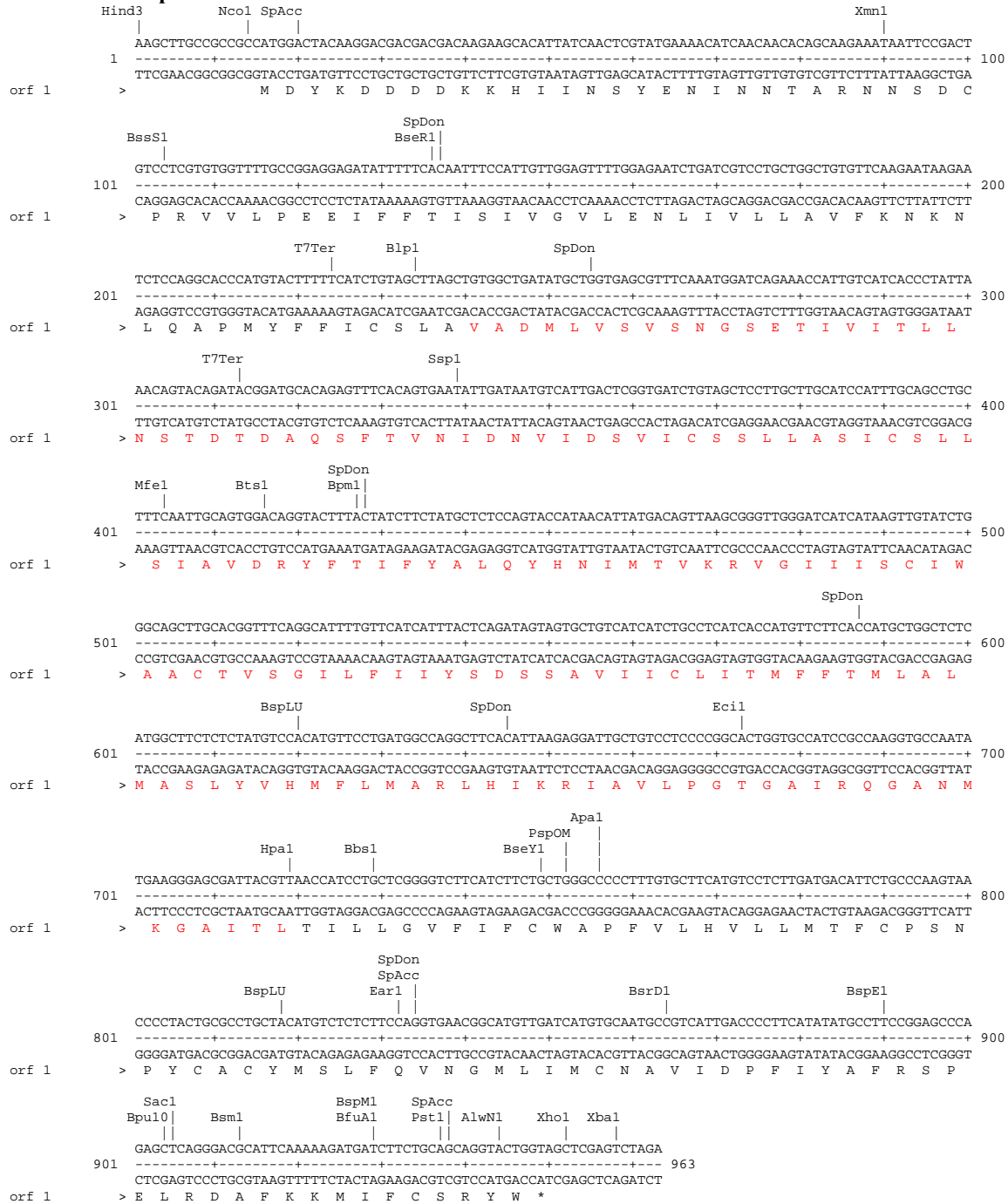


Figure B-8. Flag-hMC4R DNA Sequence

Complete Sequence of Flag-hMC4R in pcDNA3

AAGCTTGGTACCGAGCTCGGATCCACTAGTCTCAGTGTGGTGAATTCGGCTTGCCTGCCCGCCACTGGACTACAAGGACGACGACGACAGAGTGAACCTCCACCCACCGTGGGATGCACACTTCTGTGCACCT
 CTGGAAACCCGACAGTTACAGACTGCACAGCAATGCCAGTGAAGTCCCTGGAAAGGCTACTCTGATGGAGGGTCTACGAGCAACTTTTGTCTCTCTGAGGTGTTTGTGACTCTGGGTGCATCAG
 CTTGTTGGAGAATATCTTGTGATTGTGGCAATAGCAAGAACAAGAATCTGCATTACCCATGTACTTTTTTCATCTGCAGCTTGGCTGTGGCTGATATGCTGTGAGCGTTTCAAATGGATCAGAAAC
 CATTGTGCATCACCCTATTAACAGTACAGATACGGATGCACAGAGTTTACAGTGAATATTGATAATGTCAATGACTCGGGTATCTGTAGCTCCTTGCTTGCATCCATTGTCAGCCCTGCTTTCAATTC
 AGTGGACAGGTACTTTACTATCTTCTATGCTCTCCAGTACCATAACTATGACAGTAAAGCGGGTTGGGATCATATAAGTTGTATCTGGCAGCTTGACAGGTTTCAGGCATTTTGTTCATCATTTA
 CTCAGATAGTAGTGTCTCATCTGCCTCATACCATGTCTTCCACCATGTGGCTCTCATGGCTTCTCTATGTCACATGTTCCTGATGGCCAGGCTTCAATTAAGAGGATGTGTCTCTCC
 CGGCACCTGGTGCATCCGCAAGGTGCAATATGAAGGGAGCGATTACCTTGACCATCTGATTGGCGTCTTGTGTCTGTGCGGCCCATCTTCTCCACTTAATATTCTACATCTCTGTCTCTCA
 GAATCCATATTGTGTGTCTCATGTCTCACTTTAAGTTGTATCTCATACTGATCATGTGAATCAATCATGATCCTCTGATTTATGCACCTCCGAGTCAAGAAGTGGAGAAACCTTCAAAGAGAT
 CATCTGTTGCTATCCCTGGGAGCCCTTTGTGACTTGTCTAGCAGATATTAATGGGGACAGACGCAATATAGAAGCCGAATTTGCAGATATCCAGCACAGTGGCGGCCCTCGAGTCTAGA

Restriction Map

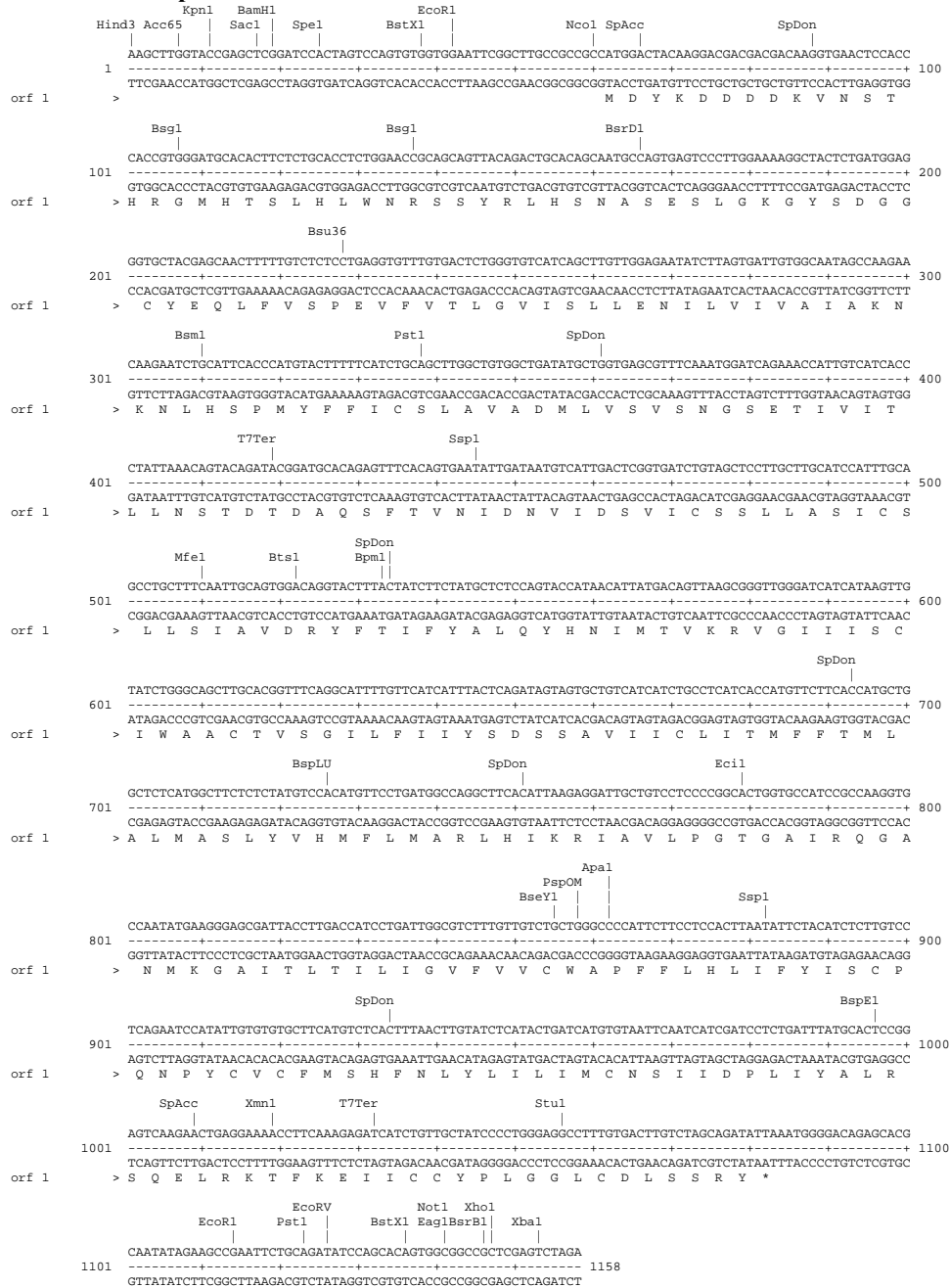


Figure B-9. Chimera 4C1 DNA Sequence

Complete sequence of Flag-hMC4R/4C1/pcDNA3

AAGCTTGGCCGCGCCATGGACTACAAGGACGACGACGACAAGAAGCACATTATCAACTCGTATGAAAACATCAACAACACAGCAAGAATAATTCGGACTGTCCTCGTGGTTTTGCCGGAGGAGATA
 TTTTTCACAAATTCATTTGGAGTTTGGAGAACTGATCGTCTGCTGGCTGGTTCAAGAATAAGAATCTCCAGGCACCCATGTACTTTTTTCATCTGTAGCTTAGCTGGCTGATATGCTGGTG
 AGCGTTTTCAATGGATCAGAAACCATTGTATCACCCCTATTAACAGTACAGATACGGATGCACAGAGTTTACAGTGAATATTGATAATNTCATTGACTCGGTGATCTGTAGCTCCTTGGCTGCATCC
 ATTTGCAGCTGCTTTCAATTCAGTGGACAGGTACTTTACTATCTTCTATGCTCTCCAGTACCATAAACATTATGACAGTTAAGCGGGTTGGGATCATATAAGTTGATCTGGGCAGCTTGCACGGTT
 TCAGGCATTTTGGTTCATTTACTCAGATAGTGTGCTGCATCATCTGCCATCACCATTGTTCTTACCATGCTGGCTCTCATGGCTTCTCTATGTCACATGTTCCCTGATGGCCAGGCTTCC
 ATTAAGAGGATGCTGCTCCCGGCACTGGTGCATCCGCCAAGTGCCAAATATGAAGGGAGCGATTACCTTGACCATCTGATGGCTCTTTGTTGCTGCTGGGCCCACTTCTTCCACTTA
 ATATTCTACATCTTGTGCTCAGAATCCATATTGTGTGCTTCAATGCTCACTTAACTTGTATCTCATACTGATCATGTGAATCAATCATCGATCCTCTGATTTATGCACTCCGGAGTCAAGAA
 CTGAGGAAACCTTCAAAGAGATCATCTGTTGCTATCCCTGGGAGCCCTTGTGACTTGTCTAGCAGATATTAATGGGGACAGACGCAATATAGAAGCCGAATTCGACGATATCCAGCACAGT
 GCGCGCGCTCGAGTCTAGA

Restriction Map

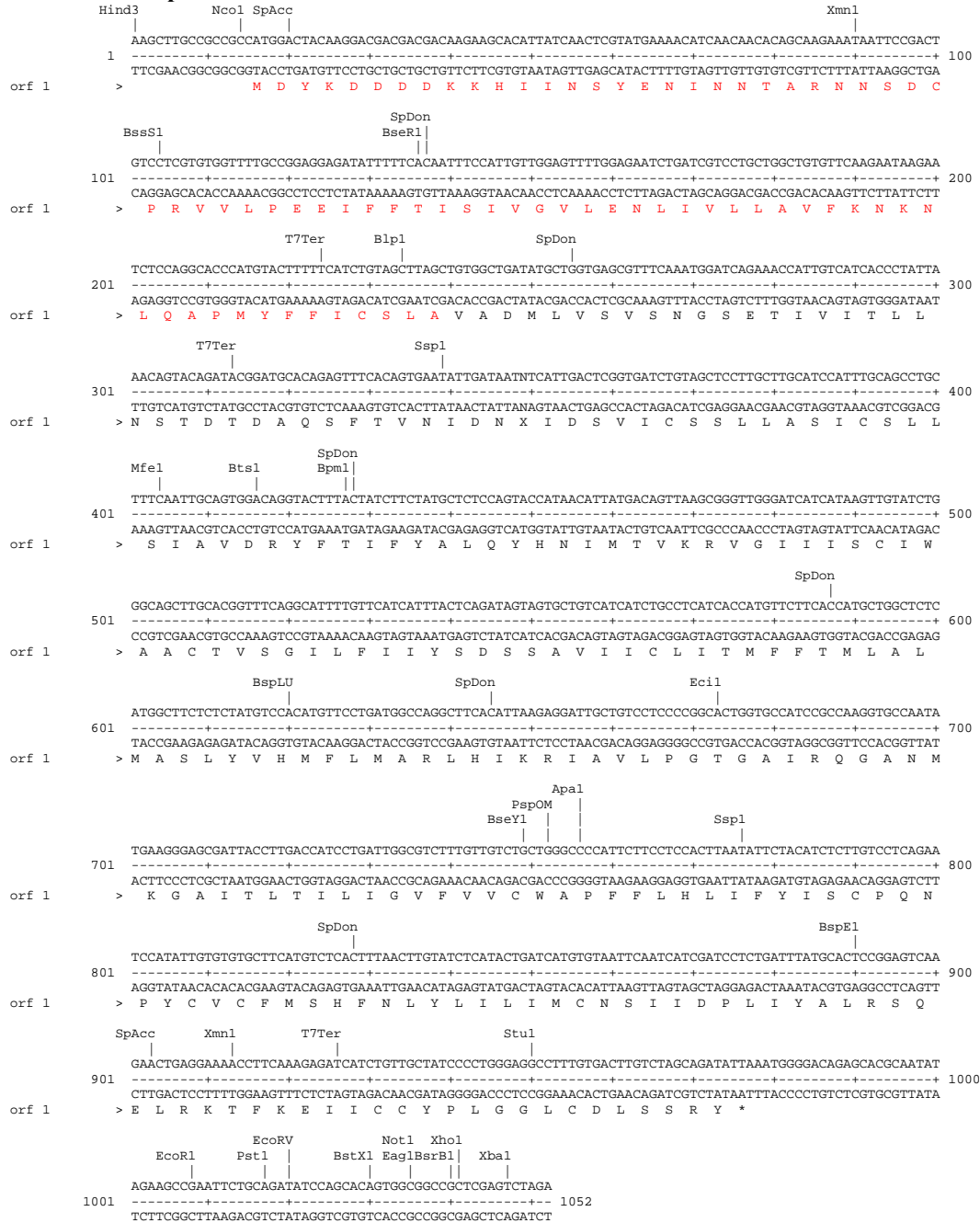


Figure B-10. Chimera 4C2 DNA Sequence

Complete sequence of Flag-hMC4R/4C2/pcDNA3

AAGCTTGGTACCGAGCTCGGATCCACTAGTCTCAGTGTGGTGAATTCGGCTTGGCCGCCCATGGACTACAGGACGACGACGACAGGTTGAAGTCCACCCACCGTGGGATGCACACTTCTGTCACCT
 CTGGAACCCGACGAGTTACAGACTGCACAGCAATGCCAGTGAATTCCTGGAAAGGCTACTCTGATGGAGGGTGTCTACGAGCAACTTTTGTCTCTCTGAGGTGTTTGTGACTCTGGGTGCATCAG
 CTTGTTGGAGAATATCTTAGTGATTGTGGCAATAGCAAGAACAAGAACTGCATTACCCATGTACTTTTTCATCTGCAGCTTAGCCATATCTGATATGCTGGCCAGCCTATATAAGATCTTGGAAAA
 TATCTCGATCATATTTGAGAAACATGGGCTATCTCAAGCCACGTTGGCAGTTTGAAGAACACAGCCGATGACATCATCGACTCCCTGTTTGTCTCTCCCTGGCTGGCTCCACTTTCAGCCCTGTCTGTGAT
 TGCTGGCCAGCCGTTACTTTACTATCTTCTATGCTCTCCAGTACCATAACATTATGACAGTTAAGCGGGTGGGATCATATAAGTTGTATCTGGGCAGCTTGCACGGTTTCAGGCAATTTTGTTCATCAT
 TTAATCAGATAGTAGTGTCTCATCATCTGCCTCATCACCATTGTTTCCACCATGCTGGCTCTCATGGCTTCTCTCATATGTCACATGTTCTGATGGCCAGGCTTACATTAAGAGGATTTGCTGTCT
 CCCCAGCAGTGTGCCATCCGCCAAGGTGCCAATATGAAGGGAGCGATTACCTTGACCATCTGATGGCGTCTTGTGTCTGCTGGGCCCATTTCTCCACCTTAATATTACATCTCTGTCT
 TCAGAAATCCATATTGTGTGCTTCACTTAACTTGTATCTCACTGATCATGTTAATCAATCATCGATCTCTGATTTATGCACTCCGGAGTCAAGAACTGAGGAAAACCTTCAAGA
 GATCATCTGTTGCTATCCCTGGGAGGCCTTTGTGACTTGTCTAGCAGATATTAATGGGACAGAGCACCAATATAGAAGCCGAATTTGTCAGATATCCAGCACAGTGGCCGCCCTCGAGTCTAGA

Restriction Map

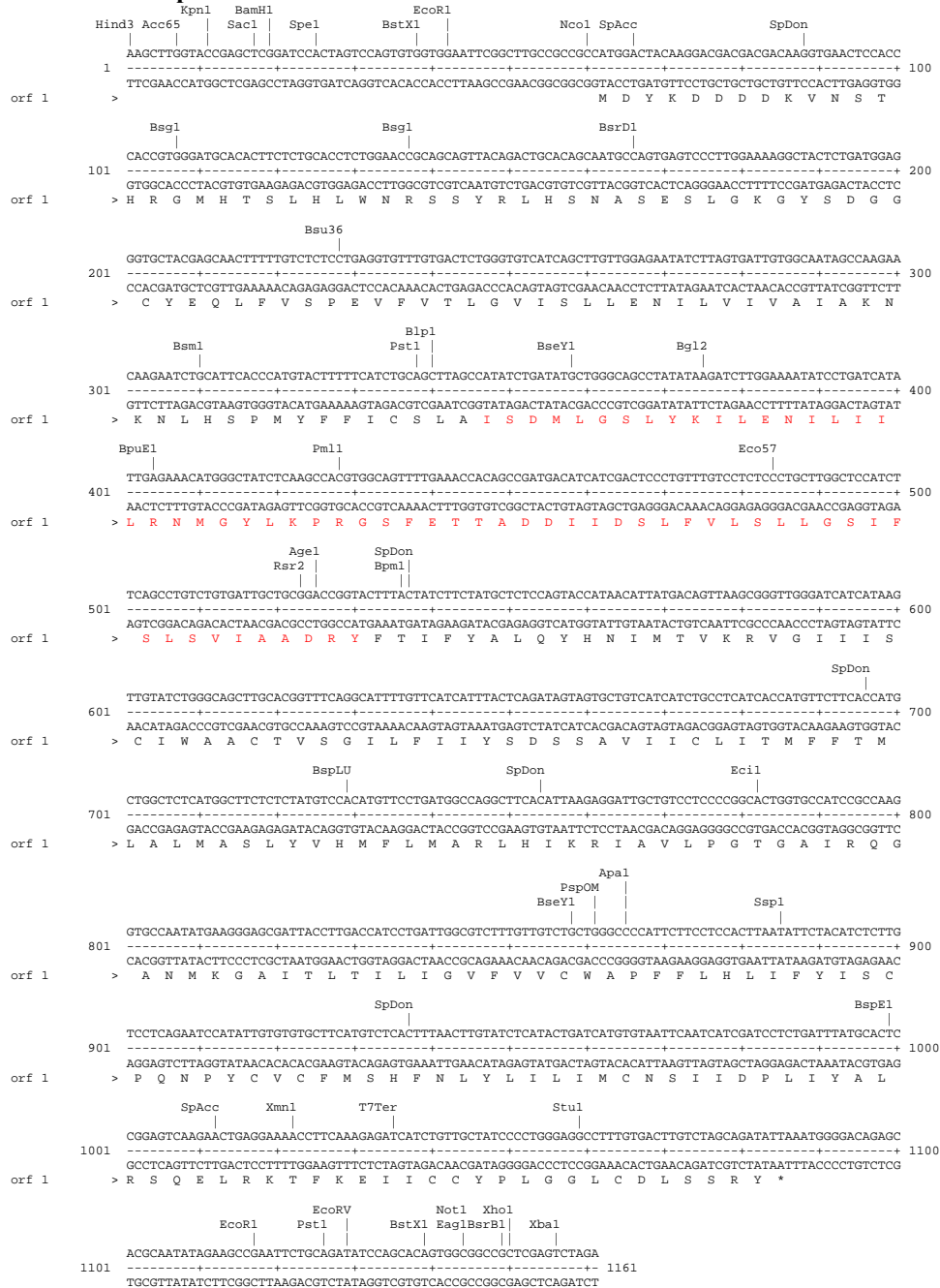


Figure B-12. Chimera 4C4 DNA Sequence

Complete sequence of Flag-hMC4R/4C4/pcDNA3

AAGCTTGGTACCGAGCTCGGATCCACTAGTCCAGTGTGGTGAATTCGGCTTGGCCGCCCATGGACTACAAGGACGACGACGACAAAGTGAAGTCCACCCACCGTGGGATGCACACTTCTGTGCACCT
 CTGGAAACCAGCAGTTACAGACTGCACAGCAATGCCAGTGAATTCCTGGAAAGAGCTACTCTGATGGAGGGTGTCTACGAGCAACTTTTGTCTCTCTCTAGGTGGTGGTGTGATCAG
 CTTGTGGAGAATATCTTGTGATTTGGCAATAGCCAAAGAAACAAAGATCTGCATTACCCATGTACTTTTTTCATCTGCAGCTTGGCTGTGGCTGATATGTCTGGTGGAGCTTTCAAATGGATCAGAAAC
 CATTGTCTACACCCCTATTAACAGTACAGATACGGATGCACAGAGTTTCACAGTGAATATTGATAATGTCAATGACTCGGGTATCTGTAGCTCCTTGGCTTGCATCCATTTCAGCCCTGCTTTCAATTC
 AGTGGACAGGTACTTTACTATCTTCTATGCTCTCCAGTACCATAAACATTATGACAGTTAAGGGGTTGGGATCATATAAGTTGATCTGGGACGCTGCACGGTTTCAGGCATTTTGTTCATCATT
 CTCAGATAGTAGTCTGTATCTCTGCCTCATACCATGTCTTCCACATGGCTCTCATGGCTCTCTCTATGTCCACATGTTCTCTGATGGCCAGGCTTCACATTAAAGAGGATGTGTCTCTCC
 CGGCACCTGGTGCATCCGCAAGGTGCAATATGAAGGGAGCGATTAC**TTAACCATCTCTGCTGGGGTCTTCATCTCTGCTGGGCCCTTTGTGCTTCATGCTCCTTGTGATGACATTCTGCCAAG**
TAACCCCTACTGCGCTGTACATGCTCTCTCCAGGTGAACGGCATGTTGATCATGTGCAATGCCGTCATTGACCCCTTCATATATGCCTCCGGAGCCAGAGCTCAGGGACGATTCAAAGAT
GATCTTCTGCAGCAGGTAAGTGTAGCTCGAGTCTAGA

Restriction Map

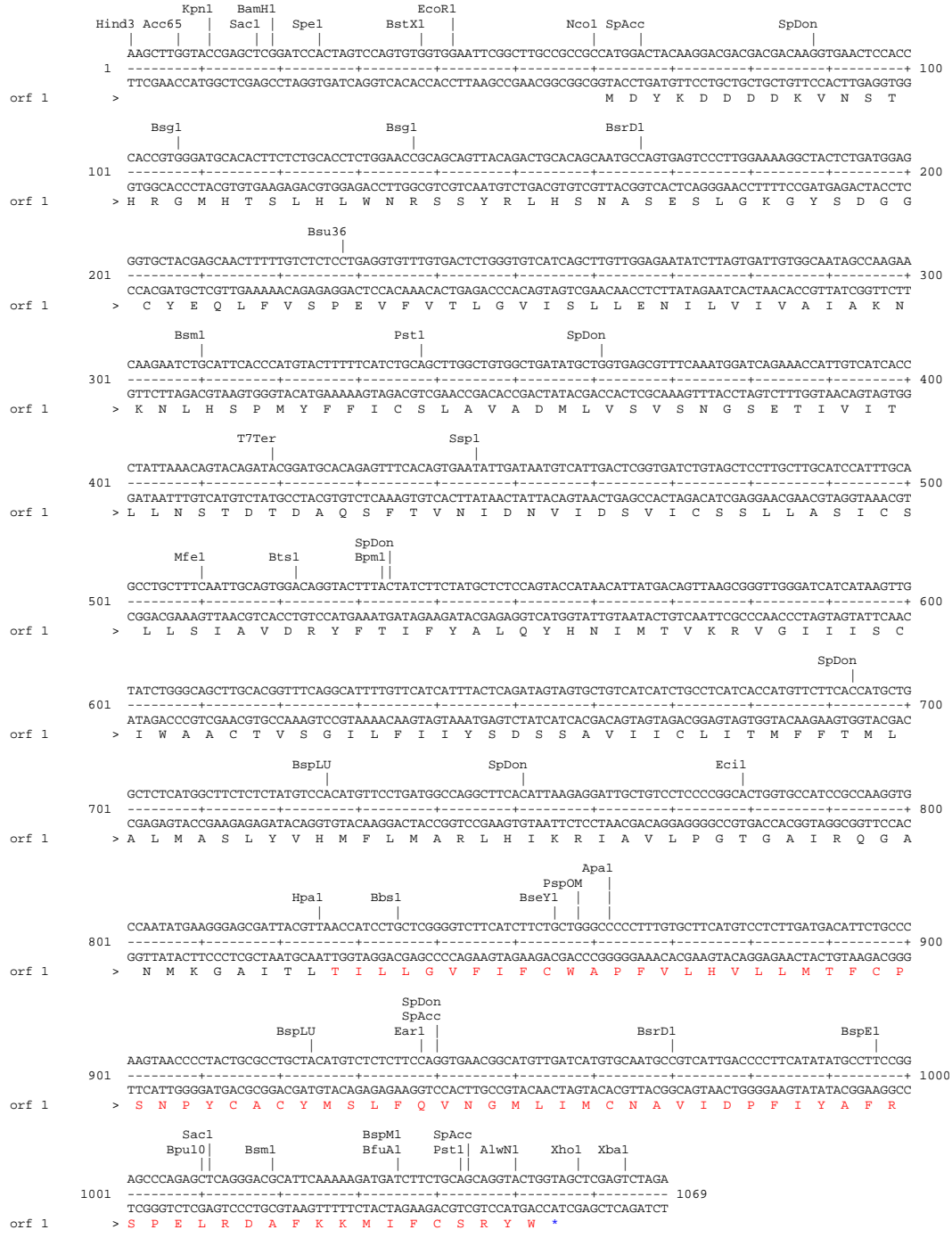


Figure B-13. Chimera 4C5 DNA Sequence

Complete sequence of Flag-hMC4R/4C5/pcDNA3

AAGCTTGGTACCGAGCTCGGATCCACTAGTCTCAGTGTGGTGAATTCGGCTTGCCTGCCCGCCATGGACTACAGGACGACGACGACAGGTTGAAGTCCACCCACCGTGGGATGCACACTTCTGACCT
 CTGGAAACCCAGCAGTGTACAGACTGCACAGCAATGCCAGTGAATTCCTGGAAAGGCTACTCTGATGGAGGGTGTCTACGAGCAACTTTTGTCTCCTGAGGTGTTTGTGACTCTGGGTGCATCAG
 CTTGTTGGAGAATATCTTAGTGATTGTGGCAATAGCCAAGAACAAGAAATCTGCATTACCCATGTACTTTTTCATCTGCAGCTTAGCCATATCTGATATGTCTGGCCAGCCTATATAAGATCTTGGAAAA
 TATCTGATCATATTTGAGAAACATGGGCTATCTCAAGCCACGTTGGCAGTTTGAACCACAGCCGATGACATCATCGACTCCCTGTTTGTCTCCTCCCTGGCTGGCTCCATCTTCCAGCCTGTCTGTGAT
 TGCTGGGACCGCTACATCACCCTTTCCACGCACTGCGGTACCAAGCATCGTACCATGCGCCGCACTGTGGTGGTCTTACGGTCACTGGACGTTCTGCACGGGACTGGCATCACCATGGTGT
 CTCTCCCATCATGTGCCACAGTATCACCTTACGTCGCTGTCCCGCTGATGCTGTCTTATCTCTGTGCCTCTATGTGCACATGTTCTGCTGGCTCGATCCACACAGGAAGATCTCCACCCT
 CCCAGAGCCAACATGAAGGGGCCATCACGTTAACCATCTGATTGGCGCTTTTGTGTCTGCTGGGCCCATCTCTCCTCCACTTAATATCTACATCTCTTGTCTCAGAACTCCATATTTGTGTGTG
 CTTTCATGCTCACTTAACTGTATCTCACTGATCATGTGTAATTCATCATCGATCCTCTGATTTATGACATCCGGAGTCAAGAAGTGAAGAAACCTTCAAGAGATCATCTGTTCTATCCCT
 GGGAGCCTTTGTGACTTGTCTAGCAGATATAAATGGGGACAGACGCAATATAGAAGCCGAATTCGAGATATCCAGCAGTGGCGGCCCTCGAGTCTAGA

Restriction Map

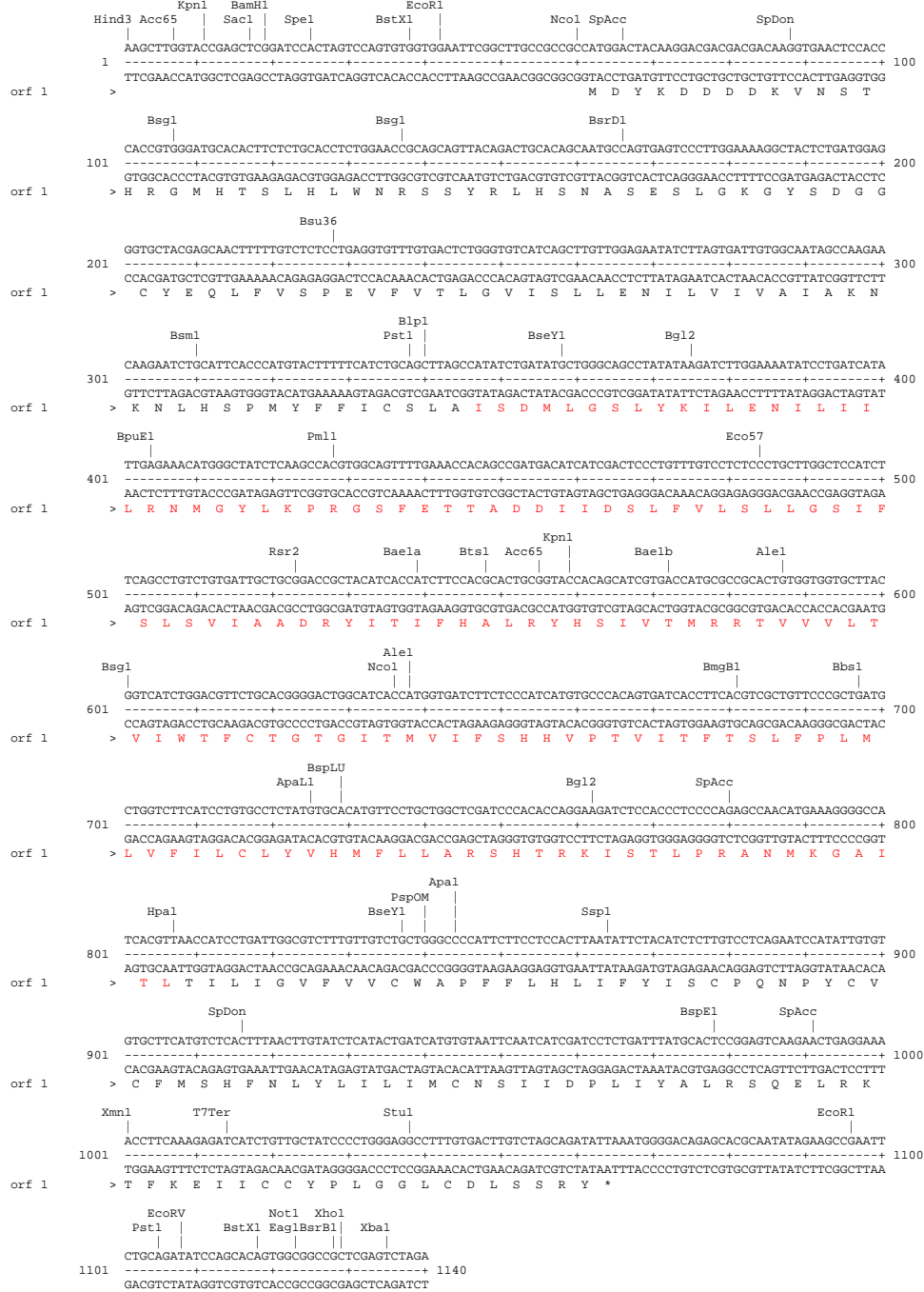
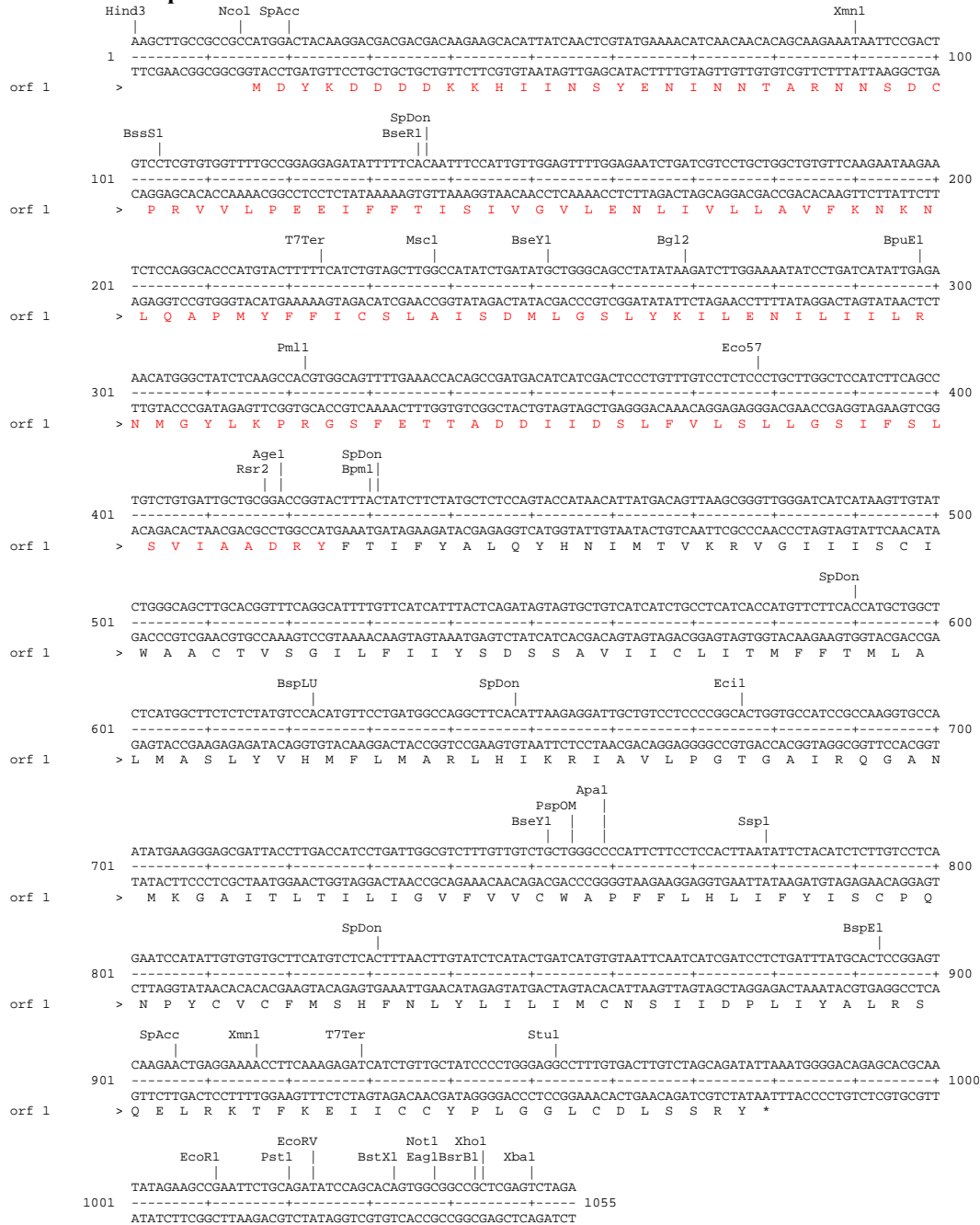


Figure B-14. Chimera 4C6 DNA Sequence

Complete sequence of Flag-hMC4R/4C6/pcDNA3

AAGCTTGGCCGCGCATGGACTACAAGGACGACGACGACAAGAAGCACATTATCAACTCGTATGAAAACATCAACAACACAGCAAGAATAATCCGACTGTCCTCGTGGTTTTGCCGGAGGAGATATTTTCACAA
 TTTCATTTGGAGTTTTGGAGAACTGATCGTCTGGCTTCAAGAAATAAGAACTCCAGGCACCCATGTACTTTTCATCTGTAGCTTGGCCATATCTGATATGCTGGCAGCCTATATAAGATCTTGA
 AAATATCCTGATCATATTGAGAAACATGGGCTATCTCAAGCCACGTGGCAGTTTTGAAACCACAGCCGATGACATCATCGACTCCCTGTTTGTCTCTCCCTGCTTGGCTCCATCTTCAGCCTGTCTGTGATTGCTGCG
 GACCCGGTACTTTACTATCTTCTATGCTCTCCAGTACCATAACATATGACAGTTAAGCGGGTTGGGATCATCATAAGTTGATCTGGGCAGCTTGCACGGTTTCAGGCATTTTGTTCATATTTACTCAGATAGTAGTG
 CTGTCAATCATCTGCCTCATCACCATGTTCTTCCACATGCTGGCTCTCATGGCTTCTCTATGTCACACATGTTCTGTATGGCCAGGTTACACATTAAGAGGATTGCTGTCCCTCCCGGCATGGTGCCATCCGCCAAGG
 TGCCAAATGAAGGGAGCGATTACCTTGACCATCCTGATTGGCGTCTTTGTGTCTGCTGGGCCCATCTTCTCCACTTAATATTTCTACATCTCTGTCTCAGAAATCCATATTGTGTGTGCTCATGTCTCACTTT
 AACTTGTATCTCATACTGATCATGTGTAATCAATCATGATCCTCTGATTTATGCACTCCGGAGTCAAGAACTGAGGAAAACCTTCAAAGAGATCATCTGTGTCTATCCCTGGGAGGCCTTTGTGACTTGTCTAGCA
 GATATTAATGGGACAGAGCACGAATATAGAAGCCGAATCTGCAGATATCCAGCACAGTGGCGCCGCTCGAGTCTAGA

Restriction Map



APPENDIX C
HISTOGRAMS OF FACS CHIMERA DATA

Histogram statistics were calculated relative to the isotype control as background.

M1 = No label and isotype control peaks.

M2 = Surface and total expression, peak only.

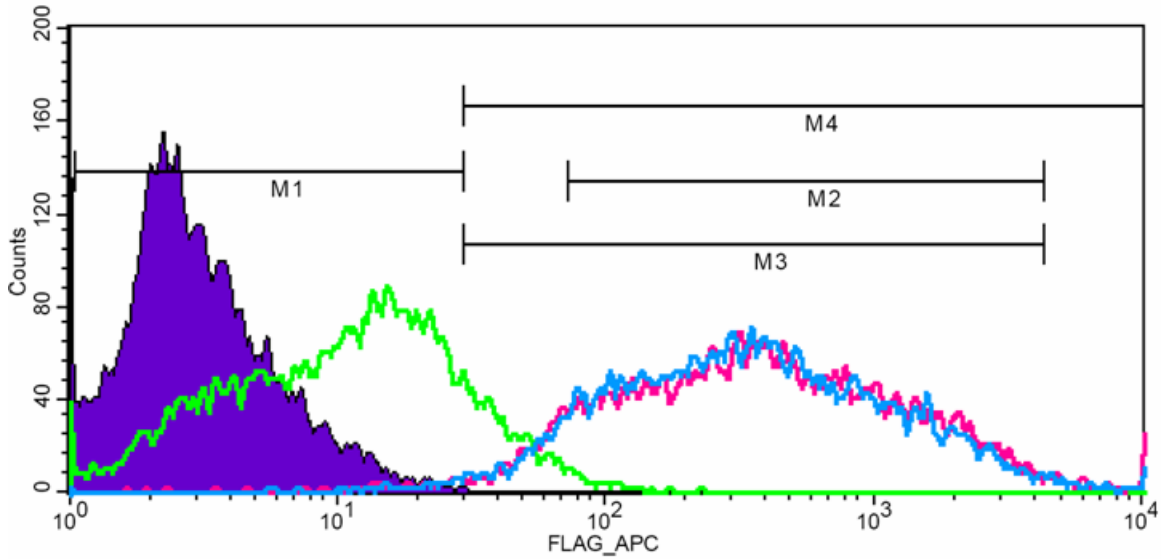
M3 = Surface and total expression peaks + low end.

M4 = Surface and total expression peaks + high and low ends.

Color Key:

- Purple (filled) peak = No label
- Green = Isotype control
- Pink = Surface labeled with Anti-Flag-APC
- Total = Surface and intracellular labeled with Anti-FLAG-APC

Figure C-1. Flag-hMC2R in HEK cells FACS Histogram



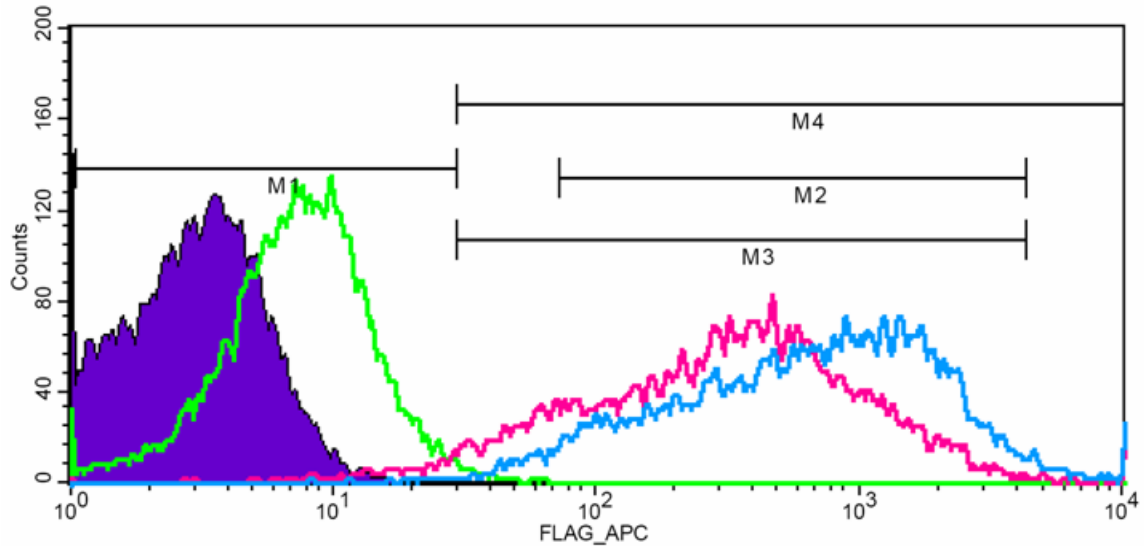
Surface Statistics:

Marker	Left, Right	Events	% Gated	% Total	Mean	Geo Mean	CV	Median	Peak Ch
All	1, 9910	20000	50.10	100.00	725.55	348.37	150.04	349.12	313
M1	1, 30	422	1.06	2.11	16.26	12.67	53.27	16.55	28
M2	72, 4294	17692	44.31	88.46	691.57	421.65	107.95	392.42	313
M3	30, 4294	19252	48.22	96.26	640.00	356.84	115.07	352.27	313
M4	30, 9910	19578	49.04	97.89	740.84	374.43	147.84	358.66	313

Total Statistics:

Marker	Left, Right	Events	% Gated	% Total	Mean	Geo Mean	CV	Median	Peak Ch
All	1, 9910	20000	50.10	100.00	644.21	326.62	146.58	321.97	336
M1	1, 30	368	0.92	1.84	18.49	15.88	43.24	19.46	29
M2	72, 4294	17908	44.86	89.54	629.97	388.82	110.54	365.17	336
M3	30, 4294	19400	48.59	97.00	585.70	333.51	117.19	324.88	336
M4	30, 9910	19640	49.19	98.20	655.69	345.56	144.74	333.76	336

Figure C-2. Chimera 2C1 in HEK cells FACS Histogram



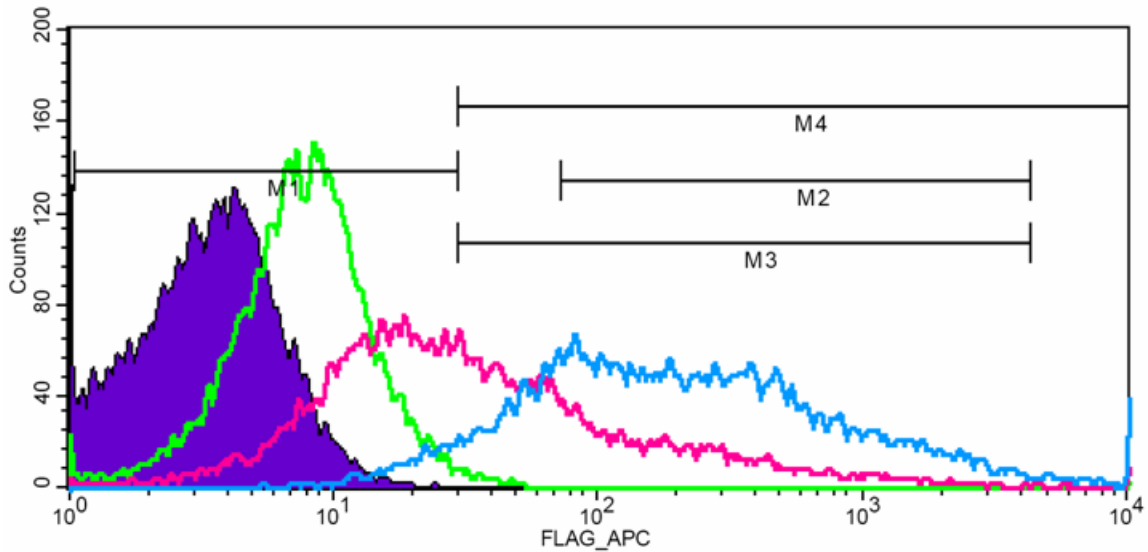
Surface Statistics:

Marker	Left, Right	Events	% Gated	% Total	Mean	Geo Mean	CV	Median	Peak Ch
All	1, 9910	20000	50.06	100.00	535.55	275.22	145.93	316.23	461
M1	1, 30	844	2.11	4.22	17.44	14.92	45.40	17.31	26
M2	72, 4294	16858	42.19	84.29	578.21	389.20	100.45	385.42	461
M3	30, 4294	19050	47.68	95.25	517.54	306.95	110.46	333.76	461
M4	30, 9910	19166	47.97	95.83	558.11	312.78	141.67	336.78	461

Total Statistics:

Marker	Left, Right	Events	% Gated	% Total	Mean	Geo Mean	CV	Median	Peak Ch
All	1, 9910	20000	50.06	100.00	1029.62	583.71	114.53	667.14	922
M1	1, 30	132	0.33	0.66	19.17	17.46	37.31	20.26	21
M2	72, 4294	18694	46.79	93.47	948.73	621.41	87.41	691.58	922
M3	30, 4294	19422	48.61	97.11	915.19	566.52	90.82	655.25	922
M4	30, 9910	19868	49.72	99.34	1036.33	597.48	113.89	673.17	922

Figure C-3. Chimera 2C2 in HEK cells FACS Histogram



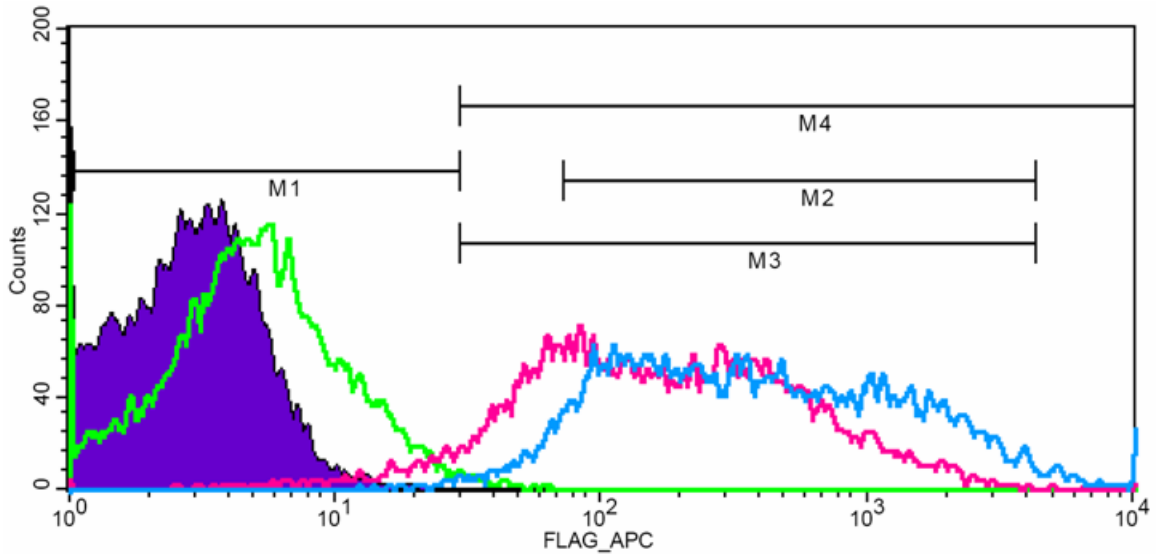
Surface Statistics:

Marker	Left, Right	Events	% Gated	% Total	Mean	Geo Mean	CV	Median	Peak Ch
All	1, 9910	20000	50.07	100.00	121.59	33.46	392.48	26.90	18
M1	1, 30	10684	26.75	53.42	14.77	12.68	48.79	13.95	18
M2	72, 4294	4632	11.60	23.16	358.19	220.21	136.15	182.69	82
M3	30, 4294	9310	23.31	46.55	201.57	99.12	187.38	71.69	46
M4	30, 9910	9366	23.45	46.83	243.00	101.65	278.68	72.34	46

Total Statistics:

Marker	Left, Right	Events	% Gated	% Total	Mean	Geo Mean	CV	Median	Peak Ch
All	1, 9910	20000	50.07	100.00	520.71	198.23	206.64	179.43	9910
M1	1, 30	1268	3.17	6.34	20.19	18.89	31.37	21.10	29
M2	72, 4294	14938	37.40	74.69	523.27	306.52	125.73	271.39	80
M3	30, 4294	18404	46.07	92.02	434.43	217.88	142.90	194.56	80
M4	30, 9910	18748	46.94	93.74	554.15	232.01	199.10	199.89	9910

Figure C-4. Chimera 2C3 in HEK cells FACS Histogram



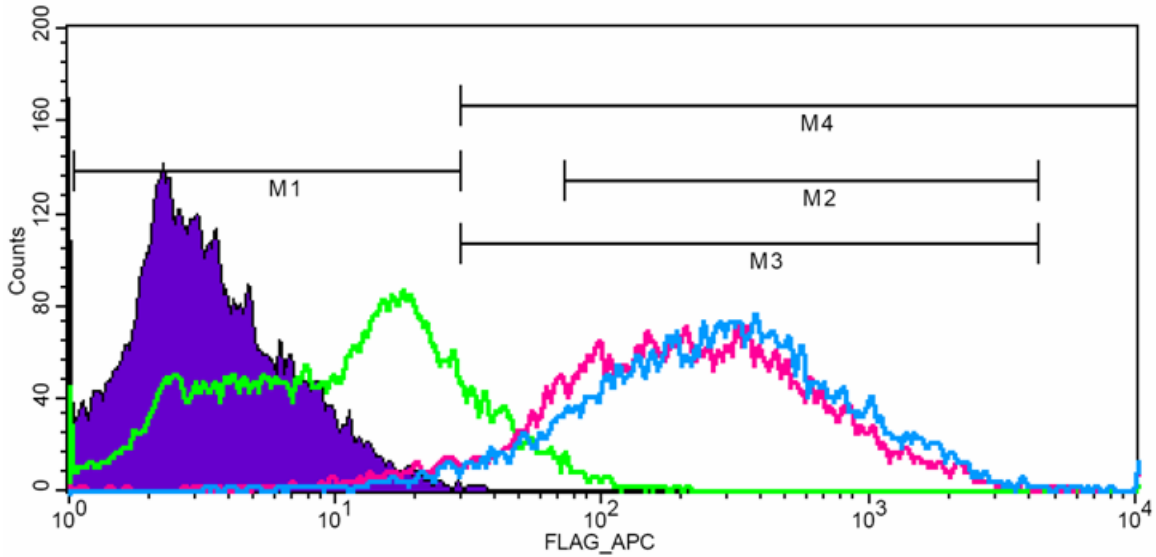
Surface Statistics:

Marker	Left, Right	Events	% Gated	% Total	Mean	Geo Mean	CV	Median	Peak Ch
All	1, 9910	20000	50.01	100.00	323.19	160.70	153.15	156.79	68
M1	1, 30	1346	3.37	6.73	17.39	14.87	45.30	18.11	22
M2	72, 4294	14644	36.62	73.22	411.07	272.27	110.72	259.46	81
M3	30, 4294	18624	46.57	93.12	334.31	189.94	128.51	177.83	68
M4	30, 9910	18658	46.65	93.29	345.21	191.15	146.39	177.83	68

Total Statistics:

Marker	Left, Right	Events	% Gated	% Total	Mean	Geo Mean	CV	Median	Peak Ch
All	1, 9910	20000	50.01	100.00	783.37	369.20	147.31	336.78	171
M1	1, 30	192	0.48	0.96	20.35	18.54	36.29	22.27	26
M2	72, 4294	18134	45.34	90.67	720.90	410.63	112.29	371.80	171
M3	30, 4294	19420	48.56	97.10	676.83	359.07	118.13	330.77	171
M4	30, 9910	19812	49.54	99.06	790.62	379.87	146.35	342.89	171

Figure C-5. Chimera 2C4 in HEK cells FACS Histogram



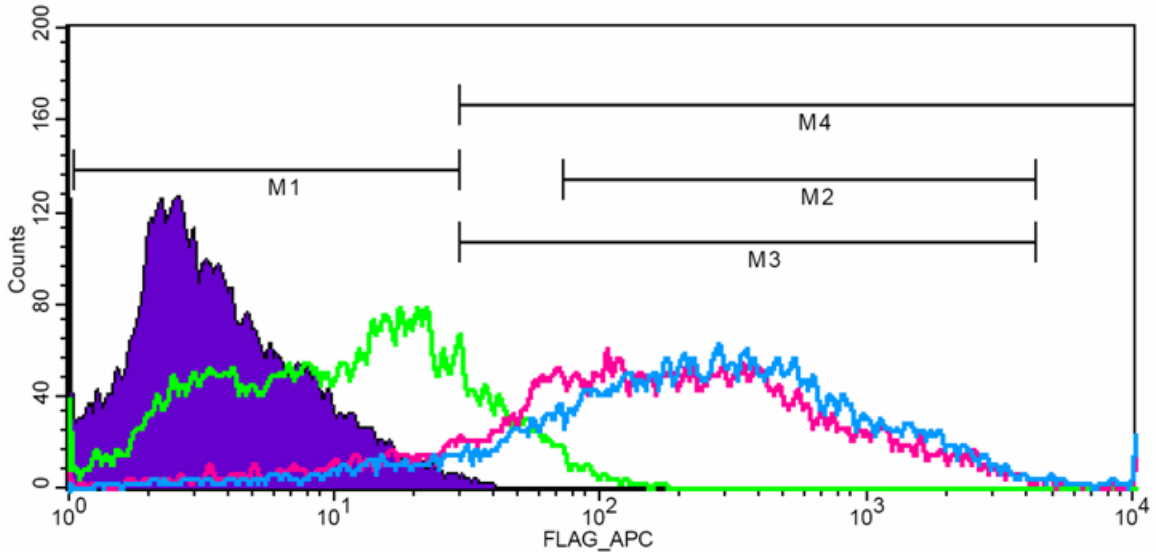
Surface Statistics:

Marker	Left, Right	Events	% Gated	% Total	Mean	Geo Mean	CV	Median	Peak Ch
All	1, 9910	20000	50.03	100.00	378.15	195.45	167.39	201.69	339
M1	1, 30	1160	2.90	5.80	16.76	14.00	47.15	17.31	24
M2	72, 4294	16326	40.84	81.63	420.41	282.78	111.13	264.16	339
M3	30, 4294	18770	46.95	93.85	372.64	226.87	121.54	218.70	339
M4	30, 9910	18844	47.14	94.22	400.33	229.96	161.25	220.67	339

Total Statistics:

Marker	Left, Right	Events	% Gated	% Total	Mean	Geo Mean	CV	Median	Peak Ch
All	1, 9910	20000	50.03	100.00	466.21	252.16	152.10	266.55	365
M1	1, 30	728	1.82	3.64	17.79	15.04	45.31	19.20	26
M2	72, 4294	17366	43.44	86.83	490.35	329.70	105.87	310.59	365
M3	30, 4294	19182	47.98	95.91	448.83	275.92	113.72	276.32	365
M4	30, 9910	19278	48.22	96.39	483.01	280.40	148.41	278.81	365

Figure C-6. Chimera 2C5 in HEK cells FACS Histogram



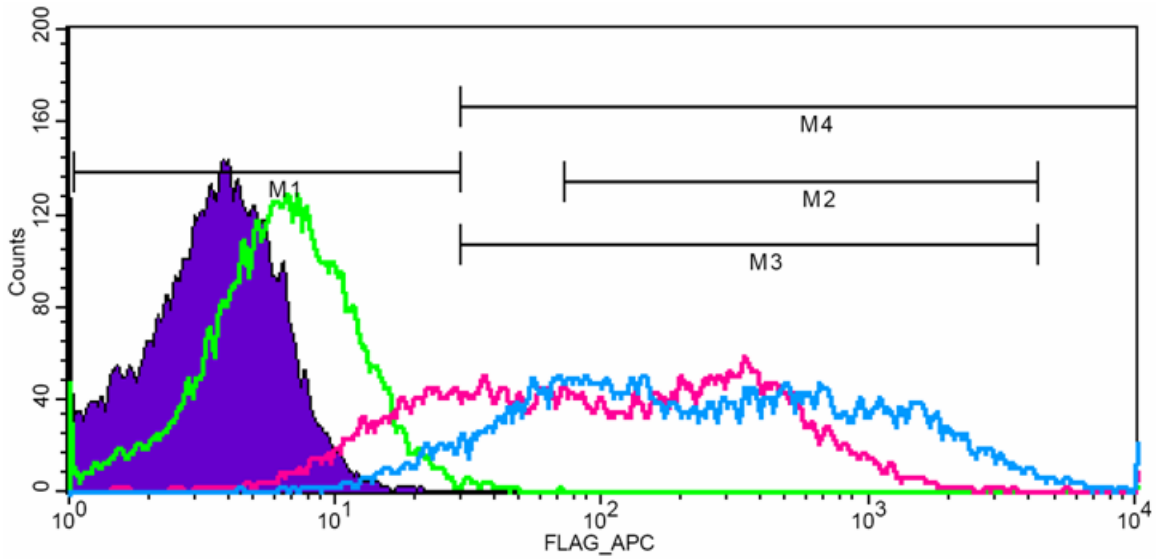
Surface Statistics:

Marker	Left, Right	Events	% Gated	% Total	Mean	Geo Mean	CV	Median	Peak Ch
All	1, 9910	20000	50.00	100.00	419.94	152.59	189.60	162.53	103
M1	1, 30	2612	6.53	13.06	13.57	10.37	62.25	12.30	27
M2	72, 4294	14100	35.25	70.50	515.77	311.11	122.30	278.81	103
M3	30, 4294	17258	43.15	86.29	430.87	222.90	138.73	205.35	103
M4	30, 9910	17396	43.49	86.98	480.80	228.93	174.07	209.08	103

Total Statistics:

Marker	Left, Right	Events	% Gated	% Total	Mean	Geo Mean	CV	Median	Peak Ch
All	1, 9910	20000	50.00	100.00	543.71	214.59	177.45	239.28	271
M1	1, 30	1902	4.75	9.51	13.85	10.78	59.35	13.22	14
M2	72, 4294	15688	39.22	78.44	578.04	358.60	113.07	330.77	271
M3	30, 4294	17868	44.67	89.34	513.76	281.76	123.85	273.84	271
M4	30, 9910	18108	45.27	90.54	599.09	293.82	166.56	281.33	271

Figure C-7. Chimera 2C6 in HEK cells FACS Histogram



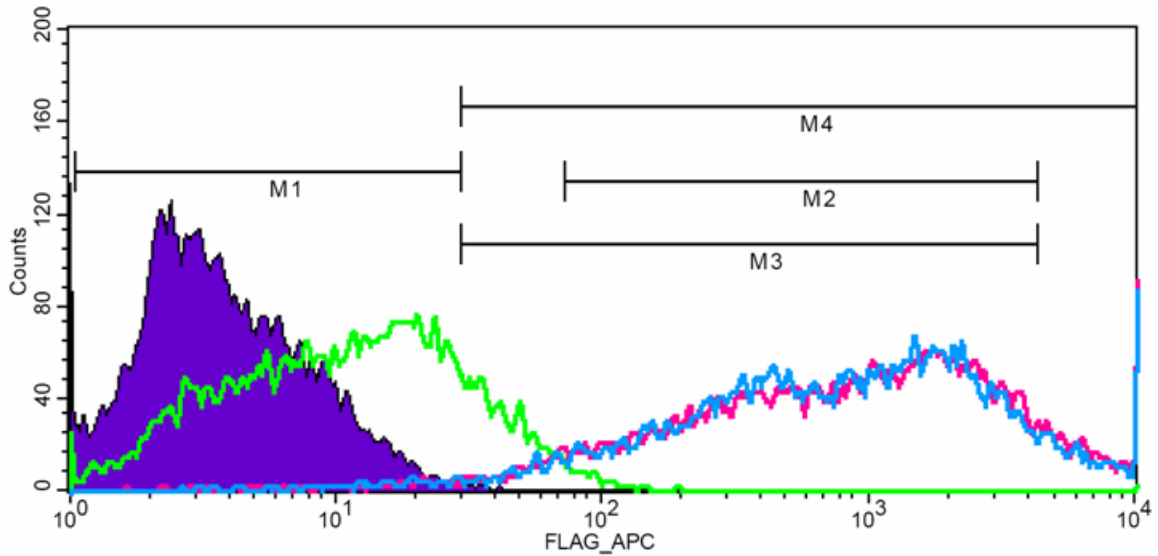
Surface Statistics:

Marker	Left, Right	Events	% Gated	% Total	Mean	Geo Mean	CV	Median	Peak Ch
All	1, 9910	20000	50.08	100.00	226.99	93.73	197.79	94.75	330
M1	1, 30	4898	12.26	24.49	17.11	15.30	40.59	17.15	17
M2	72, 4294	11126	27.86	55.63	361.03	264.68	97.33	264.16	330
M3	30, 4294	15102	37.82	75.51	278.50	166.94	119.13	176.24	330
M4	30, 9910	15132	37.89	75.66	294.54	168.23	168.96	176.24	330

Total Statistics:

Marker	Left, Right	Events	% Gated	% Total	Mean	Geo Mean	CV	Median	Peak Ch
All	1, 9910	20000	50.08	100.00	630.92	239.30	163.02	226.71	637
M1	1, 30	1408	3.53	7.04	20.15	18.72	32.07	21.10	29
M2	72, 4294	14994	37.55	74.97	711.57	406.42	110.59	399.54	637
M3	30, 4294	18348	45.94	91.74	590.77	276.38	127.94	264.16	637
M4	30, 9910	18622	46.63	93.11	676.14	289.28	155.58	273.84	637

Figure C-8. Flag-hMC4R in HEK cells FACS Histogram



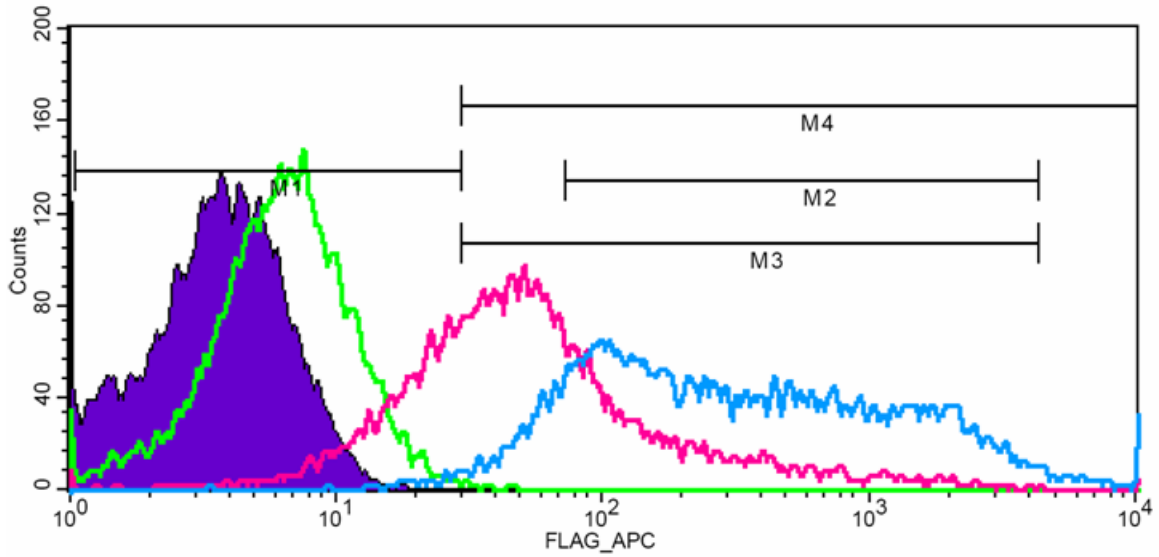
Surface Statistics:

Marker	Left, Right	Events	% Gated	% Total	Mean	Geo Mean	CV	Median	Peak Ch
All	1, 9910	20000	50.06	100.00	1548.88	715.65	121.02	873.79	9910
M1	1, 30	498	1.25	2.49	14.67	11.45	57.06	14.99	17
M2	72, 4294	17044	42.66	85.22	1187.28	746.61	87.42	850.53	1074
M3	30, 4294	17886	44.77	89.43	1133.88	658.27	91.83	777.37	1074
M4	30, 9910	19508	48.83	97.54	1587.58	794.82	118.53	922.24	9910

Total Statistics:

Marker	Left, Right	Events	% Gated	% Total	Mean	Geo Mean	CV	Median	Peak Ch
All	1, 9910	20000	50.06	100.00	1454.93	688.74	123.43	813.12	9910
M1	1, 30	520	1.30	2.60	15.19	12.38	53.21	15.06	23
M2	72, 4294	17318	43.35	86.59	1133.81	724.19	87.45	805.84	1684
M3	30, 4294	18066	45.22	90.33	1089.04	649.00	91.31	749.89	1684
M4	30, 9910	19482	48.76	97.41	1493.22	766.47	120.81	850.53	9910

Figure C-9. Chimera 4C1 in HEK cells FACS Histogram



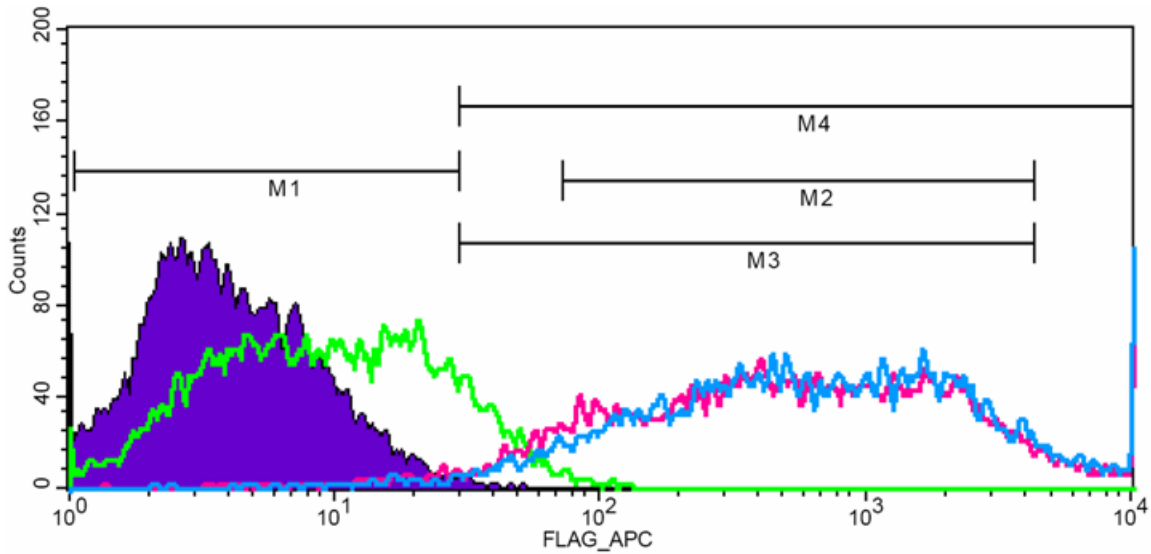
Surface Statistics:

Marker	Left, Right	Events	% Gated	% Total	Mean	Geo Mean	CV	Median	Peak Ch
All	1, 9910	20000	50.05	100.00	139.37	52.51	318.61	46.14	49
M1	1, 30	6034	15.10	30.17	18.48	16.60	38.30	19.11	27
M2	72, 4294	6032	15.09	30.16	336.64	193.29	150.61	142.02	75
M3	30, 4294	13964	34.94	69.82	172.33	85.47	210.53	63.21	49
M4	30, 9910	14002	35.04	70.01	191.23	86.49	273.07	63.78	49

Total Statistics:

Marker	Left, Right	Events	% Gated	% Total	Mean	Geo Mean	CV	Median	Peak Ch
All	1, 9910	20000	50.05	100.00	737.09	306.10	161.33	261.80	101
M1	1, 30	366	0.92	1.83	19.66	17.45	37.95	20.54	25
M2	72, 4294	16986	42.50	84.93	702.22	381.96	116.43	342.89	101
M3	30, 4294	19236	48.13	96.18	626.44	303.18	127.07	261.80	101
M4	30, 9910	19638	49.14	98.19	750.32	322.73	159.40	273.84	101

Figure C-10. Chimera 4C2 in HEK cells FACS Histogram



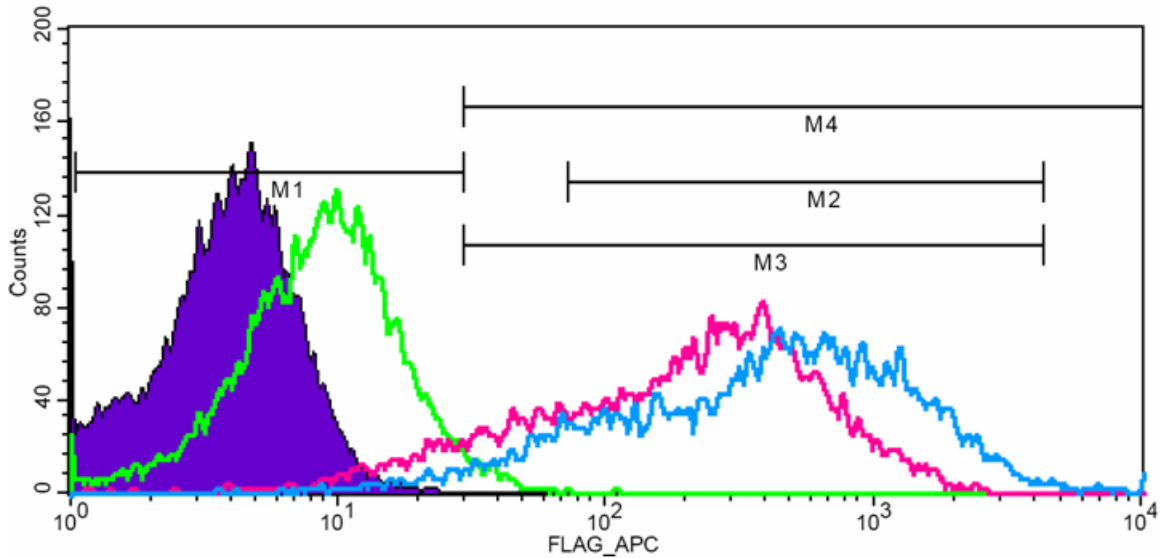
Surface Statistics:

Marker	Left, Right	Events	% Gated	% Total	Mean	Geo Mean	CV	Median	Peak Ch
All	1, 9910	20000	50.09	100.00	1127.63	461.14	144.73	491.37	9910
M1	1, 30	708	1.77	3.54	15.49	12.54	53.20	15.40	28
M2	72, 4294	16902	42.33	84.51	938.52	554.61	99.76	557.31	286
M3	30, 4294	18338	45.93	91.69	869.20	460.75	106.97	478.29	286
M4	30, 9910	19300	48.34	96.50	1167.98	526.10	141.03	528.03	9910

Total Statistics:

Marker	Left, Right	Events	% Gated	% Total	Mean	Geo Mean	CV	Median	Peak Ch
All	1, 9910	20000	50.09	100.00	1269.28	544.86	139.96	577.72	9910
M1	1, 30	540	1.35	2.70	14.86	11.93	54.87	15.33	16
M2	72, 4294	17184	43.04	85.92	988.50	599.25	96.91	604.30	486
M3	30, 4294	18266	45.75	91.33	933.04	517.67	102.37	542.47	486
M4	30, 9910	19462	48.74	97.31	1303.96	605.85	137.15	609.76	9910

Figure C-11. Chimera 4C3 in HEK cells FACS Histogram



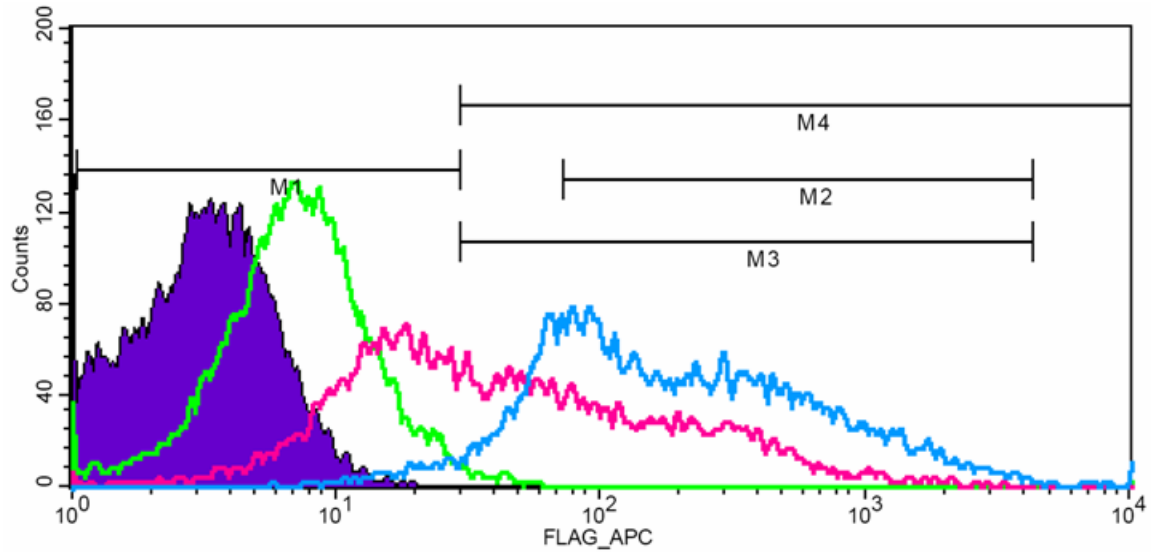
Surface Statistics:

Marker	Left, Right	Events	% Gated	% Total	Mean	Geo Mean	CV	Median	Peak Ch
All	1, 9910	20000	50.06	100.00	310.43	169.19	116.63	210.97	375
M1	1, 30	2058	5.15	10.29	17.30	15.09	42.63	17.62	28
M2	72, 4294	15120	37.85	75.60	395.44	296.86	86.51	296.93	375
M3	30, 4294	17946	44.92	89.73	340.92	222.60	99.27	245.82	375
M4	30, 9910	17954	44.94	89.77	343.84	222.94	106.90	245.82	375

Total Statistics:

Marker	Left, Right	Events	% Gated	% Total	Mean	Geo Mean	CV	Median	Peak Ch
All	1, 9910	20000	50.06	100.00	698.24	361.34	126.24	429.35	437
M1	1, 30	710	1.78	3.55	18.28	16.05	41.47	19.28	26
M2	72, 4294	17376	43.49	86.88	730.84	484.32	93.42	504.81	437
M3	30, 4294	19116	47.85	95.58	669.05	394.25	101.57	445.08	437
M4	30, 9910	19300	48.31	96.50	722.90	404.67	122.78	453.16	437

Figure C-12. Chimera 4C4 in HEK cells FACS Histogram



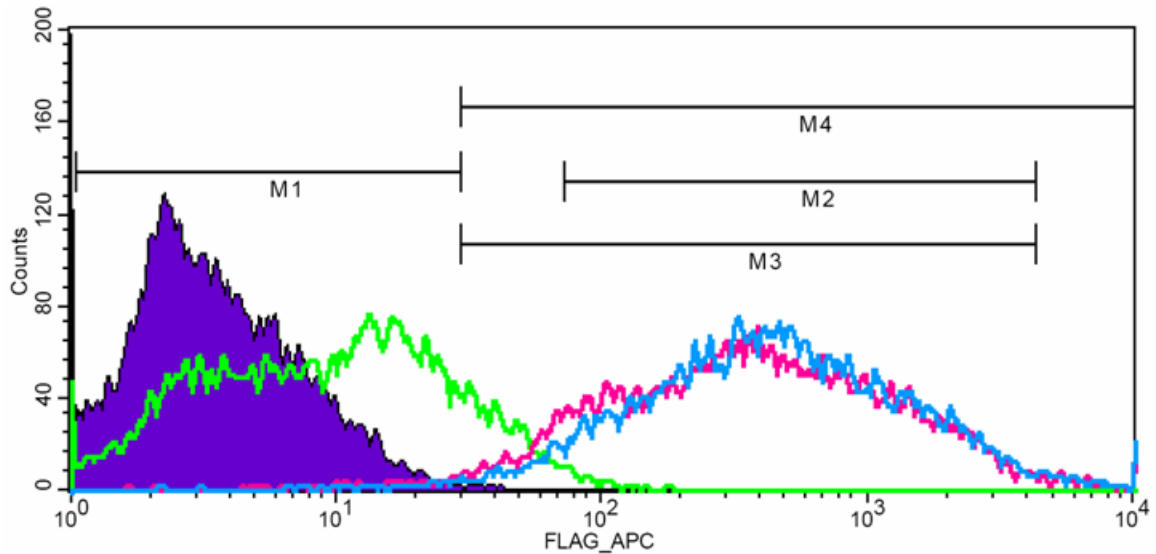
Surface Statistics:

Marker	Left, Right	Events	% Gated	% Total	Mean	Geo Mean	CV	Median	Peak Ch
All	1, 9910	20000	50.04	100.00	119.33	42.77	232.64	34.60	12
M1	1, 30	9182	22.97	45.91	15.16	13.29	45.44	14.59	12
M2	72, 4294	6566	16.43	32.83	301.32	209.60	120.41	189.38	104
M3	30, 4294	10834	27.10	54.17	201.15	114.89	153.44	95.60	30
M4	30, 9910	10848	27.14	54.24	207.29	115.45	170.65	95.60	30

Total Statistics:

Marker	Left, Right	Events	% Gated	% Total	Mean	Geo Mean	CV	Median	Peak Ch
All	1, 9910	20000	50.04	100.00	405.64	186.51	176.27	162.53	64
M1	1, 30	840	2.10	4.20	19.19	17.74	34.34	19.63	22
M2	72, 4294	15272	38.21	76.36	475.40	284.55	123.77	257.13	88
M3	30, 4294	19086	47.75	95.43	391.20	203.15	141.28	174.66	64
M4	30, 9910	19176	47.97	95.88	422.26	206.51	171.85	176.24	64

Figure C-13. Chimera 4C5 in HEK cells FACS Histogram



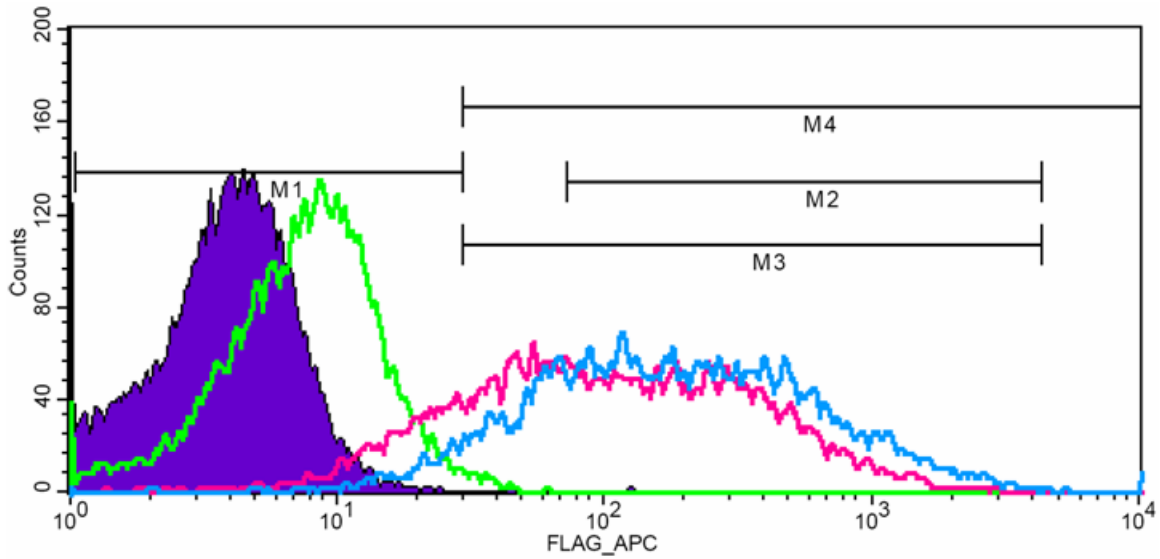
Surface Statistics:

Marker	Left, Right	Events	% Gated	% Total	Mean	Geo Mean	CV	Median	Peak Ch
All	1, 9910	20000	49.96	100.00	689.24	343.08	140.47	355.45	286
M1	1, 30	520	1.30	2.60	15.47	12.62	52.59	15.54	17
M2	72, 4294	17674	44.15	88.37	678.95	425.46	104.41	403.15	286
M3	30, 4294	19214	47.99	96.07	628.86	359.79	111.43	361.90	286
M4	30, 9910	19488	48.68	97.44	706.95	374.30	137.86	368.47	286

Total Statistics:

Marker	Left, Right	Events	% Gated	% Total	Mean	Geo Mean	CV	Median	Peak Ch
All	1, 9910	20000	49.96	100.00	771.91	404.74	139.34	414.18	316
M1	1, 30	372	0.93	1.86	15.44	11.78	58.68	14.86	27
M2	72, 4294	18322	45.76	91.61	710.33	456.46	102.46	441.09	316
M3	30, 4294	19256	48.10	96.28	678.47	410.82	106.69	414.18	316
M4	30, 9910	19632	49.04	98.16	786.09	432.56	137.46	421.70	316

Figure C-14. Chimera 4C6 in HEK cells FACS Histogram



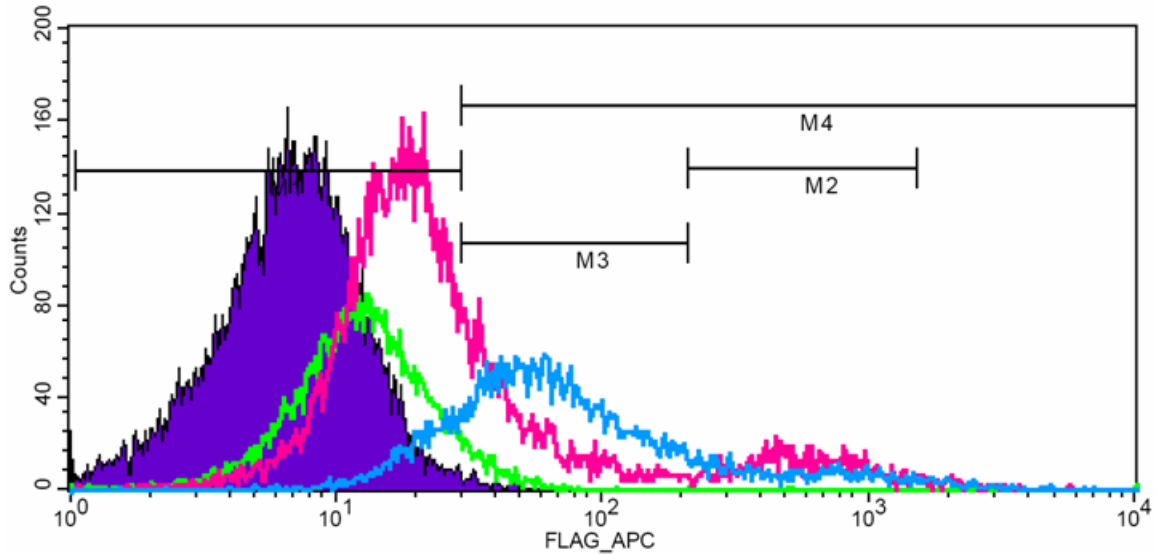
Surface Statistics:

Marker	Left, Right	Events	% Gated	% Total	Mean	Geo Mean	CV	Median	Peak Ch
All	1, 9910	20000	50.09	100.00	206.40	97.06	172.79	94.75	44
M1	1, 30	3652	9.15	18.26	17.98	16.03	39.44	18.43	25
M2	72, 4294	11466	28.71	57.33	323.28	231.91	106.76	216.74	235
M3	30, 4294	16348	40.94	81.74	241.37	144.46	130.58	133.35	44
M4	30, 9910	16366	40.98	81.83	248.26	145.06	153.80	134.56	44

Total Statistics:

Marker	Left, Right	Events	% Gated	% Total	Mean	Geo Mean	CV	Median	Peak Ch
All	1, 9910	20000	50.09	100.00	358.05	174.97	168.23	171.54	115
M1	1, 30	1250	3.13	6.25	19.57	17.32	37.54	20.72	29
M2	72, 4294	15070	37.74	75.35	431.08	282.25	112.73	259.46	115
M3	30, 4294	18700	46.83	93.50	357.34	201.48	129.12	189.38	115
M4	30, 9910	18766	46.99	93.83	380.32	203.96	161.79	191.10	115

Figure C-15. Flag-hMC2R in OS3 cells FACS Histogram



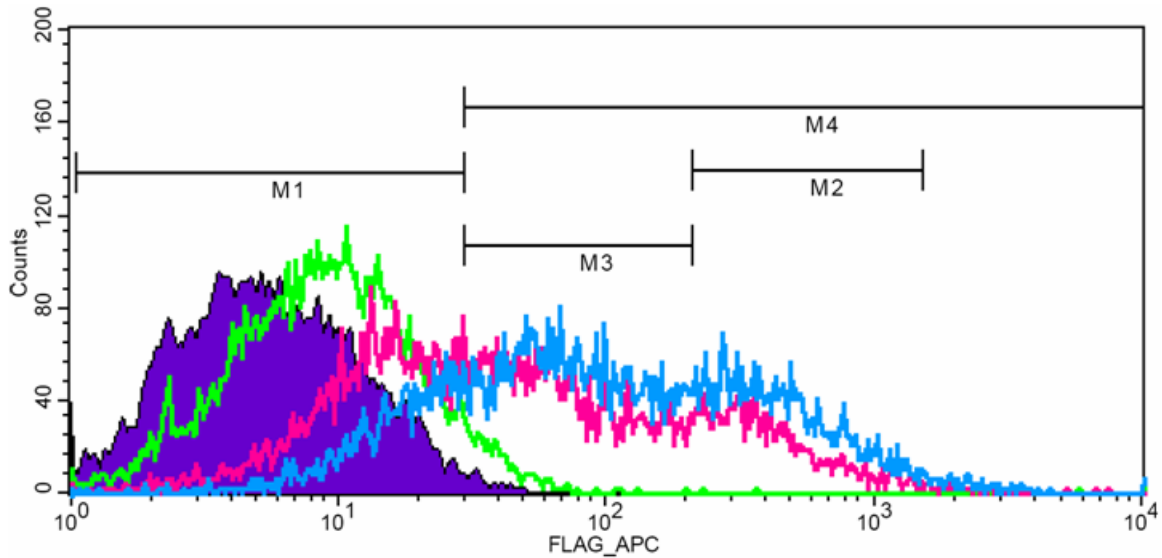
Surface Statistics:

Marker	Left, Right	Events	% Gated	% Total	Mean	Geo Mean	CV	Median	Peak Ch
All	1, 9910	20000	200.00	200.00	82.47	26.08	291.67	19.63	20
M1	1, 30	14524	145.24	145.24	16.59	15.39	36.07	16.11	20
M2	209, 1526	1540	15.40	15.40	618.27	555.50	47.11	549.84	437
M3	30, 209	3900	39.00	39.00	55.51	49.01	60.79	42.17	33
M4	30, 9910	5554	55.54	55.54	254.02	103.80	161.15	57.25	33

Total Statistics:

Marker	Left, Right	Events	% Gated	% Total	Mean	Geo Mean	CV	Median	Peak Ch
All	1, 9910	10000	100.00	100.00	155.36	72.07	214.36	59.89	58
M1	1, 30	1703	17.03	17.03	21.25	20.41	25.42	21.67	26
M2	209, 1526	1213	12.13	12.13	585.09	491.93	59.82	478.29	224
M3	30, 209	6992	69.92	69.92	74.93	65.89	54.52	62.08	58
M4	30, 9910	8323	83.23	83.23	182.40	93.04	196.82	71.69	58

Figure C-16. Chimera 2C1 in OS3 cells FACS Histogram



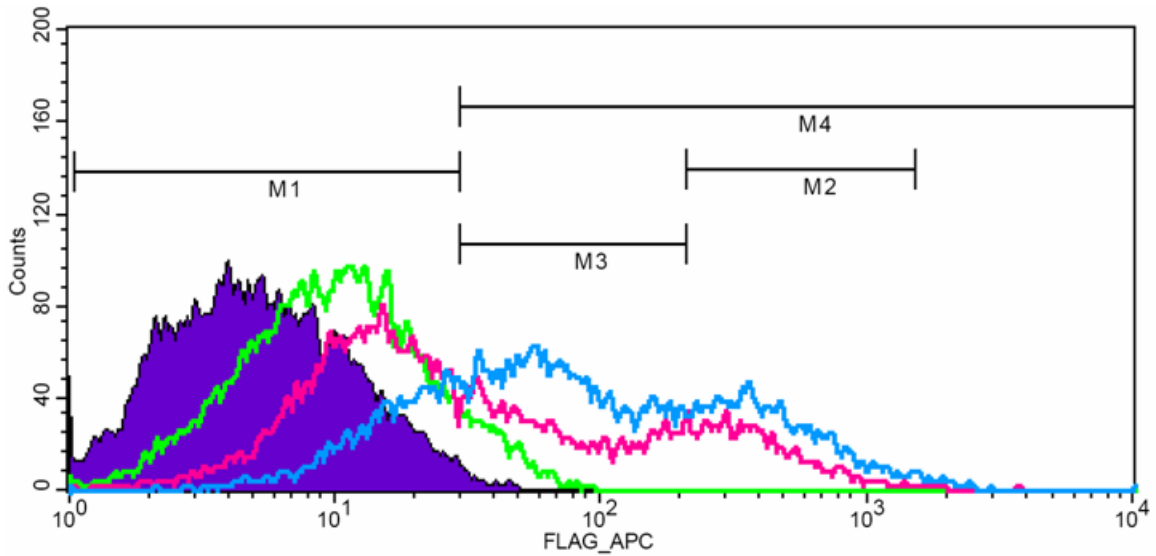
Surface Statistics:

Marker	Left, Right	Events	% Gated	% Total	Mean	Geo Mean	CV	Median	Peak Ch
All	1, 9910	20000	49.73	100.00	123.95	45.93	202.05	38.89	13
M1	1, 30	8578	21.33	42.89	14.96	13.03	47.53	14.07	13
M2	209, 1526	3452	8.58	17.26	440.69	391.83	56.11	358.66	349
M3	30, 209	7956	19.78	39.78	79.19	67.83	58.92	62.08	40
M4	30, 9910	11472	28.53	57.36	205.04	117.76	149.44	96.47	40

Total Statistics:

Marker	Left, Right	Events	% Gated	% Total	Mean	Geo Mean	CV	Median	Peak Ch
All	1, 9910	20000	49.73	100.00	214.11	94.04	170.30	85.05	66
M1	1, 30	4268	10.61	21.34	18.08	16.56	36.76	18.11	24
M2	209, 1526	5858	14.57	29.29	487.23	429.37	55.56	403.15	266
M3	30, 209	9754	24.25	48.77	87.73	75.58	55.71	71.69	66
M4	30, 9910	15766	39.20	78.83	266.78	150.19	147.84	135.77	66

Figure C-17. Chimera 2C2 in OS3 cells FACS Histogram



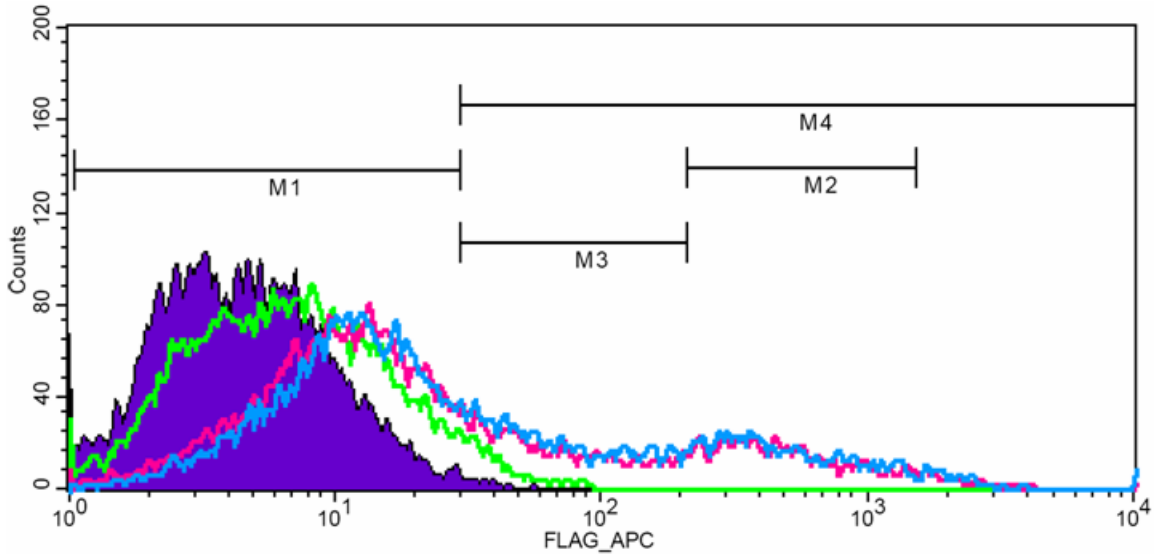
Surface Statistics:

Marker	Left, Right	Events	% Gated	% Total	Mean	Geo Mean	CV	Median	Peak Ch
All	1, 9910	20000	50.12	100.00	109.15	33.84	245.34	23.29	12
M1	1, 30	11214	28.10	56.07	13.52	11.66	50.04	12.52	12
M2	209, 1526	3104	7.78	15.52	429.23	385.98	52.94	355.45	324
M3	30, 209	5660	14.18	28.30	83.56	69.48	62.86	62.08	34
M4	30, 9910	8832	22.13	44.16	230.18	131.17	160.29	128.64	34

Total Statistics:

Marker	Left, Right	Events	% Gated	% Total	Mean	Geo Mean	CV	Median	Peak Ch
All	1, 9910	20000	50.12	100.00	197.90	81.45	185.42	70.41	47
M1	1, 30	5030	12.60	25.15	17.38	15.65	39.93	17.31	25
M2	209, 1526	5322	13.34	26.61	489.23	430.62	56.37	399.54	349
M3	30, 209	9530	23.88	47.65	83.68	71.95	57.02	67.93	47
M4	30, 9910	15002	37.59	75.01	258.07	141.50	157.40	121.88	47

Figure C-18. Chimera 2C3 in OS3 cells FACS Histogram



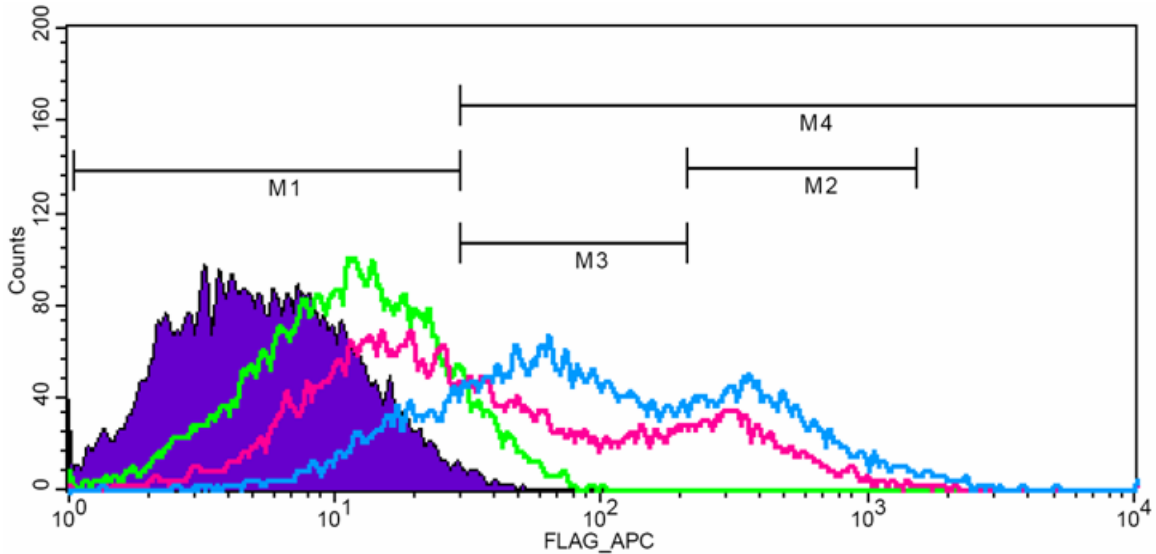
Surface Statistics:

Marker	Left, Right	Events	% Gated	% Total	Mean	Geo Mean	CV	Median	Peak Ch
All	1, 9910	20000	50.02	100.00	141.45	25.31	289.26	15.68	12
M1	1, 30	13286	33.22	66.43	11.45	9.33	59.79	10.00	12
M2	209, 1526	2880	7.20	14.40	548.21	473.39	58.07	441.09	339
M3	30, 209	3536	8.84	17.68	78.85	66.24	62.45	58.82	33
M4	30, 9910	6738	16.85	33.69	397.45	182.57	158.74	189.38	33

Total Statistics:

Marker	Left, Right	Events	% Gated	% Total	Mean	Geo Mean	CV	Median	Peak Ch
All	1, 9910	20000	50.02	100.00	163.24	30.63	312.01	18.43	11
M1	1, 30	12290	30.73	61.45	12.14	10.15	55.58	10.94	11
M2	209, 1526	3174	7.94	15.87	546.17	470.46	57.95	429.35	266
M3	30, 209	4186	10.47	20.93	79.55	67.04	61.43	60.43	33
M4	30, 9910	7732	19.34	38.66	403.07	177.87	188.49	172.32	33

Figure C-19. Chimera 2C4 in OS3 cells FACS Histogram



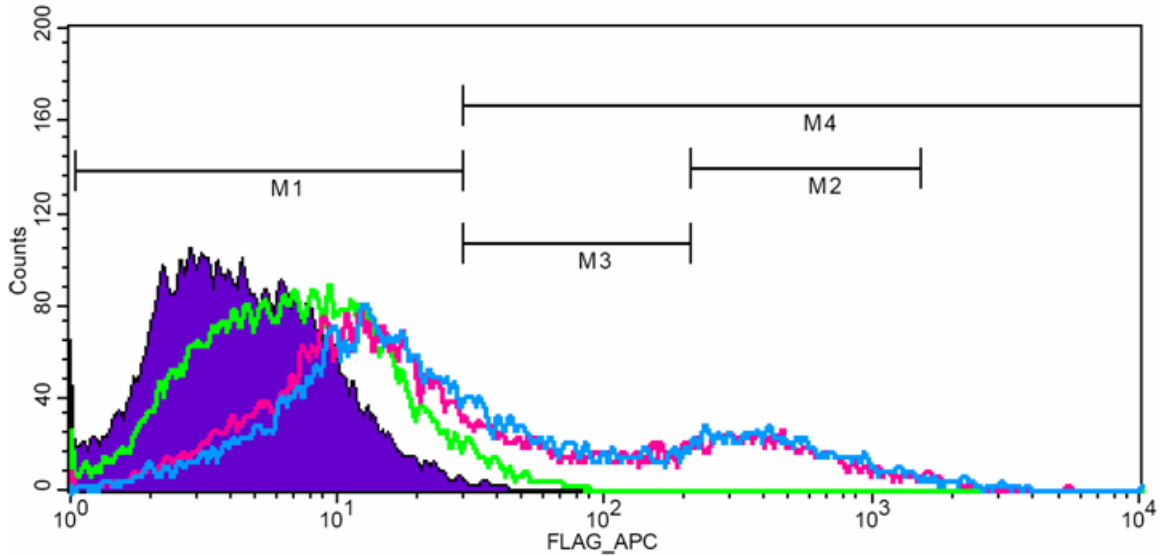
Surface Statistics:

Marker	Left, Right	Events	% Gated	% Total	Mean	Geo Mean	CV	Median	Peak Ch
All	1, 9910	20000	50.07	100.00	112.73	36.88	237.67	26.66	13
M1	1, 30	10524	26.34	52.62	13.94	11.94	50.63	12.98	13
M2	209, 1526	3356	8.40	16.78	425.04	381.56	53.85	345.99	278
M3	30, 209	6130	15.34	30.65	82.18	68.73	62.18	60.98	30
M4	30, 9910	9520	23.83	47.60	221.58	128.41	161.57	124.09	30

Total Statistics:

Marker	Left, Right	Events	% Gated	% Total	Mean	Geo Mean	CV	Median	Peak Ch
All	1, 9910	20000	50.07	100.00	227.31	95.44	185.59	85.05	62
M1	1, 30	4058	10.16	20.29	17.49	15.73	39.89	17.31	16
M2	209, 1526	5910	14.79	29.55	491.12	432.73	55.78	403.15	333
M3	30, 209	9806	24.55	49.03	84.66	73.23	55.37	70.41	62
M4	30, 9910	15986	40.02	79.93	280.03	150.34	163.18	129.80	62

Figure C-20. Chimera 2C5 in OS3 cells FACS Histogram



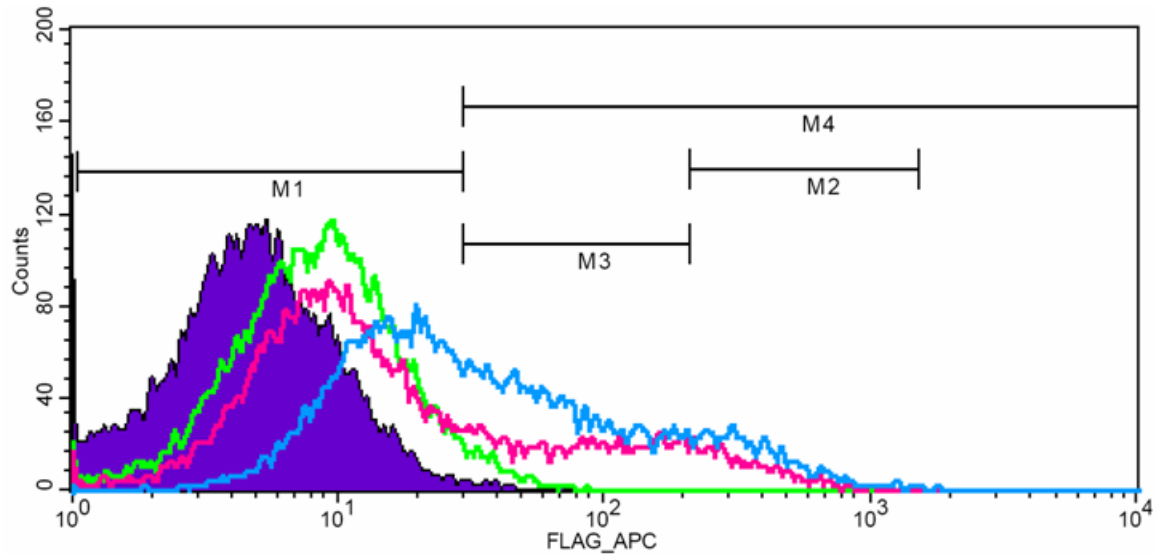
Surface Statistics:

Marker	Left, Right	Events	% Gated	% Total	Mean	Geo Mean	CV	Median	Peak Ch
All	1, 9910	20000	50.02	100.00	136.16	27.30	276.64	16.85	10
M1	1, 30	12820	32.06	64.10	11.60	9.49	58.89	10.27	10
M2	209, 1526	3220	8.05	16.10	514.12	450.86	55.85	425.51	445
M3	30, 209	3736	9.34	18.68	84.12	70.17	61.70	63.78	34
M4	30, 9910	7188	17.98	35.94	358.29	181.54	157.33	196.32	445

Total Statistics:

Marker	Left, Right	Events	% Gated	% Total	Mean	Geo Mean	CV	Median	Peak Ch
All	1, 9910	20000	50.02	100.00	155.61	32.55	272.18	19.99	12
M1	1, 30	11946	29.87	59.73	12.56	10.44	55.25	11.55	12
M2	209, 1526	3570	8.93	17.85	531.21	462.64	56.53	429.35	230
M3	30, 209	4264	10.66	21.32	78.46	65.66	63.18	58.29	31
M4	30, 9910	8086	20.22	40.43	366.47	174.99	165.77	186.01	31

Figure C-21. Chimera 2C6 in OS3 cells FACS Histogram



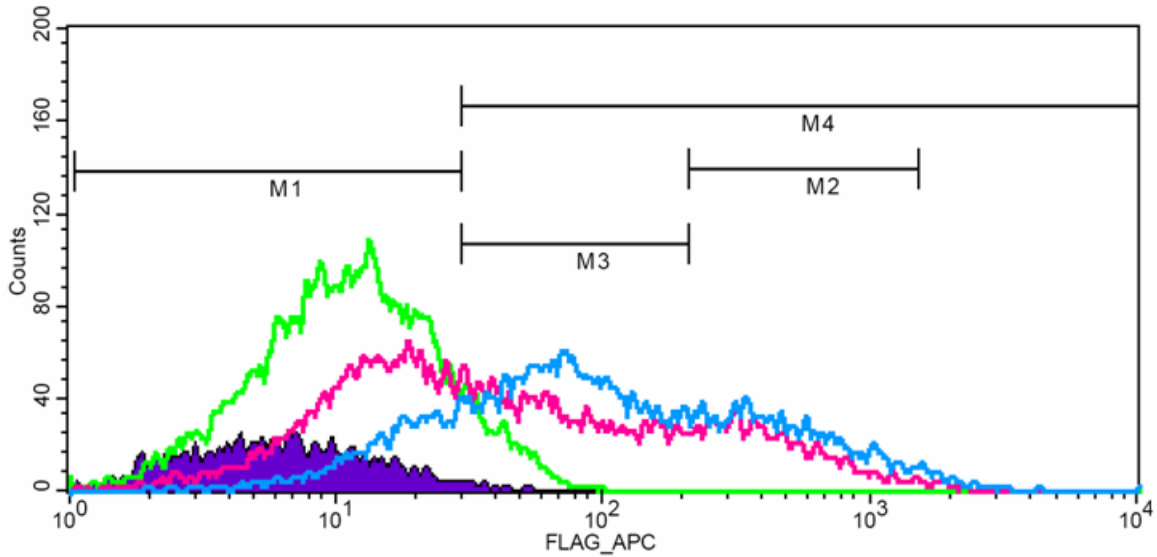
Surface Statistics:

Marker	Left, Right	Events	% Gated	% Total	Mean	Geo Mean	CV	Median	Peak Ch
All	1, 9910	20000	50.08	100.00	52.61	17.08	234.51	11.65	7
M1	1, 30	14520	36.36	72.60	10.19	8.49	60.18	8.66	7
M2	209, 1526	1372	3.44	6.86	367.84	337.56	50.36	307.81	209
M3	30, 209	4102	10.27	20.51	91.34	77.20	56.88	78.44	33
M4	30, 9910	5456	13.66	27.28	165.82	112.18	117.68	109.41	33

Total Statistics:

Marker	Left, Right	Events	% Gated	% Total	Mean	Geo Mean	CV	Median	Peak Ch
All	1, 9910	20000	50.08	100.00	87.94	36.33	195.61	28.13	19
M1	1, 30	10308	25.81	51.54	15.31	13.73	43.40	14.46	19
M2	209, 1526	2374	5.94	11.87	405.99	367.65	52.40	336.78	385
M3	30, 209	7368	18.45	36.84	78.09	66.51	60.06	60.98	35
M4	30, 9910	9750	24.41	48.75	164.39	101.67	135.01	82.79	35

Figure C-22. Flag-hMC4R in OS3 cells FACS Histogram



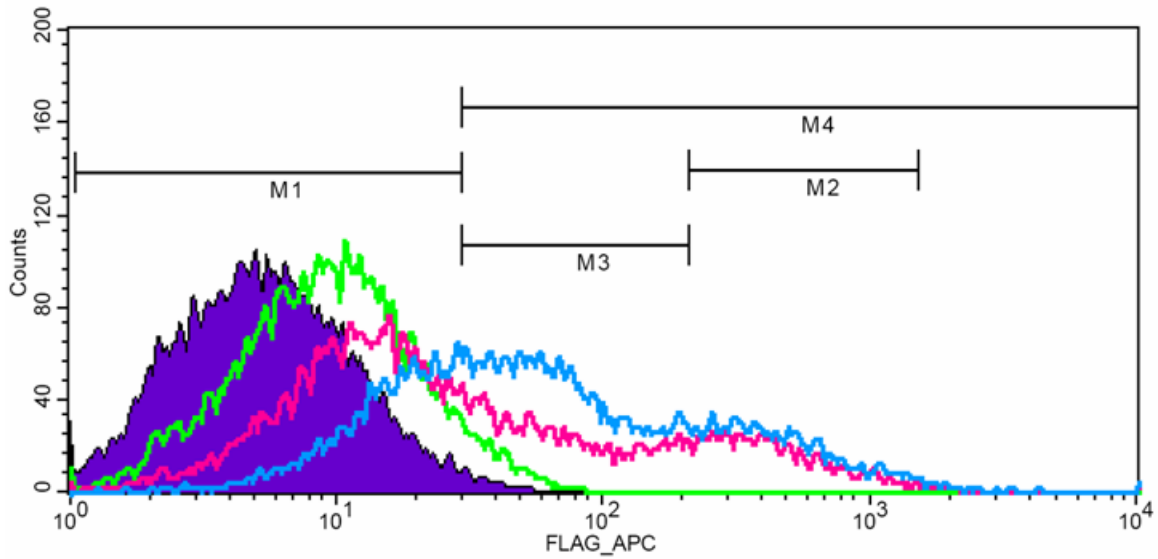
Surface Statistics:

Marker	Left, Right	Events	% Gated	% Total	Mean	Geo Mean	CV	Median	Peak Ch
All	1, 9910	20000	50.07	100.00	139.36	44.64	222.45	34.91	12
M1	1, 30	9256	23.17	46.28	14.29	12.20	50.15	13.46	12
M2	209, 1526	3736	9.35	18.68	475.83	418.88	56.77	381.97	257
M3	30, 209	6968	17.44	34.84	82.62	70.29	58.67	65.23	37
M4	30, 9910	10806	27.05	54.03	245.86	135.28	159.18	119.71	37

Total Statistics:

Marker	Left, Right	Events	% Gated	% Total	Mean	Geo Mean	CV	Median	Peak Ch
All	1, 9910	18180	45.51	90.90	239.20	97.37	178.13	85.05	63
M1	1, 30	3604	9.02	18.02	17.49	15.58	40.63	17.78	28
M2	209, 1526	5090	12.74	25.45	534.82	463.49	57.50	429.35	228
M3	30, 209	9208	23.05	46.04	86.11	75.05	53.62	72.99	63
M4	30, 9910	14612	36.58	73.06	293.37	152.55	156.55	124.09	63

Figure C-23. Chimera 4C1 in OS3 cells FACS Histogram



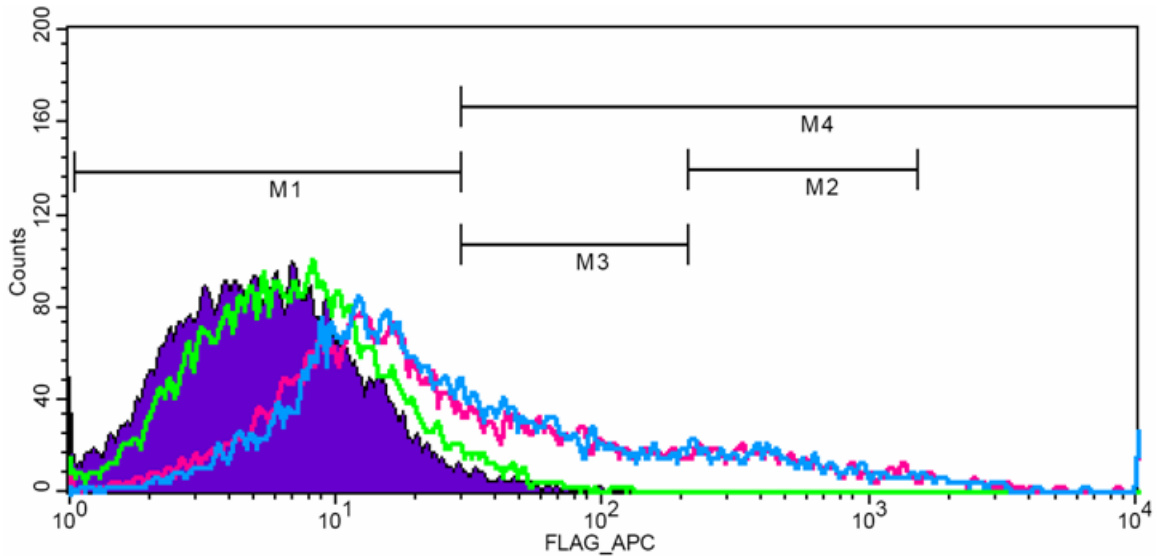
Surface Statistics:

Marker	Left, Right	Events	% Gated	% Total	Mean	Geo Mean	CV	Median	Peak Ch
All	1, 9910	20000	50.01	100.00	112.16	30.38	255.75	20.54	15
M1	1, 30	11856	29.65	59.28	12.71	10.65	54.81	11.50	15
M2	209, 1526	3038	7.60	15.19	475.43	420.42	55.13	388.91	250
M3	30, 209	5052	12.63	25.26	81.68	68.61	61.61	62.08	34
M4	30, 9910	8166	20.42	40.83	256.38	139.78	159.08	132.16	34

Total Statistics:

Marker	Left, Right	Events	% Gated	% Total	Mean	Geo Mean	CV	Median	Peak Ch
All	1, 9910	20000	50.01	100.00	166.68	61.29	227.83	50.94	29
M1	1, 30	6712	16.78	33.56	16.89	15.08	41.64	16.85	29
M2	209, 1526	4008	10.02	20.04	504.00	440.09	57.52	404.97	252
M3	30, 209	9208	23.02	46.04	78.29	67.27	58.69	62.64	29
M4	30, 9910	13366	33.42	66.83	241.11	123.52	185.05	93.90	29

Figure C-24. Chimera 4C2 in OS3 cells FACS Histogram



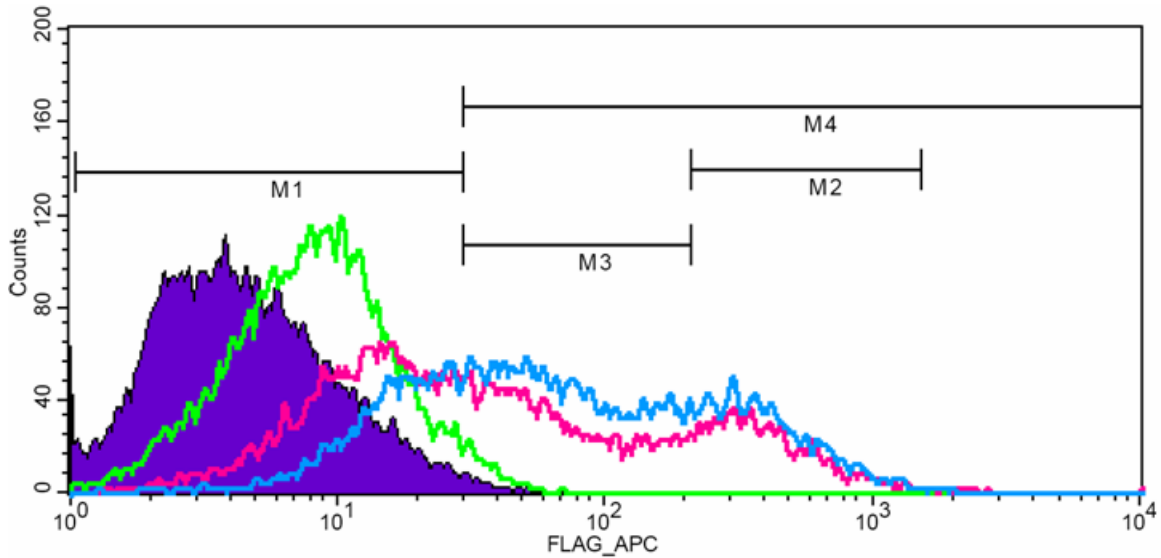
Surface Statistics:

Marker	Left, Right	Events	% Gated	% Total	Mean	Geo Mean	CV	Median	Peak Ch
All	1, 9910	20000	50.06	100.00	174.68	29.70	384.06	18.77	12
M1	1, 30	12218	30.58	61.09	12.20	10.19	55.55	11.14	12
M2	209, 1526	2564	6.42	12.82	545.25	467.55	59.58	429.35	313
M3	30, 209	4790	11.99	23.95	79.50	68.00	58.64	63.21	30
M4	30, 9910	7810	19.55	39.05	428.39	159.36	238.85	122.98	30

Total Statistics:

Marker	Left, Right	Events	% Gated	% Total	Mean	Geo Mean	CV	Median	Peak Ch
All	1, 9910	20000	50.06	100.00	175.50	31.49	395.05	20.35	11
M1	1, 30	11954	29.92	59.77	13.04	11.11	52.24	11.86	11
M2	209, 1526	2490	6.23	12.45	547.93	468.94	59.86	429.35	271
M3	30, 209	5168	12.93	25.84	77.01	65.54	60.84	59.89	44
M4	30, 9910	8078	20.22	40.39	415.35	147.44	251.78	107.46	9910

Figure C-25. Chimera 4C3 in OS3 cells FACS Histogram



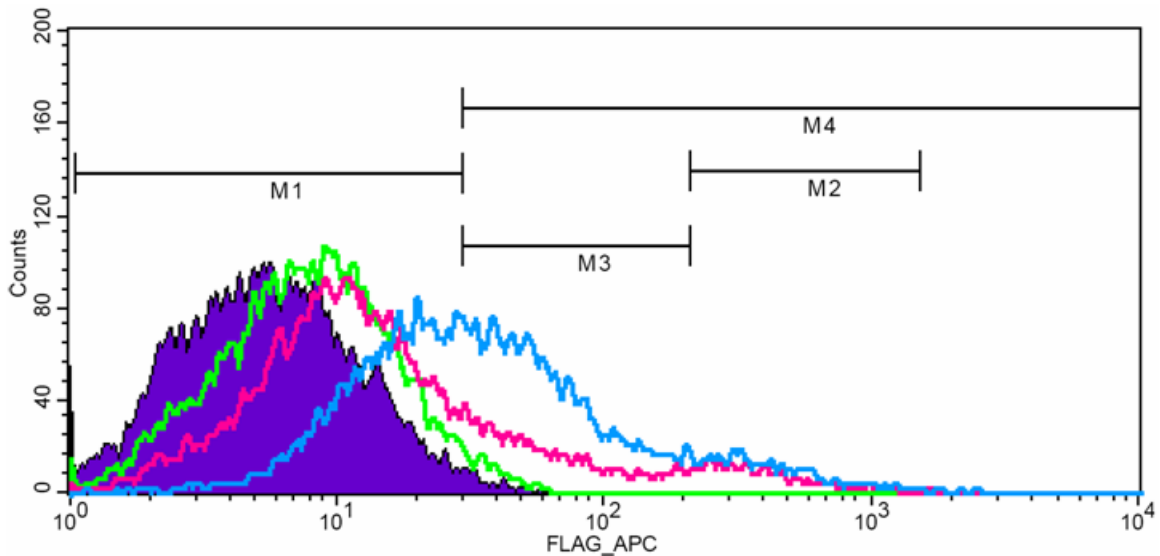
Surface Statistics:

Marker	Left, Right	Events	% Gated	% Total	Mean	Geo Mean	CV	Median	Peak Ch
All	1, 9910	20000	50.06	100.00	123.44	39.38	232.72	29.96	15
M1	1, 30	9964	24.94	49.82	13.83	11.78	51.58	12.75	15
M2	209, 1526	3610	9.03	18.05	434.62	390.64	53.03	358.66	333
M3	30, 209	6394	16.00	31.97	79.04	66.77	61.71	59.35	35
M4	30, 9910	10074	25.21	50.37	231.51	129.75	161.79	117.57	35

Total Statistics:

Marker	Left, Right	Events	% Gated	% Total	Mean	Geo Mean	CV	Median	Peak Ch
All	1, 9910	20000	50.06	100.00	154.90	67.67	169.30	58.82	29
M1	1, 30	6032	15.10	30.16	17.07	15.34	39.89	17.00	24
M2	209, 1526	4664	11.67	23.32	439.50	395.09	52.15	365.17	296
M3	30, 209	9292	23.26	46.46	83.83	71.39	58.43	66.71	29
M4	30, 9910	13994	35.02	69.97	214.08	128.11	137.47	115.48	29

Figure C-26. Chimera 4C4 in OS3 cells FACS Histogram



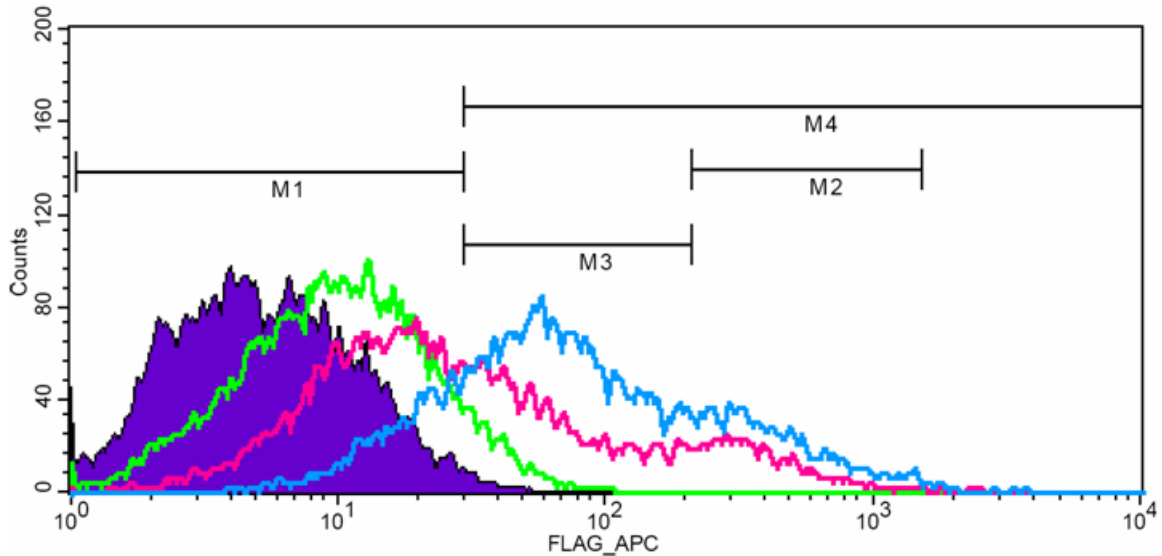
Surface Statistics:

Marker	Left, Right	Events	% Gated	% Total	Mean	Geo Mean	CV	Median	Peak Ch
All	1, 9910	20000	50.03	100.00	48.09	15.48	289.95	12.08	10
M1	1, 30	15584	38.98	77.92	11.03	9.10	59.20	9.56	10
M2	209, 1526	1198	3.00	5.99	422.20	378.84	53.33	342.89	388
M3	30, 209	3244	8.11	16.22	70.74	60.20	63.33	52.80	29
M4	30, 9910	4456	11.15	22.28	177.61	100.52	144.16	74.99	29

Total Statistics:

Marker	Left, Right	Events	% Gated	% Total	Mean	Geo Mean	CV	Median	Peak Ch
All	1, 9910	20000	50.03	100.00	82.55	36.02	243.04	31.06	19
M1	1, 30	9658	24.16	48.29	16.41	14.64	42.44	16.11	19
M2	209, 1526	1732	4.33	8.66	459.68	406.37	56.81	371.80	228
M3	30, 209	8636	21.60	43.18	68.12	59.41	58.87	53.76	37
M4	30, 9910	10406	26.03	52.03	143.62	83.05	183.63	62.08	37

Figure C-27. Chimera 4C5 in OS3 cells FACS Histogram



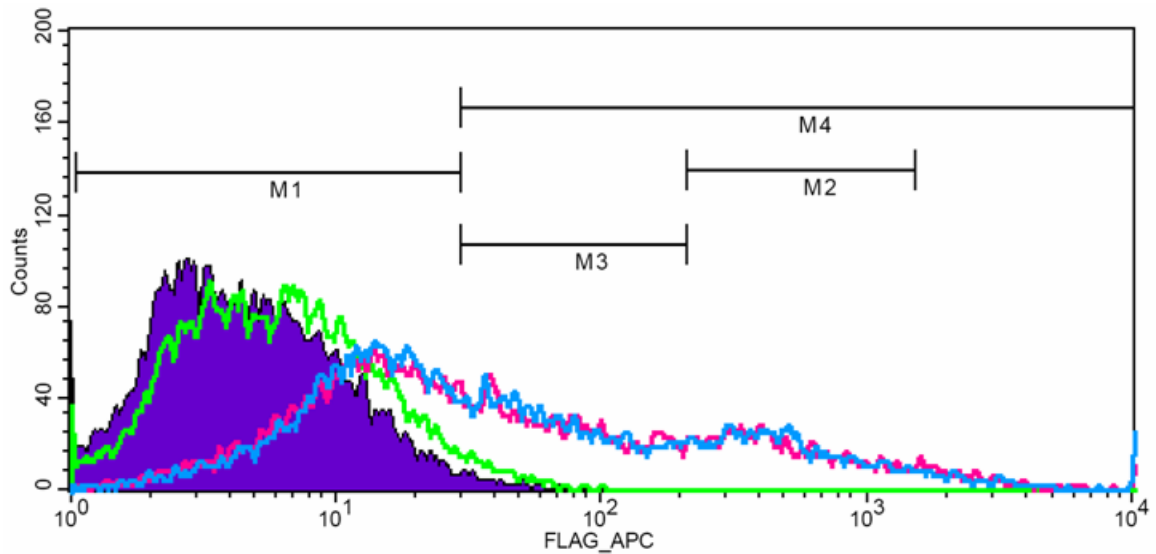
Surface Statistics:

Marker	Left, Right	Events	% Gated	% Total	Mean	Geo Mean	CV	Median	Peak Ch
All	1, 9910	20000	50.02	100.00	85.93	29.90	260.99	23.50	18
M1	1, 30	11438	28.60	57.19	13.98	11.99	50.52	12.86	18
M2	209, 1526	2216	5.54	11.08	420.00	377.77	54.02	344.44	371
M3	30, 209	6338	15.85	31.69	72.80	61.79	62.99	54.25	34
M4	30, 9910	8604	21.52	43.02	181.33	100.99	175.19	75.67	34

Total Statistics:

Marker	Left, Right	Events	% Gated	% Total	Mean	Geo Mean	CV	Median	Peak Ch
All	1, 9910	20000	50.02	100.00	164.78	77.16	192.36	66.71	55
M1	1, 30	4172	10.43	20.86	18.67	17.22	35.46	19.11	25
M2	209, 1526	4118	10.30	20.59	470.23	412.32	58.04	371.80	278
M3	30, 209	11652	29.14	58.26	80.63	70.13	55.54	66.12	55
M4	30, 9910	15876	39.70	79.38	202.76	114.10	170.53	88.96	55

Figure C-28. Chimera 4C6 in OS3 cells FACS Histogram



Surface Statistics:

Marker	Left, Right	Events	% Gated	% Total	Mean	Geo Mean	CV	Median	Peak Ch
All	1, 9910	20000	50.07	100.00	231.48	43.47	296.72	29.69	13
M1	1, 30	10024	25.09	50.12	13.04	10.77	55.73	11.86	13
M2	209, 1526	3604	9.02	18.02	551.33	473.75	59.00	429.35	310
M3	30, 209	5764	14.43	28.82	81.18	69.04	59.30	64.94	36
M4	30, 9910	10012	25.06	50.06	449.48	175.89	204.79	151.25	36

Total Statistics:

Marker	Left, Right	Events	% Gated	% Total	Mean	Geo Mean	CV	Median	Peak Ch
All	1, 9910	20000	50.07	100.00	227.97	44.05	320.81	29.96	13
M1	1, 30	9976	24.97	49.88	13.45	11.35	52.32	12.52	13
M2	209, 1526	3678	9.21	18.39	548.93	474.45	58.03	441.09	406
M3	30, 209	5838	14.61	29.19	79.14	67.44	59.85	62.08	35
M4	30, 9910	10054	25.17	50.27	440.26	169.60	224.10	139.49	35

LIST OF REFERENCES

- (1) Hruba, V. J.; Li, G.; Haskell-Luevano, C.; Shenderovich, M. Design of peptides, proteins, and peptidomimetics in chi space. *Biopolymers* **1997**, *43*, 219-266.
- (2) Haskell-Luevano, C.; Sawyer, T. K.; Hendrata, S.; North, C.; Panahinia, L. et al. Truncation studies of alpha-melanotropin peptides identify tripeptide analogues exhibiting prolonged agonist bioactivity. *Peptides* **1996**, *17*, 995-1002.
- (3) Sahm, U. G.; Olivier, G. W.; Branch, S. K.; Moss, S. H.; Pouton, C. W. Synthesis and biological evaluation of alpha-MSH analogues substituted with alanine. *Peptides* **1994**, *15*, 1297-1302.
- (4) Sawyer, T. K.; Sanfilippo, P. J.; Hruba, V. J.; Engel, M. H.; Heward, C. B. et al. 4-Norleucine, 7-D-phenylalanine-alpha-melanocyte-stimulating hormone: a highly potent alpha-melanotropin with ultralong biological activity. *Proc. Natl. Acad. Sci. U. S. A.* **1980**, *77*, 5754-5758.
- (5) Bednarek, M. A.; Silva, M. V.; Arison, B.; MacNeil, T.; Kalyani, R. N. et al. Structure-function studies on the cyclic peptide MT-II, lactam derivative of alpha-melanotropin. *Peptides* **1999**, *20*, 401-409.
- (6) Holder, J. R.; Bauzo, R. M.; Xiang, Z.; Haskell-Luevano, C. Structure-activity relationships of the melanocortin tetrapeptide Ac-His-DPhe-Arg-Trp-NH(2) at the mouse melanocortin receptors. 1. Modifications at the His position. *J. Med. Chem.* **2002**, *45*, 2801-2810.
- (7) Holder, J. R.; Bauzo, R. M.; Xiang, Z.; Haskell-Luevano, C. Structure-activity relationships of the melanocortin tetrapeptide Ac-His-DPhe-Arg-Trp-NH(2) at the mouse melanocortin receptors: part 2 modifications at the Phe position. *J. Med. Chem.* **2002**, *45*, 3073-3081.
- (8) Holder, J. R.; Xiang, Z.; Bauzo, R. M.; Haskell-Luevano, C. Structure-activity relationships of the melanocortin tetrapeptide Ac-His-D-Phe-Arg-Trp-NH2 at the mouse melanocortin receptors. 4. Modifications at the Trp position. *J. Med. Chem.* **2002**, *45*, 5736-5744.
- (9) Holder, J. R.; Xiang, Z.; Bauzo, R. M.; Haskell-Luevano, C. Structure-activity relationships of the melanocortin tetrapeptide Ac-His-DPhe-Arg-Trp-NH2 at the mouse melanocortin receptors. Part 3: modifications at the Arg position. *Peptides* **2003**, *24*, 73-82.
- (10) Ramachandran, G. N.; Ramakrishnan, C.; Sasisekharan, V. Stereochemistry of polypeptide chain configurations. *J Mol Biol* **1963**, *7*, 95-99.

- (11) Hadley, M. E.; Anderson, B.; Heward, C. B.; Sawyer, T. K.; Hruby, V. J. Calcium-dependent prolonged effects on melanophores of [4-norleucine, 7-D-phenylalanine]-alpha-melanotropin. *Science* **1981**, *213*, 1025-1027.
- (12) Irani, B. G.; Holder, J. R.; Todorovic, A.; Wilczynski, A. M.; Joseph, C. G. et al. Progress in the development of melanocortin receptor selective ligands. *Curr. Pharm. Des.* **2004**, *10*, 3443-3479.
- (13) Adessi, C.; Soto, C. Converting a peptide into a drug: strategies to improve stability and bioavailability. *Curr Med Chem* **2002**, *9*, 963-978.
- (14) Fischer, P. M. The design, synthesis and application of stereochemical and directional peptide isomers: a critical review. *Curr Protein Pept Sci* **2003**, *4*, 339-356.
- (15) Johannesson, P.; Erdelyi, M.; Lindeberg, G.; Frandberg, P. A.; Nyberg, F. et al. AT2-selective angiotensin II analogues containing tyrosine-functionalized 5,5-bicyclic thiazabicycloalkane dipeptide mimetics. *J Med Chem* **2004**, *47*, 6009-6019.
- (16) Johannesson, P.; Lindeberg, G.; Tong, W.; Gogoll, A.; Karlen, A. et al. Bicyclic tripeptide mimetics with reverse turn inducing properties. *J Med Chem* **1999**, *42*, 601-608.
- (17) Johannesson, P.; Lindeberg, G.; Tong, W.; Gogoll, A.; Synnergren, B. et al. Angiotensin II analogues encompassing 5,9- and 5,10-fused thiazabicycloalkane tripeptide mimetics. *J Med Chem* **1999**, *42*, 4524-4537.
- (18) Rose, G. D.; Gierasch, L. M.; Smith, J. A. Turns in peptides and proteins. *Adv Protein Chem* **1985**, *37*, 1-109.
- (19) Pauling, L.; Corey, R. B.; Branson, H. R. The structure of proteins; two hydrogen-bonded helical configurations of the polypeptide chain. *Proc Natl Acad Sci U S A* **1951**, *37*, 205-211.
- (20) Pauling, L.; Corey, R. B. The pleated sheet, a new layer configuration of polypeptide chains. *Proc Natl Acad Sci U S A* **1951**, *37*, 251-256.
- (21) Venkatachalam, C. M. Stereochemical criteria for polypeptides and proteins. V. Conformation of a system of three linked peptide units. *Biopolymers* **1968**, *6*, 1425-1436.
- (22) Milner-White, E.; Ross, B. M.; Ismail, R.; Belhadj-Mostefa, K.; Poet, R. One type of gamma-turn, rather than the other gives rise to chain-reversal in proteins. *J Mol Biol* **1988**, *204*, 777-782.
- (23) Lindman, S.; Lindeberg, G.; Nyberg, F.; Karlen, A.; Hallberg, A. Comparison of three gamma-turn mimetic scaffolds incorporated into angiotensin II. *Bioorg Med Chem* **2000**, *8*, 2375-2383.

- (24) Andreu, D.; Albericio, F.; Sole, N. A.; Munson, M. C.; Farrer, M. et al. Formation of Disulfide Bonds in Synthetic Peptides and Proteins. *Peptide Synthesis Protocols*; Humana Press Inc.: Totowa, New Jersey, 1994; pp 91-169.
- (25) Stewart, J. M.; Young, J. D. *Solid Phase Peptide Synthesis*; 2 ed.; Pierce Chemical Company: Rockford, 1984.
- (26) Haskell-Luevano, C.; Rosenquist, A.; Souers, A.; Khong, K. C.; Ellman, J. A. et al. Compounds that activate the mouse melanocortin-1 receptor identified by screening a small molecule library based upon the beta-turn. *J Med Chem* **1999**, *42*, 4380-4387.
- (27) Bondebjerg, J.; Xiang, Z.; Bauzo, R. M.; Haskell-Luevano, C.; Meldal, M. A solid-phase approach to mouse melanocortin receptor agonists derived from a novel thioether cyclized peptidomimetic scaffold. *J Am Chem Soc* **2002**, *124*, 11046-11055.
- (28) Sankararamakrishnan, R.; Vishveshwara, S. Conformational studies on peptides with proline in the right-handed alpha-helical region. *Biopolymers* **1990**, *30*, 287-298.
- (29) Zagari, A.; Nemethy, G.; Scheraga, H. A. The effect of the L-azetidino-2-carboxylic acid residue on protein conformation. I. Conformations of the residue and of dipeptides. *Biopolymers* **1990**, *30*, 951-959.
- (30) Yamazaki, T.; Probst, A.; Schiller, P. W.; Goodman, M. Biological and conformational studies of [Val⁴]morphiceptin and [D-Val⁴]morphiceptin analogs incorporating cis-2-aminocyclopentane carboxylic acid as a peptidomimetic for proline. *Int J Pept Protein Res* **1991**, *37*, 364-381.
- (31) Kazmierski, W.; Wire, W. S.; Lui, G. K.; Knapp, R. J.; Shook, J. E. et al. Design and synthesis of somatostatin analogues with topographical properties that lead to highly potent and specific mu opioid receptor antagonists with greatly reduced binding at somatostatin receptors. *J Med Chem* **1988**, *31*, 2170-2177.
- (32) Hausin, R. J.; Coddig, P. W. Molecular and crystal structures of MDL27,467A hydrochloride and quinapril hydrochloride, two ester derivatives of potent angiotensin converting enzyme inhibitors. *J Med Chem* **1991**, *34*, 511-517.
- (33) Boeglin, D.; Xiang, Z.; Sorenson, N. B.; Wood, M. S.; Haskell-Luevano, C. et al. Aza-scanning of the potent melanocortin receptor agonist Ac-His-D-Phe-Arg-Trp-NH₂. *Chem Biol Drug Des* **2006**, *67*, 275-283.
- (34) Holder, J. R.; Marques, F. F.; Xiang, Z.; Bauzo, R. M.; Haskell-Luevano, C. Characterization of aliphatic, cyclic, and aromatic N-terminally "capped" His-D-Phe-Arg-Trp-NH₂ tetrapeptides at the melanocortin receptors. *Eur J Pharmacol* **2003**, *462*, 41-52.

- (35) Evans, B. E.; Rittle, K. E.; Bock, M. G.; DiPardo, R. M.; Freidinger, R. M. et al. Methods for drug discovery: development of potent, selective, orally effective cholecystokinin antagonists. *J Med Chem* **1988**, *31*, 2235-2246.
- (36) Huang, S. C.; Zhang, L.; Chiang, H. C.; Wank, S. A.; Maton, P. N. et al. Benzodiazepine analogues L365,260 and L364,718 as gastrin and pancreatic CCK receptor antagonists. *Am J Physiol* **1989**, *257*, G169-174.
- (37) Evans, B.; Pipe, A.; Clark, L.; Banks, M. Identification of a potent and selective oxytocin antagonist, from screening a fully encoded differential release combinatorial chemical library. *Bioorg Med Chem Lett* **2001**, *11*, 1297-1300.
- (38) Wyatt, P. G.; Allen, M. J.; Chilcott, J.; Hickin, G.; Miller, N. D. et al. Structure-activity relationship investigations of a potent and selective benzodiazepine oxytocin antagonist. *Bioorg Med Chem Lett* **2001**, *11*, 1301-1305.
- (39) Hsu, M. C.; Schutt, A. D.; Holly, M.; Slice, L. W.; Sherman, M. I. et al. Inhibition of HIV replication in acute and chronic infections in vitro by a Tat antagonist. *Science* **1991**, *254*, 1799-1802.
- (40) Pauwels, R.; Andries, K.; Desmyter, J.; Schols, D.; Kukla, M. J. et al. Potent and selective inhibition of HIV-1 replication in vitro by a novel series of TIBO derivatives. *Nature* **1990**, *343*, 470-474.
- (41) Anzini, M.; Canullo, L.; Braile, C.; Cappelli, A.; Gallelli, A. et al. Synthesis, biological evaluation, and receptor docking simulations of 2-[(acylamino)ethyl]-1,4-benzodiazepines as kappa-opioid receptor agonists endowed with antinociceptive and anti-amnesic activity. *J Med Chem* **2003**, *46*, 3853-3864.
- (42) Xiang, Z.; Pogozeva, I. D.; Sorenson, N. B.; Wilczynski, A. M.; Holder, J. R. et al. Peptide and small molecules rescue the functional activity and agonist potency of dysfunctional human melanocortin-4 receptor polymorphisms. *Biochemistry* **2007**, *46*, 8273-8287.
- (43) Haskell-Luevano, C.; Cone, R. D.; Monck, E. K.; Wan, Y. P. Structure activity studies of the melanocortin-4 receptor by in vitro mutagenesis: identification of agouti-related protein (AGRP), melanocortin agonist and synthetic peptide antagonist interaction determinants. *Biochemistry* **2001**, *40*, 6164-6179.
- (44) Haskell-Luevano, C.; Sawyer, T. K.; Trumpp-Kallmeyer, S.; Bikker, J. A.; Humblet, C. et al. Three-dimensional molecular models of the hMC1R melanocortin receptor: complexes with melanotropin peptide agonists. *Drug Des Discov* **1996**, *14*, 197-211.
- (45) Lu, D.; Vage, D. I.; Cone, R. D. A ligand-mimetic model for constitutive activation of the melanocortin-1 receptor. *Mol Endocrinol* **1998**, *12*, 592-604.

- (46) Yang, Y. K.; Chen, M.; Lai, Y. M.; Gantz, I.; Georgeson, K. E. et al. Molecular determinants of human melanocortin-4 receptor responsible for antagonist SHU9119 selective activity. *Journal of Biological Chemistry* **2002**, *277*, 20328-20335.
- (47) Chai, B. X.; Neubig, R. R.; Millhauser, G. L.; Thompson, D. A.; Jackson, P. J. et al. Inverse agonist activity of agouti and agouti-related protein. *Peptides* **2003**, *24*, 603-609.
- (48) Wilczynski, A.; Wang, X. S.; Joseph, C. G.; Xiang, Z.; Bauzo, R. M. et al. Identification of putative agouti-related protein(87-132)-melanocortin-4 receptor interactions by homology molecular modeling and validation using chimeric peptide ligands. *J Med Chem* **2004**, *47*, 2194-2207.
- (49) Pogozheva, I. D.; Chai, B. X.; Lomize, A. L.; Fong, T. M.; Weinberg, D. H. et al. Interactions of human melanocortin 4 receptor with nonpeptide and peptide agonists. *Biochemistry* **2005**, *44*, 11329-11341.
- (50) Hogan, K.; Peluso, S.; Gould, S.; Parsons, I.; Ryan, D. et al. Mapping the binding site of melanocortin 4 receptor agonists: a hydrophobic pocket formed by I3.28(125), I3.32(129), and I7.42(291) is critical for receptor activation. *J Med Chem* **2006**, *49*, 911-922.
- (51) Chen, M.; Cai, M.; Aprahamian, C. J.; Georgeson, K. E.; Hruby, V. et al. Contribution of the conserved amino acids of the melanocortin-4 receptor in D-[Nle⁴,Phe⁷]-alpha-melanocyte-stimulating hormone binding and signaling. *J Biol Chem* **2007**, *282*, 21712-21719.
- (52) Chhajlani, V.; Wikberg, J. E. Molecular cloning and expression of the human melanocyte stimulating hormone receptor cDNA. *FEBS Lett* **1992**, *309*, 417-420.
- (53) Mountjoy, K. G.; Robbins, L. S.; Mortrud, M. T.; Cone, R. D. The cloning of a family of genes that encode the melanocortin receptors. *Science* **1992**, *257*, 1248-1251.
- (54) Roselli-Reh fuss, L.; Mountjoy, K. G.; Robbins, L. S.; Mortrud, M. T.; Low, M. J. et al. Identification of a receptor for gamma melanotropin and other proopiomelanocortin peptides in the hypothalamus and limbic system. *Proc. Natl. Acad. Sci. U. S. A.* **1993**, *90*, 8856-8860.
- (55) Mountjoy, K. G.; Mortrud, M. T.; Low, M. J.; Simerly, R. B.; Cone, R. D. Localization of the melanocortin-4 receptor (MC4-R) in neuroendocrine and autonomic control circuits in the brain. *Mol. Endocrinol.* **1994**, *8*, 1298-1308.
- (56) Gantz, I.; Miwa, H.; Konda, Y.; Shimoto, Y.; Tashiro, T. et al. Molecular cloning, expression, and gene localization of a fourth melanocortin receptor. *J. Biol. Chem.* **1993**, *268*, 15174-15179.

- (57) Gantz, I.; Shimoto, Y.; Konda, Y.; Miwa, H.; Dickinson, C. J. et al. Molecular cloning, expression, and characterization of a fifth melanocortin receptor. *Biochem. Biophys. Res. Commun.* **1994**, *200*, 1214-1220.
- (58) Cone, R. D.; Lu, D.; Koppula, S.; Vage, D. I.; Klungland, H. et al. The melanocortin receptors: agonists, antagonists, and the hormonal control of pigmentation. *Recent Prog Horm Res* **1996**, *51*, 287-317; discussion 318.
- (59) Schioth, H. B.; Chhajlani, V.; Muceniece, R.; Klusa, V.; Wikberg, J. E. Major pharmacological distinction of the ACTH receptor from other melanocortin receptors. *Life Sci.* **1996**, *59*, 797-801.
- (60) Bultman, S. J.; Michaud, E. J.; Woychik, R. P. Molecular characterization of the mouse agouti locus. *Cell* **1992**, *71*, 1195-1204.
- (61) Miller, M. W.; Duhl, D. M.; Vrieling, H.; Cordes, S. P.; Ollmann, M. M. et al. Cloning of the mouse agouti gene predicts a secreted protein ubiquitously expressed in mice carrying the lethal yellow mutation. *Genes Dev.* **1993**, *7*, 454-467.
- (62) Ollmann, M. M.; Wilson, B. D.; Yang, Y. K.; Kerns, J. A.; Chen, Y. et al. Antagonism of central melanocortin receptors in vitro and in vivo by agouti-related protein. *Science* **1997**, *278*, 135-138.
- (63) Shutter, J. R.; Graham, M.; Kinsey, A. C.; Scully, S.; Luthy, R. et al. Hypothalamic expression of ART, a novel gene related to agouti, is up-regulated in obese and diabetic mutant mice. *Genes Dev.* **1997**, *11*, 593-602.
- (64) Robbins, L. S.; Nadeau, J. H.; Johnson, K. R.; Kelly, M. A.; Roselli-Rehfuss, L. et al. Pigmentation phenotypes of variant extension locus alleles result from point mutations that alter MSH receptor function. *Cell* **1993**, *72*, 827-834.
- (65) Lu, D.; Willard, D.; Patel, I. R.; Kadwell, S.; Overton, L. et al. Agouti protein is an antagonist of the melanocyte-stimulating-hormone receptor. *Nature* **1994**, *371*, 799-802.
- (66) Riniker, B.; Sieber, P.; Rittel, W.; Zuber, H. Revised amino-acid sequences for porcine and human adrenocorticotrophic hormone. *Nat. New Biol.* **1972**, *235*, 114-115.
- (67) Valverde, P.; Healy, E.; Jackson, I.; Rees, J. L.; Thody, A. J. Variants of the melanocyte-stimulating hormone receptor gene are associated with red hair and fair skin in humans. *Nat. Genet.* **1995**, *11*, 328-330.
- (68) Pawelek, J. M. Factors regulating growth and pigmentation of melanoma cells. *J. Invest. Dermatol.* **1976**, *66*, 201-209.
- (69) Bolognia, J.; Murray, M.; Pawelek, J. UVB-induced melanogenesis may be mediated through the MSH-receptor system. *J. Invest. Dermatol.* **1989**, *92*, 651-656.

- (70) Thody, A. J.; Higgins, E. M.; Wakamatsu, K.; Ito, S.; Burchill, S. A. et al. Pheomelanin as well as eumelanin is present in human epidermis. *J. Invest. Dermatol.* **1991**, *97*, 340-344.
- (71) McNulty, J. C.; Jackson, P. J.; Thompson, D. A.; Chai, B.; Gantz, I. et al. Structures of the agouti signaling protein. *J. Mol. Biol.* **2005**, *346*, 1059-1070.
- (72) Schauer, E.; Trautinger, F.; Kock, A.; Schwarz, A.; Bhardwaj, R. et al. Proopiomelanocortin-derived peptides are synthesized and released by human keratinocytes. *J. Clin. Invest.* **1994**, *93*, 2258-2262.
- (73) Catania, A.; Lipton, J. M. The neuropeptide alpha-melanocyte-stimulating hormone: a key component of neuroimmunomodulation. *Neuroimmunomodulation* **1994**, *1*, 93-99.
- (74) Cannon, J. G.; Tatro, J. B.; Reichlin, S.; Dinarello, C. A. Alpha melanocyte stimulating hormone inhibits immunostimulatory and inflammatory actions of interleukin 1. *J. Immunol.* **1986**, *137*, 2232-2236.
- (75) Taylor, A. W.; Streilein, J. W.; Cousins, S. W. Alpha-melanocyte-stimulating hormone suppresses antigen-stimulated T cell production of gamma-interferon. *Neuroimmunomodulation* **1994**, *1*, 188-194.
- (76) Grabbe, S.; Bhardwaj, R. S.; Mahnke, K.; Simon, M. M.; Schwarz, T. et al. alpha-Melanocyte-stimulating hormone induces hapten-specific tolerance in mice. *J. Immunol.* **1996**, *156*, 473-478.
- (77) Halkerston, I. D. Cyclic AMP and adrenocortical function. *Adv Cyclic Nucleotide Res* **1975**, *6*, 99-136.
- (78) Clark, A. J.; McLoughlin, L.; Grossman, A. Familial glucocorticoid deficiency associated with point mutation in the adrenocorticotropin receptor. *Lancet* **1993**, *341*, 461-462.
- (79) Tsigos, C.; Arai, K.; Hung, W.; Chrousos, G. P. Hereditary isolated glucocorticoid deficiency is associated with abnormalities of the adrenocorticotropin receptor gene. *J Clin Invest* **1993**, *92*, 2458-2461.
- (80) Tsigos, C.; Arai, K.; Latronico, A. C.; DiGeorge, A. M.; Rapaport, R. et al. A novel mutation of the adrenocorticotropin receptor (ACTH-R) gene in a family with the syndrome of isolated glucocorticoid deficiency, but no ACTH-R abnormalities in two families with the triple A syndrome. *J Clin Endocrinol Metab* **1995**, *80*, 2186-2189.
- (81) Weber, A.; Toppari, J.; Harvey, R. D.; Klann, R. C.; Shaw, N. J. et al. Adrenocorticotropin receptor gene mutations in familial glucocorticoid deficiency: relationships with clinical features in four families. *J Clin Endocrinol Metab* **1995**, *80*, 65-71.

- (82) Wu, S. M.; Stratakis, C. A.; Chan, C. H.; Hallermeier, K. M.; Bourdony, C. J. et al. Genetic heterogeneity of adrenocorticotropin (ACTH) resistance syndromes: identification of a novel mutation of the ACTH receptor gene in hereditary glucocorticoid deficiency. *Mol Genet Metab* **1998**, *64*, 256-265.
- (83) Naville, D.; Barjhoux, L.; Jaillard, C.; Faury, D.; Despert, F. et al. Demonstration by transfection studies that mutations in the adrenocorticotropin receptor gene are one cause of the hereditary syndrome of glucocorticoid deficiency. *J Clin Endocrinol Metab* **1996**, *81*, 1442-1448.
- (84) Noon, L. A.; Franklin, J. M.; King, P. J.; Goulding, N. J.; Hunyady, L. et al. Failed export of the adrenocorticotrophin receptor from the endoplasmic reticulum in non-adrenal cells: evidence in support of a requirement for a specific adrenal accessory factor. *J Endocrinol* **2002**, *174*, 17-25.
- (85) Penhoat, A.; Naville, D.; El Mourabit, H.; Buronfosse, A.; Durand, P. et al. Functional expression of the human ACTH receptor gene. *Endocr Res* **2000**, *26*, 549-557.
- (86) Metherell, L. A.; Chapple, J. P.; Cooray, S.; David, A.; Becker, C. et al. Mutations in MRAP, encoding a new interacting partner of the ACTH receptor, cause familial glucocorticoid deficiency type 2. *Nat Genet* **2005**, *37*, 166-170.
- (87) Doufexis, M.; Storr, H. L.; King, P. J.; Clark, A. J. Interaction of the melanocortin 2 receptor with nucleoporin 50: evidence for a novel pathway between a G-protein-coupled receptor and the nucleus. *Faseb J* **2007**.
- (88) Gantz, I.; Konda, Y.; Tashiro, T.; Shimoto, Y.; Miwa, H. et al. Molecular cloning of a novel melanocortin receptor. *J. Biol. Chem.* **1993**, *268*, 8246-8250.
- (89) Butler, A. A.; Kesterson, R. A.; Khong, K.; Cullen, M. J.; Pelleymounter, M. A. et al. A unique metabolic syndrome causes obesity in the melanocortin-3 receptor-deficient mouse. *Endocrinol.* **2000**, *141*, 3518-3521.
- (90) Chen, A. S.; Marsh, D. J.; Trumbauer, M. E.; Frazier, E. G.; Guan, X. M. et al. Inactivation of the mouse melanocortin-3 receptor results in increased fat mass and reduced lean body mass. *Nat. Genet.* **2000**, *26*, 97-102.
- (91) Konda, Y.; Gantz, I.; DelValle, J.; Shimoto, Y.; Miwa, H. et al. Interaction of dual intracellular signaling pathways activated by the melanocortin-3 receptor. *J. Biol. Chem.* **1994**, *269*, 13162-13166.
- (92) Wachira, S. J.; Hughes-Darden, C. A.; Taylor, C. V.; Ochillo, R.; Robinson, T. J. Evidence for the interaction of protein kinase C and melanocortin 3-receptor signaling pathways. *Neuropeptides.* **2003**, *37*, 201-210.

- (93) Huszar, D.; Lynch, C. A.; Fairchild-Huntress, V.; Dunmore, J. H.; Fang, Q. et al. Targeted disruption of the melanocortin-4 receptor results in obesity in mice. *Cell* **1997**, *88*, 131-141.
- (94) Van der Ploeg, L. H.; Martin, W. J.; Howard, A. D.; Nargund, R. P.; Austin, C. P. et al. A role for the melanocortin 4 receptor in sexual function. *Proc. Natl. Acad. Sci. U. S. A.* **2002**, *99*, 11381-11386.
- (95) Hadley, M. E. Discovery that a melanocortin regulates sexual functions in male and female humans. *Peptides* **2005**, (*in press*).
- (96) Millington, G. W.; Tung, Y. C.; Hewson, A. K.; O'Rahilly, S.; Dickson, S. L. Differential effects of alpha-, beta- and gamma(2)-melanocyte-stimulating hormones on hypothalamic neuronal activation and feeding in the fasted rat. *Neuroscience* **2001**, *108*, 437-445.
- (97) Fan, W.; Boston, B. A.; Kesterson, R. A.; Hruby, V. J.; Cone, R. D. Role of melanocortinergic neurons in feeding and the agouti obesity syndrome. *Nature* **1997**, *385*, 165-168.
- (98) Gonzalez, M. I.; Vaziri, S.; Wilson, C. A. Behavioral effects of alpha-MSH and MCH after central administration in the female rat. *Peptides* **1996**, *17*, 171-177.
- (99) Hughes, A. M.; Everitt, B. J.; Herbert, J. The effects of simultaneous or separate infusions of some pro-opiomelanocortin-derived peptides (beta-endorphin, melanocyte stimulating hormone, and corticotrophin-like intermediate polypeptide) and their acetylated derivatives upon sexual and ingestive behaviour of male rats. *Neuroscience* **1988**, *27*, 689-698.
- (100) Dorr, R. T.; Lines, R.; Levine, N.; Brooks, C.; Xiang, L. et al. Evaluation of melanotan-II, a superpotent cyclic melanotropic peptide in a pilot phase-I clinical study. *Life Sci.* **1996**, *58*, 1777-1784.
- (101) Chen, W.; Kelly, M. A.; Opitz-Araya, X.; Thomas, R. E.; Low, M. J. et al. Exocrine gland dysfunction in MC5-R-deficient mice: evidence for coordinated regulation of exocrine gland function by melanocortin peptides. *Cell* **1997**, *91*, 789-798.
- (102) Eipper, B. A.; Mains, R. E. Analysis of the common precursor to corticotropin and endorphin. *J. Biol. Chem.* **1978**, *253*, 5732-5744.
- (103) Mains, R. E.; Eipper, B. A. Biosynthesis of adrenocorticotropin hormone in mouse pituitary tumor cells. *J. Biol. Chem.* **1976**, *251*, 4115-4120.
- (104) DeBold, C. R.; Menefee, J. K.; Nicholson, W. E.; Orth, D. N. Proopiomelanocortin gene is expressed in many normal human tissues and in tumors not associated with ectopic adrenocorticotropin syndrome. *Mol. Endocrinol.* **1988**, *2*, 862-870.

- (105) DeBold, C. R.; Nicholson, W. E.; Orth, D. N. Immunoreactive proopiomelanocortin (POMC) peptides and POMC-like messenger ribonucleic acid are present in many rat nonpituitary tissues. *Endocrinol.* **1988**, *122*, 2648-2657.
- (106) Lyons, P. D.; Blalock, J. E. Pro-opiomelanocortin gene expression and protein processing in rat mononuclear leukocytes. *J. Neuroimmunol.* **1997**, *78*, 47-56.
- (107) Nakanishi, S.; Inoue, A.; Kita, T.; Nakamura, M.; Chang, A. C. et al. Nucleotide sequence of cloned cDNA for bovine corticotropin-beta-lipotropin precursor. *Nature* **1979**, *278*, 423-427.
- (108) Saito, E.; Odell, W. D. Corticotropin/lipotropin common precursor-like material in normal rat extrapituitary tissues. *Proc. Natl. Acad. Sci. U. S. A.* **1983**, *80*, 3792-3796.
- (109) Slominski, A.; Paus, R.; Wortsman, J. On the potential role of proopiomelanocortin in skin physiology and pathology. *Mol. Cell. Endocrinol.* **1993**, *93*, C1-6.
- (110) Benjannet, S.; Rondeau, N.; Day, R.; Chretien, M.; Seidah, N. G. PC1 and PC2 are proprotein convertases capable of cleaving proopiomelanocortin at distinct pairs of basic residues. *Proc. Natl. Acad. Sci. U. S. A.* **1991**, *88*, 3564-3568.
- (111) Zhou, A.; Bloomquist, B. T.; Mains, R. E. The prohormone convertases PC1 and PC2 mediate distinct endoproteolytic cleavages in a strict temporal order during proopiomelanocortin biosynthetic processing. *J. Biol. Chem.* **1993**, *268*, 1763-1769.
- (112) Pritchard, L. E.; Turnbull, A. V.; White, A. Pro-opiomelanocortin processing in the hypothalamus: impact on melanocortin signalling and obesity. *J. Endocrinol.* **2002**, *172*, 411-421.
- (113) MacNeil, D. J.; Howard, A. D.; Guan, X.; Fong, T. M.; Nargund, R. P. et al. The role of melanocortins in body weight regulation: opportunities for the treatment of obesity. *Eur J Pharmacol* **2002**, *450*, 93-109.
- (114) Castrucci, A. M.; Hadley, M. E.; Sawyer, T. K.; Wilkes, B. C.; al-Obeidi, F. et al. Alpha-melanotropin: the minimal active sequence in the lizard skin bioassay. *Gen. Comp. Endocrinol.* **1989**, *73*, 157-163.
- (115) Hruby, V. J.; Wilkes, B. C.; Hadley, M. E.; Al-Obeidi, F.; Sawyer, T. K. et al. alpha-Melanotropin: the minimal active sequence in the frog skin bioassay. *J. Med. Chem.* **1987**, *30*, 2126-2130.
- (116) Al-Obeidi, F.; Hruby, V. J.; Castrucci, A. M.; Hadley, M. E. Design of potent linear alpha-melanotropin 4-10 analogues modified in positions 5 and 10. *J. Med. Chem.* **1989**, *32*, 174-179.

- (117) Al-Obeidi, F.; Castrucci, A. M.; Hadley, M. E.; Hruby, V. J. Potent and prolonged acting cyclic lactam analogues of alpha-melanotropin: design based on molecular dynamics. *J. Med. Chem.* **1989**, *32*, 2555-2561.
- (118) Hruby, V. J.; Lu, D.; Sharma, S. D.; Castrucci, A. L.; Kesterson, R. A. et al. Cyclic lactam alpha-melanotropin analogues of Ac-Nle4-cyclo[Asp5, D-Phe7,Lys10] alpha-melanocyte-stimulating hormone-(4-10)-NH2 with bulky aromatic amino acids at position 7 show high antagonist potency and selectivity at specific melanocortin receptors. *J. Med. Chem.* **1995**, *38*, 3454-3461.
- (119) Hruby, V. J.; Lu, D.; Sharma, S. D.; Castrucci, A. L.; Kesterson, R. A. et al. Cyclic lactam alpha-melanotropin analogues of Ac-Nle4-cyclo[Asp5, D-Phe7,Lys10] alpha-melanocyte-stimulating hormone-(4-10)-NH2 with bulky aromatic amino acids at position 7 show high antagonist potency and selectivity at specific melanocortin receptors. *J Med Chem* **1995**, *38*, 3454-3461.
- (120) Murphy, B.; Nunes, C. N.; Ronan, J. J.; Harper, C. M.; Beall, M. J. et al. Melanocortin mediated inhibition of feeding behavior in rats. *Neuropeptides* **1998**, *32*, 491-497.
- (121) Pierroz, D. D.; Ziotopoulou, M.; Ungsunan, L.; Moschos, S.; Flier, J. S. et al. Effects of acute and chronic administration of the melanocortin agonist MTII in mice with diet-induced obesity. *Diabetes* **2002**, *51*, 1337-1345.
- (122) Thiele, T. E.; van Dijk, G.; Yagaloff, K. A.; Fisher, S. L.; Schwartz, M. et al. Central infusion of melanocortin agonist MTII in rats: assessment of c-Fos expression and taste aversion. *Am. J. Physiol.* **1998**, *274*, R248-254.
- (123) Wirth, M. M.; Olszewski, P. K.; Yu, C.; Levine, A. S.; Giraud, S. Q. Paraventricular hypothalamic alpha-melanocyte-stimulating hormone and MTII reduce feeding without causing aversive effects. *Peptides*. **2001**, *22*, 129-134.
- (124) Giraud, S. Q.; Billington, C. J.; Levine, A. S. Feeding effects of hypothalamic injection of melanocortin 4 receptor ligands. *Brain Res.* **1998**, *809*, 302-306.
- (125) Chen, A. S.; Metzger, J. M.; Trumbauer, M. E.; Guan, X. M.; Yu, H. et al. Role of the melanocortin-4 receptor in metabolic rate and food intake in mice. *Transgenic Res.* **2000**, *9*, 145-154.
- (126) Marsh, D. J.; Hollopeter, G.; Huszar, D.; Laufer, R.; Yagaloff, K. A. et al. Response of melanocortin-4 receptor-deficient mice to anorectic and orexigenic peptides. *Nat. Genet.* **1999**, *21*, 119-122.
- (127) Wessells, H.; Fuciarelli, K.; Hansen, J.; Hadley, M. E.; Hruby, V. J. et al. Synthetic melanotropic peptide initiates erections in men with psychogenic erectile dysfunction: double-blind, placebo controlled crossover study. *J. Urol.* **1998**, *160*, 389-393.

- (128) Wessells, H.; Gralnek, D.; Dorr, R.; Hruby, V. J.; Hadley, M. E. et al. Effect of an alpha-melanocyte stimulating hormone analog on penile erection and sexual desire in men with organic erectile dysfunction. *Urol.* **2000**, *56*, 641-646.
- (129) Penhoat, A.; Jaillard, C.; Saez, J. M. Identification and characterization of corticotropin receptors in bovine and human adrenals. *J Steroid Biochem Mol Biol* **1993**, *44*, 21-27.
- (130) Haskell-Luevano, C.; Todorovic, A.; Gridley, K.; Sorenson, N.; Irani, B. et al. The melanocortin pathway: effects of voluntary exercise on the melanocortin-4 receptor knockout mice and ACTH(1-24) ligand structure activity relationships at the melanocortin-2 receptor. *Endocr Res* **2004**, *30*, 591-597.
- (131) Schwyzer, R. ACTH: a short introductory review. *Ann. N. Y. Acad. Sci.* **1977**, *297*, 3-26.
- (132) Balse-Srinivasan, P.; Grieco, P.; Cai, M.; Trivedi, D.; Hruby, V. J. Structure-activity relationships of gamma-MSH analogues at the human melanocortin MC3, MC4, and MC5 receptors. Discovery of highly selective hMC3R, hMC4R, and hMC5R analogues. *J. Med. Chem.* **2003**, *46*, 4965-4973.
- (133) Grieco, P.; Balse, P. M.; Weinberg, D.; MacNeil, T.; Hruby, V. J. D-Amino acid scan of gamma-melanocyte-stimulating hormone: importance of Trp(8) on human MC3 receptor selectivity. *J. Med. Chem.* **2000**, *43*, 4998-5002.
- (134) Haskell-Luevano, C.; Monck, E. K. Agouti-related protein functions as an inverse agonist at a constitutively active brain melanocortin-4 receptor. *Regul. Pept.* **2001**, *99*, 1-7.
- (135) Nijenhuis, W. A.; Oosterom, J.; Adan, R. A. AgRP(83-132) acts as an inverse agonist on the human-melanocortin-4 receptor. *Mol. Endocrinol.* **2001**, *15*, 164-171.
- (136) Graham, M.; Shutter, J. R.; Sarmiento, U.; Sarosi, I.; Stark, K. L. Overexpression of AGRT leads to obesity in transgenic mice. *Nat. Genet.* **1997**, *17*, 273-274.
- (137) Willard, D. H.; Bodnar, W.; Harris, C.; Kiefer, L.; Nichols, J. S. et al. Agouti structure and function: characterization of a potent alpha-melanocyte stimulating hormone receptor antagonist. *Biochemistry* **1995**, *34*, 12341-12346.
- (138) McNulty, J. C.; Thompson, D. A.; Bolin, K. A.; Wilken, J.; Barsh, G. S. et al. High-resolution NMR structure of the chemically-synthesized melanocortin receptor binding domain AGRP(87-132) of the agouti-related protein. *Biochemistry* **2001**, *40*, 15520-15527.
- (139) Perry, W. L.; Nakamura, T.; Swing, D. A.; Secret, L.; Eagleson, B. et al. Coupled site-directed mutagenesis/transgenesis identifies important functional domains of the mouse agouti protein. *Genetics* **1996**, *144*, 255-264.

- (140) Tota, M. R.; Smith, T. S.; Mao, C.; MacNeil, T.; Mosley, R. T. et al. Molecular interaction of Agouti protein and Agouti-related protein with human melanocortin receptors. *Biochemistry*. **1999**, *38*, 897-904.
- (141) Haskell-Luevano, C.; Monck, E. K.; Wan, Y. P.; Schentrup, A. M. The agouti-related protein decapeptide (Yc[CRFFNAFC]Y) possesses agonist activity at the murine melanocortin-1 receptor. *Peptides* **2000**, *21*, 683-689.
- (142) Wilczynski, A.; Wang, X. S.; Joseph, C. G.; Xiang, Z.; Bauzo, R. M. et al. Identification of putative agouti-related protein(87-132)-melanocortin-4 receptor interactions by homology molecular modeling and validation using chimeric peptide ligands. *J. Med. Chem.* **2004**, *47*, 2194-2207.
- (143) Flegal, K. M.; Carroll, M. D.; Ogden, C. L.; Johnson, C. L. Prevalence and trends in obesity among US adults, 1999-2000. *Jama* **2002**, *288*, 1723-1727.
- (144) Flegal, K. M.; Carroll, M. D.; Kuczmarski, R. J.; Johnson, C. L. Overweight and obesity in the United States: prevalence and trends, 1960-1994. *Int J Obes Relat Metab Disord* **1998**, *22*, 39-47.
- (145) Clinical Guidelines on the Identification, Evaluation, and Treatment of Overweight and Obesity in Adults--The Evidence Report. National Institutes of Health. *Obes Res* **1998**, *6 Suppl 2*, 51S-209S.
- (146) Tortora, G. J.; Anagnostakos, N. P. *Principles of Anatomy and Physiology*; 4 ed.; Harper and Row: New York, 1984.
- (147) Clark, A. J.; Weber, A. Adrenocorticotropin insensitivity syndromes. *Endocr Rev* **1998**, *19*, 828-843.
- (148) Merrifield, R. B. Solid Phase Peptide Synthesis .1 Synthesis of a Tetrapeptide. *Journal of the American Chemical Society* **1963**, *85*, 2149-2154.
- (149) Stewart, J. M.; Young, J. D. *Solid Phase Peptide Synthesis, Second Edition*; Pierce Chemical Company: Rockford, IL, 1984.
- (150) Merrifield, R. B. Solid Phase Peptide Synthesis 4. Synthesis of Methionyl-Lysyl-Bradykinin. *Journal of Organic Chemistry* **1964**, *29*, 3100-3102.
- (151) Merrifield, R. B. Solid Phase Peptide Synthesis 2. Synthesis of Bradykinin. *Journal of the American Chemical Society* **1964**, *86*, 304-305.
- (152) Merrifield, R. B. Solid-Phase Peptide Synthesis. 3. An Improved Synthesis of Bradykinin. *Biochemistry* **1964**, *3*, 1385-1390.

- (153) Carpino, L. A.; Han, G. Y. 9-Fluorenylthoxycarbonyl Function, a New Base-Sensitive Amino-Protecting Group. *Journal of the American Chemical Society* **1970**, *92*, 5748-5749.
- (154) Carpino, L. A.; Han, G. Y. 9-Fluorenylmethoxycarbonyl Amino-Protecting Group. *Journal of Organic Chemistry* **1972**, *37*, 3404-3405.
- (155) Wang, S. S. p-alkoxybenzyl alcohol resin and p-alkoxybenzyloxycarbonylhydrazide resin for solid phase synthesis of protected peptide fragments. *J Am Chem Soc* **1973**, *95*, 1328-1333.
- (156) Rink, H. Solid-phase synthesis of protected peptide fragments using a trialkoxy-diphenylmethylester resin. *Tetrahedron Letters* **1987**, *28*, 3787-3790.
- (157) Sieber, P. An improved method for anchoring of 9-fluorenylmethoxycarbonyl-amino acids to 4-alkoxybenzyl alcohol resins. *Tetrahedron Letters* **1987**, *28*, 6147-6150.
- (158) Barlos, K.; Chatzi, O.; Gatos, D.; Stavropoulos, G. 2-Chlorotriptyl chloride resin. Studies on anchoring of Fmoc-amino acids and peptide cleavage. *Int J Pept Protein Res* **1991**, *37*, 513-520.
- (159) Bernatowicz, M. S.; Daniels, S. B.; Koster, H. A comparison of acid labile linkage agents for the synthesis of peptide C-terminal amides. *Tetrahedron Letters* **1989**, *30*, 4645-4648.
- (160) Barlos, K.; Gatos, D.; Kallitsis, J.; Papaphotiu, G.; Sotiriu, P. et al. Darstellung geschützter peptid-fragmente unter einatz substituierter triphenylmethyl-harze. *Tetrahedron Letters* **1989**, *30*, 3943-3946.
- (161) Barlos, K.; Gatos, D.; Kapolos, S.; Papaphotiu, G.; Schafer, W. et al. Veresterung von partiell geschützten peptid-fragmenten mit harzen. Einsatz von 2-chlorotriptylchlorid zur synthese von Leu15 -gastrin I. *Tetrahedron Letters* **1989**, *30*, 3947-3950.
- (162) Grieco, P.; Gitu, P. M.; Hruby, V. J. Preparation of 'side-chain-to-side-chain' cyclic peptides by Allyl and Alloc strategy: potential for library synthesis. *J Pept Res* **2001**, *57*, 250-256.
- (163) Merrifield, R. B. Solid Phase Peptide Synthesis. 1 Synthesis of a Tetrapeptide. *Journal of the American Chemical Society* **1963**, *85*, 2149-2154.
- (164) Sheehan, J. C.; Hess, G. P. A New Method of Forming Peptide Bonds. *J. Am. Chem. Soc.* **1955**, *77*, 1067-1068.
- (165) Carpino, L. A. 1-Hydroxy-7-azabenzotriazole. An efficient peptide coupling additive. *J. Am. Chem. Soc.* **1993**, *115*, 4397-4398.
- (166) Khorana, H. G. The Chemistry of Carbodiimides. *Chem. Rev.* **1953**, *53*, 145-166.

- (167) Beyermann, M.; Henklein, P.; Klose, A.; Sohr, R.; Bienert, M. Effect of tertiary amine on the carbodiimide-mediated peptide synthesis. *Int J Pept Protein Res* **1991**, *37*, 252-256.
- (168) Bates, A. J.; Galpin, I. J.; Hallett, A.; Hudson, D.; Kenner, G. W. et al. A new reagent for polypeptide synthesis: mu-oxo-bis-(tris-(dimethylamino)-phosphonium)-bis-tetrafluoroborate. *Helv Chim Acta* **1975**, *58*, 688-696.
- (169) Barstow, L. E. H., V. J. Simple Method for Synthesis of Amides. *J Org Chem* **1971**, *36*.
- (170) Castro, B. D., J. R. Chlorotrisdimethylaminophosphonium Perchlorate - a New Reagent for Peptide Coupling. *Tetrahedron Lett* **1972**, 4747.
- (171) Coste, J. C., J. M. Esterification of Carboxylic-Acids Using Bop or Pybop. *Tetrahedron Lett* **1995**, *36*, 4253-4256.
- (172) Gawne, G. K., G. W.; Sheppard, R. C. Acyloxyphosphonium Salts as Acylating Agents, a New Synthesis of Peptides. *J Am Chem Soc* **1969**, *91*, 5669.
- (173) Yamada, S. T., Y. New Method for Synthesis of Peptides Using Adducts of Phosphorus Compounds and Tetrahalomethanes. *Tetrahedron Lett* **1971**, 3595.
- (174) Coste, J.; Campagne, J.-M. A propos de l'esterification des acides carboxyliques par le BOP ou le PyBOP. *Tetrahedron Letters* **1995**, *36*, 4253-4256.
- (175) Castro, B.; Dormoy, J. R. Le perchlorate de chlorotrisdimethylaminophosphonium: un nouveau reactif pour le couplage peptidique. *Tetrahedron Letters* **1972**, *13*, 4747-4750.
- (176) Yamada, S.-i.; Takeuchi, Y. A new method for the synthesis of peptides using the adducts of phosphorus compounds and tetrahalomethanes. *Tetrahedron Letters* **1971**, *12*, 3595-3598.
- (177) Barstow, L. E.; Hruby, V. J. Simple method for the synthesis of amides. *J. Org. Chem.* **1971**, *36*, 1305-1306.
- (178) Gawne, G.; Kenner, G. W.; Sheppard, R. C. Acyloxyphosphonium salts as acylating agents. Synthesis of peptides. *J. Am. Chem. Soc.* **1969**, *91*, 5669-5671.
- (179) Gausepolh, H.; Piele, H.; Frank, R. W. *Peptides: Chemistry, Structure, and Biology*; ESCOM: Lieden, 1992.
- (180) Schnolzer, M.; Alewood, P.; Jones, A.; Alewood, D.; Kent, S. B. In situ neutralization in Boc-chemistry solid phase peptide synthesis. Rapid, high yield assembly of difficult sequences. *Int J Pept Protein Res* **1992**, *40*, 180-193.

- (181) Castro, B.; Dormoy, J. R.; Evin, G.; Selve, C. Reactifs de couplage peptidique I (1) - l'hexafluorophosphate de benzotriazolyl N-oxytrisdimethylamino phosphonium (B.O.P.). *Tetrahedron Letters* **1975**, *16*, 1219-1222.
- (182) Kim, M. H.; Patel, D. V. "BOP" as a reagent for mild and efficient preparation of esters. *Tetrahedron Letters* **1994**, *35*, 5603-5606.
- (183) Okada, Y. Synthesis of Peptides by Solution Methods. *Current Organic Chemistry Current Organic Chemistry J1 - Current Organic Chemistry* **2001**, *5*, 1.
- (184) Coste, J.; Le-Nguyen, D.; Castro, B. PyBOP(R): A new peptide coupling reagent devoid of toxic by-product. *Tetrahedron Letters* **1990**, *31*, 205-208.
- (185) Coste, J.; Dufour, M.-N.; Pantaloni, A.; Castro, B. Brop: A new reagent for coupling N-methylated amino acids. *Tetrahedron Letters* **1990**, *31*, 669-672.
- (186) Knorr, R.; Trzeciak, A.; Bannwarth, W.; Gillessen, D. New coupling reagents in peptide chemistry. *Tetrahedron Letters* **1989**, *30*, 1927-1930.
- (187) Dourtoglou, V.; Gross, B.; Lambropoulou, V.; Zioudrou, C. O-Benzotriazolyl-N,N,N',N'-tetramethyluronium Hexafluorophosphate as Coupling Reagent for the Synthesis of Peptides of Biological Interest. *Synthesis-Stuttgart* **1984**, 572-574.
- (188) Kaiser, E. C., R. L.; Bossinger, C. D.; Cook, P.I. Color Test for Detection of Free Terminal Amino Groups in the Solid-Phase Synthesis of Peptides. *Analytical Biochemistry* **1970**, *34*, 595-598.
- (189) Christensen, T. Qualitative Test for Monitoring Coupling Completeness in Solid-Phase Peptide Synthesis Using Chloranil. *Acta Chem Scand B- Organic Chemistry and Biochemistry* **1979**, *33*, 763-766.
- (190) Horton, D. A.; Bourne, G. T.; Smythe, M. L. The combinatorial synthesis of bicyclic privileged structures or privileged substructures. *Chem Rev* **2003**, *103*, 893-930.
- (191) Hulme, C.; Peng, J.; Tang, S. Y.; Burns, C. J.; Morize, I. et al. Improved procedure for the solution phase preparation of 1,4-benzodiazepine-2,5-dione libraries via Armstrong's convertible isonitrile and the Ugi reaction. *Journal of Organic Chemistry* **1998**, *63*, 8021-8023.
- (192) Keating, T. A.; Armstrong, R. W. A remarkable two-step synthesis of diverse 1,4-benzodiazepine-2,5-diones using the Ugi four-component condensation. *Journal of Organic Chemistry* **1996**, *61*, 8935-8939.
- (193) Mayer, J. P.; Zhang, J.; Bjergarde, K.; Lenz, D. M.; Gaudino, J. J. Solid phase synthesis of 1,4-benzodiazepine-2,5-diones. *Tetrahedron Letters* **1996**, *37*, 8081-8084.

- (194) Boojamra, C. G.; Burow, K. M.; Thompson, L. A.; Ellman, J. A. Solid-phase synthesis of 1,4-benzodiazepine-2,5-diones. Library preparation and demonstration of synthesis generality. *Journal of Organic Chemistry* **1997**, *62*, 1240-1256.
- (195) Martin, P. K.; Rapoport, H.; Smith, H. W.; Wong, J. L. Synthesis of cyclophenin and isocyclophenin. *J. Org. Chem.* **1969**, *34*, 1359-1363.
- (196) Smith, H.; Wegfahrt, P.; Rapoport, H. The synthesis of cyclophenin. *J. Am. Chem. Soc* **1968**, *90*, 1668-1669.
- (197) White, J. D.; Haefliger, W. E.; Dimsdale, M. J. Stereospecific synthesis of dl-cyclophenin and dl-cyclophenol. *Tetrahedron* **1970**, *26*, 233-242.
- (198) Bunin, B. A.; Plunkett, M. J.; Ellman, J. A. Synthesis and evaluation of 1,4-benzodiazepine libraries. *Combinatorial Chemistry*, 1996; pp 448-465.
- (199) Bunin, B. A.; Plunkett, M. J.; Ellman, J. A. The Combinatorial Synthesis and Chemical and Biological Evaluation of a 1,4-Benzodiazepine Library. *Proceedings of the National Academy of Sciences of the United States of America* **1994**, *91*, 4708-4712.
- (200) Boojamra, C. G.; Burow, K. M.; Ellman, J. A. An Expedient and High-Yielding Method for the Solid-Phase Synthesis of Diverse 1,4-Benzodiazepine-2,5-Diones. *Journal of Organic Chemistry* **1995**, *60*, 5742-5743.
- (201) Bhalay, G.; Blaney, P.; Palmer, V. H.; Baxter, A. D. Solid-phase synthesis of diverse tetrahydro-1,4-benzodiazepine-2-ones. *Tetrahedron Letters* **1997**, *38*, 8375-8378.
- (202) Lee, J.; Gauthier, D.; Rivero, R. A. Solid-phase synthesis of 3,4,5-substituted 1,5-benzodiazepin-2-ones. *Journal of Organic Chemistry* **1999**, *64*, 3060-3065.
- (203) Zhang, J.; Goodloe, W. P.; Lou, B.; Saneii, H. Solid-phase synthesis of tetrahydro-1,4-benzodiazepin-2-one derivatives. *Mol Divers* **2000**, *5*, 127-130.
- (204) Christensen, T. Qualitative Test for Monitoring Coupling Completeness in Solid-Phase Peptide Synthesis Using Chloronil. *Acta Chem Scand B- Organic Chemistry and Biochemistry* **1979**, *33*, 763-766.
- (205) Kaiser, E.; Colescott, R. L.; Bossinger, C. D.; Cook, P. I. Color test for detection of free terminal amino groups in the solid-phase synthesis of peptides. *Anal Biochem* **1970**, *34*, 595-598.
- (206) Shannon, S. K.; Barany, G. Colorimetric monitoring of solid-phase aldehydes using 2,4-dinitrophenylhydrazine. *J Comb Chem* **2004**, *6*, 165-170.
- (207) Gaggini, F.; Porcheddu, A.; Reginato, G.; Rodriguez, M.; Taddei, M. Colorimetric tools for solid-phase organic synthesis. *J Comb Chem* **2004**, *6*, 805-810.

- (208) Merrifield, R. B. Solid-Phase Peptide Syntheses. *Endeavour* **1965**, *24*, 3-7.
- (209) Chen, W.; Shields, T. S.; Stork, P. J.; Cone, R. D. A colorimetric assay for measuring activation of Gs- and Gq-coupled signaling pathways. *Anal Biochem* **1995**, *226*, 349-354.
- (210) Watson, J. D.; Crick, F. H. Molecular structure of nucleic acids; a structure for deoxyribose nucleic acid. *Nature* **1953**, *171*, 737-738.
- (211) Leslie, A. G.; Arnott, S.; Chandrasekaran, R.; Ratliff, R. L. Polymorphism of DNA double helices. *J Mol Biol* **1980**, *143*, 49-72.
- (212) Mandelkern, M.; Elias, J. G.; Eden, D.; Crothers, D. M. The dimensions of DNA in solution. *J Mol Biol* **1981**, *152*, 153-161.
- (213) Benham, C. J.; Mielke, S. P. DNA mechanics. *Annu Rev Biomed Eng* **2005**, *7*, 21-53.
- (214) Wing, R.; Drew, H.; Takano, T.; Broka, C.; Tanaka, S. et al. Crystal structure analysis of a complete turn of B-DNA. *Nature* **1980**, *287*, 755-758.
- (215) Pabo, C. O.; Sauer, R. T. Protein-DNA recognition. *Annu Rev Biochem* **1984**, *53*, 293-321.
- (216) Lu, X. J.; Shakked, Z.; Olson, W. K. A-form conformational motifs in ligand-bound DNA structures. *J Mol Biol* **2000**, *300*, 819-840.
- (217) Wahl, M. C.; Sundaralingam, M. Crystal structures of A-DNA duplexes. *Biopolymers* **1997**, *44*, 45-63.
- (218) Rothenburg, S.; Koch-Nolte, F.; Haag, F. DNA methylation and Z-DNA formation as mediators of quantitative differences in the expression of alleles. *Immunol Rev* **2001**, *184*, 286-298.
- (219) Kleppe, K.; Ohtsuka, E.; Kleppe, R.; Molineux, I.; Khorana, H. G. Studies on polynucleotides. XCVI. Repair replications of short synthetic DNA's as catalyzed by DNA polymerases. *J Mol Biol* **1971**, *56*, 341-361.
- (220) Chien, A.; Edgar, D. B.; Trela, J. M. Deoxyribonucleic acid polymerase from the extreme thermophile *Thermus aquaticus*. *J Bacteriol* **1976**, *127*, 1550-1557.
- (221) Tindall, K. R.; Kunkel, T. A. Fidelity of DNA synthesis by the *Thermus aquaticus* DNA polymerase. *Biochemistry* **1988**, *27*, 6008-6013.
- (222) Lundberg, K. S.; Shoemaker, D. D.; Adams, M. W.; Short, J. M.; Sorge, J. A. et al. High-fidelity amplification using a thermostable DNA polymerase isolated from *Pyrococcus furiosus*. *Gene* **1991**, *108*, 1-6.

- (223) Sanger, F.; Nicklen, S.; Coulson, A. R. DNA sequencing with chain-terminating inhibitors. *Proc Natl Acad Sci U S A* **1977**, *74*, 5463-5467.
- (224) Graham, F. L.; Smiley, J.; Russell, W. C.; Nairn, R. Characteristics of a human cell line transformed by DNA from human adenovirus type 5. *J Gen Virol* **1977**, *36*, 59-74.
- (225) Louis, N.; Eveleigh, C.; Graham, F. L. Cloning and sequencing of the cellular-viral junctions from the human adenovirus type 5 transformed 293 cell line. *Virology* **1997**, *233*, 423-429.
- (226) Shaw, G.; Morse, S.; Ararat, M.; Graham, F. L. Preferential transformation of human neuronal cells by human adenoviruses and the origin of HEK 293 cells. *Faseb J* **2002**, *16*, 869-871.
- (227) Graham, F. L.; van der Eb, A. J. A new technique for the assay of infectivity of human adenovirus 5 DNA. *Virology* **1973**, *52*, 456-467.
- (228) Schimmer, B. P.; Kwan, W. K.; Tsao, J.; Qiu, R. Adrenocorticotropin-resistant mutants of the Y1 adrenal cell line fail to express the adrenocorticotropin receptor. *J Cell Physiol* **1995**, *163*, 164-171.
- (229) Schimmer, B. P. Adenylate cyclase activity in adrenocorticotropin hormone-sensitive and mutant adrenocortical tumor cell lines. *J Biol Chem* **1972**, *247*, 3134-3138.
- (230) Schild, H. O. pA, A new scale for the measurement of drug antagonism. *Brit. J. Pharmacol.* **1947**, *2*, 189-206.
- (231) de Wet, J. R.; Wood, K. V.; DeLuca, M.; Helinski, D. R.; Subramani, S. Firefly luciferase gene: structure and expression in mammalian cells. *Mol Cell Biol* **1987**, *7*, 725-737.
- (232) DeLuca, M.; McElroy, W. D. Two kinetically distinguishable ATP sites in firefly luciferase. *Biochem Biophys Res Commun* **1984**, *123*, 764-770.
- (233) Gorman, C. M.; Moffat, L. F.; Howard, B. H. Recombinant genomes which express chloramphenicol acetyltransferase in mammalian cells. *Mol Cell Biol* **1982**, *2*, 1044-1051.
- (234) Gorman, C. M.; Merlino, G. T.; Willingham, M. C.; Pastan, I.; Howard, B. H. The Rous sarcoma virus long terminal repeat is a strong promoter when introduced into a variety of eukaryotic cells by DNA-mediated transfection. *Proc Natl Acad Sci U S A* **1982**, *79*, 6777-6781.
- (235) Spengler, D.; Waeber, C.; Pantaloni, C.; Holsboer, F.; Bockaert, J. et al. Differential signal transduction by five splice variants of the PACAP receptor. *Nature* **1993**, *365*, 170-175.

- (236) Spengler, D.; Rupprecht, R.; Van, L. P.; Holsboer, F. Identification and characterization of a 3',5'-cyclic adenosine monophosphate-responsive element in the human corticotropin-releasing hormone gene promoter. *Mol Endocrinol* **1992**, *6*, 1931-1941.
- (237) Hollenberg, S. M.; Evans, R. M. Multiple and cooperative trans-activation domains of the human glucocorticoid receptor. *Cell* **1988**, *55*, 899-906.
- (238) Fluck, C. E.; Martens, J. W.; Conte, F. A.; Miller, W. L. Clinical, genetic, and functional characterization of adrenocorticotropin receptor mutations using a novel receptor assay. *J Clin Endocrinol Metab* **2002**, *87*, 4318-4323.
- (239) Dougherty, D. A. Cation-pi interactions in chemistry and biology: a new view of benzene, Phe, Tyr, and Trp. *Science* **1996**, *271*, 163-168.
- (240) Dougherty, D. A. Cation-pi interactions involving aromatic amino acids. *J Nutr* **2007**, *137*, 1504S-1508S; discussion 1516S-1517S.
- (241) Dennis, G. R.; Ritchie, G. L. D. Dilute-solution field gradient-induced birefringence and molecular quadrupole moment of benzene. *J. Phys. Chem.* **1991**, *95*, 656-660.
- (242) Sunner, J.; Nishizawa, K.; Kebarle, P. Ion-solvent molecule interactions in the gas phase. The potassium ion and benzene. *J. Phys. Chem.* **1981**, *85*, 1814-1820.
- (243) Rodham, D. A.; Suzuki, S.; Suenram, R. D.; Lovas, F. J.; Dasgupta, S. et al. Hydrogen bonding in the benzene-ammonia dimer. **1993**, *362*, 735-737.
- (244) Suzuki, S.; Green, P. G.; Bumgarner, R. E.; Dasgupta, S.; Goddard, W. A., 3rd et al. Benzene Forms Hydrogen Bonds with Water. *Science* **1992**, *257*, 942-945.
- (245) Shepodd, T. J.; Petti, M. A.; Dougherty, D. A. Tight, oriented binding of an aliphatic guest by a new class of water-soluble molecules with hydrophobic binding sites. *J. Am. Chem. Soc.* **1986**, *108*, 6085-6087.
- (246) Sun, D. P.; Sauer, U.; Nicholson, H.; Matthews, B. W. Contributions of engineered surface salt bridges to the stability of T4 lysozyme determined by directed mutagenesis. *Biochemistry* **1991**, *30*, 7142-7153.
- (247) Waldburger, C. D.; Schildbach, J. F.; Sauer, R. T. Are buried salt bridges important for protein stability and conformational specificity? *Nat Struct Biol* **1995**, *2*, 122-128.
- (248) Hendsch, Z. S.; Tidor, B. Do salt bridges stabilize proteins? A continuum electrostatic analysis. *Protein Sci* **1994**, *3*, 211-226.
- (249) Duffy, E. M.; Kowalczyk, P. J.; Jorgensen, W. L. Do denaturants interact with aromatic hydrocarbons in water? *J. Am. Chem. Soc.* **1993**, *115*, 9271-9275.

- (250) Mitchell, J. B.; Nandi, C. L.; McDonald, I. K.; Thornton, J. M.; Price, S. L. Amino/aromatic interactions in proteins: is the evidence stacked against hydrogen bonding? *J Mol Biol* **1994**, *239*, 315-331.
- (251) Gallivan, J. P.; Dougherty, D. A. Cation- π interactions in structural biology. *Proc Natl Acad Sci U S A* **1999**, *96*, 9459-9464.
- (252) Mecozzi, S.; West, A. P.; Dougherty, D. A. Cation- π Interactions in Simple Aromatics: Electrostatics Provide a Predictive Tool. *J. Am. Chem. Soc.* **1996**, *118*, 2307-2308.
- (253) Mecozzi, S.; West, A. P., Jr.; Dougherty, D. A. Cation- π interactions in aromatics of biological and medicinal interest: electrostatic potential surfaces as a useful qualitative guide. *Proc Natl Acad Sci U S A* **1996**, *93*, 10566-10571.
- (254) Irani, B. G. H., Jerry R.; Todorovic, Aleksandar; Wilczynski, Andrzej M.; Joseph, Christine G.; Wilson, Krista R.; Haskell-Luevano, Carrie Progress in the Development of Melanocortin Receptor Selective Ligands. *Current Pharmaceutical Designs* **2004**, *Accepted*.
- (255) Al-Obeidi, F.; Hadley, M. E.; Pettitt, B. M.; Hruby, V. J. Design of a New Class of Superpotent Cyclic alpha-Melanotropins Based on Quenched Dynamic Simulations. *J. Am. Chem. Soc.* **1989**, *11*, 3413-3416.
- (256) Willard, D. H.; Bodnar, W.; Harris, C.; Kiefer, L.; Nichols, J. S. et al. Agouti structure and function: characterization of a potent alpha-melanocyte stimulating hormone receptor antagonist. *Biochemistry*. **1995**, *34*, 12341-12346.
- (257) Schioth, H. B.; Muceniece, R.; Mutulis, F.; Prusis, P.; Lindeberg, G. et al. Selectivity of Cyclic [-Nal7] and [-Phe7] Substituted MSH Analogues for the Melanocortin Receptor Subtypes. *Peptides* **1997**, *18*, 1009-1013.
- (258) Hruby, V. J.; Lu, D. S.; Sharma, S. D.; Castrucci, A. D.; Kesterson, R. A. et al. Cyclic Lactam Alpha-Melanotropin Analogs of Ac-Nle(4)- Cyclo[Asp(5),D-Phe(7),Lys(10)] Alpha-Melanocyte-Stimulating Hormone-(4-10)-NH₂ with Bulky Aromatic-Amino-Acids at Position- 7 Show High Antagonist Potency and Selectivity at Specific Melanocortin Receptors. *Journal of Medicinal Chemistry* **1995**, *38*, 3454-3461.
- (259) Schioth, H. B.; Mutulis, F.; Muceniece, R.; Prusis, P.; Wikberg, J. E. Discovery of novel melanocortin4 receptor selective MSH analogues. *Br. J. Pharmacol.* **1998**, *124*, 75-82.
- (260) Kask, A.; Mutulis, F.; Muceniece, R.; Pakla, R.; Mutule, I. et al. Discovery of a novel superpotent and selective melanocortin-4 receptor antagonist (HS024): evaluation in vitro and in vivo. *Endocrinol.* **1998**, *139*, 5006-5014.

- (261) Grieco, P.; Lavecchia, A.; Cai, M.; Trivedi, D.; Weinberg, D. et al. Structure-activity studies of the melanocortin peptides: discovery of potent and selective affinity antagonists for the hMC3 and hMC4 receptors. *J. Med. Chem.* **2002**, *45*, 5287-5294.
- (262) al-Obeidi, F.; Hruby, V. J.; Hadley, M. E.; Sawyer, T. K.; Castrucci, A. M. Design, synthesis, and biological activities of a potent and selective alpha-melanotropin antagonist. *Int J Pept Protein Res* **1990**, *35*, 228-234.
- (263) Hruby, V. J.; Sharma, S. D.; Toth, K.; Jaw, J. Y.; al-Obeidi, F. et al. Design, synthesis, and conformation of superpotent and prolonged acting melanotropins. *Ann N Y Acad Sci* **1993**, *680*, 51-63.
- (264) Kask, A.; Mutulis, F.; Muceniece, R.; Pakkla, R.; Mutule, I. et al. Discovery of a novel superpotent and selective melanocortin-4 receptor antagonist (HS024): Evaluation in vitro and in vivo. *Endocrinology* **1998**, *139*, 5006-5014.
- (265) Bednarek, M. A.; MacNeil, T.; Kalyani, R. N.; Tang, R.; Van der Ploeg, L. H. T. et al. Analogs of Lactam Derivatives of [alpha]-Melanotropin with Basic and Acidic Residues. *Biochemical and Biophysical Research Communications* **2000**, *272*, 23-28.
- (266) Bednarek, M. A.; MacNeil, T.; Kalyani, R. N.; Tang, R.; Van der Ploeg, L. H. T. et al. Selective, High Affinity Peptide Antagonists of α -Melanotropin Action at Human Melanocortin Receptor 4: Their Synthesis and Biological Evaluation in Vitro. *J. Med. Chem.* **2001**, *44*, 3665-3672.
- (267) Chen, M.; Georgeson, K. E.; Harmon, C. M.; Haskell-Luevano, C.; Yang, Y. Functional characterization of the modified melanocortin peptides responsible for ligand selectivity at the human melanocortin receptors. *Peptides* **2006**, *27*, 2836-2845.
- (268) Haskell-Luevano, C.; Lim, S.; Yuan, W.; Cone, R. D.; Hruby, V. J. Structure activity studies of the melanocortin antagonist SHU9119 modified at the 6, 7, 8, and 9 positions. *Peptides* **2000**, *21*, 49-57.
- (269) Grieco, P.; Cai, M.; Han, G.; Trivedi, D.; Campiglia, P. et al. Further structure-activity studies of lactam derivatives of MT-II and SHU-9119: Their activity and selectivity at human melanocortin receptors 3, 4, and 5. *Peptides* **2007**, *28*, 1191-1196.
- (270) Grieco, P.; Rossi, C.; Gatti, S.; Colombo, G.; Carlin, A. et al. Design and Synthesis of Melanocortin Peptides with Candidacidal and Anti-TNF- α Properties. *J. Med. Chem.* **2005**, *48*, 1384-1388.
- (271) Grieco, P.; Han, G.; Weinberg, D.; MacNeil, T.; Van der Ploeg, L. H. T. et al. Design and Synthesis of Highly Potent and Selective Melanotropin Analogues of SHU9119 Modified at Position 6. *Biochemical and Biophysical Research Communications* **2002**, *292*, 1075-1080.

- (272) Kask, A.; Rago, L.; Mutulis, F.; Pahkla, R.; Wikberg, J. E. et al. Selective antagonist for the melanocortin 4 receptor (HS014) increases food intake in free-feeding rats. *Biochem. Biophys. Res. Commun.* **1998**, *245*, 90-93.
- (273) Schioth, H. B.; Muceniece, R.; Mutulis, F.; Bouiffour, A. A.; Mutule, I. et al. Further pharmacological characterization of the selective melanocortin 4 receptor antagonist HS014: comparison with SHU9119. *Neuropeptides* **1999**, *33*, 191-196.
- (274) Cheung, A. W.; Danho, W.; Swistok, J.; Qi, L.; Kurylko, G. et al. Structure-activity relationship of linear peptide Bu-His-DPhe-Arg-Trp-Gly-NH(2) at the human melanocortin-1 and -4 receptors: arginine substitution. *Bioorg Med Chem Lett* **2002**, *12*, 2407-2410.
- (275) Sahm, U. G.; Olivier, G. W. J.; Branch, S. K.; Moss, S. H.; Pouton, C. W. Synthesis and biological evaluation of [alpha]-MSH analogues substituted with alanine. *Peptides* **1994**, *15*, 1297-1302.
- (276) Singh, J.; Thornton, J. M. SIRIUS. An automated method for the analysis of the preferred packing arrangements between protein groups. *J Mol Biol* **1990**, *211*, 595-615.
- (277) Shi, Z.; Olson, C. A.; Kallenbach, N. R. Cation-pi interaction in model alpha-helical peptides. *J Am Chem Soc* **2002**, *124*, 3284-3291.
- (278) Li, H.; Ilin, S.; Wang, W.; Duncan, E. M.; Wysocka, J. et al. Molecular basis for site-specific read-out of histone H3K4me3 by the BPTF PHD finger of NURF. *Nature* **2006**, *442*, 91-95.
- (279) Pena, P. V.; Davrazou, F.; Shi, X.; Walter, K. L.; Verkhusha, V. V. et al. Molecular mechanism of histone H3K4me3 recognition by plant homeodomain of ING2. *Nature* **2006**, *442*, 100-103.
- (280) Gromiha, M. M.; Santhosh, C.; Ahmad, S. Structural analysis of cation-pi interactions in DNA binding proteins. *Int J Biol Macromol* **2004**, *34*, 203-211.
- (281) Mian, I. S.; Bradwell, A. R.; Olson, A. J. Structure, function and properties of antibody binding sites. *J Mol Biol* **1991**, *217*, 133-151.
- (282) Golinelli-Pimpaneau, B.; Goncalves, O.; Dintinger, T.; Blanchard, D.; Knossow, M. et al. Structural evidence for a programmed general base in the active site of a catalytic antibody. *Proc Natl Acad Sci U S A* **2000**, *97*, 9892-9895.
- (283) Shulman, H.; Makarov, C.; Ogawa, A. K.; Romesberg, F.; Keinan, E. Chemically Reactive Immunogens Lead to Functional Convergence of the Immune Response. *J. Am. Chem. Soc.* **2000**, *122*, 10743-10753.

- (284) Gromiha, M. M.; Suwa, M. Structural analysis of residues involving cation- π interactions in different folding types of membrane proteins. *Int J Biol Macromol* **2005**, *35*, 55-62.
- (285) Gromiha, M. M. Influence of cation- π interactions in different folding types of membrane proteins. *Biophys Chem* **2003**, *103*, 251-258.
- (286) Sussman, J. L.; Harel, M.; Frolow, F.; Oefner, C.; Goldman, A. et al. Atomic structure of acetylcholinesterase from *Torpedo californica*: a prototypic acetylcholine-binding protein. *Science* **1991**, *253*, 872-879.
- (287) Lester, H. A.; Dibas, M. I.; Dahan, D. S.; Leite, J. F.; Dougherty, D. A. Cys-loop receptors: new twists and turns. *Trends Neurosci* **2004**, *27*, 329-336.
- (288) Sine, S. M.; Engel, A. G. Recent advances in Cys-loop receptor structure and function. *Nature* **2006**, *440*, 448-455.
- (289) Zhong, W.; Gallivan, J. P.; Zhang, Y.; Li, L.; Lester, H. A. et al. From ab initio quantum mechanics to molecular neurobiology: a cation- π binding site in the nicotinic receptor. *Proc Natl Acad Sci U S A* **1998**, *95*, 12088-12093.
- (290) Beene, D. L.; Brandt, G. S.; Zhong, W.; Zacharias, N. M.; Lester, H. A. et al. Cation- π interactions in ligand recognition by serotonergic (5-HT_{3A}) and nicotinic acetylcholine receptors: the anomalous binding properties of nicotine. *Biochemistry* **2002**, *41*, 10262-10269.
- (291) Brejc, K.; van Dijk, W. J.; Klaassen, R. V.; Schuurmans, M.; van Der Oost, J. et al. Crystal structure of an ACh-binding protein reveals the ligand-binding domain of nicotinic receptors. *Nature* **2001**, *411*, 269-276.
- (292) Cashin, A. L.; Petersson, E. J.; Lester, H. A.; Dougherty, D. A. Using physical chemistry to differentiate nicotinic from cholinergic agonists at the nicotinic acetylcholine receptor. *J Am Chem Soc* **2005**, *127*, 350-356.
- (293) Melis, C.; Chau, P. L.; Price, K. L.; Lummis, S. C.; Molteni, C. Exploring the binding of serotonin to the 5-HT₃ receptor by density functional theory. *J Phys Chem B* **2006**, *110*, 26313-26319.
- (294) Spier, A. D.; Lummis, S. C. The role of tryptophan residues in the 5-Hydroxytryptamine(3) receptor ligand binding domain. *J Biol Chem* **2000**, *275*, 5620-5625.
- (295) Lummis, S. C.; D, L. B.; Harrison, N. J.; Lester, H. A.; Dougherty, D. A. A cation- π binding interaction with a tyrosine in the binding site of the GABAC receptor. *Chem Biol* **2005**, *12*, 993-997.

- (296) Boileau, A. J.; Evers, A. R.; Davis, A. F.; Czajkowski, C. Mapping the agonist binding site of the GABAA receptor: evidence for a beta-strand. *J Neurosci* **1999**, *19*, 4847-4854.
- (297) Leite, J. F.; Cascio, M. Structure of ligand-gated ion channels: critical assessment of biochemical data supports novel topology. *Mol Cell Neurosci* **2001**, *17*, 777-792.
- (298) Padgett, C. L.; Hanek, A. P.; Lester, H. A.; Dougherty, D. A.; Lummis, S. C. Unnatural amino acid mutagenesis of the GABA(A) receptor binding site residues reveals a novel cation-pi interaction between GABA and beta 2Tyr97. *J Neurosci* **2007**, *27*, 886-892.
- (299) Ma, J. C.; Dougherty, D. A. The Cationminus signpi Interaction. *Chem Rev* **1997**, *97*, 1303-1324.
- (300) Inoue, Y.; Nakamura, N.; Inagami, T. A review of mutagenesis studies of angiotensin II type 1 receptor, the three-dimensional receptor model in search of the agonist and antagonist binding site and the hypothesis of a receptor activation mechanism. *J Hypertens* **1997**, *15*, 703-714.
- (301) Khandelia, H.; Kaznessis, Y. N. Cation-pi interactions stabilize the structure of the antimicrobial peptide indolicidin near membranes: molecular dynamics simulations. *J Phys Chem B* **2007**, *111*, 242-250.
- (302) Yamada, S. Intramolecular cation-pi interaction in organic synthesis. *Org Biomol Chem* **2007**, *5*, 2903-2912.
- (303) Sawyer, T. K.; Hruby, V. J.; Wilkes, B. C.; Draelos, M. T.; Hadley, M. E. et al. Comparative biological activities of highly potent active-site analogues of alpha-melanotropin. *J. Med. Chem.* **1982**, *25*, 1022-1027.
- (304) Ellman, J. A. Design, Synthesis, and Evaluation of Small-Molecule Libraries. *Acc. Chem. Res.* **1996**, *29*, 132-143.
- (305) Gordon, E. M.; Barrett, R. W.; Dower, W. J.; Fodor, S. P. A.; and Gallop, M. A. Applications of Combinatorial Technologies to Drug Discovery. 2. Combinatorial Organic Synthesis, Library Screening Strategies, and Future Directions. *J. Med Chem.* **1994**, *37*, 1385-1401.
- (306) Terrett, N. K.; Gardner, M.; Gordon, D. W.; Kobylecki, R. J.; Steele, J. Combinatorial synthesis-The design of compound libraries and their application to drug discovery. *Tetrahedron* **1995**, *51*, 1385-1401.
- (307) Nicolaou, K. C.; Pfefferkorn, J. A.; Roecker, A. J.; Cao, G. Q.; Barluenga, S. et al. Natural product-like combinatorial libraries based on privileged structures. 1. General principles and solid-phase synthesis of benzopyrans. *Journal of the American Chemical Society* **2000**, *122*, 9939-9953.

- (308) Nikiforovich, G. V.; Sharma, S. D.; Hadley, M. E.; Hruby, V. J. Studies of conformational isomerism in alpha-melanocyte stimulating hormone by design of cyclic analogues. *Biopolymers* **1998**, *46*, 155-167.
- (309) Prabhu, N. V.; Perkyns, J. S.; Pettitt, B. M. Modeling of alpha-MSH conformations with implicit solvent. *J Pept Res* **1999**, *54*, 394-407.
- (310) Prabhu, N. V.; Perkyns, J. S.; Pettitt, B. M.; Hruby, V. J. Structure and dynamics of alpha-MSH using DRISM integral equation theory and stochastic dynamics. *Biopolymers* **1999**, *50*, 255-272.
- (311) Willoughby, C. A.; Hutchins, S. M.; Rosauer, K. G.; Dhar, M. J.; Chapman, K. T. et al. Combinatorial synthesis of 3-(amidoalkyl) and 3-(aminoalkyl)-2-arylindole derivatives: discovery of potent ligands for a variety of G-protein coupled receptors. *Bioorg Med Chem Lett* **2002**, *12*, 93-96.
- (312) Bondensgaard, K.; Ankersen, M.; Thogersen, H.; Hansen, B. S.; Wulff, B. S. et al. Recognition of privileged structures by G-protein coupled receptors. *J Med Chem* **2004**, *47*, 888-899.
- (313) Dyck, B.; Parker, J.; Phillips, T.; Carter, L.; Murphy, B. et al. Aryl piperazine melanocortin MC4 receptor agonists. *Bioorg Med Chem Lett* **2003**, *13*, 3793-3796.
- (314) Arasasingham, P. N.; Fotsch, C.; Ouyang, X.; Norman, M. H.; Kelly, M. G. et al. Structure-activity relationship of (1-aryl-2-piperazinylethyl)piperazines: antagonists for the AGRP/melanocortin receptor binding. *J Med Chem* **2003**, *46*, 9-11.
- (315) Richardson, T. I.; Ornstein, P. L.; Briner, K.; Fisher, M. J.; Backer, R. T. et al. Synthesis and structure-activity relationships of novel arylpiperazines as potent and selective agonists of the melanocortin subtype-4 receptor. *J. Med. Chem.* **2004**, *47*, 744-755.
- (316) Xi, N.; Hale, C.; Kelly, M. G.; Norman, M. H.; Stec, M. et al. Synthesis of novel melanocortin 4 receptor agonists and antagonists containing a succinamide core. *Bioorg. Med. Chem. Lett.* **2004**, *14*, 377-381.
- (317) Sebhat, I. K.; Martin, W. J.; Ye, Z.; Barakat, K.; Mosley, R. T. et al. Design and pharmacology of N-[(3R)-1,2,3,4-tetrahydroisoquinolinium-3-ylcarbonyl]-(1R)-1-(4-chlorobenzyl)-2-[4-cyclohexyl-4-(1H-1,2,4-triazol-1-ylmethyl)piperidin-1-yl]-2-oxoethylamine (1), a potent, selective, melanocortin subtype-4 receptor agonist. *J Med Chem* **2002**, *45*, 4589-4593.
- (318) Herpin, T. F.; Yu, G.; Carlson, K. E.; Morton, G. C.; Wu, X. et al. Discovery of tyrosine-based potent and selective melanocortin-1 receptor small-molecule agonists with anti-inflammatory properties. *J Med Chem* **2003**, *46*, 1123-1126.

- (319) Ujjainwalla, F.; Warner, D.; Walsh, T. F.; Wyvratt, M. J.; Zhou, C. et al. Design and syntheses of melanocortin subtype-4 receptor agonists: evolution of the pyridazinone archetype. *Bioorg Med Chem Lett* **2003**, *13*, 4431-4435.
- (320) Kulesza, A.; Ebetino, F. H.; Mishra, R. K.; Cross-Doersen, D.; Mazur, A. W. Synthesis of 2,4,5-trisubstituted tetrahydropyrans as peptidomimetic scaffolds for melanocortin receptor ligands. *Org Lett* **2003**, *5*, 1163-1166.
- (321) Mazur, A. W.; Kulesza, A.; Mishra, R. K.; Cross-Doersen, D.; Russell, A. F. et al. Novel tetrahydropyran-based peptidomimetics from a bioisosteric transformation of a tripeptide. Evidence of their activity at melanocortin receptors. *Bioorg Med Chem* **2003**, *11*, 3053-3063.
- (322) Pan, K.; Scott, M. K.; Lee, D. H.; Fitzpatrick, L. J.; Crooke, J. J. et al. 2,3-Diaryl-5-anilino[1,2,4]thiadiazoles as melanocortin MC4 receptor agonists and their effects on feeding behavior in rats. *Bioorg Med Chem* **2003**, *11*, 185-192.
- (323) Vos, T. J.; Caracoti, A.; Che, J. L.; Dai, M.; Farrer, C. A. et al. Identification of 2-[2-[2-(5-bromo-2-methoxyphenyl)-ethyl]-3-fluorophenyl]-4,5-dihydro-1H-imidazole (ML00253764), a small molecule melanocortin 4 receptor antagonist that effectively reduces tumor-induced weight loss in a mouse model. *J Med Chem* **2004**, *47*, 1602-1604.
- (324) Cain, J. P.; Mayorov, A. V.; Cai, M.; Wang, H.; Tan, B. et al. Design, synthesis, and biological evaluation of a new class of small molecule peptide mimetics targeting the melanocortin receptors. *Bioorg Med Chem Lett* **2006**, *16*, 5462-5467.
- (325) Al-Obeidi, F.; O'Connor, S. D.; Job, C.; Hruby, V. J.; Pettitt, B. M. NMR and quenched molecular dynamics studies of superpotent linear and cyclic alpha-melanotropins. *J Pept Res* **1998**, *51*, 420-431.
- (326) Hata, M.; Marshall, G. R. Do benzodiazepines mimic reverse-turn structures? *J Comput Aided Mol Des* **2006**, *20*, 321-331.
- (327) Ripka, A. S.; Rich, D. H. Peptidomimetic design. *Curr Opin Chem Biol* **1998**, *2*, 441-452.
- (328) Richardson, T. I.; Ornstein, P. L.; Briner, K.; Fisher, M. J.; Backer, R. T. et al. Synthesis and structure-activity relationships of novel arylpiperazines as potent and selective agonists of the melanocortin subtype-4 receptor. *J Med Chem* **2004**, *47*, 744-755.
- (329) Xi, N.; Hale, C.; Kelly, M. G.; Norman, M. H.; Stec, M. et al. Synthesis of novel melanocortin 4 receptor agonists and antagonists containing a succinamide core. *Bioorg Med Chem Lett* **2004**, *14*, 377-381.
- (330) Bunin, B. A.; Plunkett, M. J.; Ellman, J. A.; Bray, A. M. The synthesis of a 1680 member 1,4-benzodiazepine library. *New Journal of Chemistry* **1997**, *21*, 125-130.

- (331) Liesch, J. M.; Hensens, O. D.; Springer, J. P.; Chang, R. S.; Lotti, V. J. Asperlicin, a novel non-peptidal cholecystokinin antagonist from *Aspergillus alliaceus*. Structure elucidation. *J Antibiot (Tokyo)* **1985**, *38*, 1638-1641.
- (332) Goetz, M. A.; Lopez, M.; Monaghan, R. L.; Chang, R. S.; Lotti, V. J. et al. Asperlicin, a novel non-peptidal cholecystokinin antagonist from *Aspergillus alliaceus*. Fermentation, isolation and biological properties. *J Antibiot (Tokyo)* **1985**, *38*, 1633-1637.
- (333) Chang, R. S.; Lotti, V. J.; Monaghan, R. L.; Birnbaum, J.; Stapley, E. O. et al. A potent nonpeptide cholecystokinin antagonist selective for peripheral tissues isolated from *Aspergillus alliaceus*. *Science* **1985**, *230*, 177-179.
- (334) Migaud, M.; Roques, B. P.; Durieux, C. Effects of cholecystokinin octapeptide and BC 264, a potent and selective CCK-B agonist on aspartate and glutamate release from rat hippocampal slices. *Neuropharmacology* **1994**, *33*, 737-743.
- (335) Durieux, C.; Ruiz-Gayo, M.; Roques, B. P. In vivo binding affinities of cholecystokinin agonists and antagonists determined using the selective CCKB agonist [³H]pBC 264. *Eur J Pharmacol* **1991**, *209*, 185-193.
- (336) Lin, C. W.; Holladay, M. W.; Barrett, R. W.; Wolfram, C. A.; Miller, T. R. et al. Distinct requirements for activation at CCK-A and CCK-B/gastrin receptors: studies with a C-terminal hydrazide analogue of cholecystokinin tetrapeptide (30-33). *Mol Pharmacol* **1989**, *36*, 881-886.
- (337) Lin, C. W.; Holladay, M. W.; Witte, D. G.; Miller, T. R.; Wolfram, C. A. et al. A71378: a CCK agonist with high potency and selectivity for CCK-A receptors. *Am J Physiol* **1990**, *258*, G648-651.
- (338) Lin, C. W.; Shiosaki, K.; Miller, T. R.; Witte, D. G.; Bianchi, B. R. et al. Characterization of two novel cholecystokinin tetrapeptide (30-33) analogues, A-71623 and A-70874, that exhibit high potency and selectivity for cholecystokinin-A receptors. *Mol Pharmacol* **1991**, *39*, 346-351.
- (339) Shiosaki, K.; Lin, C. W.; Kopecka, H.; Craig, R.; Wagenaar, F. L. et al. Development of CCK-tetrapeptide analogues as potent and selective CCK-A receptor agonists. *J Med Chem* **1990**, *33*, 2950-2952.
- (340) Cheng, M. F.; Fang, J. M. Liquid-phase combinatorial synthesis of 1,4-benzodiazepine-2,5-diones as the candidates of endothelin receptor antagonism. *J Comb Chem* **2004**, *6*, 99-104.
- (341) Lu, D.; Haskell-Luevano, C.; Våge, D. I.; Cone, R. Functional variants of the MSH receptor (MC1R), agouti, and their effects on mammalian pigmentation. *G-proteins, receptors, and disease*; The Humana Press, Inc.: New Jersey, 1997; pp 231-259.

- (342) Chai, B. X.; Pogozeva, I. D.; Lai, Y. M.; Li, J. Y.; Neubig, R. R. et al. Receptor-antagonist interactions in the complexes of agouti and agouti-related protein with human melanocortin 1 and 4 receptors. *Biochemistry* **2005**, *44*, 3418-3431.
- (343) Vecchietti, V.; Clarke, G. D.; Colle, R.; Giardina, G.; Petrone, G. et al. (1S)-1-(aminomethyl)-2-(arylacetyl)-1,2,3,4-tetrahydroisoquinoline and heterocycle-condensed tetrahydropyridine derivatives: members of a novel class of very potent kappa opioid analgesics. *J Med Chem* **1991**, *34*, 2624-2633.
- (344) Barlow, J. J.; Blackburn, T. P.; Costello, G. F.; James, R.; Le Count, D. J. et al. Structure/activity studies related to 2-(3,4-dichlorophenyl)-N-methyl-N-[2-(1-pyrrolidinyl)-1-substituted-ethyl]acetamides: a novel series of potent and selective kappa-opioid agonists. *J Med Chem* **1991**, *34*, 3149-3158.
- (345) Clark, C. R.; Halfpenny, P. R.; Hill, R. G.; Horwell, D. C.; Hughes, J. et al. Highly selective kappa opioid analgesics. Synthesis and structure-activity relationships of novel N-[(2-aminocyclohexyl)aryl]acetamide and N-[(2-aminocyclohexyl)aryloxy]acetamide derivatives. *J Med Chem* **1988**, *31*, 831-836.
- (346) Lavecchia, A.; Greco, G.; Novellino, E.; Vittorio, F.; Ronsisvalle, G. Modeling of kappa-opioid receptor/agonists interactions using pharmacophore-based and docking simulations. *J Med Chem* **2000**, *43*, 2124-2134.
- (347) Wilczynski, A.; Wilson, K. R.; Scott, J. W.; Edison, A. S.; Haskell-Luevano, C. Structure-activity relationships of the unique and potent agouti-related protein (AGRP)-melanocortin chimeric Tyr-c[beta-Asp-His-DPhe-Arg-Trp-Asn-Ala-Phe-Dpr]-Tyr-NH₂ peptide template. *J Med Chem* **2005**, *48*, 3060-3075.
- (348) Vamvakopoulos, N. C.; Rojas, K.; Overhauser, J.; Durkin, A. S.; Nierman, W. C. et al. Mapping the human melanocortin 2 receptor (adrenocorticotrophic hormone receptor; ACTHR) gene (MC2R) to the small arm of chromosome 18 (18p11.21-pter). *Genomics* **1993**, *18*, 454-455.
- (349) Slominski, A.; Ermak, G.; Mihm, M. ACTH receptor, CYP11A1, CYP17 and CYP21A2 genes are expressed in skin. *J Clin Endocrinol Metab* **1996**, *81*, 2746-2749.
- (350) Lin, C. J.; Jorge, A. A.; Latronico, A. C.; Marui, S.; Fragoso, M. C. et al. Origin of an ovarian steroid cell tumor causing isosexual pseudoprecocious puberty demonstrated by the expression of adrenal steroidogenic enzymes and adrenocorticotropin receptor. *J Clin Endocrinol Metab* **2000**, *85*, 1211-1214.
- (351) Boston, B. A.; Cone, R. D. Characterization of melanocortin receptor subtype expression in murine adipose tissues and in the 3T3-L1 cell line. *Endocrinology* **1996**, *137*, 2043-2050.

- (352) Begeot, M.; Saez, J. M. Melanocortins and Adrenocortical Function. *The Melanocortin Receptors*; Humana Press, Inc.: Totowa, NJ, 2000; pp 75-107.
- (353) Hofmann, K.; Wingender, W.; Finn, F. M. Correlation of adrenocorticotrophic activity of ACTH analogs with degree of binding to an adrenal cortical particulate preparation. *Proc. Natl. Acad. Sci. U S A* **1970**, *67*, 829-836.
- (354) McLatchie, L. M.; Fraser, N. J.; Main, M. J.; Wise, A.; Brown, J. et al. RAMPs regulate the transport and ligand specificity of the calcitonin-receptor-like receptor. *Nature* **1998**, *393*, 333-339.
- (355) Christopoulos, G.; Perry, K. J.; Morfis, M.; Tilakaratne, N.; Gao, Y. et al. Multiple amylin receptors arise from receptor activity-modifying protein interaction with the calcitonin receptor gene product. *Mol Pharmacol* **1999**, *56*, 235-242.
- (356) Hilairret, S.; Belanger, C.; Bertrand, J.; Laperriere, A.; Foord, S. M. et al. Agonist-promoted internalization of a ternary complex between calcitonin receptor-like receptor, receptor activity-modifying protein 1 (RAMP1), and beta-arrestin. *J Biol Chem* **2001**, *276*, 42182-42190.
- (357) Hilairret, S.; Foord, S. M.; Marshall, F. H.; Bouvier, M. Protein-protein interaction and not glycosylation determines the binding selectivity of heterodimers between the calcitonin receptor-like receptor and the receptor activity-modifying proteins. *J Biol Chem* **2001**, *276*, 29575-29581.
- (358) Leuthauser, K.; Gujer, R.; Aldecoa, A.; McKinney, R. A.; Muff, R. et al. Receptor-activity-modifying protein 1 forms heterodimers with two G-protein-coupled receptors to define ligand recognition. *Biochem J* **2000**, *351 Pt 2*, 347-351.
- (359) Kuwasako, K.; Shimekake, Y.; Masuda, M.; Nakahara, K.; Yoshida, T. et al. Visualization of the calcitonin receptor-like receptor and its receptor activity-modifying proteins during internalization and recycling. *J Biol Chem* **2000**, *275*, 29602-29609.
- (360) Foord, S. M.; Marshall, F. H. RAMPs: accessory proteins for seven transmembrane domain receptors. *Trends Pharmacol Sci* **1999**, *20*, 184-187.
- (361) Xu, A.; Choi, K. L.; Wang, Y.; Permana, P. A.; Xu, L. Y. et al. Identification of novel putative membrane proteins selectively expressed during adipose conversion of 3T3-L1 cells. *Biochem Biophys Res Commun* **2002**, *293*, 1161-1167.
- (362) Roy, S.; Rached, M.; Gallo-Payet, N. Differential regulation of the human adrenocorticotropin receptor [melanocortin-2 receptor (MC2R)] by human MC2R accessory protein isoforms alpha and beta in isogenic human embryonic kidney 293 cells. *Mol Endocrinol* **2007**, *21*, 1656-1669.

- (363) Xiang, Z.; Litherland, S. A.; Sorensen, N. B.; Proneth, B.; Wood, M. S. et al. Pharmacological characterization of 40 human melanocortin-4 receptor polymorphisms with the endogenous proopiomelanocortin-derived agonists and the agouti-related protein (AGRP) antagonist. *Biochemistry* **2006**, *45*, 7277-7288.
- (364) Proneth, B.; Xiang, Z.; Pogosheva, I. D.; Litherland, S. A.; Gorbatyuk, O. S. et al. Molecular mechanism of the constitutive activation of the L250Q human melanocortin-4 receptor polymorphism. *Chem Biol Drug Des* **2006**, *67*, 215-229.
- (365) Chubet, R. G.; Brizzard, B. L. Vectors for expression and secretion of FLAG epitope-tagged proteins in mammalian cells. *Biotechniques* **1996**, *20*, 136-141.
- (366) Blondet, A.; Doghman, M.; Durand, P.; Begeot, M.; Naville, D. An E-box-containing region is involved in the tissue-specific expression of the human MC2R gene. *J Mol Endocrinol* **2004**, *32*, 811-823.
- (367) Frigeri, C.; Tsao, J.; Czerwinski, W.; Schimmer, B. P. Impaired steroidogenic factor 1 (NR5A1) activity in mutant Y1 mouse adrenocortical tumor cells. *Mol Endocrinol* **2000**, *14*, 535-544.
- (368) Gummow, B. M.; Scheys, J. O.; Cancelli, V. R.; Hammer, G. D. Reciprocal regulation of a glucocorticoid receptor-steroidogenic factor-1 transcription complex on the Dax-1 promoter by glucocorticoids and adrenocorticotrophic hormone in the adrenal cortex. *Mol Endocrinol* **2006**, *20*, 2711-2723.
- (369) Chen, M.; Cai, M.; Aprahamian, C. J.; Georgeson, K. E.; Hruby, V. et al. Contribution of the conserved amino acids of the melanocortin-4 receptor in [corrected] [Nle⁴,D-Phe⁷]-alpha-melanocyte-stimulating [corrected] hormone binding and signaling. *J Biol Chem* **2007**, *282*, 21712-21719.
- (370) Yang, Y. K.; Fong, T. M.; Dickinson, C. J.; Mao, C.; Li, J. Y. et al. Molecular determinants of ligand binding to the human melanocortin-4 receptor. *Biochemistry*. **2000**, *39*, 14900-14911.
- (371) Zhang, X.; Firestein, S. The olfactory receptor gene superfamily of the mouse. *Nat Neurosci* **2002**, *5*, 124-133.
- (372) Young, J. M.; Shykind, B. M.; Lane, R. P.; Tonnes-Priddy, L.; Ross, J. A. et al. Odorant receptor expressed sequence tags demonstrate olfactory expression of over 400 genes, extensive alternate splicing and unequal expression levels. *Genome Biol* **2003**, *4*, R71.
- (373) Young, J. M.; Friedman, C.; Williams, E. M.; Ross, J. A.; Tonnes-Priddy, L. et al. Different evolutionary processes shaped the mouse and human olfactory receptor gene families. *Hum Mol Genet* **2002**, *11*, 535-546.

- (374) Mural, R. J.; Adams, M. D.; Myers, E. W.; Smith, H. O.; Miklos, G. L. et al. A comparison of whole-genome shotgun-derived mouse chromosome 16 and the human genome. *Science* **2002**, *296*, 1661-1671.
- (375) Gibbs, R. A.; Weinstock, G. M.; Metzker, M. L.; Muzny, D. M.; Sodergren, E. J. et al. Genome sequence of the Brown Norway rat yields insights into mammalian evolution. *Nature* **2004**, *428*, 493-521.
- (376) Behrens, M.; Bartelt, J.; Reichling, C.; Winnig, M.; Kuhn, C. et al. Members of RTP and REEP gene families influence functional bitter taste receptor expression. *J Biol Chem* **2006**, *281*, 20650-20659.

BIOGRAPHICAL SKETCH

Krista Renner Wilson was born in Ocala, Florida in 1981 to Robert and Janice Renner. Krista attended St. John Lutheran School in Ocala from kindergarten through 12th grade. At the age of eight Krista joined the 4-H Club, which quickly became a very important part of her life and education. She raised and showed lambs and hogs and also developed a flourishing rabbitry. Through 4-H Krista learned showmanship, responsibility, record-keeping and business skills which have been very valuable in academics and life. Krista graduated high school in 1999 with highest honors and received multiple scholarships for college. For 2 years, Krista attended Central Florida Community College in Ocala, FL where she majored in biology. Krista graduated in 2001 summa cum laude from the Honors Program and was also awarded the prestigious Science Student of the Year Award in 2001. Krista then traveled to Gainesville, FL to the University of Florida where she majored in animal science with a specialization in animal biology and a minor in chemistry. During the undergraduate years Krista was a part of the University Scholars Program where she worked with Dr. Carrie Haskell-Luevano to gain research experience. After graduation in 2003 with highest honors and receiving the J. Wayne Reitz Award given to the Outstanding Senior in the College of Agriculture and Life Sciences, Krista was married to Brandon Wilson and settled down in Gainesville to earn her doctorate in medicinal chemistry continuing to work with Dr. Carrie Haskell-Luevano. Krista was supported by the University of Florida Alumni Fellowship. She received her Ph. D. in 2008 and plans to take time off to raise her children before pursuing a career in academia.